Oles Honchar Dnipro National University

V.I. Lipovskyi

«APPLIED DESIGN TASKS OF A TOP CHARGING ARRANGEMENT FOR A BLAST FURNACE»

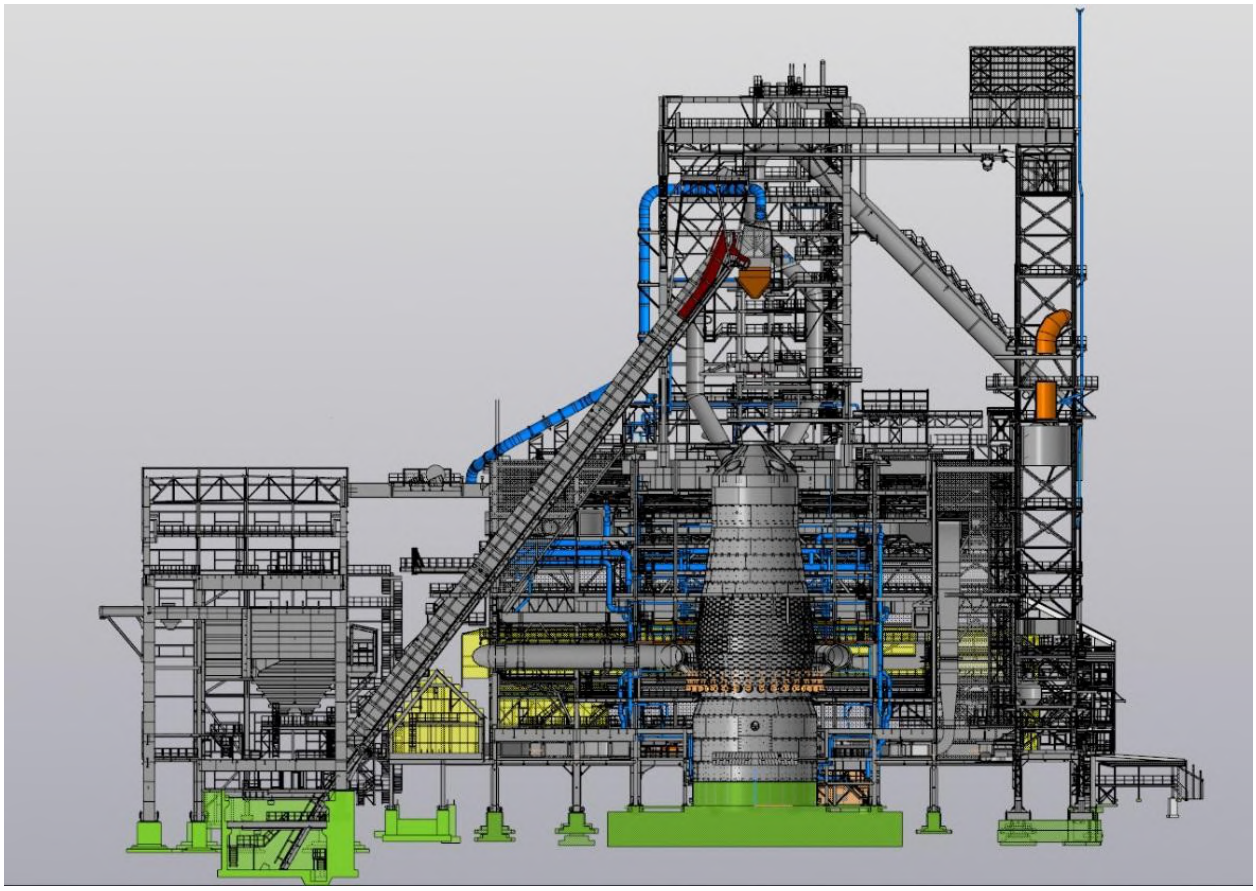

Dnipro
2025

UDC 669.162.215.2:539.3]
L79

Рекомендовано до друку Вченою радою
Дніпровського національного університету імені Олеся Гончара
(від 25 вересня 2025року протокол № 5)

Reviewers:

Baiul Kostiantyn, Doctor of Engineering Sciences, Senior Researcher, Technological Equipment & Control Systems Dept., Z.I. Nekrasov Iron & Steel Institute of National Academy of Sciences of Ukraine, Dnipro, Ukraine.

Belodedenko Serhii, Doctor of Engineering's Sciences, Professor, Head of Department of Industrial Mechanical Engineering, Dnipro Metallurgical Institute, Ukrainian State University of Science and Technologies.

L79 Lipovskyi V.L. Applied design tasks of a top charging arrangement for a blast furnace/ DNU [electronic resource]. Dnipro, 2025. 230 p.

Ліповський В.І. Прикладні задачі проектування колошникового завантажувального пристрою доменної печі/ ДНУ ім. О.Гончара [електронний ресурс]**.** Дніпро, 2025. 230с.

The monograph contains the results of solving the design problems of structures without a conical blast furnace charging device. All design cases of structural loads, namely, normal operating conditions, wind loads, and seismic effects, are considered. The results of calculation of the main elements of the charging device, namely: charge hoppers, centering device, and charging devices, are presented. The results were obtained by means of finite element modeling implemented in the ANSYS CAE system

Монографія містить результати рішень задач проектування конструкцій без конусного колошникового завантажувального пристрою доменної печі. Розглянуті всі розрахункові випадки навантажень конструкцій, а саме нормальних умов експлуатації, вітрового навантаження та сейсмічного впливу. Представлено результати розрахунку основних елементів завантажувального пристрою, а саме: бункерів шихти, центрувача, завантажувальних пристроїв. Результати отримані за допомогою моделювання методом скінченних елементів реалізованого в CAE системі ANSYS.

.

УДК 669.162.215.2:539.3]=111

INTRODUCTION

A distinctive feature of human development is continuous improvement of existing technologies and creation of fundamentally new ones. The history of technology demonstrates that replacement of old technologies with new ones is a natural process driven by the accumulation of knowledge, the development of tools, and the emergence of more efficient solutions. The introduction of new technologies transforms every sphere of human activity, ensuring sustainable development and improving quality of life.

Real-world examples in medicine, energy, information technology, space exploration, aviation and transportation, materials science, construction, agriculture, ecology, industry, and manufacturing illustrate this development trend. Each new step is determined by the level of scientific progress as a method of understanding and advancement of tools for modeling complex systems and phenomena, as well as for creation of innovative results.

Technological development is closely linked to progress in science and engineering. This process is inevitable, as technology not only addresses current needs but also serves as a driving force for the evolution of society.

Today, numerical methods and modeling play a crucial role in creation of new technologies and optimization of existing processes. They enable precise calculations, prediction of behavior of systems and materials, and reduction of experimental cost. With the advancement of artificial intelligence and quantum computing, the world is preparing for a new leap forward. These technologies are already being applied in development of complex simulations, optimization of production processes, and creation of materials with predefined properties.

Modern engineering education has widely integrated and applied CAD (Computer-Aided Design) systems, CAE (Computer-Aided Engineering), CAM (Computer-Aided Manufacturing), and Product Lifecycle Management (PLM) systems. Regardless of the industry, numerical calculations and modeling have become the foundation of innovation, driving technological progress and sustainable development.

Metallurgy, one of the oldest industries, vividly illustrates the evolution of technology in the context of scientific progress and introduction of new tools. This sector has progressed from traditional oresmelting methods in primitive furnaces to modern innovative technologies such as Direct Reduced Iron (DRI) and Electric Arc Furnace (EAF) metallurgy.

In its early stages, humanity relied on blast furnaces, which remained the foundation of the iron and steel industry for centuries. These furnaces enabled the processing of iron ore into pig iron, which was then converted into steel. However, high energy consumption, significant CO_2 emissions, and limited efficiency necessitated the development of new technologies. The cycles of technological change are illustrated in Figure 0.1 [1].

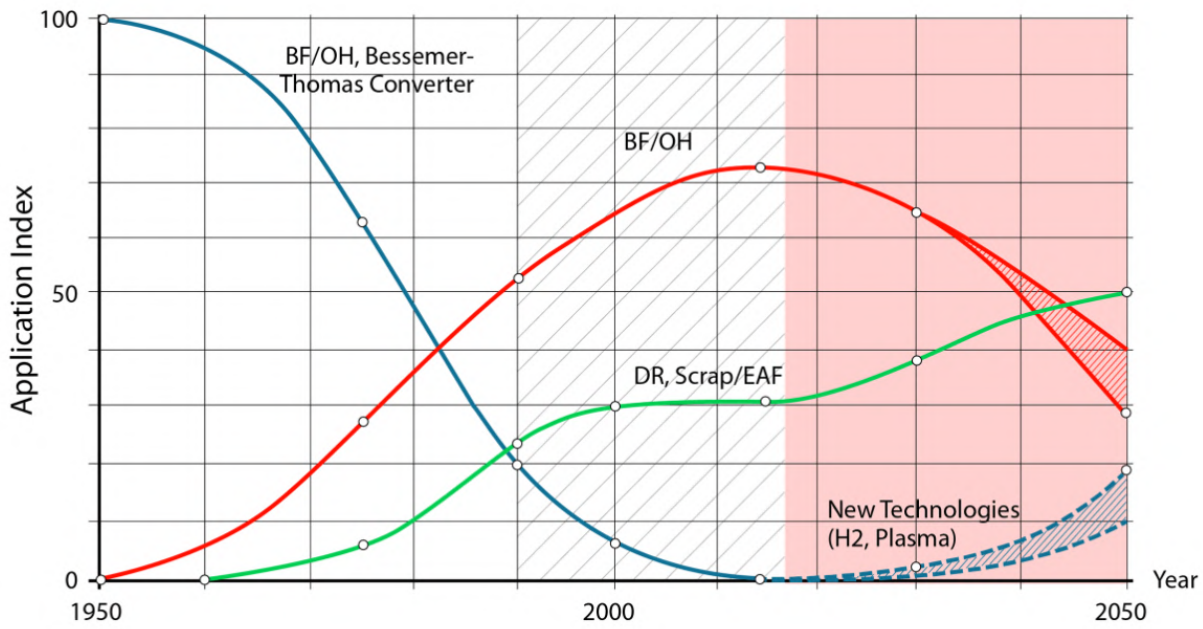

Fig. 0.1 Technology Transition Cycle in Metallurgy

The BF/OH technology refers to the steelmaking process that uses two types of furnaces: blast furnaces (BF) and open-hearth furnaces (OH). The Bessemer-Thomas Converter was the primary steel production method in the 19th and early 20th centuries. The invention of the Bessemer converter in the 19th century was revolutionary, enabling mass steel production from pig iron. This process significantly reduced steel production costs, fueling industrialization. These

methods paved the way for modern basic oxygen furnace (BOF) technologies, which are more efficient and environmentally friendly.

However, due to numerical modeling, automation, and new raw material processing methods and technologies are being implemented:

1. **Direct Reduced Iron (DRI) – DR (Direct Reduction):** This technology involves direct reduction of iron ore into sponge iron using natural gas or hydrogen. Currently, plants in India and the Middle East actively use DRI due to the availability of natural gas. This method significantly reduces CO_2 emissions compared to blast furnaces.
2. **Electric Arc Furnaces (EAF) – Scrap/EAF (Electric Arc Furnace):** This method produces steel from scrap metal or DRI using electricity. In the U.S. and Europe, steel plants frequently use Scrap/EAF as their primary steel production method. In Ukraine, the ArcelorMittal Kryvyi Rih plant [2] is implementing EAF to recycle scrap metal, minimizing its carbon footprint.
3. **Metal 3D Printing:** This technology enables the production of metal parts using layer-by-layer powder deposition. Metallurgical companies like GE Additive [3] use 3D printing to manufacture aircraft engine components that are both lighter and stronger than traditional parts.
4. **Hydrogen-Based Blast Furnaces:** Projects like HYBRIT [4] in Sweden are replacing coal with hydrogen, virtually eliminating CO_2 emissions. Given the global environmental agenda, the metallurgy industry is striving to reduce its carbon footprint.

Transition from blast furnaces to DRI and EAF demonstrates that technology change is not only natural but also necessary for ensuring sustainable development. Metallurgy clearly illustrates how the combination of scientific progress, numerical modeling, and new technologies contributes to creation of more efficient, cost-effective, and environmentally friendly solutions.

This study examines the **design challenges of the blast furnace top charging system**. The results were obtained using finite element modeling within the ANSYS

CAE system. The study presents design calculations of the main components of the charging system [5]. The models are designed to meet technological requirements to minimize harmful emissions in blast furnace production.

Design Object: Blast Furnace Top Charging System

An essential component for the operation of a blast furnace is the **top charging system**. According to the *Encyclopedic Metallurgical Dictionary*, it is a multi-level metal structure. It is designed to accommodate a complex set of mechanisms and equipment that ensure loading of charge materials into blast furnace, gas extraction, as well as installation and dismantling of charging apparatus and other equipment during furnace maintenance [5].

Configuration and composition of the top charging system are determined by the size of blast furnace, the type of supporting metal structures, and the type of charging apparatus. It consists of:

- Charging system
- Burden level measurement sensors
- Gas extraction ducts
- Atmospheric valves
- Lifting mechanisms for equipment installation and maintenance
- Load-bearing steel structures and service platforms for mechanism maintenance

A general view of the charging system including a section of the blast furnace is shown in Fig. 0.2 and on the title page of the monograph [6].

Operating Conditions and Types of Charging Systems

The charging system operates under extremely harsh conditions, being exposed to large amounts of abrasive burden materials, dust-laden gas, excess pressure, and high, uneven heating. There are several types of such systems:

2.1 **Bell-type charging systems**

2.2 **Bell-less charging systems**

2.3 **Cascade charging systems**

2.4 Combined systems

Bell-less charging systems are the most widely used due to their high precision and efficiency in burden distribution, which is especially important for large blast furnaces. Their application provides several advantages:

- **Reduction in fuel consumption**
- **Decrease in CO_2 emissions**
- **Extended service life of the furnace lining**

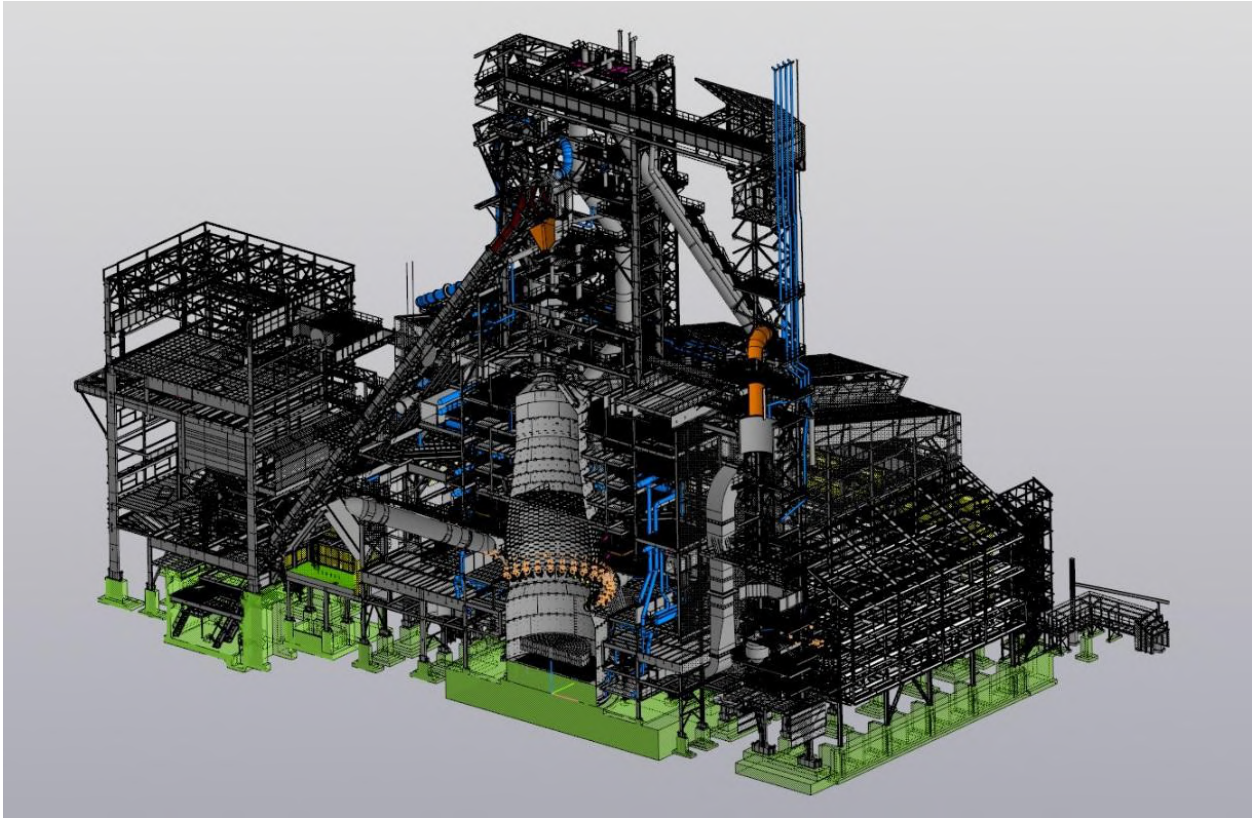

Fig. 0.2 General View of the Charging System with a Section of the Blast Furnace

Currently, European companies such as **Paulus (Germany)** [7], **Danieli Corus (Italy)** [8], **and Primetals Technologies (Austria)** [9] are designing and implementing modern charging system projects.

Paulus focuses on upgrading bell-less charging systems by integrating automated control systems.

Danieli Corus specializes in high-performance bell-less charging systems with a minimal carbon footprint.

Primetals Technologies is developing innovative AI-powered bell-less systems for load analysis and optimization.

Ukraine is actively modernizing its metallurgy sector [10]. As a result, it is adopting these technologies. Notable implementations in the country include projects at **Zaporizhstal** and **ArcelorMittal Kryvyi Rih**:

– At **Zaporizhstal**, a **Danieli Corus** bell-less charging system has been introduced [11].

– At **ArcelorMittal Kryvyi Rih**, charge management technologies, including bell-less systems, have been implemented to enhance efficiency [12].

The general view of the **Danieli Corus** bell-less charging system is shown in Fig. 0.3. This illustration does not provide detailed depictions of charge level sensors, gas extraction ducts, atmospheric valves, lifting mechanisms for equipment installation and maintenance, load-bearing steel structures, or service platforms.

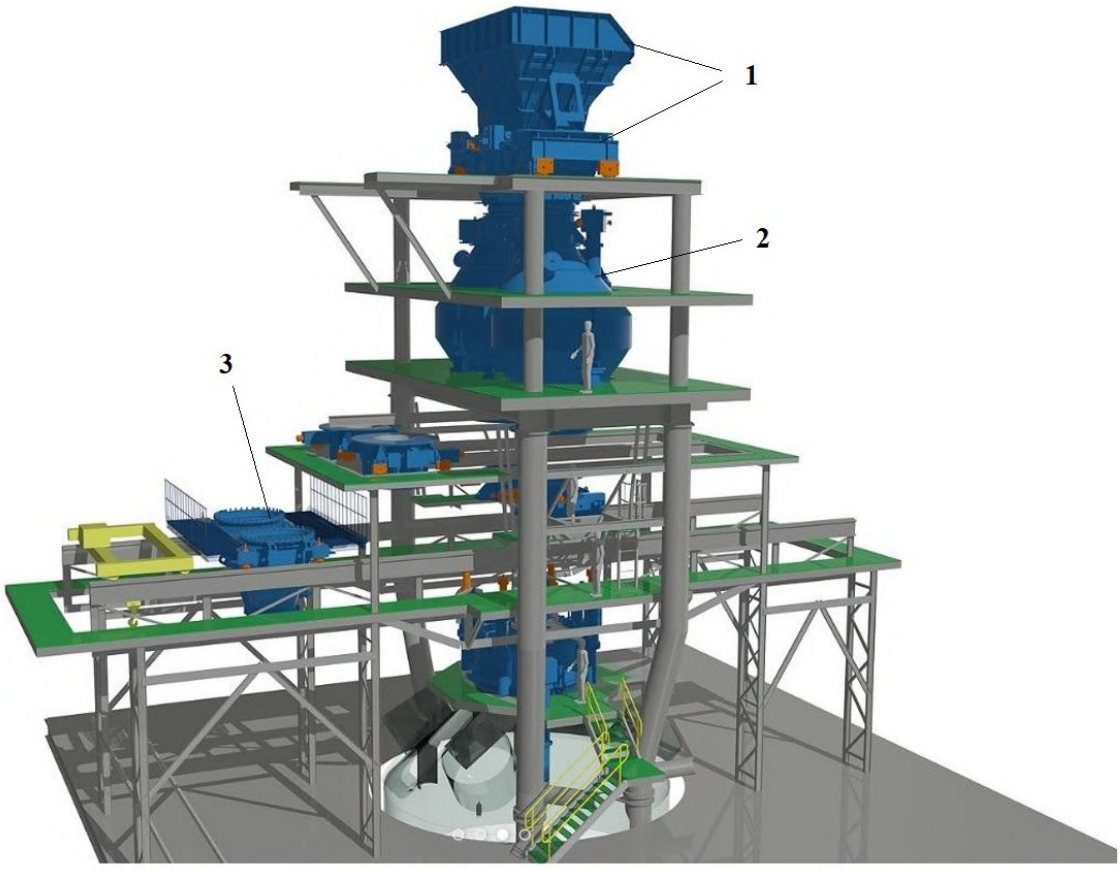

Fig. 0.3 Bell-less Charging System by Danieli Corus [13].

The main components of the charging system include:

– Upper and lower hoppers (1)

– Charge bunker (2)

– Centering top-charging unit (3)

These structures are designed for specific technological and operational conditions. The design of these components will be discussed in this study.

Fig. 0.4 Bell-less Charging System by Danieli Corus [13].

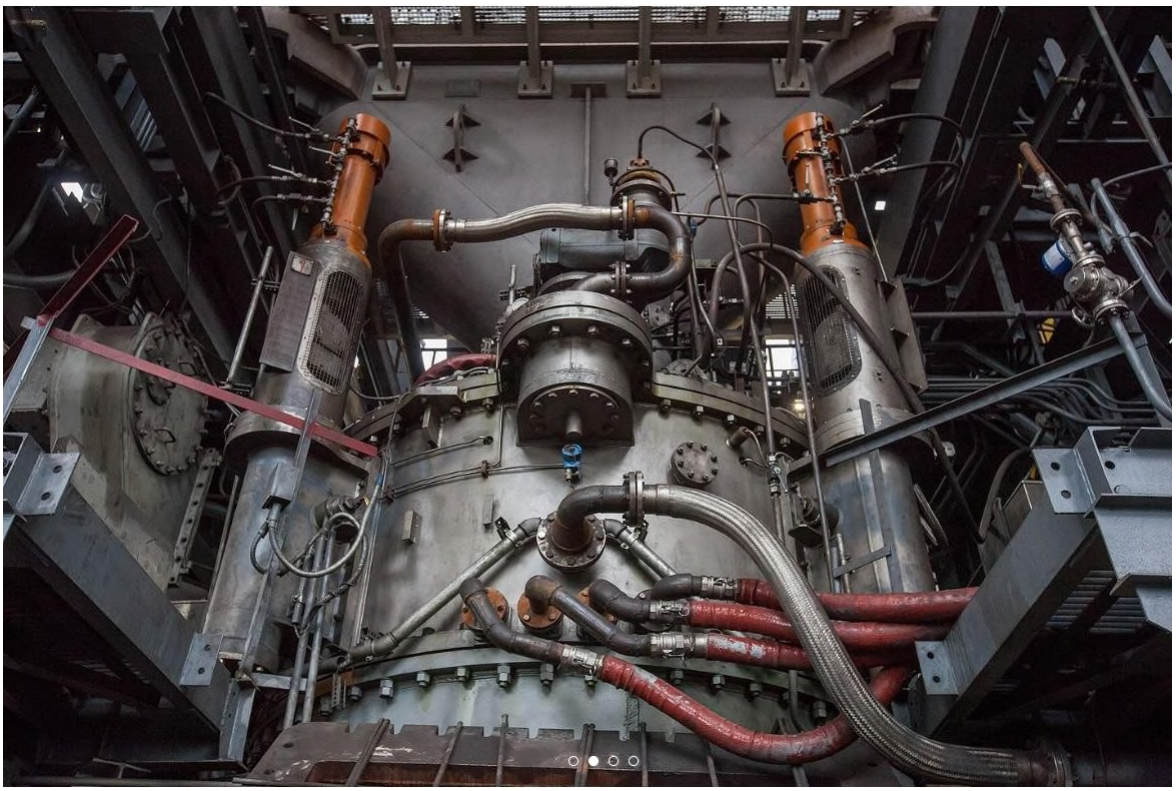

Fig. 0.5 Bell-less Charging System by Danieli Corus [13].

Figs. 0.4 – 0.5 show photographs of parts of the Danieli Corus bell-less charging system [13].

Methodology for Design Calculations

As the initial geometric data for design calculations of receiving hoppers, charge hoppers, and centering unit, drawings of prototype structures were used. The calculations were performed for all loading scenarios considering technological features of the equipment's operation conditions and placement.

At the first stage, material selection for these structures was conducted. The choice of material was based on a numerical experiment performed for the charge hopper under normal stating conditions (NSC). A comparison was made between two materials: 09G2S (S355 analogue) and 10HSND.

Normal operating conditions correspond to a scenario of combined loading, including:

- Internal pressure of 0.23 MPa,
- Thermal load of 450°C,
- Full hopper load with charge material.

The charge material may consist of coke, sinter, or pellets. The material properties used in the calculations are provided in Table 0.1 [14]. The material with the highest density was selected for the calculations.

Table 1.1 Typical Burden Data

Description	Bulk Densities (dry basis), (t/m^3)	Sizes, (mm)
Coke	0.50	Avg. : 25–70 Max.: 125
Sinter	1.70	Avg.: 5–50 Max.: 125
Pellet	2.10	Avg.: 9–16 Max: 125

Based on a comparison of the calculation results for all designed structures, 09G2S was selected. All loading scenarios were determined, including:

- Normal stating conditions (NSC)
- NSC plus wind load from various wind directions

- NSC plus seismic load combined with wind load

A separate sub-modeling method was used to analyze the strength of lifting lugs and flange connections.

For prototype structures with known geometric parameters, design adjustments were made based on fundamental strength calculations. If any localized failure in the designed structure was identified, modifications were applied to that specific area. The geometry was refined iteratively until all structural integrity requirements were met.

Load Considerations Based on Project Location

Step-by-step design refinement followed an adaptive approach using the prototype structure to meet specific loading conditions. Seismic and wind load factors were applied considering the location of the designed structures in Zaporizhzhia, Ukraine. Themeteorological data for Zaporizhzhia is as follows:

- **Ambient temperature**: Maximum: +40.2°C; Minimum: -29.3°C
- **Relative humidity**: Maximum: 100%; Minimum: 32%
- **Climate and precipitation**: Climate: Moderate;
  - Maximum daily precipitation: 128 mm
  - Average annual precipitation: 510 mm
- **Wind:** Average wind speed: 28.8 m/s
- **Elevation:**
  - Average elevation above sea level: 140 m
  - Seismic zone: MSK-64 classification

The final calculation results for structurally sound components are presented as stress and strain contour plots, deformation diagrams, and safety factor distributions for each component of the bell-less charging system.

CHAPTER I

1.1 ASSESSMENT OF THE STRENGTH OF THE CHARGE BUNKER

1.1.1 Design features

The design calculation and strength assessment of the pressurized bin of the blast furnace top charging device were carried out based on the original prototype drawing. This bin is an integral part of the blast furnace charging system. The structural features of the bins and its operation are determined by the following factors:

–overall weight of the entire structure shall not exceed 100000kg, and the volume of material bin equals to 27 m3;

–bottom elevation of the structure is at the level of 47748mm, and the top elevation is at the level of 53028mm. The top elevation is the place for the upper sealing valve weighing 12,500kg fixed to the silo's flange. The entire structure is fitted with 3 external supports holding, both the bin itself and the upper sealing valve;

–the bin operates under conditions of steady-state thermal loading at the temperature of 450°C;

–the structure operators under conditions of alternate loading with asymmetry coefficient equal to 0;

–the design pressure in the bin equals to 2.3Bar (0.23 MPa), and annual oscillation quantity there of equals to 57000;

– operational lifetime is 20 years;

– the functional purpose of the bin is batch mixture intake and charging thereof into the blast furnace. The calculations use the batch mixture (pellets) with maximum density of 2100 kg/m3as an example of a material to be charged;

– the blast furnace top-charging unit is located in Zaporozhye, Ukraine. The altitude of the land is 140 m, seismic zone corresponds to MSK-64.

1.2 INITIAL DATA, DEISGN CASES AND DESIGN ARRANGEMENT OF THE BIN

1.2.1 Characteristics of bin design

The geometrical dimensions of the bin's structure are specified according to the prototype drawing, presented in Fig. 1.1;

The material of walls, bearing flanges, supporting brackets, upper weld-on linings and transportation lugs: plate steel 09G2S as per GOST19281-89.

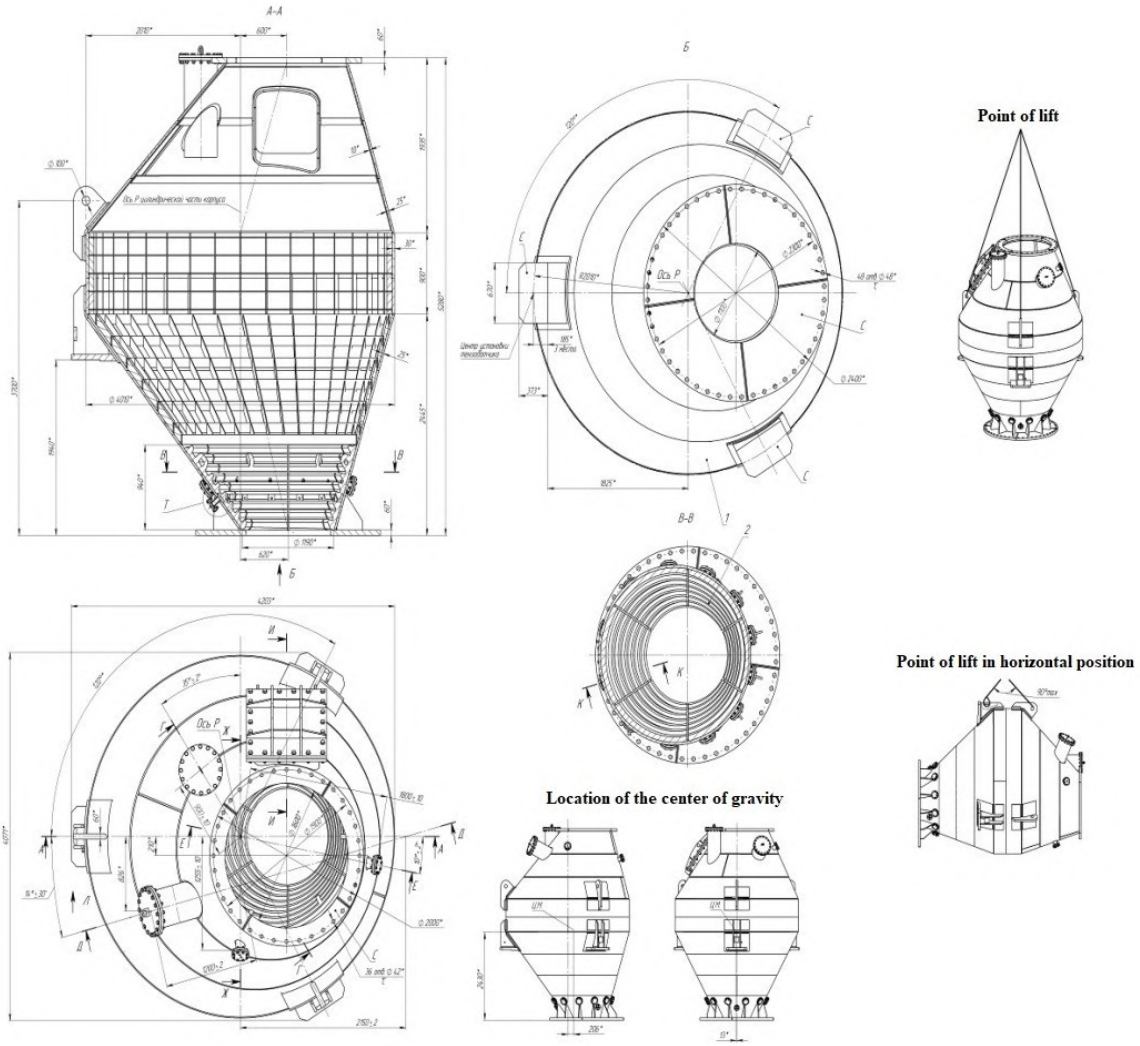

Fig. 1.1 Drawing of the prototype of bin structure

1.2.2 Physical and mechanical properties of materials. The operating conditions of the structure considered are determined by thermal steady-state field at the temperature of 450°C.The mechanical performance of 09G2S steel per GOST1050-88 at the temperature of 450°C are as follows:

–Yield strength, σ_{02} 157 MPa;

–Tensile strength, σ_v 392 MPa;

–Elasticity modulus 180 GPa;

–Poisson's ratio 0.3;

–Fatigue strength 210 MPa;

–Linear thermal expansion rate 1.38×10^{-5} deg^{-1};

– Rated density value 7850 kg/m^3;

– Yield strength, σ_{02} at 20°C 245 MPa.

For the purpose of assessment of structure's fatigue strength, the Wehler curve data have been used as obtained for the case of symmetrical case of loading with asymmetry coefficient ***R = –1.*** The data were taken from the reference guide V.T. Troschenko, L.A. Sosnovskiy "Endurance strength of metals and alloys", Part1 and normative document PNAE G-7-002-86, Fig.5.6, item 5.6.

1.2.3 Loads and design loading cases

Loads, recommended design cases of bin design and strength standards are regulated on the basis of the following normative documents:

− DBN V.1.2-2:2006 "LOADS AND EFFECTS: Design rules";

− SNiP 2.09.03-85: "Construction facilities of industrial enterprises: Bulk material container facilities";

– STP 0.03.082-2009. Qualification of seismic impact safety-related equipment. General requirements.

– SNiP 2.04.12-86. Construction codes and regulations. Strength calculation of steel pipelines.

– SNiP 2.01.07-85. Loads and effects.

− GOST30546.1-98, GOST 30546.2-98, GOST 30546.3-98. Interstate standards with supplements on seismic strength of machines, devices and other engineering items adopted in Ukraine in 2000.

− GOST R 51282-99. Processing equipment for launching and technical sites of rocket and space complexes. Design and testing rules.

− PNAE G-7-002-86. Strength calculation code for equipment and pipelines of nuclear power units;

− PNAE G-7-008-89. Rules for design and safe operation of equipment and pipelines of nuclear power units.

Besides thermal effect, the structure is further affected by the following loadings:

– internal design pressure;

– weight of metal structure ***Gκ=20294 kg*** and batch mixture. Total weight of the entire structure with batch mixture shall not exceed 100000kg;

– loose material loads acting on bin's walls;

– wind effect;

– seismic impact.

1.2.3.1 Loose material loads on bin's walls.

The calculation of loose material loads acting on hopper's walls is performed as per SNiP 2.09.03-85. Load safety factors g_f for structure's dead weight, service loads on flooring, snow load and wind effect are taken as per SNiP 2.01.07-85 and are equal to:

– for horizontal and vertical pressures of loose materials $g_f = 1.3$;

– for specified angle of loose material internal friction $g_f = 1.1$.

The loose design material vertical pressure onto horizontal plane shall be determined by the equation $p = 1.3\gamma h$, where γ is material specific weight, h is material layer elevation above the given point.

The design horizontal pressure onto horizontal plane is specified with the equation $p_h = 1.3\lambda\gamma h$, where λ is the lateral pressure factor that is taken as equal to the ratio of horizontal pressure to vertical one, i.e. $\lambda = p_h / p_a = tg^2(45^0 - \phi / (2\, g_f))$. Also, ϕ is material internal friction. For the types of loose materials used the rated value of ϕ angle equals to $35°$ (customer requirements-35). The design value of the rated internal pressure angle is determined as the rated internal friction angle deleted by the load safety factor $g_f = 1.1$. The value is $\lambda = 0.309564$.

Since the pressure from the loose material is determined by the maximum possible bin filling degree, i.e. when material is over the bin's top elevation at the natural degree of repose, the bin is under effect of the following loads:

–loose material pressure onto the vertical wall of the bin's cylindrical part. The rated horizontal pressure for the case of maximum possible loose material filling degree is determined by the equation $p_h = n \times \gamma \times z \times cos2\psi$, where n is the dynamic response factor (Table 1, Guidelines on calculation and designing of reinforced concrete, steel and combined bunkers, Moscow, Stroyizdat, 1983, 200 ps.). $n=1.2$, $\gamma=2100$, $\psi=35°$ (loose material repose angle), $cos^2\psi= 0.671$, skip capsule volume $9m^3$;

–loose material pressure onto sloping wall in bin's conical part. The angle of structure's wall slope is adopted as constant and equal to $\alpha=60°$. The rated normal pressure onto the sloping wall for the case of maximum possible loose material filling degree is determined as follows $p_h = n \times \gamma \times (z+h_0) \times cos^2\alpha + n \times \gamma \times z \times cos^2\psi \times sin^2\alpha$; where $h_0 = 1.295$ m, $n = 1.2$, $\gamma = 2100$, $\psi=35°$, $\alpha=60°$, and z is the coordinate of layer elevation from the top edge of bin's cylindrical part;

–bin hopper pressure at lower flange aperture area shall be determined by the equation $p_\alpha = p_h / \lambda$. The pressures $p_h = n \times \gamma \times z \times cos^2\psi$, shall be determined by the value of bin hopper's coordinate from the top edge of bin's cylindrical part $z=3.345$ m. Value $p_h = 55489$ Pa, $p_\alpha = 179248.9$ Pa.

The calculations use the material with maximum specific weight of $2100 kG/m^3$ as the batch mixture (pellets).

As per initial data the bin's walls are under effect of the following loose material loads, namely:

–the pressure on vertical wall in bin's cylindrical part, equaling to $p_h = 1691 \times z$ N/m2, where z is level elevation coordinate from the top edge of bin's cylindrical part;

–pressure on sloping walls in bin's conical part, equaling to $p_h = 1898.2 \times z + 815.85$ N/m^2, where z is level elevation coordinate from the top edge of bin's cylindrical part $0.9 \text{ m} \leq z \leq 3.345 \text{ m}$;

–the bin hopper at bin's lower flange aperture area is under effect of the pressure equaling to p_α = ***179248.9 Pa***. This value determines hopper bottom response reaction. The force is determined as the product of pressure and aperture's area and equals to ***Q=170346 N.***

1.2.3.2 Wind effect

The wind effect is an alternate load, for which two design values are set:

– limit design value;

– operating design value.

With respect to the norm the wind effect on the structure is set out as normal pressure preconditioned by general resistance of construction facility along *x* and *z* axes, and is conditionally applied to structure's projection on a plane square with appropriate axis. The limit design value of wind effect has been considered.

The limit design value of wind effect is determined by the formula:

$$W_m=\zeta_{FM} \times W_0 \times C,$$

where, ζ_{FM} is the safety factor for the limit value of wind effect, determined by the time of equipment operation. The value of this factor is determined by the Table 9.1 of DBN V.1.2-2:2006 and is taken equal to ζ_{FM} = ***0.90***;

W_0 is characteristic value of wind effect, and is defined by the wind region map 3 (Fig.1, annex E to design rules). For the city of Zaporozhye the wind effect characteristic value equals to ***460 Pa***.

Coefficient ***C*** is calculated by the equation:

$$C=C_{aer}\times C_h\times C_{alt}\times C_{rel}\times C_{dir}\times C_d,$$

where, C_{aer} is the aerodynamic factor of general frontal resistance. C_{aer} is calculated by pressure profile for construction facility with circular cylindrical surface as presented in sketch 12b of normative document (Fig. 1.2). Factor ***k*** is take equal to ***k=0.925*** (by the table for construction facility with circular cylindrical surface).

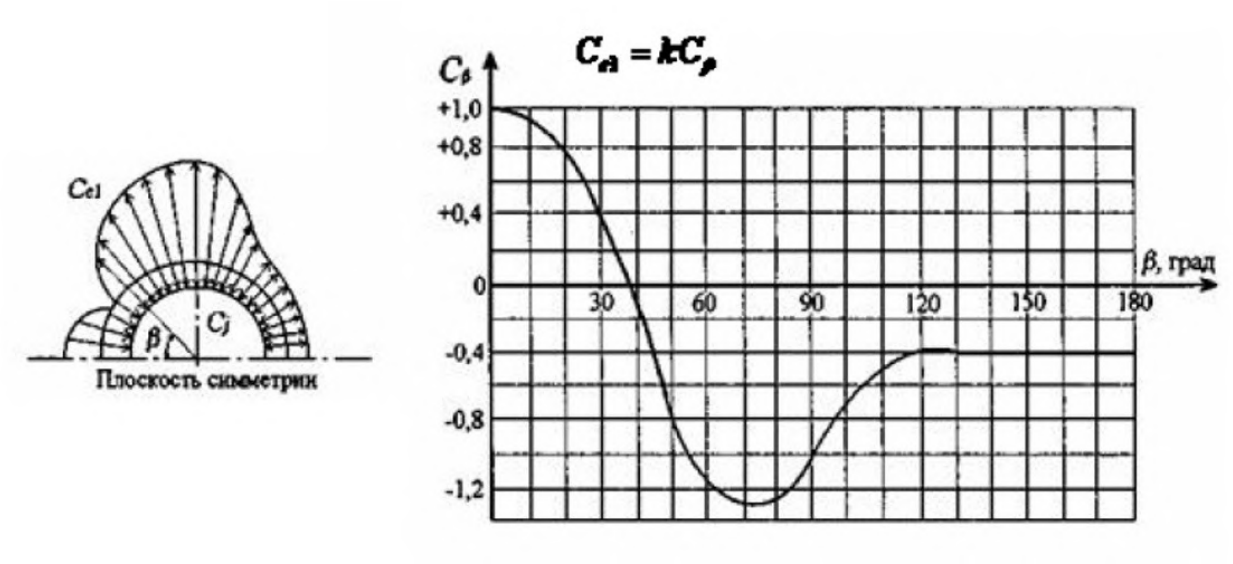

Fig. 1.2 Pressure profile at circular cylindrical surface

C_h is the coefficient of construction facility height, determined by the annex 1 of the normative document and equals to $C_h = 2.2125$;

C_{alt} is the coefficient of geographic height, equal to ***1.0,*** since the geographic height of the facility is H=150m above sea level and under [H] = 500m;

C_{rel} is the terrain relief factor, equal to ***1.0***;

C_{dir} is the coefficient of direction, equal ***1.0***;

C_d is the dynamic response factor, determined by Fig.9.9 of design rules for vertical vessels with lining by the maximal diameter and equals to ***1.05***.

The value of load factor defines the alternate pressure around the circular cylindrical surface dependent upon C_β, as follows:

$$C=0.925 \times C_\beta \times 2.125 \times 1.0 \times 1.0 \times 1.0 \times 1.05 = 2.064 \times C_\beta$$

The limit design value of wind effect alternating around circular cylindrical surface equals to:

$$W_m=0.9 \times 460 \times 2.064 \times C_\beta = 854.5 \times C_\beta \text{ Pa.}$$

This dependence is presented in the design model as discrete piecewise-constant distribution of pressure around bin's side surface at the pitch of 10° from plane of symmetry.

1.2.3.3 Seismic impact

The initial data for calculation of seismic strength of equipment designed are the seismic risk zoning of Ukraine (OSR-2004-A-B-C) developed by the Institute of Geophysics of the National Academy of Sciences of Ukraine. On the basis of construction norms "DBN V1.1-12:2006 Construction in seismic regions of Ukraine" the calculations are carried out for special load combination with consideration of seismic impact, i.e. design-basis earthquake (DE) and maximum design earthquakes (MDE). The location of the facility in Zaporozhye determines the seismic impact intensity values, namely:

– DE intensity –5 points as per MSK-64;

– MDE intensity –6 points as per MSK-64.

The calculations have been carried out for maximum design earthquakes MDE. Accelerograms and initial parameters for calculation are obtained on the basis of the following normative documents:

− PNAE G-7-002-86. Strength calculation code for equipment and pipelines of nuclear power units;

− PNAE G-7-008-89. Rules for design and safe operation of equipment and pipelines of nuclear power units.

The acceleration values for the given level of equipment mounting are determined by the method of linear interpolation in terms of vertical and horizontal oscillations with damping factor ***K = 0.02*** and site seismic intensity of 9 points (Fig. P9.1, Fig. P9.2 PNAE G-7-002-86). For seismic intensity of 6 points these parameters are multiplied by conversion factor equal to 0.12 (table P9.1). The initial parameters of accelerations for calculation on MDE are presented in Tables 1.1-1.3. The marks *43.323 m* and *57.648 m* correspond to centering unit, left material bin and loading module of top-charging unit.

Table 1.1 shows the generalized spectrum of horizontal oscillation response with damping factor 0.02 for the marks of equipment designed.

Table 1.1

Frequency, *f*, *Hz*	**0**	**3**	**4**	**6**	**10**	**12**	**15**	**24**	**30**
Mark *42.323 m*	**0,95**	**2,875**	**5,35**	**6,654**	**4,92**	**4,889**	**2,286**	**1,87**	**1,762**
Mark *47.748 m*	**1,06**	**2,116**	**9,201**	**9,584**	**3,773**	**3,695**	**2,72**	**2,035**	**1,789**
Mark *53.898 m*	**1,1**	**1,8**	**10,8**	**10,8**	**3,9**	**3,2**	**2,9**	**2,1**	**1,8**

Table 1.2

Frequency, *f*, *Hz*	**0**	**3**	**4**	**6**	**10**	**12**	**15**	**24**	**30**
Mark *42.323 m*	**0.492**	**1.207**	**1.78**	**2.25**	**2.365**	**2.566**	**2.25**	**2.3**	**3.403**
Mark *47.748 m*	**0.492**	**0.99**	**2.43**	**3.77**	**3.8**	**3.86**	**2.72**	**2.658**	**2.944**
Mark *53.898 m*	**0.492**	**0.9**	**2.7**	**4.4**	**4.4**	**4.4**	**2.912**	**2.805**	**2.75**

Table 1.3

Frequency, *f*, *Hz*	**0**	**3**	**4**	**6**	**10**	**12**	**15**	**24**	**30**
Mark *42.323 m*	**3.403**	**4.993**	**5.96**	**5.93**	**5.907**	**3.349**	**2.718**	**2.242**	**3.403**
Mark *47.748 m*	**2.944**	**2.76**	**3.54**	**3.457**	**3.378**	**2.52**	**2.144**	**1.781**	**2.944**
Mark *53.898 m*	**2.75**	**2.595**	**2.54**	**2.43**	**2.328**	**2.169**	**1.906**	**1.59**	**2.75**

The tables 1.2 and 1.3 show the generalized spectrum of vertical vacillation response with damping factor equal to 0.02 for the marks of the equipment designed.

1.1.1.1. Permissible stresses and design loading cases

According to PNAE G-7-002-86 (i. 3.4) for calculations the nominal permissible stress in elements of equipment and pipelines under internal pressure shall be taken equal to minimal from the following values:

$$[\sigma] = \min\{\sigma_в/2.6;\ \sigma_{02}/1.5\} = 104.7\ MPa.$$

Equipment static strength design and assessment of structure's operational capacity under normal service conditions (PNAE G-7-002-86, item 5.4) shall be performed according to the following groups of permissible groups:

– permissible membrane stresses (from action of design pressure)

$$[\sigma]_1 = [\sigma] = 104.7\ MPa;$$

– permissible reduced stresses determined by sums of membrane and bending stresses (design pressure + container facility dead weight + external loads, in accordance with normal service conditions):

$$[\sigma]_2=1.3[\sigma]= 136.1\ MPa.$$

For calculation of seismic strength for the loading type "normal service conditions plus maximum design earthquakes" (NSC + MDE) according to PNAEG7-002-86, i.5.11, the permissible reduced stresses to be used are as follows:

$$[\sigma]_2=1.4[\sigma]= 146.6\ MPa.$$

Consideration of wind effect is made for the loading type "normal service conditions plus limit design plus wind effect limit design value (NSC+LWE) for permissible reduced stresses:

$$[\sigma]_2=1.3[\sigma].$$

The nominal permissible stress in bolts of flanged joints are calculated as per i.3.5 PNAE G 7-002-86 $[\sigma] = \sigma_в/n_t$. Bolts of strength class 8.8 are made of steel 35. Tensile strength of this steel at the temperature of 350°C is $\sigma_в=500MPa$. Since the service temperature of bolts exceeds the rated value then according to section 3.2 of the normative document $n_t = 3$, the permissible stress equals to:

$$[\sigma] = 166.67MPa.$$

The nominative permissible stress at the temperature of 20°C is taken equal to material yield strength at this temperature and reduced by material safety factor. Material safety factor $\gamma_м$ is determined by the table 2 and as per GOST27772-88 and TU 14-1-3023-80 equals to $\gamma_м = 1.025;\ [\sigma] = \sigma_{02}/\gamma_м= 239\ MPa.$

Assessment of performance capacity of bin structure's elements is made by permissible stresses of each structural element at design temperature. The nominal permissible stress for each element is calculated in accordance with PNAE G 7-002-86 by material yield strength at design temperature. Tensile strength at design temperature is take equal to material yield strength at the temperature of 20°C reduced by correction safety factors for materials and temperature. The material safety factor is taken equal to $\gamma_м= 1.025$. Temperature correction factor is taken from PNAE G 7-002-86 and equals to the ratio of yield strength at 20°C to yield strength

at the temperature of 450°C for steel 09G2S: $\gamma_m = 245/157 = 1.56$. Yield strength values for structure's elements at 20°C are taken from quality certificates for materials whereof the bin is made: No.21189dd. Oct.15, 2016. "Ilyich Iron and Steel Works";No. 108-19382 dd. May 20, 2016 "Magnitogorsk Iron and Steel Works";No.10524 dd. May 21, 2016 "Ilyich Iron and Steel Works"; No.09-3752 dd. Mar. 27, 2016 Azovstal Iron & Steel Works; No.EN10204-3.1 dd. May 01, 2016 Research and Production Enterprise "Steelservice". The certificates served to provide the minimal yield strength values σ_{02}. For each structure's element the yield strength at the temperature of 450°C is determined as follows $[\sigma_{02}]_m = \sigma_{02}/(\gamma_м\gamma_m)$ and presented in Table 1.4.

Table 1.4

Structural member of material bin	Element thickness (mm)	Stresses (MPa)				
		σ_{02}	$[\sigma_{02}]_m$	$[\sigma]_1$	$1.3[\sigma]_1$	$1.4[\sigma]_1$
Cylindrical wall	**30**	**365**	**228.2**	**152.1**	**197.7**	**212.9**
Conical wall	**25**	**359**	**224.5**	**149.6**	**194.4**	**209.4**
Top flange	**60**	**310**	**193.8**	**129.2**	**167.9**	**180.8**
Bottom flange	**60**	**310**	**193.8**	**129.2**	**167.9**	**180.8**
Branch/flange	**10/30**	**375/365**	**234.5/ 228.2**	**156.3/ 152.1**	**203.1/ 197.7**	**218.8/ 212.9**
Hatch/flange	**25/40**	**359/350**	**224.5/ 218.8**	**149.6/ 145.8**	**194.4/ 189.5**	**209.4/ 204.1**
Support's lug	**60**	**310**	**193.8**	**129.2**	**167.9**	**180.8**

Consideration of corrosion affecting the permissible stress for each bin's structural element is made through reduction of design permissible stresses by the of corrosion factor n_k. Reduction in size Δ of any element due to corrosion is taken equal to 3mm; the corrosion factor is taken equal to $n_k = \Delta/(\Delta-3)$, and $[\sigma_{02}]_m = \sigma_{02}/(\gamma_м\gamma_m n_k)$ the table 1.5 shows adjusted permissible stresses. For cylindrical and conical bin's parts $n_k = 1$, since for the design bin's model these thicknesses are reduced as compared to design values by 3 mm and equal to 27 and 22 mm accordingly.

Permissible stresses for material bin's bolt joints are taken equal to

$$[\sigma] = 166.7 MPa.$$

The required assessments of structure performance capacity define the following design cases and design loading patterns:

– structural design under effect of design internal pressure;

– structural design under conditions of NSC;

– structural design under conditions of NSC + LWE;

– structural design under conditions of seismic impact NSC + MDE.

Table 1.5

Structural member of material bin	Element thickness (mm)	Stresses (MPa)				
		σ_{02}	$[\sigma_{02}]_m$	$[\sigma]_1$	$1.3[\sigma]_1$	$1.4[\sigma]_1$
Cylindrical wall	**30**	**365**	**228.2**	**152.1**	**197.7**	**212.9**
Conical wall	**25**	**359**	**224.5**	**149.6**	**194.4**	**209.4**
Top flange	**60/57**	**310**	**184.1**	**122.7**	**159.5**	**171.8**
Bottom flange	**60/57**	**310**	**184.1**	**122.7**	**159.5**	**171.8**
Branch/flange	**10/30**	**375/365**	**205.4/ 164.1**	**136.9/ 109.4**	**178.0 /142.2**	**191.6 /153.2**
Hatch/flange	**25/40**	**359/350**	**202.3 /197.6**	**134.9 /131.7**	**175.4 /171.2**	**188.8 /184.3**
Support's lug	**60/57**	**310**	**184.1**	**122.7**	**159.5**	**171.8**

1.2.3.5 Design case for normal service conditions

The bin's operation corresponds to two load cases: operation under pressure and operation under no pressure. The design case for normal service conditions (NSC) is defined by the following loads acting on bin's structure:

– sealing valve weight force acting on bin's top flange and equal to:

$G_{кл}$= 12500 kg = 122625 N;

–bottom sealing flange weight force acting on bin's bottom flange:

$G_{н}$= 14500 kg = 142245 N;

–design internal pressure in the bin equals to ***p =0.23MPa;***

–structure's bulk weight force. Bin's weight taken into consideration is ***$G_{К}$=20294 kG***;

–forces of design internal pressure acting on:

a) sloping and vertical standard DN 400 flanges with aperture's diameter of 400mm, and equaling to ***29780 N;***

b) top nonstandard flange with aperture's diameter of 1600 mm, and equaling to ***462432 N;***

c) bottom nonstandard flange with diameter of 110 mm, and equaling to ***218576 N;***

d) flange of lateral inspection manhole, and equaling to ***182022 N***. This force in the design model is replaced with ***379505 Pa;***

– thermal stress at steady-state heating of the structure up to 450°C;

–loose material pressure onto vertical wall in bin's cylindrical part $p_h = 2730 \times z$;

– loose material pressure onto sloping wall in bin's conical part $p_h = 1220.5 \times z$;

– loose material force onto bin hopper ***Q = 170346 N.*** This force is taken into account only in shut-off condition of the sealing valve.

For design case of bin operation under no pressure all loads caused by acting design pressure are disregarded.

The design model of material bin under normal service conditions is presented in Fig. 1.3. The pattern of loose material pressure application onto bin's cylindrical and conical walls is presented in Fig. 1.4.

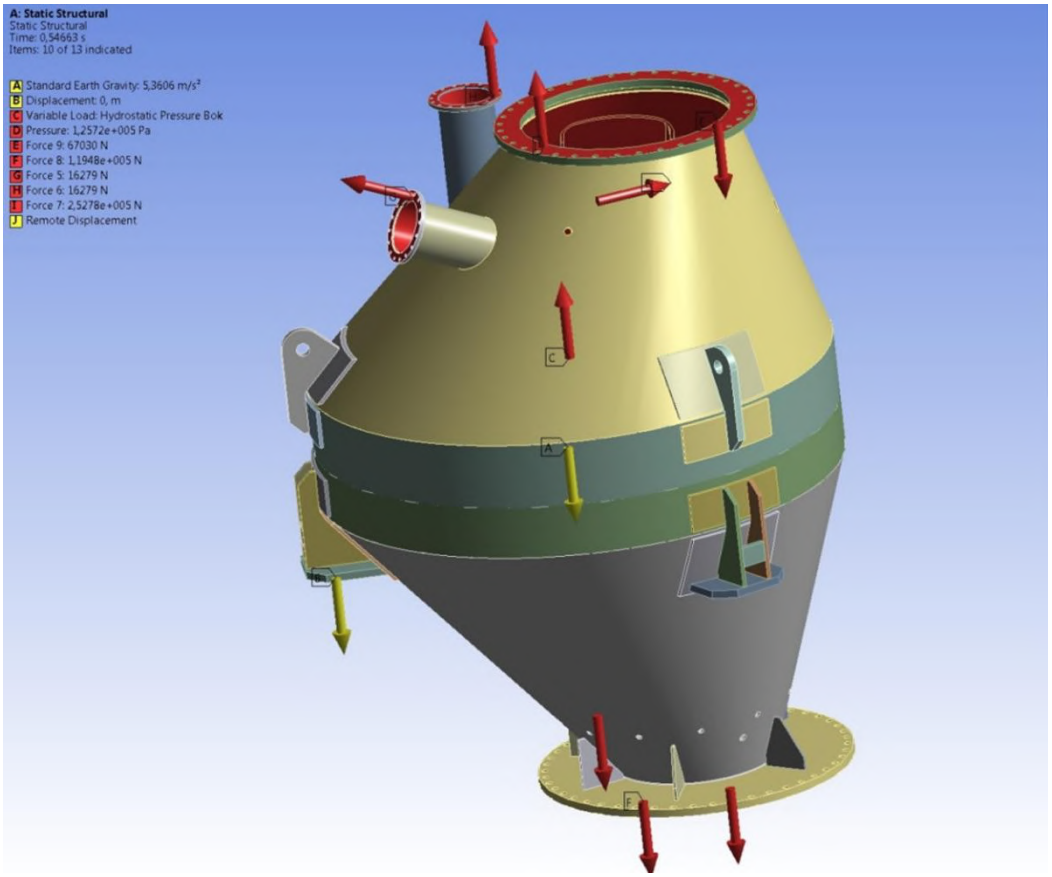

Fig. 1.3 Design loading pattern of the bin under NSC

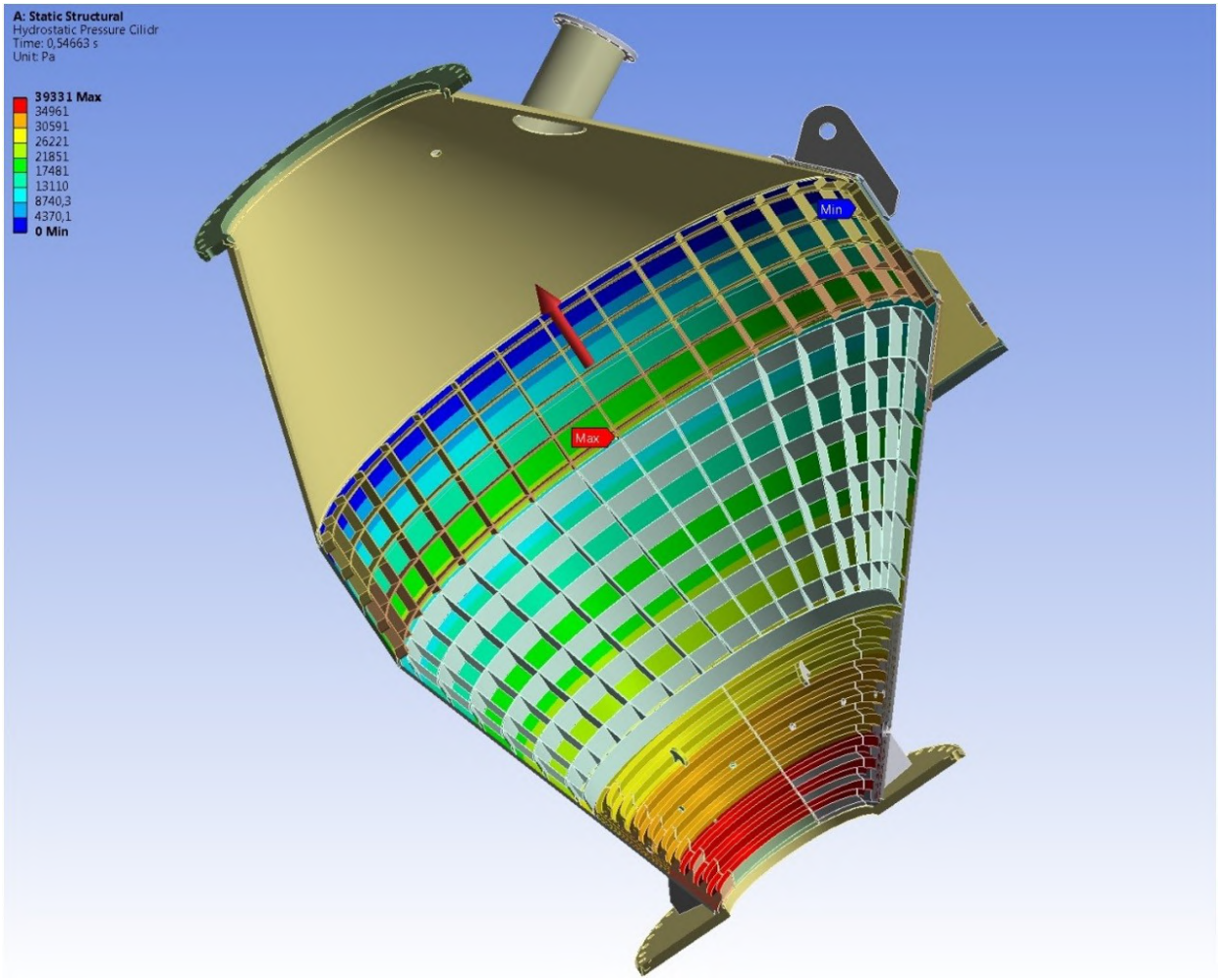

Fig. 1.4 Loose material pressure distribution on bin's walls

1.1.2. Fundamental principles performing calculations and analyzing and calculation results

When performing calculations, the following features are to be taken into consideration:

– the structure's geometrical model shall take into consideration all structure's stress risers caused by fillets and chamfers of component parts, as well as corrosion. On recommendations of the customer the consideration of corrosion is made with reduction of load-bearing cover thickness of structure's design by 3 mm. Thickness of cylindrical part is ***27 mm***, and for conical part the value is ***22 mm***;

– on customer's demand the bin is released of all internal ribs and linings. Weight of these elements (grid + lining = ***4573.39 kg***), as well as the weight of manhole lid with ribs (weighing ***398.05 kg***), is added to entire structure. The total

weight equals to ***19358.44 kg*** and the volume is ***1,8328 m^3***. The entire weight has been increased by safety factor ***1.05*** in relation to loads and equals to ***20294 kg***. The calculations specify this weight with the material density value equaling to ***11090 kg/m^3*** for the volume in question.

– structure's materials shall be considered as nonlinear elastic isotropic materials with mechanical characteristics corresponding to service temperature of 450°C. The calculations shall employ the bilinear deformation curve for the service temperature;

– an ideal contact interaction is adopted for all welded structure's surfaces;

– for structure's materials the sketch presentation of Wehler curve with physical endurance limit σ is to be adopted as per Baskvin's equation;

– the value of endurance limit reduction factor K_f is to be determined with consideration of surface roughness factor $K_{F\sigma}$ and cross-section full size response factor $K_{d\sigma}$;

– roughness effect is to be taken into account as per the procedure set out in GOST 25.504-82. Assuming that structure's surface has roughness from 0.8 to 1.6 μm the factor $K_{F\sigma} = 0.92$;

– cross-section full size response factor is to be determined by the nomographic chart presented in the reference guide "Machine part strength design: reference guide / I.A. Birger, B.F. Shor, G.B. Iosilevich". For sheet thickness of 30 mm the factor is $K_{d\sigma} = 0.92$. In this case the endurance limit reduction factor K_f is adopted in the calculation equal to 0.846;

– to determine the fatigue resistance in the presence of local stress risers the equation of Morrow-Manson is to be used;

– the obtained load history characteristics for components of stress tensor are brought to damage-equivalent characteristics under conditions of single-axis loading. The transition to reduced stresses (damage-equivalent, single-axis) by amplitude and average values of load cycle stresses is to be made by the value of specific distortion energy;

– the obtained load history characteristics with asymmetry coefficient $\boldsymbol{R = 0}$ are to be brought to damage-equivalent characteristics under conditions of symmetric cycle loading. To perform this transition, the formulas for the amplitude of equivalent symmetrical cycle stress loading $\sigma_{аэкв}$ are used on the basis of Goodman's law;

– the assessment of service lifespan of a unit is to be performed by the number of cycles till failure. This assessment is carried out using the stress cycle behavior function by Wehler curve described;

– as strength criterion the IV – th theory of strength is to be used.

– with regards for all erection and transportation operations with material bin the design patterns shall adopt the value of overload factor as per GOST R 51282-99 (table 10) equal to 1.2.

– when analyzing the calculation results the local extremums of equivalent stresses are not to be considered, if the act in areas within a finite element. This recommendation is related to numerical singularity of finite element method and can be removed by means of structure submodelling in the given area and corrective remeshing of the finite element model. The structure submodelling in such an area can be made for selected bin structure elements.

1.2.5 Description of bin designing procedure.

Structure's geometric modeling has been performed using three-dimensional presentation of the bin in SolidWorks software-package. Physical modeling has been carried out in ANSYS software-package. The calculation procedure of structure's stress-strain state is the finite-element method implemented by ANSYS WORKBENCH calculation package.

The bin structure's finite-element model and fragments thereof is presented in Fig. 1.5.

Fig. 1.5 Finite-element model for material bin designing

The model consists of 2815764 nodes united by 798557 elements. The mesh quality is 0.83. Dimension of a finite element side does not exceed 25mm.

1.3 BIN DESIGN CALCULATION

1.3.1 Structural design under estimated loading

Results of bin designing for the load case of internal design pressure are presented in a form of stress and strain patterns, and fatigue design parameters in Fig. 1.6 – 1.19.

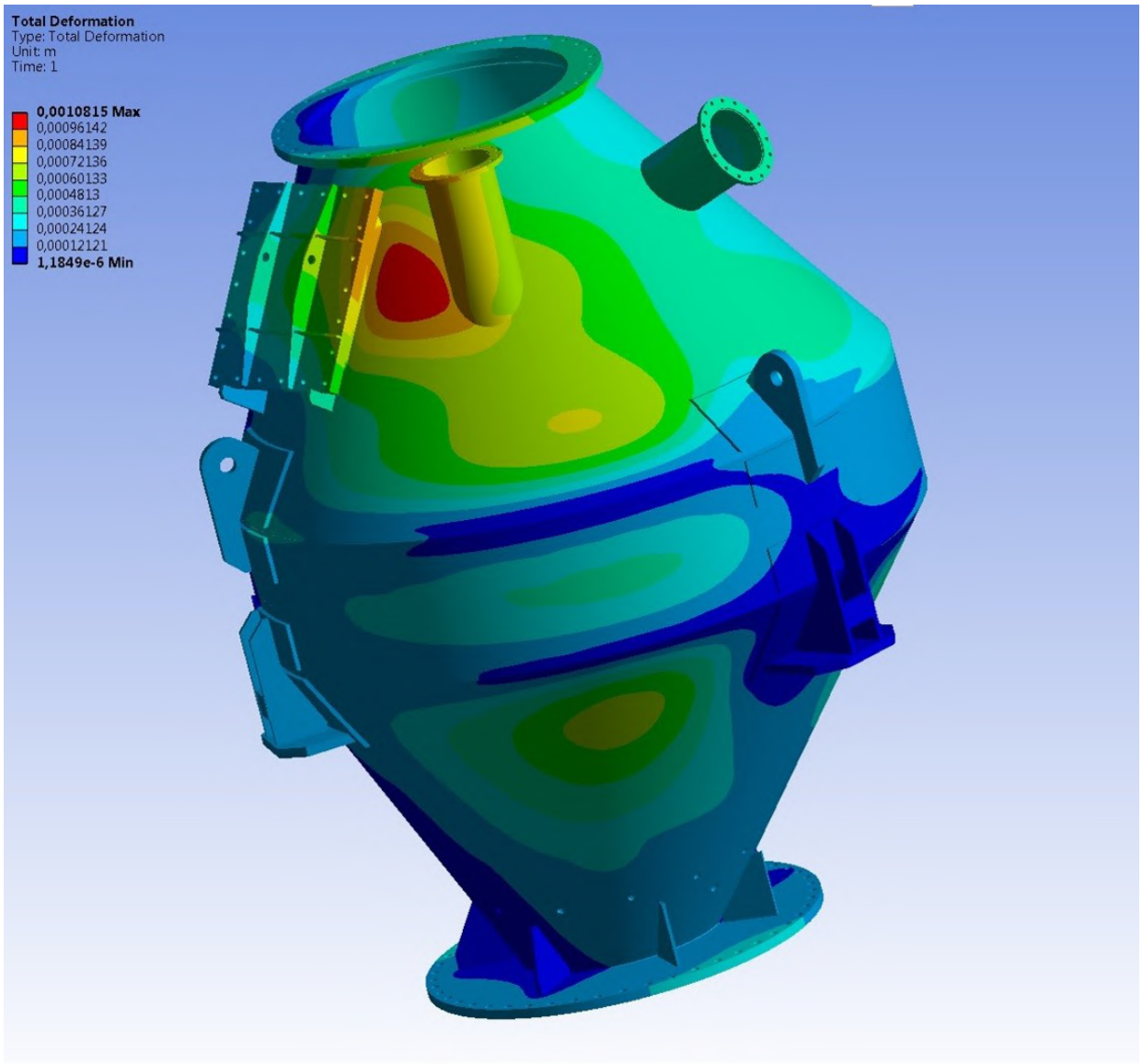

Fig. 1.6 Distribution of total strains arising in the structure

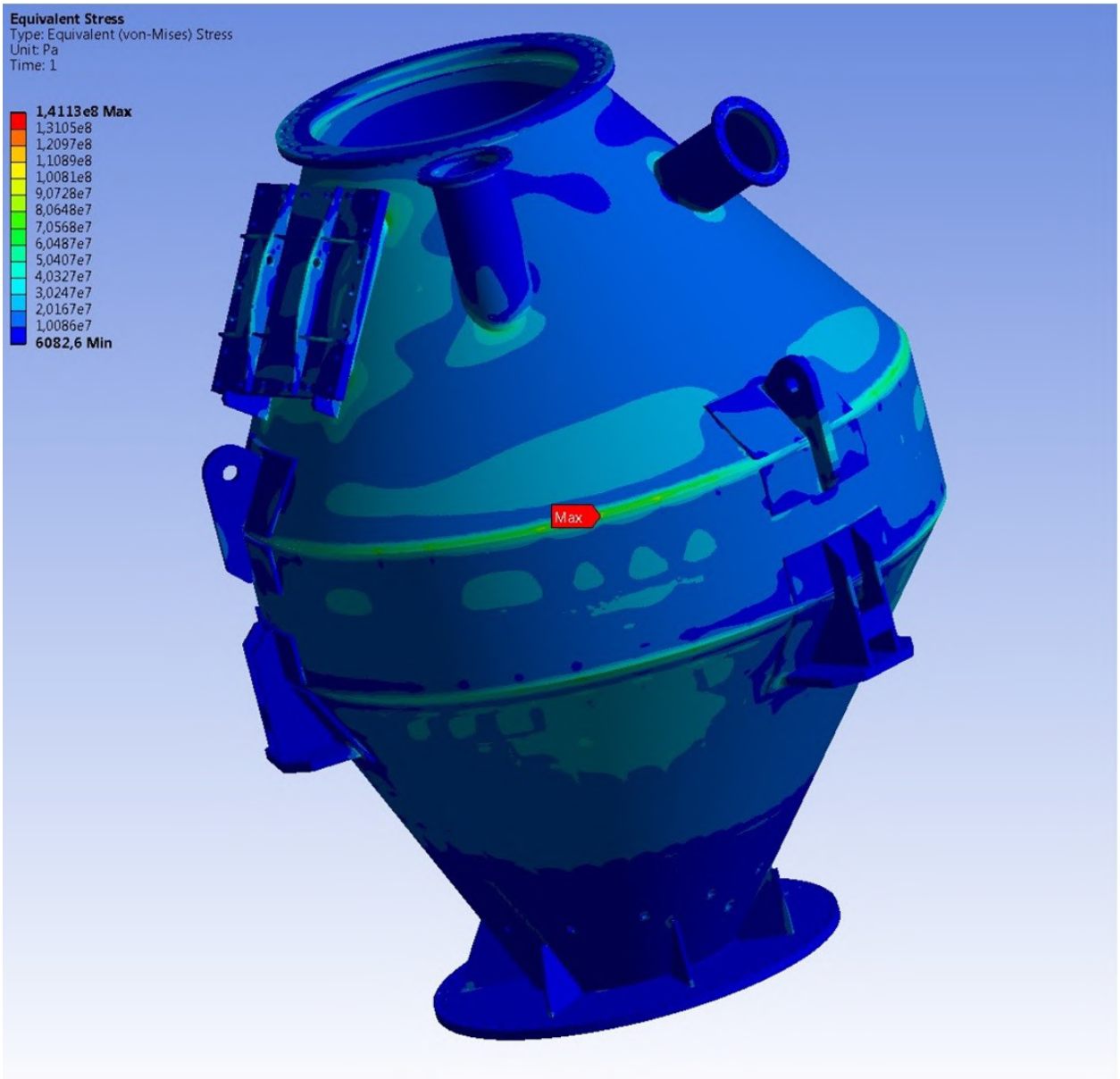

Fig. 1.7 Distribution of von Mises equivalent strains arising in the structure

The biggest stresses arise in the support. These stresses are local in nature and are within the finite element. The Fig. 1.8 shows an area of maximal stress in the support. This is the result a numerical singularity in the given area of bin's finite element model. Stresses in this area can be made specific by means of structure modeling. Submodeling of a support's structure is made by predesigned displacement fields at the border of a given structure. The submodeling is presented as a design pattern in Fig. 1.9. For the given part of a structure the border strains represent the submodel border conditions.

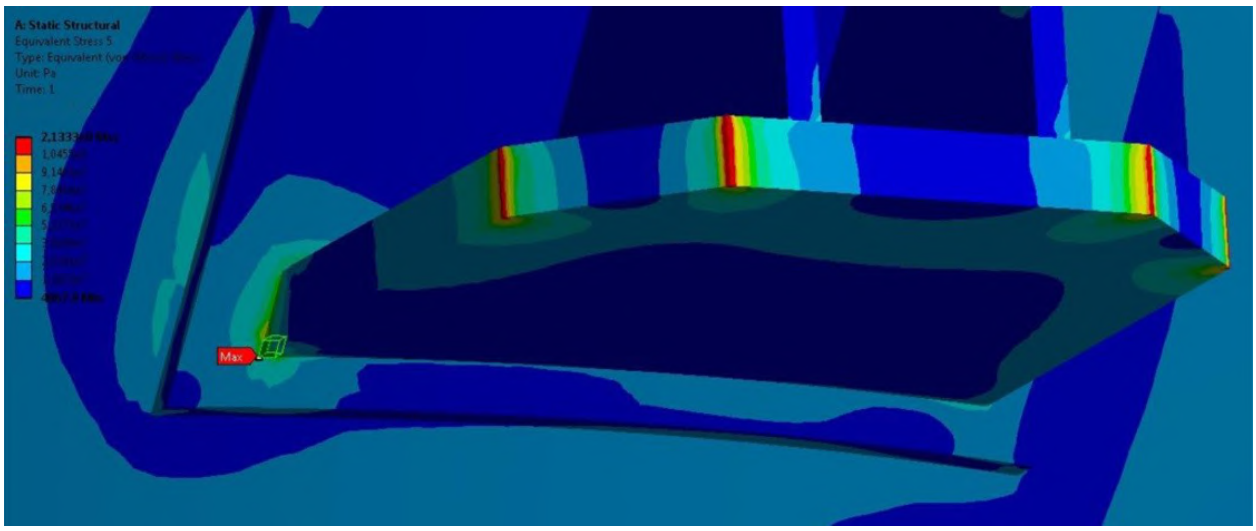

Fig. 1.8 Distribution of maximal stresses in the structure

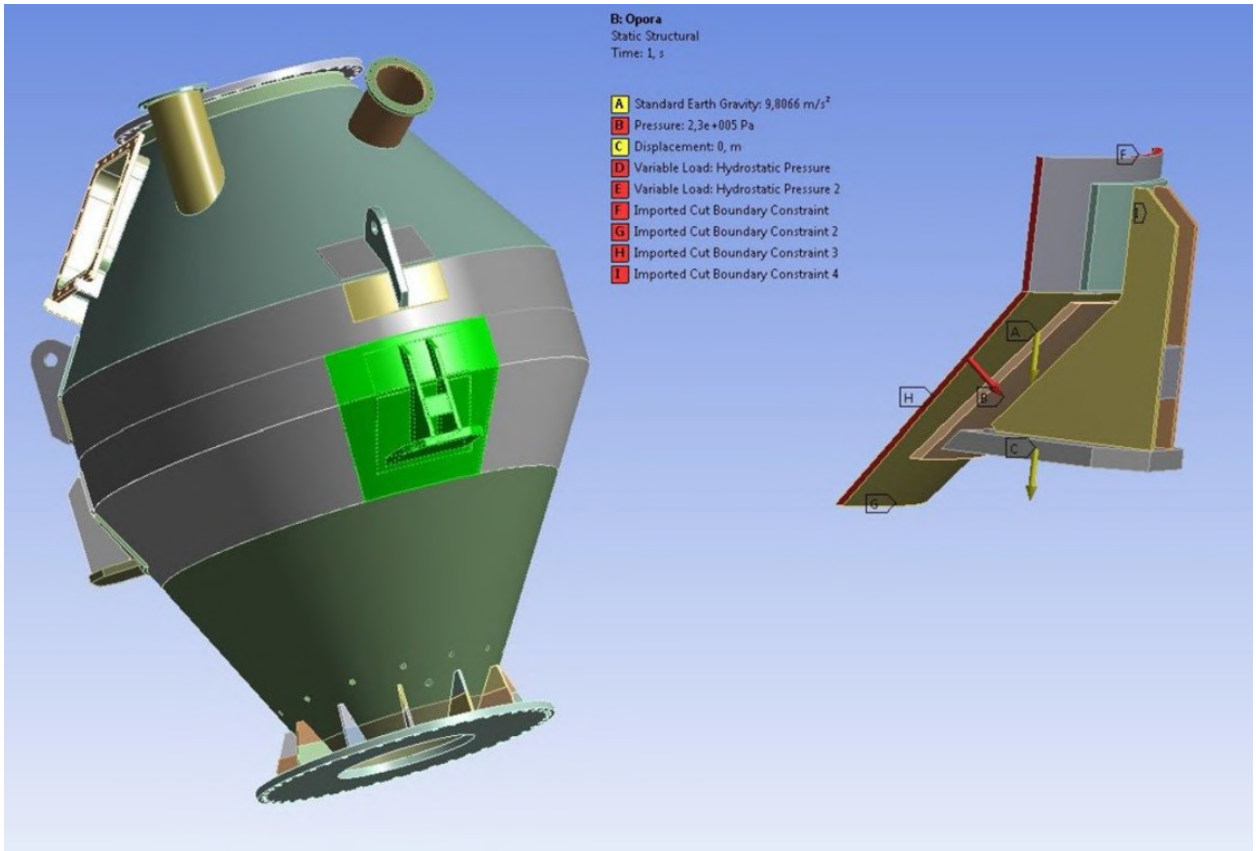

Fig. 1.9 Design pattern for calculation of stresses in material bin's support

Fig. 1.10 – Fig. 1.12 represent imported strains for a submodel, distribution of strains and von Mises equivalent stresses in the support.

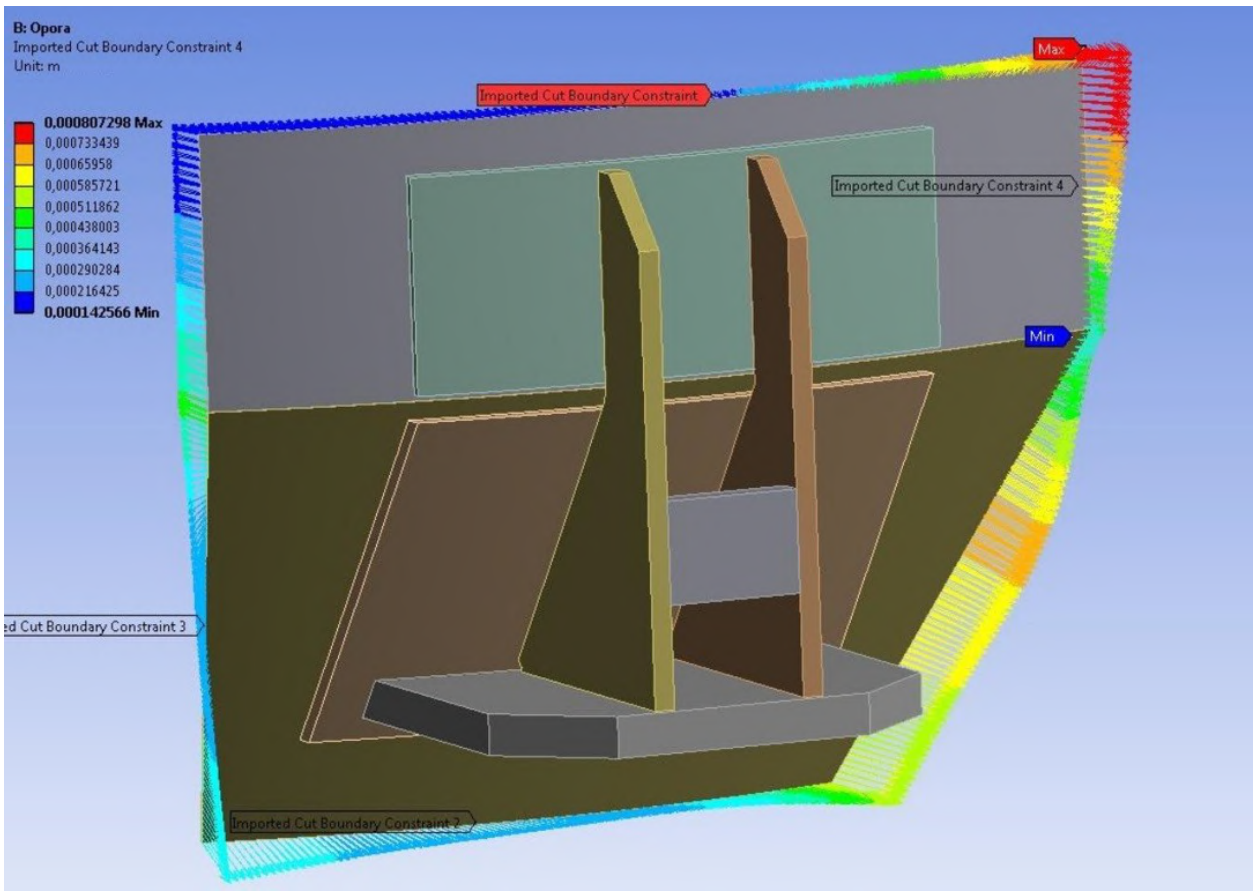

Fig. 1.10 Imported strains in submodel of the support

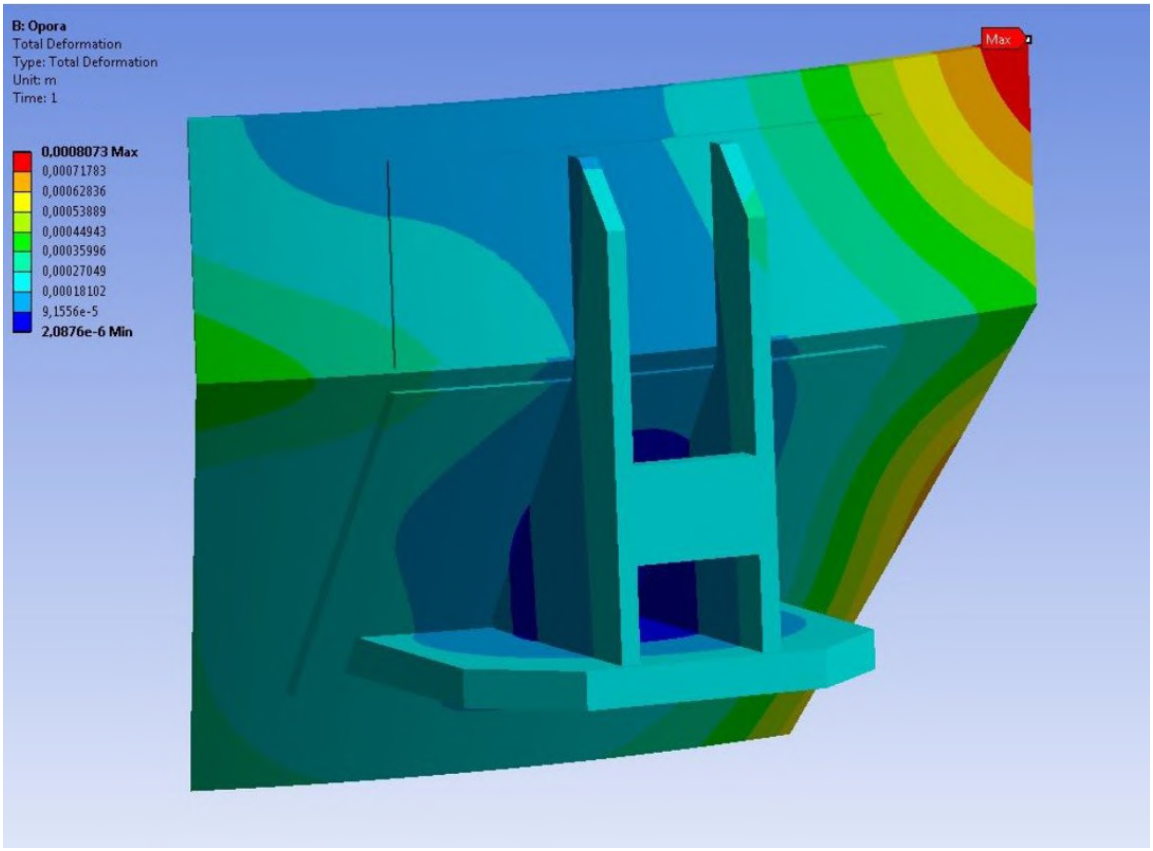

Fig. 1.11 Total strains in the support

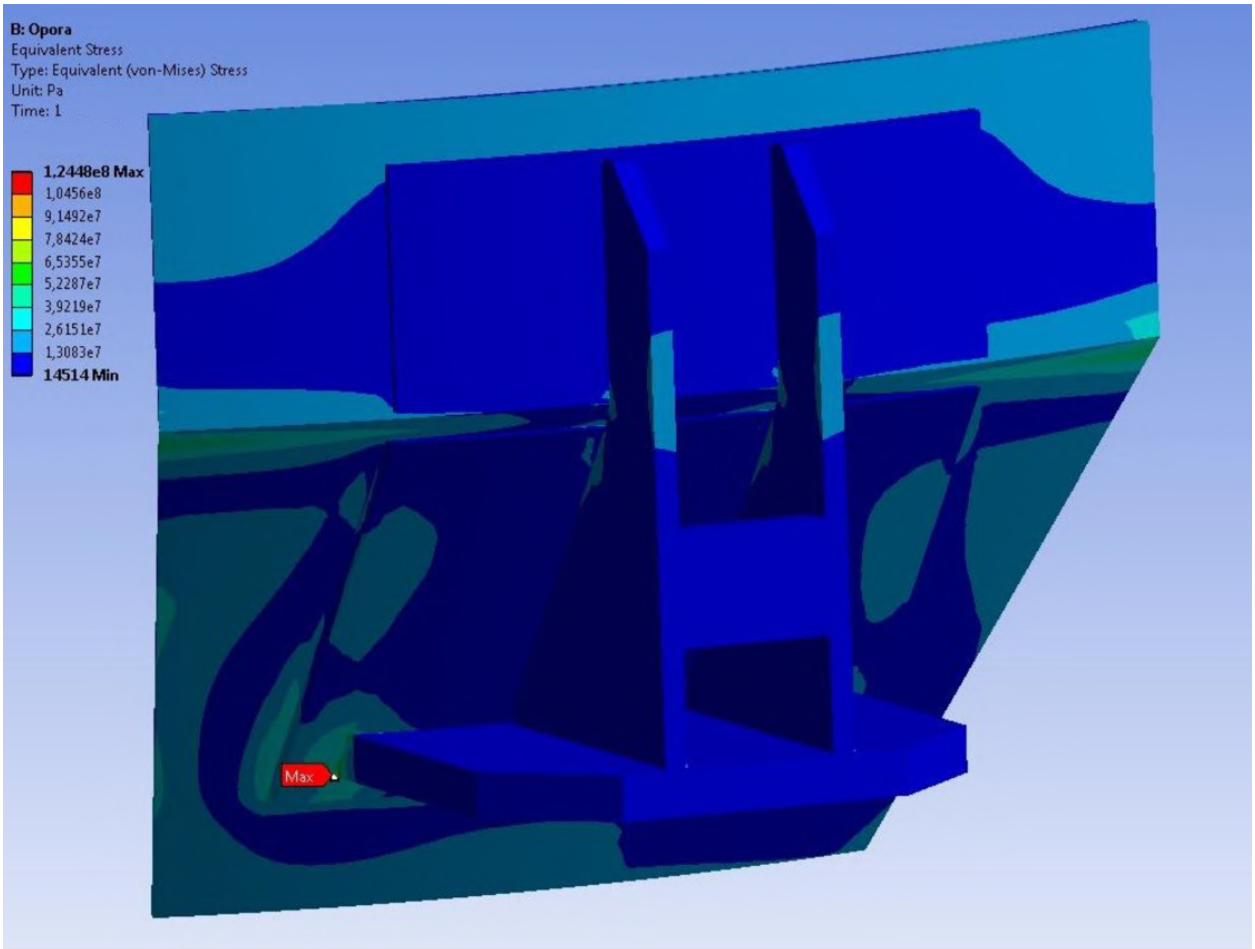

Fig. 1.12. Distribution of von Mises equivalent stresses in the support

Bin's support, the most distant one from the bin hopper, is the most load-bearing one of structure's supports.

The bin's load-bearing cover does not exceed 101.6MPa. Fig. 1.13 – Fig. 1.14 show distribution of stresses in load-bearing cover. These stresses are maximal inside the bin in the area of joining the cylindrical and upper conical part of the structure under the vertical branch pipe. The area of rounding off of the internal surface of bin structure's lateral flange shows arising of stresses that do not exceed 124.7 MPa. The Fig. 1.15 presents distribution von Mises equivalent stresses bin's lateral flange. The assessment of service lifespan of load-bearing elements of the bin and correctness of assessment in question is presented in Fig. 1.16 – Fig. 1.19.

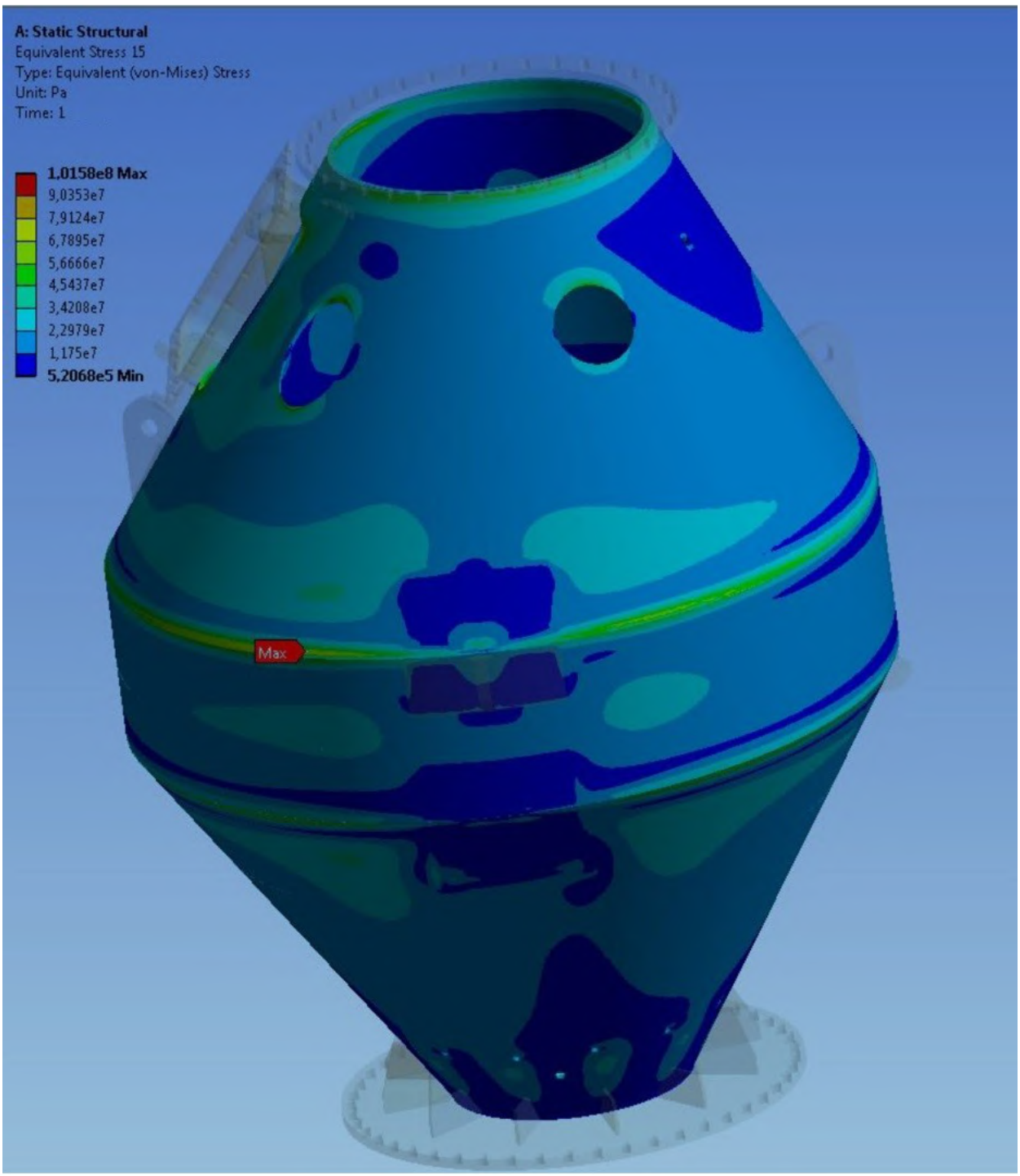

Fig. 1.13 Distribution of von Mises equivalent stresses arising in bin's load-bearing cover

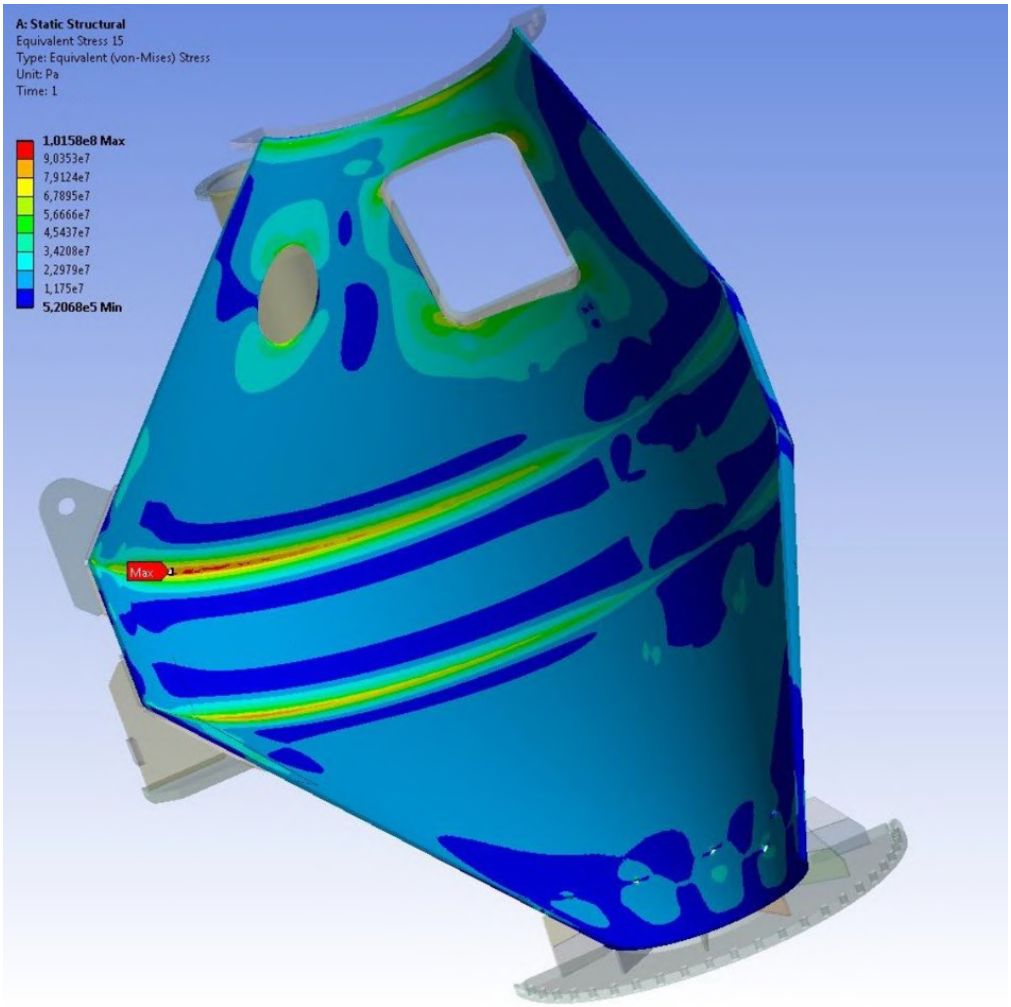

Fig. 1.14 Distribution of von Mises equivalent stresses arising in silo's load-bearing cover

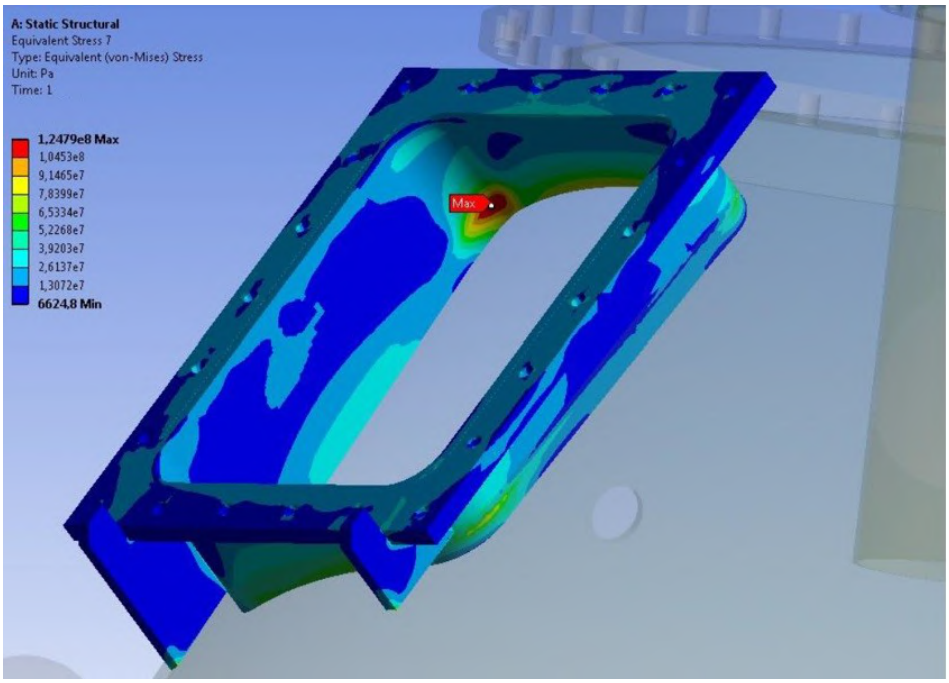

Fig. 1.15 Distribution of equivalent stresses arising in the bin's lateral flange

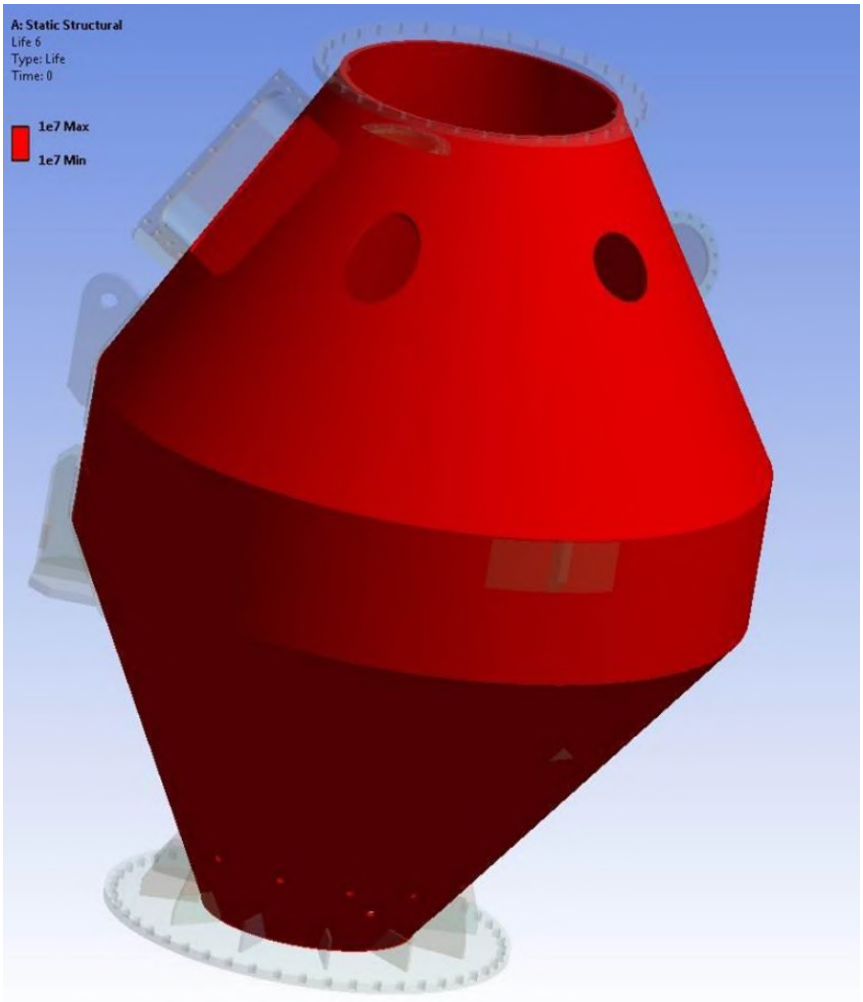

Fig. 1.16 Distribution of bin's load-bearing cover lifespan by Wehler SN curve

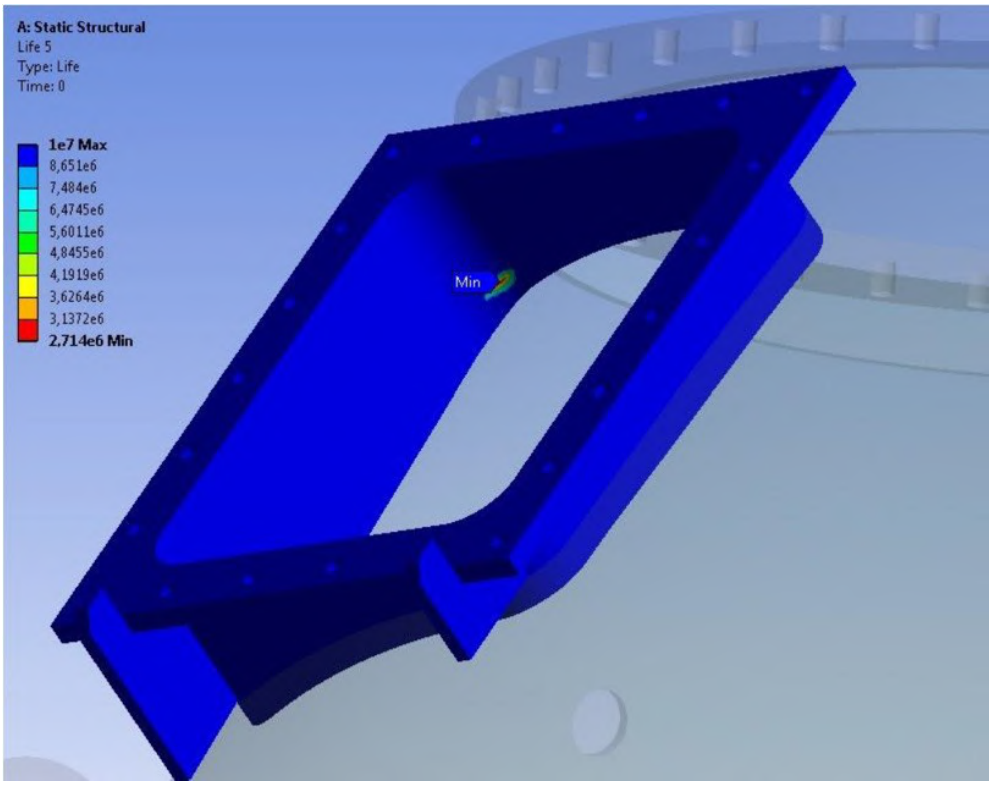

Fig. 1.17 Distribution of bin's lateral flange lifespan by Wehler SN curve

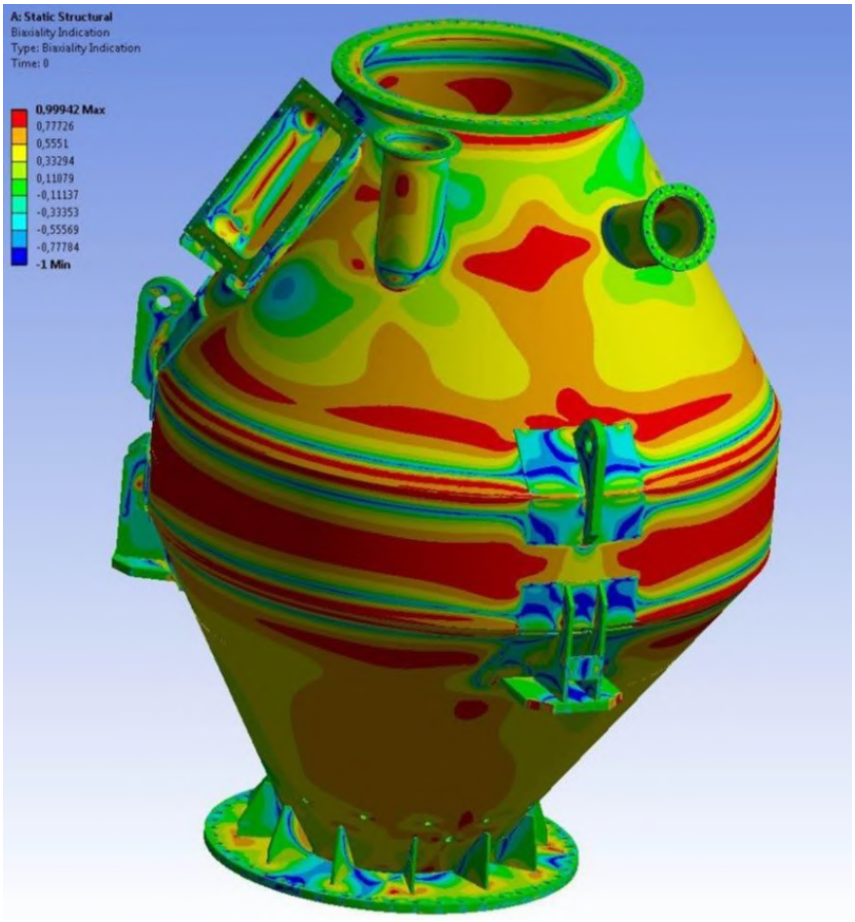

Fig. 1.18 Distribution of stress-state nature in the bin by Wehler SN curve

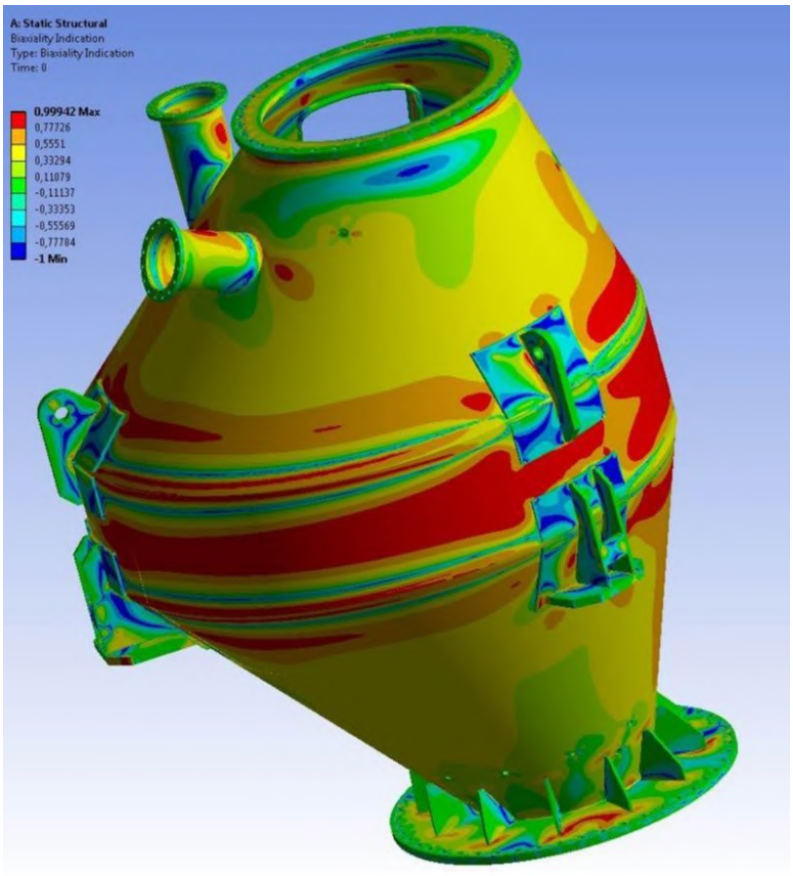

Fig. 1.19 Distribution of stress-state nature in the bin by Wehler SN curve

1.3.2 Structural design for normal service conditions (NSC)

The results of hopper designing for normal service conditions are presented as patterns of stresses, strains and fatigue calculation parameters in figures 1.20-1.31.

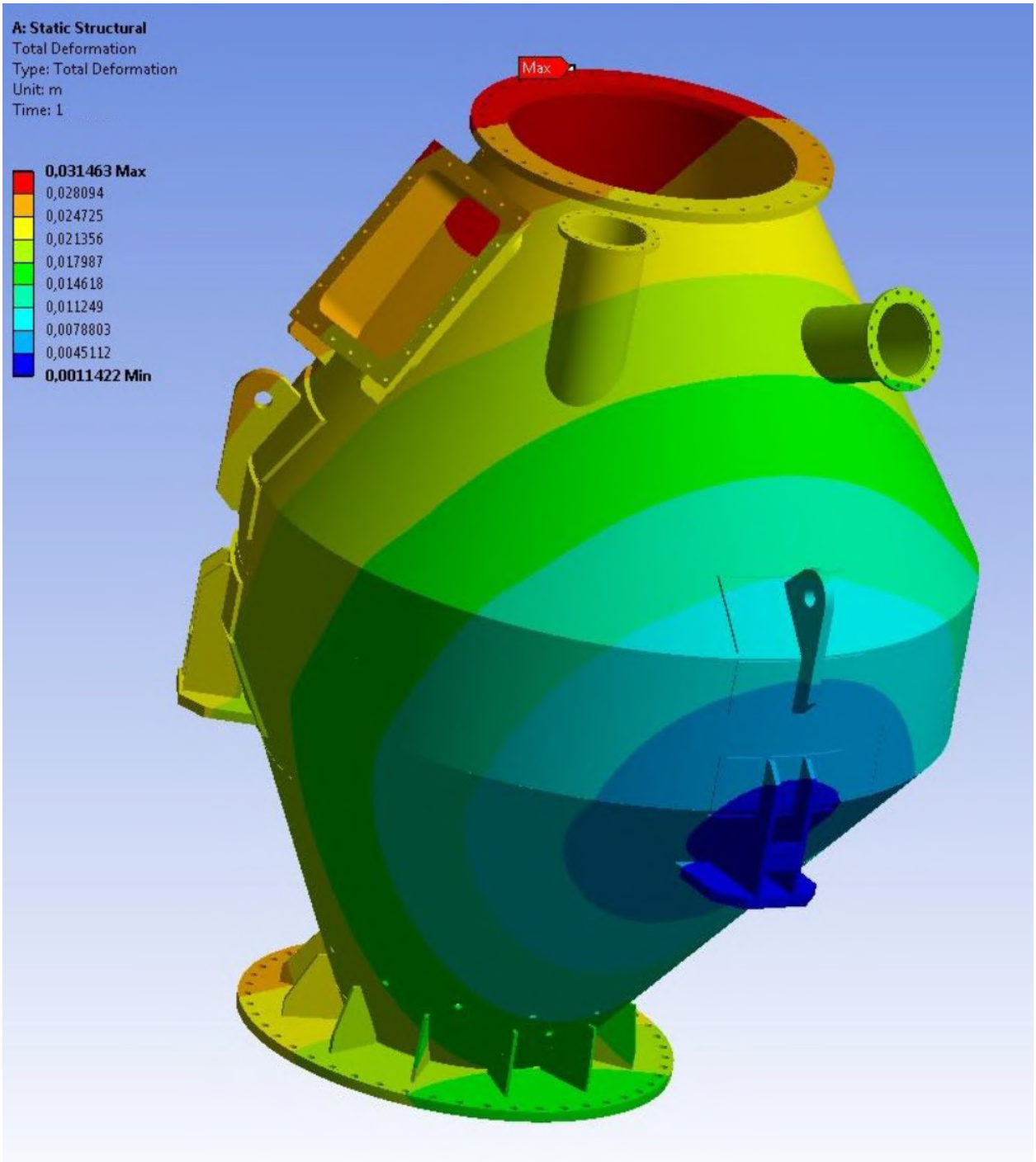

Fig. 1.20 Distribution of total strain arising in a structure

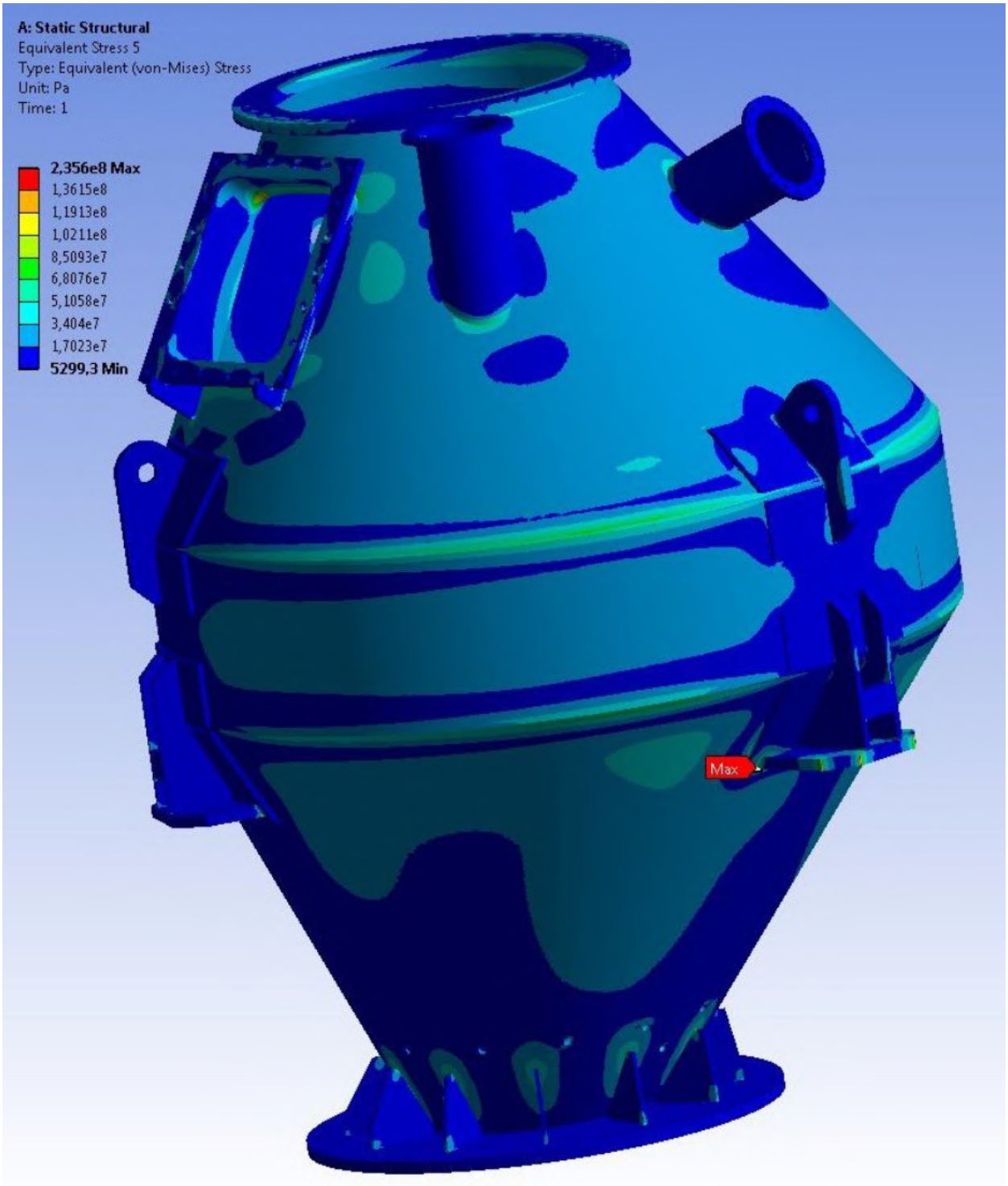

Fig. 1.21 Distribution of von Mises equivalent stresses arising in the structure

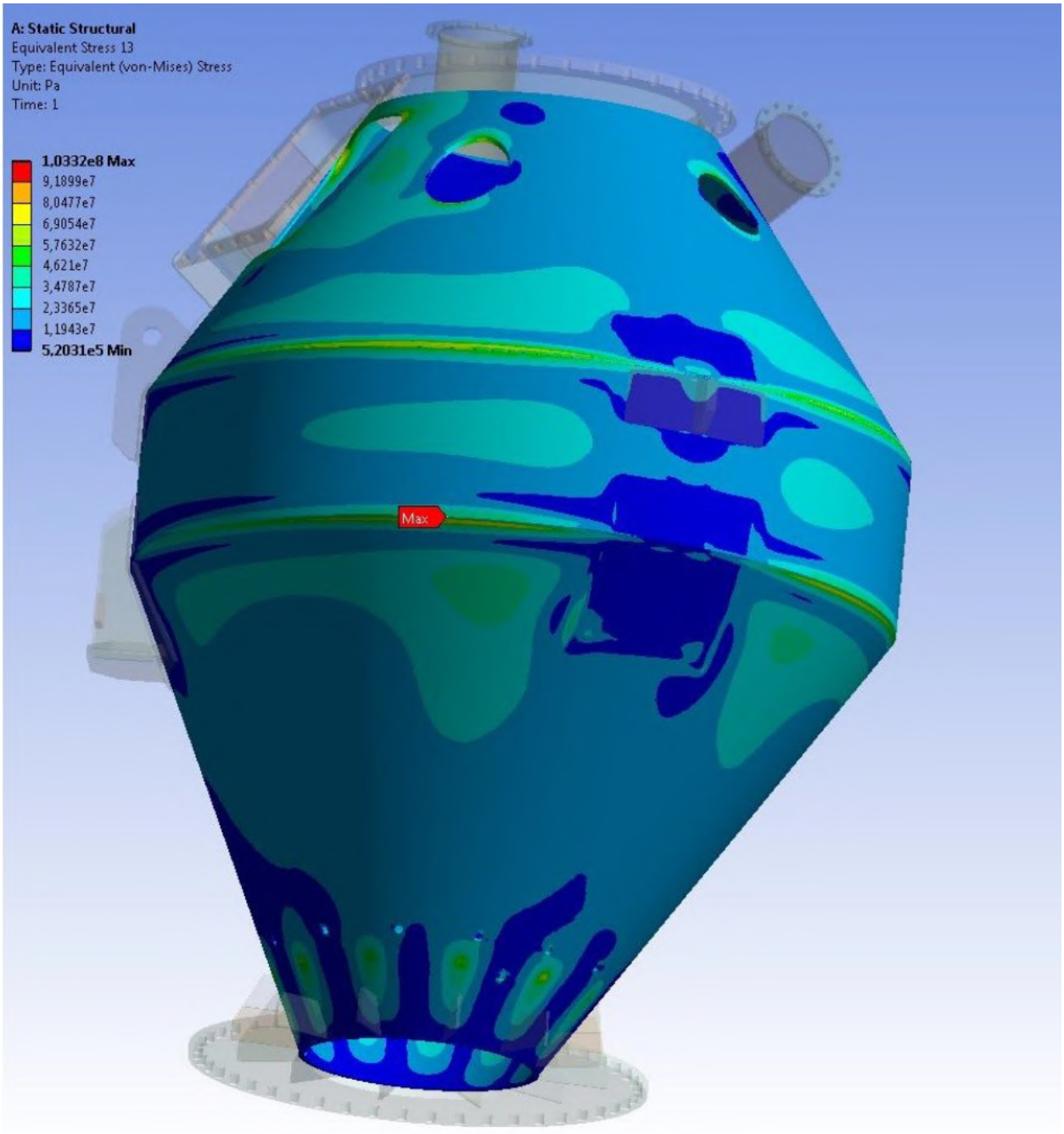

Fig. 1.22 Distribution of von Mises equivalent stresses arising in structure's load-bearing cover

The area of maximal stress in the cover is located inside the structure at the border of joining the conical and cylindrical bin's parts.

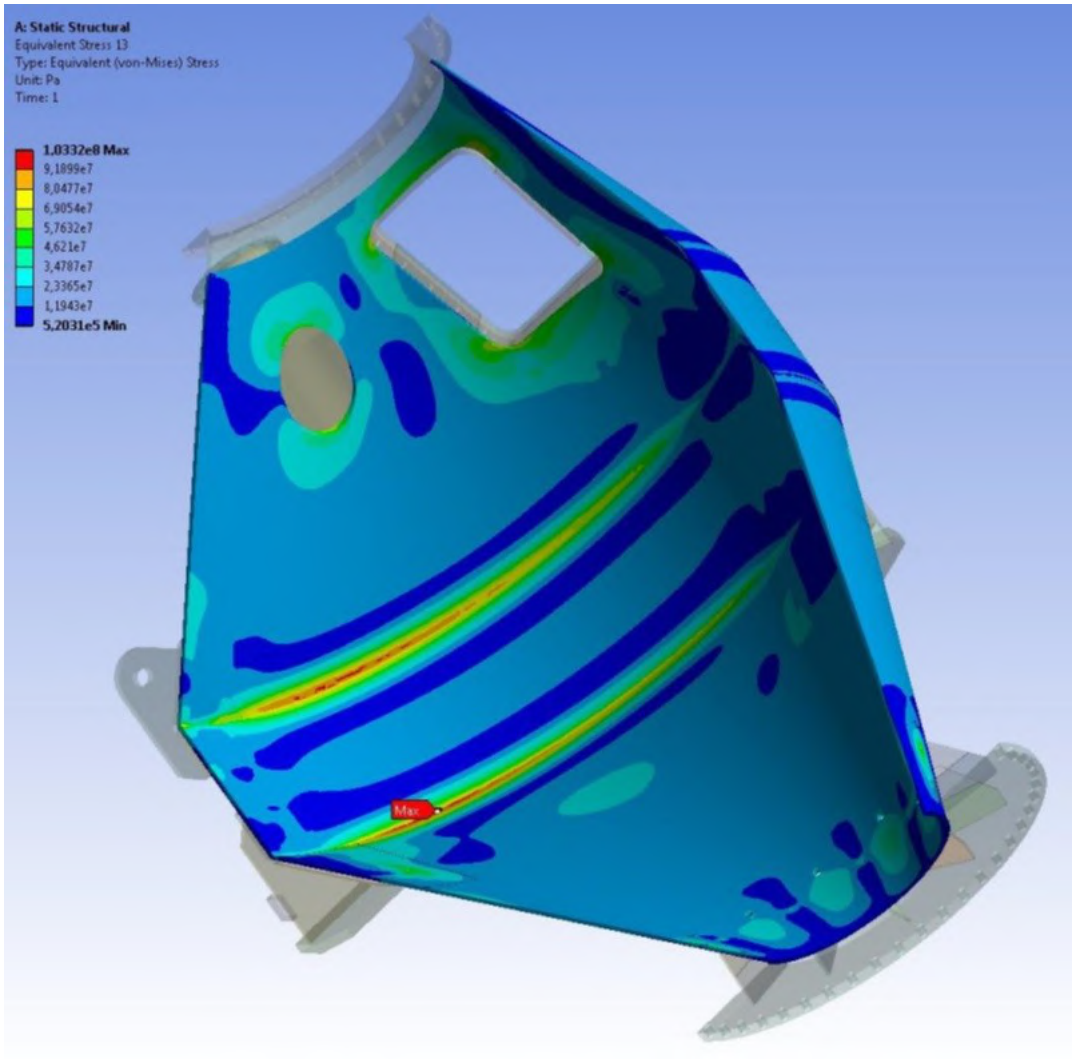

Fig. 1.23 Distribution of von Mises equivalent stresses arising in structure's load-bearing cover

Stresses in this area can be made specific by means of structure modeling. Submodeling of a support's structure is made by predesigned displacement fields at the border of a specified structure's part. The submodeling is presented in Fig. 1.24. For the given part of a structure the border strains represent the submodel border conditions.

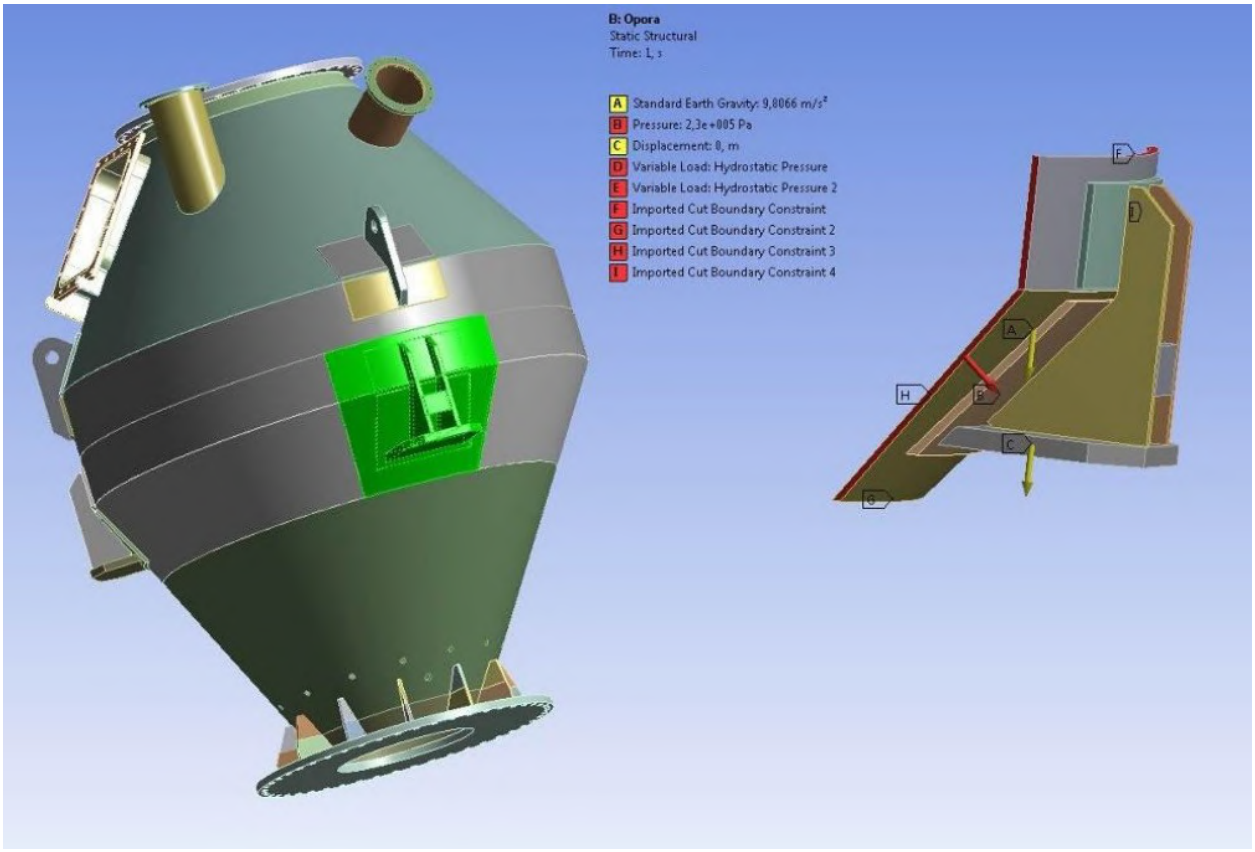

Fig. 1.24 Submodeling of bin's support

Fig. 1.25-1.27 represent imported strains for a submodel, distribution of strains and von Mises equivalent stresses in the support.

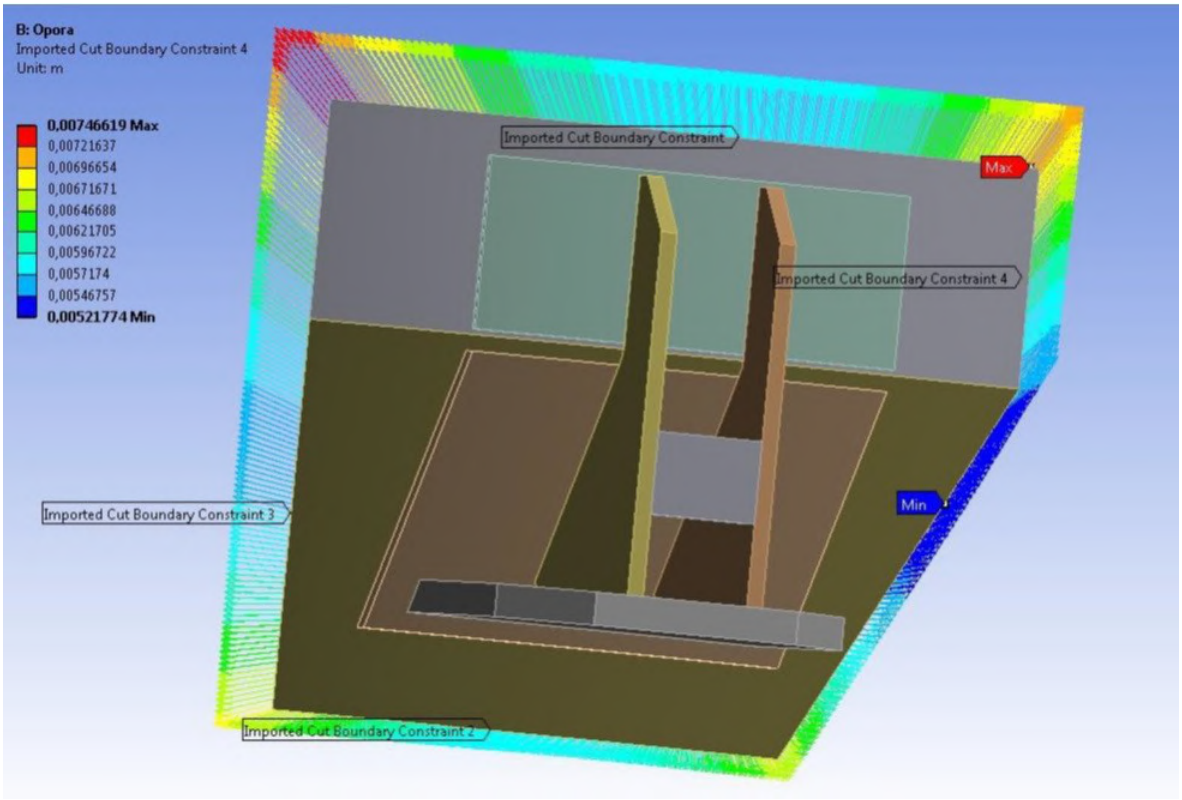

Fig. 1.25 Imported strains in support's submodel

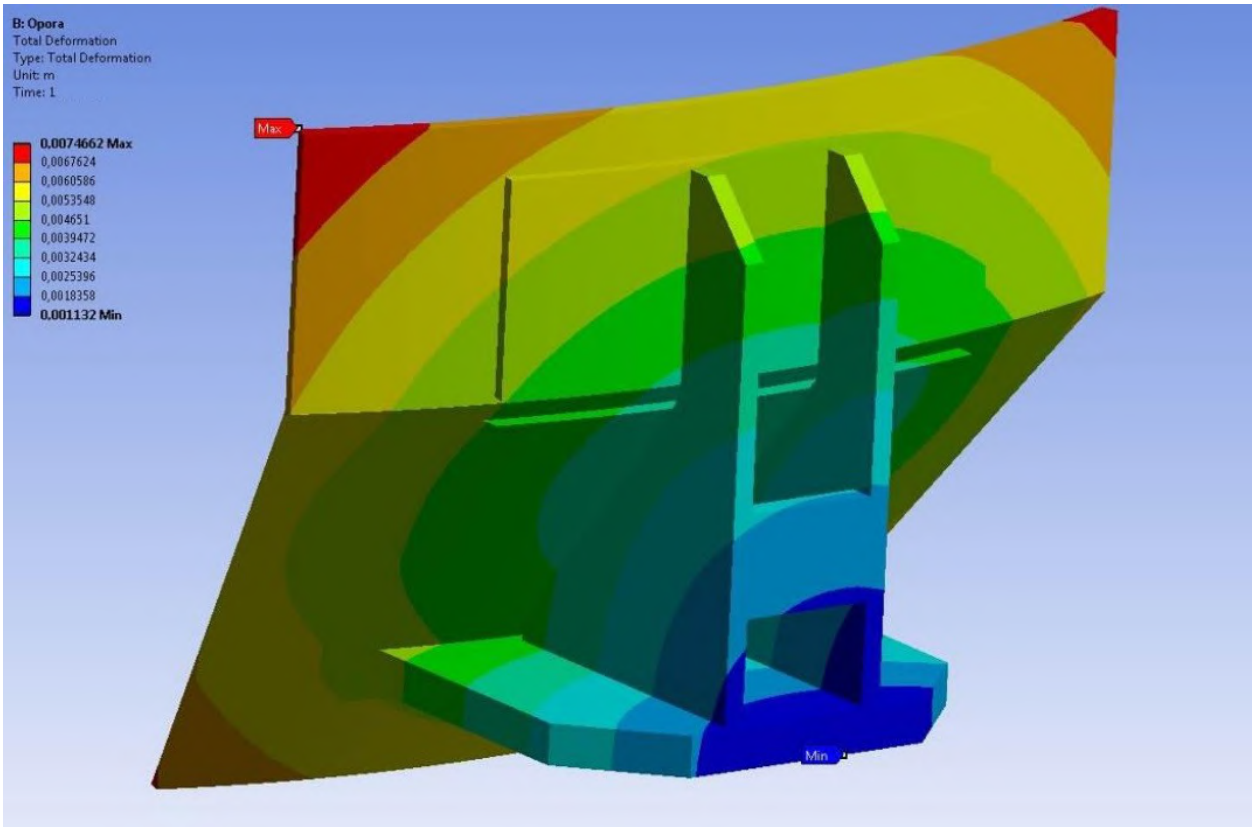

Fig. 1.26 Total strains in the support

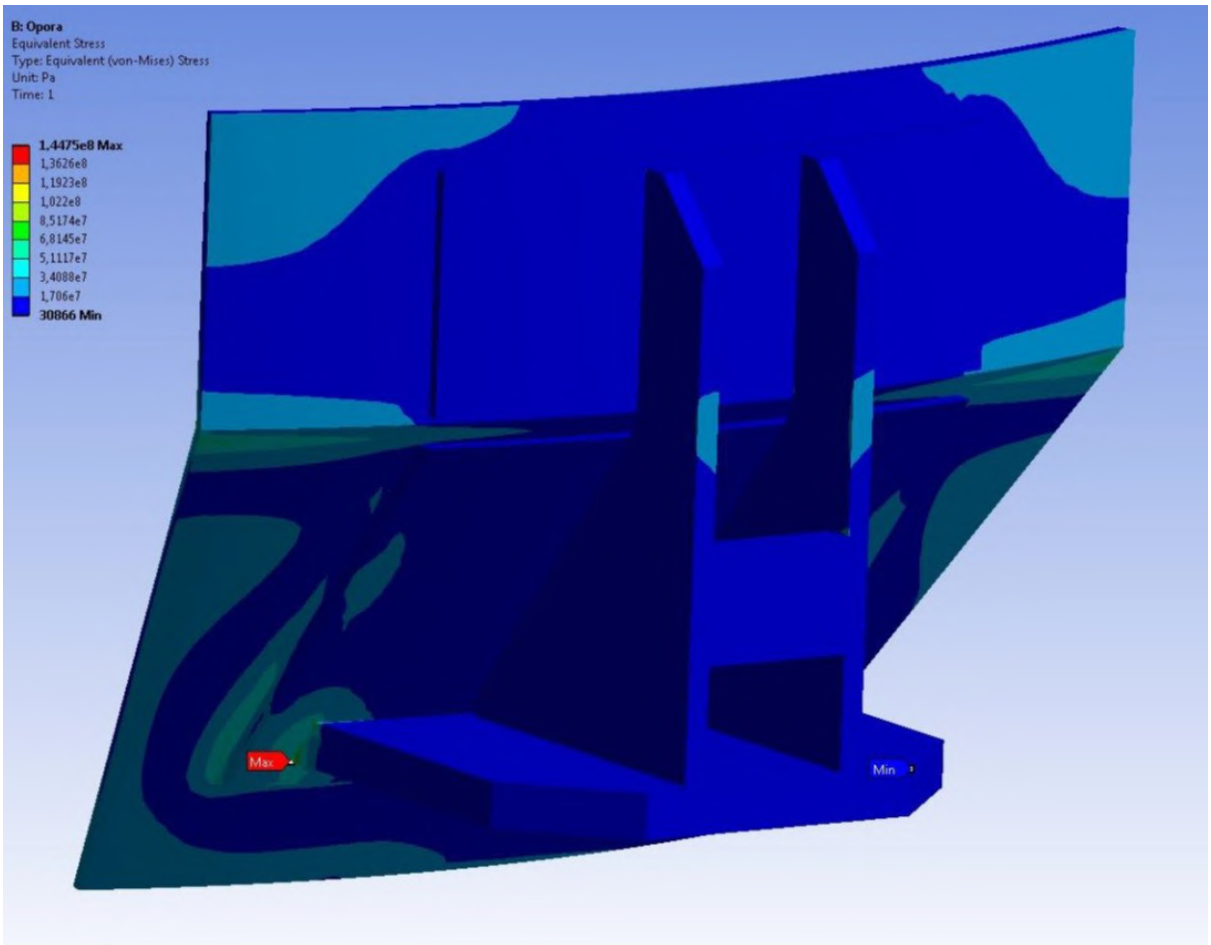

Fig. 1.27 Distribution of von Mises equivalent stresses in the support

Bin's support, the most distant one from the bin hopper, is the most load-bearing one of structure's supports.

The bin's load-bearing cover does not exceed 103.3MPa. These stresses are maximal inside the bin in the area of joining the cylindrical and upper conical part of the structure under the vertical branch pipe. The area of rounding off of the internal surface of bin structure's lateral flange shows arising of stresses that do not exceed 120.2 MPa. The Fig. 1.28 presents distribution von Mises equivalent stresses bin's lateral flange. The assessment of service lifespan of load-bearing elements of the bin and correctness of assessment in question is presented in Fig. 1.29-1.33.

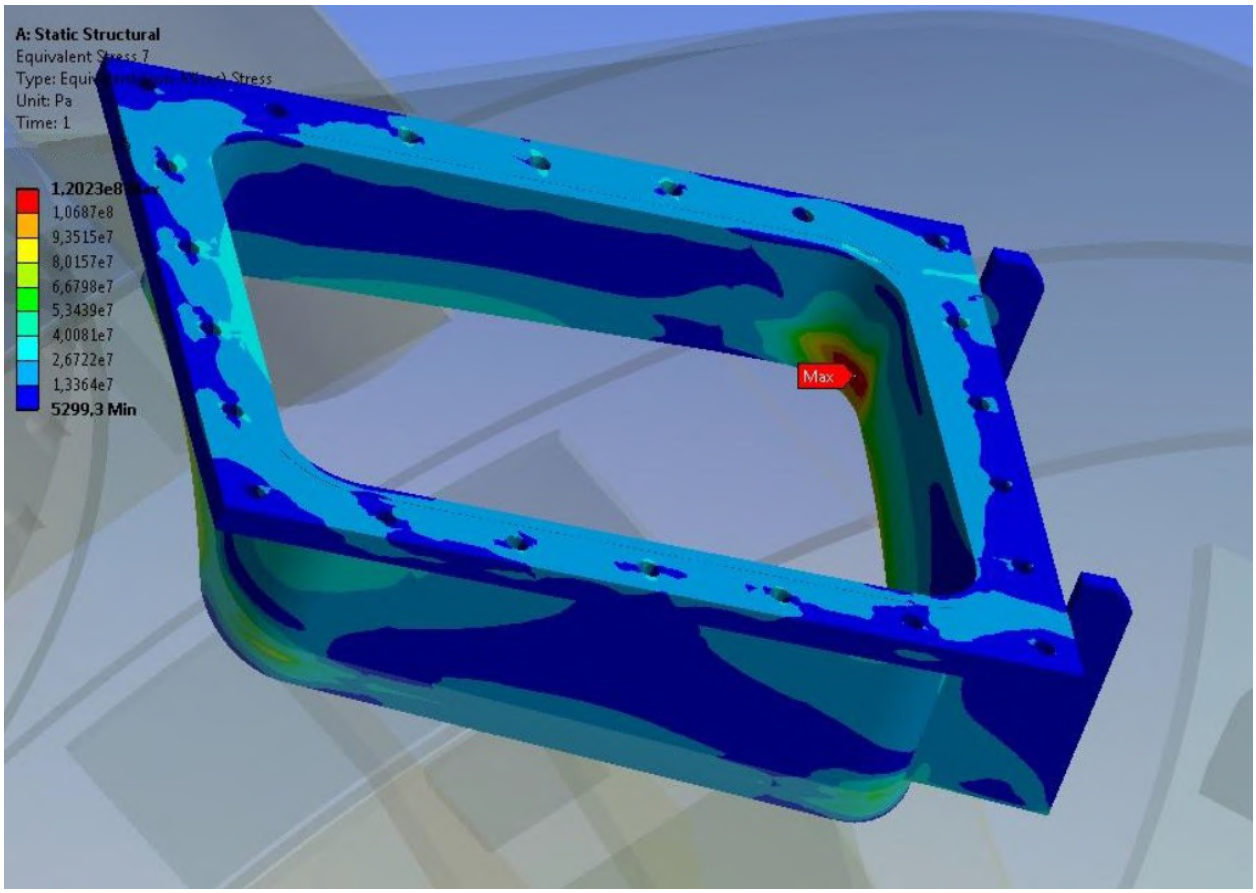

Fig. 1.28 Distribution of equivalent stresses in bin's lateral flange

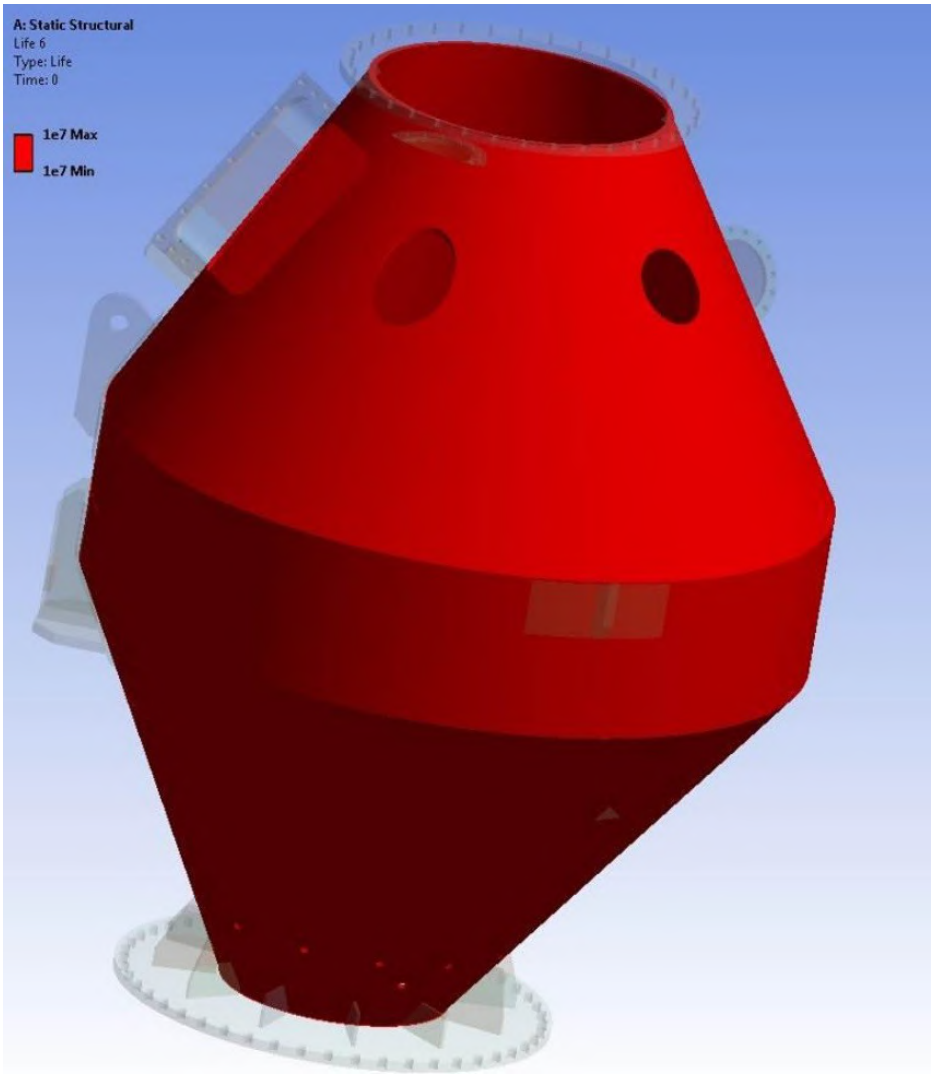

Fig. 1.29 Distribution of bin's load-bearing lifespan by Wehler SN curve

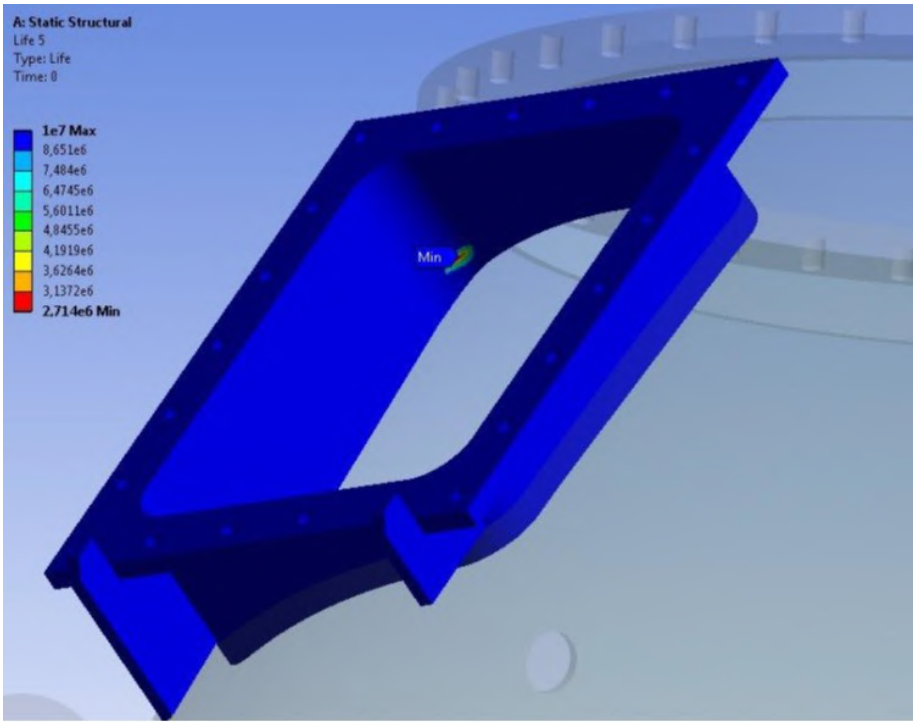

Fig. 1.30 Distribution of bin's load-bearing lifespan by Wehler SN curve

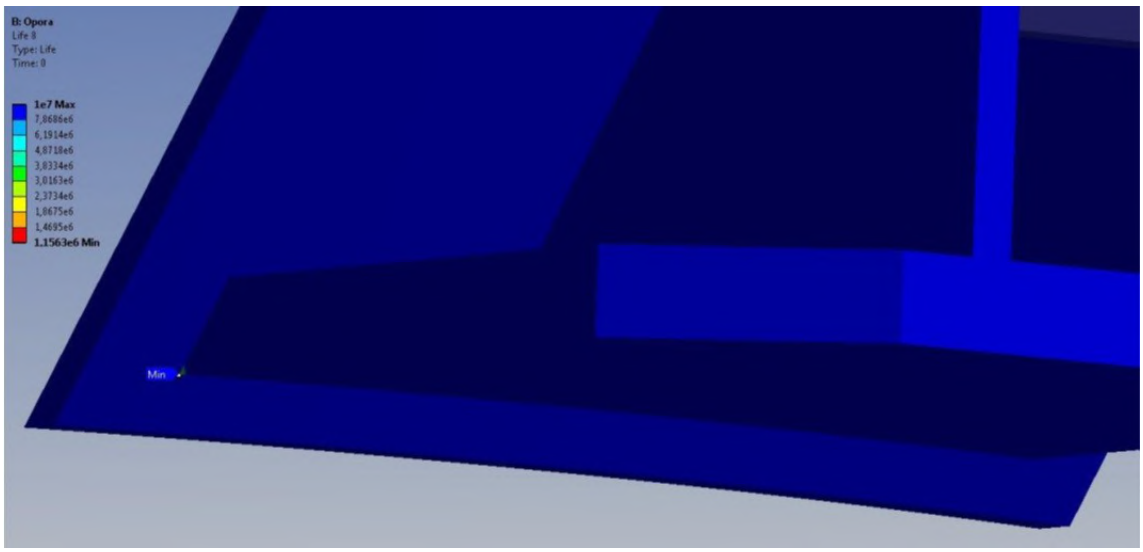

Fig. 1.31 Distribution of bin's support lifespan by Wehler SN curve

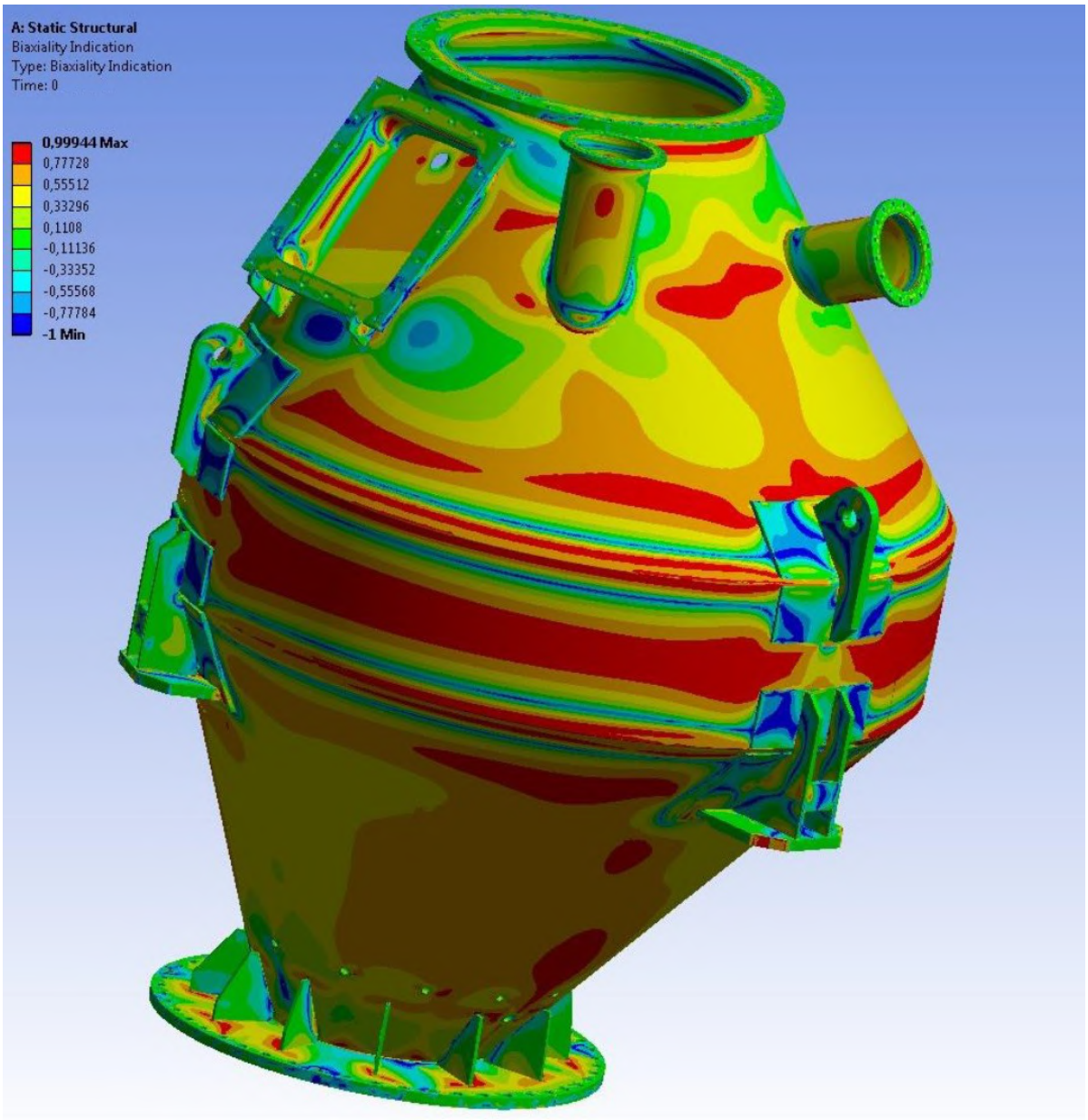

Fig. 1.32 Distribution of stress-state nature in the bin by Wehler SN curve

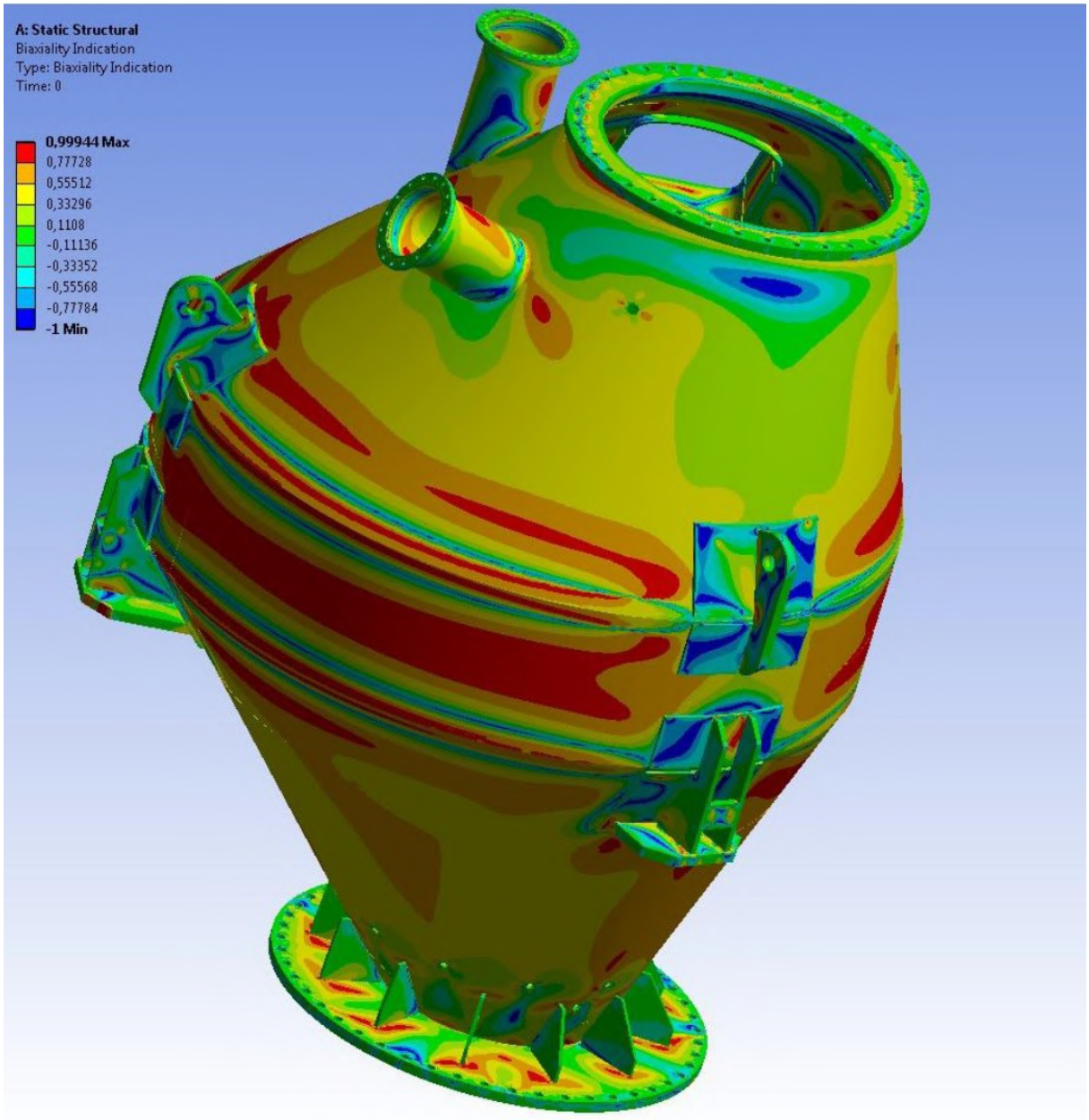

Fig. 1.33 Distribution of stress-state nature in the bin by Wehler SN curve

1.3.3 Structural design for seismic impact

Seismic impact calculation is performed using the response spectrum method. The initial data is the spectrum of structure's response to dynamic effect. The bin's response spectrum is taken to mean the absolute values of maximal response acceleration of linear-elastic system depending on impact frequency. The bin's response spectrum is specified with accelerograms and is presented in Tables 1.2-1.4 for the 47.748m mark. To define this loading the structure's natural oscillation modes and quantity thereof shall be determined. The number of frequencies shall be

determined out of the condition that the frequencies in question correspond to 90% of structure's reduced mass in accordance with the method of reduction. The values of natural oscillation and modes are determined out of structure's modal analysis.

1.3.3.1 Structure's modal analysis

Calculation results of modal analysis showed that it is sufficient to take into consideration the first 100 natural oscillation harmonics, and these are presented in Fig. 1.34.

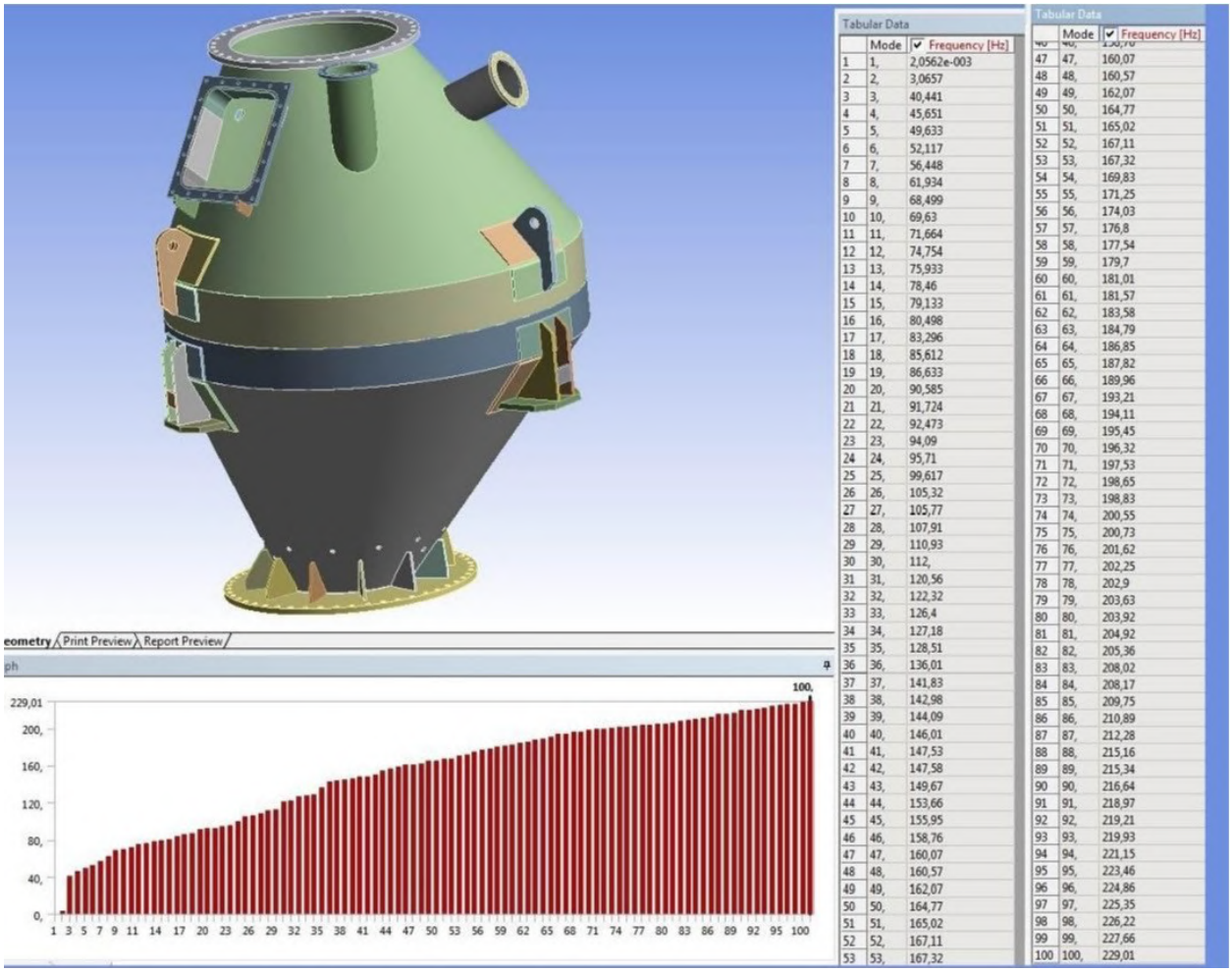

Fig. 1.34 Values of the first 100 natural oscillation frequencies of the structure

Oscillation modes for certain natural frequencies are presented in Fig. 1.35.

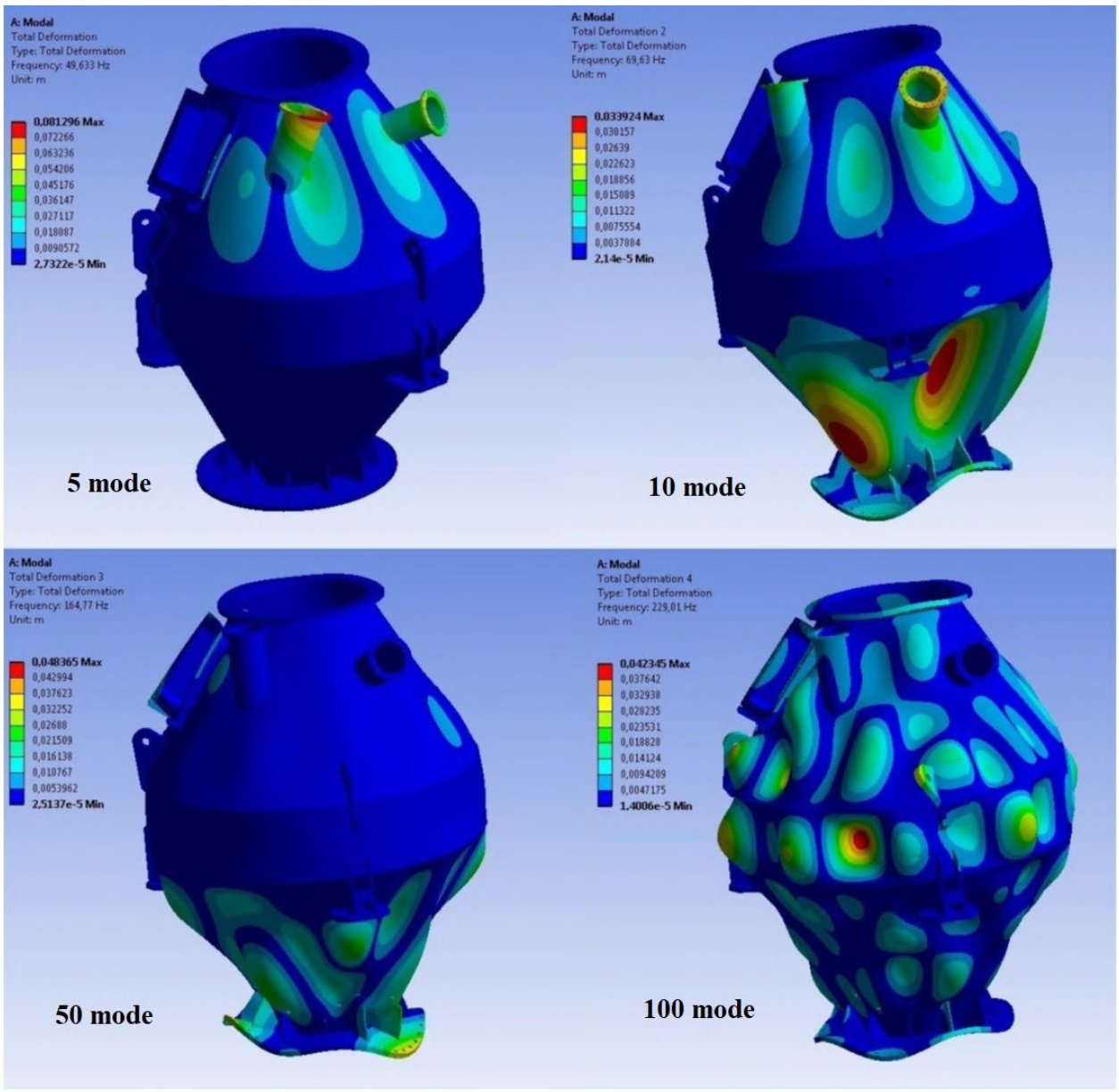

Fig. 1.35 Oscillation modes for 1, 10, 50 and 100 natural frequencies

When carrying out the linear-spectrum analysis the calculation results are obtained using the method of square-root out of sum of squares (SRSS). According to calculation results the bin being under seismic impact shows arising of much less stresses caused by internal pressure. Field distribution of von Mises equivalent stresses is presented in Fig. 1.36-1.38.

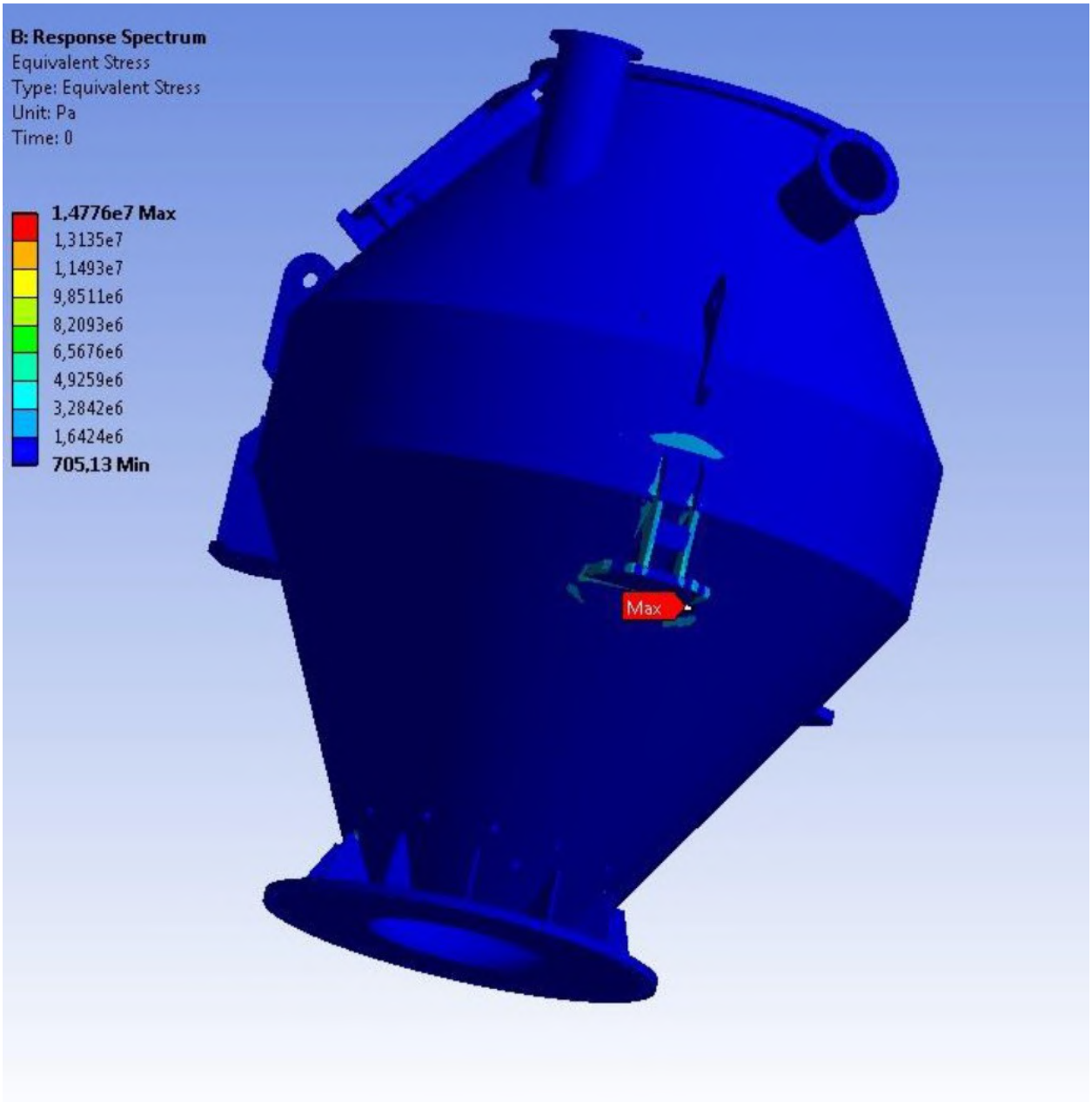

Fig. 1.36 Distribution of von Mises stresses in the bin under seismic impact

The biggest stresses arise in the area of structure's fixation, i.e. on supports. In the case under study the magnitude thereof does not exceed 17% of stresses for the case of normal service conditions.

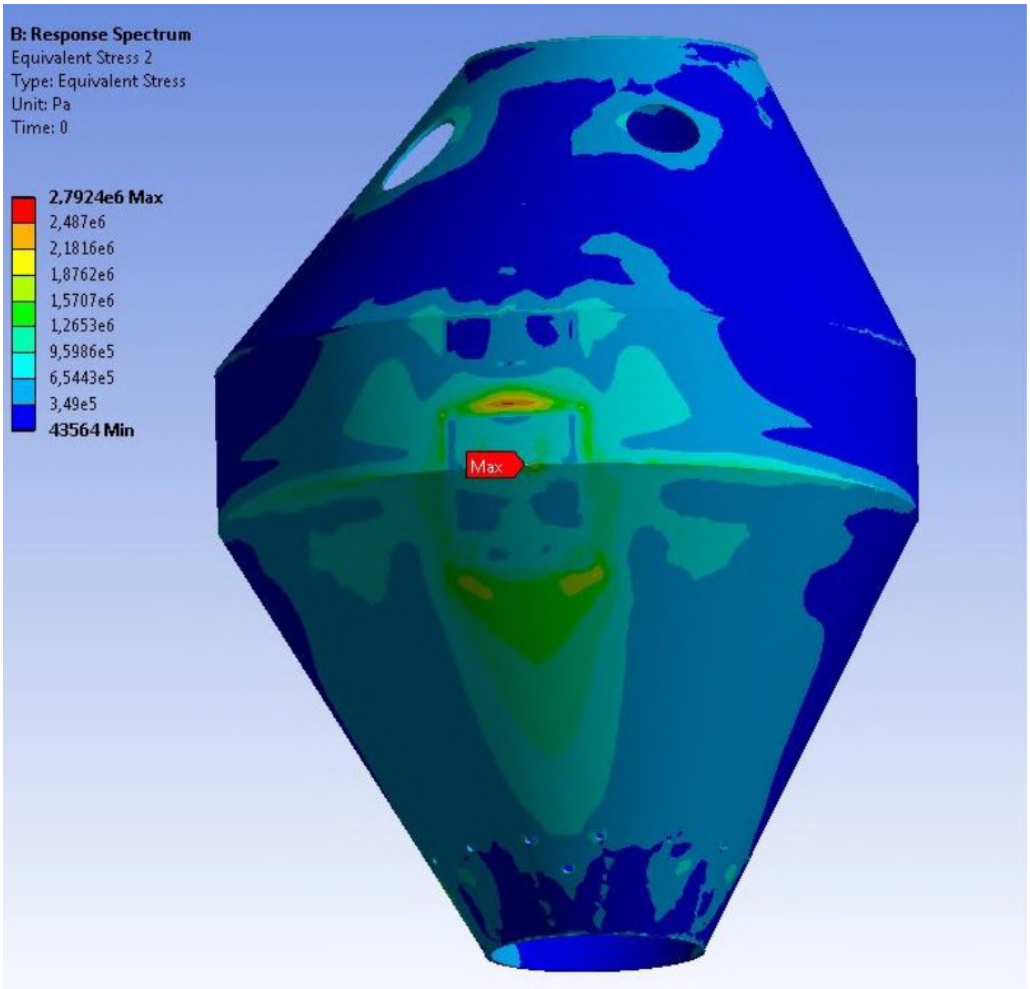

Fig. 1.37 Distribution of von Mises equivalent stresses in bin's load-bearing cover under seismic impact

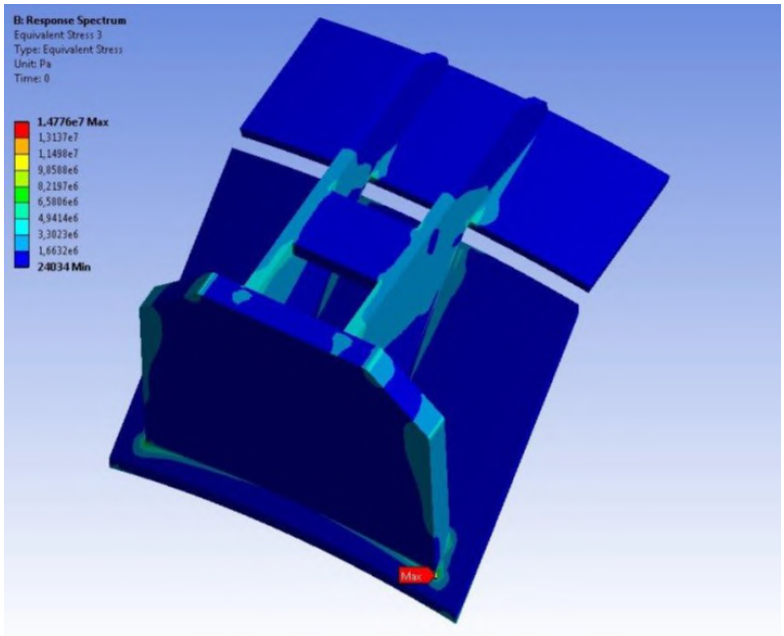

Fig. 1.38 Distribution of von Mises equivalent stresses in the support under seismic impact

1.3.4 Structural design for wind effect conditions and normal service conditions

The conical part of bin's rotation body has a symmetry plane. This geometry feature of bin's structure defines three design cases of wind effect direction. Wind effect direction is presented in Fig. 1.39.

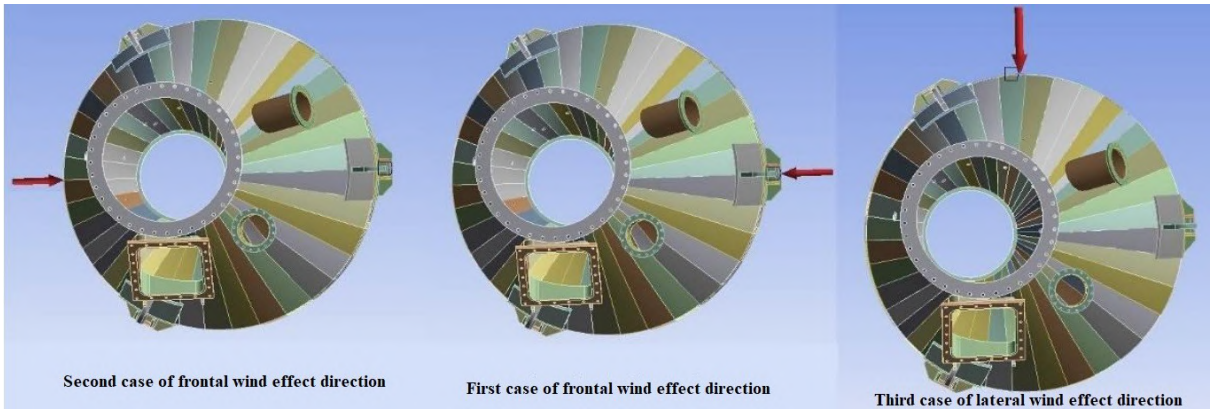

Fig. 1.39 Wind effect direction

First case of frontal wind effect direction

Results of bin designing under wind effect and normal service conditions for the first case of wind direction are presented as patterns of stresses, strains and fatigue calculation parameters in figures 1.40-1.45.

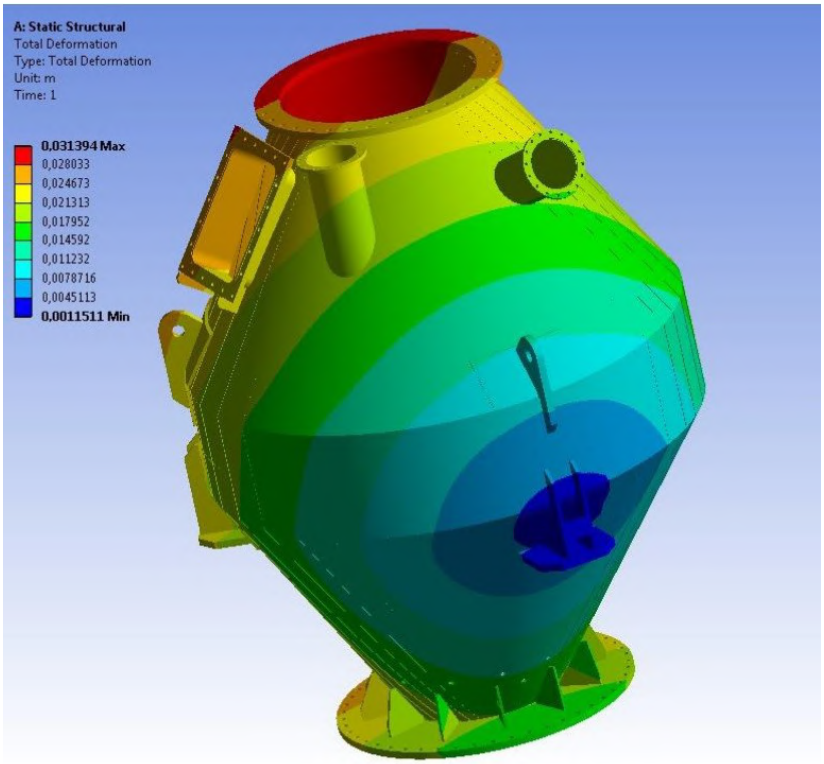

Fig. 1.40 Distribution of total strain arising in the bin

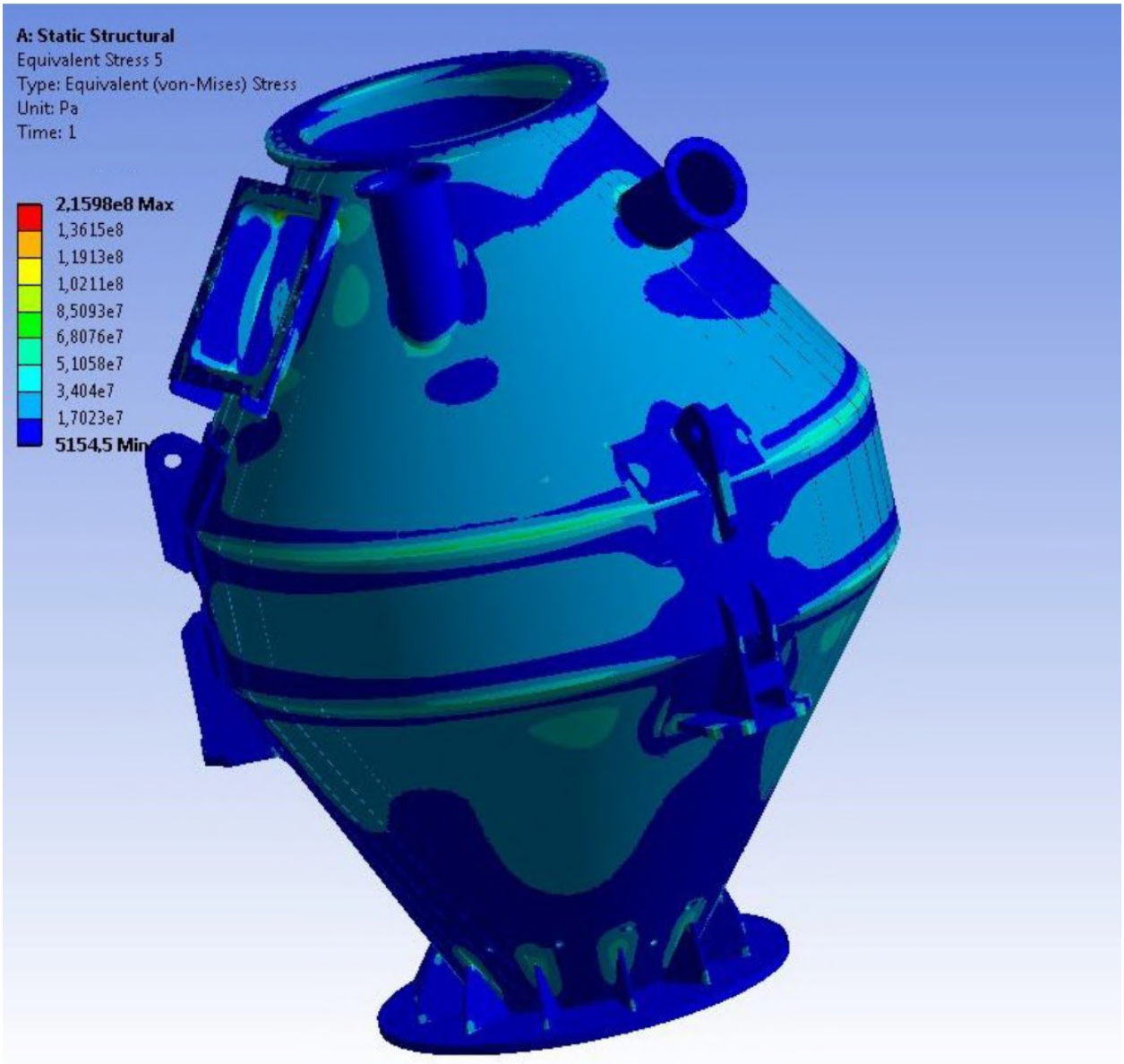

Fig. 1.41 Distribution of von Mises equivalent stresses arising in material bin

The biggest stresses in the structure arise in bin's support, the most distant one from aperture's axis. The load-bearing cover has the biggest stresses inside the area of joining the bin's conical and cylindrical parts. Fig. 1.42-1.44 presents the distribution of stresses in bin's load-bearing cover. The maximal stresses in the load-bearing cover do not exceed 106MPa.

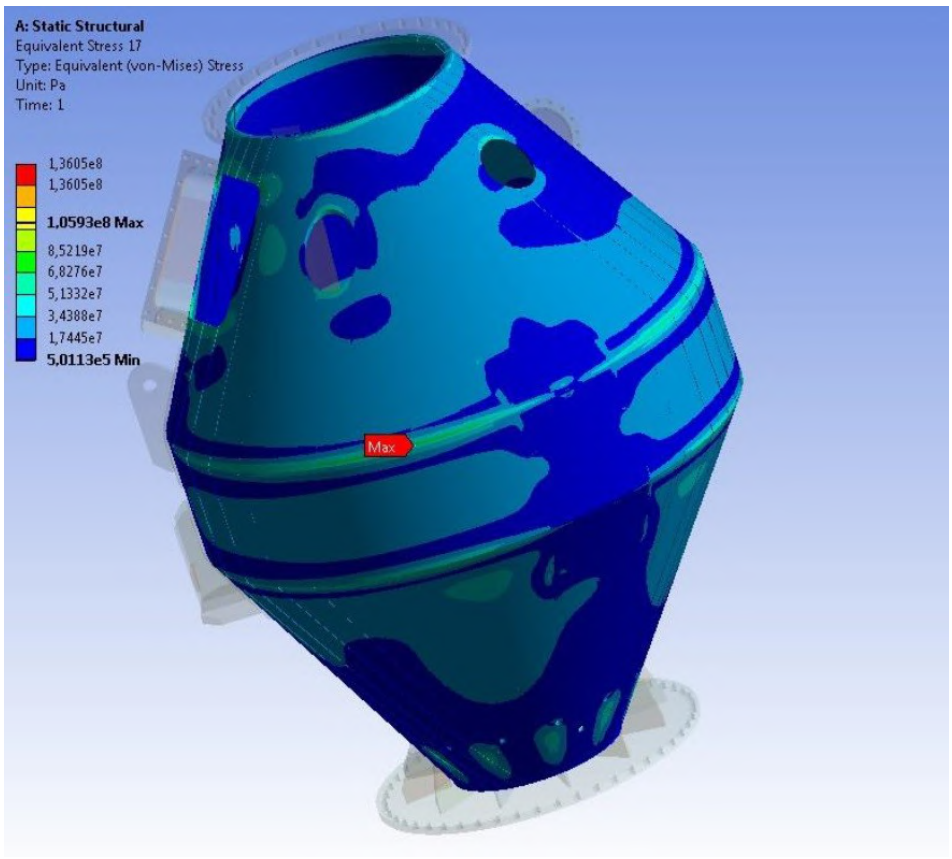

Fig. 1.42 Distribution of von Mises equivalent stresses arising in bin's load-bearing cover

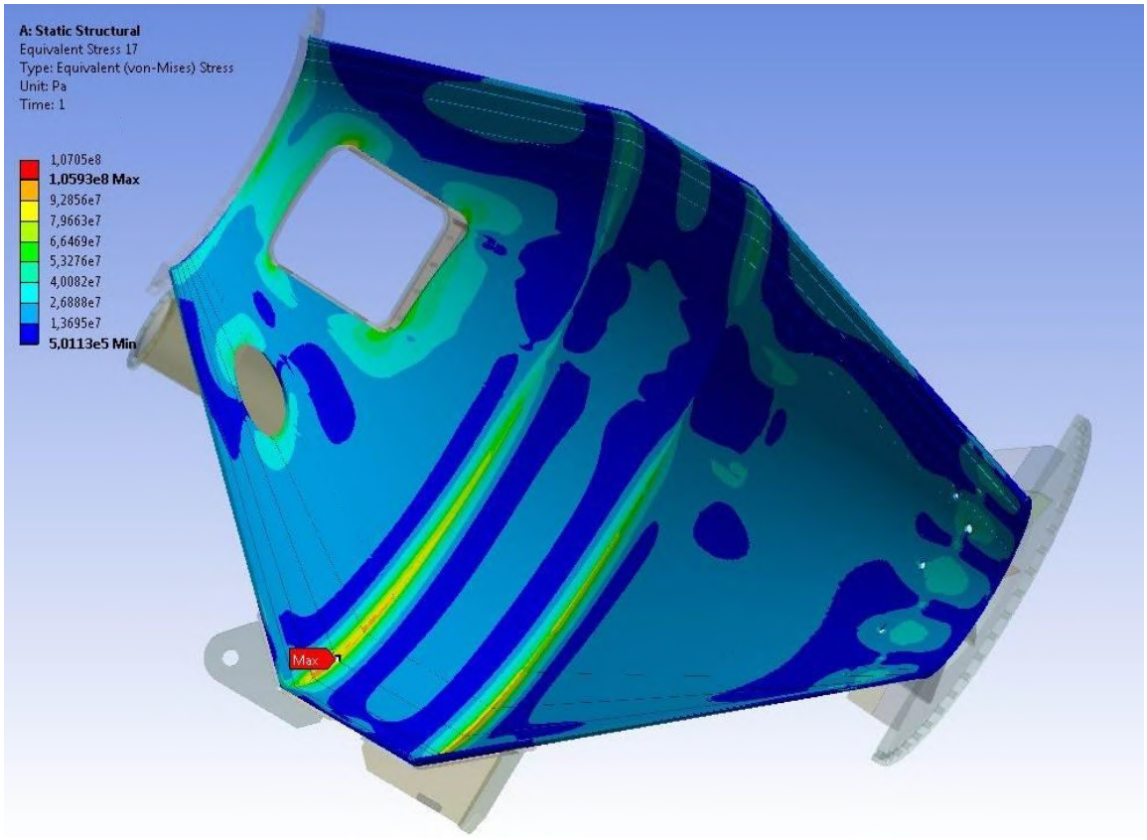

Fig. 1.43 Distribution of von Mises equivalent stresses arising inside the bin

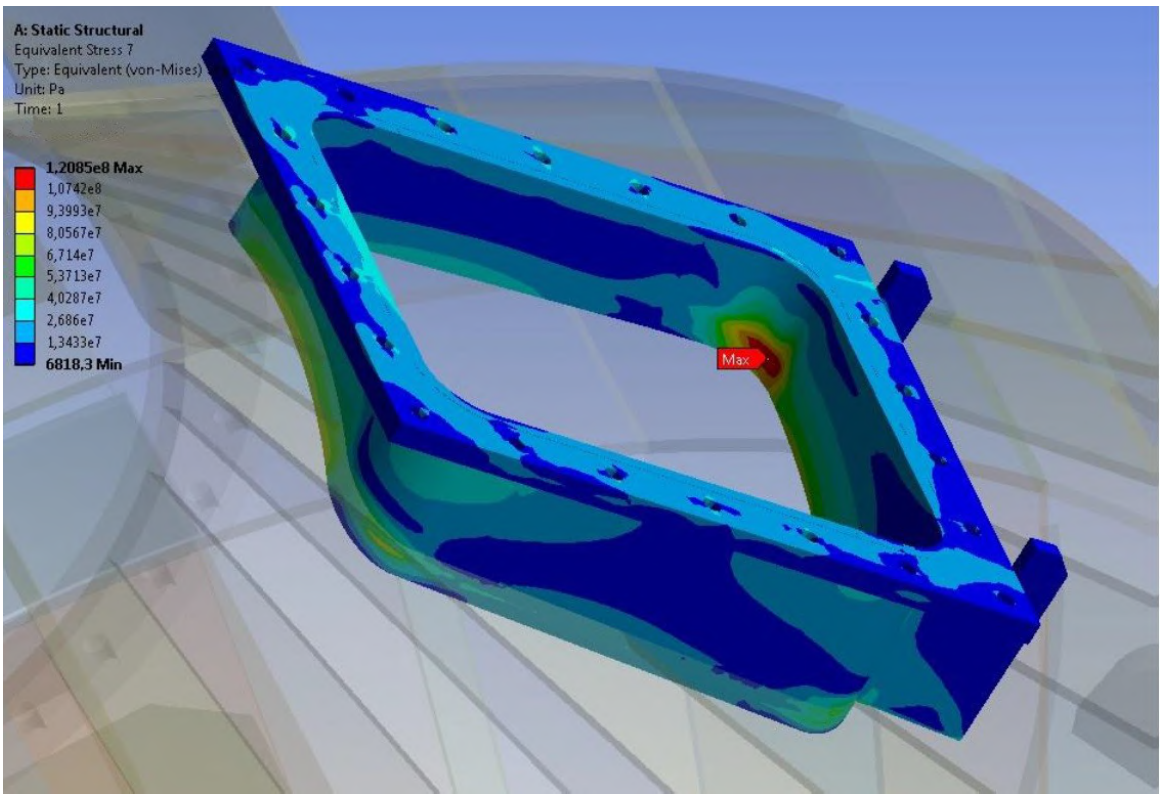

Fig. 1.44 Distribution of equivalent stresses in bin's lateral flange

Definition of stresses as more specific for the support has been made after submodeling of the structure. Distribution of stresses in the support is presented in Fig. 1.45.

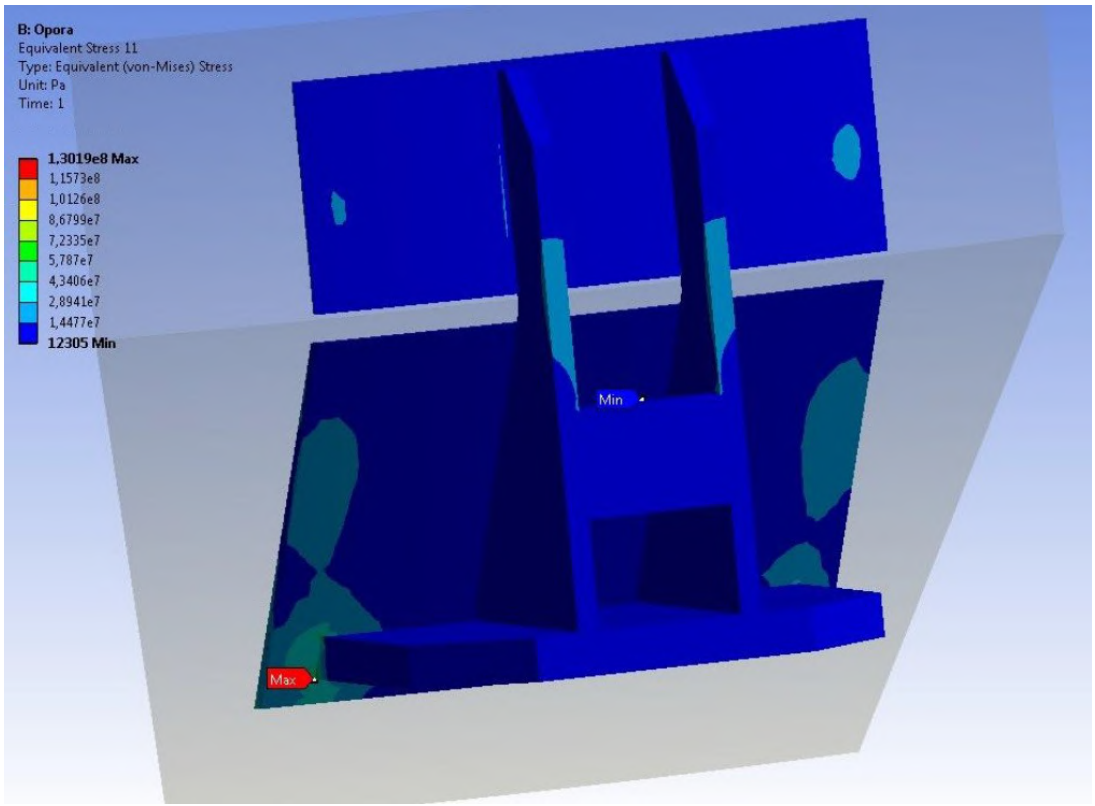

Fig. 1.45 Distribution of equivalent stresses in bin's support

Second case of frontal wind effect direction.

Results of bin designing under wind effect and normal service conditions for the second case of wind direction are presented as patterns of stresses, strains and fatigue calculation parameters in figures 1.46-1.55.

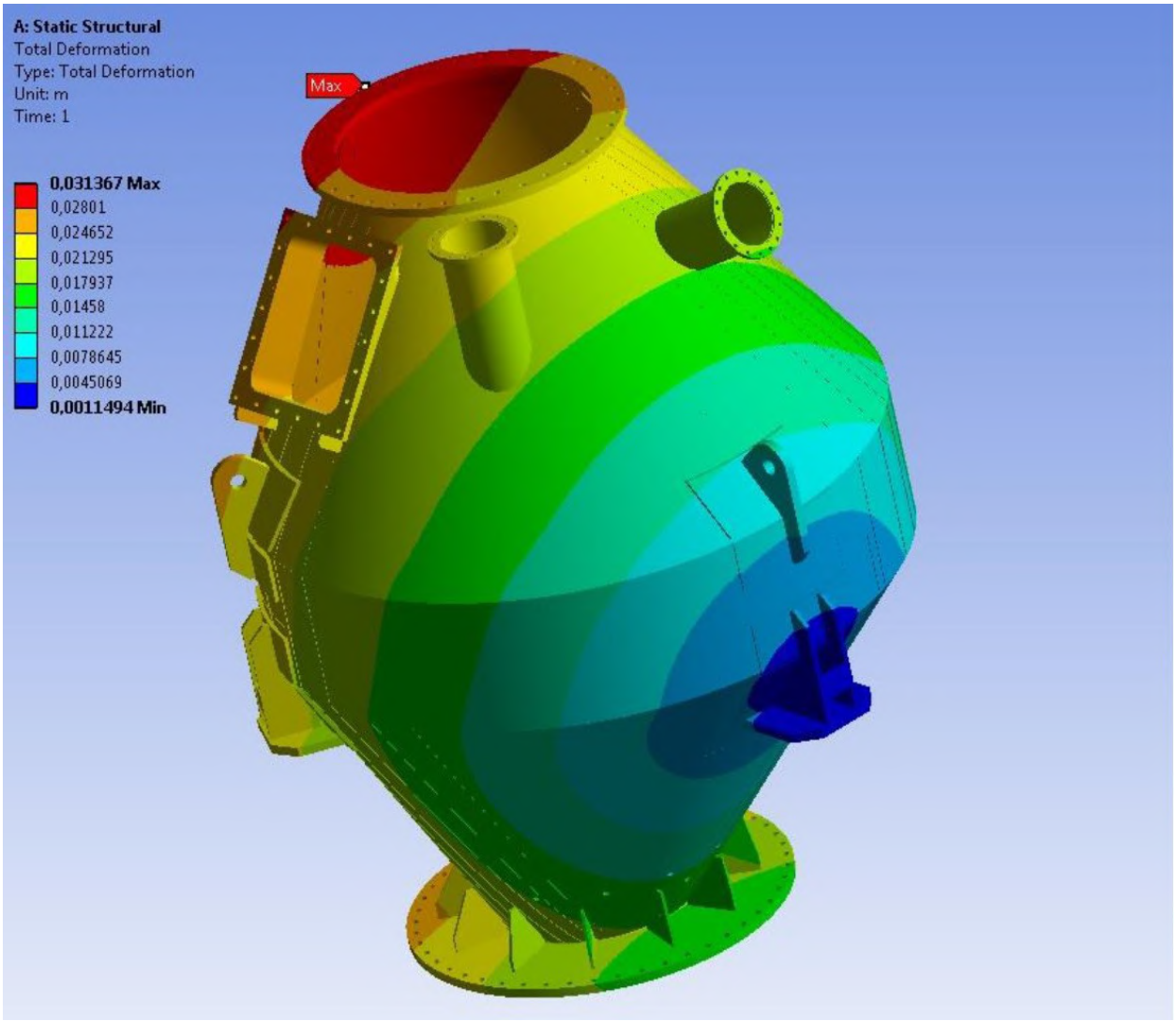

Fig. 1.46 Distribution of total strain arising in the bin

The biggest stresses in the structure arise in bin's support, the most distant one from aperture's axis.

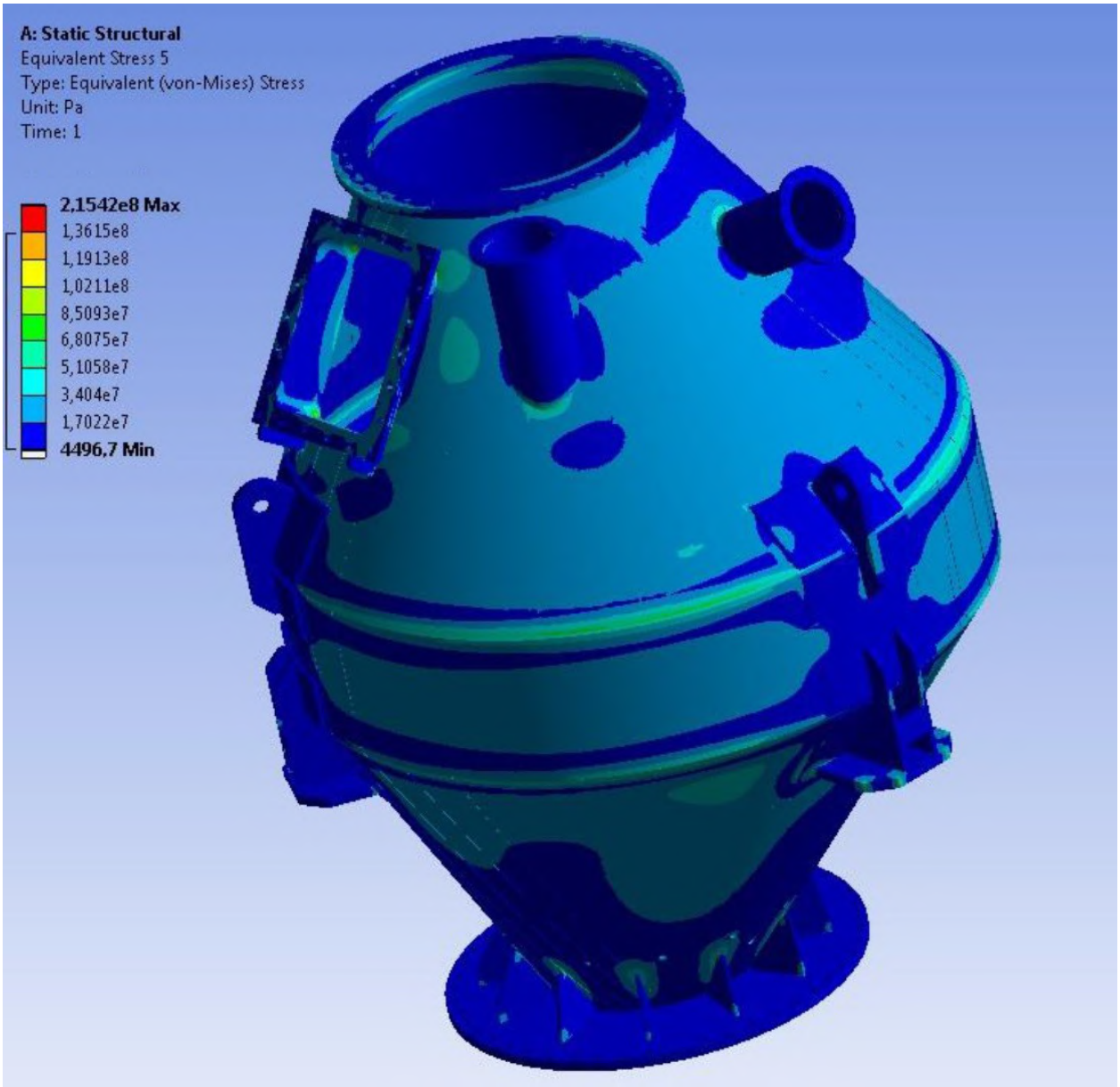

Fig. 1.47 Distribution of von Mises equivalent stresses arising in the material bin

The load-bearing cover has the biggest stresses inside the area of joining the bin's conical and cylindrical parts. Fig. 1.48-1.50 presents the distribution of stresses in bin's load-bearing cover. The maximal stresses in the load-bearing cover do not exceed 106.3MPa.

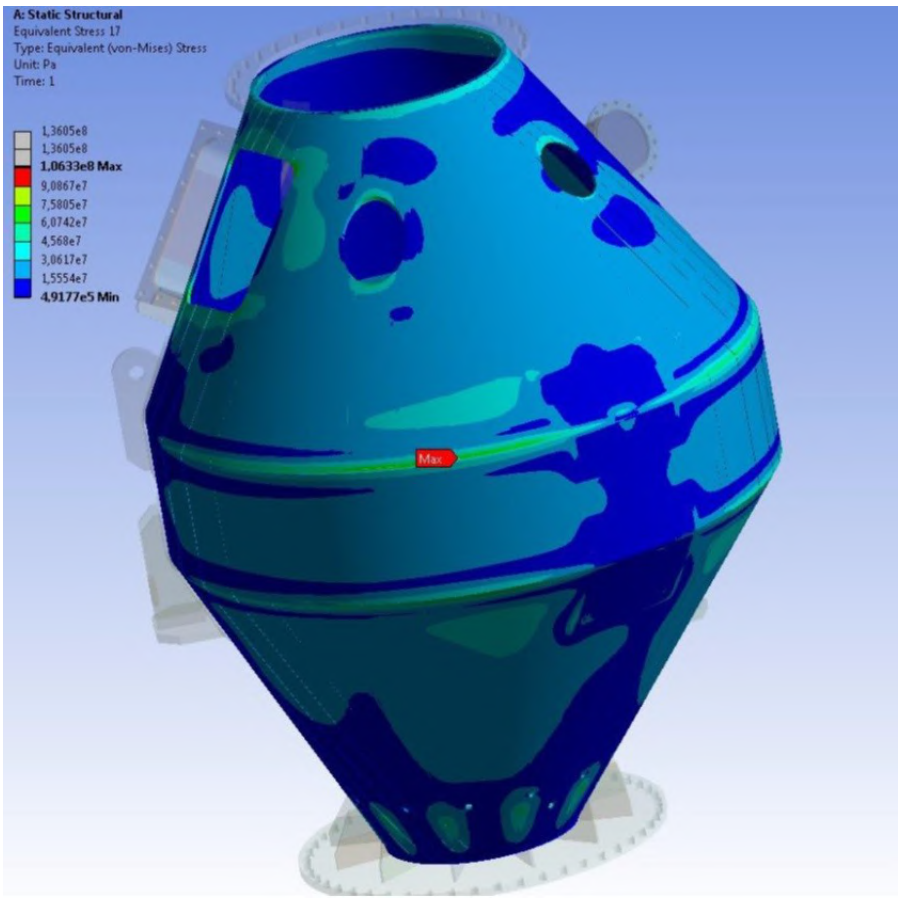

Fig. 1.48 Distribution of von Mises equivalent stresses arising in bin's load-bearing cover

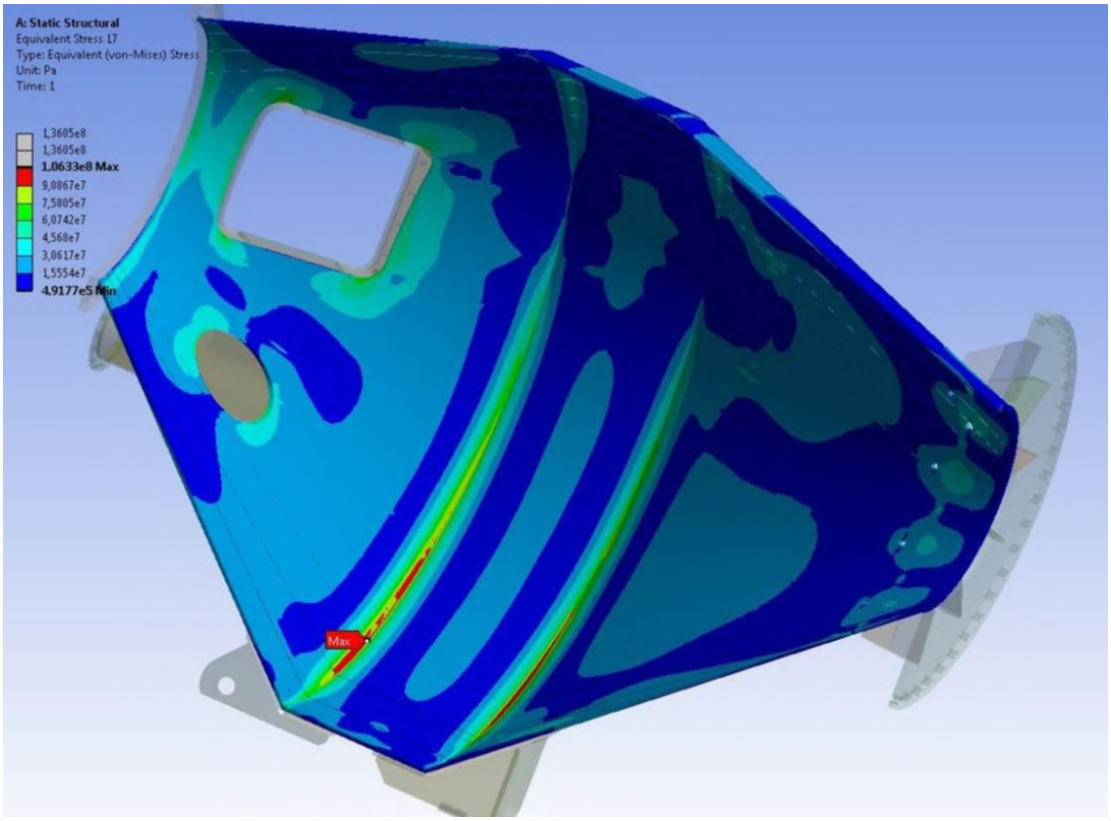

Fig. 1.49 Distribution of von Mises equivalent stresses inside the bin

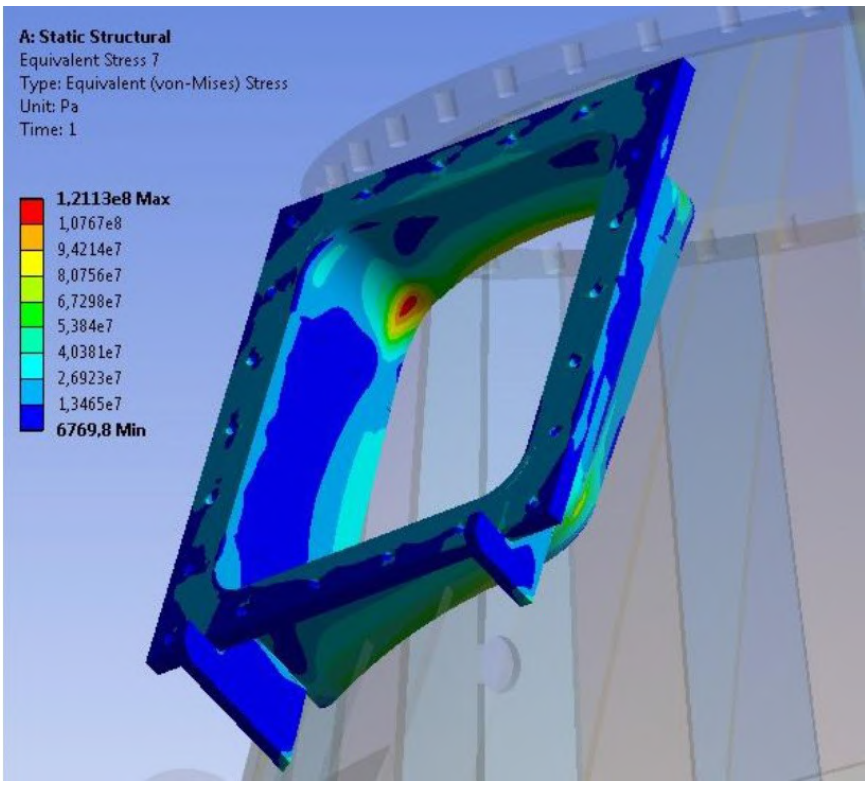

Fig. 1.50 Distribution of von Mises equivalent stresses in bin's lateral flange

Definition of stresses as more specific for the support has been made after submodeling of the structure. Distribution of stresses in the support is presented in Fig. 1.52.

Import of displacements and distribution of stresses in the support are presented in Fig. 1.51-1.52.

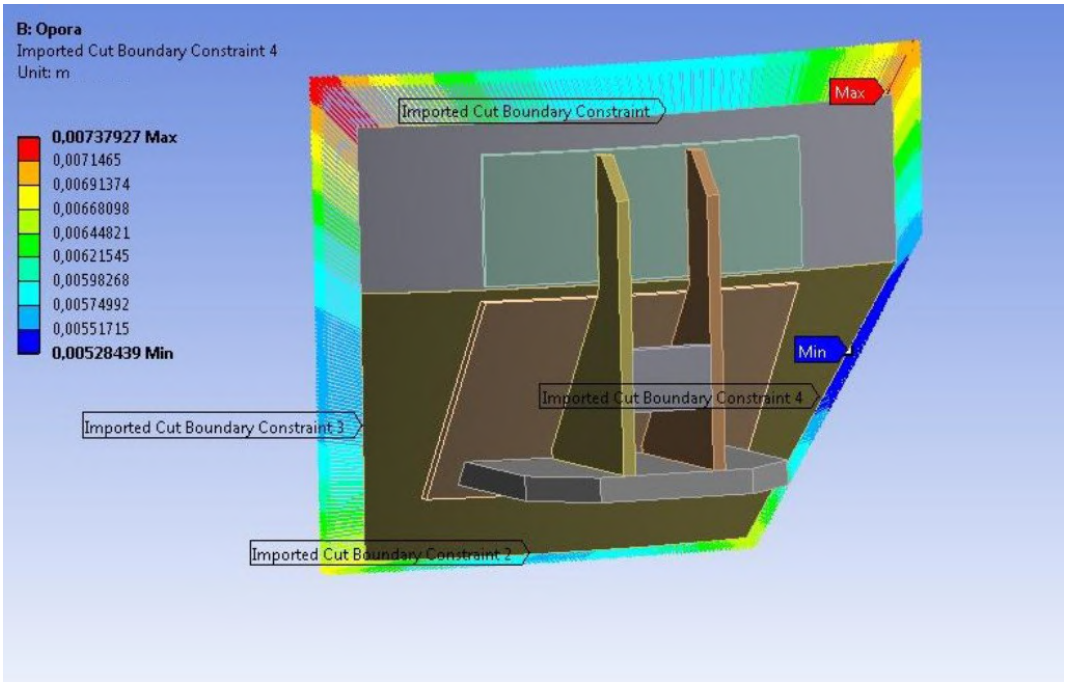

Fig. 1.51 Imported strains in support's submodel

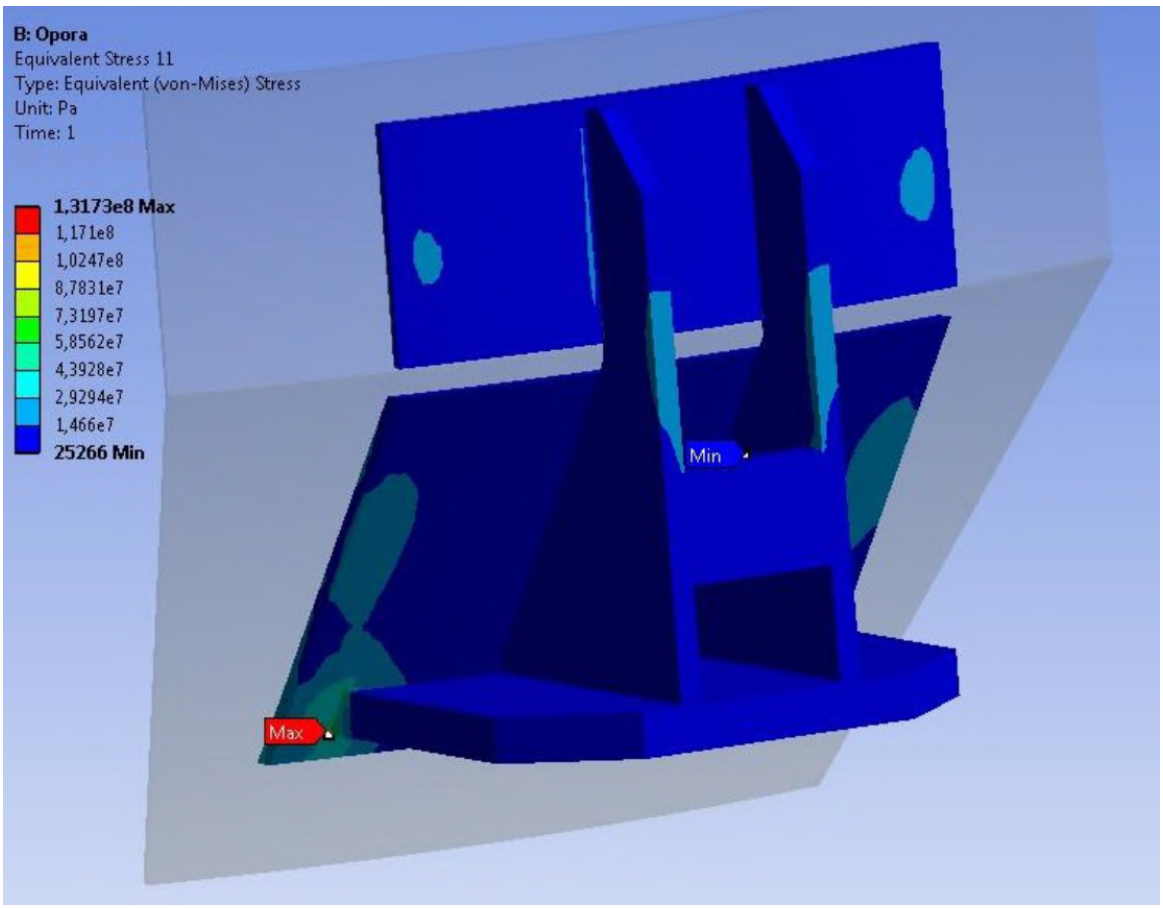

Fig. 1.52 Distribution of equivalent stresses in bin's support

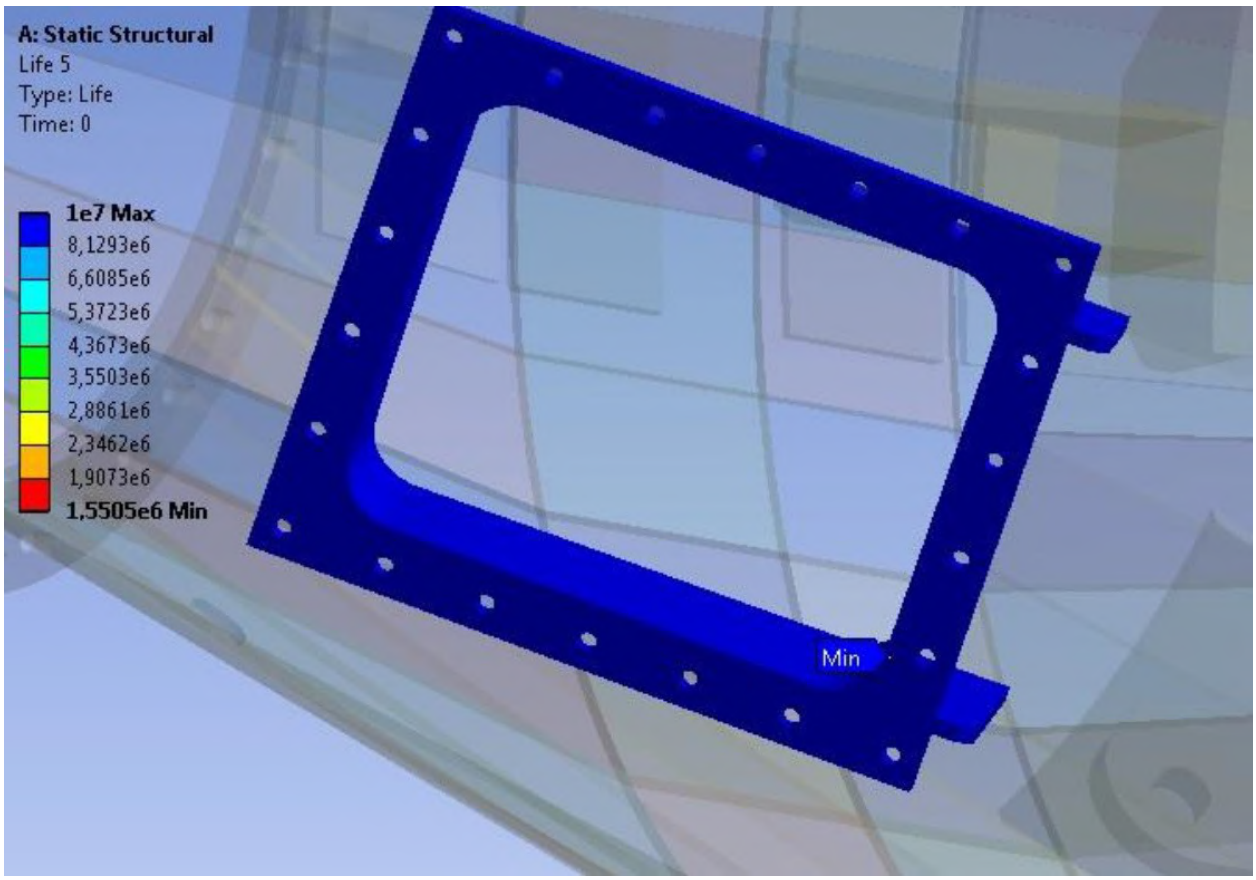

Fig. 1.53 Distribution of bin's lateral flange lifespan by Wehler SN curve

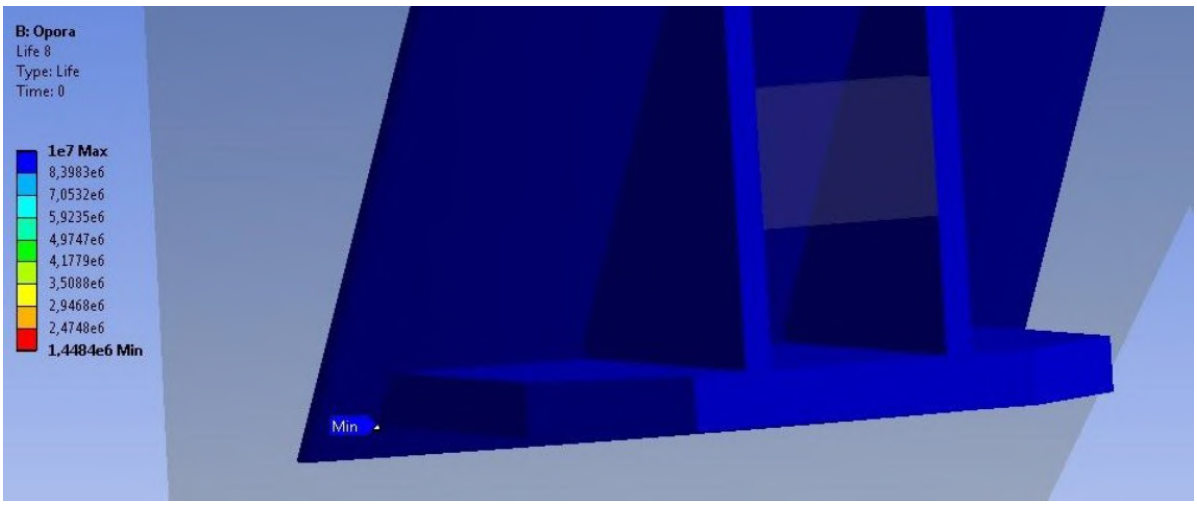

Fig. 1.54 Distribution of bin's support lifespan by Wehler SN curve

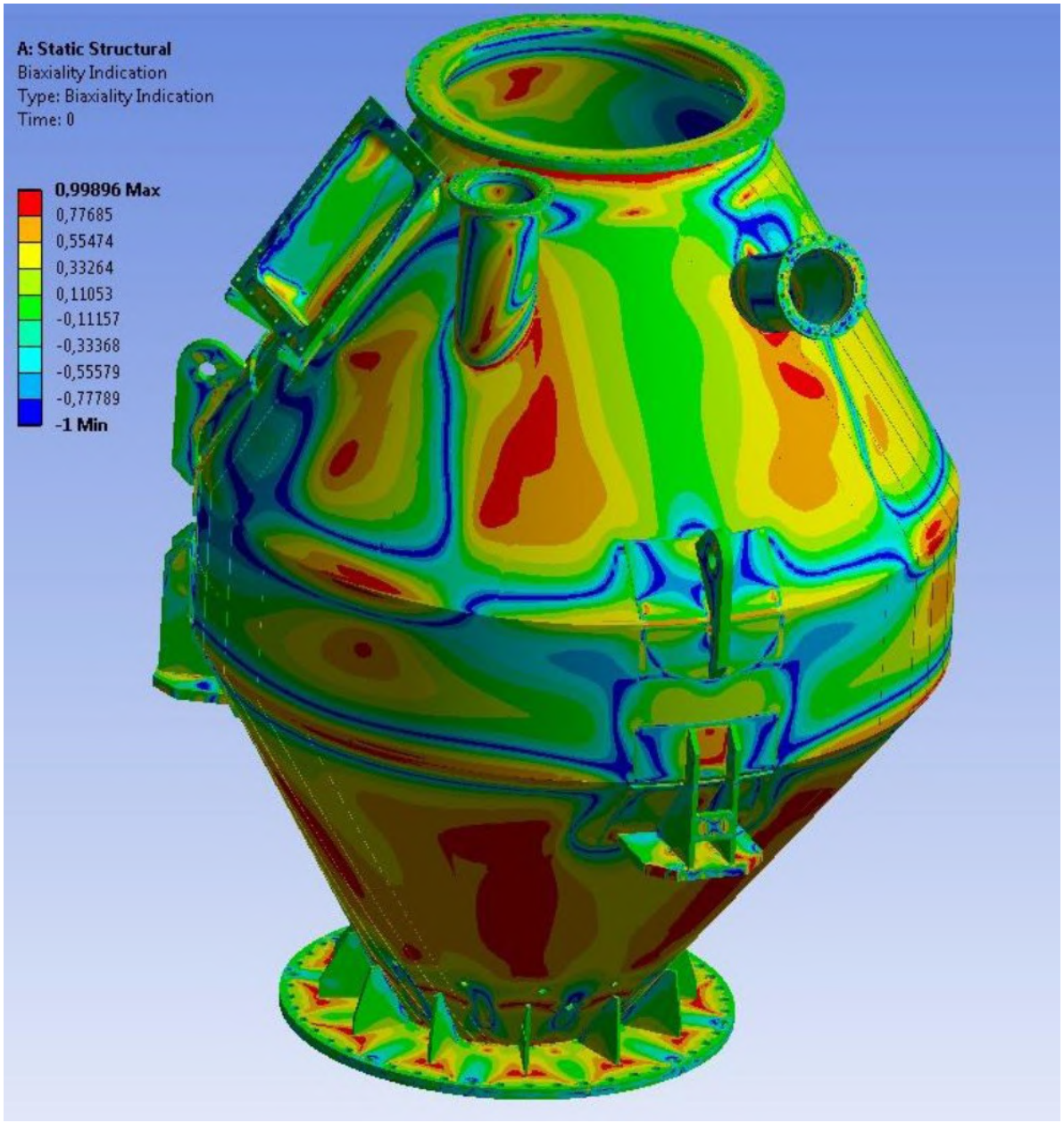

Fig. 1.55 Distribution of stress-state nature in the bin by Wehler SN curve

Third case of lateral wind effect direction.

Results of bin designing under wind effect and normal service conditions for the third case of wind direction are presented as patterns of stresses, strains and fatigue calculation parameters in figures 1.56-1.63.

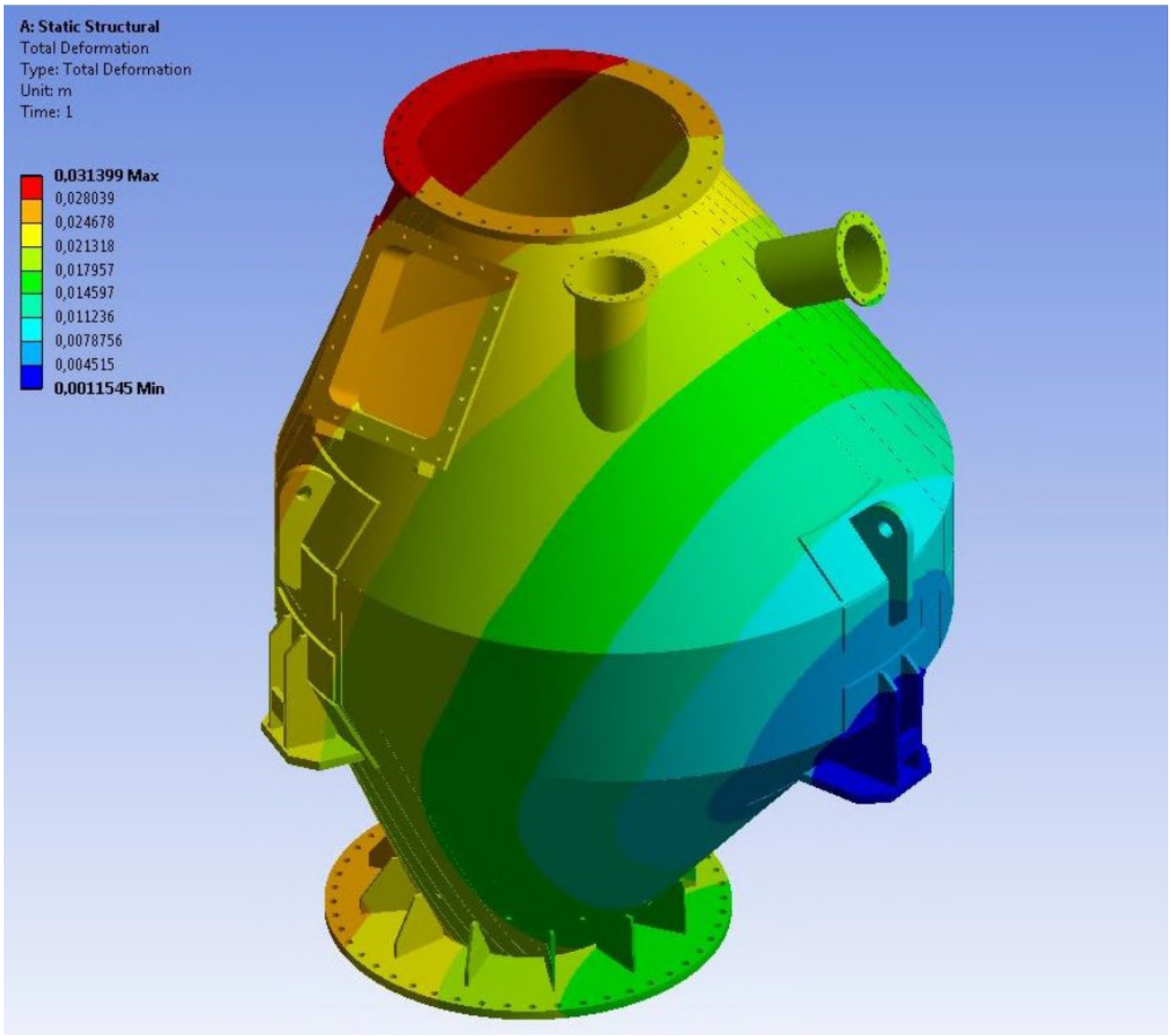

Fig. 1.56 Distribution of total strain arising in the bin

The biggest stresses in the structure arise in bin's support, the most distant one from aperture's axis. This bin's support is the most load-bearing one of structure's supports. Fig. 1.57-1.58 present von Mises equivalent stresses for the entire structure and in bin's supports.

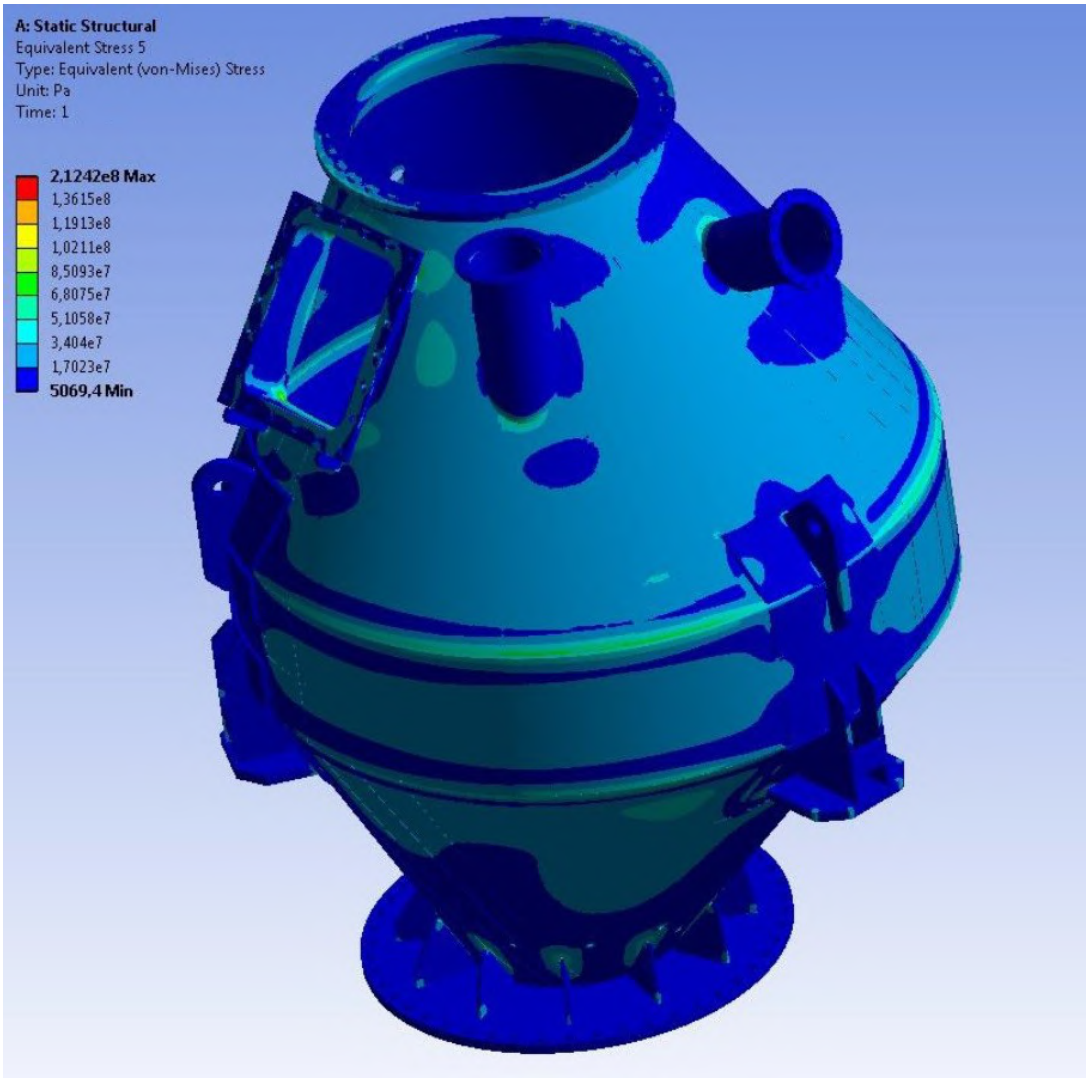

Fig. 1.57 Distribution of von Mises stresses arising in material bin

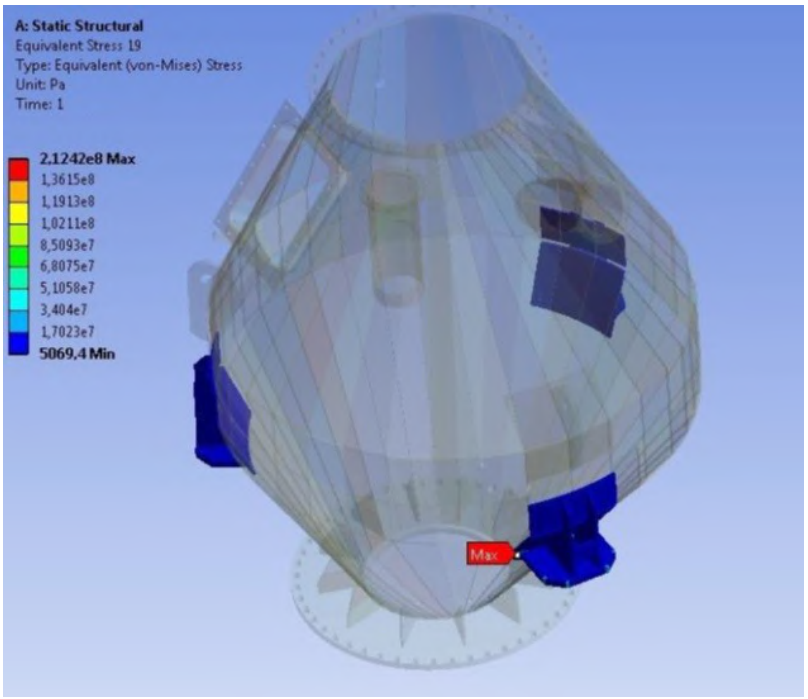

Fig. 1.58 Distribution of von Mises equivalent stresses in supports

Regarding the load-bearing cover the biggest stresses arise in the area of joining the upper conical and cylindrical parts of the bin. Fig. 1.59-1.60 present the distribution of stresses in bin's load-bearing cover. Bin's support, the most distant one from the bin hopper, is the most load-bearing one of structure's supports. The maximal stresses in the load-bearing cover do not exceed 106.6MPa.

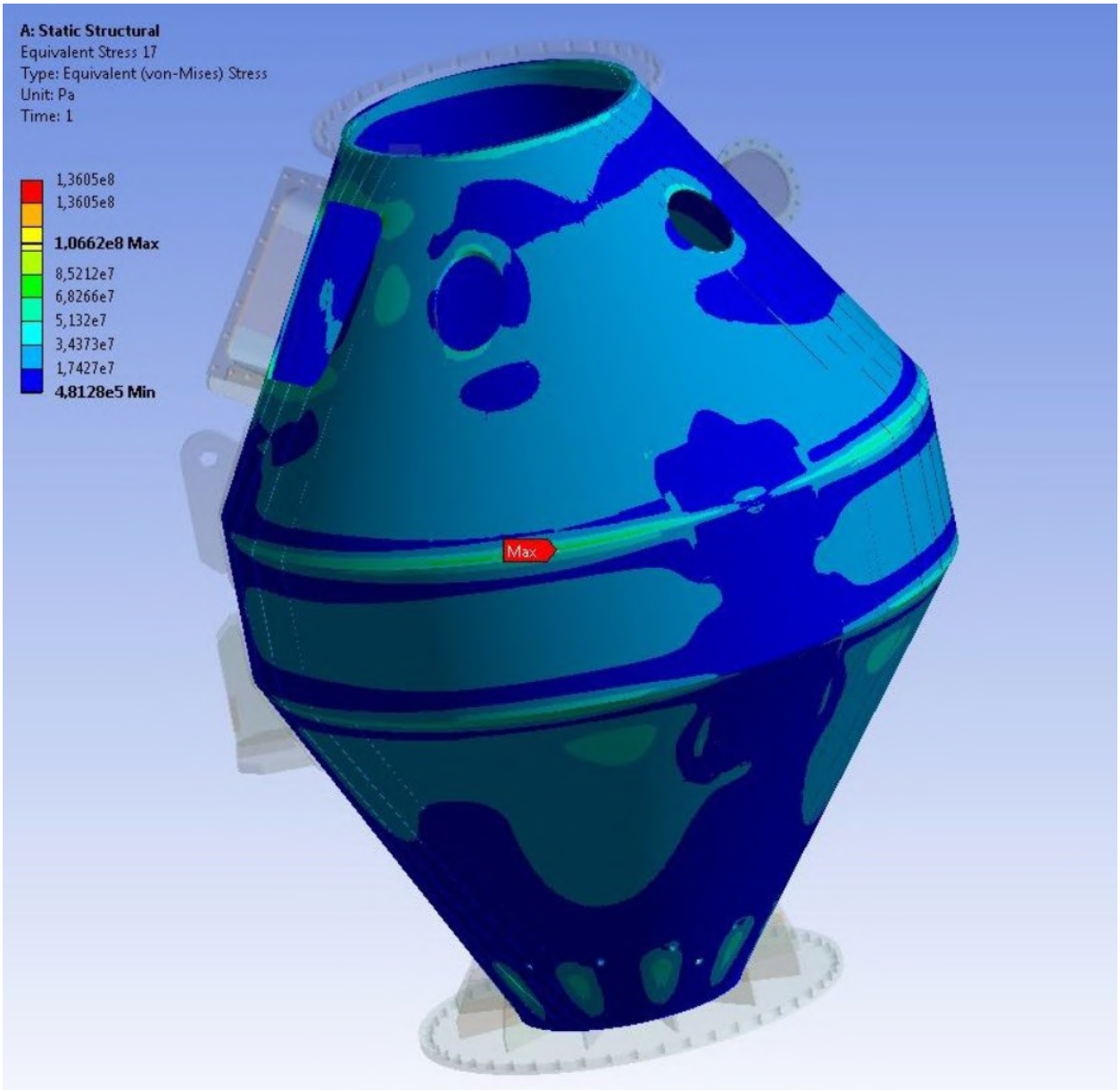

Fig. 1.59 Distribution of von Mises equivalent stresses arising in bin's load-bearing cover

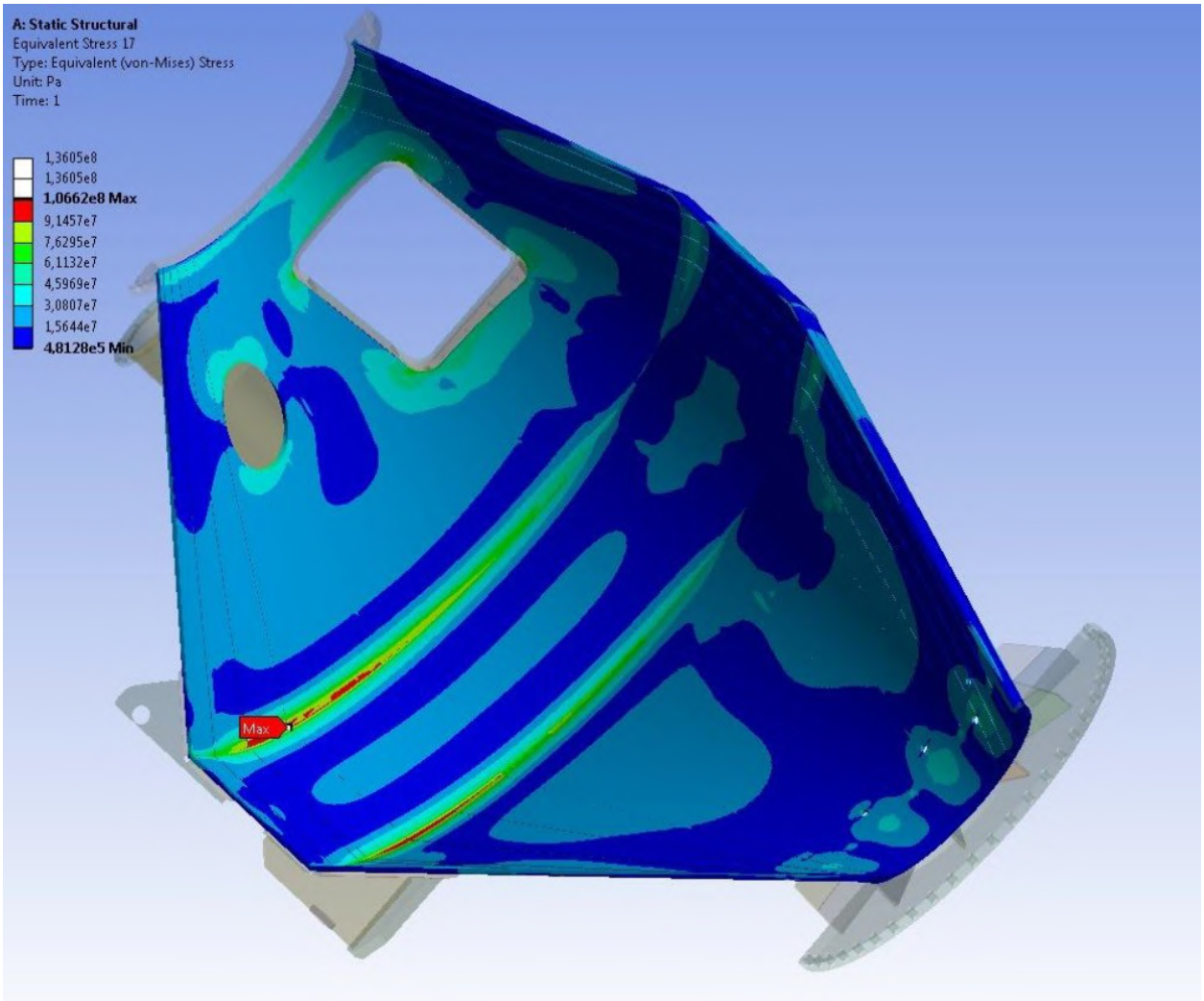

Fig. 1.60 Distribution of von Mises equivalent stresses inside the bin

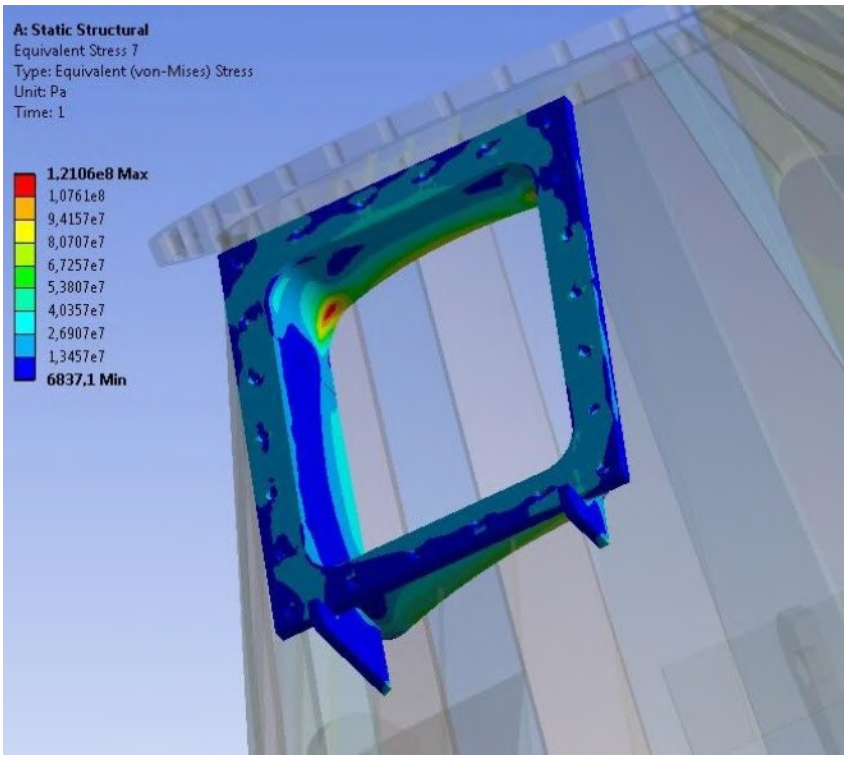

Fig. 1.61 Distribution of equivalent stresses in bin's lateral flange

Definition of stresses as more specific for the most load-bearing support has been made after submodeling of the structure. Distribution of stresses in the support is presented in Fig. 1.45. Import of strains and more specific distribution of stresses in the support are presented in Fig. 1.62-1.63.

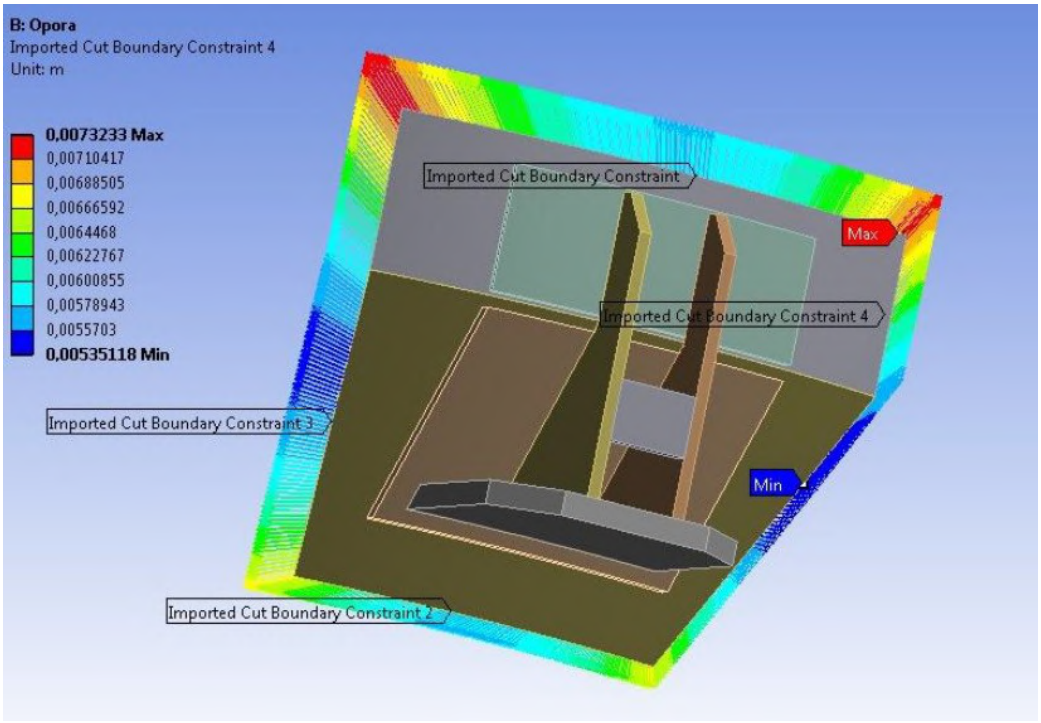

Fig. 1.62 Imported strains in support's submodel

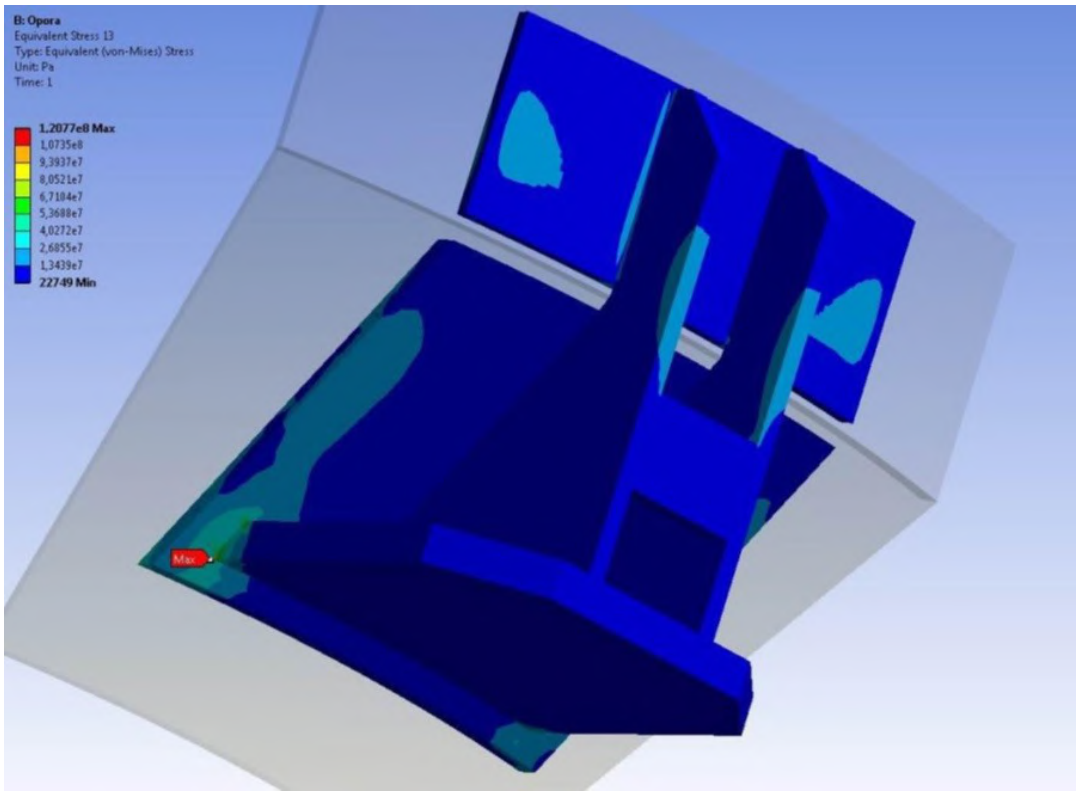

Fig. 1.63 Distribution of equivalent stresses in bin's support

Stresses arising in bin's structure elements from wind effect are presented in Table 1.6.

Table 1.6

Structural elements of material bin	Obtained results of stresses from wind effect design cases (MPa)			Maximal stress (MPa)
	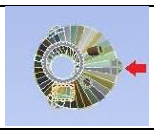		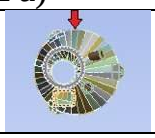	
Cylindrical wall	**105.9**	**106.3**	**106.6**	**106.6**
Conical wall	**105.9**	**106.3**	**106.6**	**106.6**
Top flange	**51.0**	**51.0**	**51.0**	**51.0**
Bottom flange	**68.0**	**68.0**	**68.0**	**68.0**
Branch/flange	**83.8/28.0**	**83.8/28.0**	**83.9/28.0**	**83.9/28.0**
Hatch/flange	**120.8/40.2**	**121.1/40.3**	**121.0/40.3**	**121.1/40.3**
Support's lug	**130.1**	**131.7**	**120.7**	**131.7**

The conducted calculations allow presenting the stress state of bin hopper structural elements for considered load combinations as the table 1.7 and single out the design case of maximum load.

Table 1.7

Structural members of material bin	Obtained stresses from design load cases (МПа)				Maximal stress (MPa)
	Design pressure + weight	NSC	NSC + LWE	NSC + MDE	
Cylindrical wall	**101.5**	**103.2**	**106.6**	**106.1**	**106.6**
Conical wall	**101.5**	**103.2**	**106.6**	**106.1**	**106.6**
Top flange	**52.2**	**59.1**	**51.0**	**60.7**	**60.7**
Bottom flange	**65.3**	**66.1**	**68.1**	**67.7**	**68.1**
Branch/flange	**81.0/27.0**	**81.2/27.1**	**83.9/28.0**	**82.8/28.7**	**83.9/28.7**
Hatch/flange	**124.7/ 39.2**	**120.2/ 40.0**	**121.1/ 40.3**	**121.8/ 41.6**	**124.7/ 39.2**
Support's lug	**124.4**	**144.2**	**131.7**	**158.9**	**158.9**

The most load-bearing structure element is support's lug. The operational lifespan value for this element is 1.156×106cycles or 20.3 years of service.

1.3.5 Designing the bin structural members

Irregular flanged connections of charging bin's structure are designed using the submodelling procedure. Designing of each flanged connection is performed as per sub-model. Each sub-model is obtained by splitting the master model with a plane located at the distance of 3-4 cover thicknesses from the flange. Using the master model for a given case of designing the stress patterns are determined along splitting planes. These strains serve as boundary conditions for the flanged connection being designed. Each flanged connection is completed with a lid and bolts securing the lid. The design pattern is built on the basis of acting loads and boundary conditions of strain patterns. Designing of bin's structural members has been performed the most loaded design case.

1.3.5.1 Designing the upper flanged connection

The design pattern of upper flanged connection submodel is presented in Fig. 1.64.

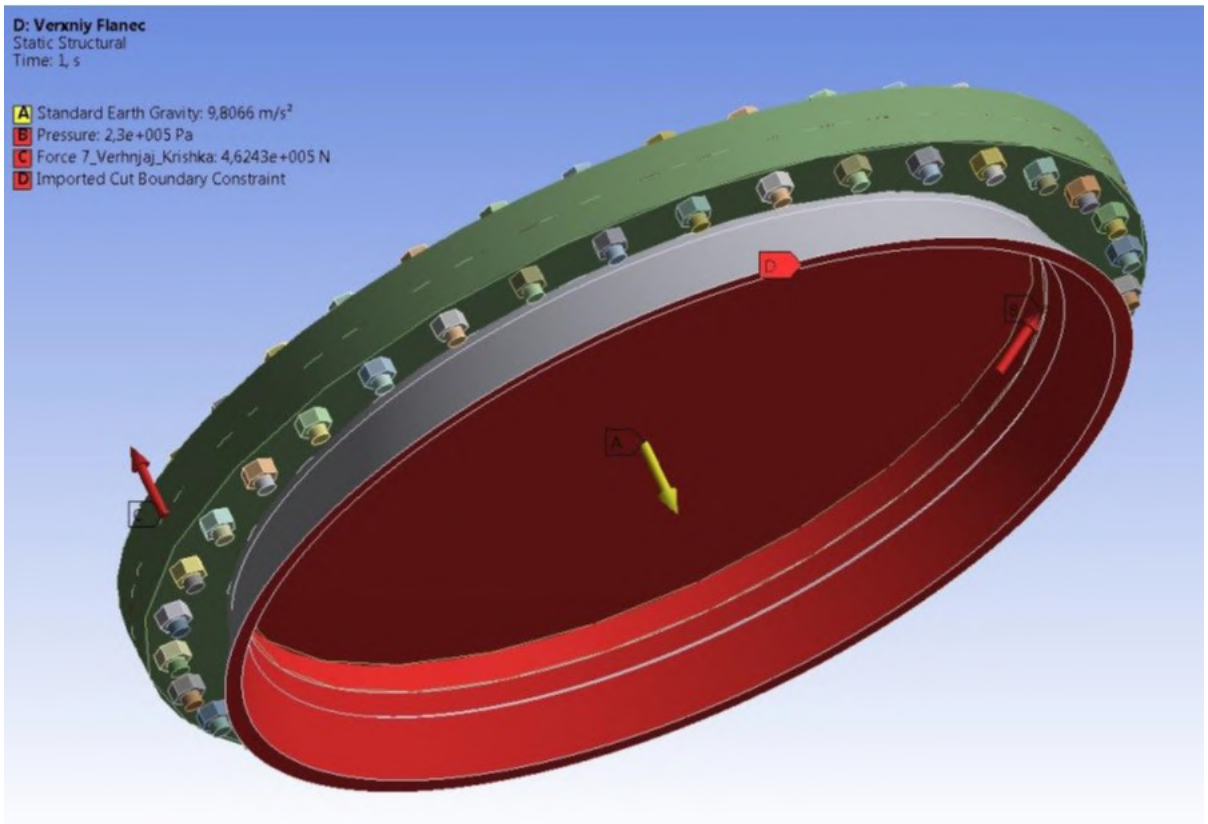

Fig. 1.64 Design case of upper flange loading

Fig. 1.65 depicts imported strains from the general bin's model.

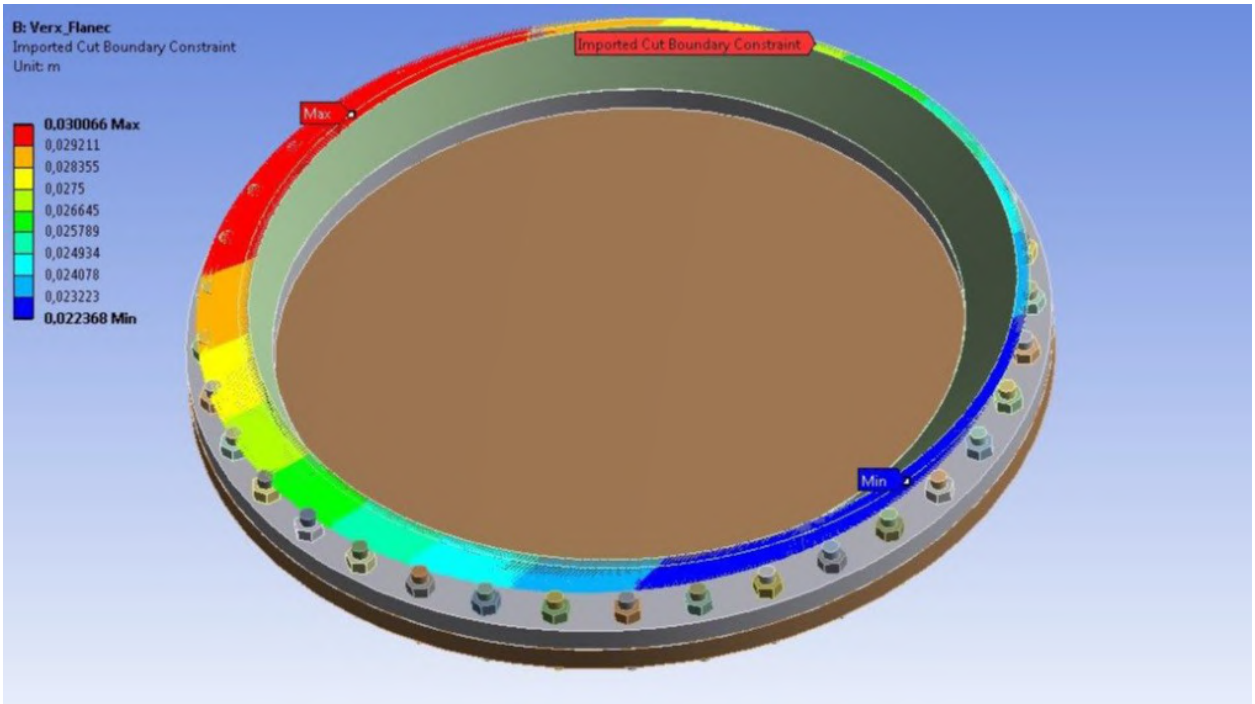

Fig. 1.65 Distribution of imported strain patterns in the upper flanged connection

The finite-element model is presented in Fig. 1.66.

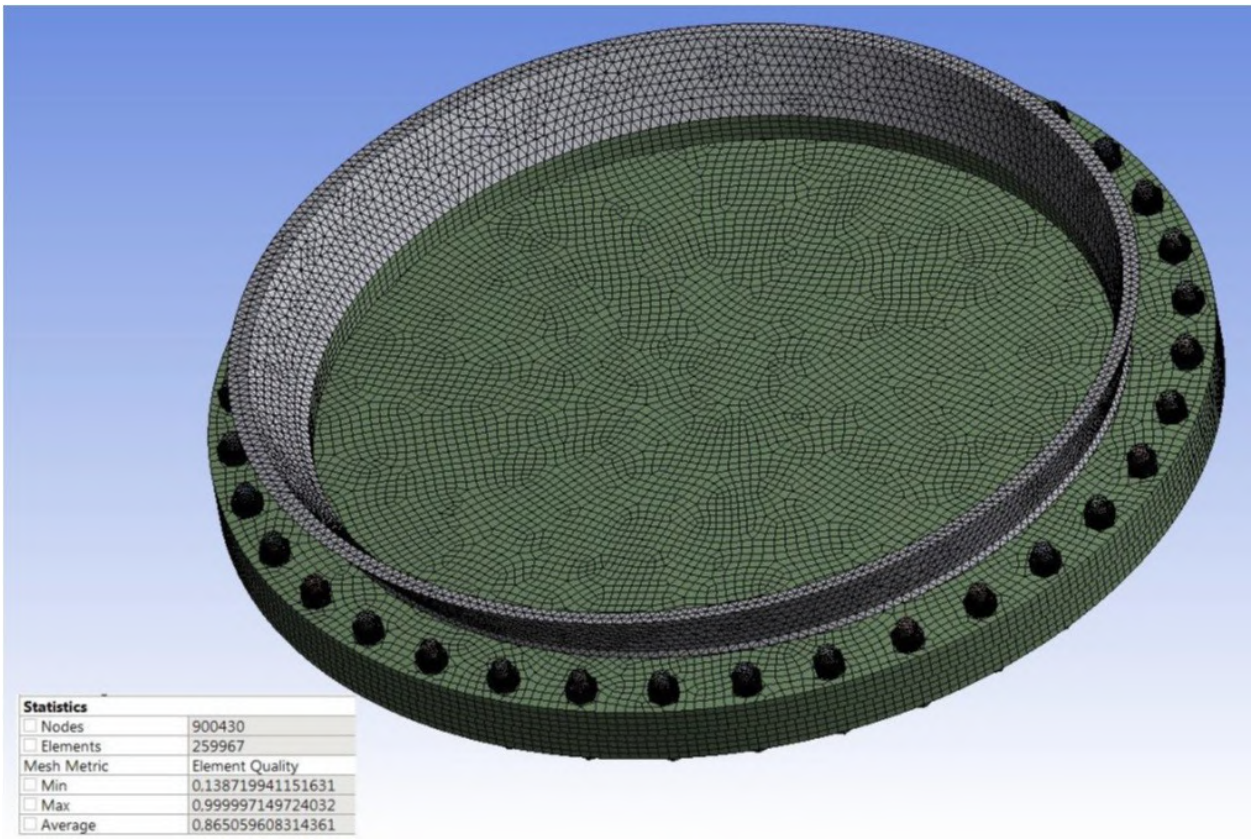

Fig. 1.66 Finite-element model of upper flanged connection

Calculation results of stress-strain state are presented in Fig. 1.67-1.71.

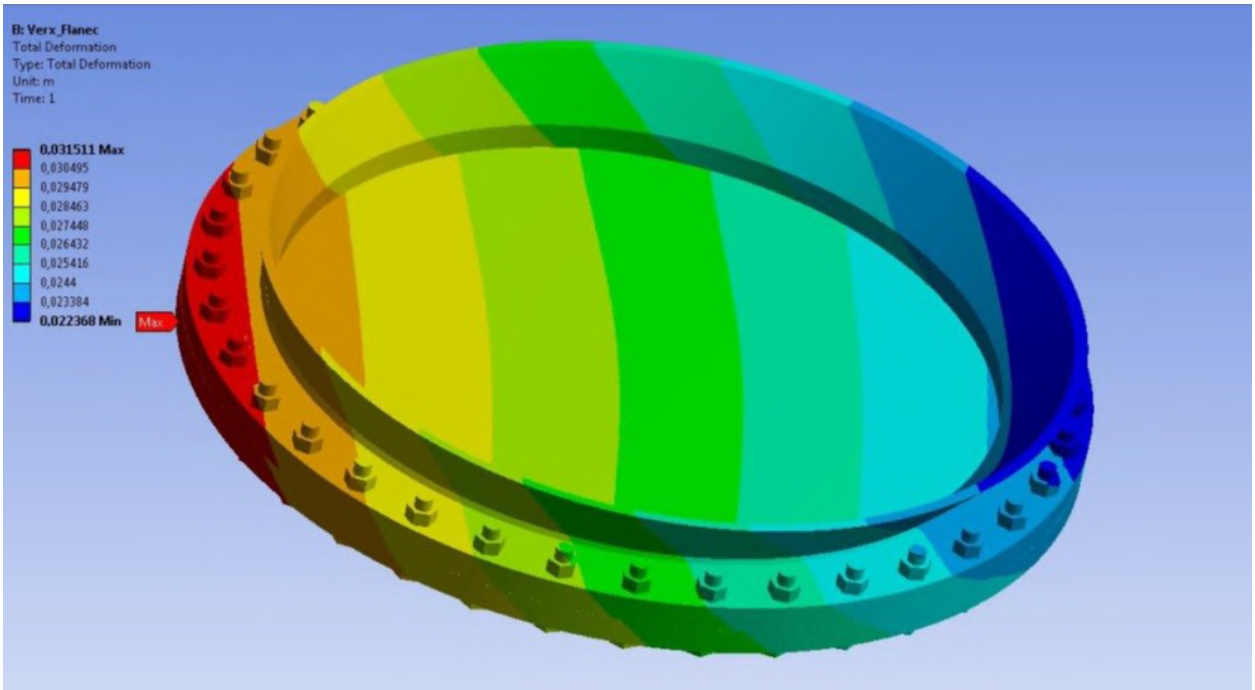

Fig. 1.67 Distribution of total strain arising in the structure

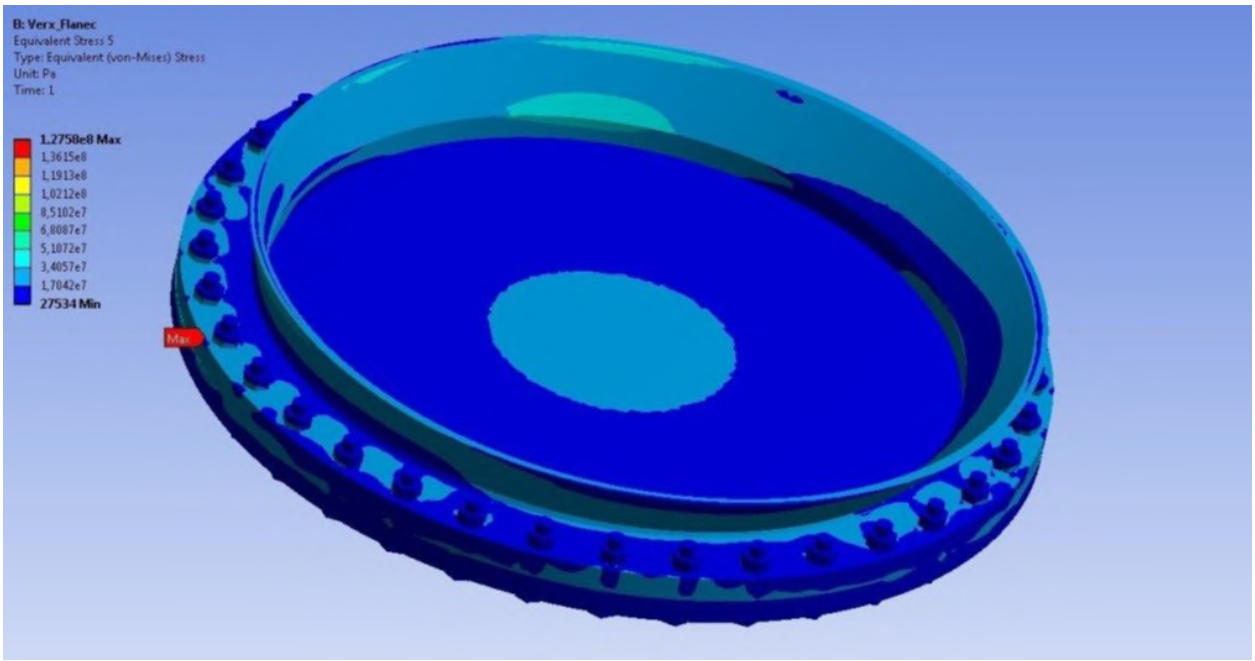

Fig. 1.68 Distribution of von Mises equivalent stresses

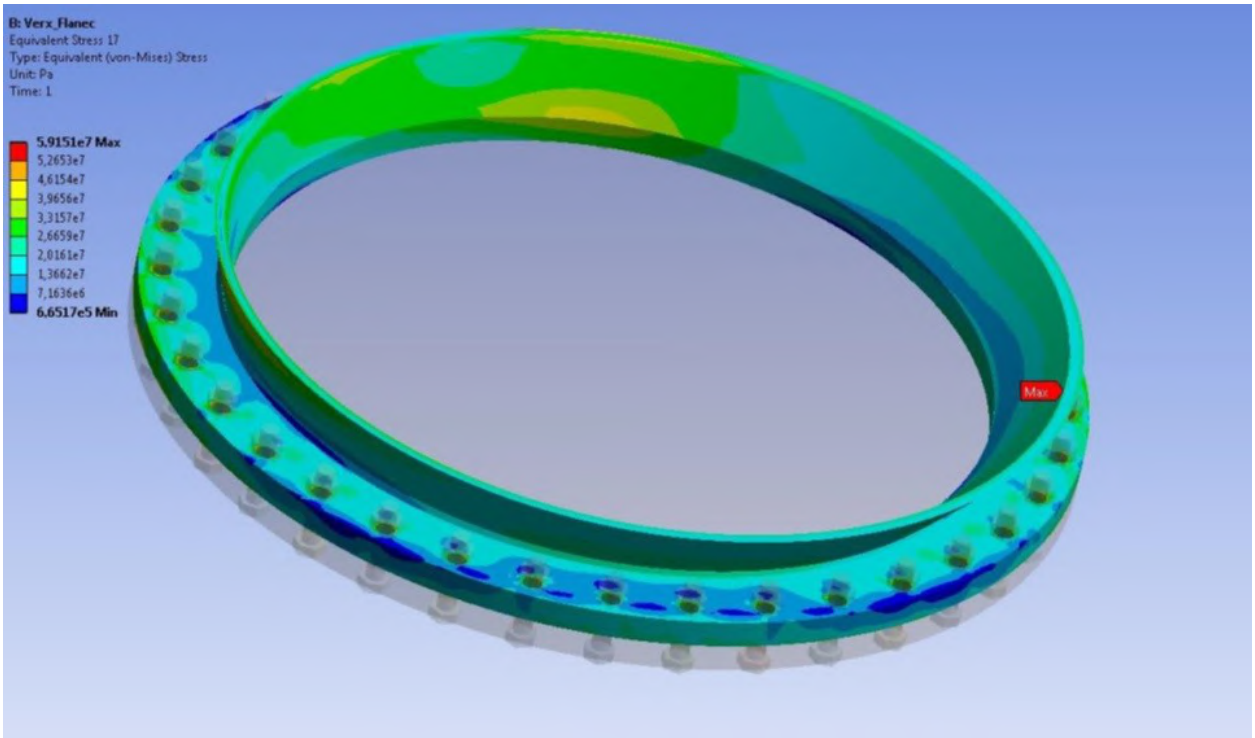

Fig. 1.69 Distribution of von Mises equivalent stresses in the flange

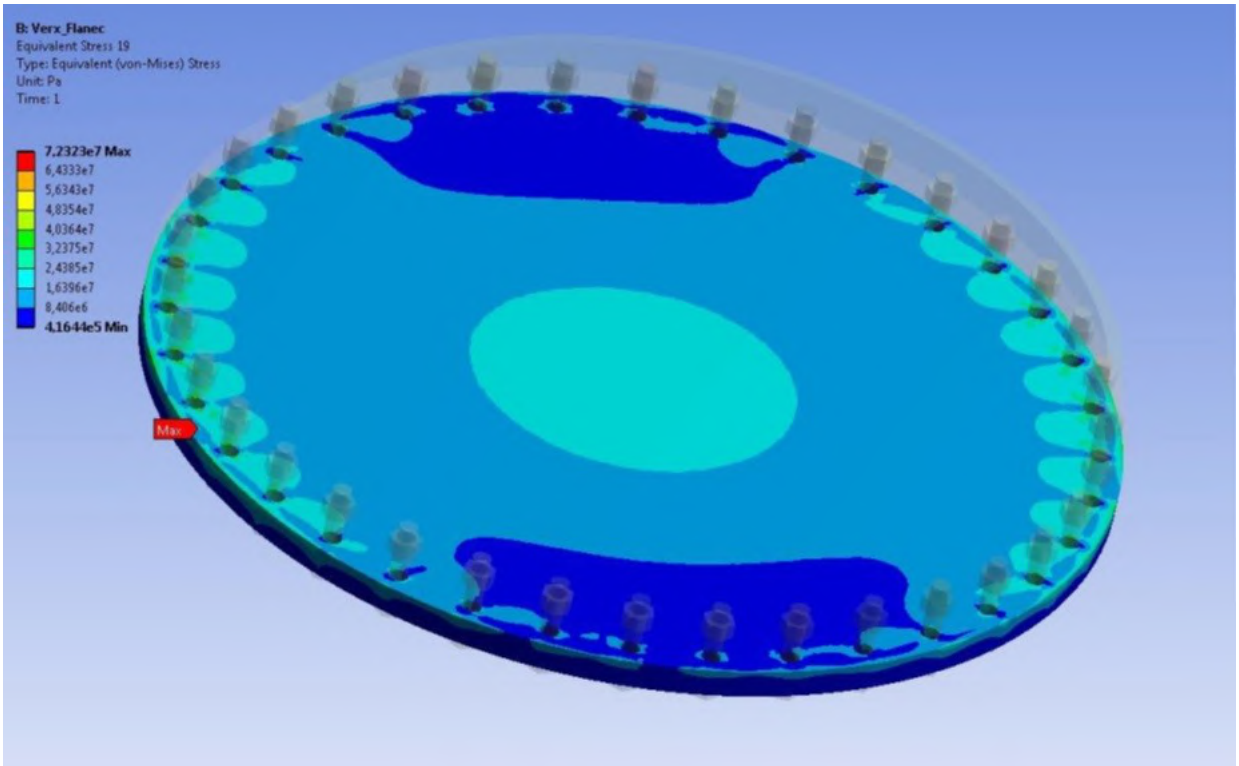

Fig. 1.70 Distribution of von Mises equivalent stresses in the lid

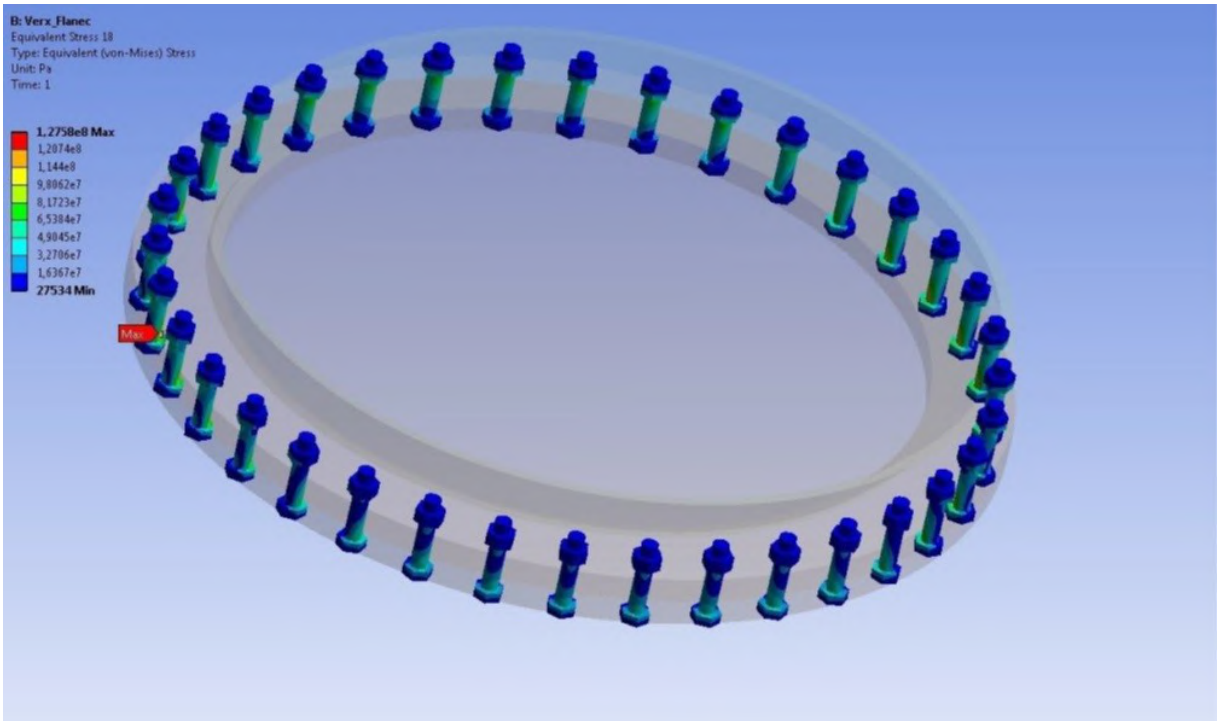

Fig. 1.71 Distribution of von Mises equivalent stresses in bolts

1.3.5.2 Designing the lower flanged connection

The design pattern of lower flanged connection submodel is presented in fig. 1.72.

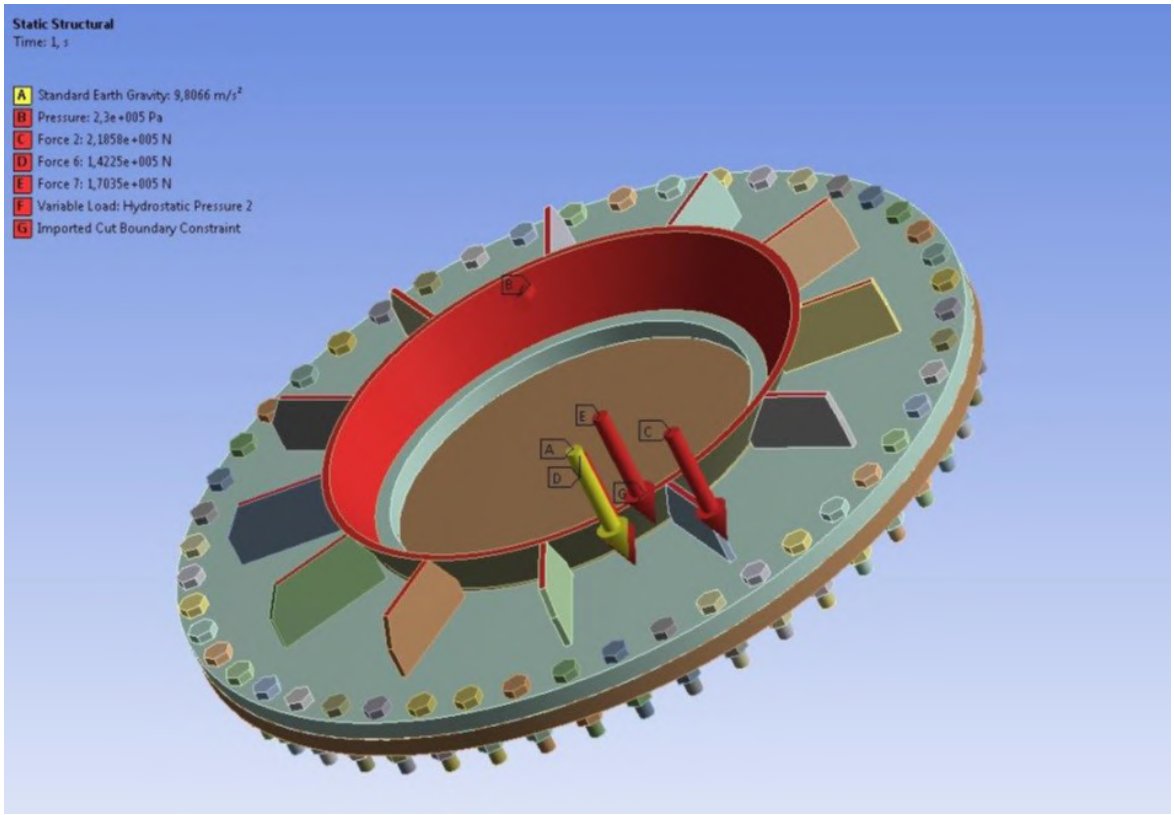

Fig. 1.72 Design case of lower flange loading

Fig. 1.73 depicts imported strains from the general bin's model.

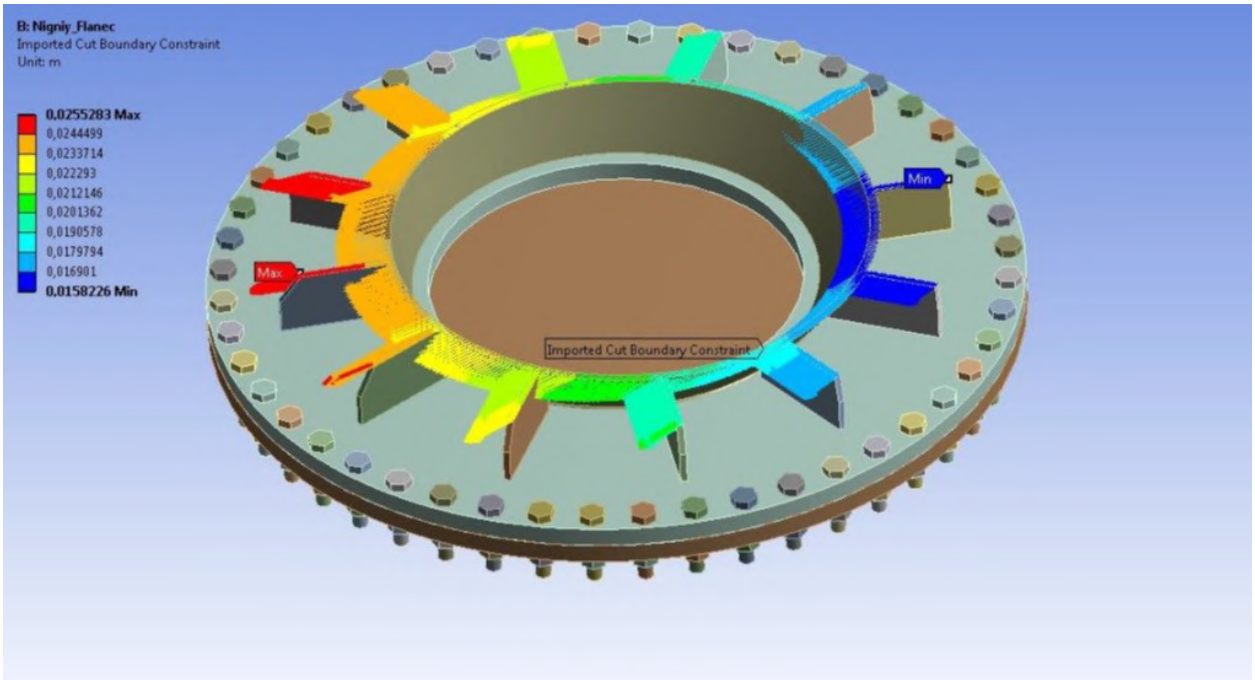

Fig. 1.73 Distribution of imported strain patterns in the lower flanged connection

The finite-element model is presented in Fig. 1.74.

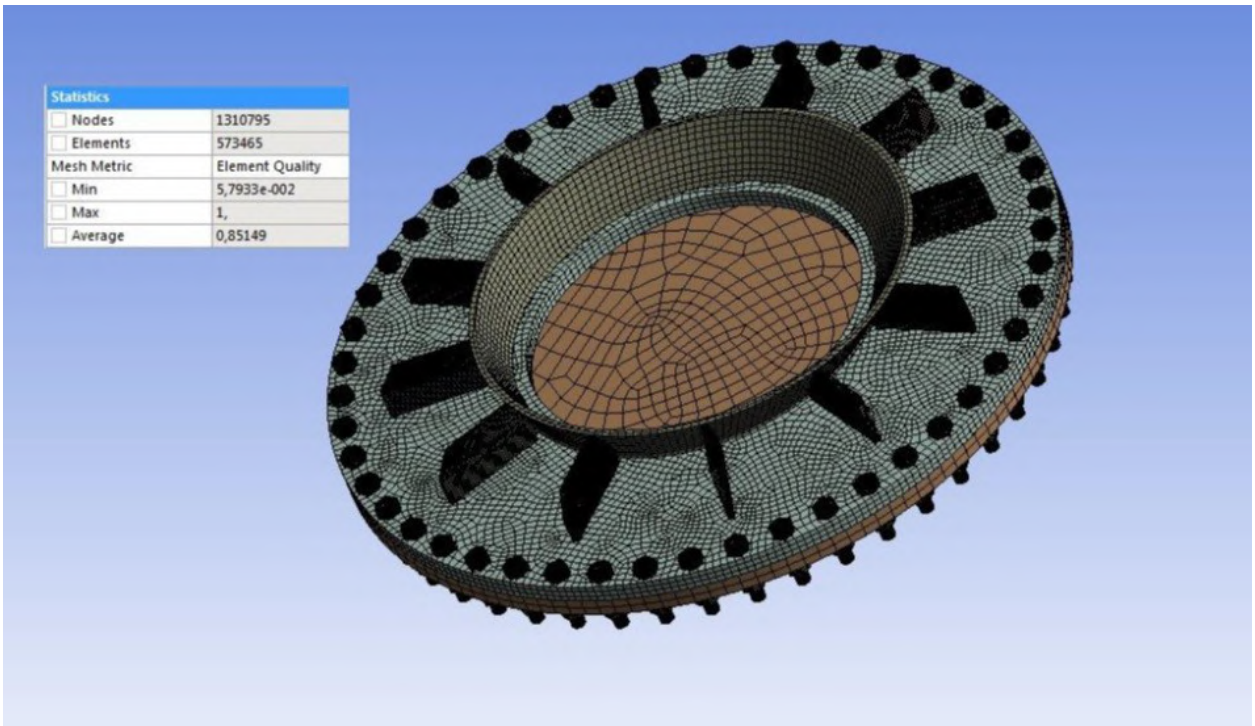

Fig. 1.74 Finite-element model of lower flanged connection

Calculation results of stress-strain state are presented in Fig. 1.75-1.79.

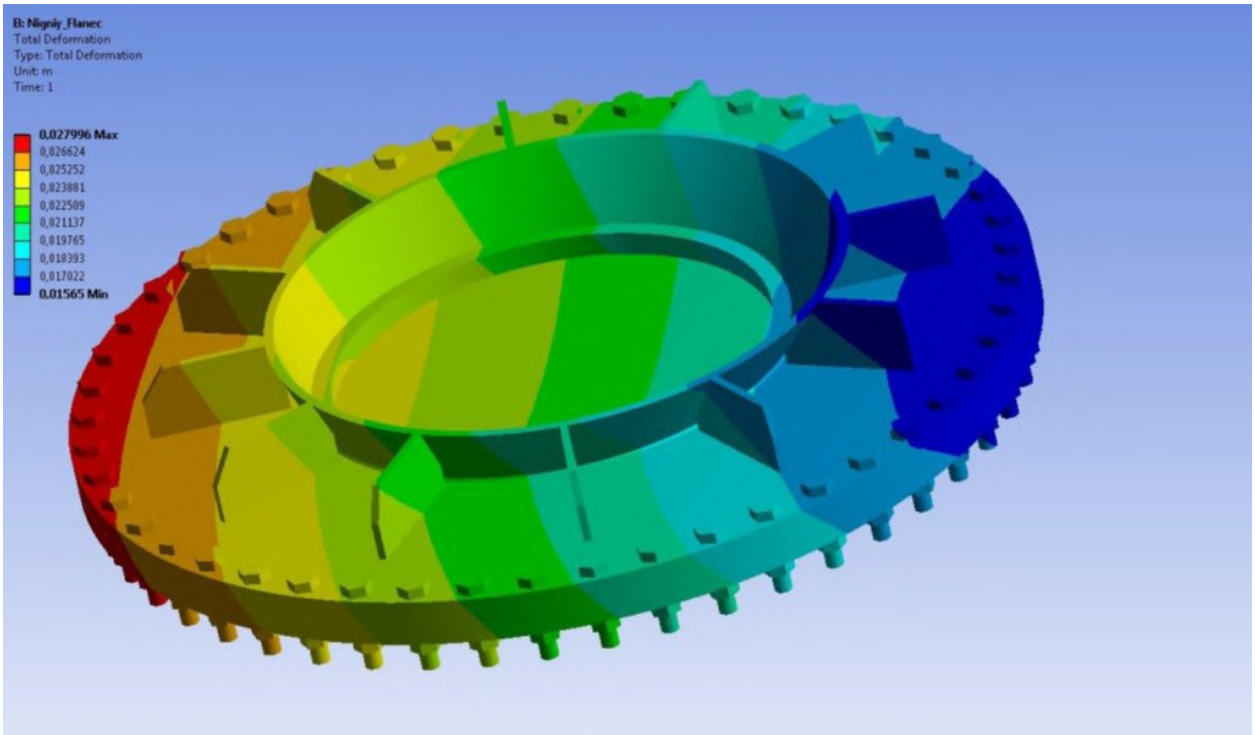

Fig. 1.75 Distribution of total strain arising in the structure

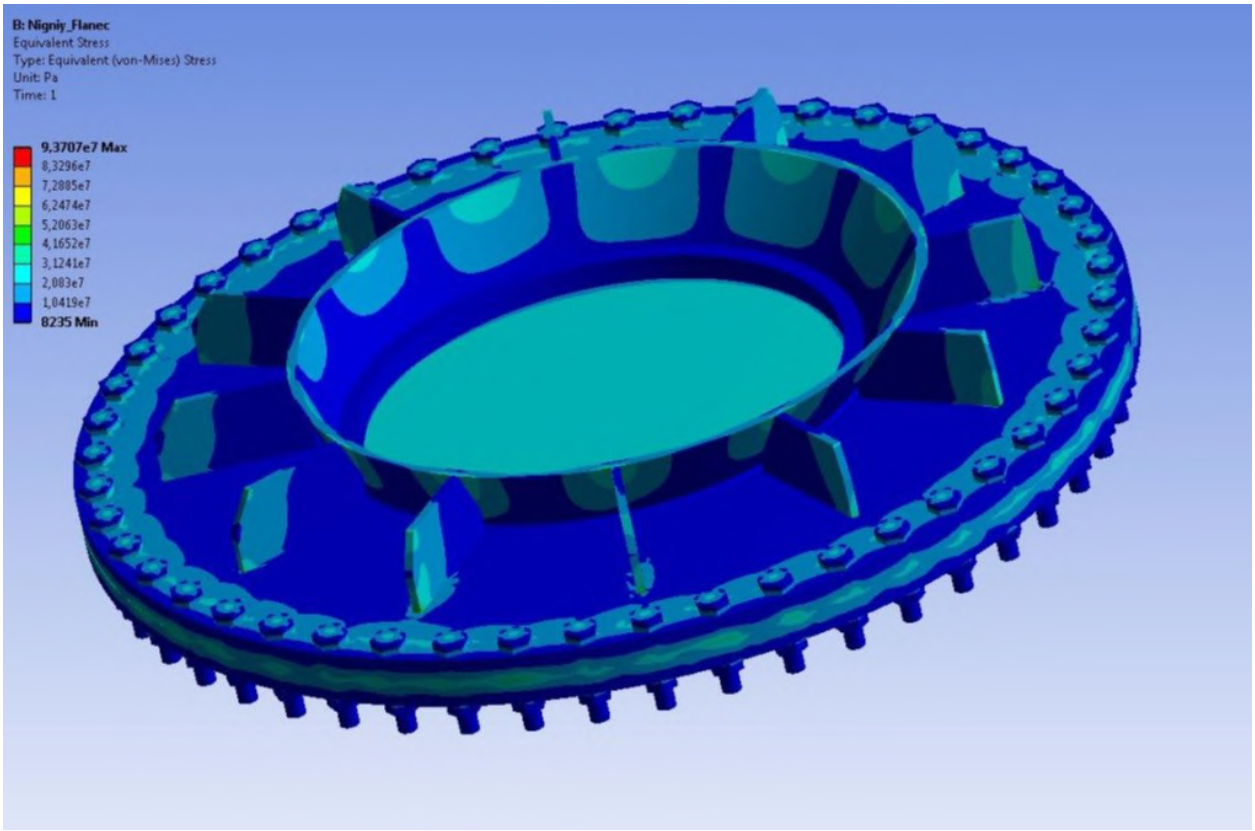

Fig. 1.76 Distribution of von Mises equivalent stresses

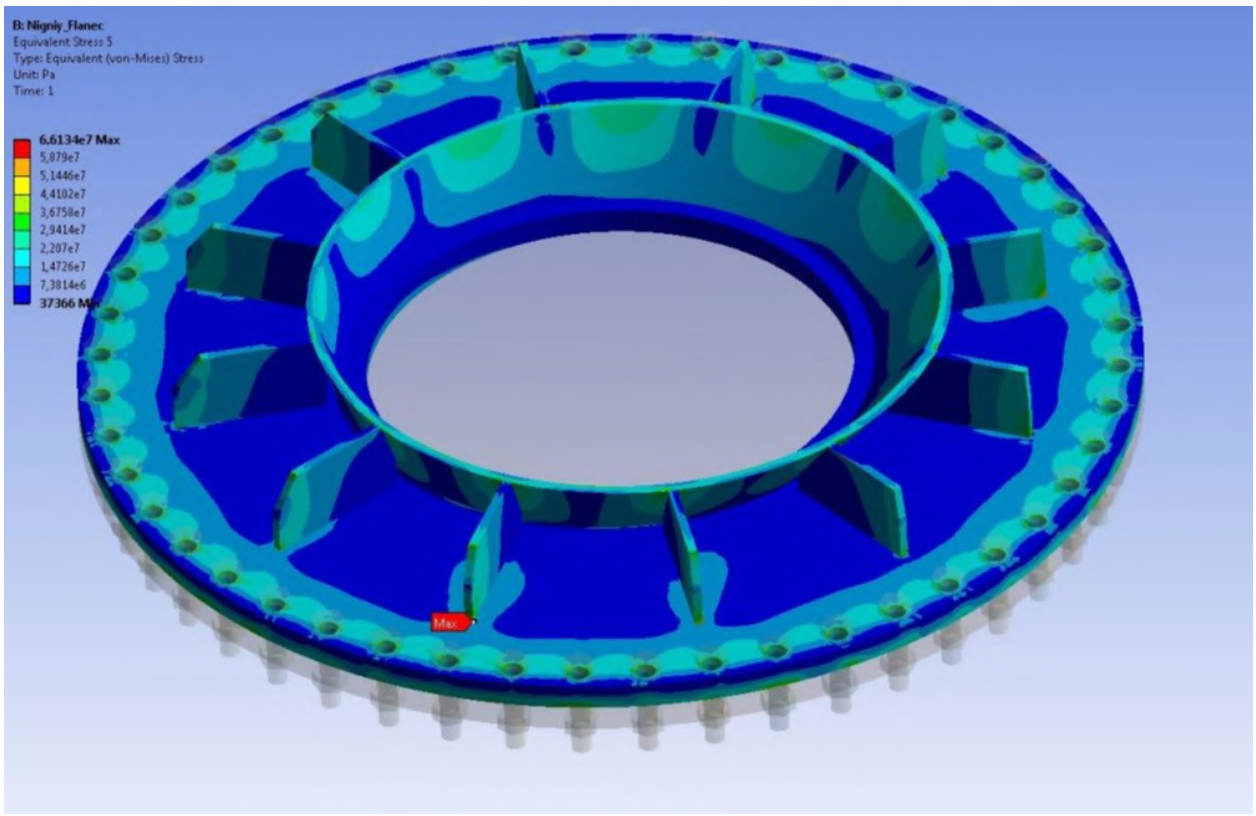

Fig. 1.77 Distribution of von Mises equivalent stresses in the flange

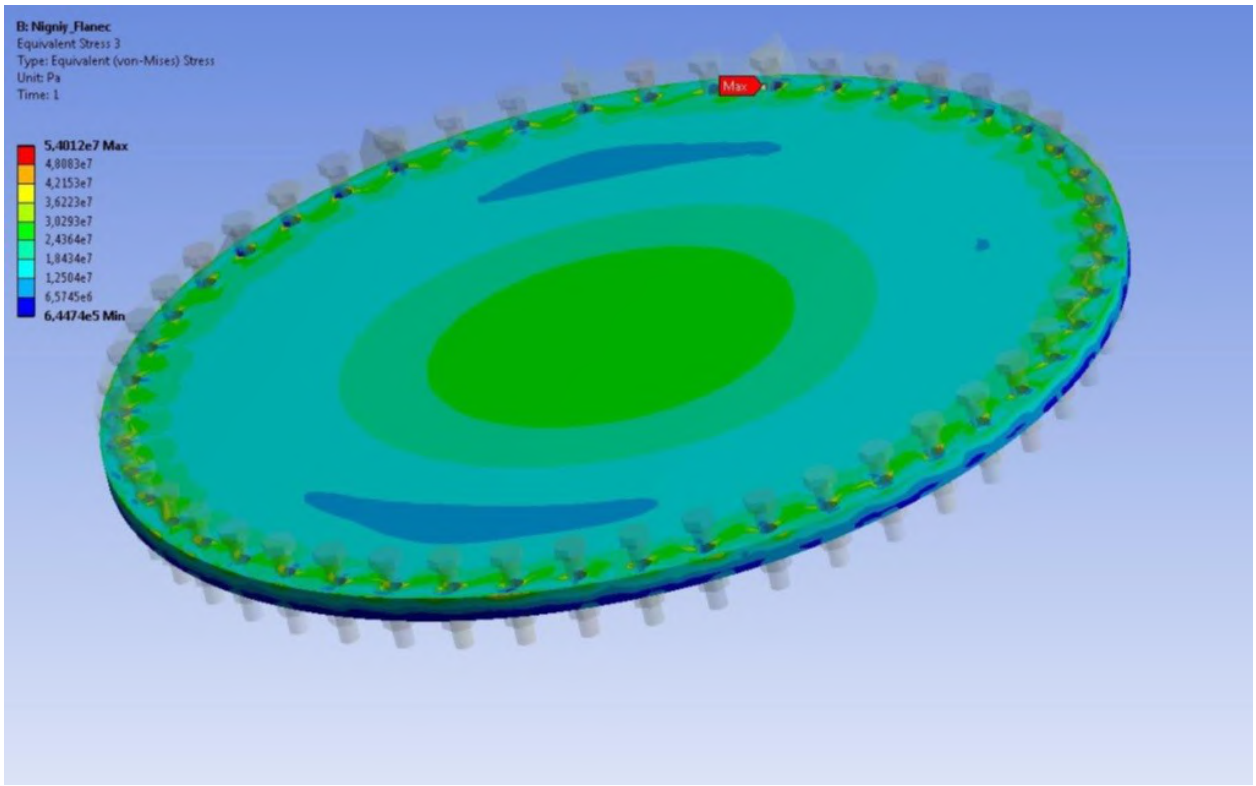

Fig. 1.78 Distribution of von Mises equivalent stresses in the lid

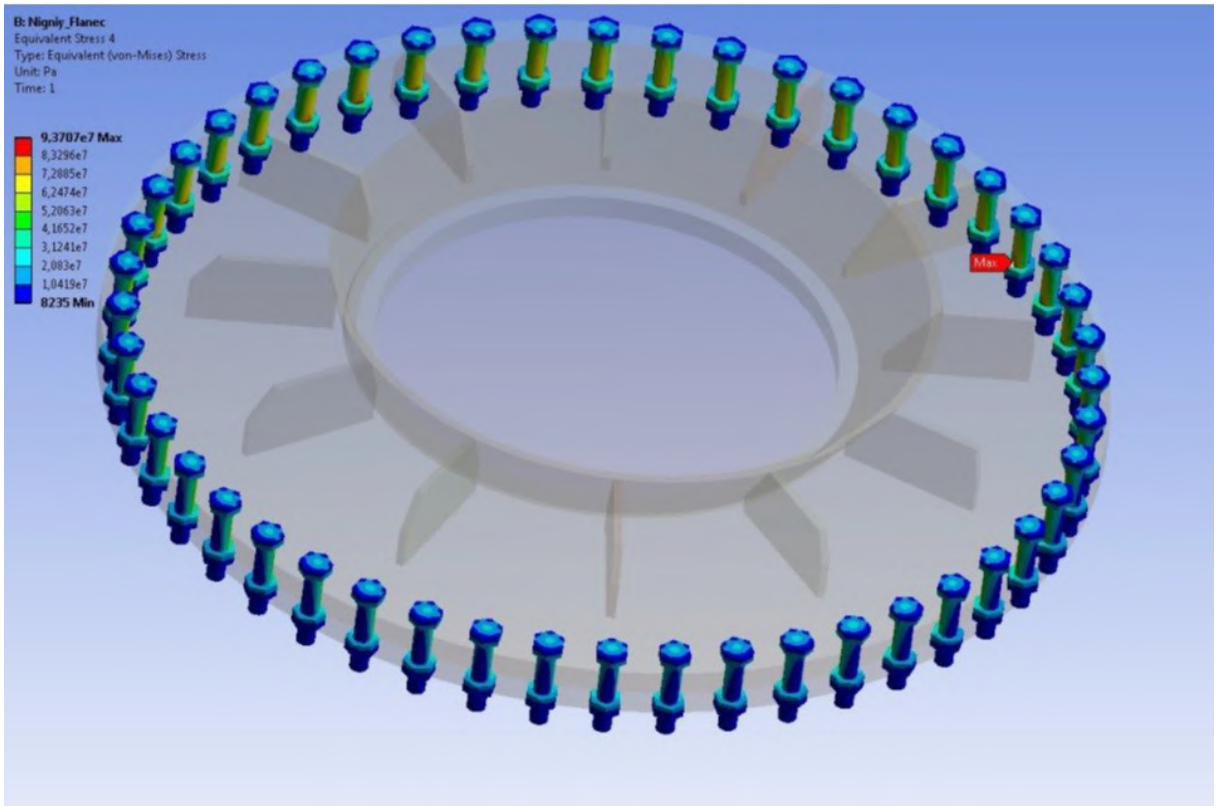

Fig. 1.79 Distribution of von Mises equivalent stresses in bolts

1.3.5.3 Designing the lateral flanged connection

The submodeling pattern and design pattern of lower flanged connection sub-model is presented in Fig.1.80.

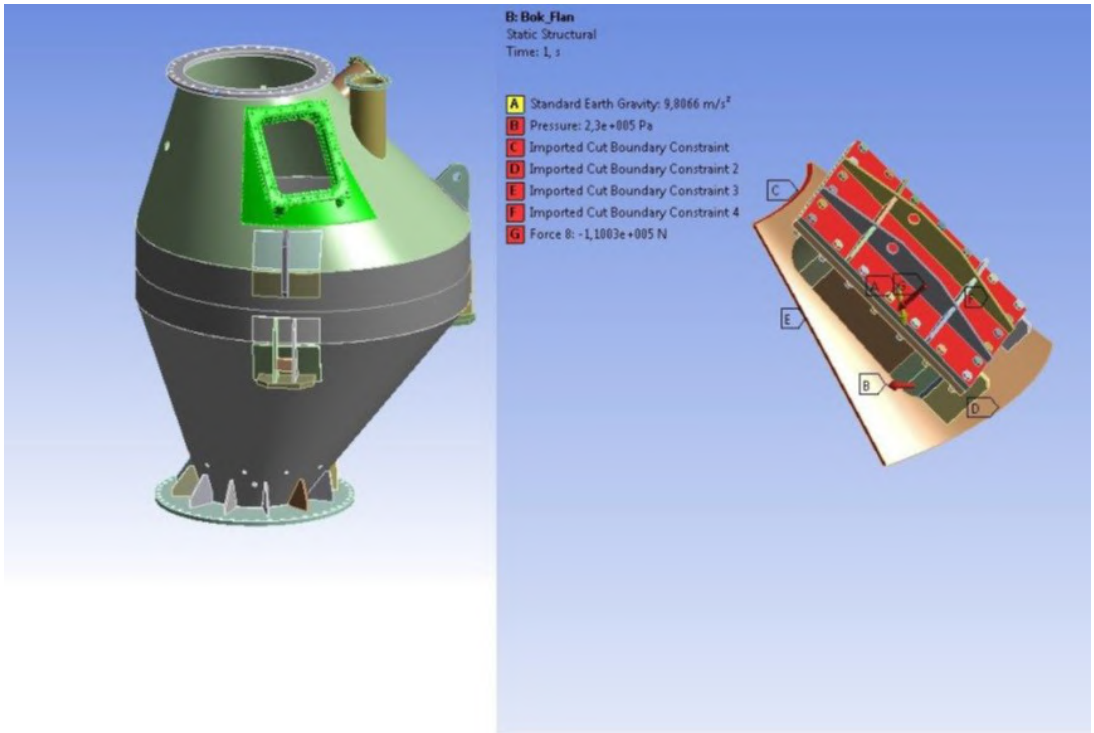

Fig. 1.80 Submodeling pattern and design pattern of lateral flange

Fig. 1.81 depicts imported strains from the general bin's model.

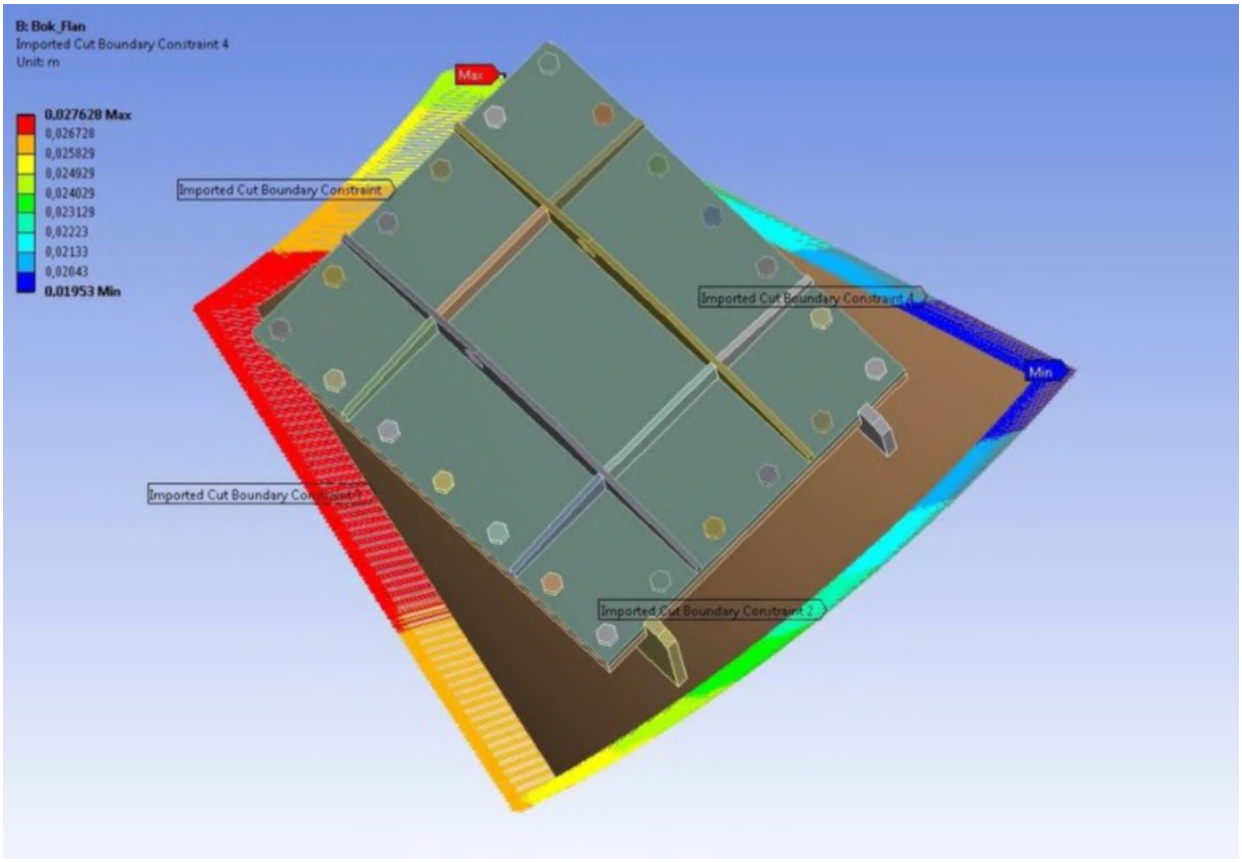

Fig. 1.81 Distribution of imported strain patterns in the lateral flanged connection

The finite-element model is presented in Fig. 1.82.

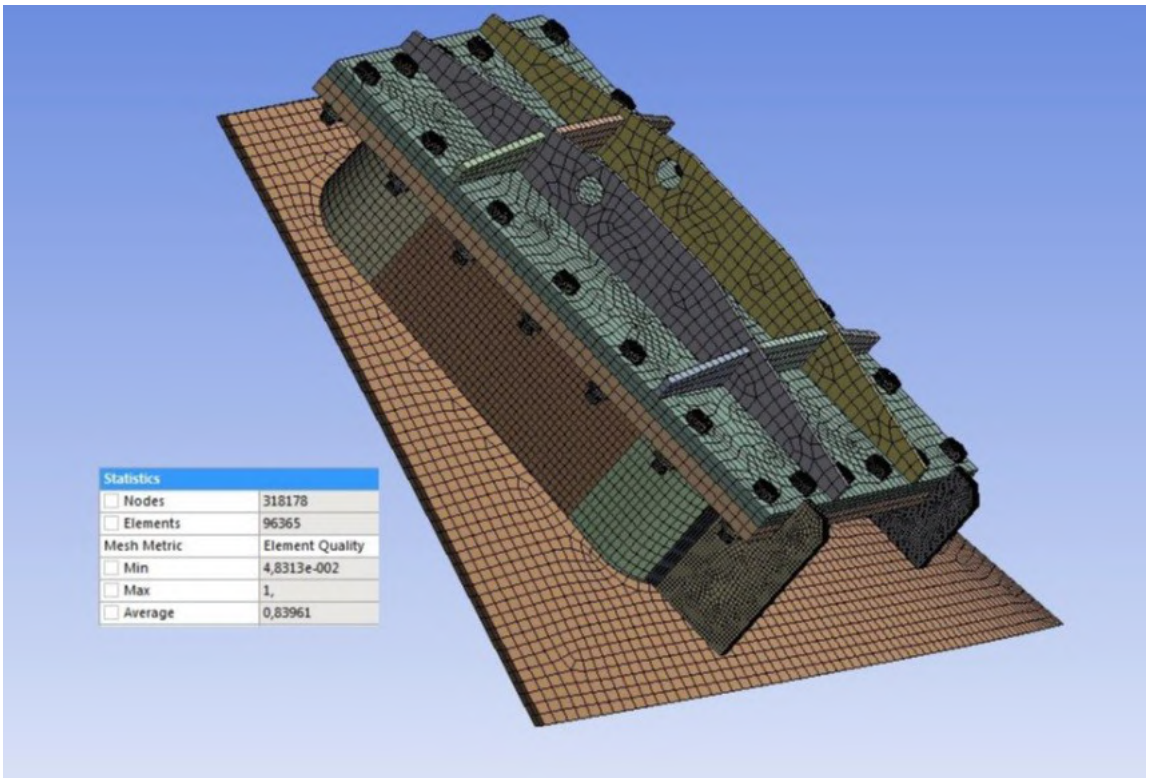

Fig. 1.82 Finite-element model of lateral flanged connection

Calculation results of stress-strain state are presented in Fig. 1.83-1.87.

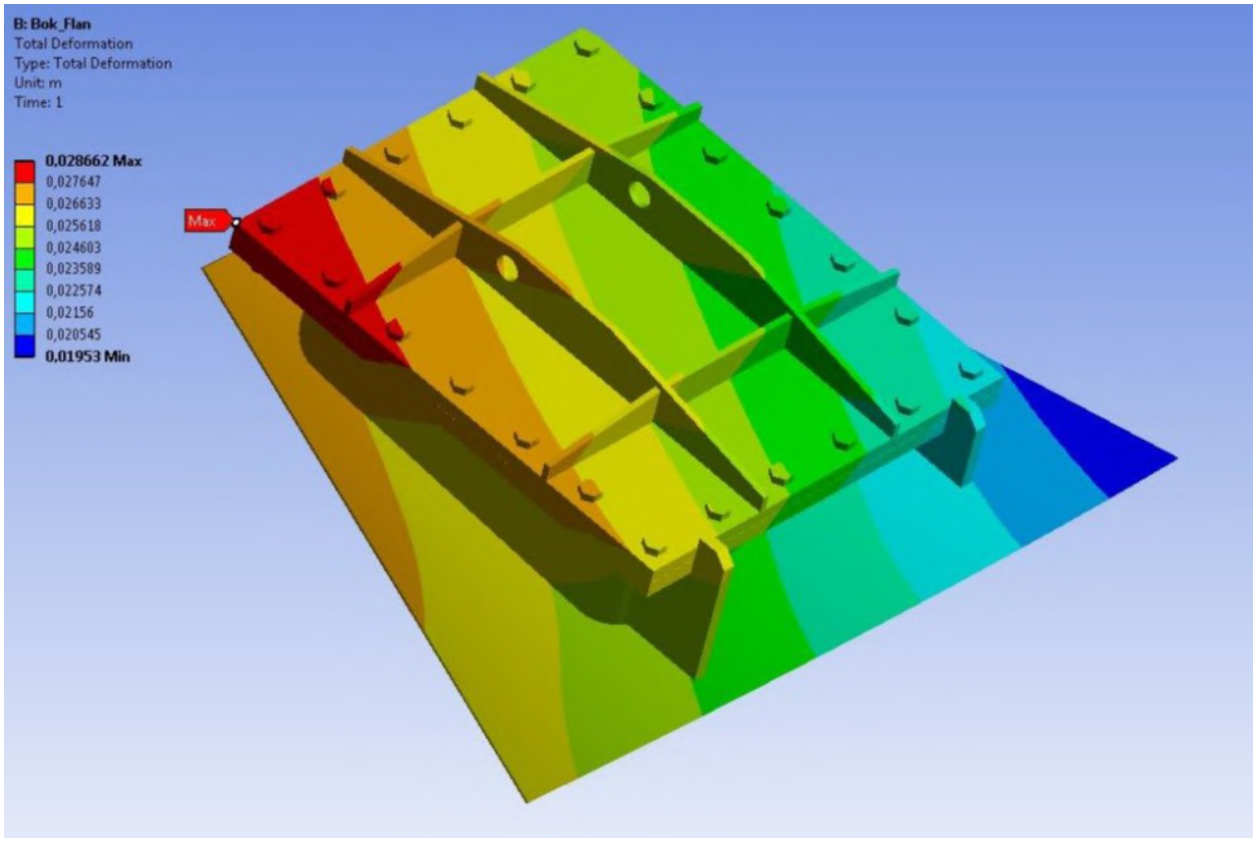

Fig. 1.83 Distribution of total strain arising in the structure

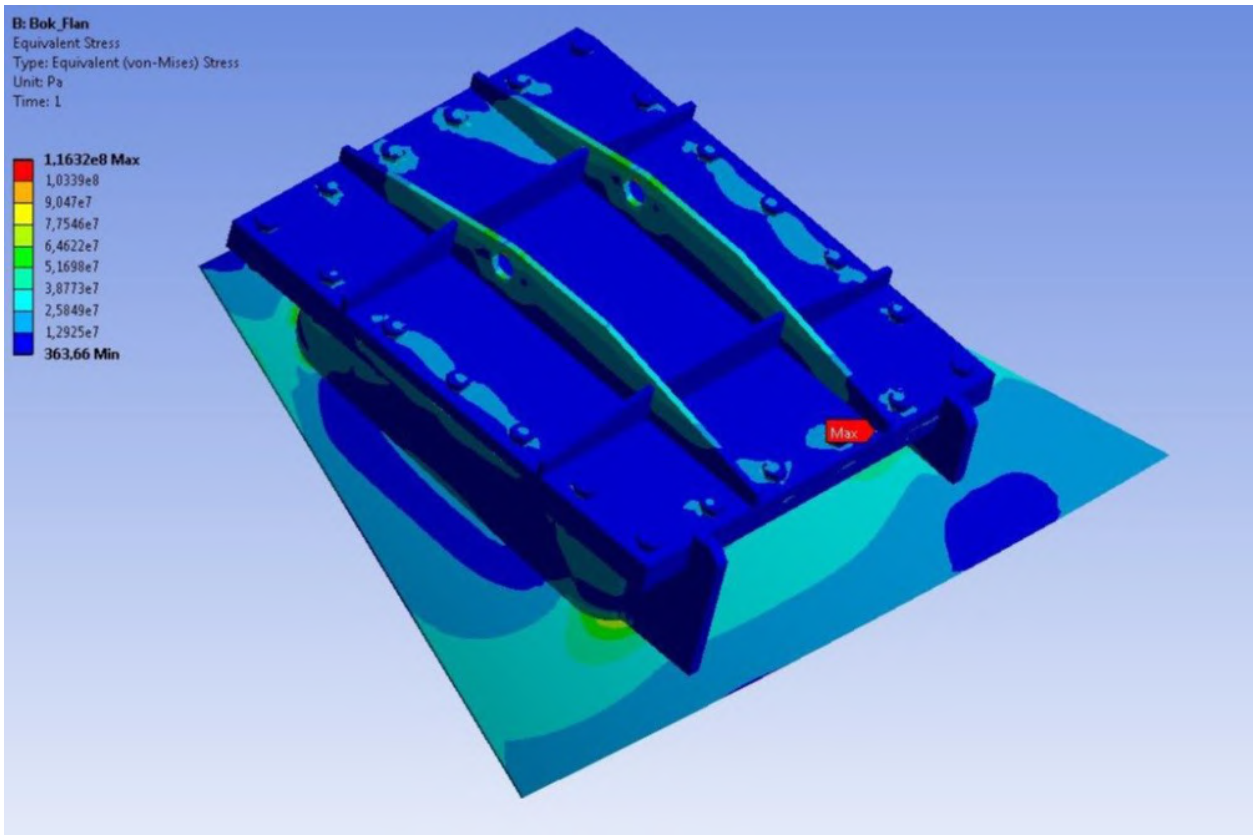

Fig. 1.84 Distribution of von Mises equivalent stresses

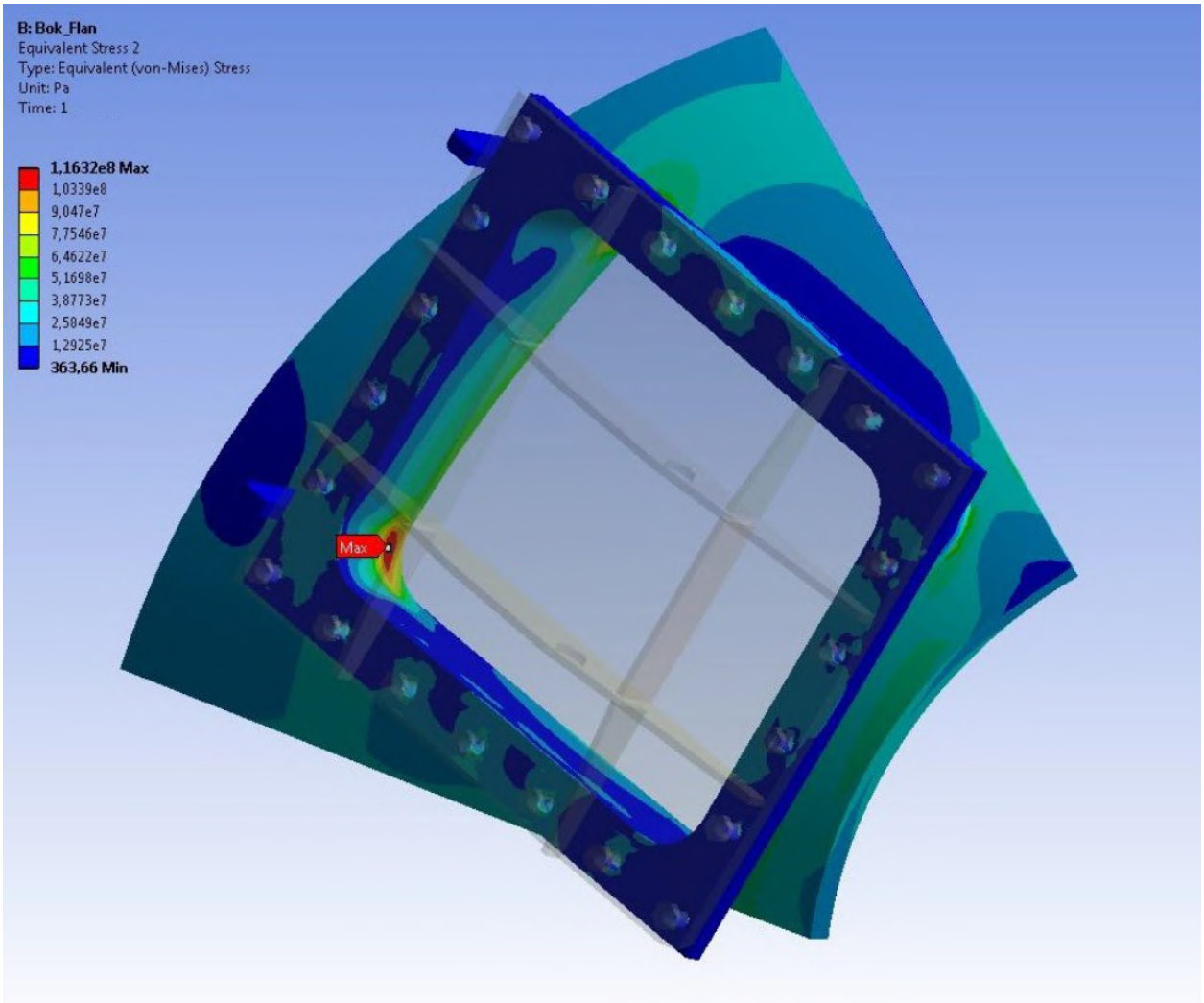

Fig. 1.85 Distribution of von Mises equivalent stresses in the flange

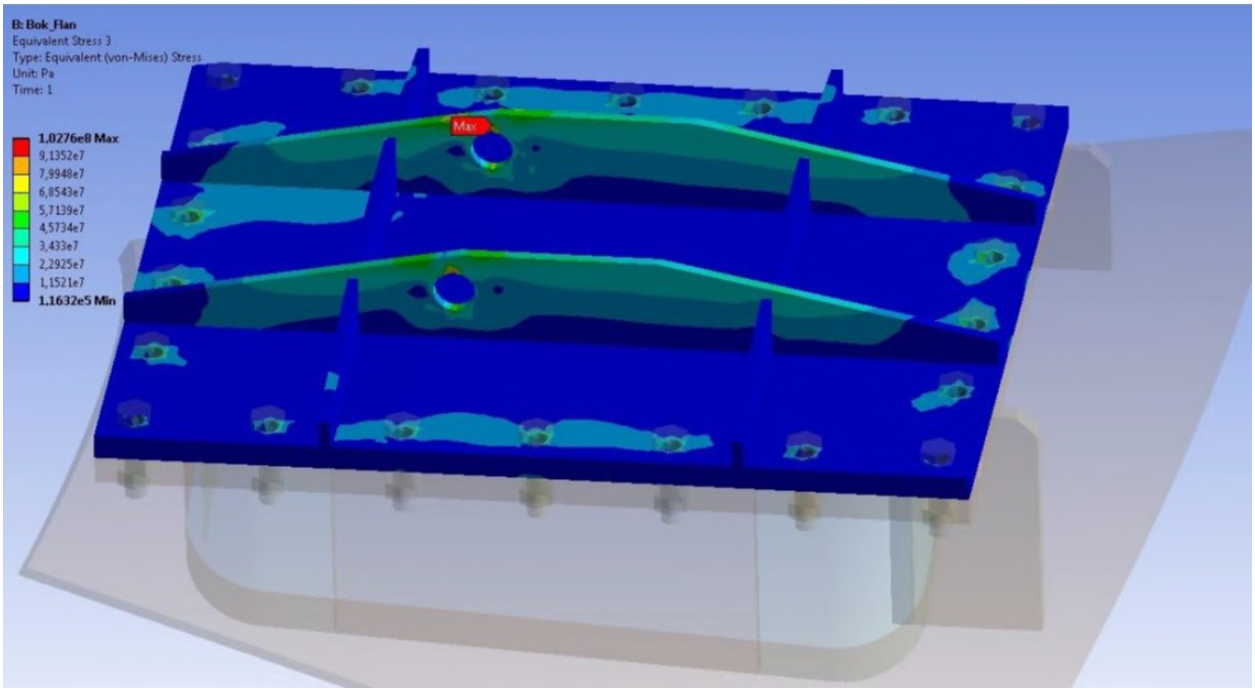

Fig. 1.86 Distribution of von Mises equivalent stresses in the lid

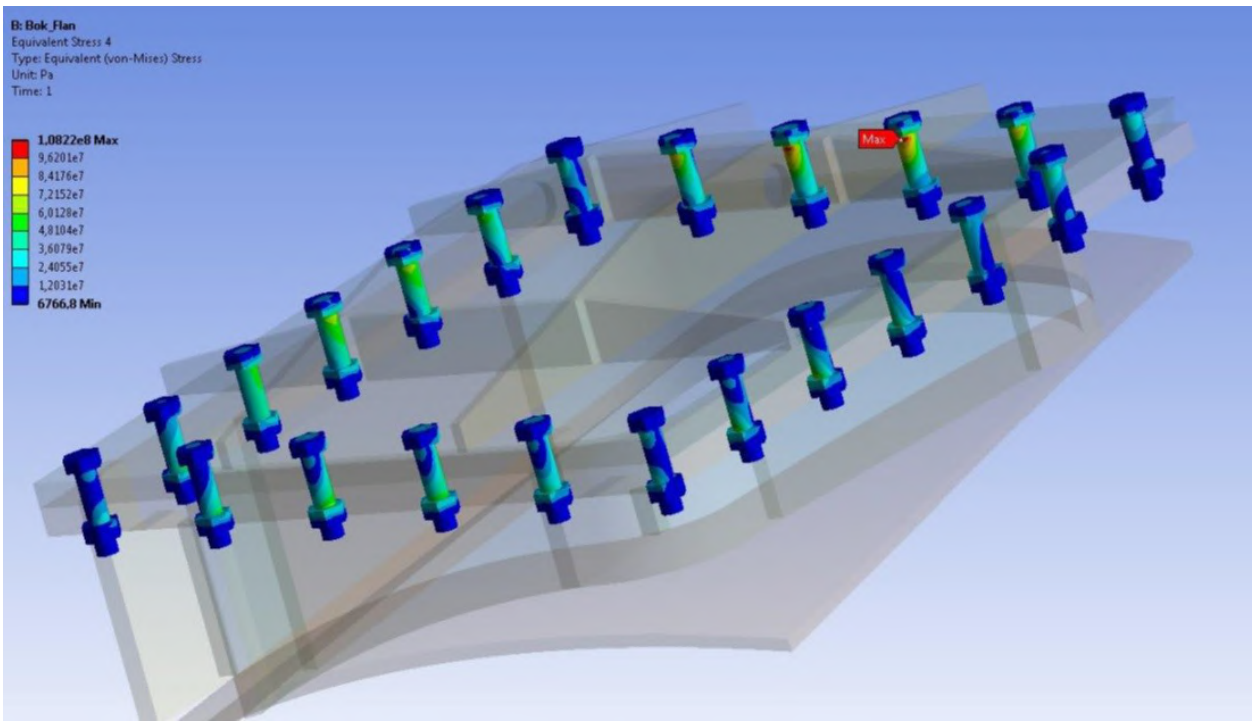

Fig. 1.87 Distribution of von Mises equivalent stresses in bolts

1.3.6 Strength calculation of bin design lugs

To assess the strength of bin's lugs two design cases have been considered, namely the case of crane lift in vertical and horizontal positions of the bin. Fig. 1.88 presented cases of bin slinging.

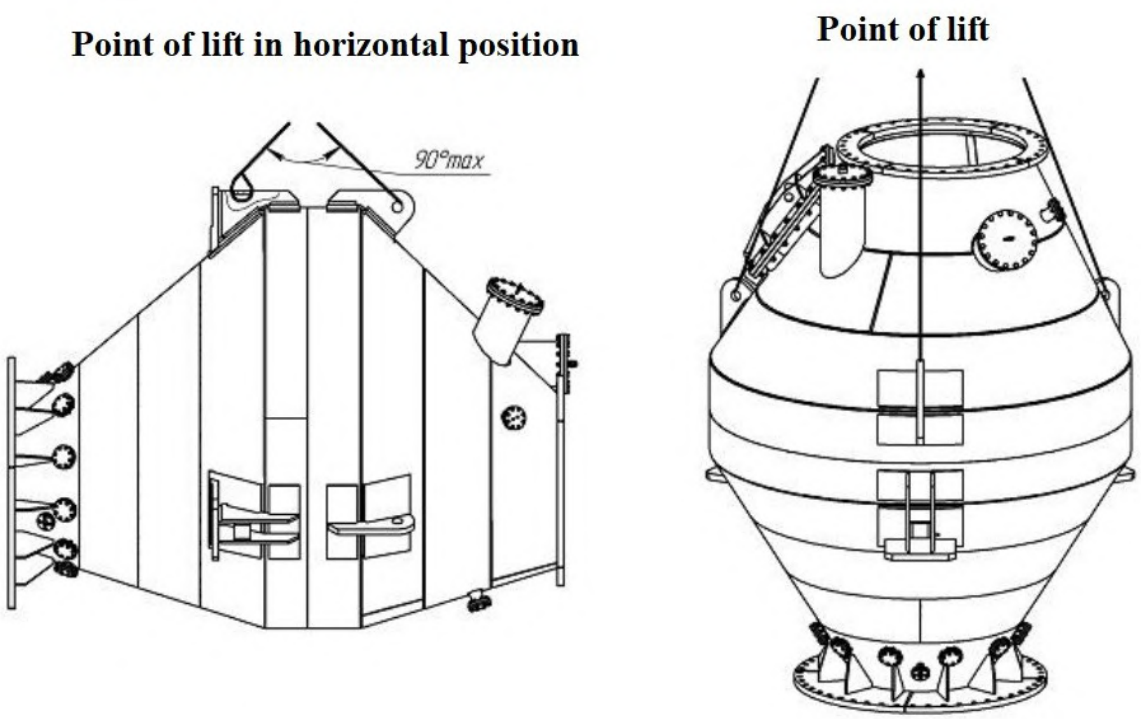

Fig. 1.88 Bin's sling arrangement

In the course of crane-lifting the bin in vertical position the bin is fastened by ear lugs. The design model sets border shift conditions in all their lugs in form of cylindrical fixation. The design load case for vertical lift of the hopper is presented in Fig. 1.89. When lifting in horizontal position the design model sets border conditions as cylindrical fixation by the ear lug and securing the transverse plate of the support. The design loading pattern for bin's horizontal lift is presented in Fig. 1.90. All design cases take into consideration the additional load equal to bin's weight.

Calculation results of stress-strain state for bin's vertical lift in horizontal position are presented in Fig. 1.91-1.95.

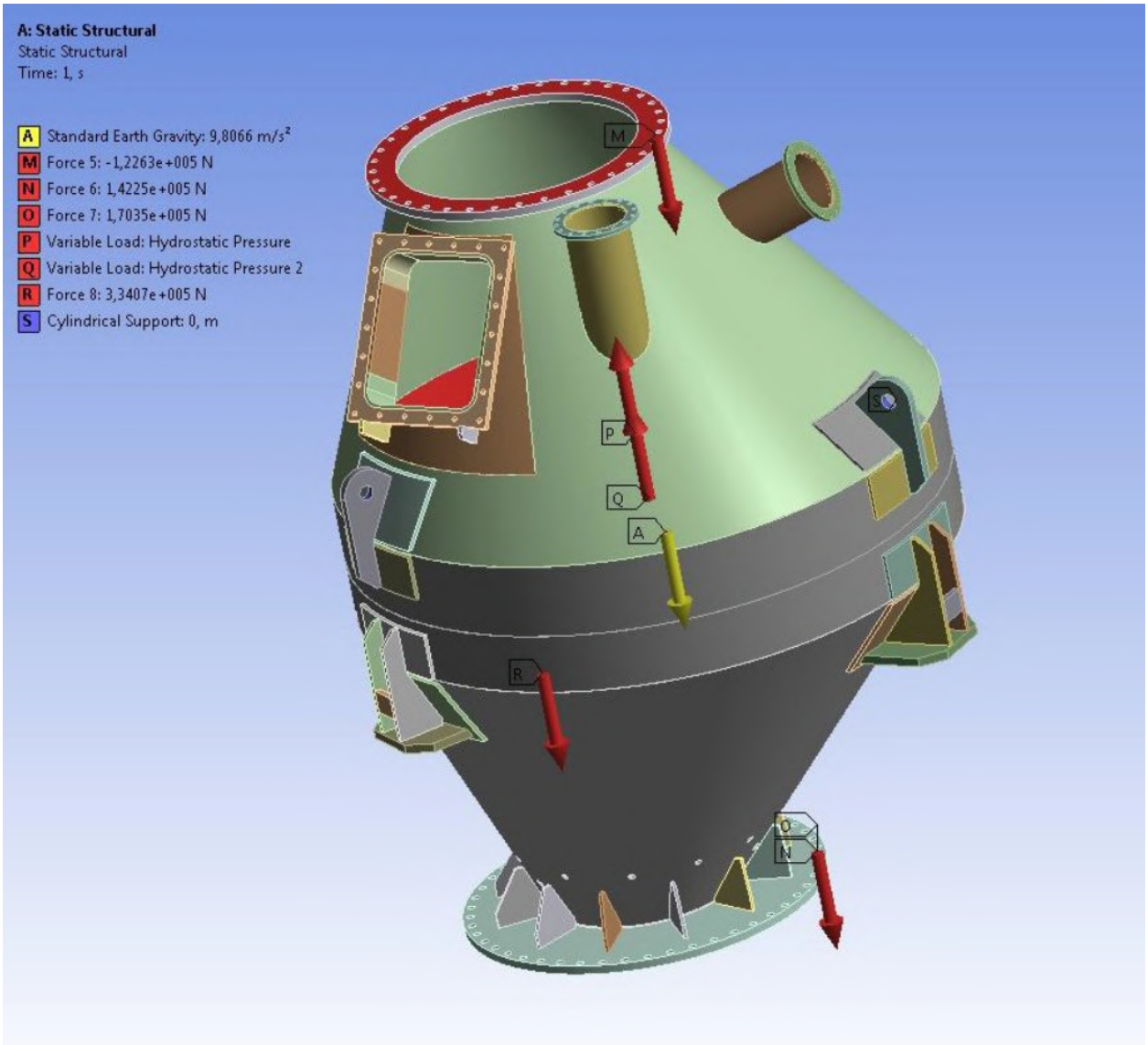

Fig. 1.89 Design case of bin's loading for calculation of lugs

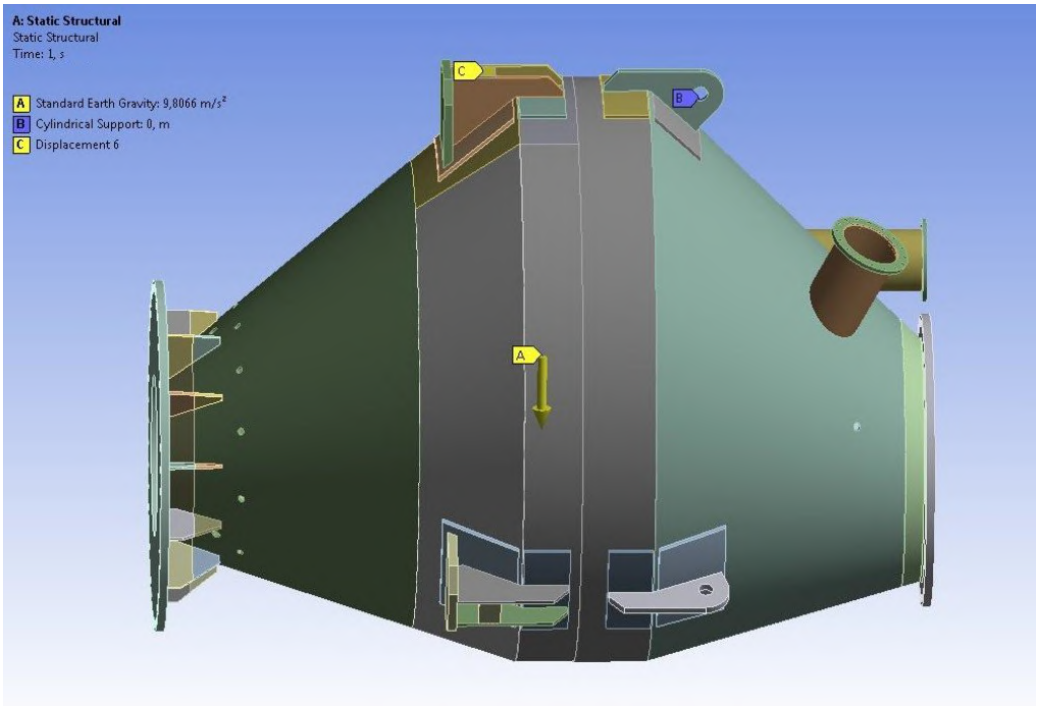

Fig. 1.90 Design case of bin's loading for calculation of lugs

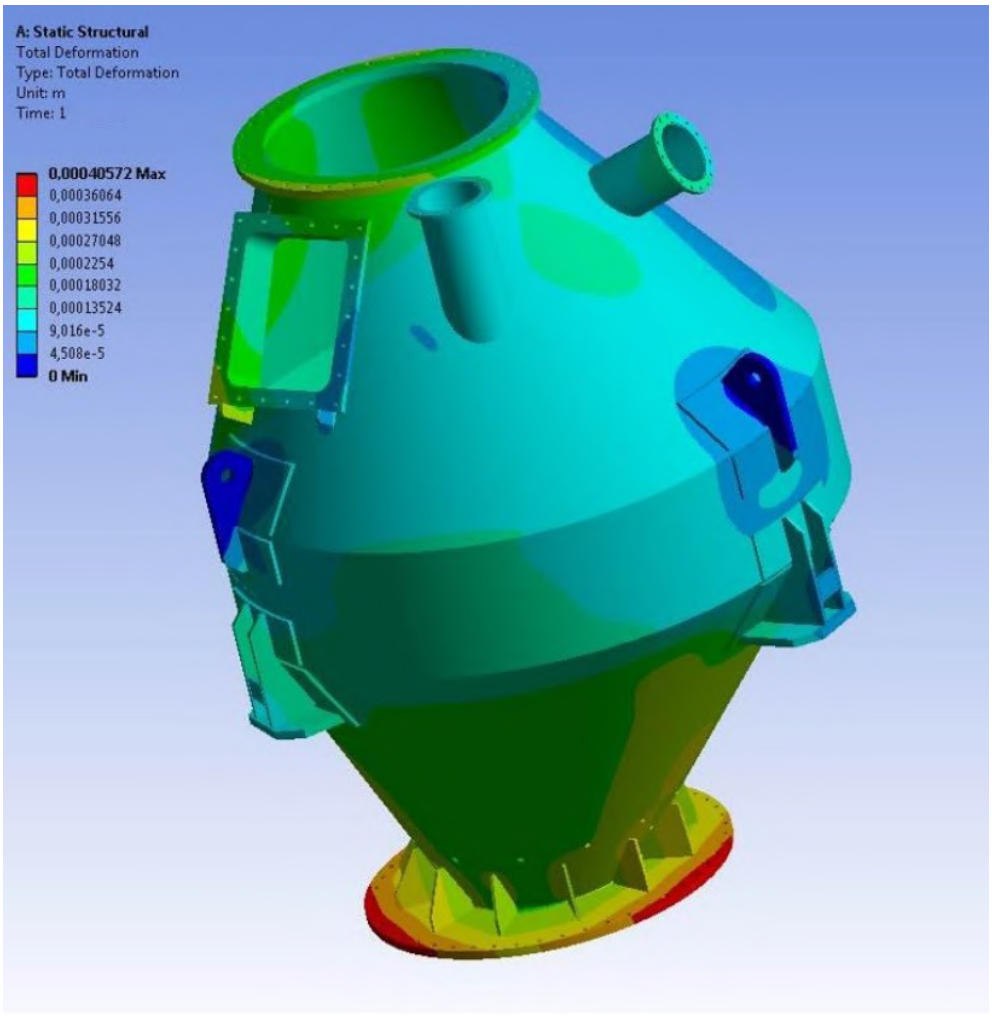

Fig. 1.91 Distribution of total strain arising in the structure when lifting in vertical position

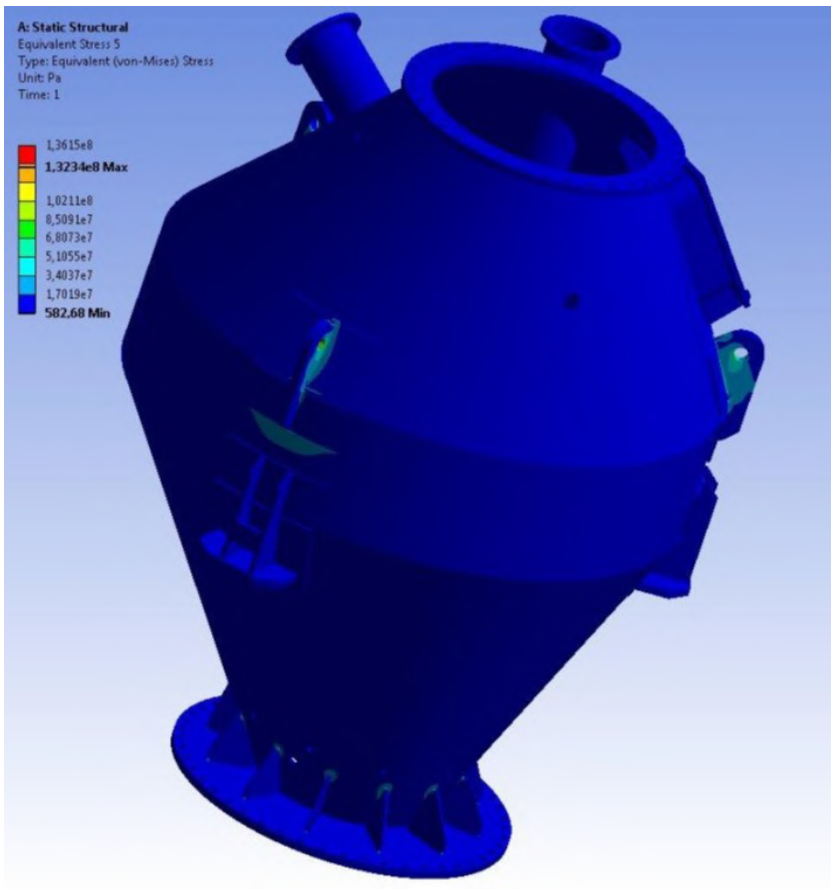

Fig. 1.92 Distribution of von Mises equivalent stresses when lifting in vertical position

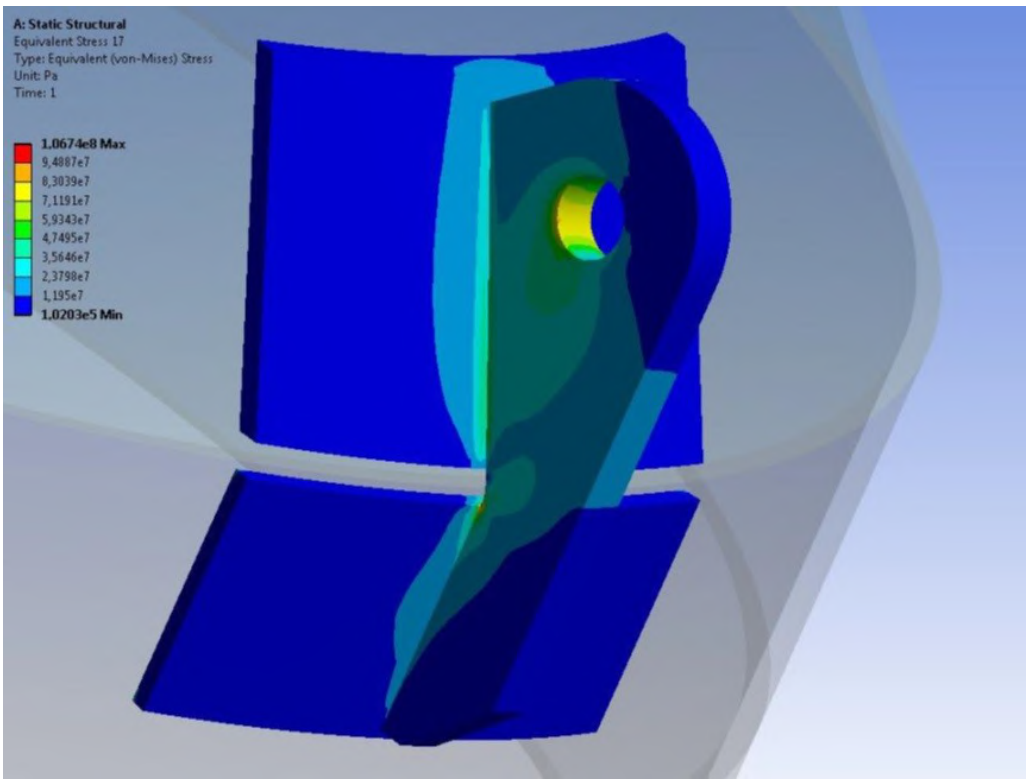

Fig. 1.93 Distribution of von Mises equivalent stresses in the lug under lateral hatch when lifting in vertical position

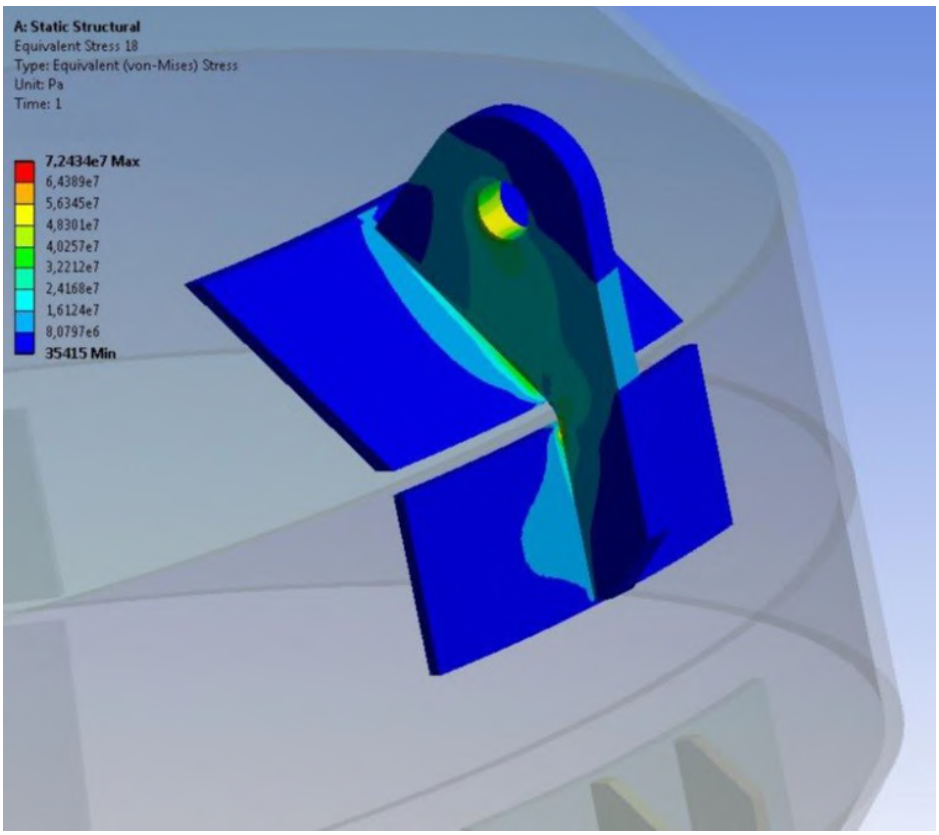

Fig. 1.94 Distribution of von Mises equivalent stresses in the lug, the most distant one from symmetry axis when lifting in vertical position

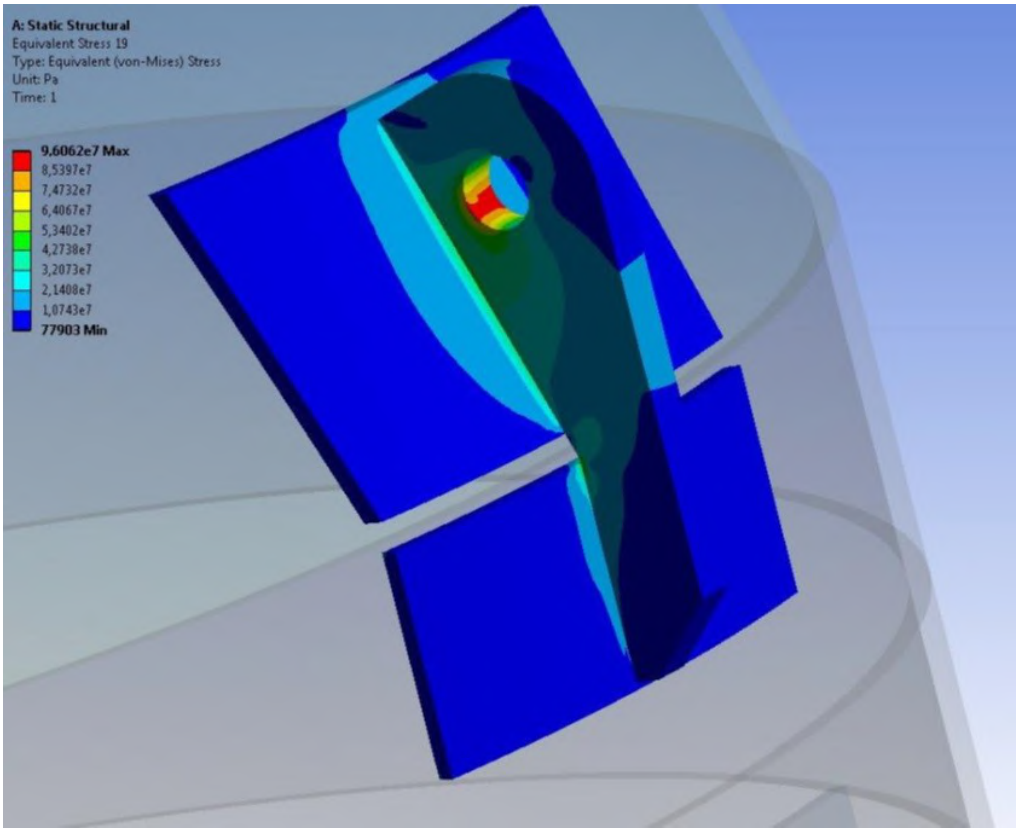

Fig. 1.95 Distribution of von Mises equivalent stresses in the third lug when lifting in vertical position

Calculation results of stress-strain state for bin's vertical lift in horizontal position are presented in Fig. 1.96-1.97.

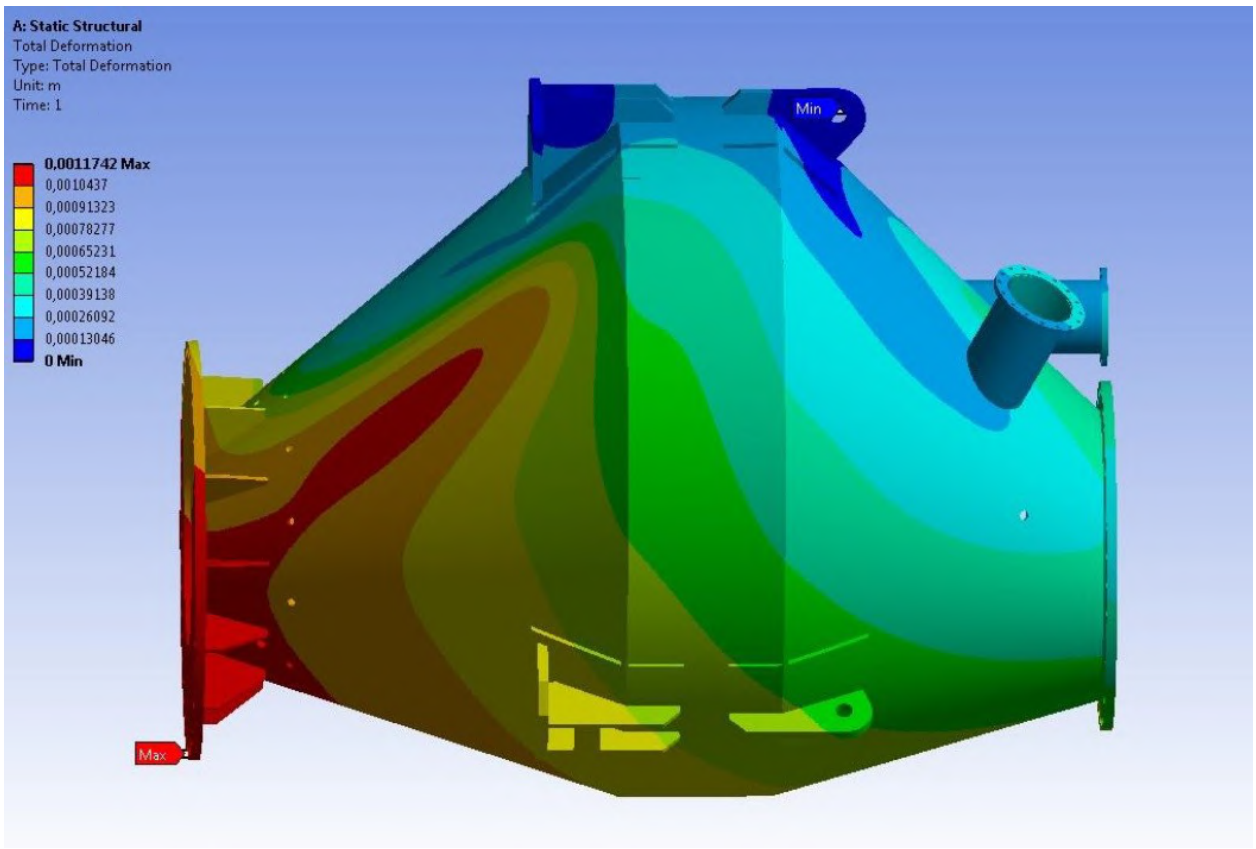

Fig. 1.96 Distribution of total strains arising in the structure

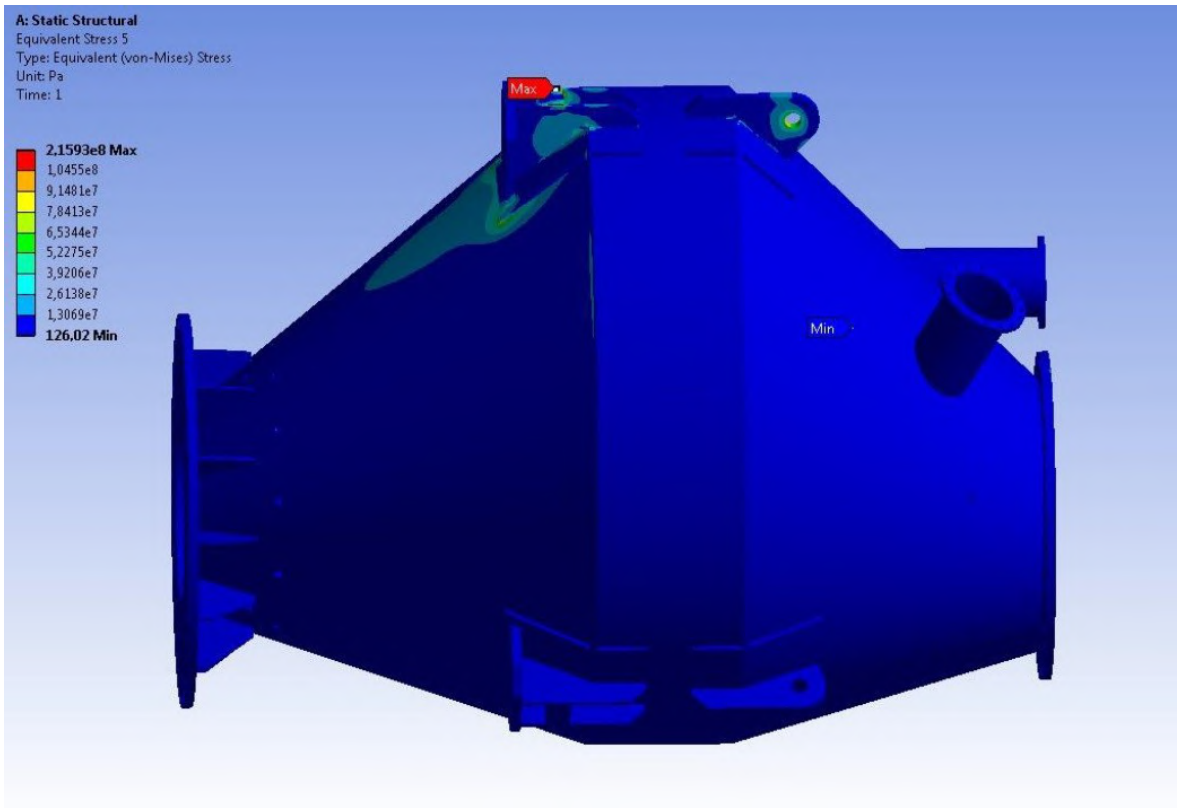

Fig. 1.97 Distribution of von Mises equivalent stresses

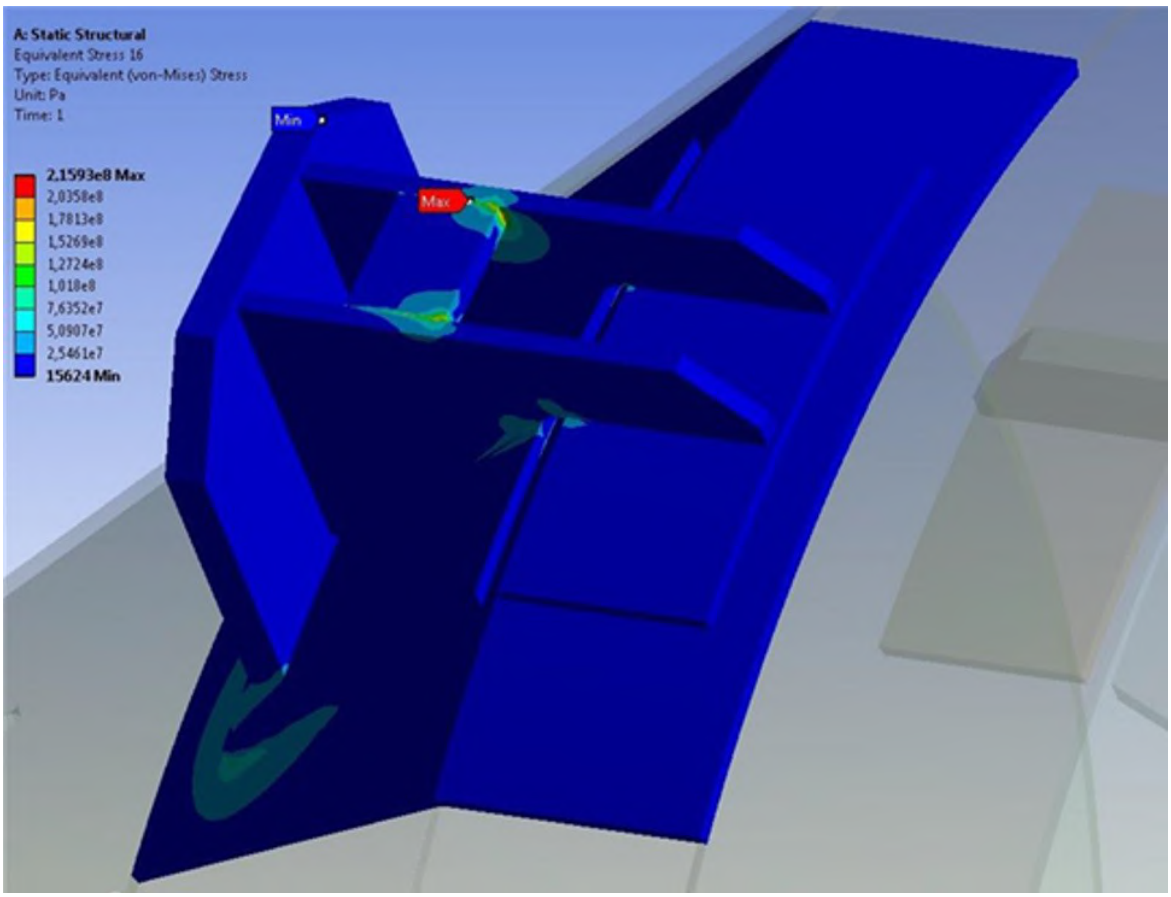

Fig. 1.98 Distribution of von Mises equivalent stresses in the support

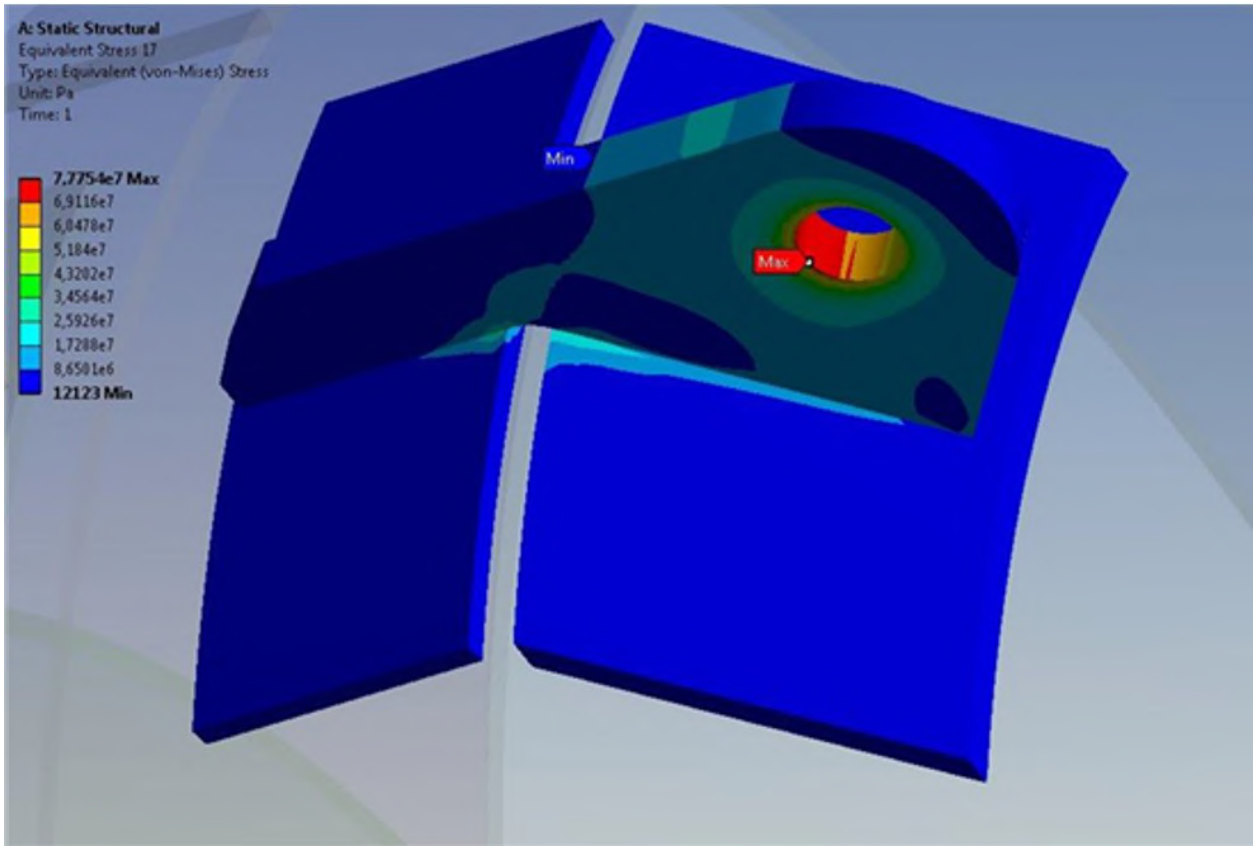

Fig. 1.99 Distribution of von Mises equivalent stresses in the lug

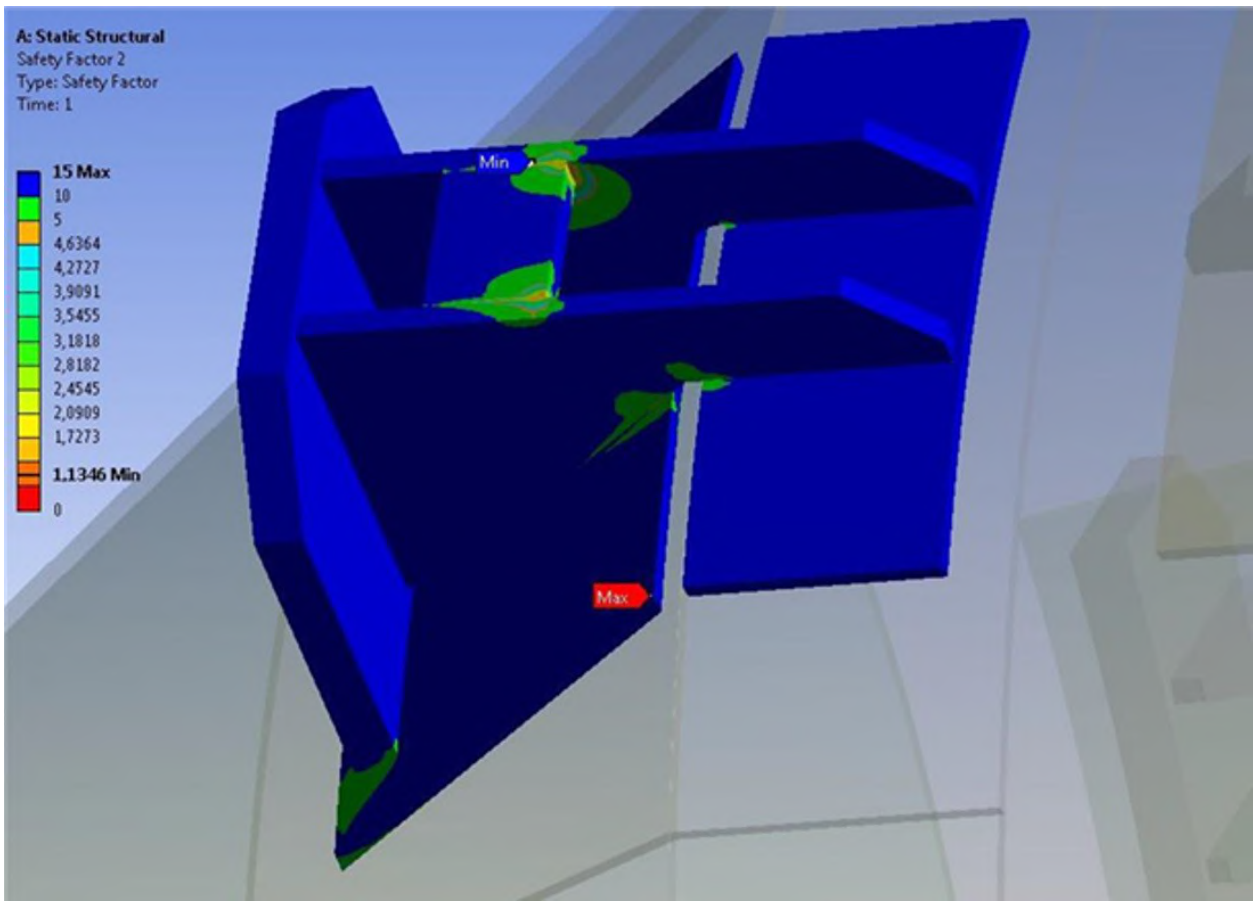

Fig. 1.100 Distribution of safety factor through the support

Bin's design meets strength and stiffness requirements when performing erection and transportation operations.

1.3.7 Design collective results

Calculation results obtained are presented as the summary Table 1.8. The table uses the following designations:

σ_{max} , the maximal stresses arising in structural member of material bin;

[σ], permissible stresses in structural member of the bin;

n, safety factor of a structural member of material bin;

N, operational lifespan or number of cycles before appearance of fatigue cracks in bin's structure members. Time-related operational lifespan is calculated on the condition of making 57000 load cycles annually.

Table 1.8

Structural members of material bin	***σmax (MPa)***	***[σ] (MPa)***	***n***	***N***
Cylindrical wall	**106.6**	**197.7**	**1.85**	**1×10^7**
Conical wall	**106.6**	**194.4**	**1.82**	**1×10^7**
Top flange	**60.7**	**159.5**	**2.62**	**1×10^7**
Bottom flange	**68.1**	**159.5**	**2.34**	**1×10^7**
Branch/flange	**83.9/28.7**	**142.2/178.0**	**1.69/6.2**	**1×10^7**
Hatch/flange	**124.7/39.2**	**131.7/134.9**	**1.06/3.4**	**2.714×10^6**
Support's lug	**158.9**	**180.8**	**1.13**	**1.156×10^6. 20.3 years**
Bottom flange bolts	**93.7**	**166.7**	**1.77**	**1×10^7**
Top flange bolts	**127.5**	**166.7**	**1.3**	**2.516×10^6**
Hatch bolts	**108.2**	**166.7**	**1.54**	**1×10^7**

The presented results of designing show that charging bin's structure meets strength and stiffness requirements for all design loading cases. Structure's operation-al lifespan meets requirements of structure's period of operation. Since the charging bin operates under conditions of alternating load with symmetry factor equal to zero the structure's lifespan assessment has been carried out. Initiation of fatigue cracking is designed using SN-approach to description of Wehler curve. It should be noted that the biggest stresses in the structure arise in bin's support lug parts under conditions of joint loading due to maximal design earthquake of 6 points and normal service conditions. Operational lifespan of this part is lower as compared to operational lifespan of hopper body's load-bearing coverб but meets the requirements of service lifespan. Verification of selected Wehler SN curve is made on correspondence of the type of experimental dependence employed for lifespan assessment, and the type of stress state arising in the structure under study. These dependencies are presented for each design case in figures 19-20, 33-34 and 56-57. Data presented in these figures show that for entire structure practically, and danger zones in particular, stress state corresponds to tension state. This result means that employment of selected fatigue curve data obtained for the case of cyclic bending was correct. Besides of that, the structure operates under conditions of tension for all design cases, thus allowing not to perform structure buckling analysis.

The definitive design load case of the structure is limit wind effect loading under normal service conditions, wherein the maximal stresses arise in the load-bearing bin's cover.

1.4 CHAPTER CONCLUSIONS

Results of numerical calculation of the material bin are as follows:

– the structure of the bin meets requirements to strength and stiffness;

– the most undesired design case of structure service is wind effect loading under normal service conditions;

–the biggest stresses in bin's load-bearing cover arise at the joining of cylindrical and vertical conical part of the bin in the area of DN400 cylindrical offset;

– the minimal value of structure's service lifespan till initiation of first fatigue cracking is 20.3 years (in support lugs), thus meeting the service lifespan requirement.

CHAPTER II

2.1 ASSESSMENT OF THE STRENGTH OF THE CENTERING TOP-CHARGING UNIT OF THE BLAST FURNACE

2.1.1 Design features.

The purpose of this work is to calculate the strength of pressurized centering unit of top-charging unit designed were carried out based on the original prototype drawing. This bin is an integral part of the blast furnace charging system. The reference of the centering unit to other parts of the entire charging unit is presented on customer figure 0.3. The design features of the centering unit, and operational service thereof, are determined by the following factors:

–overall weight of the entire structure equals to 27000 kg;

–bottom elevation of the structure is at the level of 42188 mm, and the top elevation is at the level of 45168 mm. The top elevation for each flange of the centering unit is the place for the upper sealing valve weighing 12500kg.The entire structure is fitted with 4 supports holding, both the centering units itself and the upper sealing valves;

– the centering units operates under conditions of steady-state thermal loading at the temperature of 450°C;

– the structure operates under conditions of alternate loading with asymmetry factor equal to 0;

– the design pressure in the bin equals to 2.3Bar (0.23 MPa), and annual oscillation quantity thereof equals to 57000;

– the functional purpose of the centering unit is batch mixture supply to the blast furnace. The calculations use the batch mixture (pellets) with maximum density of 2100 kg/m^3 as an example of a material to be charged;

– operational lifetime is 20 years;

– the blast furnace top-charging unit is located in Zaporozhye, Ukraine. The altitude of the land is 140 m, seismic zone corresponds to MSK-64.

2.2 INITIAL DATA, DEISGN CASES AND DESIGN ARRANGEMENT OF THE BIN

2.2.1 Characteristics of bin design

The geometrical dimensions of the bin's structure are specified according to the prototype drawing, presented in Fig. 2.1;

The material of walls, bearing flanges, supporting brackets, upper weld-on linings and transportation lugs: plate steel 09G2S as per GOST19281-89;

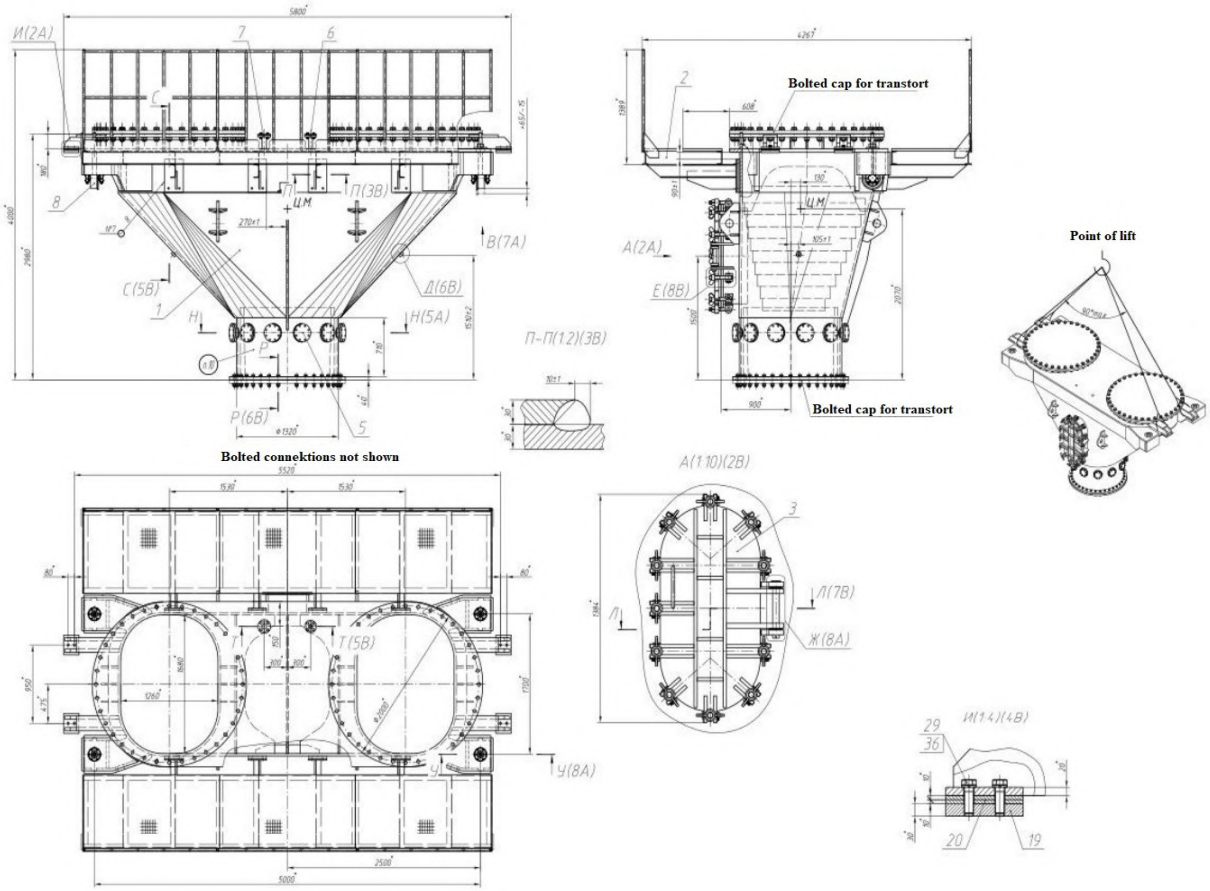

Fig. 2.1 Drawing of the prototype of bin structure

2.2.2 The material properties and loading cases of the centering top-charging unit

The operating conditions of the structure considered are determined by thermal steady-state field at the temperature of 450°C. The mechanical features of steel 09G2S based on GOST 1050-88 at 450°C are outlined in paragraph 1.2.2 of this work.

The normative documents mentioned in paragraph 1.2.3 of this work are used to determine loads, recommended design cases for centering top-charging unit and strength standards.

Beside thermal effect, the structure is further affected by the following loadings:

– internal design pressure;

– weight of metal structure $G_к$***=15767 kg*** and batch mixture. Total weight of the entire structure with batch mixture shall not exceed ***27000 kg;***

– loose material loads acting on centering unit's walls;

– wind effect;

– seismic impact.

2.2.2.1 Loose material loads on the centering top-charging unit walls

The calculation of loose material loads acting on centering unit's walls is performed as per SNiP 2.09.03-85. Load safety factors g_f for structure' dead weight, service loads on flooring; snow load and wind effects are taken as per SNiP 2.01.07-85 and are equal to:

– for horizontal and vertical pressures of loose materials g_f ***= 1.3;***

– for specified angle of loose material internal friction g_f ***= 1.1.***

The loose design material vertical pressure onto horizontal plane shall be deter-mined by the equation $p = 1.3 \times \gamma h$, where γ is material specific weight, h is material layer elevation above the given point.

The loose material pressure onto vertical wall in cylindrical part of the centering unit is specified with the equation $p_h = n \times \lambda \times \gamma \times h$, where λ is the lateral pressure factor that is taken as equal to the ratio of horizontal pressure to vertical one, i.e. $\lambda = p_h / p_\alpha = tg^2(45° - \phi/(2\, g_f))$. Also, ϕ is material internal friction. For the types of loose materials used the rated value of ϕ angle equals to $35°$. The design value of the rated internal pressure angle is determined as the rated internal friction angle deleted by the load safety factor $g_f = 1.1$. The value is $\lambda = 0.309564$, and n is the dynamic response factor (Table 1, Guidelines on calculation and designing of

reinforced concrete, steel and combined bunkers, Moscow, Stroyizdat, 1983, 200 ps.) ***n=1.2***, skip capsule volume is ***9 m^3;***

The calculations use the material with maximum specific weight of ***2100 kG/m^3*** as the batch mixture (pellets).

The rated normal pressure onto bin's sloping wall and bin hopper is determined as follows $p_\alpha = n \times m_o \times \gamma \times h$, где $m_o = \cos^2\alpha + \lambda \sin^2\alpha$; α is the angle of plane inclination to horizon. For the centering unit designed the curved surface is split to segments with constant angle of inclination. For each surface of a segment the design normal pressure is specified as follows:

Surface 1**:** $\alpha = 60°; \lambda = 0.309564, m_o = 0.482173, p_h = 1215.1 \times z;$

Surface 2**:** $\alpha = 67.5°; \lambda = 0.309564, m_o = 0.410676, p_h = 1034{,}91 \times z;$

Surface 3**:** $\alpha = 75°; \lambda = 0.309564, m_o = 0.355814, p_h = 896.65 \times z;$

Surface 4**:** $\alpha = 90°; \lambda = 0.309564, m_o = 0.309564, p_h = 780.1 \times z;$

Surface 5**:** $\alpha = 45°; \lambda = 0.309564, m_o = 0.654782; p_h = 1650.1 \times z;$

z is measured off from the top level of centering unit's cylindrical surface.

According to initial data, the centering unit's walls are under effect of the following loose material loads, namely:

– in cylindrical part of the centering unit the pressure onto vertical wall is as follows $p_h = 780.1 \times z\ N/m^2$, where *z* is the coordinate of layer elevation from the top edge of centering unit’s cylindrical part;

– in curved part of the centering unit the pressure onto sloping segments is as follows $p_\alpha = 1215.15 \times z\ N/m^2$, $p_h = 1034.91 \times z\ N/m^2$, $p_h = 896.65 \times z\ N/m^2$, $p_h = 1650.1 \times z\ N/m^2$, where *z* is the coordinate of layer elevation from the top edge of centering unit 's cylindrical part;

– the bin hopper of the centering unit at bottom flange aperture area is under effect of the following pressure $p_\alpha = 73669.2$ ***Pa***. This pressure determines the force of loose material acting onto the bottom flange. The force is found as the product of pressure at aperture area and equals to ***Q = 94790.2 H***.

2.2.2.2 Wind effect

The wind effect is an alternate load, for which two design values are set:

– limit design value;

– operating design value.

With respect to the norm the wind effect on the structure is set out as normal pressure preconditioned by general resistance of construction facility along *x* and *z* axes, and is conditionally applied to structure's projection on a plane square with appropriate axis. The limit design value of wind effect has been considered.

The limit design value of wind effect is determined by the formula:

$$W_m = \zeta_{FM} \times W_0 \times C,$$

where, ζ_{FM} is the safety factor for the limit value of wind effect, determined by the time of equipment operation. The value of this factor is determined from the Table 9.1 of DBNV. 1.2-2:2006 and is adopted equal to $\zeta_{FM} = 0.90$.

W_0 is characteristic value of wind effect, and is defined by the wind region map 3 (Fig.1, annex E to design rules). For the city of Zaporozhye the wind effect characteristic value equals to 460Pa.

Coefficient C is calculated by the equation:

$$C = C_{aer} \times C_h \times C_{alt} \times C_{rel} \times C_{dir} \times C_d,$$

where C_{aer} is the aerodynamic factor of general air drag adopted as per DBNV.1.2-2:2006, and equals to 1.4;

C_h is the coefficient of construction facility height, determined by the annex 1 of the normative document and equals to $C_h = 2.215$;

C_{alt} is the coefficient of geographic height, equal to 1.0, since the geographic height of the construction facility is H=150m above sea level and under [H]=500m;

C_{rel} is the terrain relief factor, equal to 1.0;

C_{dir} is the coefficient of direction, equal 1.0;

C_d is the dynamic response factor, determined by Fig.9.6 of design rules and equals to 1.075. The value *C* is determined as follows:

$$C = 1.4 \times 2.125 \times 1.0 \times 1.0 \times 1.0 \times 1.075 = 3.198$$

The limit design value of wind effect equals to:

$$W_m = 0.9 \times 460 \times 3.198 = 1324 \text{ Pa.}$$

The calculations adopt the value of wind effect pressure equal to ***1324 Pa***.

2.2.2.3 Seismic impact, permissible stresses and design loading cases

The initial data for calculation of seismic strength of equipment designed are the seismic risk zoning of Ukraine (OSR-2004-A-B-C) developed by the Institute of Geophysics of the National Academy of Sciences of Ukraine. On the basis of construction norms "DBNV1.1-12:2006 Construction in seismic regions of Ukraine" the calculations are carried out for special load combination with consideration of seismic impact, i.e. design-basis earthquake (DE) and maximum design earthquakes (MDE). The seismic impact, permissible stresses and design loading cases are outlined in paragraphs 1.2.3.3-1.2.3.4 of this work.

Table 2.1

Structural member of material bin	Element thickness (mm)	Stresses (MPa)				
		σ_{02}	$[\sigma_{02}]_m$	$[\sigma]_1$	$1.3[\sigma]_1$	$1.4[\sigma]_1$
Cylindrical wall	**30**	**365**	**228.2**	**152.1**	**197.7**	**212.9**
Conical wall	**30**	**365**	**228.2**	**152.1**	**197.7**	**212.9**
Top flange	**40/30**	**350/365**	**218.8/ 228.2**	**145.8/ 152.1**	**189.5/ 197.7**	**204.1/ 212.9**
Bottom flange	**40/20**	**350/410**	**218.8/ 256.4**	**145.8/ 170.9**	**189.5/ 222.2**	**204.1/ 239.2**
Branch/flange	**25/30**	**359/365**	**224.5/ 228.2**	**149.6/ 152.1**	**194.4/ 197.7**	**209.4/ 212.9**
Hatch/flange	**40**	**350**	**218.8**	**145.8**	**189.5**	**204.1**
Support's lug	**40**	**350**	**218.8**	**145.8**	**189.5**	**204.1**

For each structure's element the yield strength at the temperature of 450°C is determined as follows $[\sigma_{02}]_m = \sigma_{02}/(\gamma_м \gamma_m)$ and presented in Table 2.1. Consideration of corrosion affecting the permissible stress for each bin's structural element is made through reduction of design permissible stresses by the of corrosion factor n_k. Reduction in size Δ of any element due to corrosion is taken equal to 3mm; the corrosion factor is taken equal to $n_k = \Delta/(\Delta-3)$, and $[\sigma_{02}]_m = \sigma_{02}/(\gamma_м \gamma_m n_k)$. The table 2.5 shows adjusted permissible stresses.

Table 2.5

Structural member of material bin	Corrosion factor, n_k	Stresses (MPa)				
		σ_{02}	$[\sigma_{02}]_m$	$[\sigma]_1$	$1.3[\sigma]_1$	$1.4[\sigma]_1$
Cylindrical wall	**1.11**	**365**	**205.4**	**136.9**	**178.0**	**191.6**
Conical wall	**1.11**	**365**	**205.4**	**136.9**	**178.0**	**191.6**
Top flange	**1.08/1.11**	**350/365**	**202.3/ 205.4**	**134.9/ 136.9**	**175.4/ 178.0**	**188.8/ 191.6**
Bottom flange	**1.08/1.17**	**350/410**	**202.3/ 218.0**	**134.9/ 145.3**	**175.4/ 188.9**	**188.8/ 203.4**
Branch/flange	**1.13/1.11**	**359/365**	**197.6/ 205.4**	**131.7/ 136.9**	**171.2/ 178.0**	**184.4/ 191.6**
Hatch/flange	**1.08**	**350**	**202.3**	**134.9**	**175.4**	**188.8**
Support's lug	**1.08**	**350**	**202.3**	**134.9**	**175.4**	**188.8**

Permissible stresses for material bin's bolt joints are taken equal to ***[σ] = 166.7 MPa.*** The required assessments of structure performance capacity define the following design cases and design loading patterns:

– structural design under effect of design internal pressure;

– structural design under conditions of NSC;

– structural design under conditions of NSC + LWE;

– structural design under conditions of seismic impact NSC + MDE.

2.2.2.4 Design case for normal service conditions

The centering unit's operation corresponds to two load cases: operation under pressure and operation under no pressure. The design case for normal service conditions (NSC) is defined by the following loads acting on bin's structure:

– sealing valve weight force acting on bin's top flanges and equal to $G_{кл}$ = ***25000 + 2000 = 27000 kg.*** This load is caused by the pressure acting on the top flanges. The area of flanges is ***2.463m²***, and the pressure is ***107 539 Pa***;

– design internal pressure in the centering unit equals to ***p = 0.23 MPa;***

– structure's bulk weight force equals to. Bin's weight taken into consideration is $G_к$***=15767 kg***;

– forces caused by internal design pressure acting on:

a) bottom nonstandard flange with aperture diameter of 1280 mm, and equaling to ***295 963 N;***

b) top nonstandard flange, and equaling to ***427 140 N;***

c) flange of lateral inspection manhole. Manhole's area is ***0.4935m^2***. The force acting on the flange equals to ***113 523 N.***

– thermal stress at steady-state heating of the structure up to 450°C;

– loose material pressure onto vertical wall in centering unit's cylindrical part ***p_h=780.1×z;***

– loose material pressure onto curved wall in centering unit's conical part:

surface 1**:** ***α = 60^0,*** ***p_h = 1215.1×z;*** surface 2: ***α = 67.5^0, p_h = 1034.91×z;***

surface 3: ***α=75^0 ,*** ***p_h = 896.65×z;*** surface 4: ***α=45^0,*** ***p_h = 1650.1×z;***

– load on cantilever beams for observation deck mounting.

Dimensions of deck 1 are ***5.3×1.0=5.3 m^2***. Load per 1 m^2 as rated equals to ***4000 N.*** Weight of the deck is ***5000 N***. The force equals to ***21200 + 5000 = 26200 N.*** One cantilever beam is under effect of the force of ***6550N;***

– loose material force acting onto bin hopper, as applied to bottom flange of the centering unit and equal to ***94790 N***.

The design model of the centering unit under normal service conditions (NSC) is presented in Fig. 2.2.

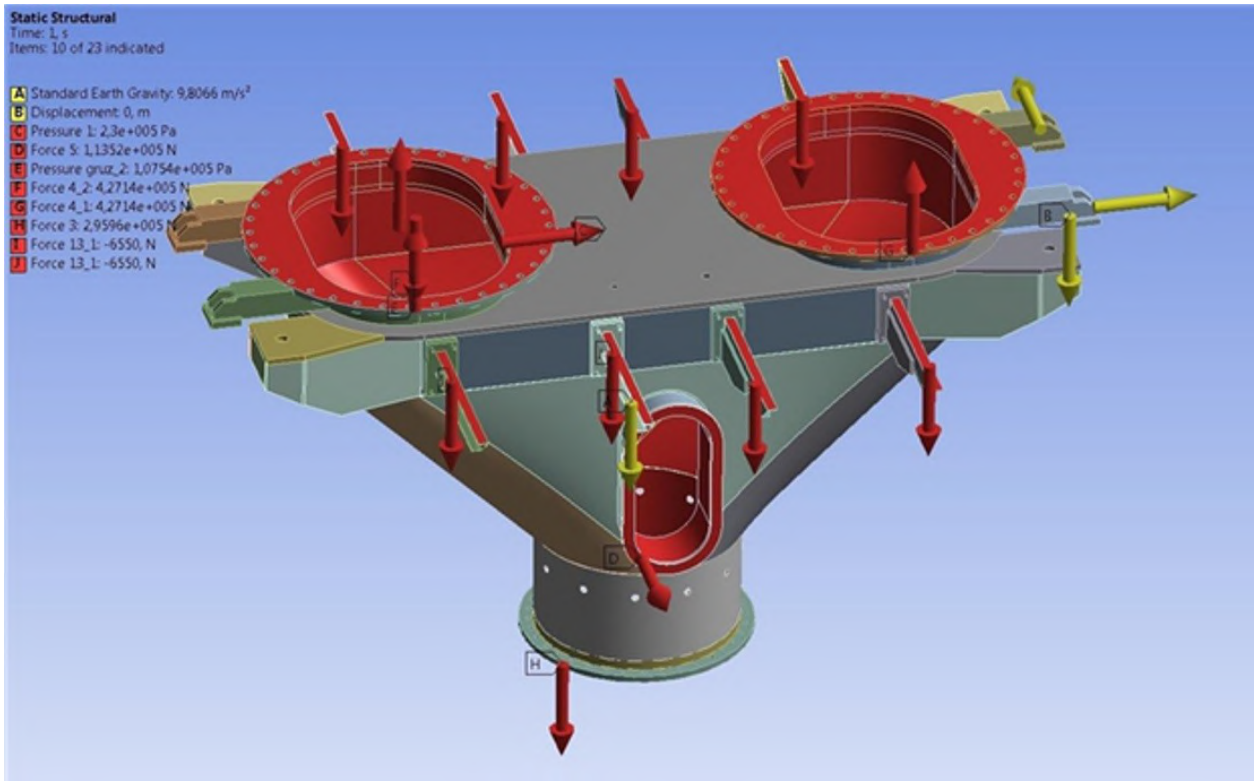

Fig. 2.2 Design pattern of centering unit under NSC.

2.2.3 Fundamental principles for carrying out calculations and analyzing and calculation results.

When performing calculations, the following features are to be taken into consideration:

– the structure's geometrical model shall take into consideration all structure's stress risers caused by fillets and chamfers of component parts;

– on customer's demand the centering unit is released of all internal ribs and linings. Weight of these elements (grid + lining = ***2 684.5 kg***), as well as the weight of man-hole lid with ribs (weighing ***330 kg***), is added to entire structure. The total weight equals to ***15 016.0 kg*** and the volume is ***1,3103 m^3***. The entire weight has been in-creased by safety factor ***1.05*** in relation to loads and equals to ***15 767 kg.*** The calculations specify this weight with the material density value equaling to ***11 090 kg/m^3*** for the volume in question. The calculations specify this weight with the material density value equaling to ***11 460 kg/m^3*** for the volume in question;

– structure's materials shall be considered as nonlinear elastic isotropic materials with mechanical characteristics corresponding to service temperature of 450°C. The calculations shall employ the bilinear deformation curve for the service temperature;

– an ideal contact interaction is adopted for all welded structure's surfaces;

– for structure's materials the sketch presentation of Wehler curve with physical endurance limit σ_R is to be adopted as per Baskvin's equation;

– the value of endurance limit reduction factor K_f is to be determined with consideration of surface roughness factor $K_{F\sigma}$ and cross-section full size response factor $K_{d\sigma}$;

– roughness effect is to be taken into account as per the procedure set out in GOST 25.504-82. Assuming that structure's surface has roughness from 0.8 to 1.6 μm the factor $K_{F\sigma}$ = ***0.92;***

– cross-section full size response factor is to be determined by the nomographic chart presented in the reference guide "Machine part strength design:

reference guide / I.A. Birger, B.F. Shor, G.B. Iosilevich". For sheet thickness of 30 mm the factor is $K_{d\sigma}$ **= *0.92***. In this case the endurance limit reduction factor K_f is adopted in the calculation equal to ***0.846;***

– to determine the fatigue resistance in the presence of local stress risers the equation of Morrow-Manson is to be used;

– the obtained load history characteristics for components of stress tensor are brought to damage-equivalent characteristics under conditions of single-axis loading. The transition to reduced stresses (damage-equivalent, single-axis) by amplitude and average values of load cycle stresses is to be made by the value of specific distortion energy;

– the obtained load history characteristics with asymmetry coefficient $R = 0$ are to be brought to damage-equivalent characteristics under conditions of symmetric cycle loading. To perform this transition, the formulas for the amplitude of equivalent symmetrical cycle stress loading $\sigma_{аэкв}$ are used on the basis of Goodman's law;

– the assessment of service lifespan of a unit is to be performed by the number of cycles till failure and the level of full strains. These assessments are carried out using the stress cycle behavior function by Wehler SN curve described;

– as strength criterion the IV-th theory of strength is to be used.

– with regards for all erection and transportation operations with material bin the design patterns shall adopt the value of overload factor as per GOST R 51282-99 (table 10) equal to 1.2.

– when analyzing the calculation results the local extremes of equivalent stresses are not to be considered, if they act in areas within a finite element. This recommendation is related to numerical singularity of finite element method and can be removed by means of structure submodelling in the given area and corrective remeshing of the finite element model. The structure submodelling in such an area can be made for selected bin structure elements.

2.2.4 Description of bin designing procedure

Structure's geometric modeling has been performed using three-dimensional presentation of the centering unit in SolidWorks software-package. Physical modeling has been carried out in ANSYS software-package. The calculation procedure of structure's stress-strain state is the finite-element method implemented by ANSYS WORKBENCH calculation package.

The structure's finite-element model is presented in fig. 2.3 and consists of 2506898 nodes united by 927493 elements. The mesh quality is 0.82. Dimension of a finite element side does not exceed 20mm.

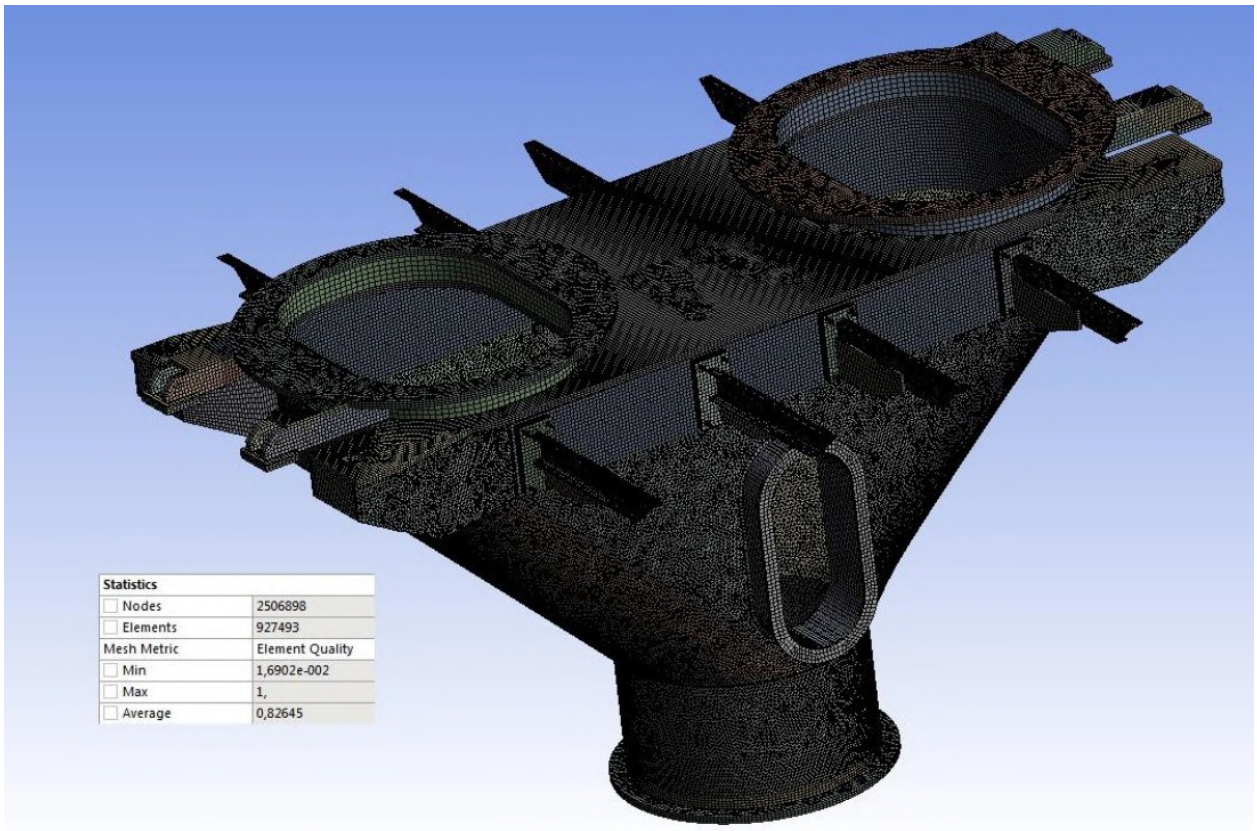

Fig. 2.3 Finite-element model of the centering unit.

2.3 CENTERING UNIT DESIGN CALCULATION

2.3.1 Structural design under estimated loading

Results of centering unit designing for the load case of internal design pressure and structure's weight are presented in a form of stress and strain patterns, and fatigue design parameters in Fig. 2.4-2.18.

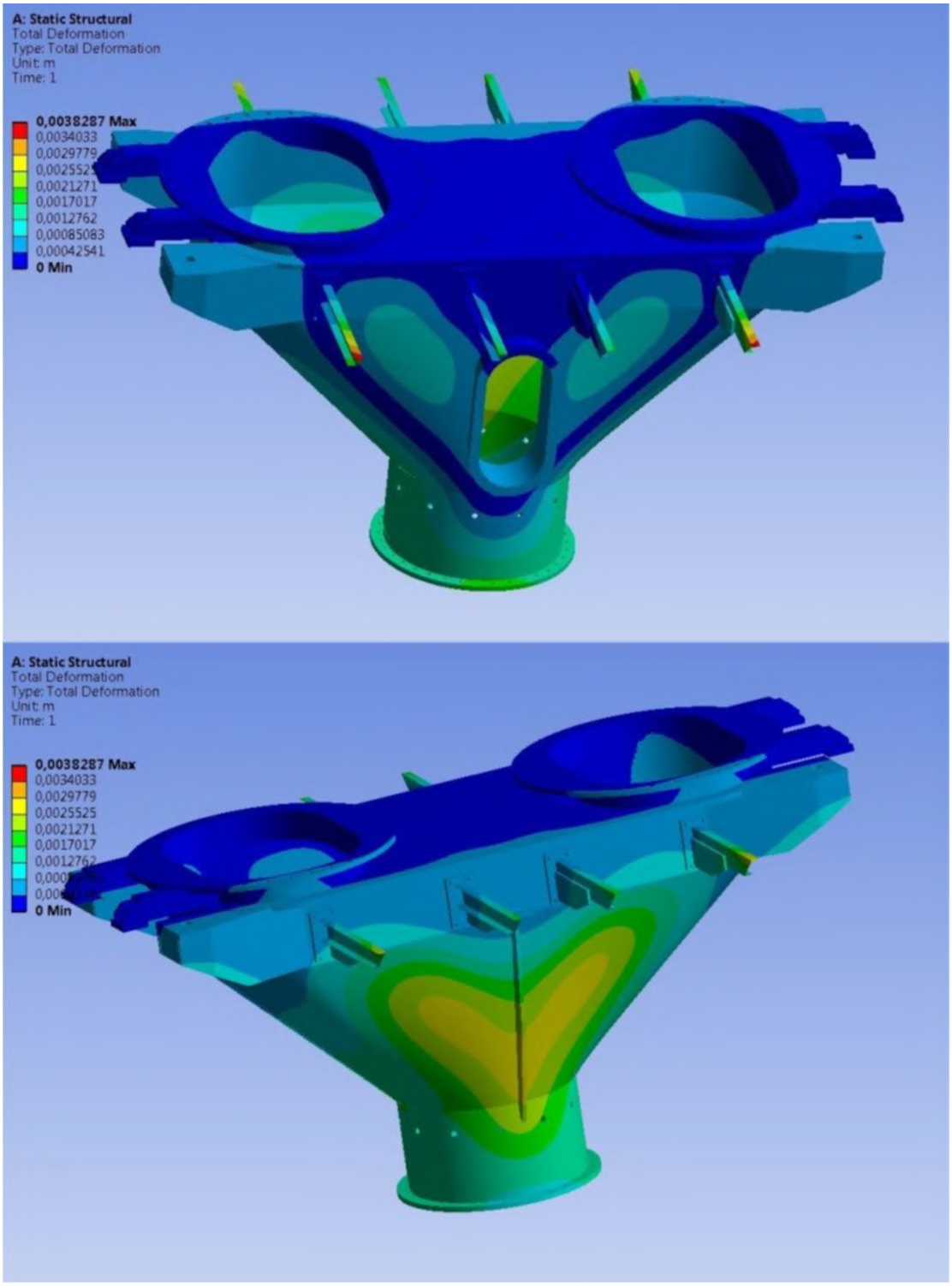

Fig. 2.4 Distribution of total strains arising in the structure.

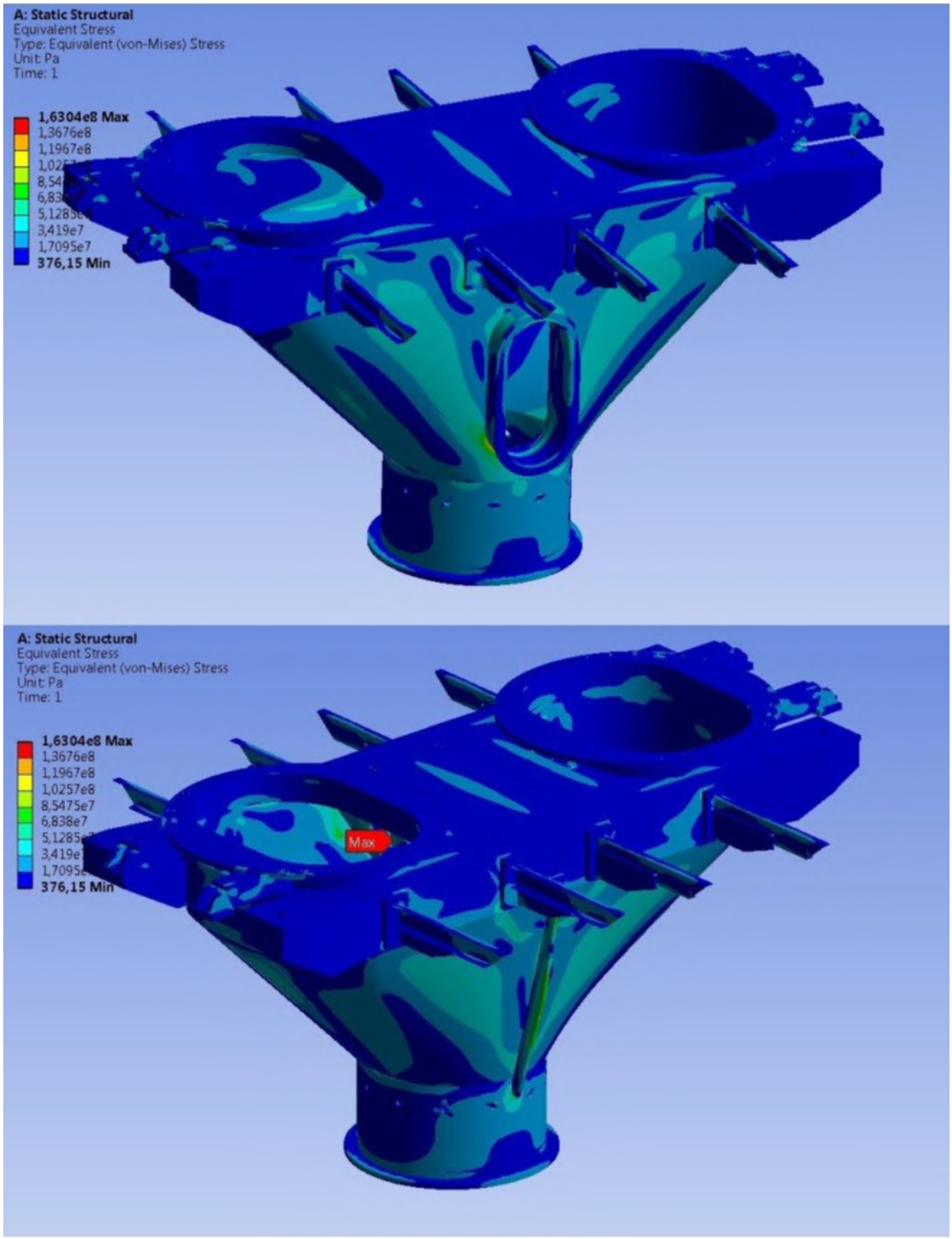

Fig. 2.5 Distribution of von Mises equivalent strains arising in the structure.

The biggest stresses arise in inner ribs of the centering unit. These stresses are local in nature and are within the finite element. Fig. 2.6 shows distribution of von Mises stresses inside the centering unit.

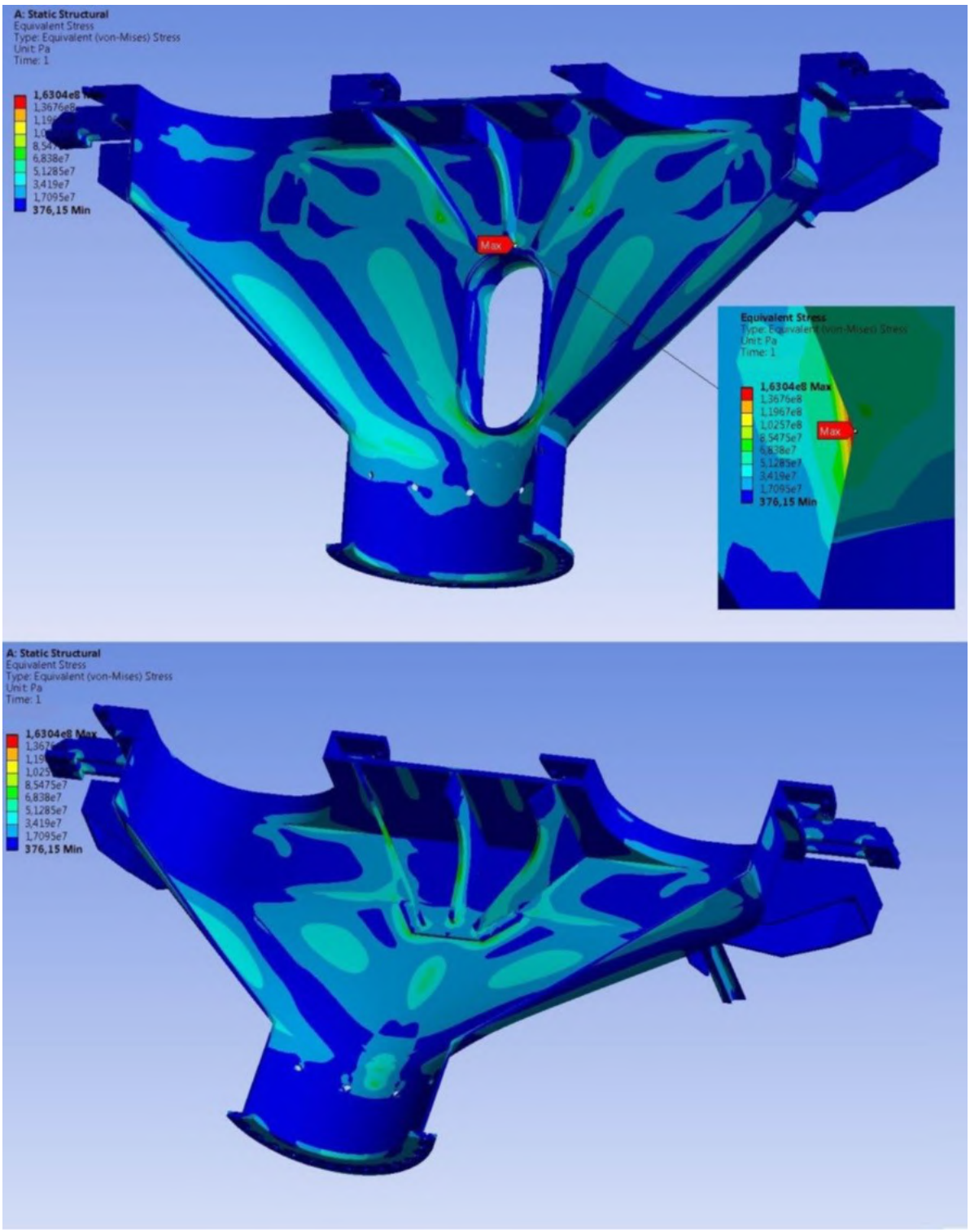

Fig. 2.6 Distribution of stresses inside the structure.

Distribution of stresses in centering unit's structural members is presented in Fig. 2.7-2.12.

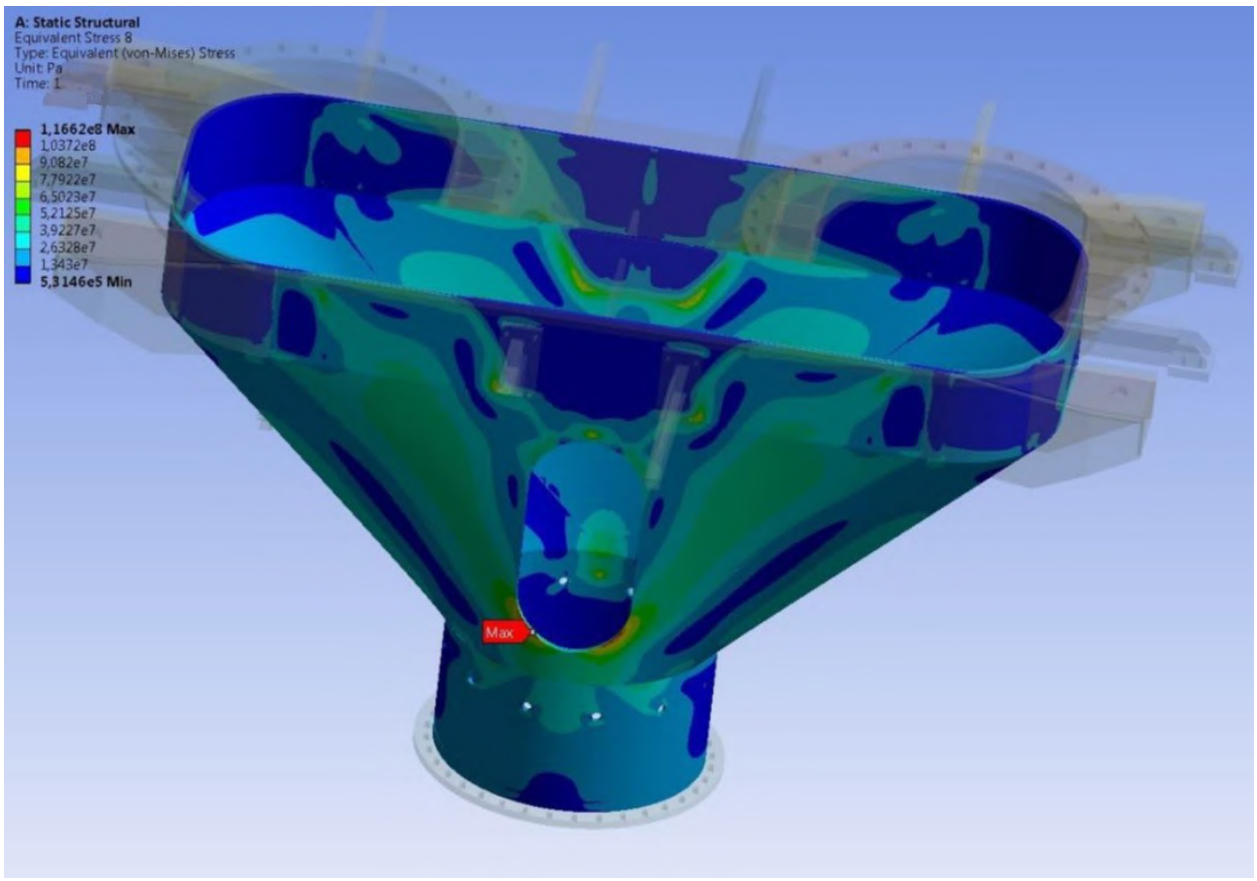

Fig. 2.7 Distribution of stresses arising in the load-bearing cover.

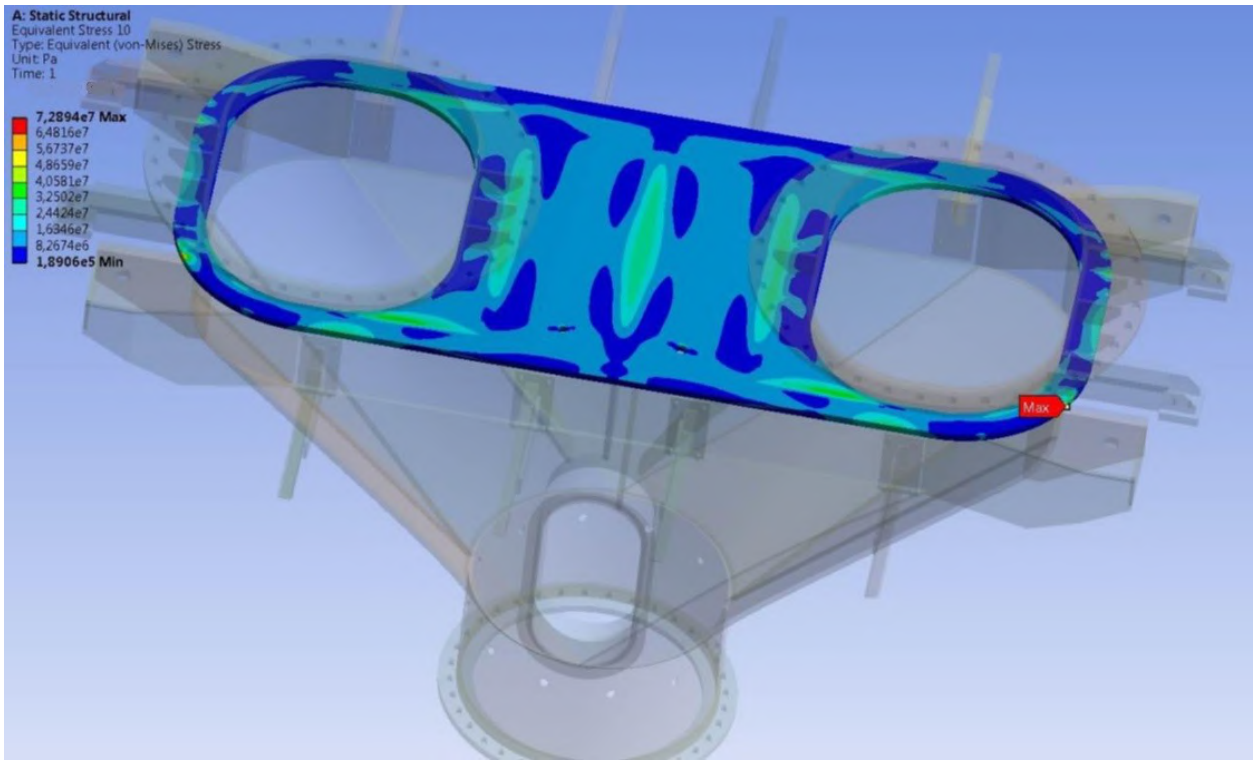

Fig. 2.8 Distribution of stresses arising in the top plate.

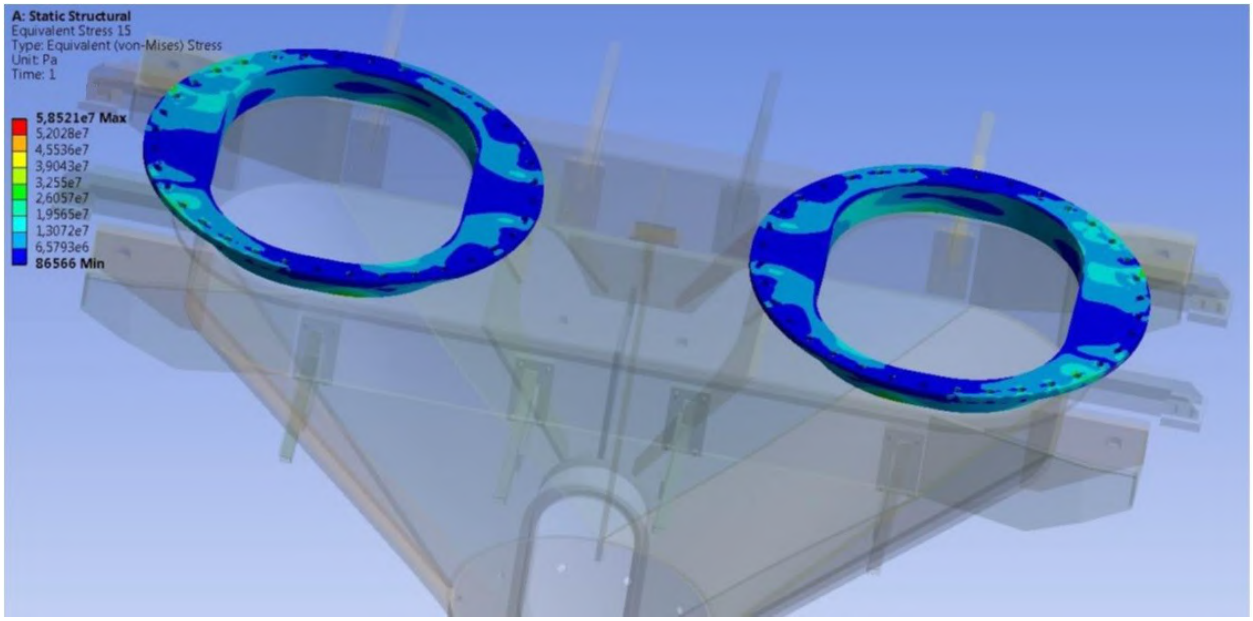

Fig. 2.9 Distribution of equivalent stresses in top flanges.

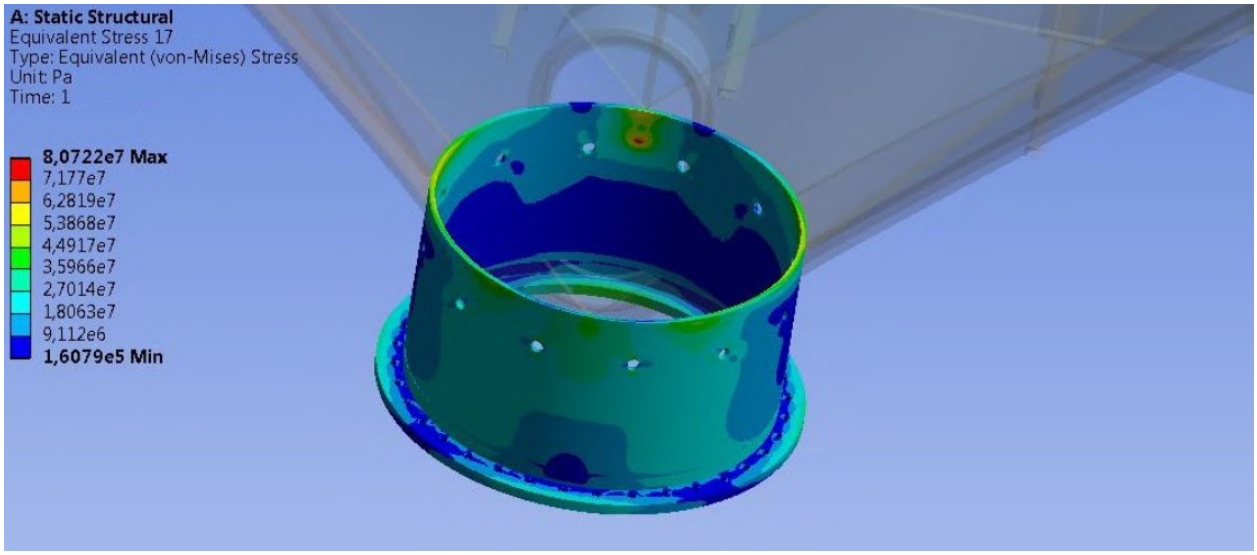

Fig. 2.10 Distribution of equivalent stresses in the bottom flange.

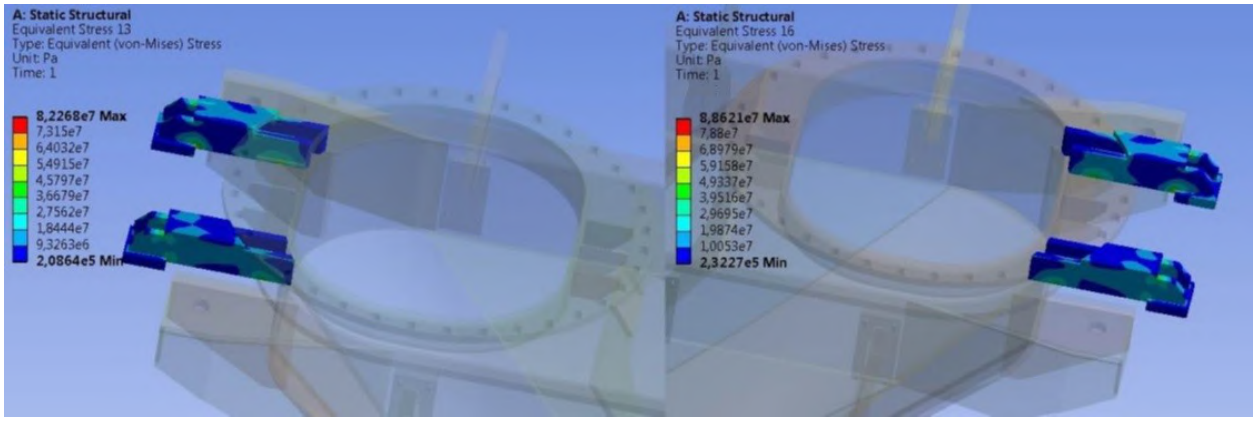

Fig. 2.11 Distribution of equivalent stresses in supports.

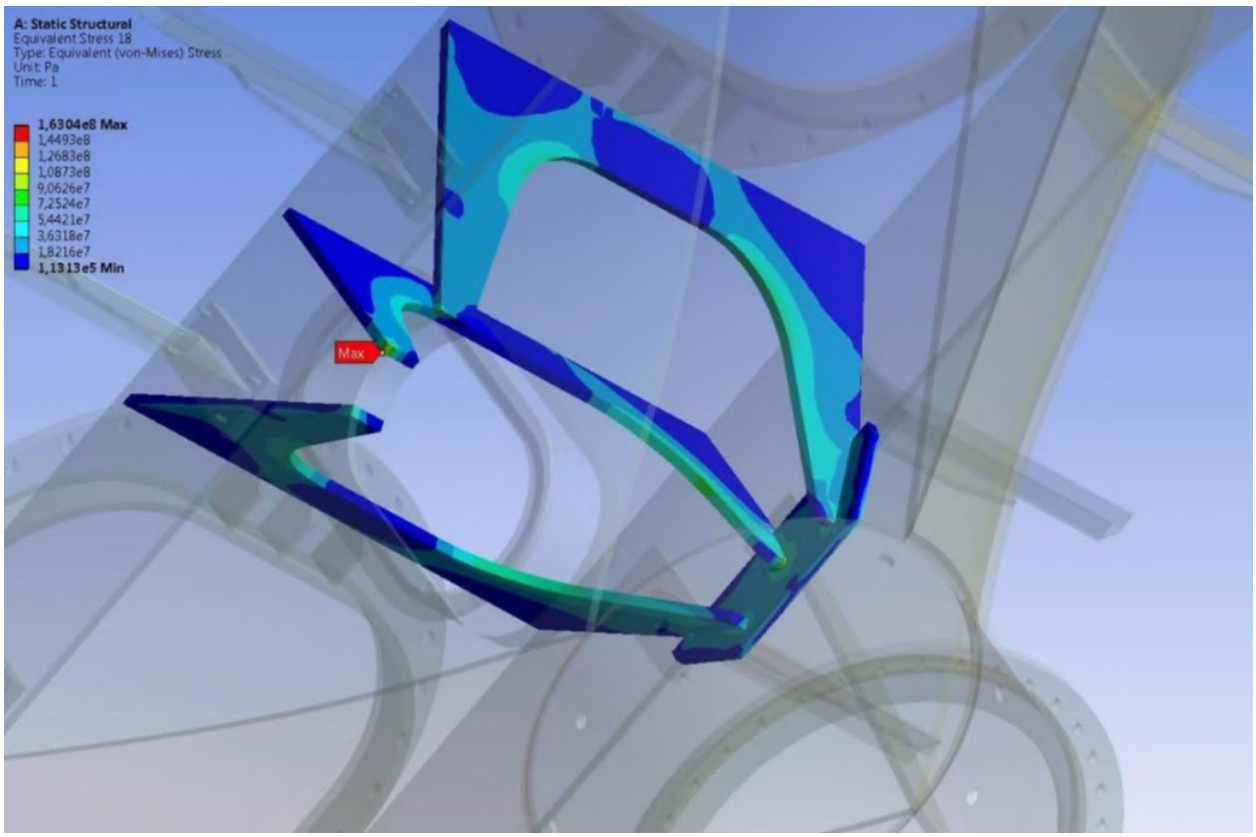

Fig. 2.12 Distribution of equivalent stresses in centering unit's ribs.

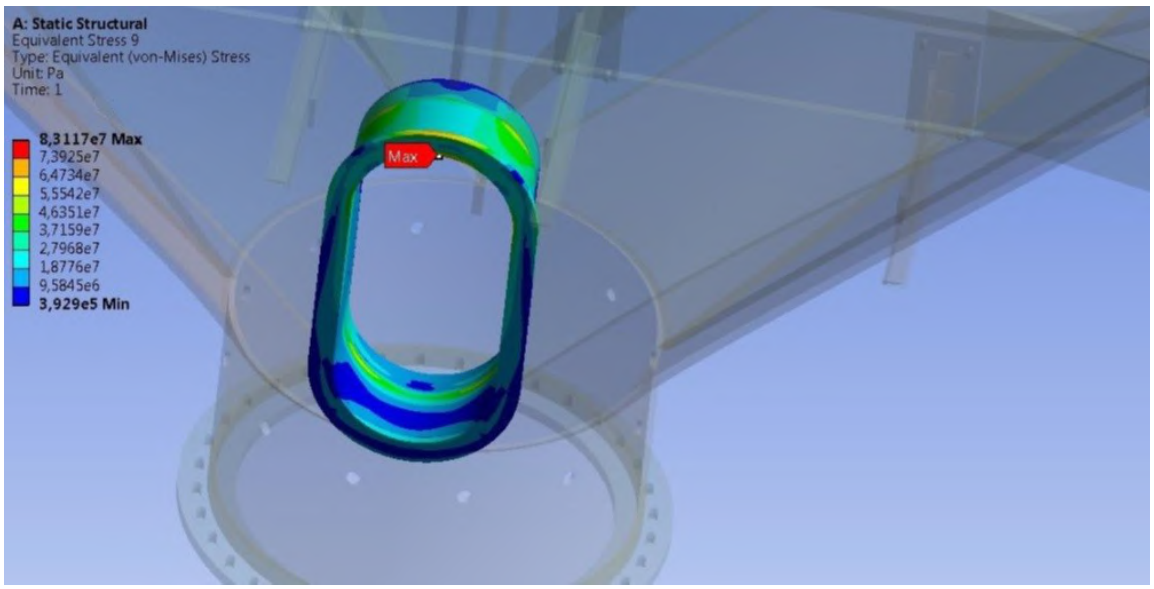

Fig. 2.13 Distribution of equivalent stresses in the centering unit's lateral manhole.

The stresses in centering unit's load-bearing cover do not exceed 116.6MPa. Fig. 2.7 shows distribution of stresses in load-bearing cover. These stresses are maximal in the area of joining the centering unit's bottom conical part and the cover of the lateral manhole. The assessment of service lifespan of load-bearing elements of the bin and correctness of assessment in question is presented in Fig. 2.14-2.18.

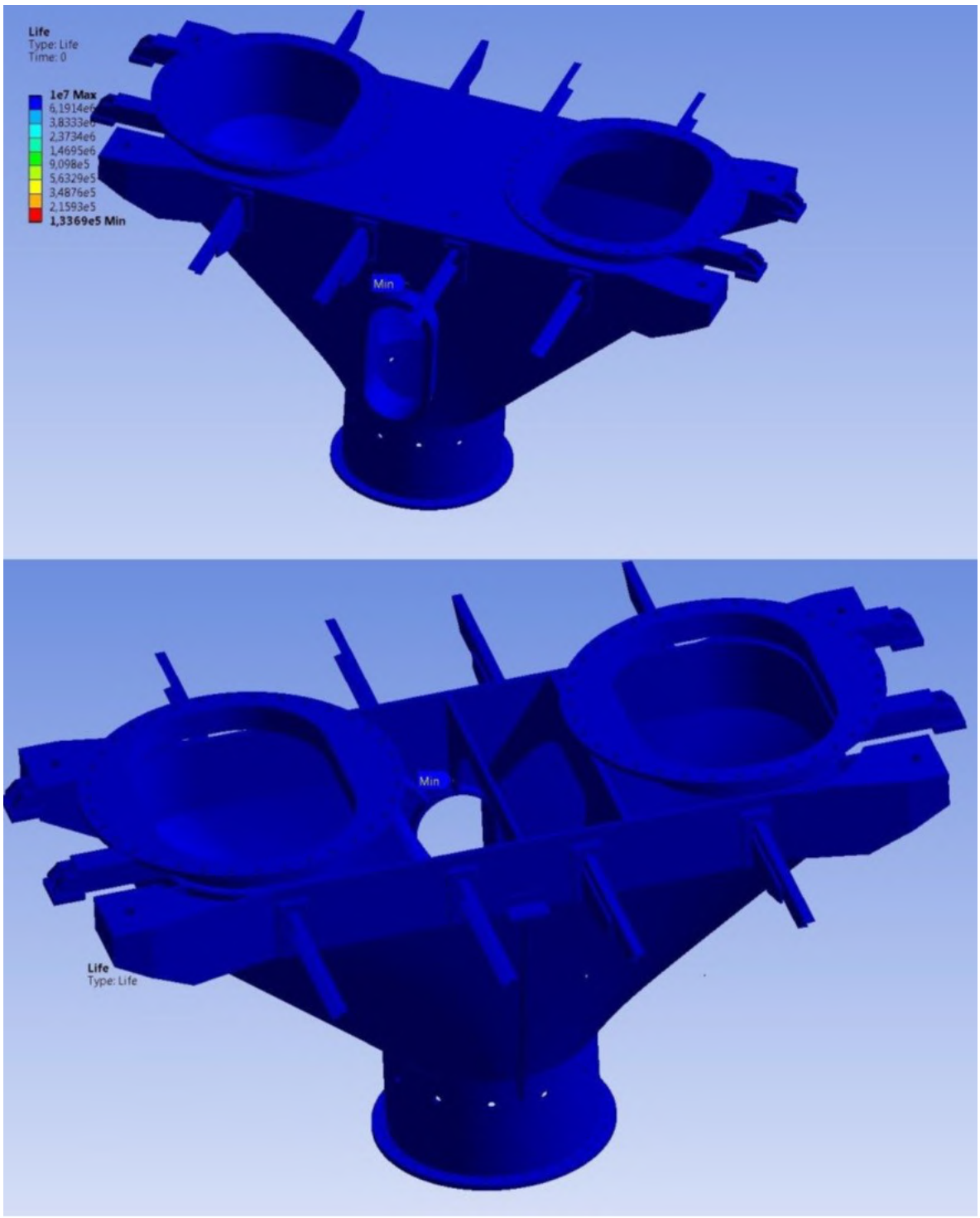

Fig. 2.14 Distribution of centering unit lifespan by Wehler SN curve

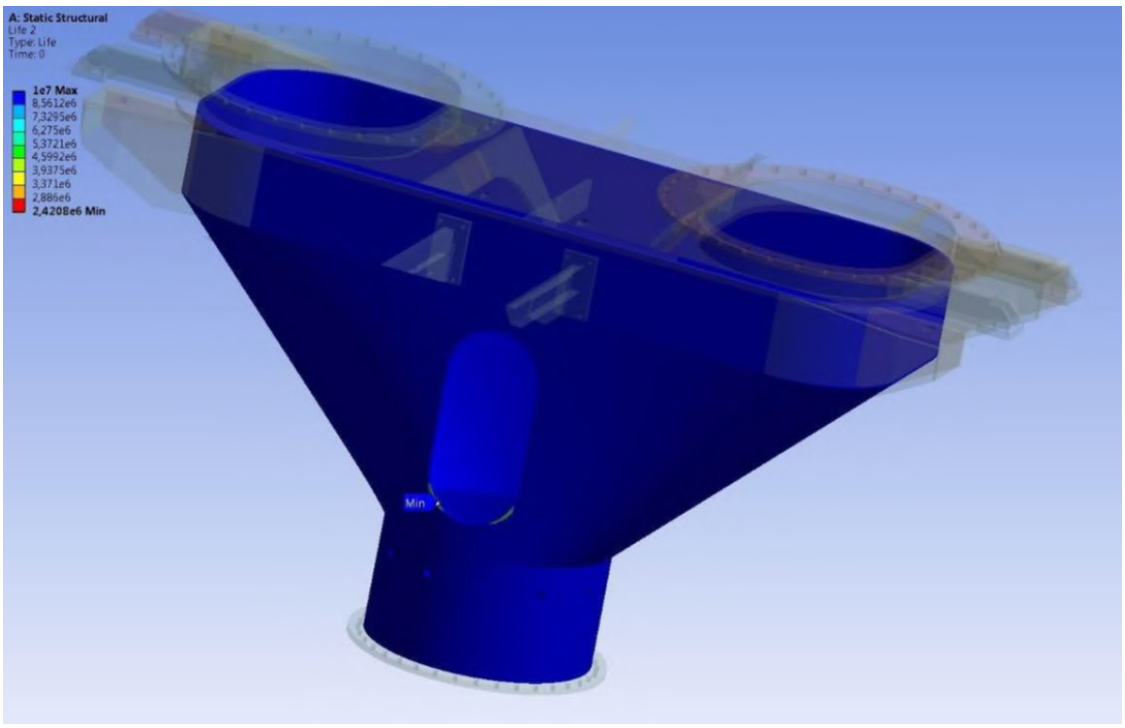

Fig. 2.15 Distribution of lifespan of centering unit's load-bearing cover by Wehler SN curve

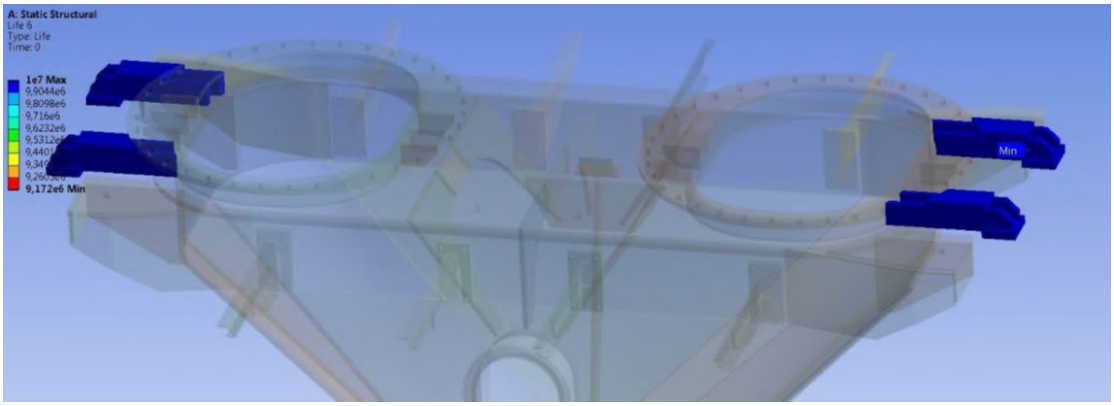

Fig. 2.16 Distribution of lifespan of centering unit's supports by Wehler SN curve

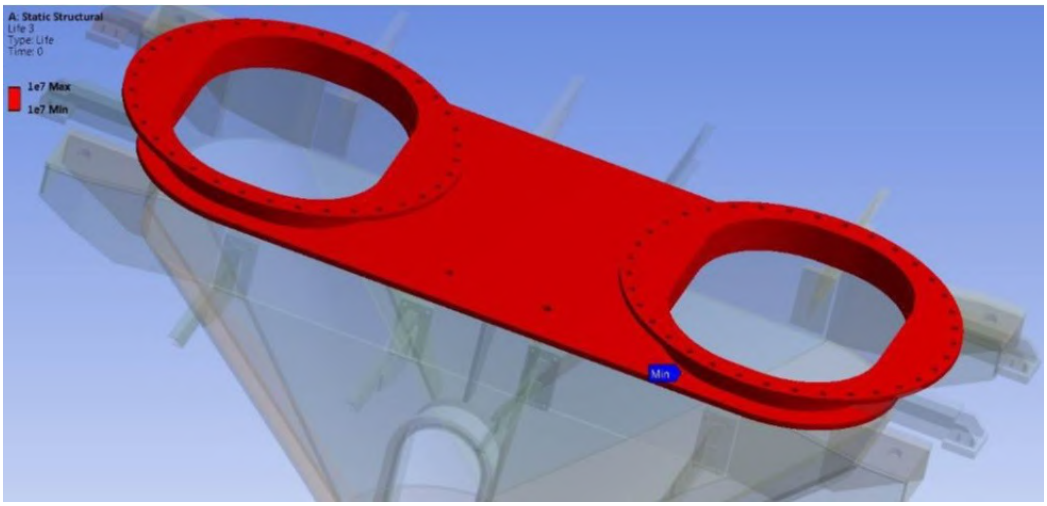

Fig. 2.17 Distribution of lifespan of centering unit's plate by Wehler SN curve

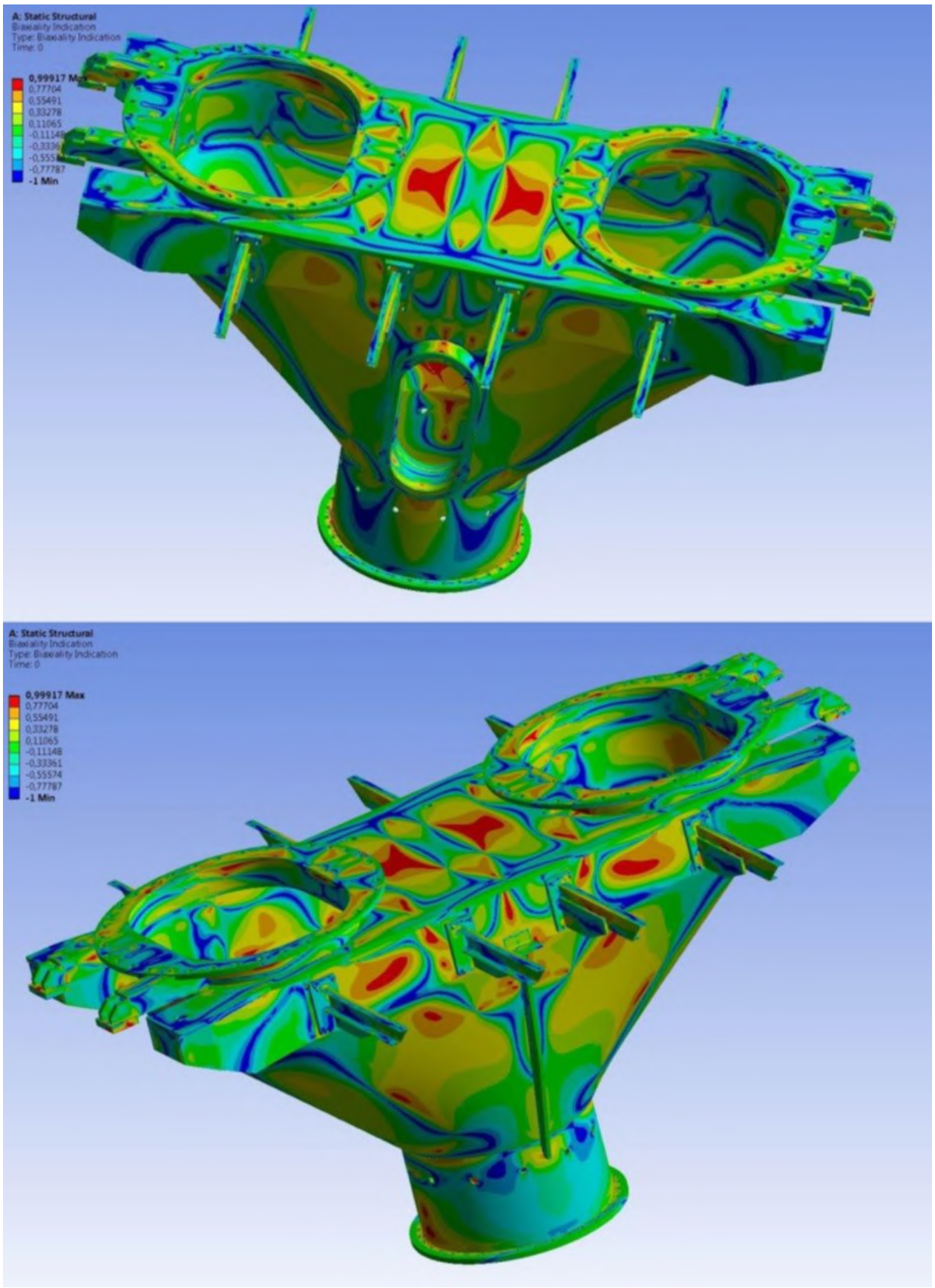

Fig. 2.18 Distribution of stress-strain nature in the bin by Wehler SN curve.

2.3.2 Structural design for normal service conditions (NSC)

The results of bin designing for normal service conditions are presented as pat-terns of stresses, strains and fatigue calculation parameters in figures 2.19-2.31.

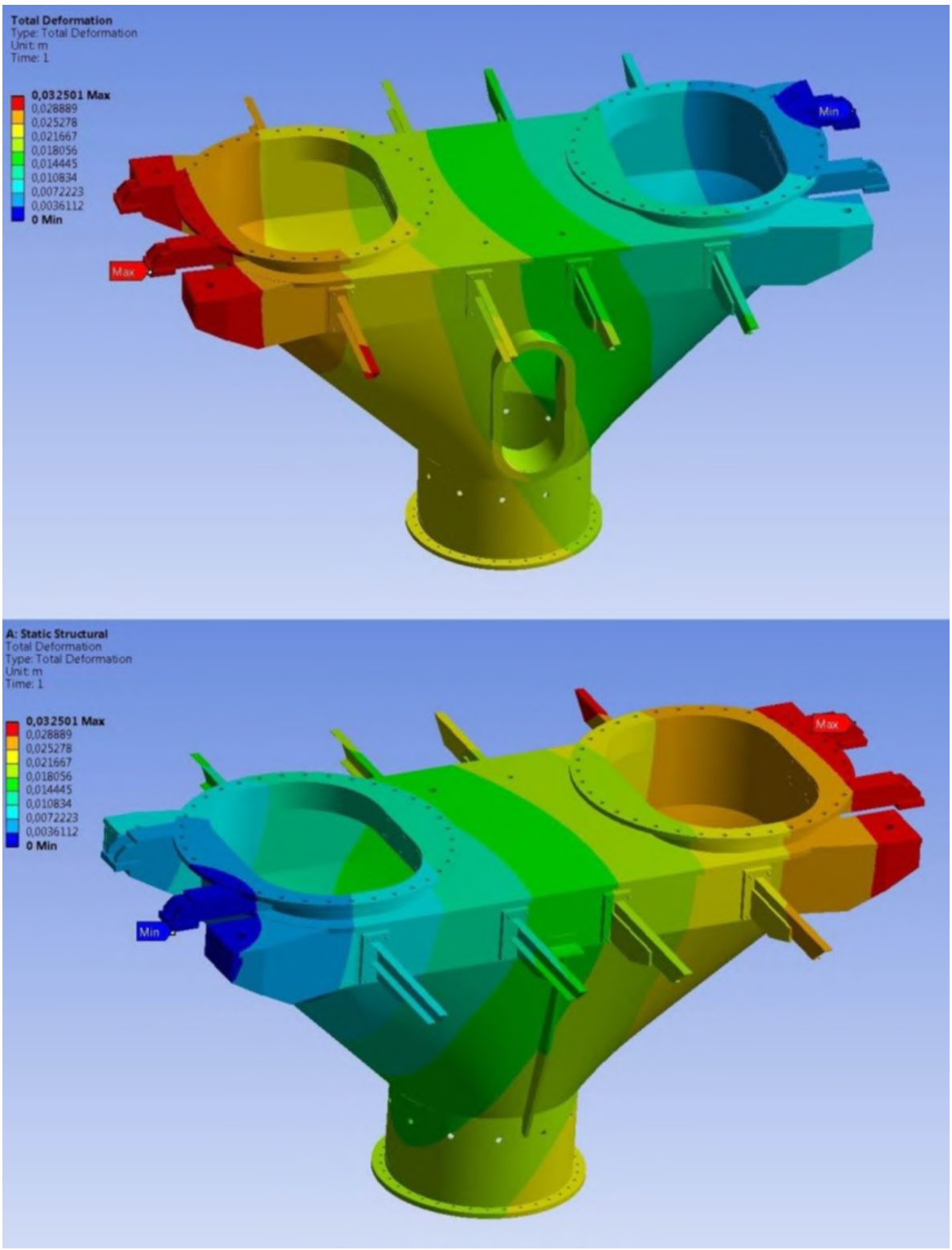

Fig. 2.19 Distribution of total strain arising in the structure.

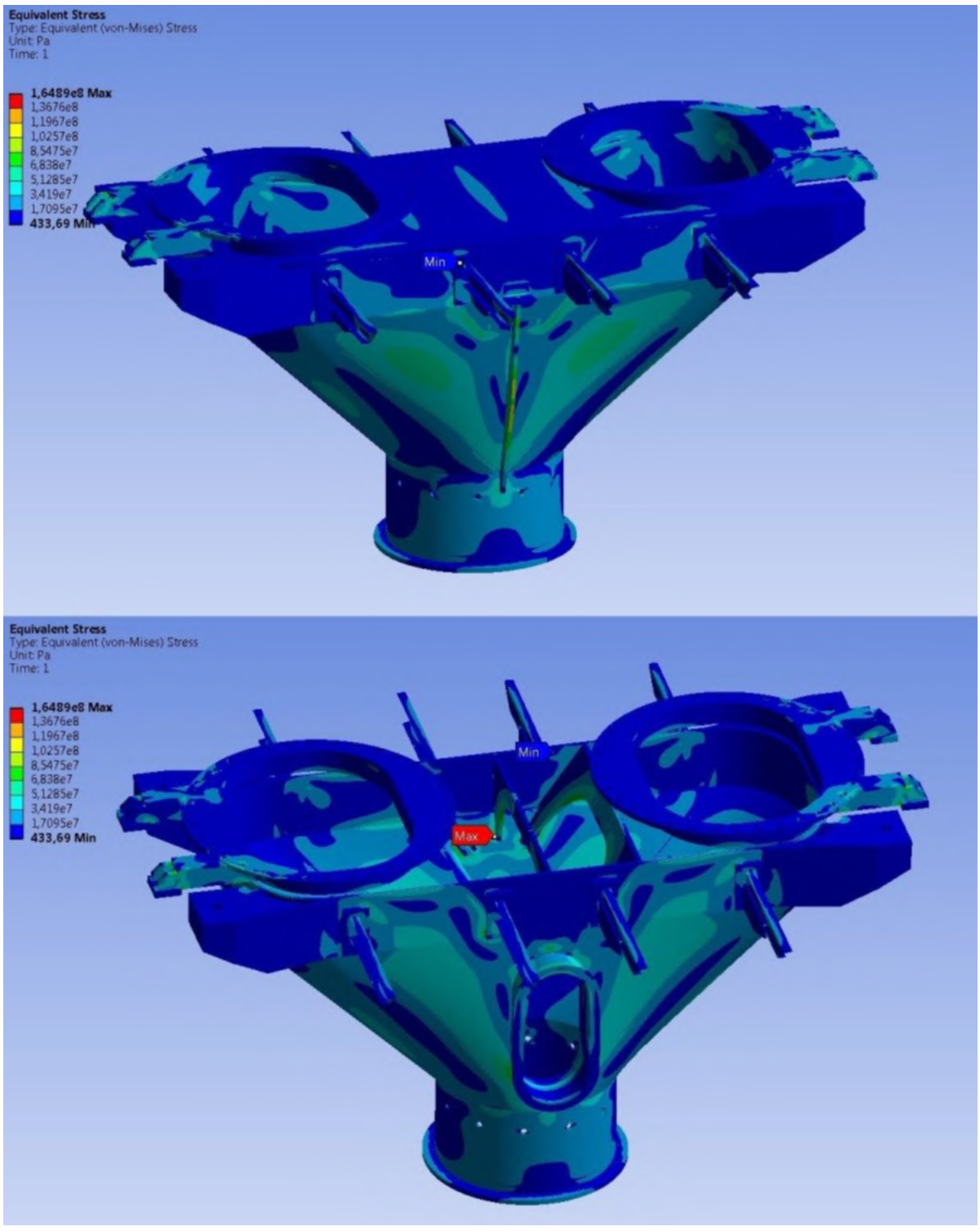

Fig. 2.20 Distribution of von Mises equivalent stresses arising in the structure.

The biggest stresses arise in centering unit's internal ribs. These stresses are local in nature and are within the finite element. The Fig. 2.21 shows distributions of von Mises equivalent stresses inside the centering unit.

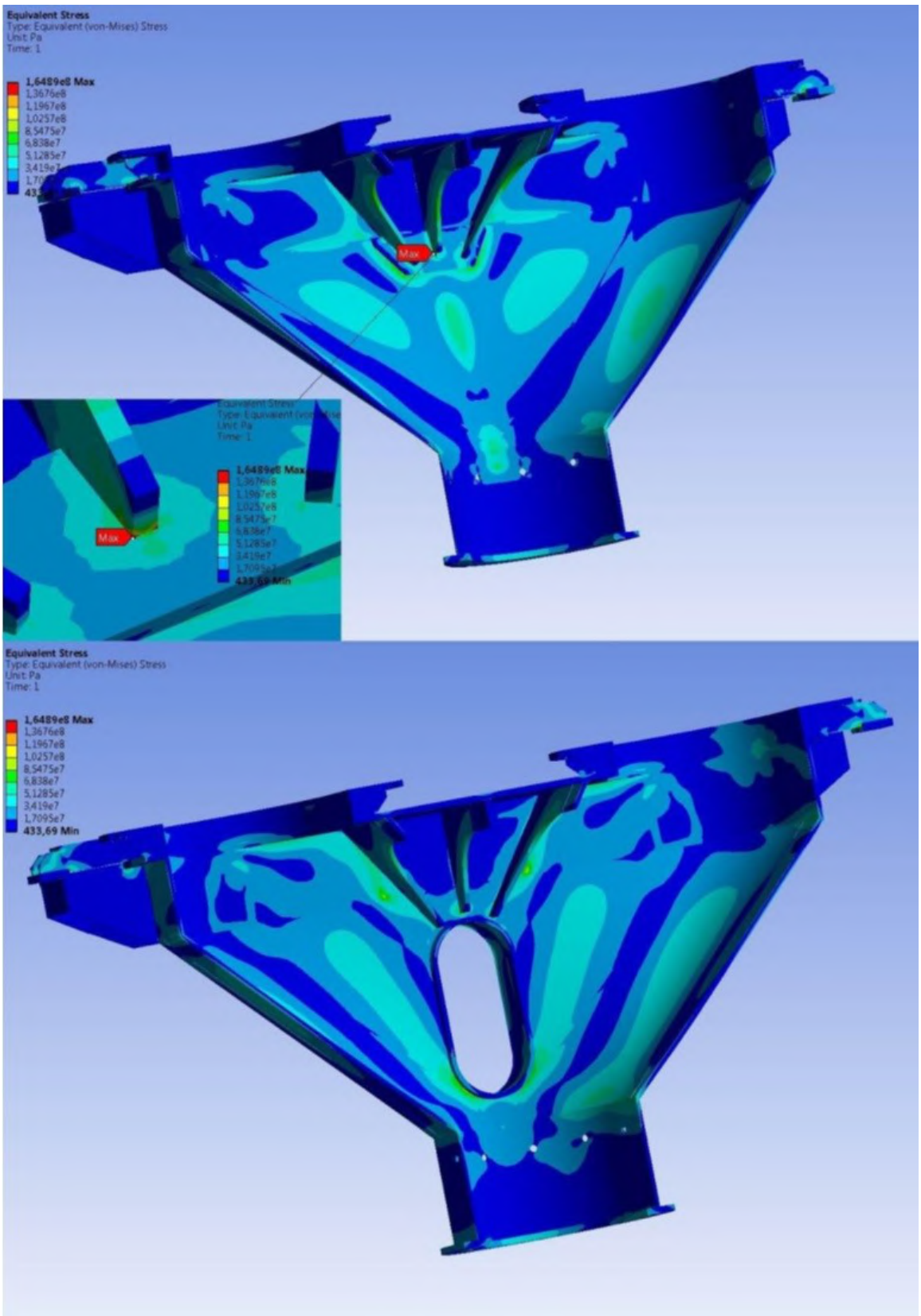

Fig. 2.21 Distribution of stresses arising in the structure.

Distribution of stresses in of centering unit's structural members is presented in Fig. 2.22-2.28.

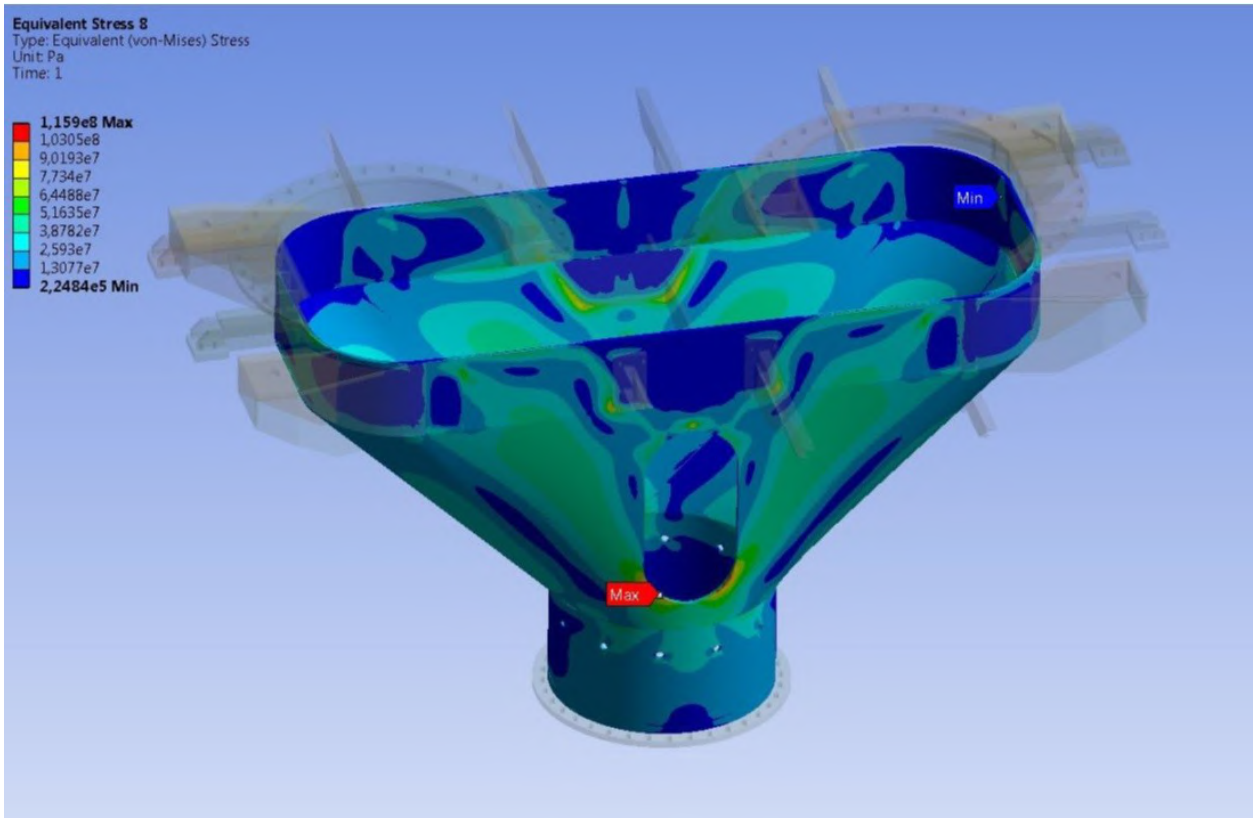

Fig. 2.22 Distribution of stresses arising in the load-bearing cover.

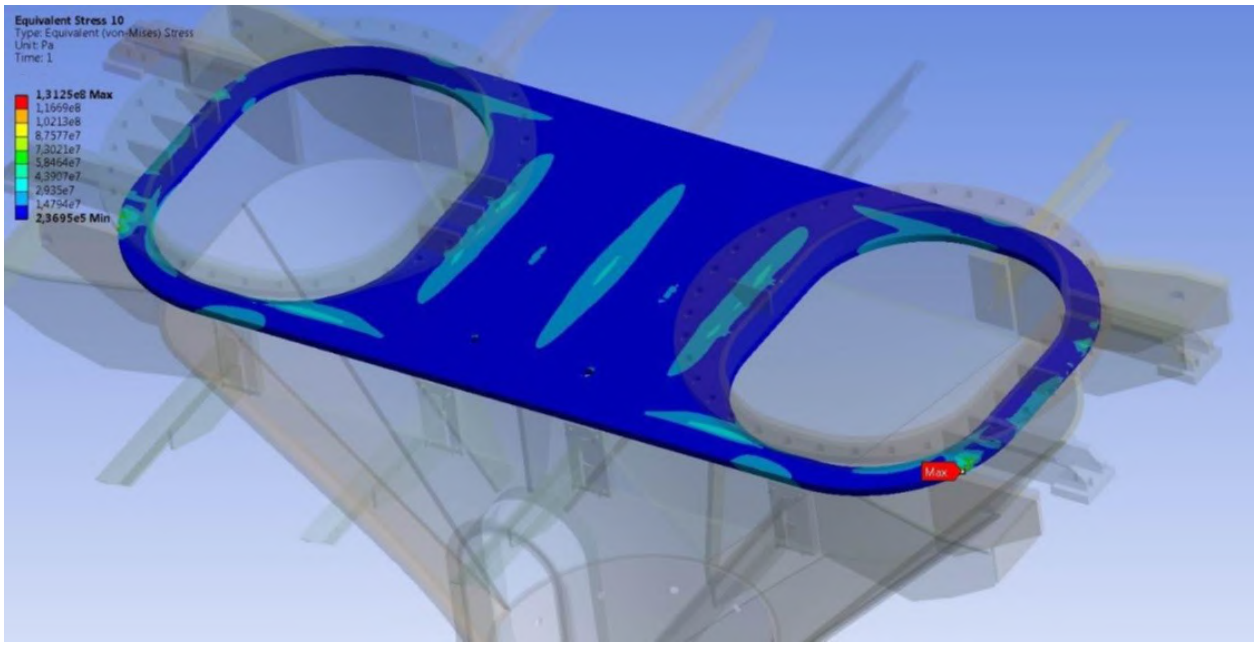

Fig. 2.23 Distribution of stresses arising in the top plate.

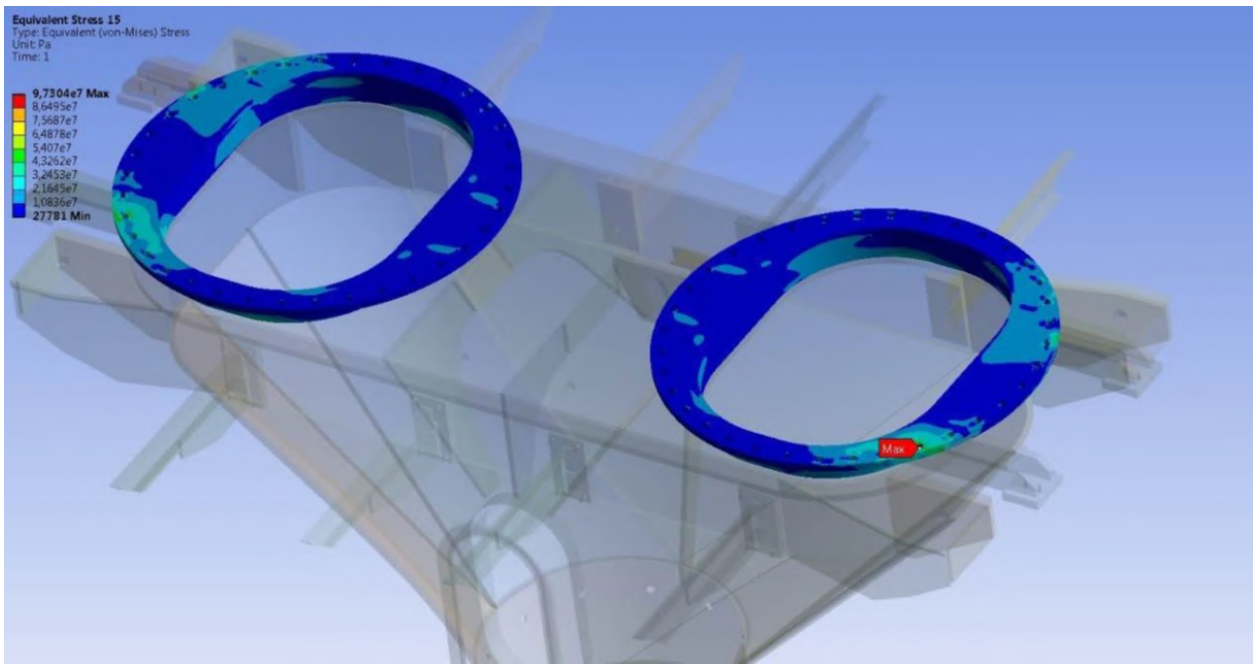

Fig. 2.24 Distribution of equivalent stresses in top flanges.

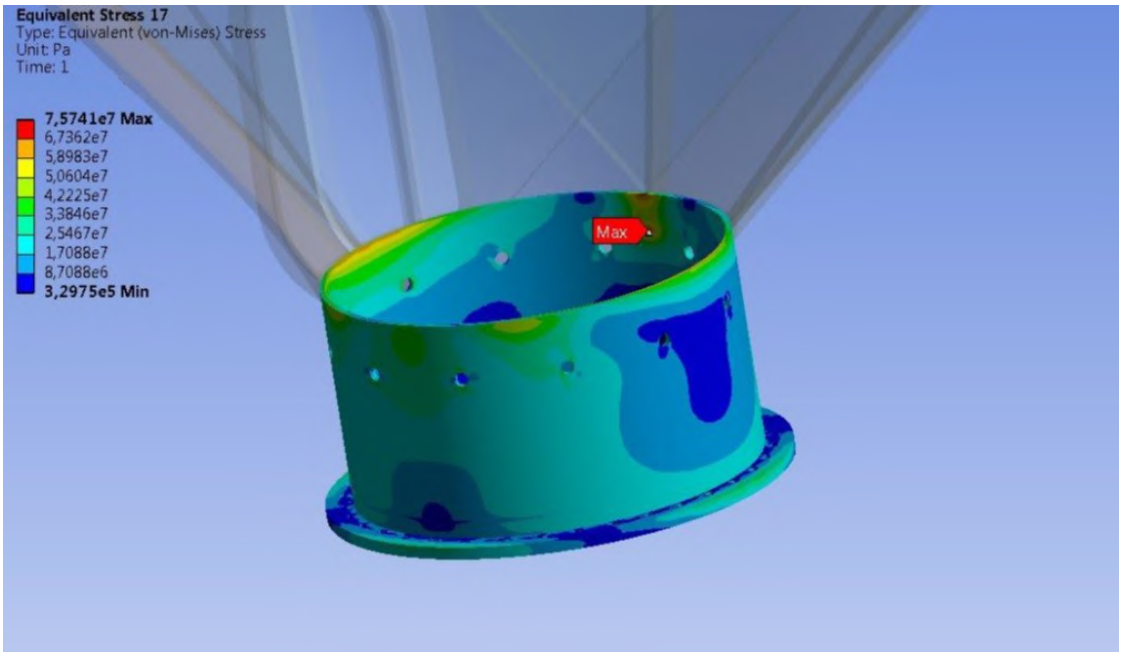

Fig. 2.25 Distribution of equivalent stresses in the bottom flange.

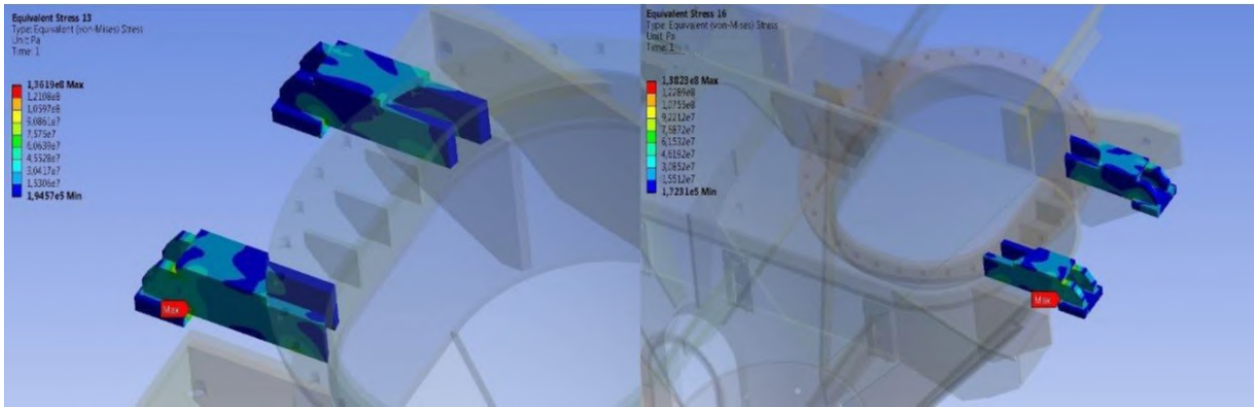

Fig. 2.26 Distribution of equivalent stresses in supports.

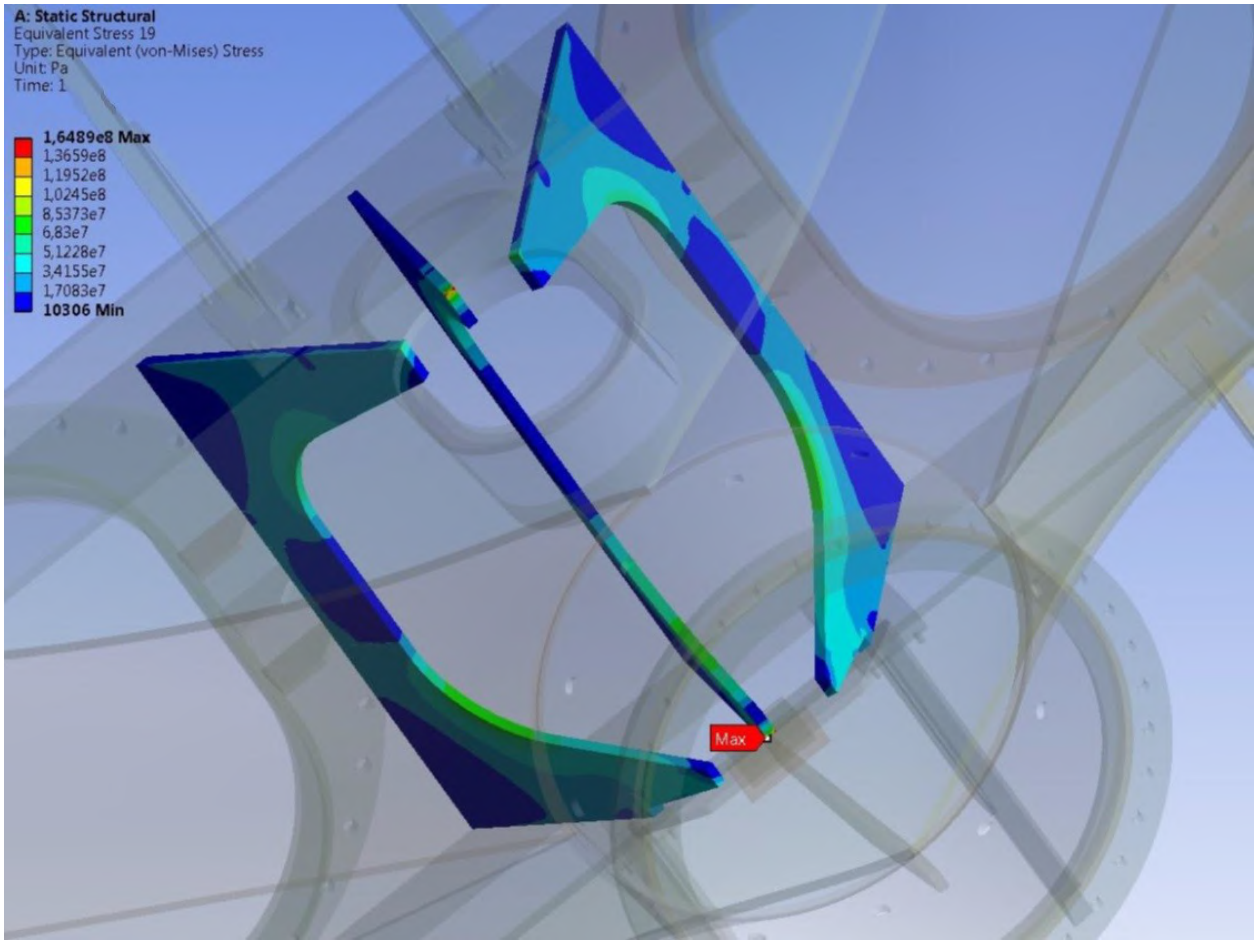

Fig. 2.27 Distribution of equivalent stresses in centering unit's ribs.

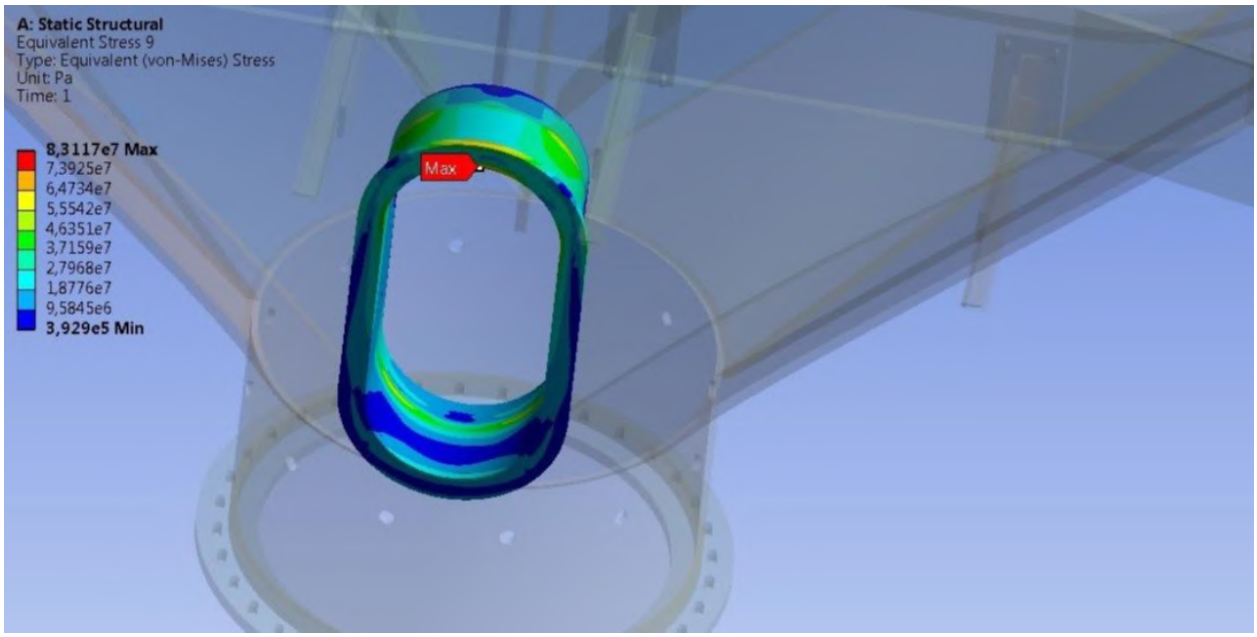

Fig. 2.28 Distribution of equivalent stresses in centering unit's lateral manhole.

The stresses in centering unit's load-bearing cover do not exceed 115.9MPa. Fig. 2.22 shows distribution of stresses in load-bearing cover. These stresses are

maxi-mal in the area of joining the centering unit's bottom conical part and the cover of the lateral manhole. The assessment of service lifespan of load-bearing elements of the bin and correctness of assessment in question is presented in Fig. 2.29-2.33.

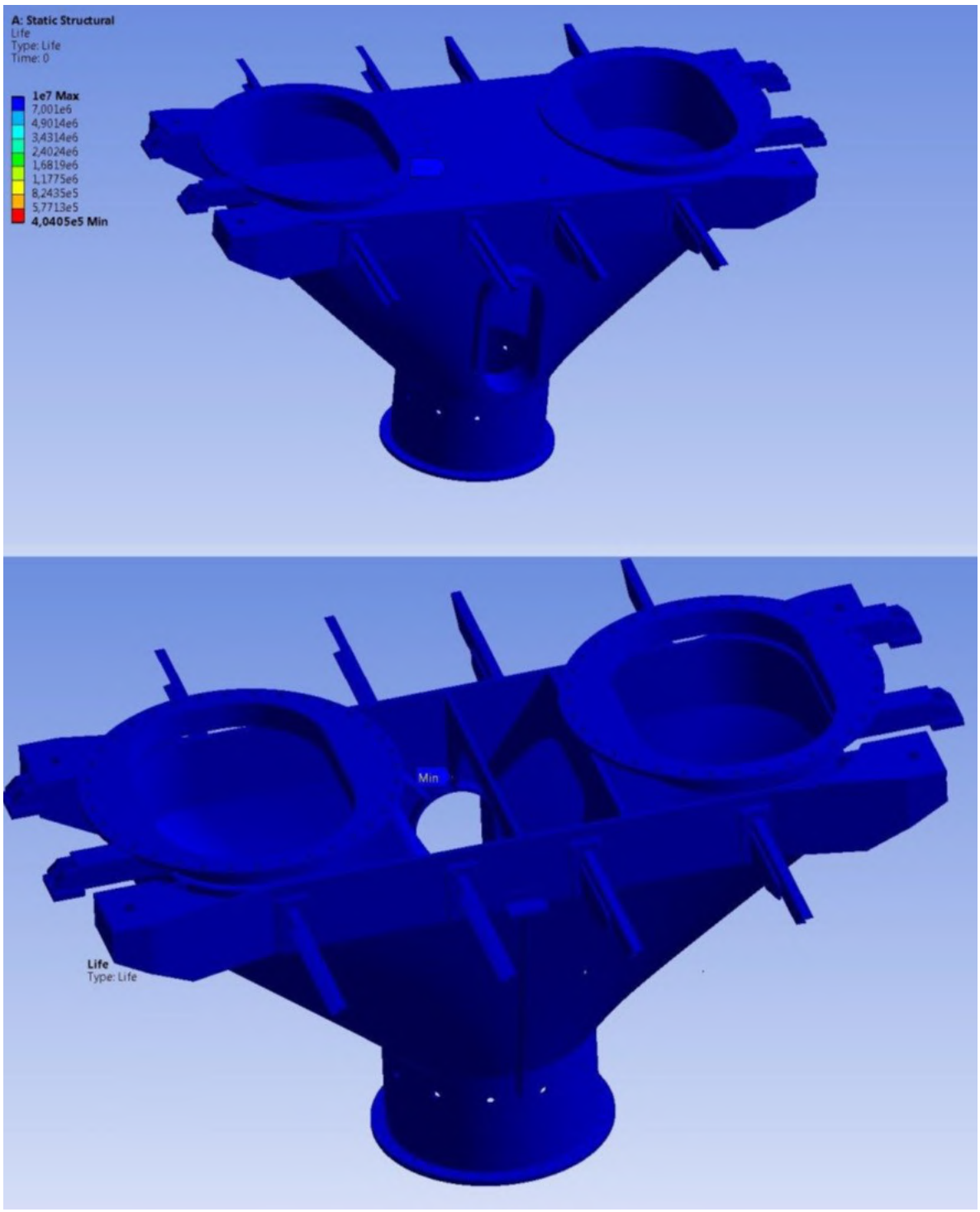

Fig. 2.29 Distribution of centering unit lifespan by Wehler SN curve.

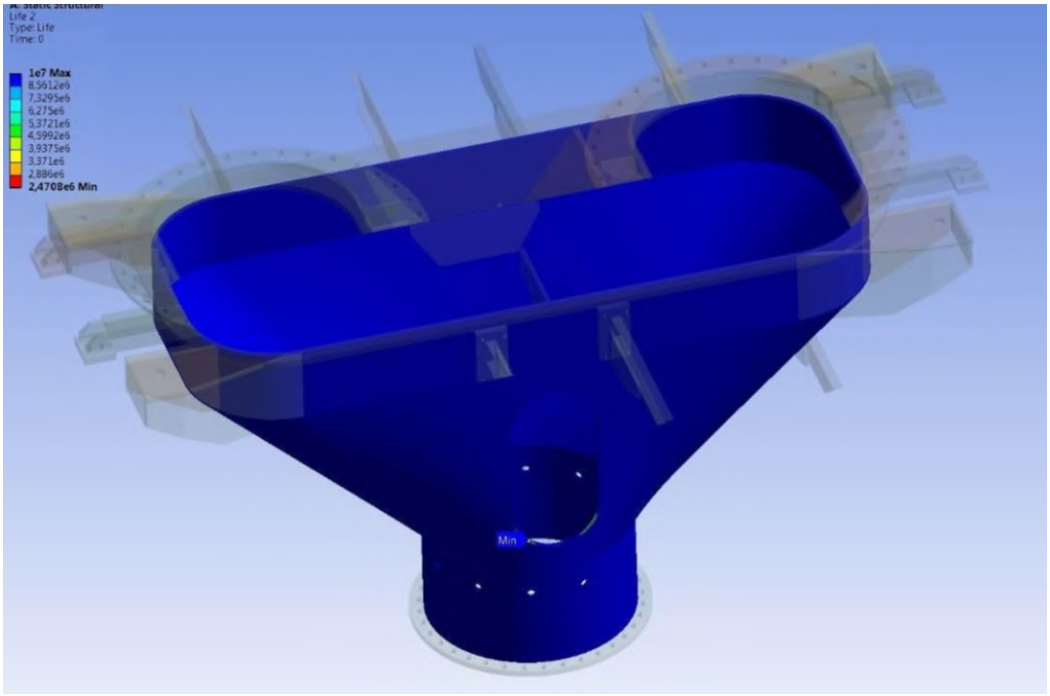

Fig. 2.30 Distribution of lifespan of centering unit's load-bearing cover.

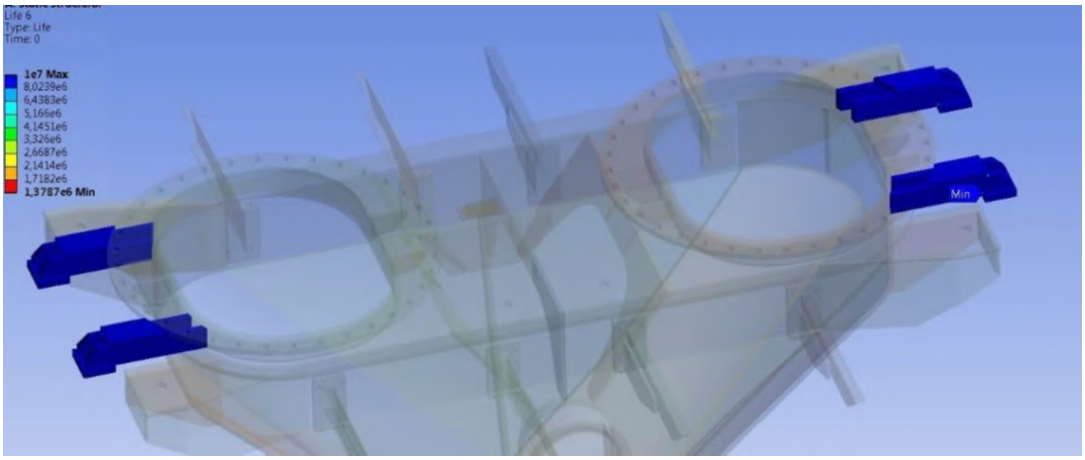

Fig. 2.31 Distribution of lifespan of centering unit's supports by Wehler SN curve.

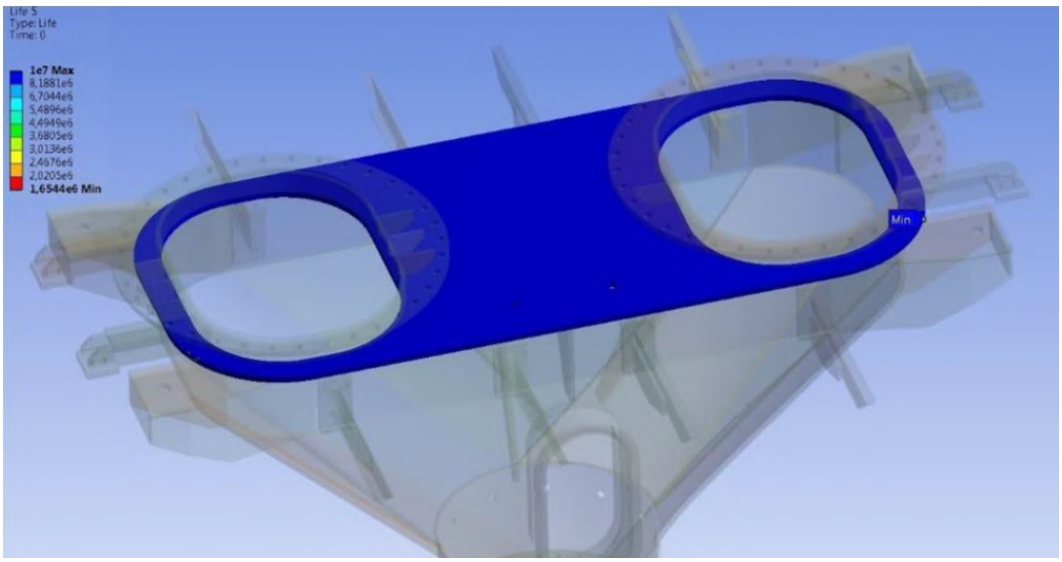

Fig. 2.32 Distribution of lifespan of centering unit's top plate.

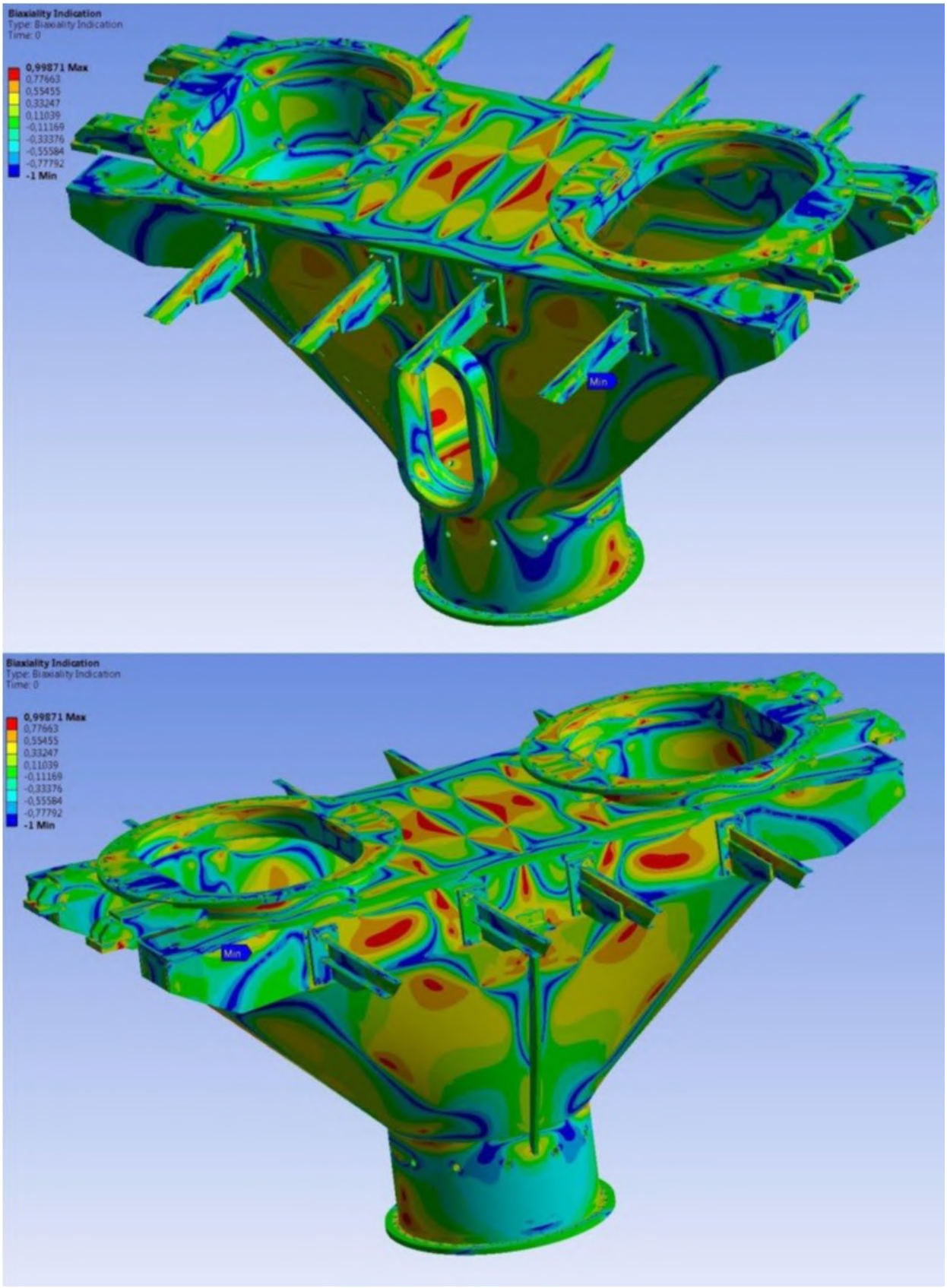

Fig. 2.33 Distribution of stress-strain nature in the bin by Wehler SN curve.

2.3.3 Structural design for seismic impact

Seismic impact calculation is performed using the response spectrum method. The initial data is the spectrum of structure's response to dynamic effect. The response spectrum is taken to mean the combination of absolute values of maximal response accelerations of linear-elastic system depending on impact frequency. The bin's response spectrum is specified with accelerograms and is presented in Tables 1.1- 1.3 paragraph 1.2.3.3 for the 47.748 m mark. To define this loading the structure's natural oscillation modes and quantity thereof shall be determined. The number of frequencies shall be determined out of the condition that the frequencies in question correspond to 90% of structure's reduced mass in accordance with the method of reduction. The values of natural oscillations and modes are determined out of structure's modal analysis.

2.3.3.1 Structure's modal analysis

Calculation results of modal analysis showed that it is sufficient to take into consideration the first 100 natural oscillation harmonics, and these are presented in Fig. 2.34.

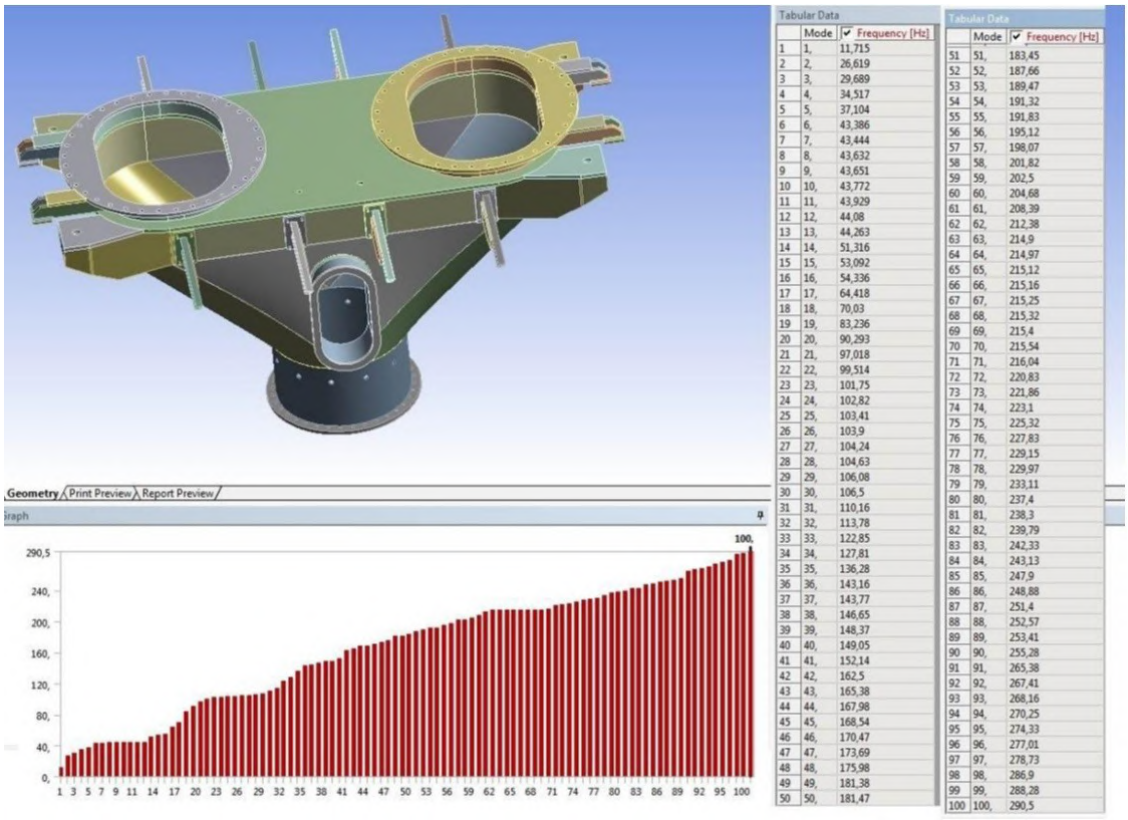

Fig. 2.34. Values of the first 100 natural oscillation frequencies of the structure.

Oscillation modes for certain natural frequencies are presented in Fig. 2.35.

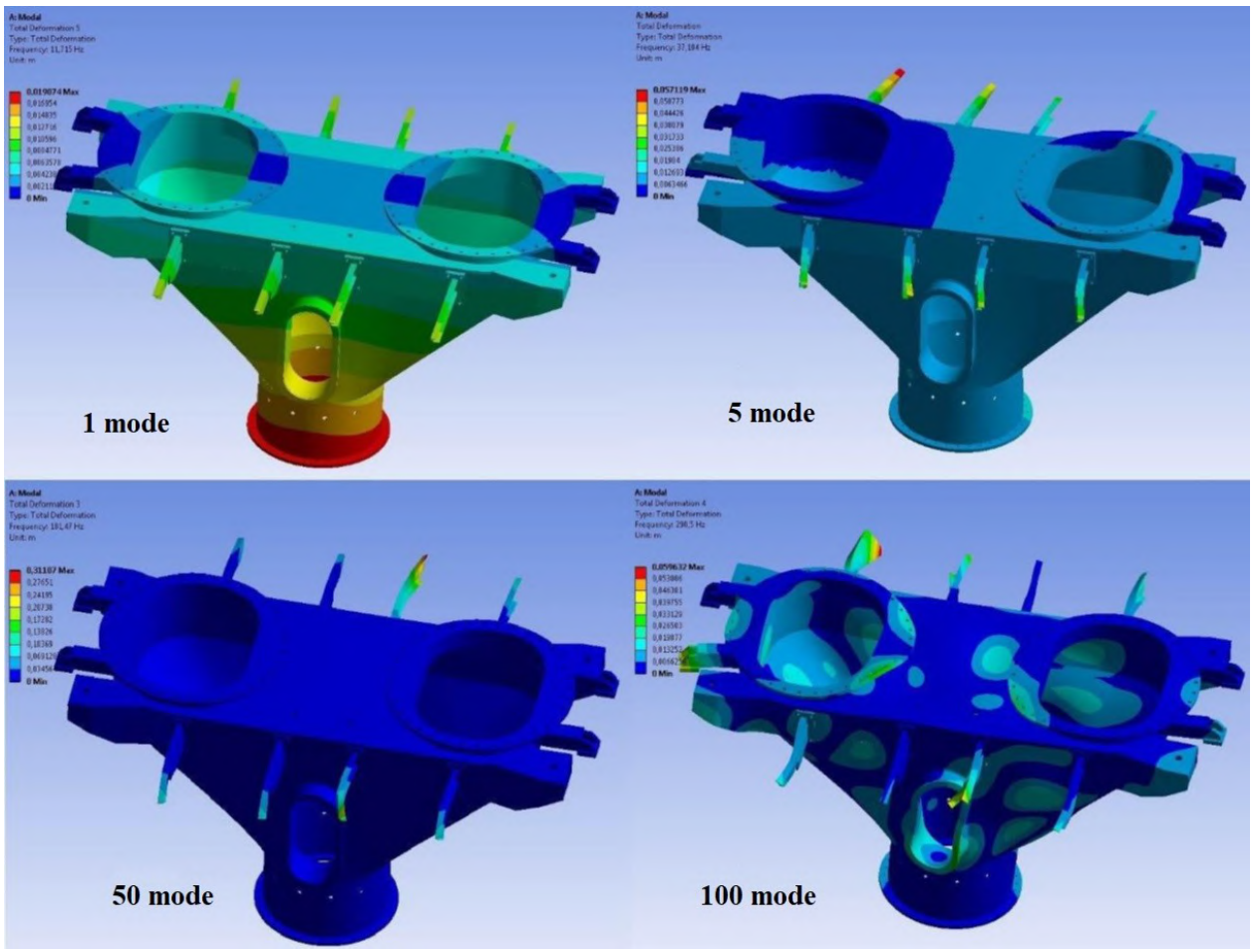

Fig. 2.35. Oscillation modes for 1, 10, 50 and 100 natural frequencies.

When carrying out the linear-spectrum analysis the calculation results are obtained using the method of square-root out of sum of squares (SRSS). According to calculation results the bin being under seismic impact shows arising of much less stresses caused by internal pressure. Field distribution of von Mises equivalent stresses is presented in Fig. 2.36. The biggest stresses arise in the area of structure's fixation, i.e. on supports. In the case under study the magnitude thereof does not exceed 10% of stresses for the case of normal service conditions. Distribution of stresses caused by seismic impact to centering unit's structural members is presented in Fig. 2.37-2.42.

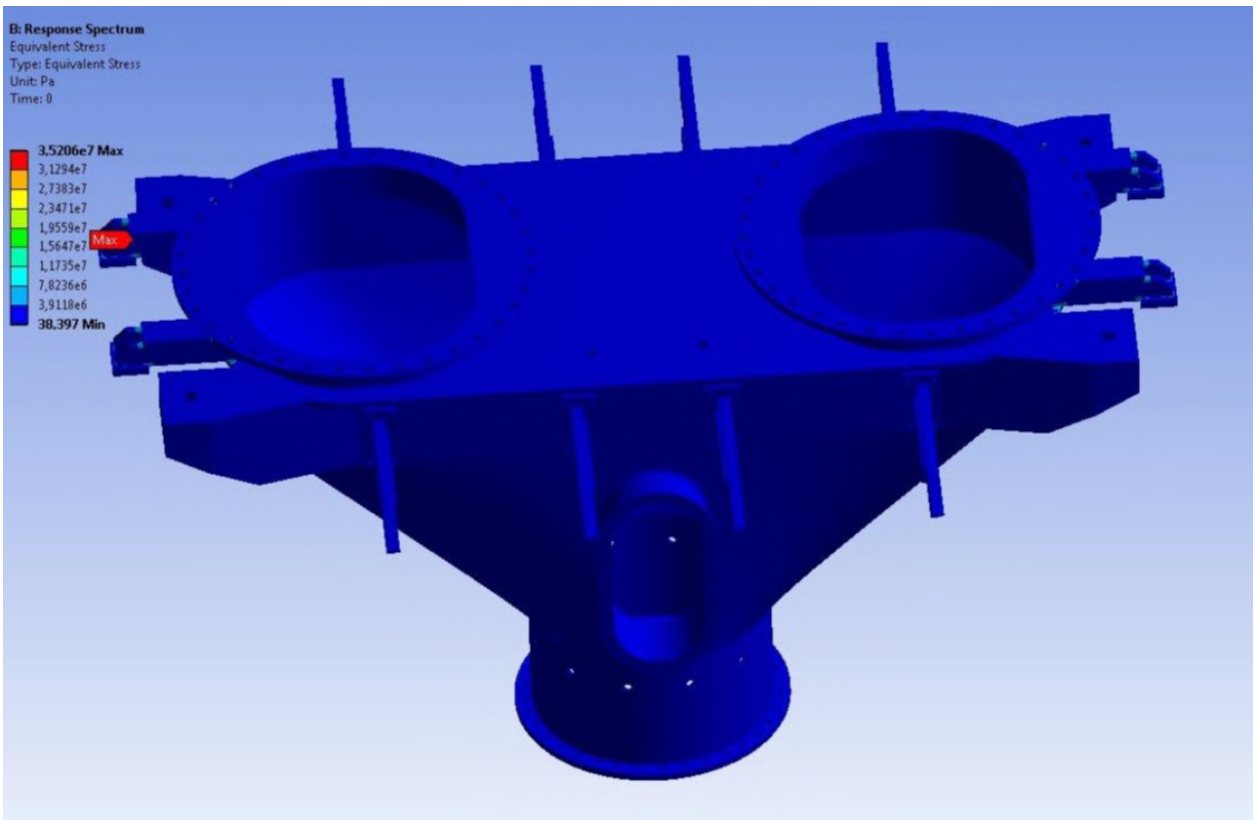

Fig. 2.36 Distribution of von Mises equivalent stresses in the bin under seismic impact.

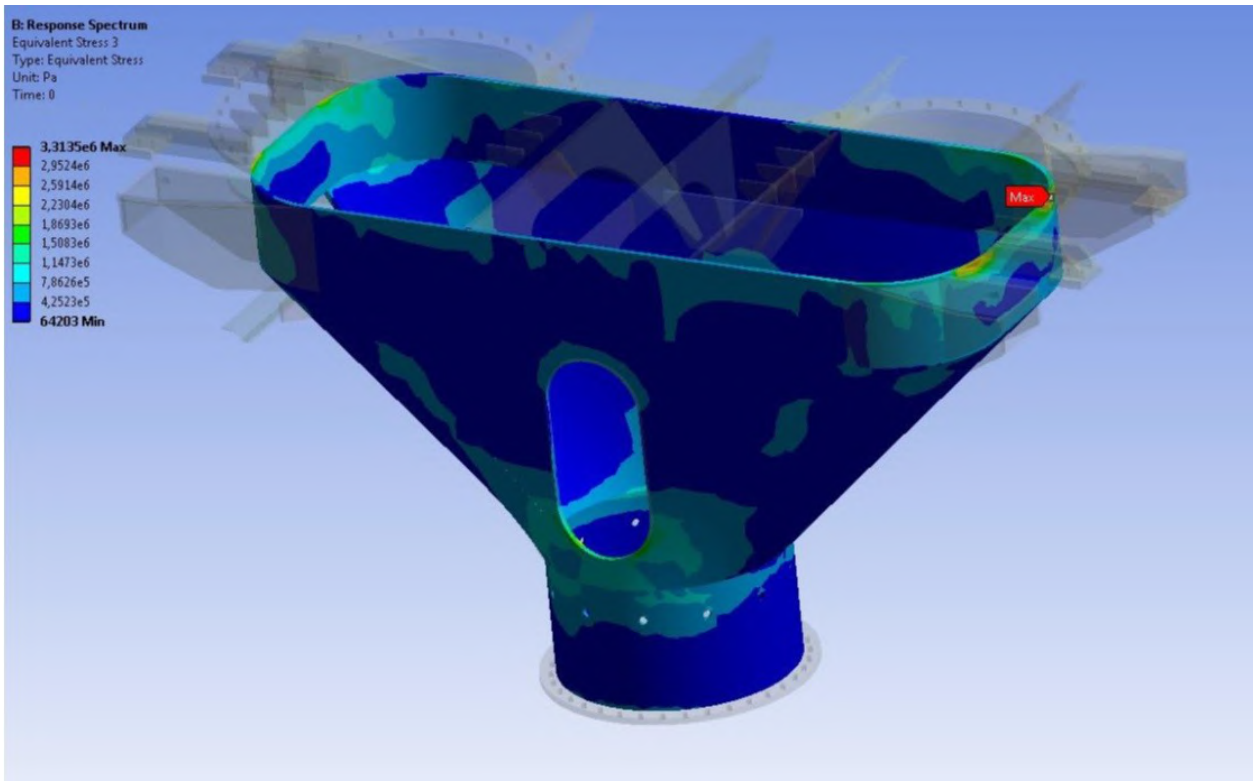

Fig. 2.37 Distribution of equivalent stresses in centering unit's load-bearing cover.

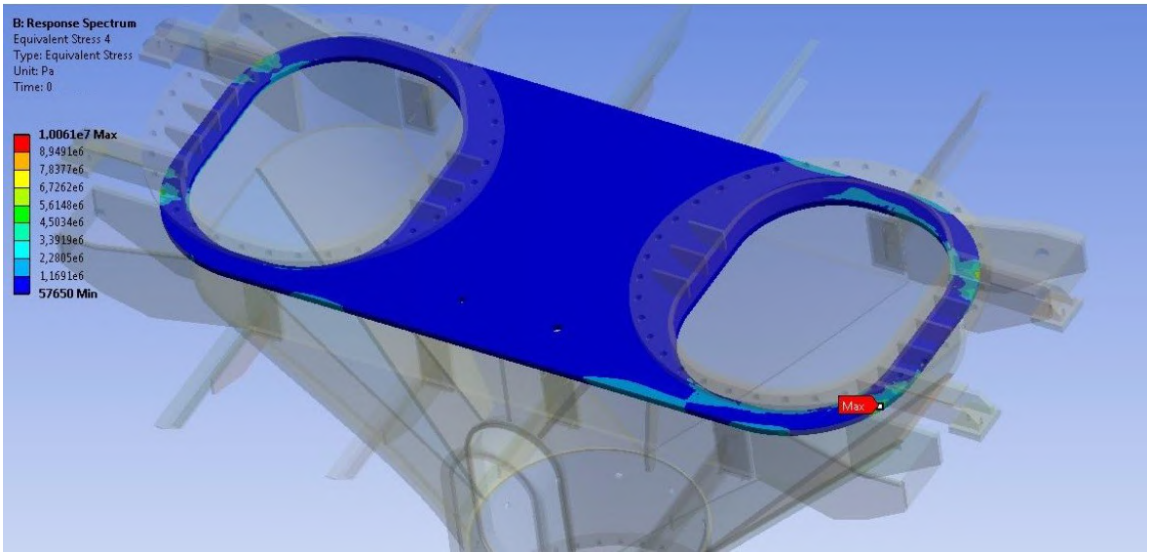

Fig. 2.38 Distribution of von Mises equivalent stresses in the top plate.

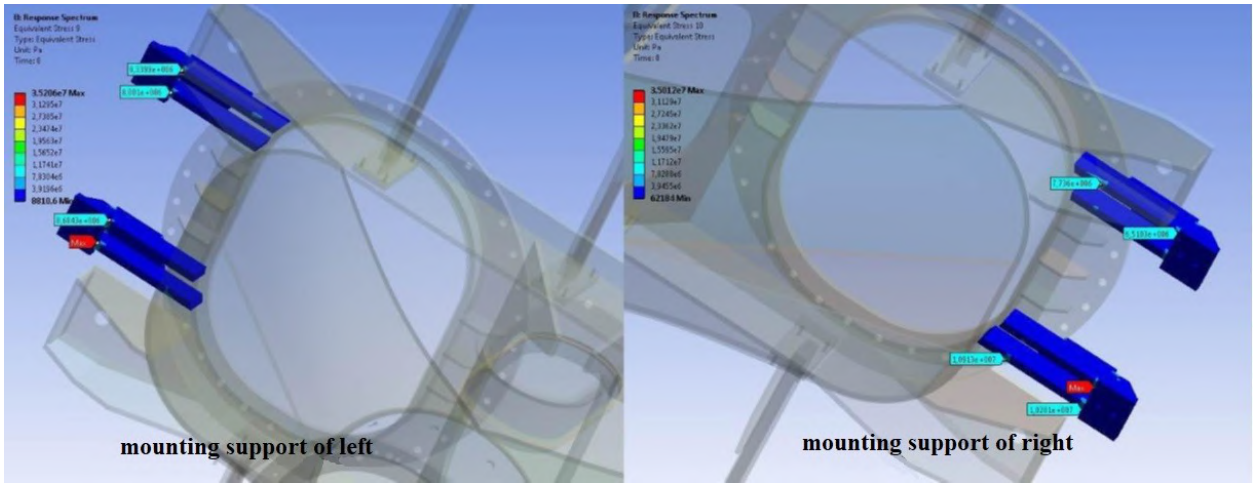

Fig. 2.39 Distribution of equivalent stresses in centering unit's support.

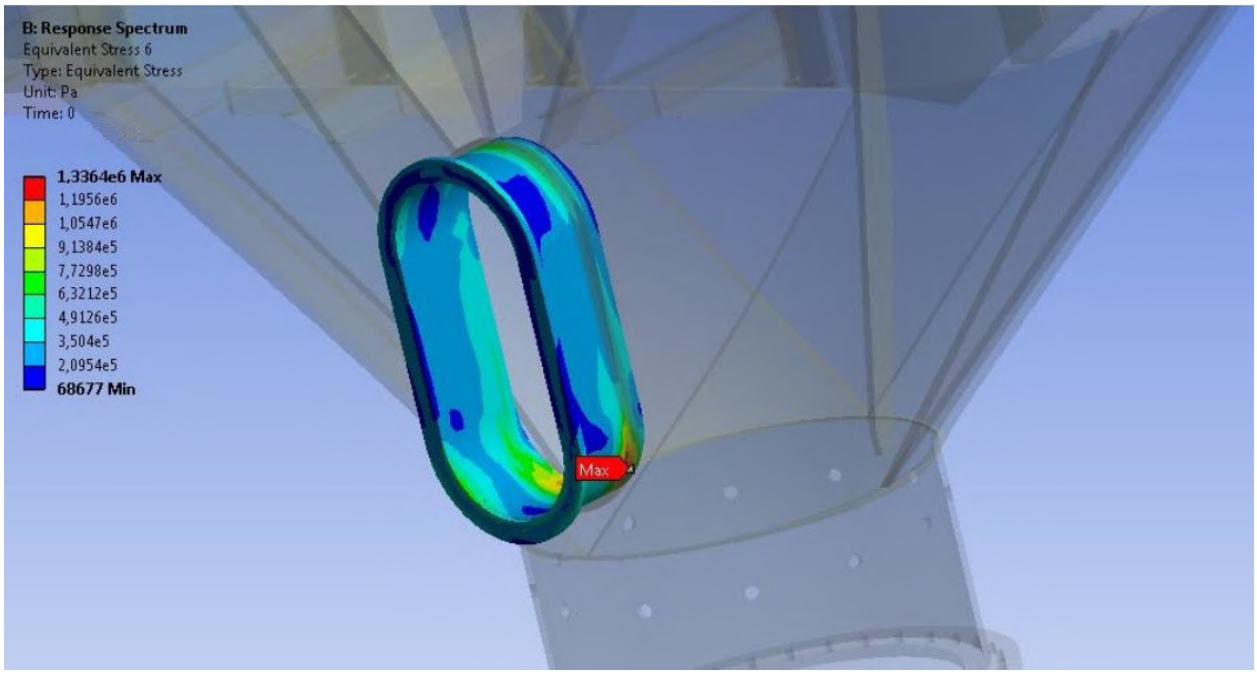

Fig. 2.40 Distribution of equivalent stresses in the lateral flange.

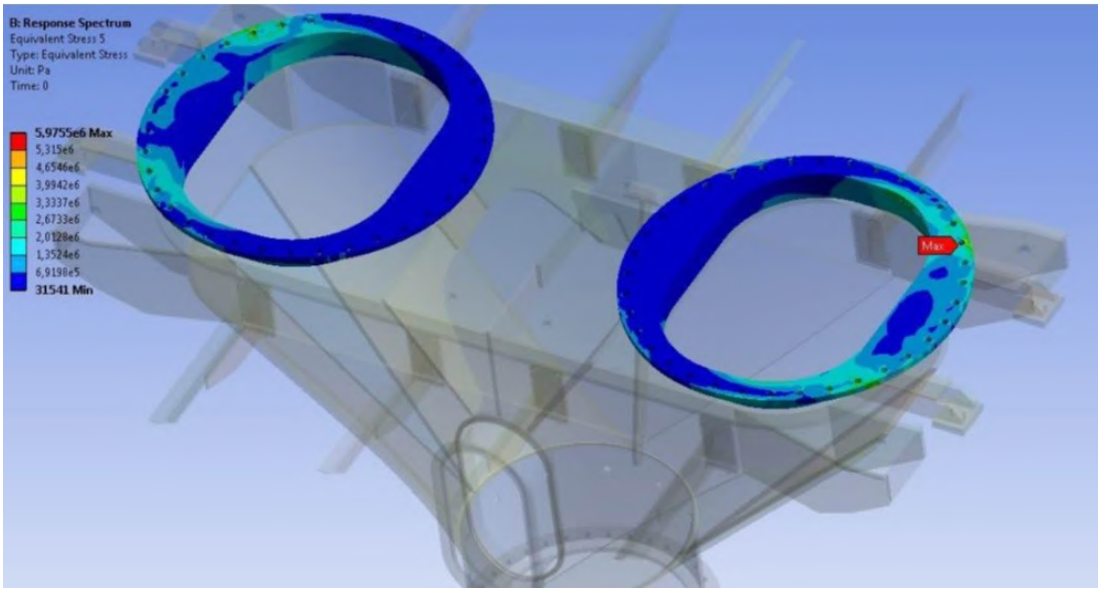

Fig. 2.41 Distribution of equivalent stresses in top flanges.

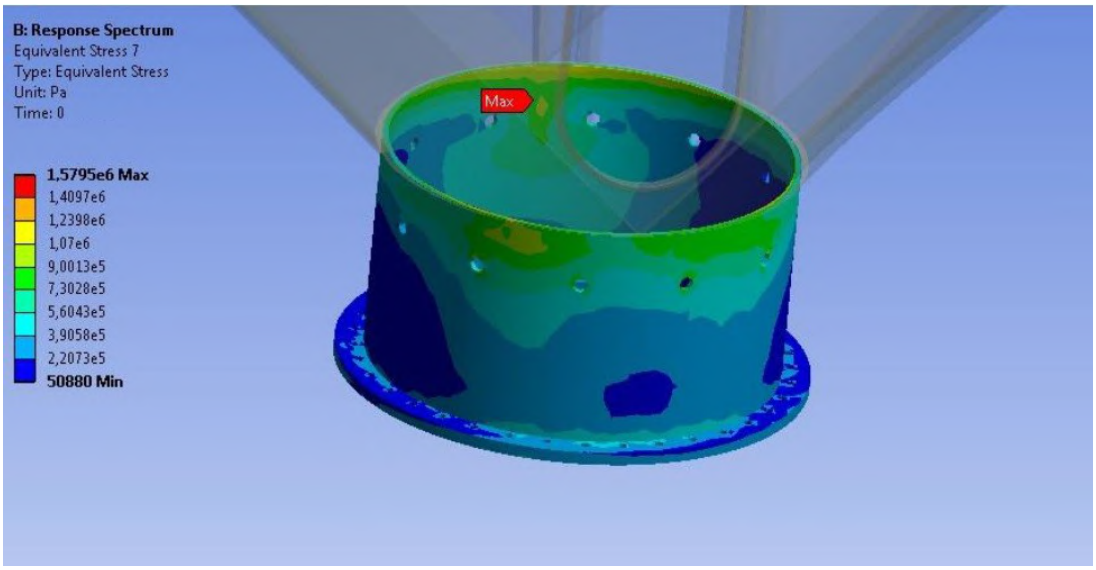

Fig. 2.42 Distribution of equivalent stresses in the bottom flange.

2.3.4 Structural design for wind effect conditions and normal service conditions

This geometry feature of structure unit's structure defines two design cases of wind effect direction. Wind effect direction is presented in Fig. 2.43.

2.3.4.1 First case of frontal wind effect direction.

Results of centering unit designing under frontal wind effect and normal service conditions are presented as patterns of stresses, strains and fatigue calculation parameters in figures 2.44-2.50. The biggest stresses in inner ribs of the centering unit. These stresses are local in nature and are within the finite element. The Fig. 2.46 shows distribution of von Mises equivalent stresses inside the

centering unit. Distribution of stresses in centering unit's structural elements is presented in Fig. 2.43-2.53.

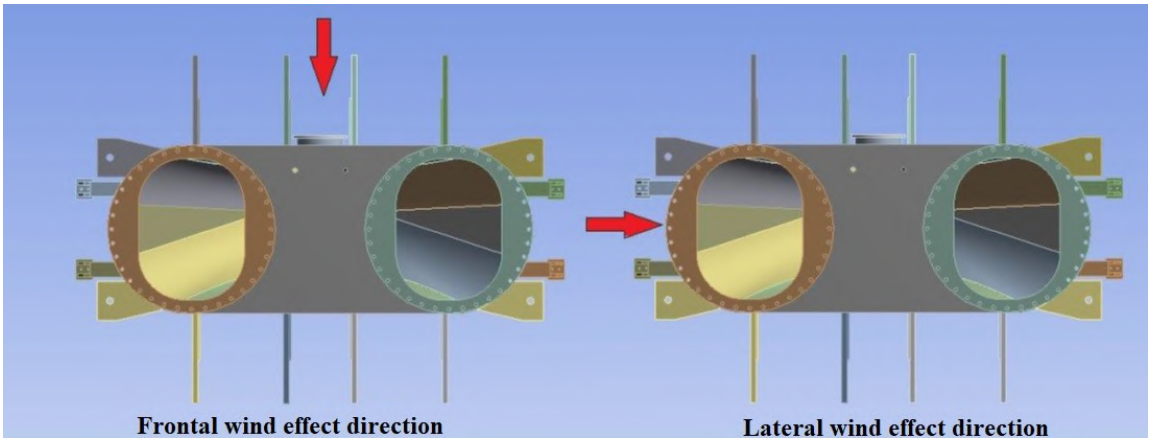

Fig. 2.43 Wind effect direction.

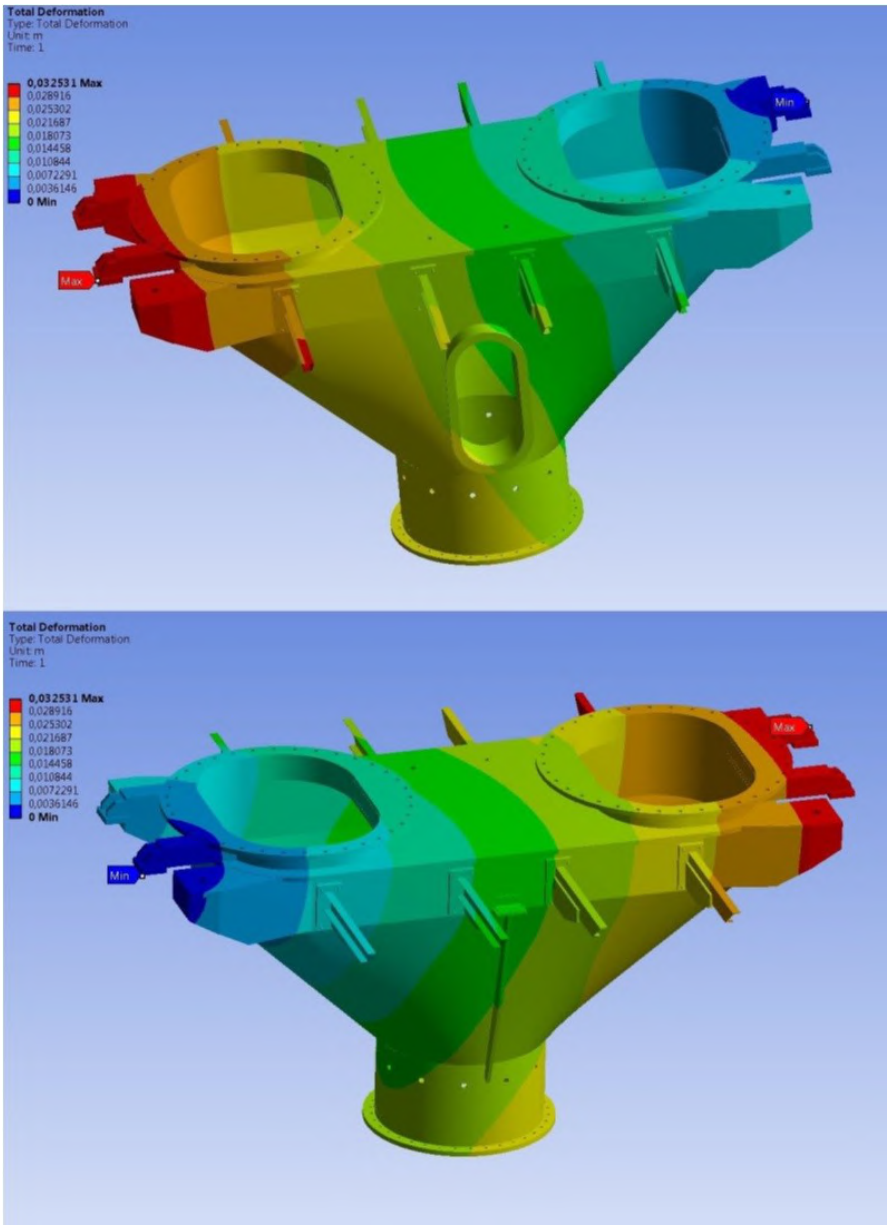

Fig. 2.44 Distribution of total strain arising in the centering unit.

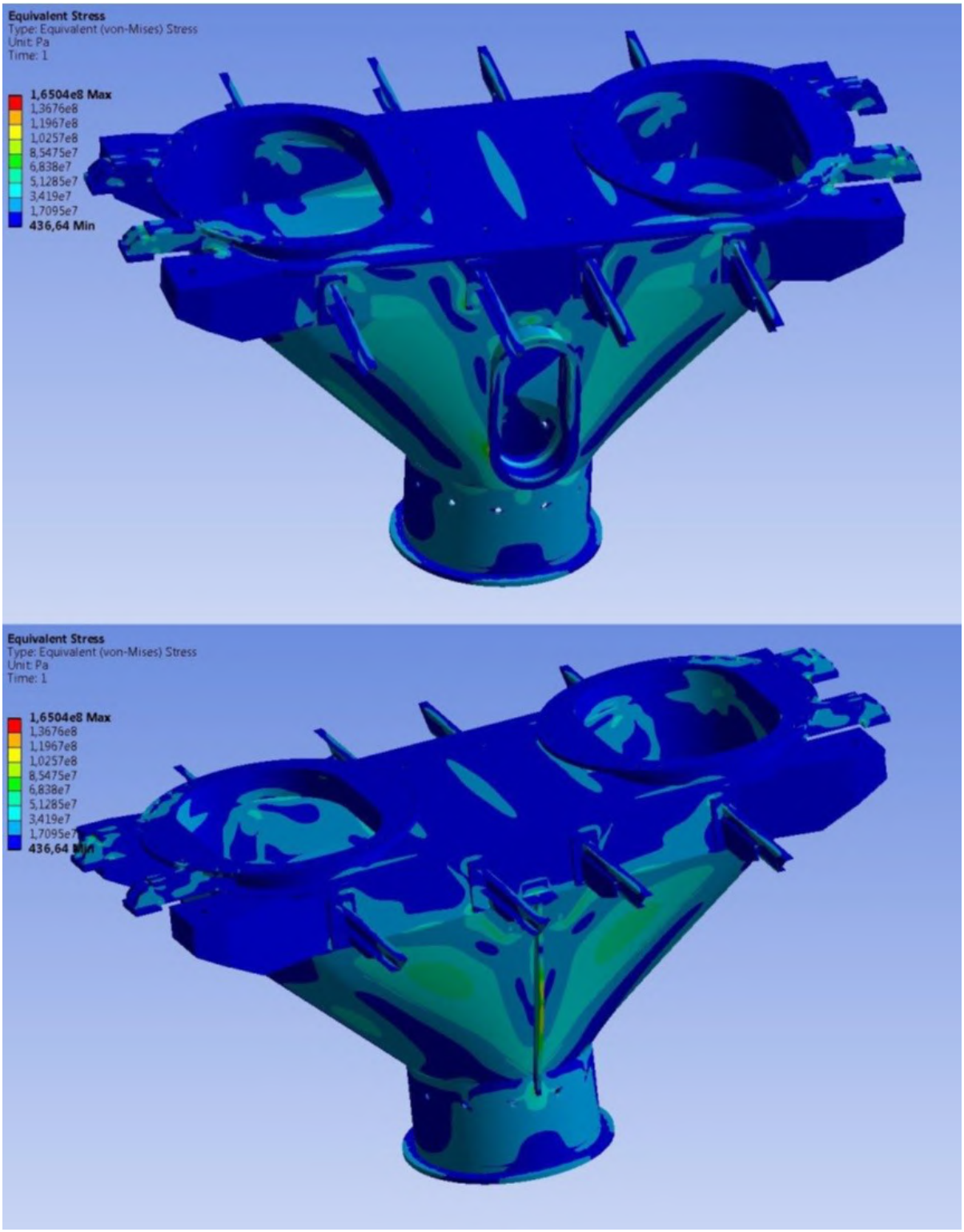

Fig. 2.45 Distribution of von Mises equivalent stresses arising in the centering unit.

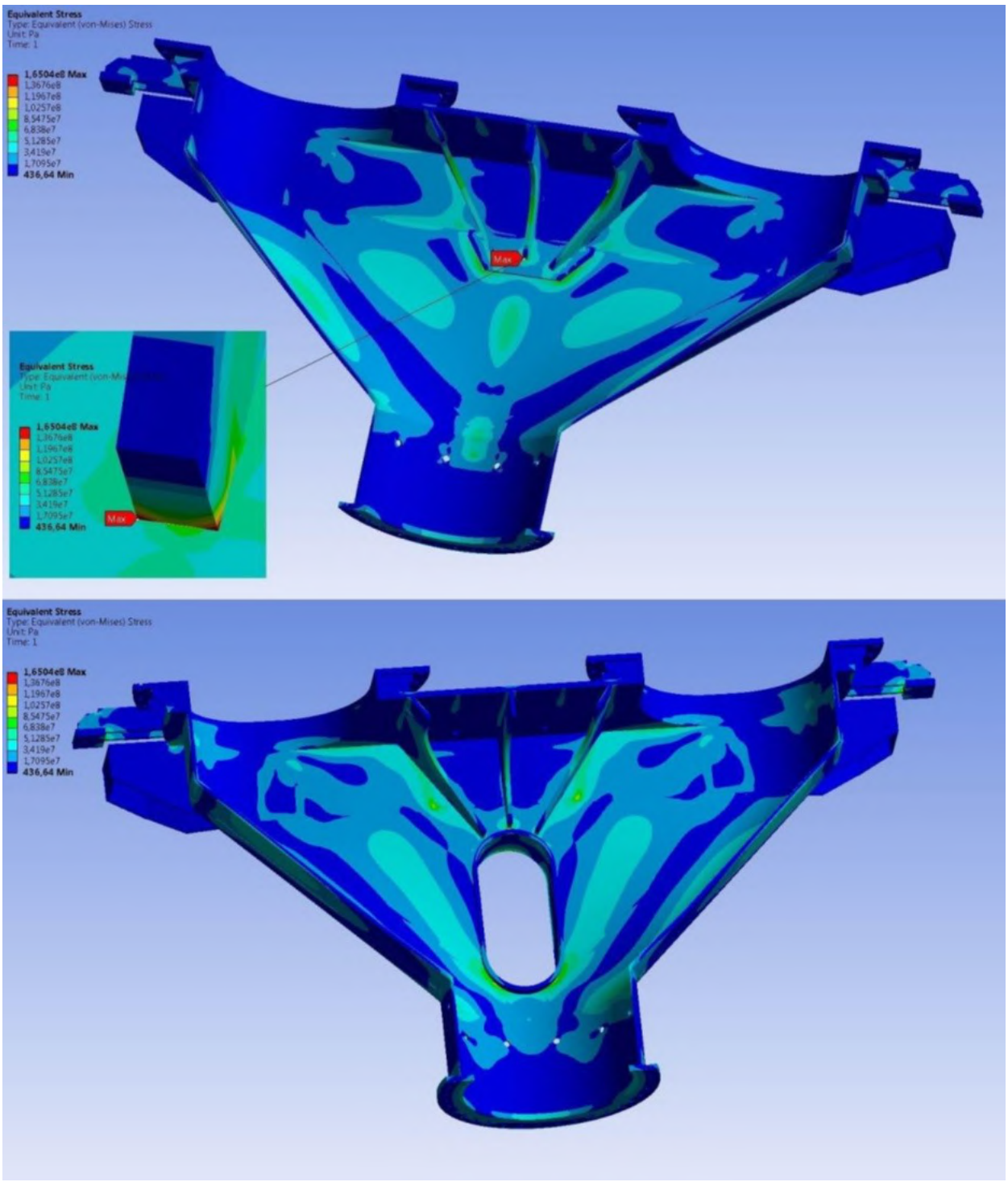

Fig. 2.46 Distribution of von Mises equivalent stresses arising in the centering unit.

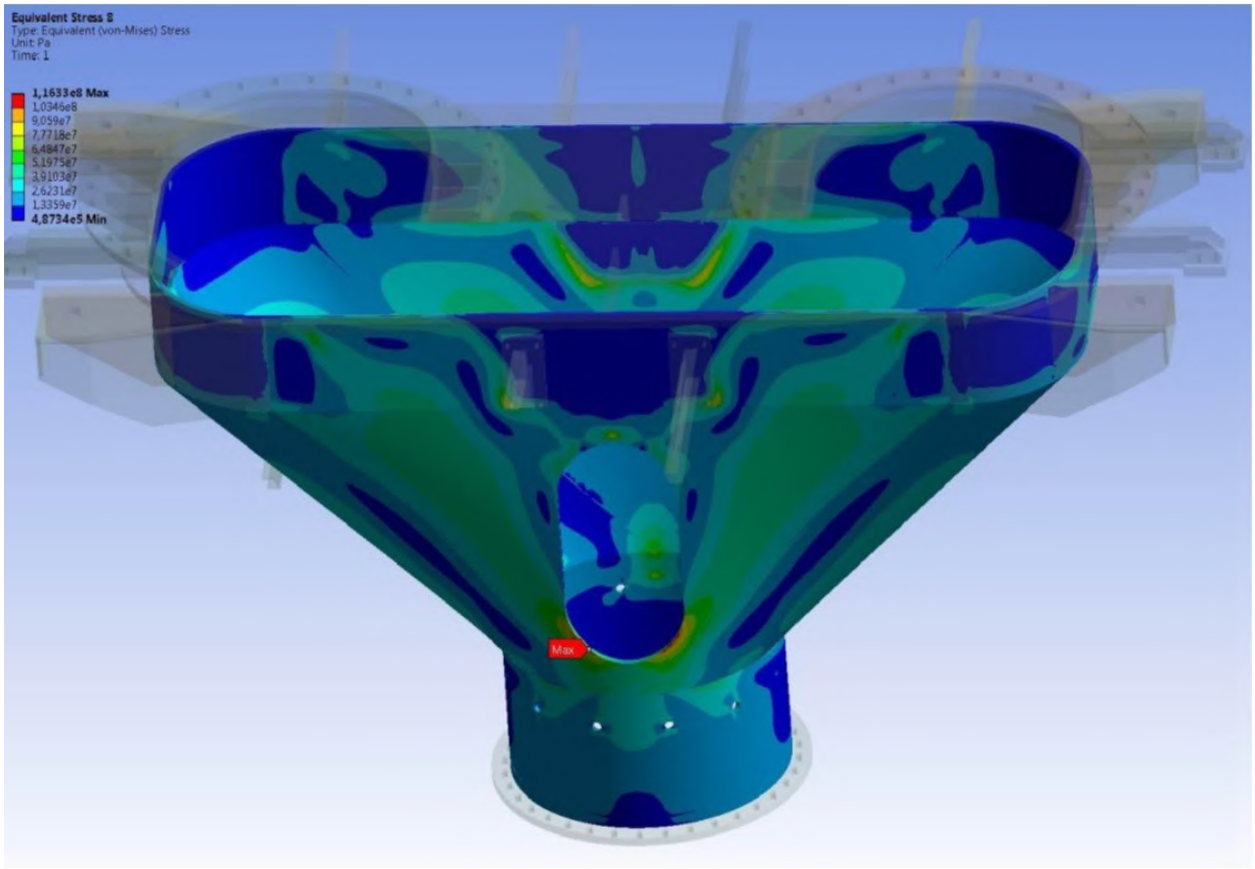

Fig. 2.47 Distribution of von Mises equivalent stresses arising in centering unit's load-bearing cover.

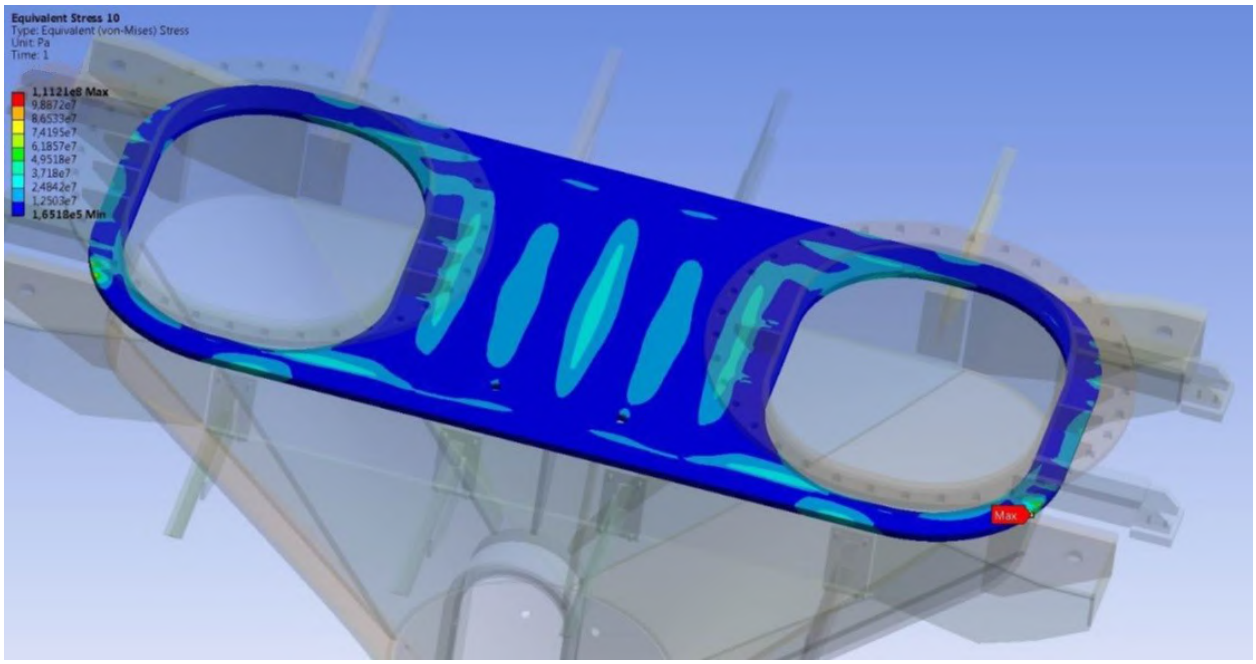

Fig. 2.48 Distribution of stresses arising in the top plate.

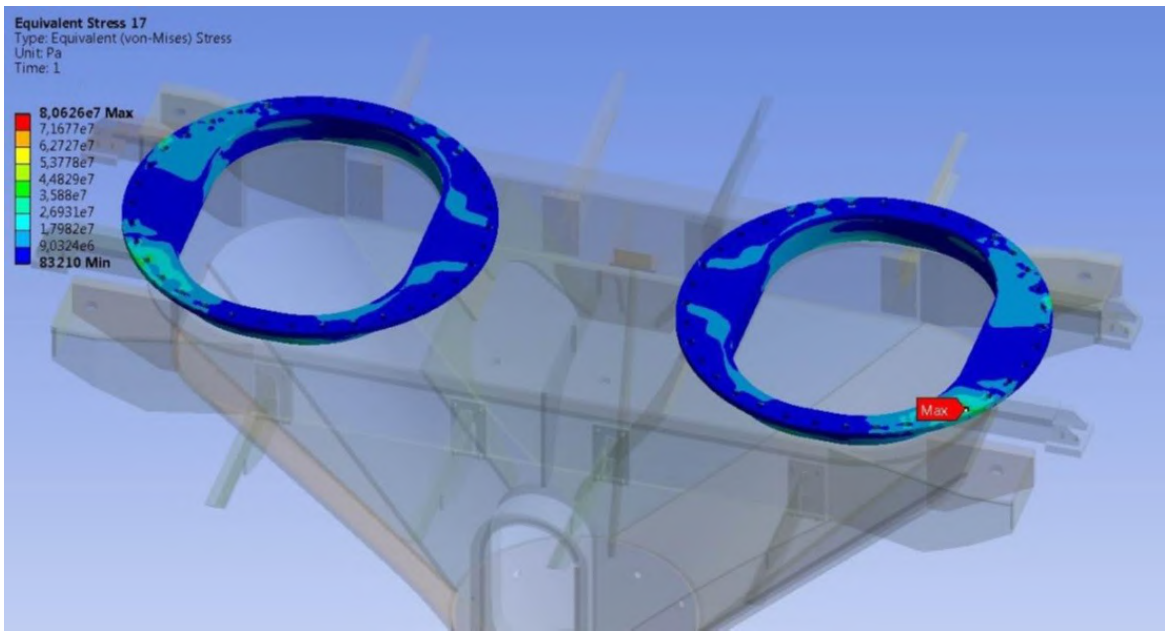

Fig. 2.49 Distribution of equivalent stresses in top flanges.

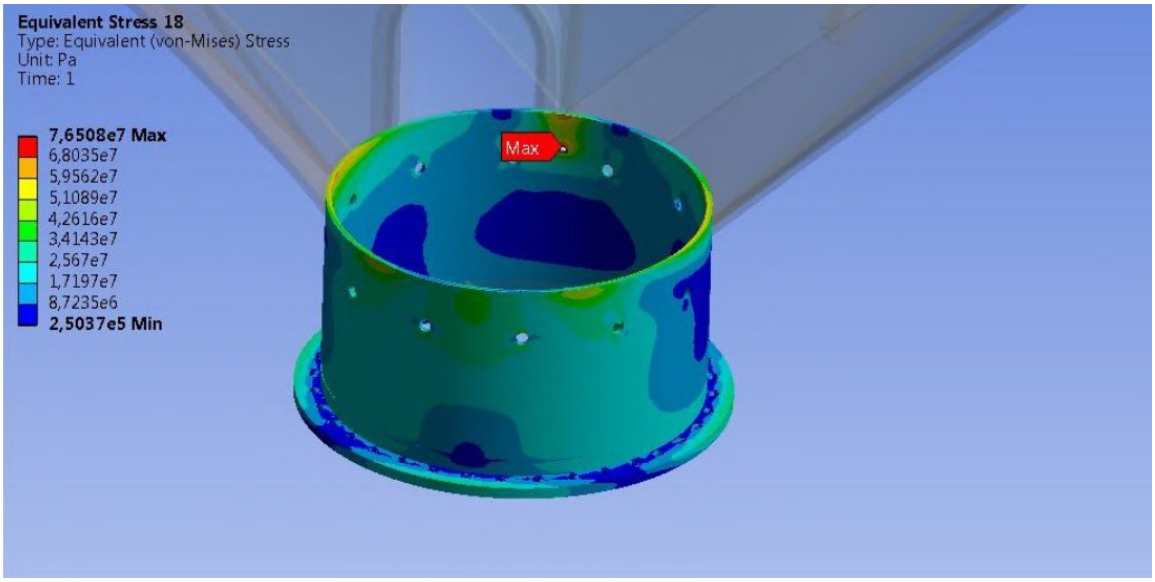

Fig. 2.50 Distribution of equivalent stresses in the bottom flange.

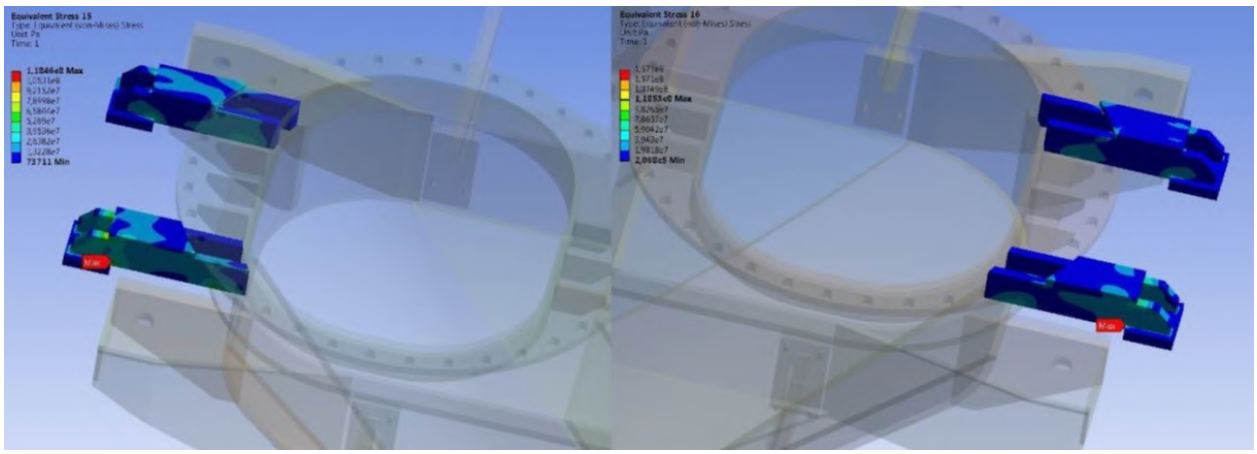

Fig. 2.51 Distribution of equivalent stresses in supports.

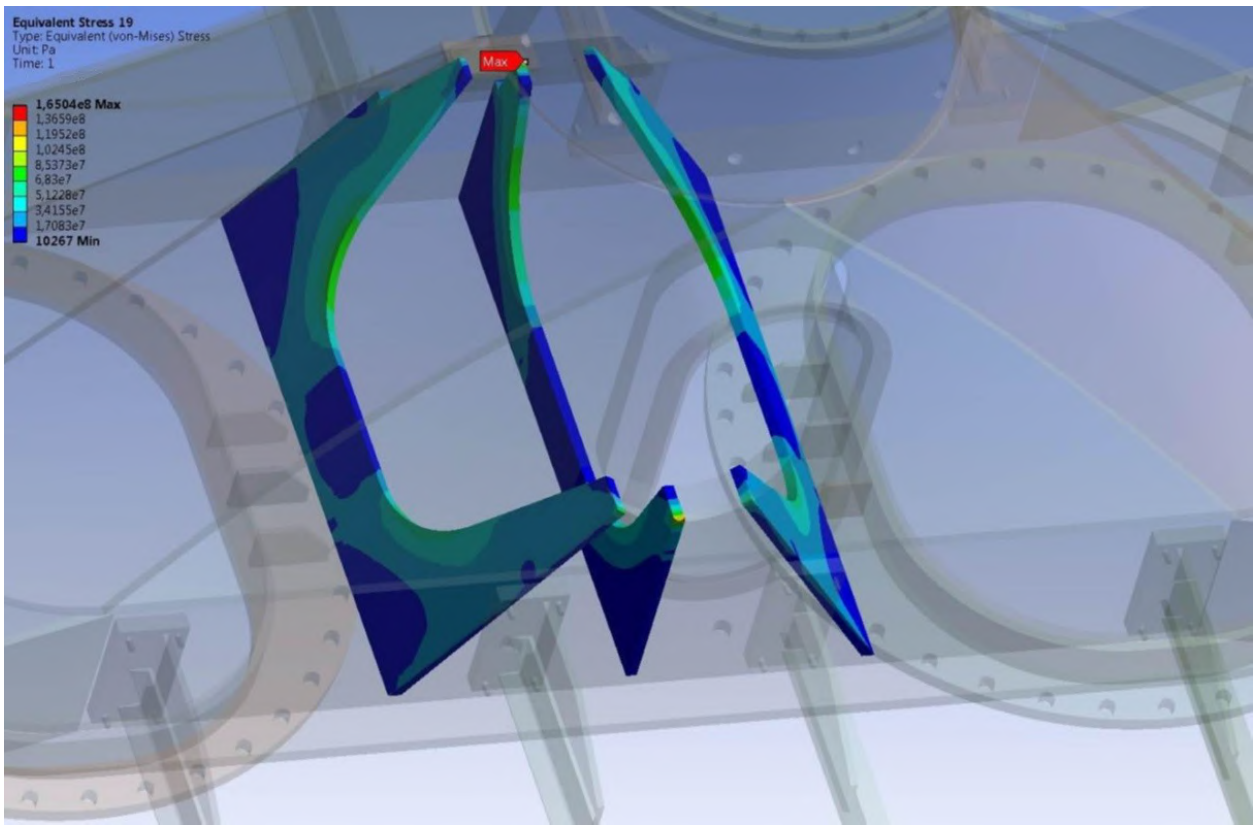

Fig. 2.52 Distribution of equivalent stresses in centering unit's ribs.

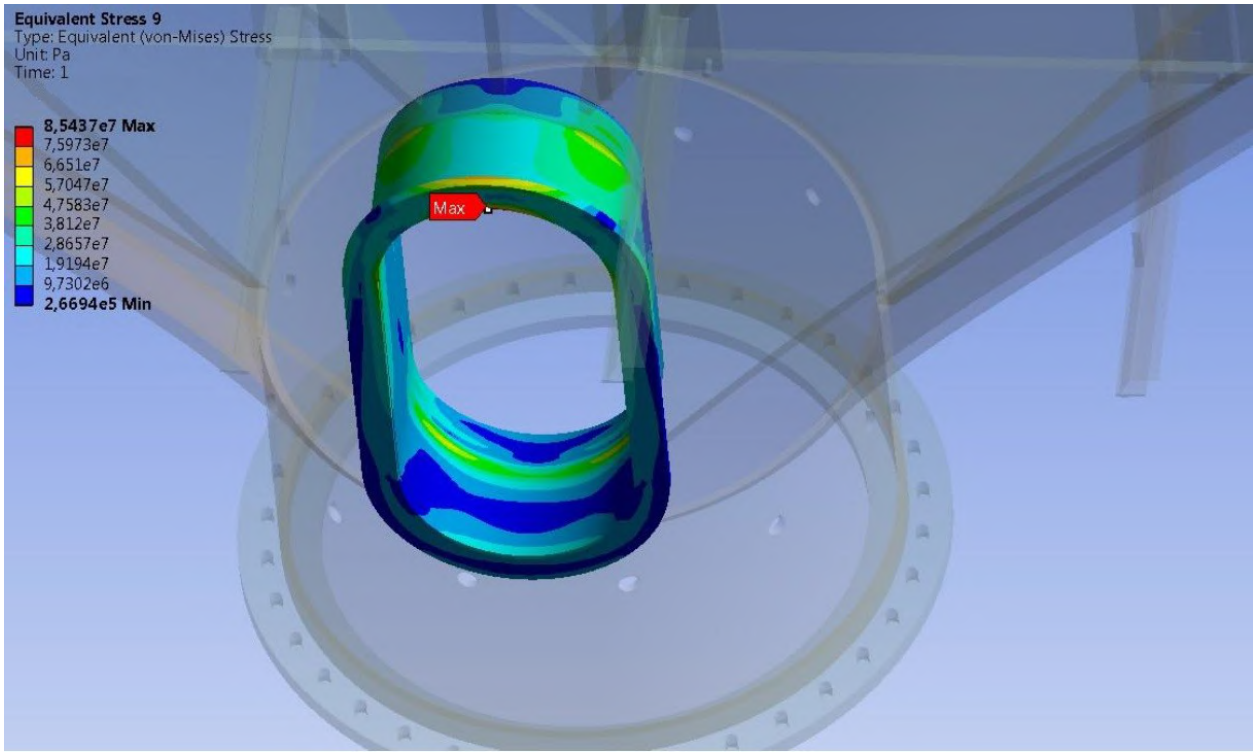

Fig. 2.53 Distribution of equivalent stresses in centering unit's lateral manhole.

The stresses in centering unit's load-bearing cover do not exceed 116.3MPa. Fig. 48 shows distribution of stresses in load-bearing cover. These stresses are maximal in the area of joining the centering unit's bottom conical part and the cover of

the lateral manhole. The assessment of service lifespan of load-bearing elements of the bin and correctness of assessment in question is presented in Fig. 2.54-2.59.

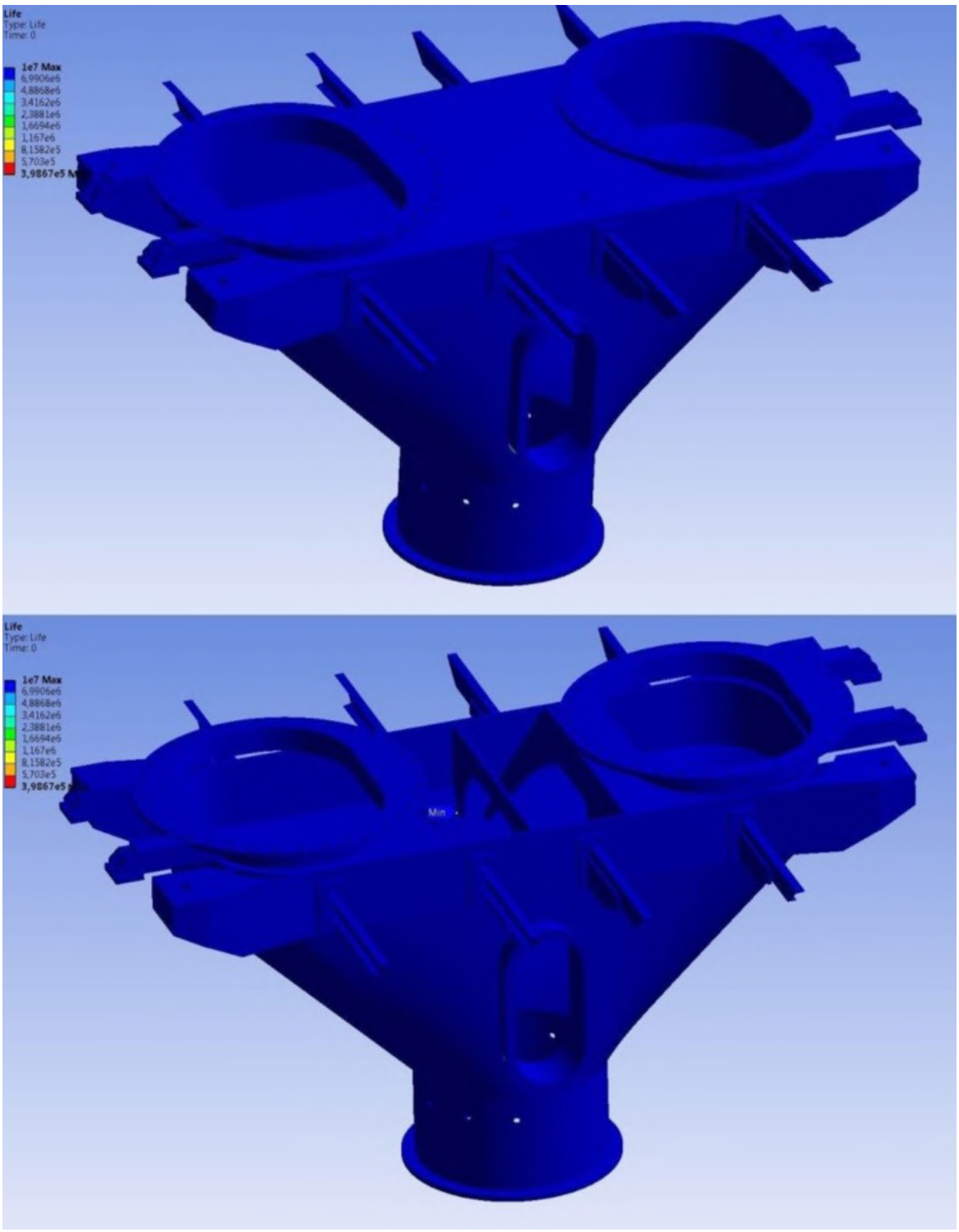

Fig. 2.54 Distribution of centering unit lifespan by Wehler SN curve.

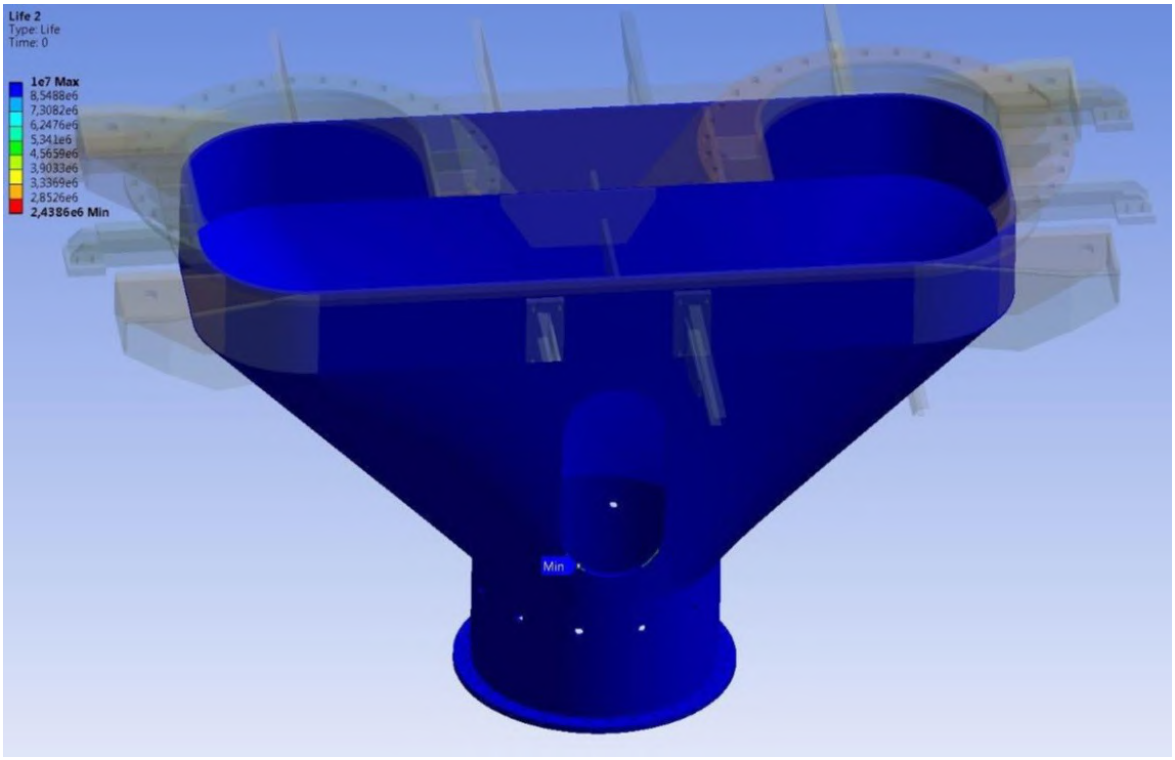

Fig. 2.55 Distribution of lifespan of centering unit's load-bearing cover.

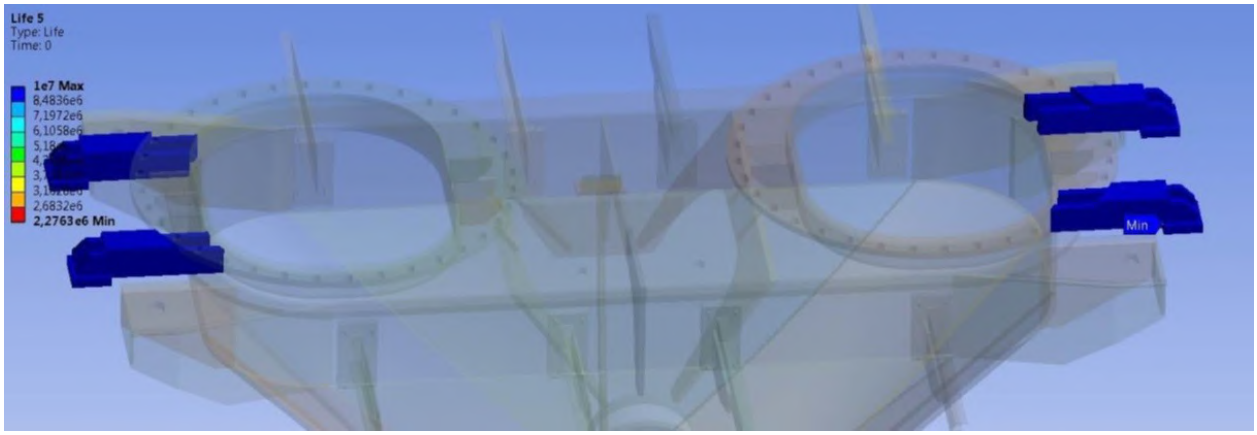

Fig. 2.56 Distribution of lifespan of centering unit's supports by Wehler SN curve.

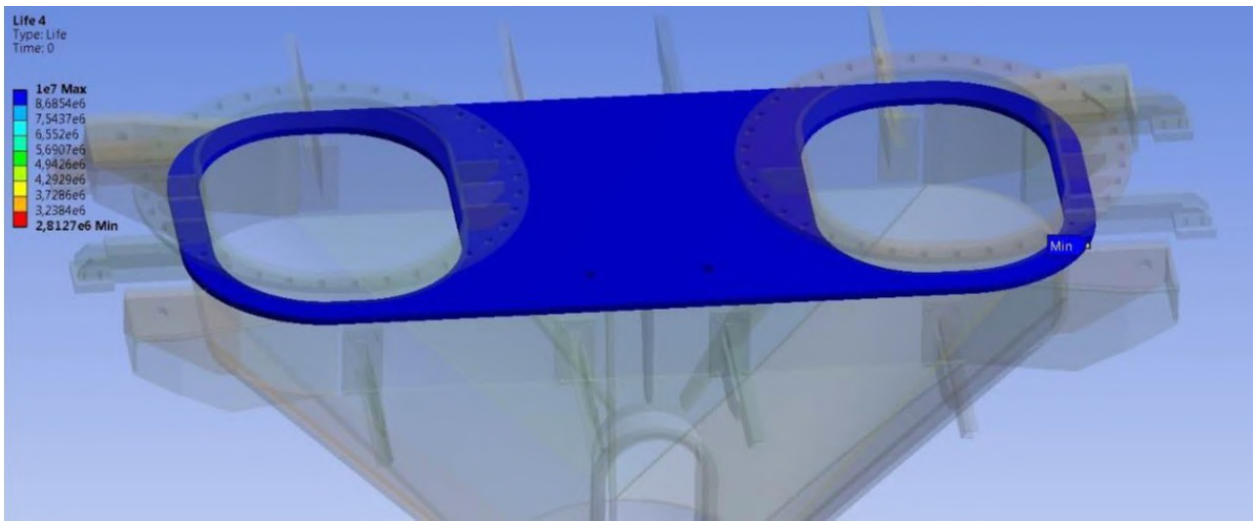

Fig. 2.57 Distribution of lifespan of centering unit's top plate.

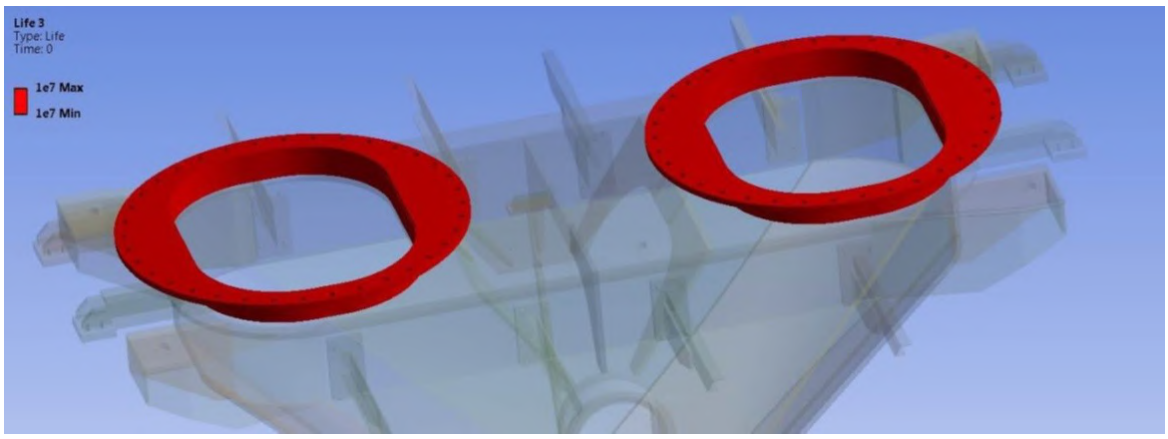

Fig. 2.58 Distribution of lifespan of centering unit's top flanges.

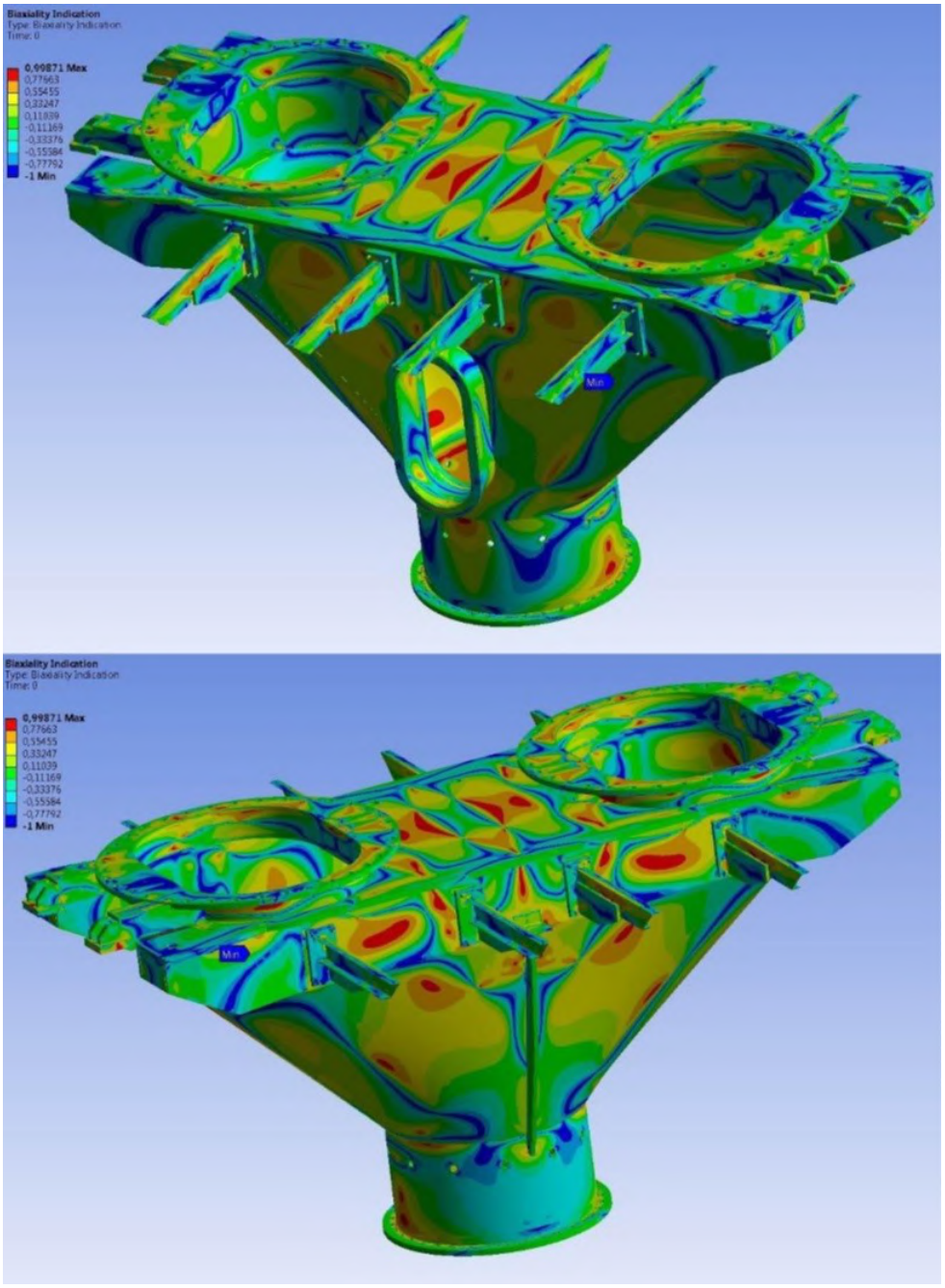

Fig. 2.59 Distribution of stress-state nature in the bin by Wehler SN curve.

2.3.4.2 Second case of lateral wind effect direction.

Results of bin designing under wind effect and normal service conditions for the second case of wind direction are presented as patterns of stresses, strains and fatigue calculation parameters in figures 2.60-2.61.

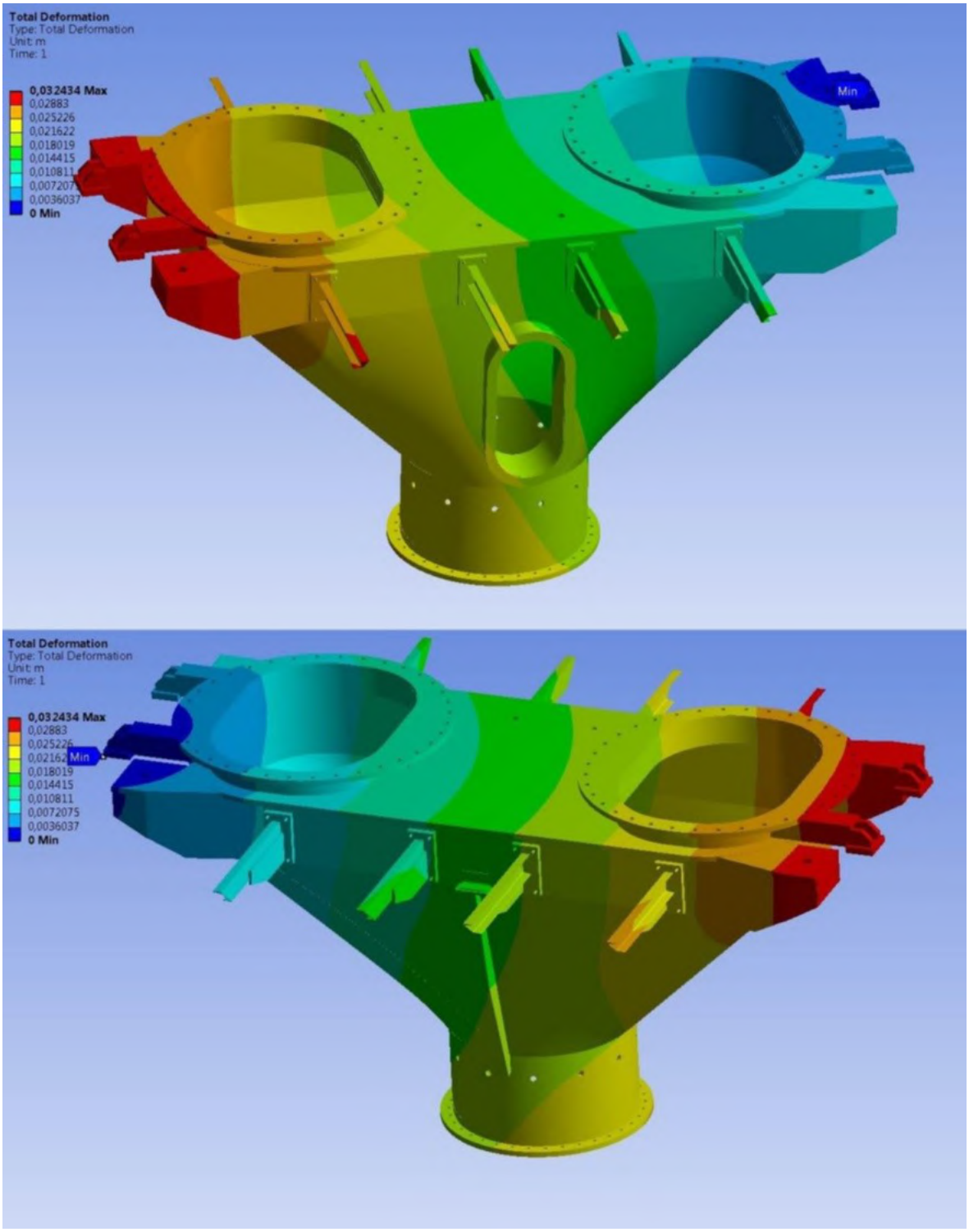

Fig. 2.60 Distribution of total strain arising in the bin.

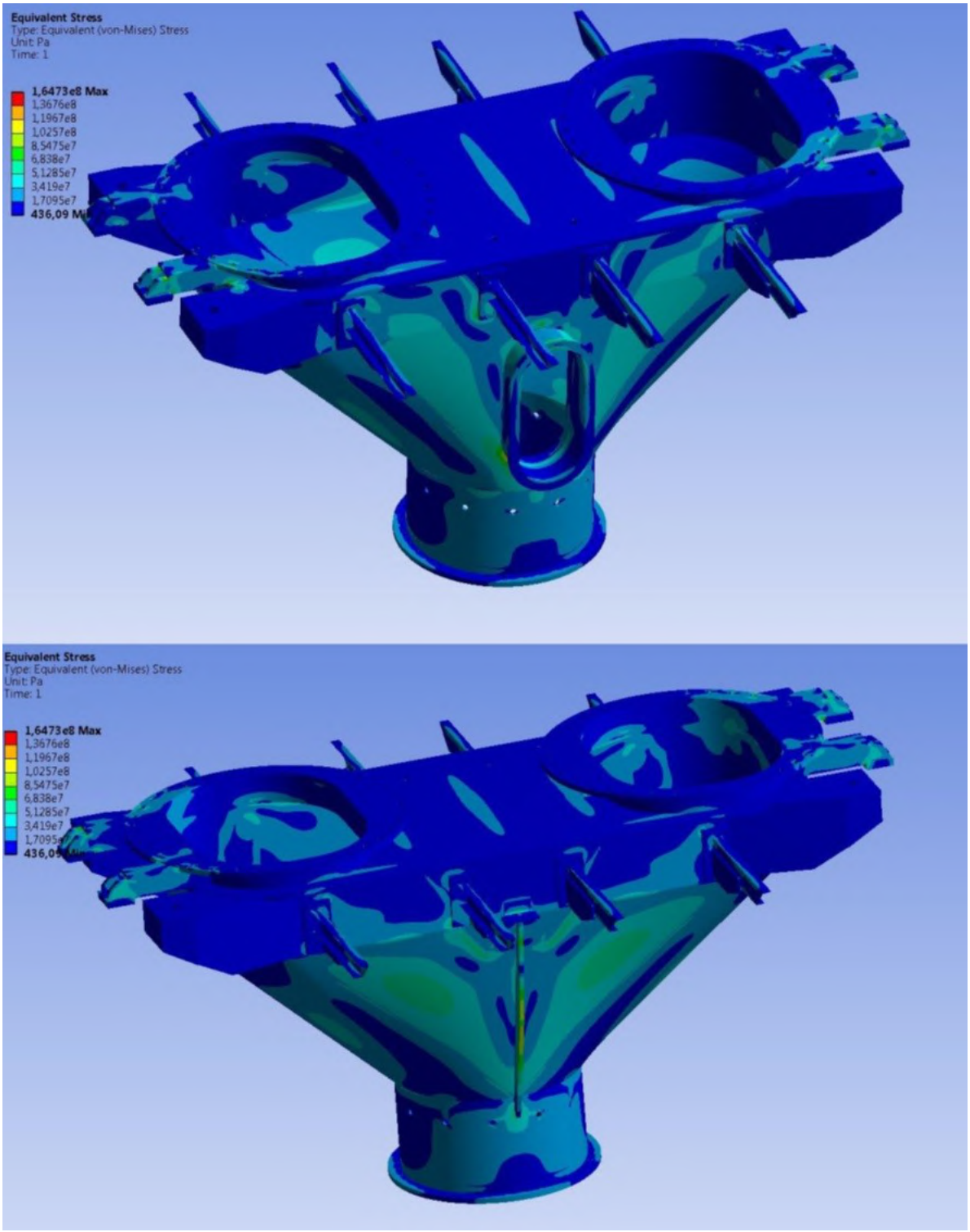

Fig. 2.61 Distribution of von Mises equivalent stresses arising in the structure.

The biggest stresses arise in inner ribs of the centering unit. These stresses are local in nature and are within the finite element. The Fig. 2.62 shows distribution of von Mises equivalent stresses inside the centering unit.

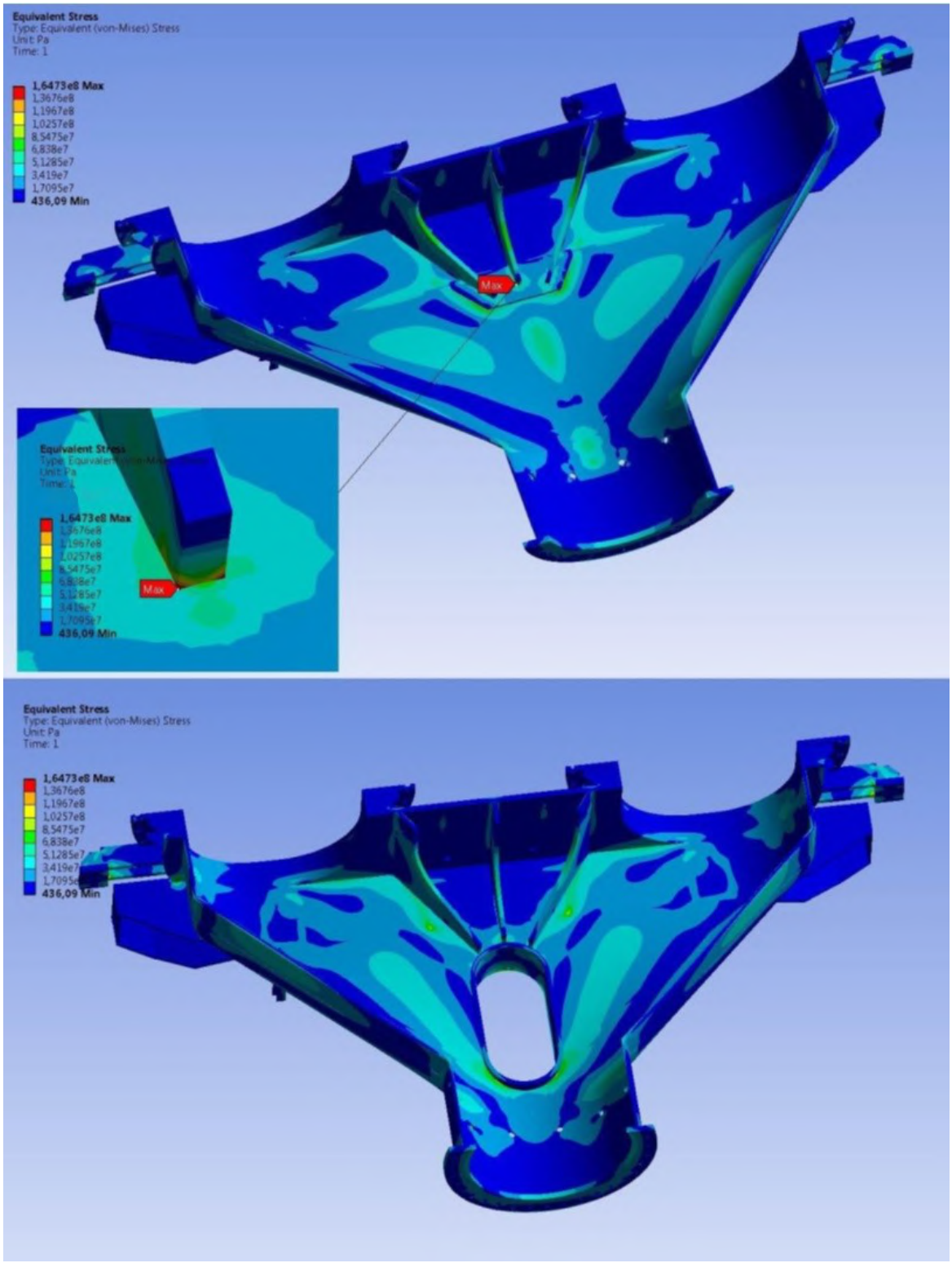

Fig. 2.62 Distribution of stresses arising inside the structure.

Distribution of stresses in centering unit's structural members is presented in Fig. 2.63-2.69.

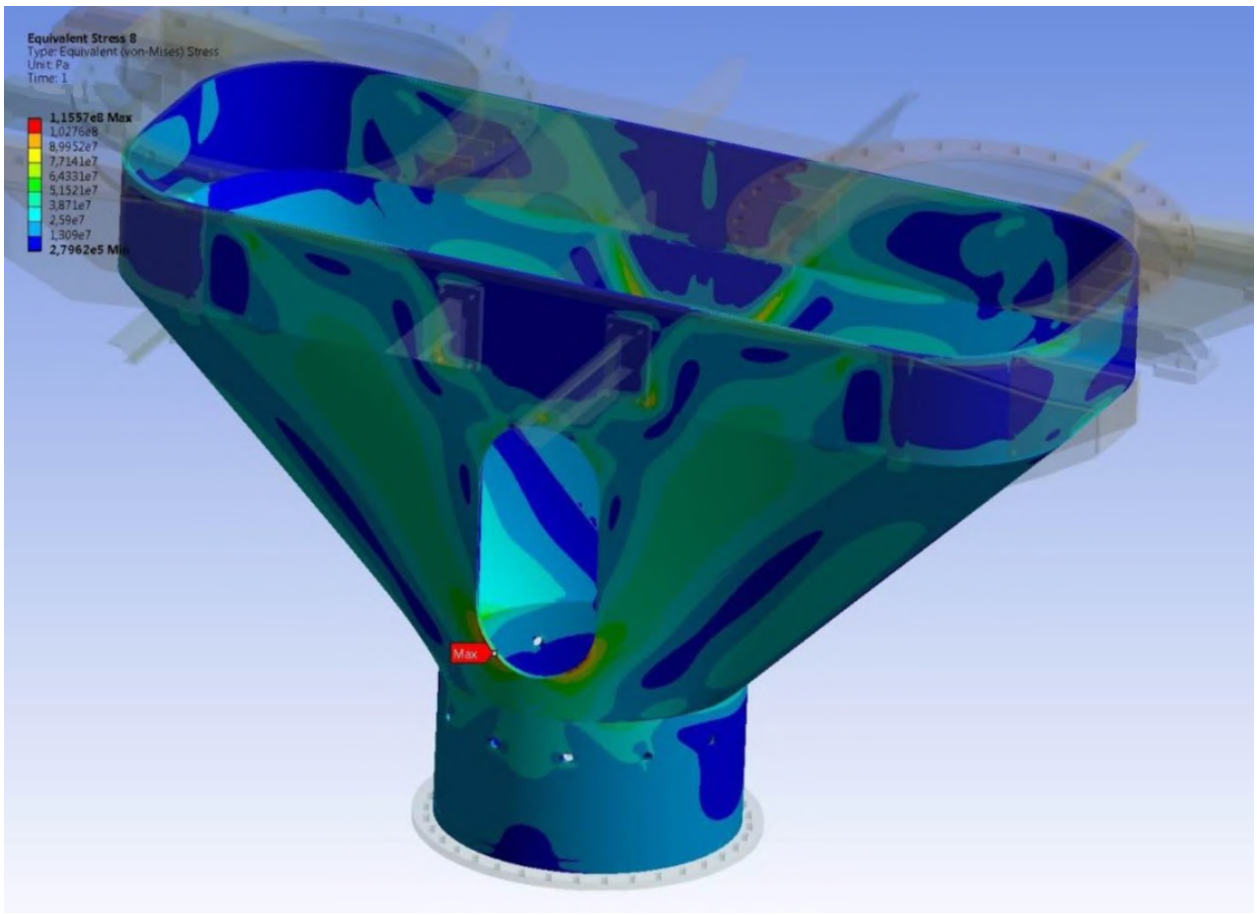

Fig. 2.63 Distribution of stresses arising in the load-bearing cover.

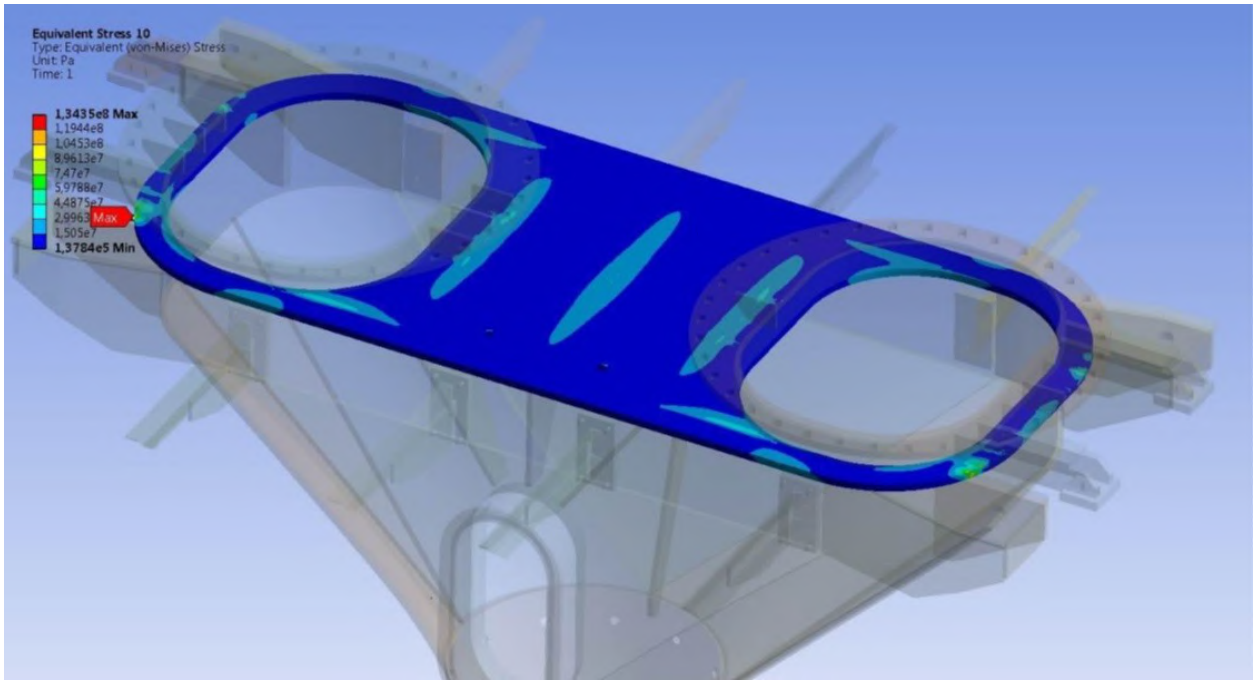

Fig. 2.64 Distribution of stresses arising in the top plate.

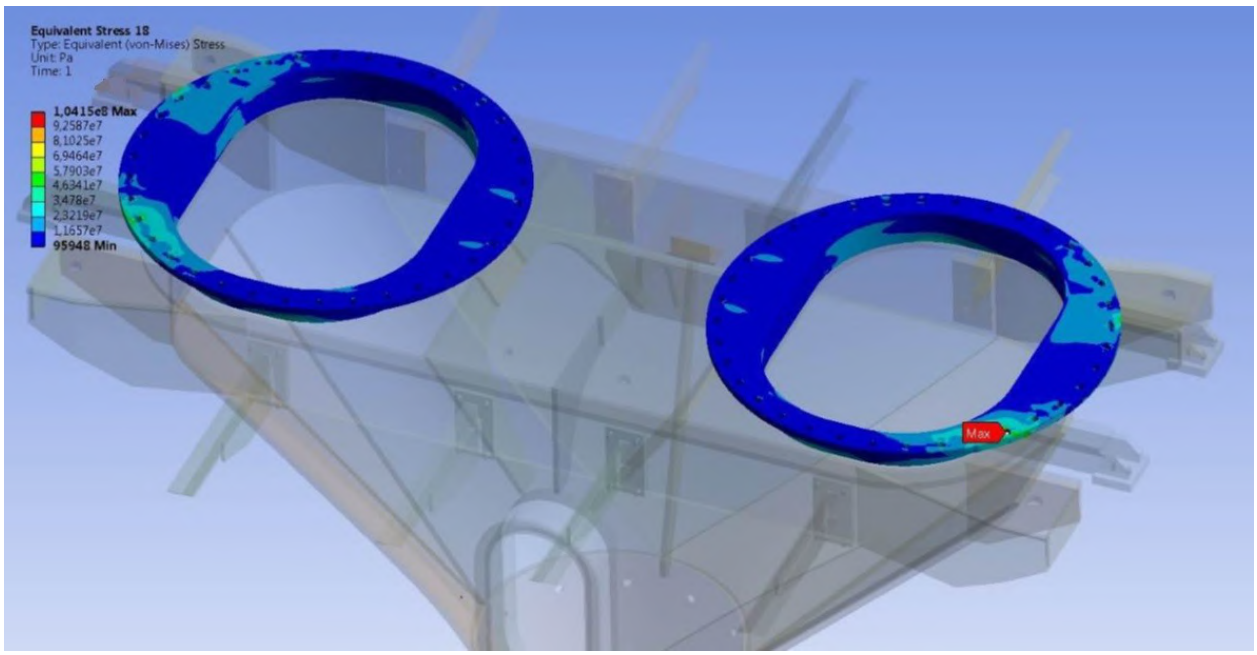

Fig. 2.65 Distribution of equivalent stresses in top flanges.

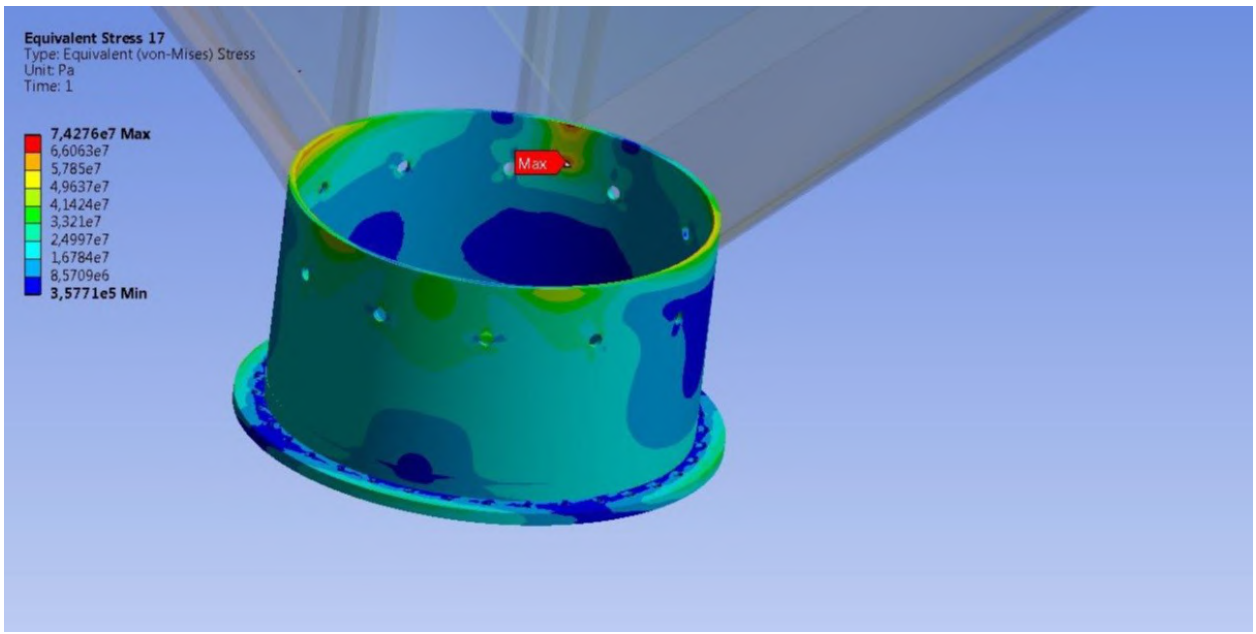

Fig. 2.66 Distribution of equivalent stresses in the bottom flange.

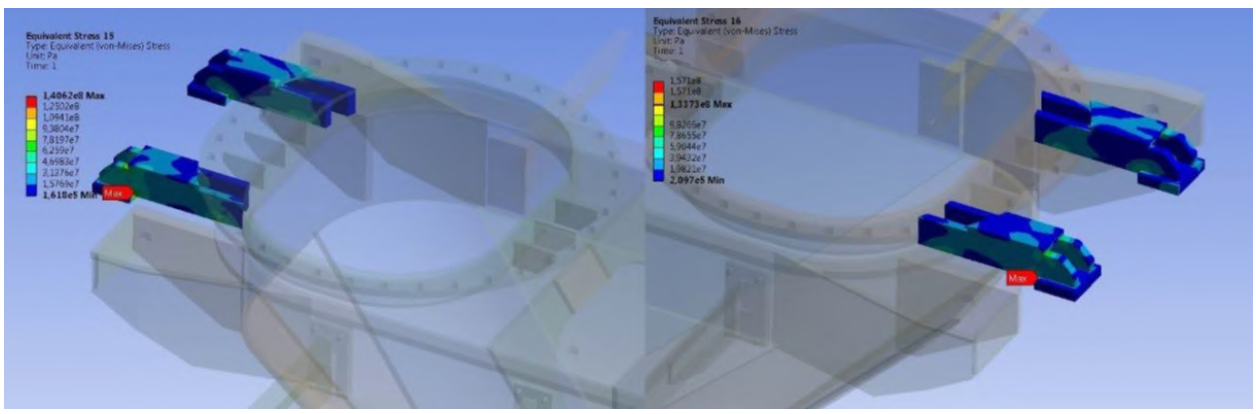

Fig. 2.67 Distribution of equivalent stresses in supports.

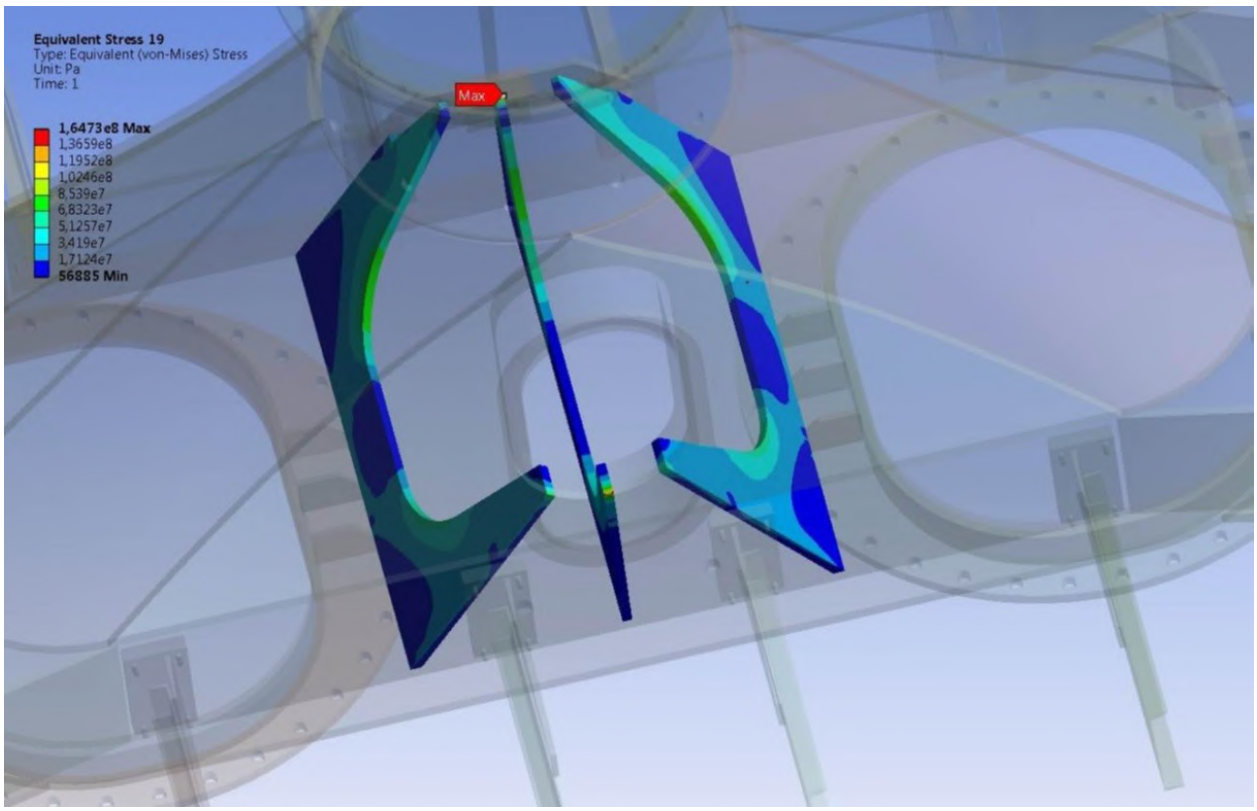

Fig. 2.68 Distribution of equivalent stresses in centering unit's ribs.

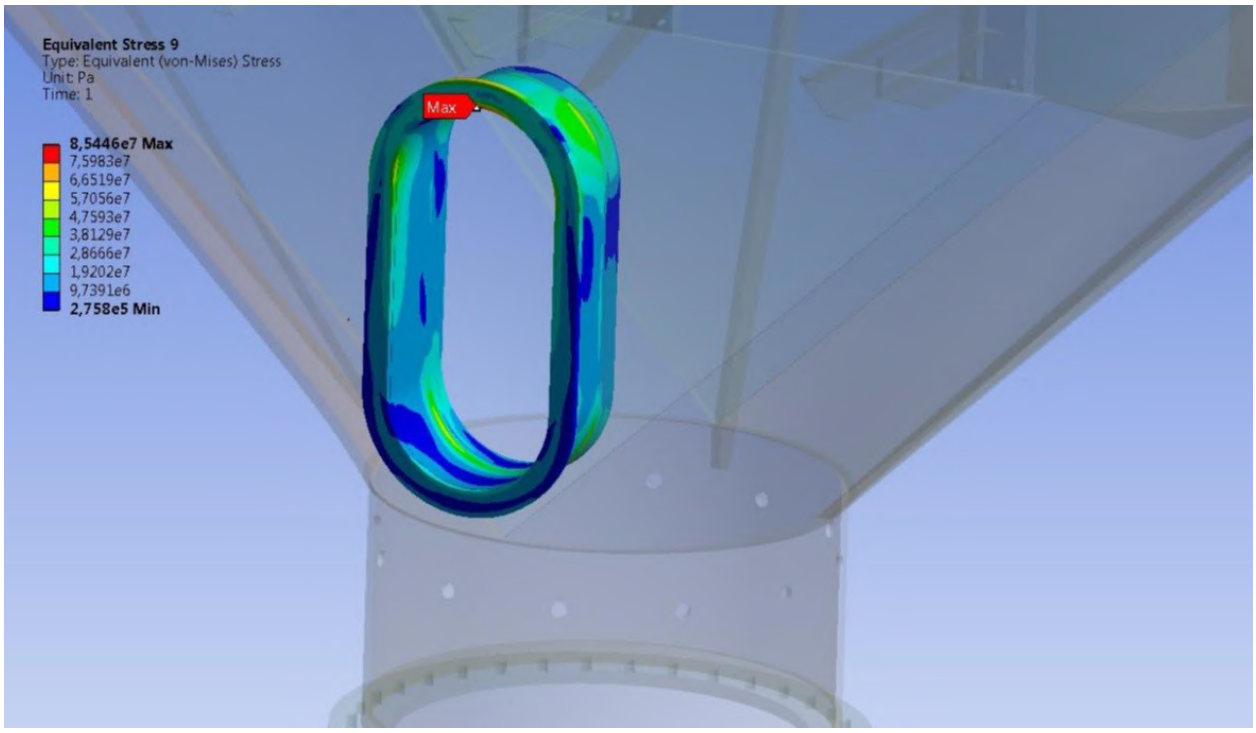

Fig. 2.69 Distribution of equivalent stresses in the centering unit's lateral manhole.

The stresses in centering unit's load-bearing cover do not exceed 115.9MPa. Fig. 2.63 shows distribution of stresses in load-bearing cover. These stresses are maxi mal in the area of joining the centering unit's bottom conical part and the cover

of the lateral manhole. The assessment of service lifespan of load-bearing elements of the bin and correctness of assessment in question is presented in Fig. 2.70-2.75.

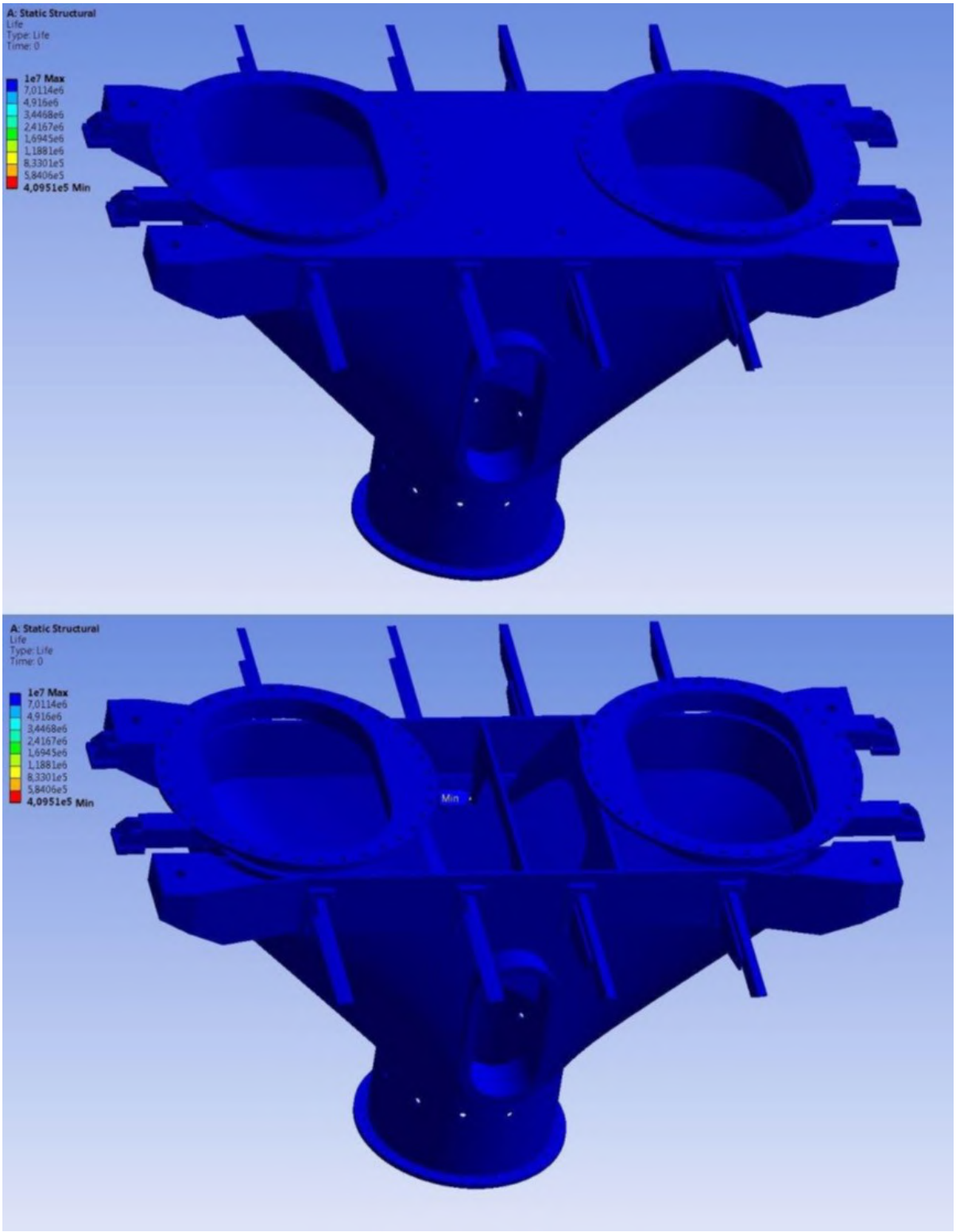

Fig. 2.70 Distribution of centering unit lifespan by Wehler SN curve.

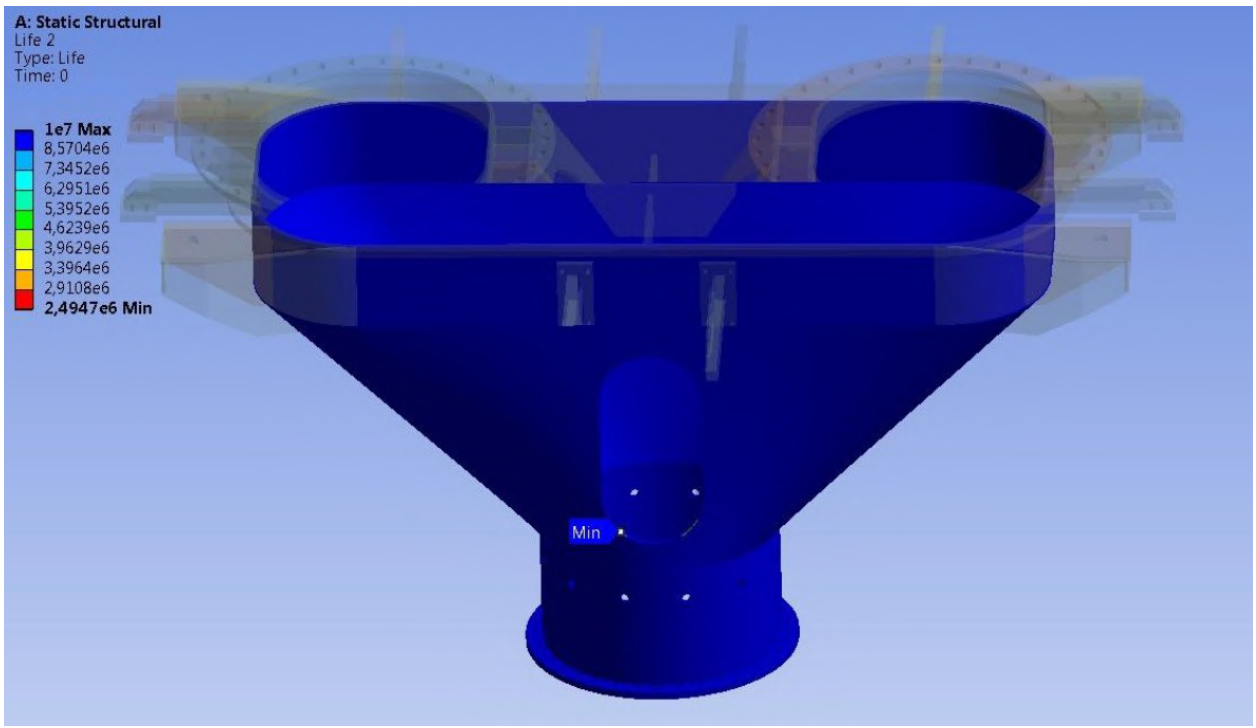

Fig. 2.71 Distribution of lifespan of centering unit's load-bearing cover.

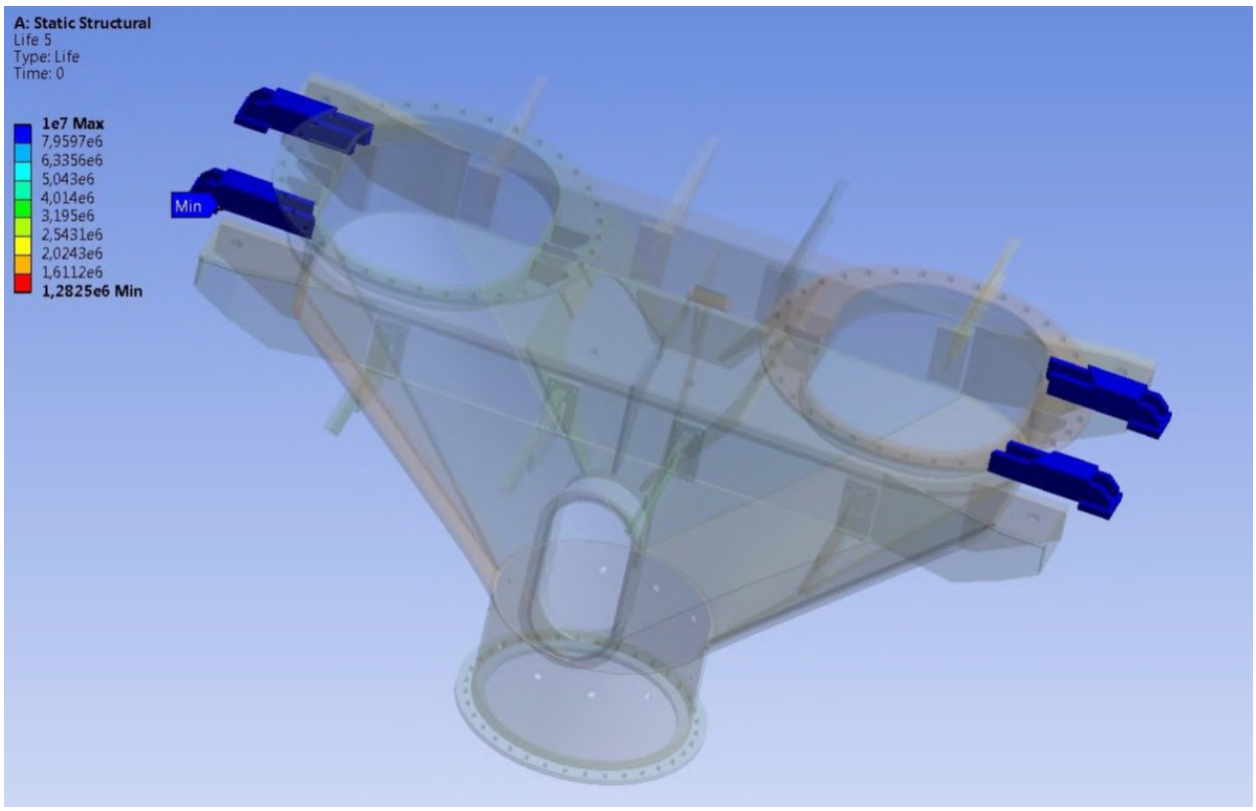

Fig. 2.72 Distribution of lifespan of centering unit's supports by Wehler SN curve.

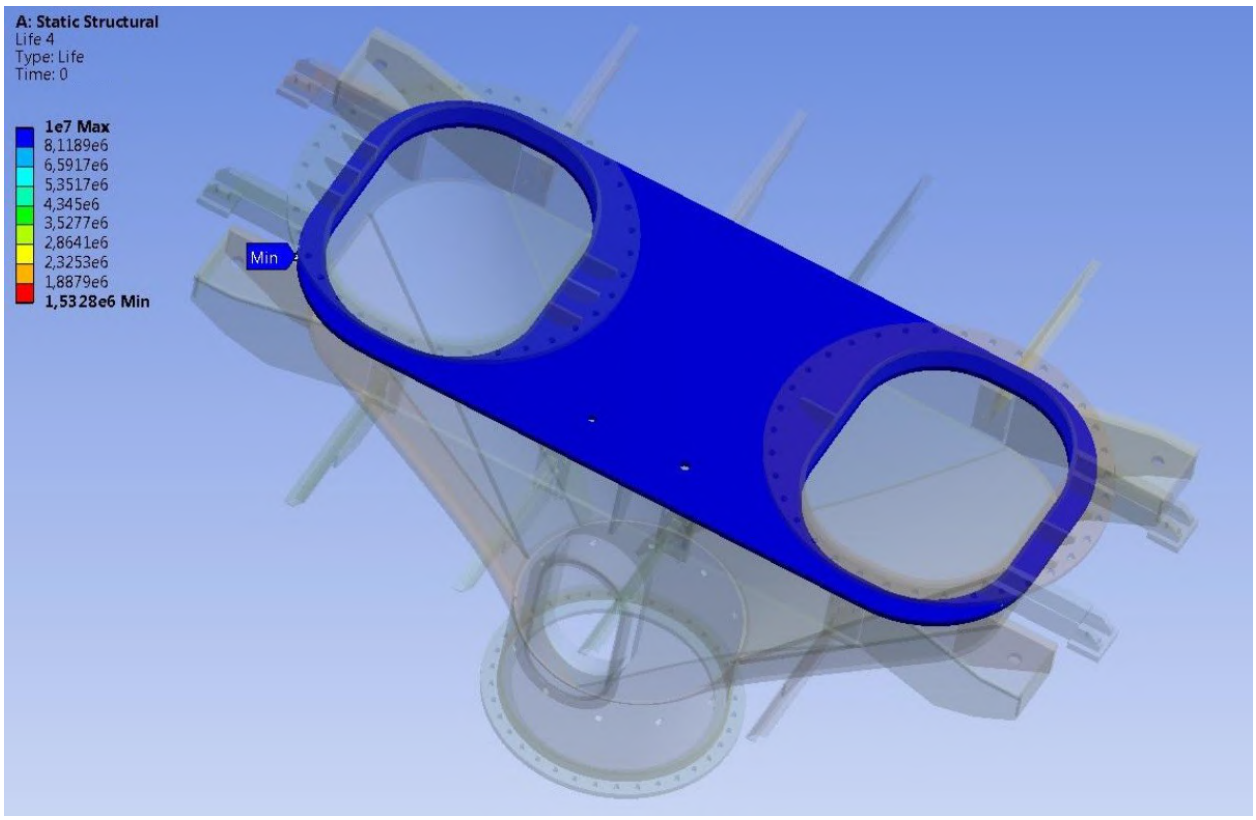

Fig. 2.73 Distribution of lifespan of centering unit's top plate.

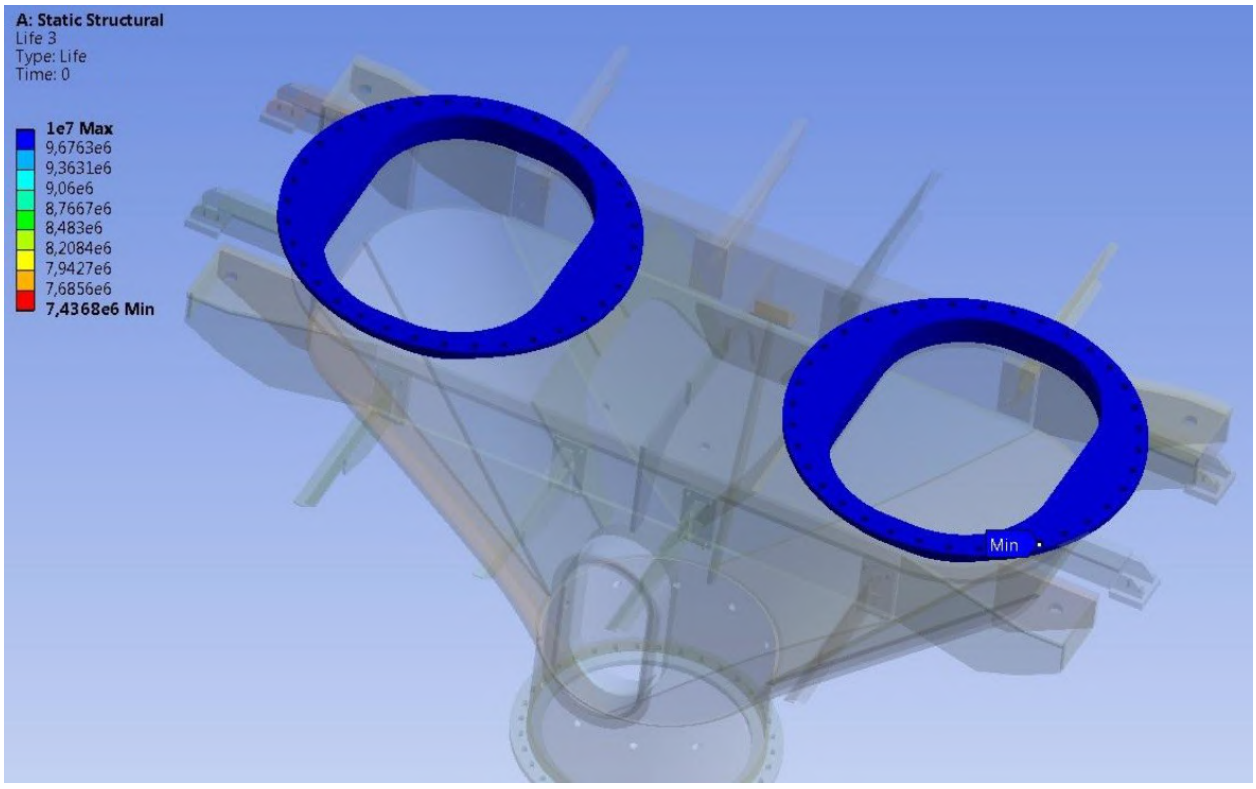

Fig. 2.74 Distribution of lifespan of centering unit's top flanges.

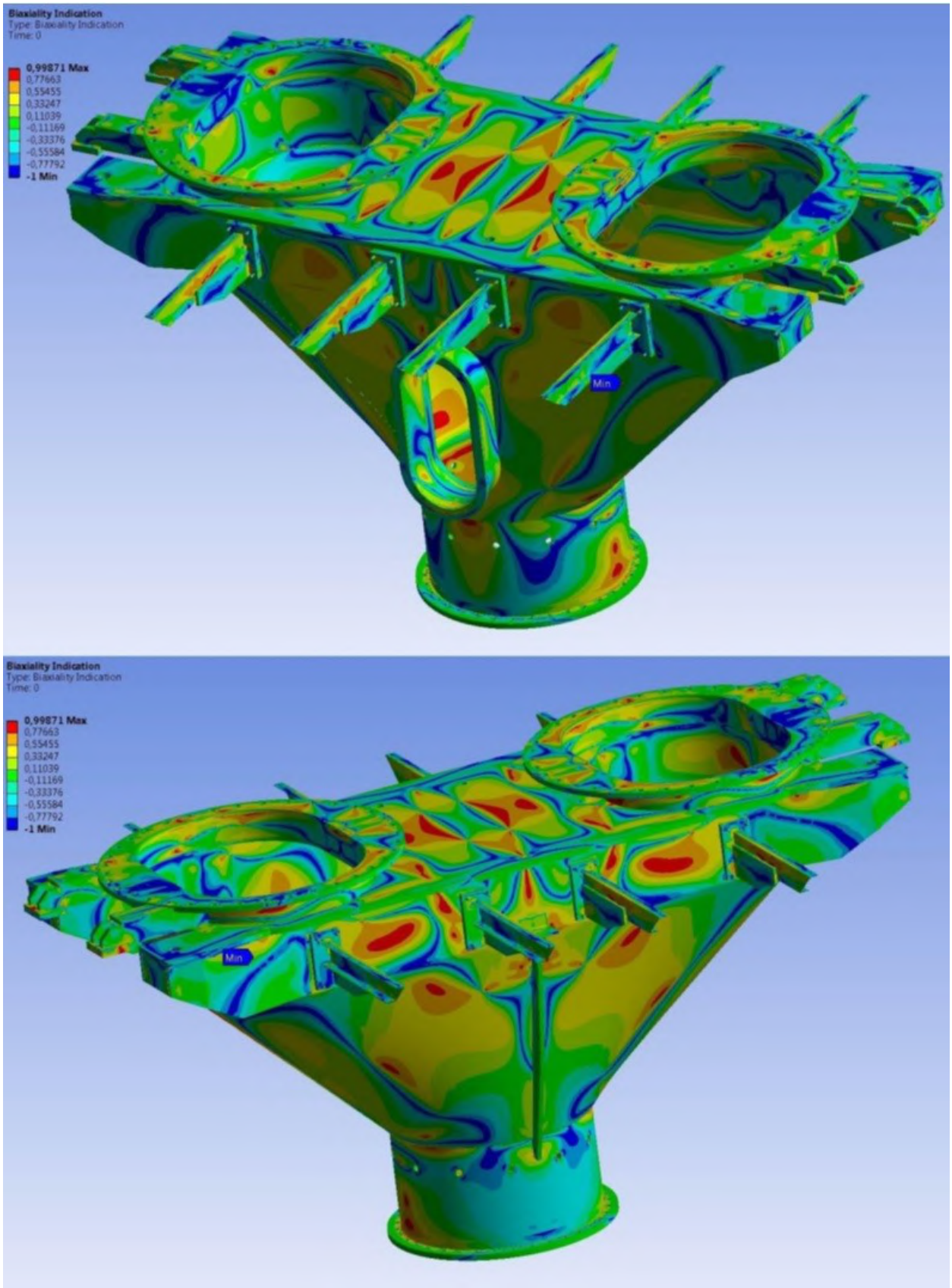

Fig. 2.75 Distribution of stress-state nature in the bin by Wehler SN curve.

Stresses arising in bin's structure elements from wind effect are presented in Table 2.6.

Table 2.6.

Structural elements of material bin	Obtained results of stresses from wind effect design cases (MPa)		Maximal stress (MPa)
	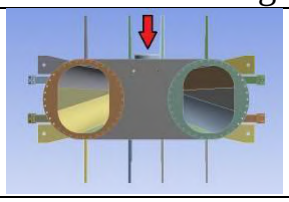	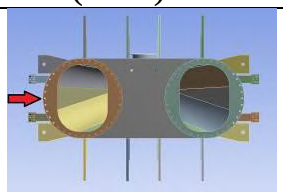	
Cylindrical wall	**90.5**	**89.9**	**90.,5**
Curved wall (cover)	**116.3**	**115.5**	**116.3**
Top flange/ flange's cover	**80.6/35.8**	**104.1/46.3**	**104.1/46.3**
Bottom flange / flange's cover	**42.6/76.5**	**41.4/74.2**	**42.6/76.5**
Lateral flange / flange's cover	**85.4/57.0**	**85.4/57.0**	**85.4/57.0**
Top plate of the body frame	**111.2**	**134.3**	**134.3**
Support's lug (left/right)	**118.4/118.5**	**140.8/133.7**	**140.8/133.7**

The conducted calculations allow presenting the stress state of bin hopper's structural members for considered load combinations as the table 2.7 and single out the design case of maximum load.

Table 2.7.

Structural elements of material bin	Obtained stresses from design load cases (MPa)				Maximal stress (MPa)
	Design pressure + weight	NSC	NSC + LWE	NSC + MDE	
Cylindrical wall	**90.8**	**90.1**	**90.5**	**90.6**	**90.8**
Curved wall (cover)	**116.6**	**115.9**	**116.3**	**117.4**	**117.4**
Top flange/ flange's cover	**58.5/39.0**	**97.3/43.0**	**104.1/46.30**	**109.1**	**109.1**
Bottom flange / flange's cover	**44.9/80.7**	**50.6/75.7**	**41.4/74.2**	**52.1/75.8**	**52.1/75.8**
Lateral flange / flange's cover	**83.1/55.4**	**85.3/66.4**	**85.4/57.0**	**86.7/57.7**	**86.7/57.7**
Top plate of the body frame	**72.8**	**131.20**	**134.3**	**144.3**	**144.3**
Support's lug (left/right)	**82.6/88.6**	**136.1/138.2**	**140.8/133.7**	**149.6/152.7**	**149.6/152.7**

The most load-bearing structural member is right support's lug. The operational lifespan value for this element is 1.3787×10^{6}cycles or 22.5 years of service.

2.3.5 Designing the bin structural members

Irregular flanged connections of charging bin's structure are designed using the sub-modelling procedure. Designing of each flanged connection is performed as per sub-model. Each sub-model is obtained by splitting the master model with a plane located at the distance of 3-4 cover thicknesses from the flange. Using the master mod-el for a given case of designing the stress patterns are determined along splitting planes. These strains serve as boundary conditions for the flanged connection being designed. Each flanged connection is completed with a lid and bolts securing the lid. The design pattern is built on the basis of acting loads and boundary conditions of strain patterns. Designing of bin's structural members has been performed the most loaded design case.

2.3.5.1 Designing the upper flanged connection

The structure's upper part has two top flanged connections. The acting temperature load causes various stress states in left and right top flanges. Let's carry out the submodeling for the left and right flanges. The submodel's design pattern for right upper flanged connection is presented in Fig. 2.76. The finite-element model and imported strain fields are presented in Fig. 2.77-2.78. Calculation results of stress-strain state is presented in Fig. 2.79-2.83.

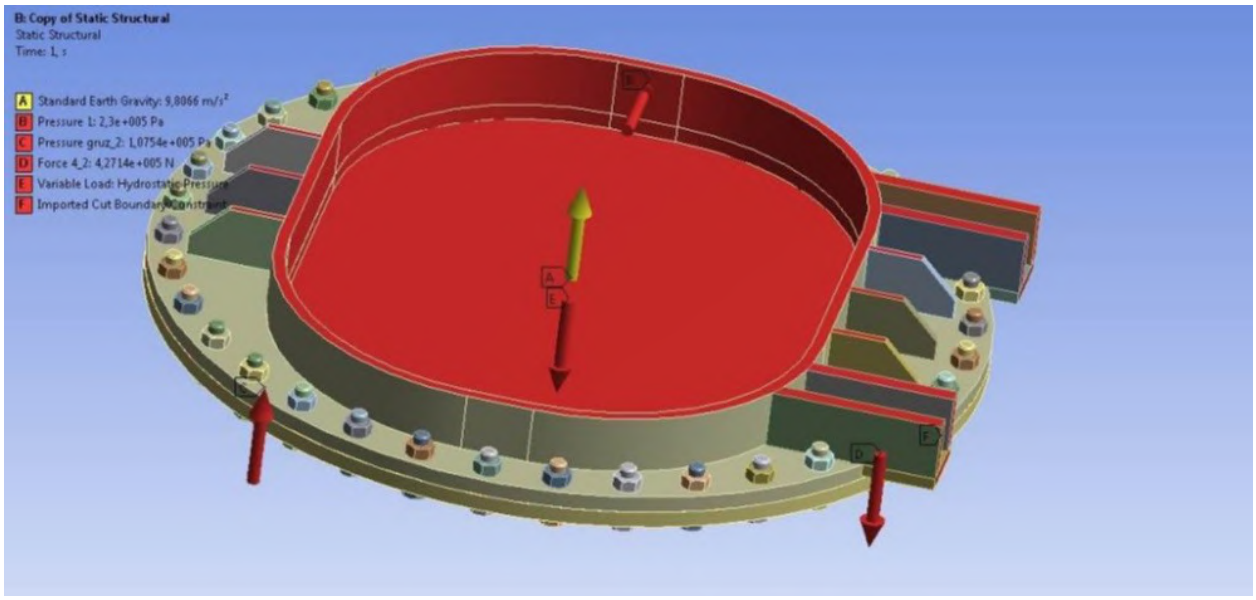

Fig. 2.76 Design pattern of loading the right flanged connection.

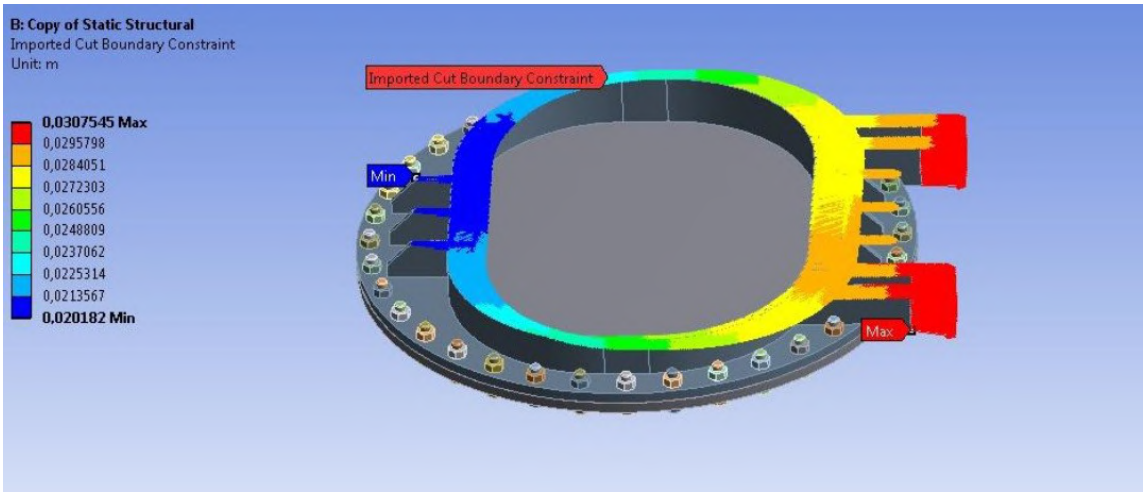

Fig. 2.77 Distribution of imported strain patterns in right upper flanged connection.

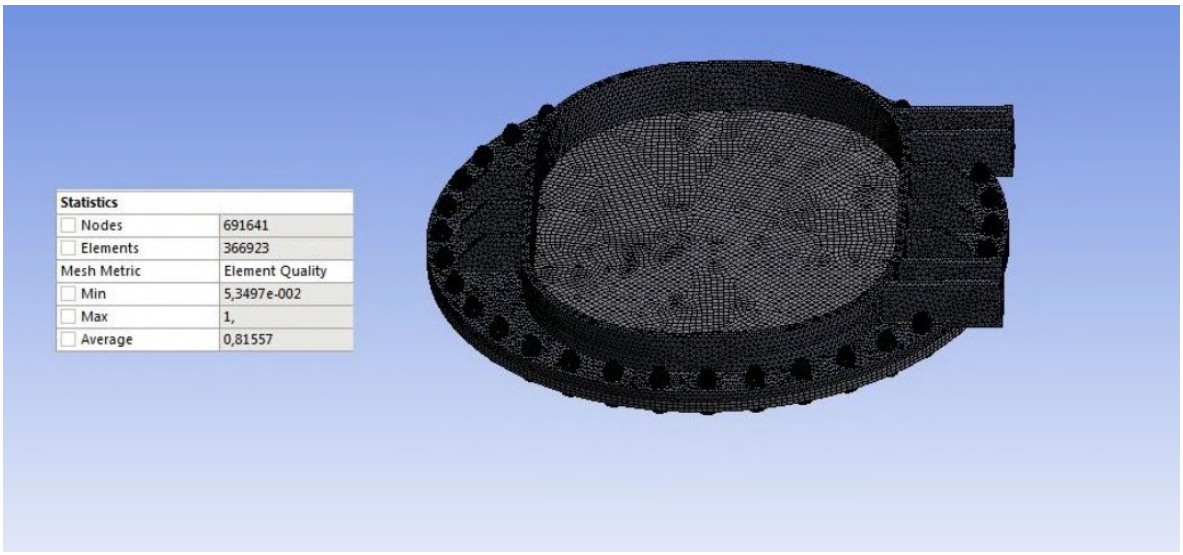

Fig. 2.78 Finite-element model of right upper-flanged connection.

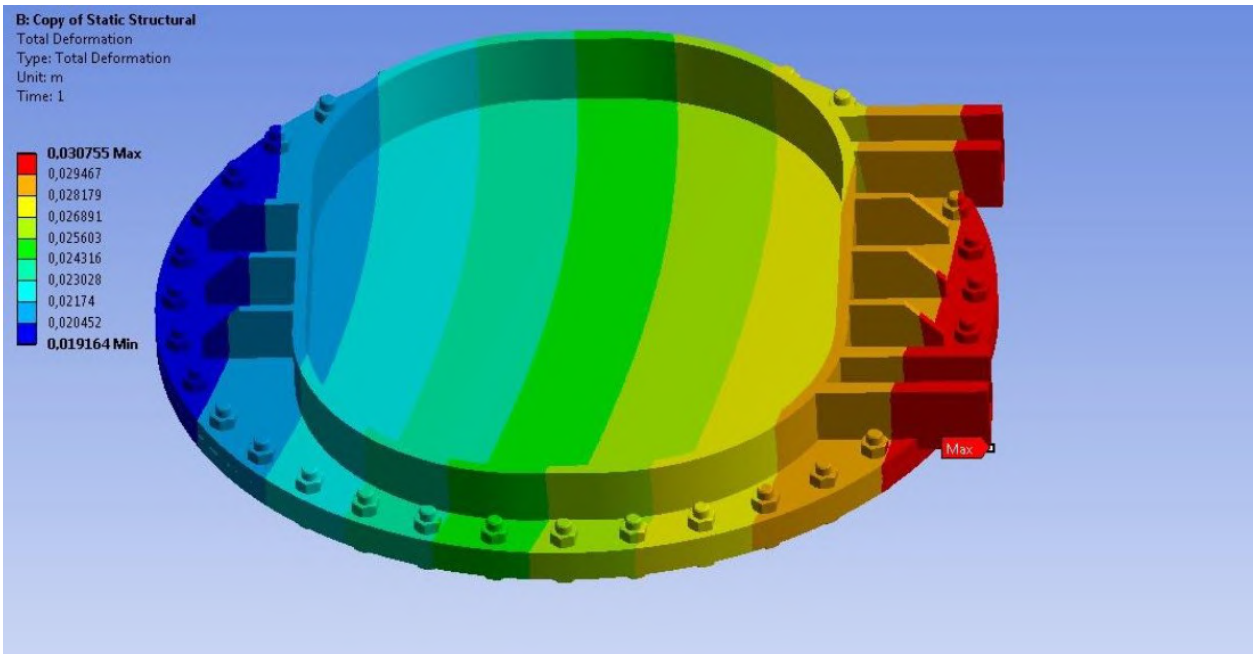

Fig. 2.79 Distribution of total strain arising in the structure.

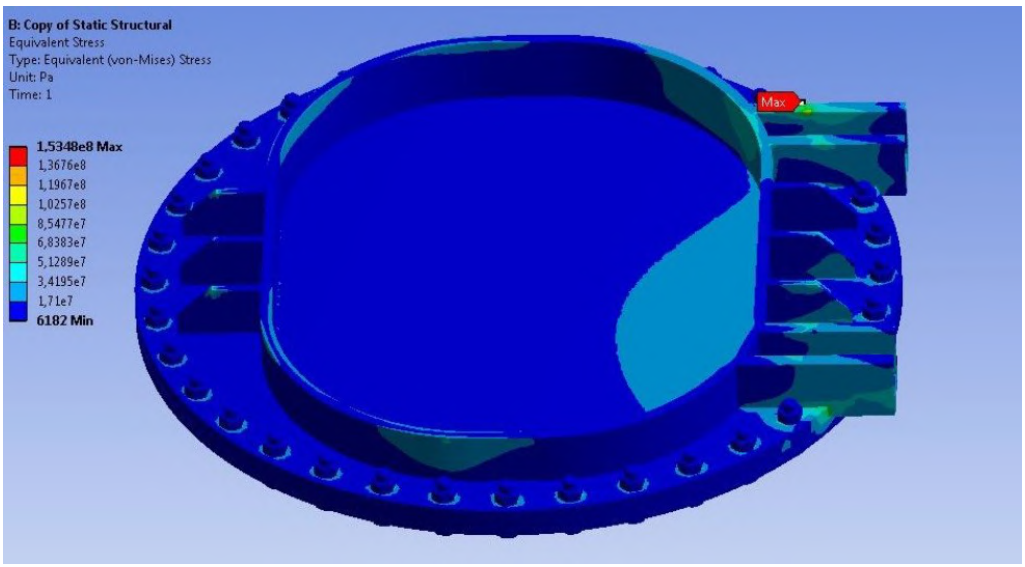

Fig. 2.80 Distribution of von Mises equivalent stresses in right upper connection.

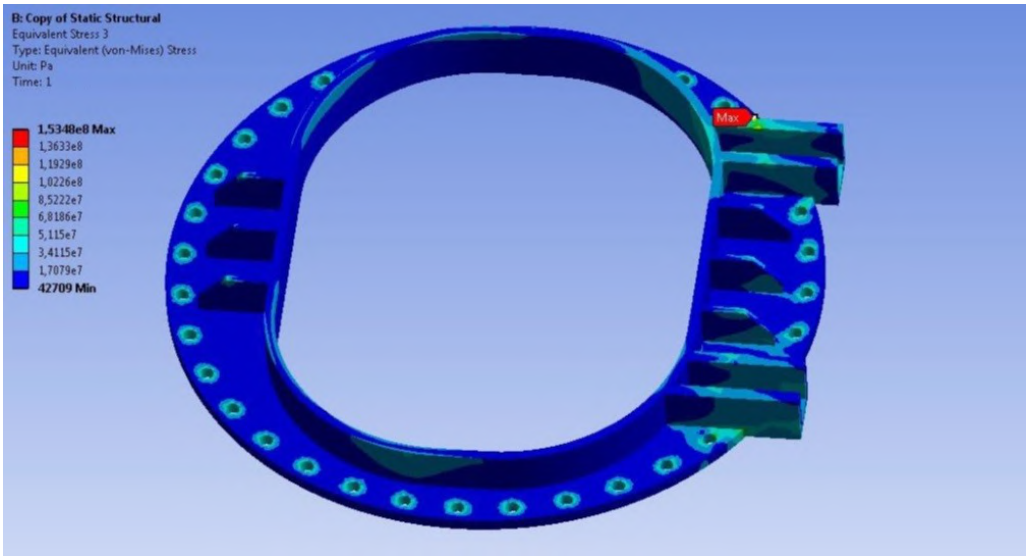

Fig. 2.81 Distribution of von Mises equivalent stresses in the flange.

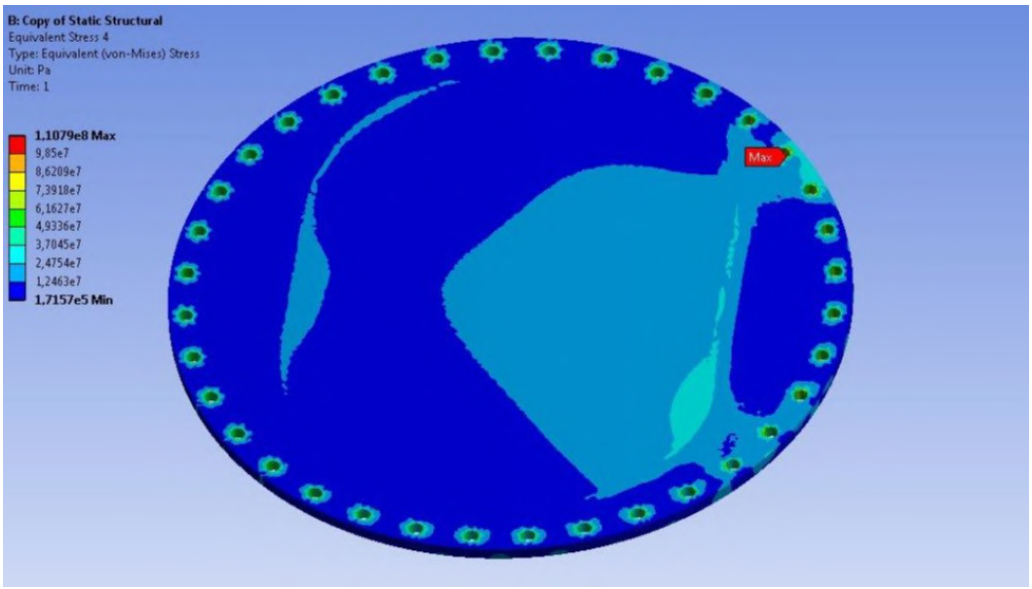

Fig. 2.82 Distribution of von Mises equivalent stresses in the lid.

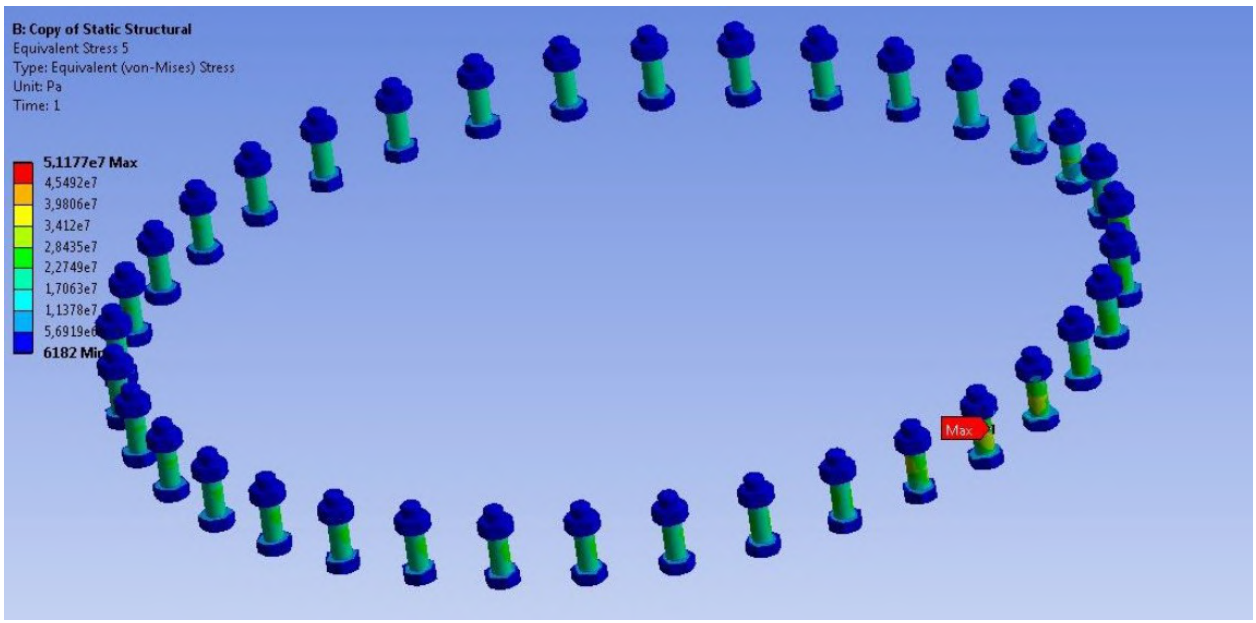

Fig. 2.83 Distribution of von Mises equivalent stresses in bolts.

By analogy let's carry out the calculation of upper left flanged connection. The design pattern of upper flanged connection's submodel is presented in Fig. 2.84.

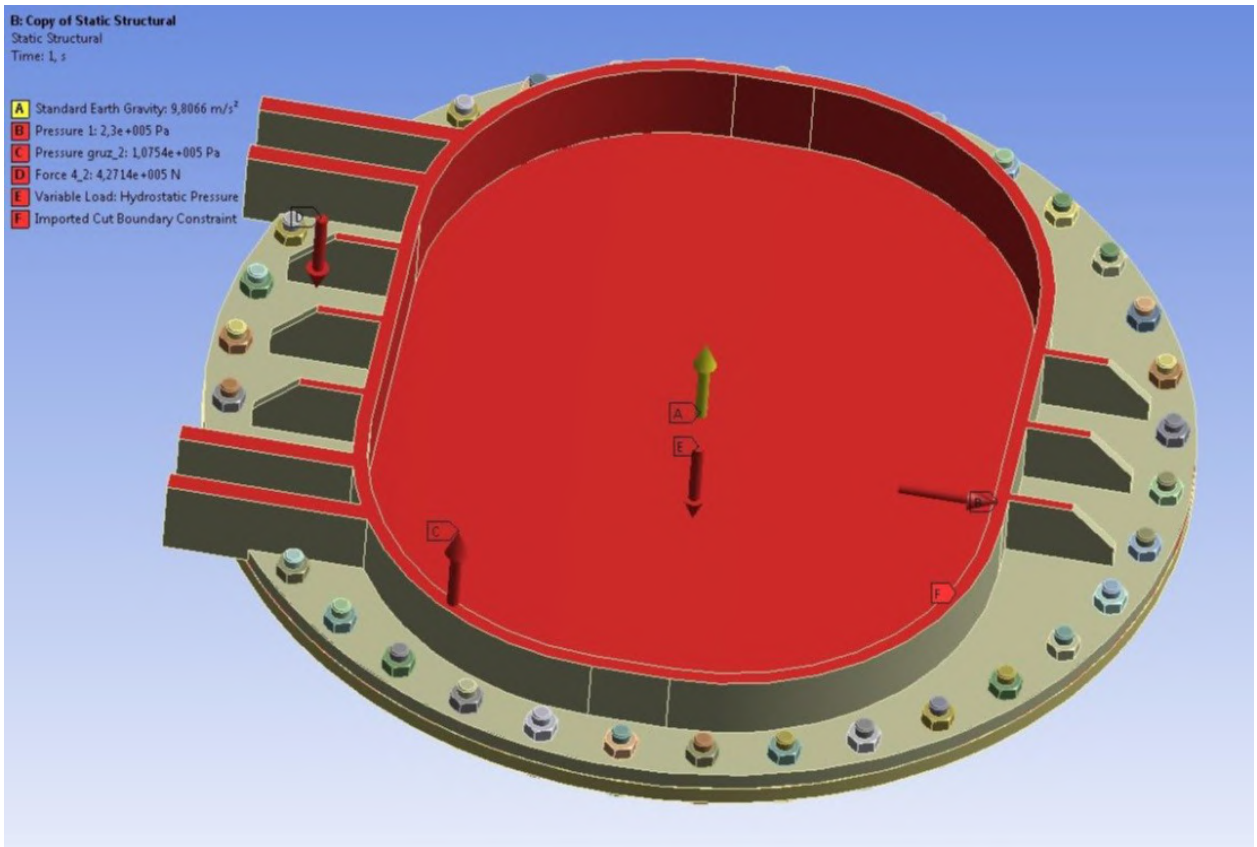

Fig.2.84 Design pattern of loading the upper left flanged connection.

Fig. 2.85 depicts imported strains for a general centering unit's model for upper left flanged connection.

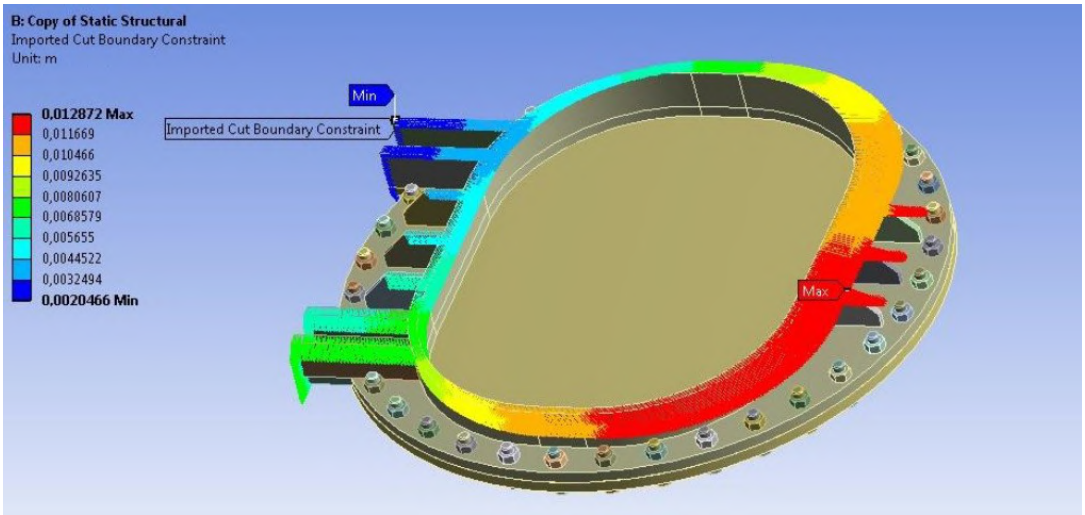

Fig. 2.85 Distribution of imported strain patterns in the upper left flanged connection.

The finite-element model is presented in Fig. 2.86.

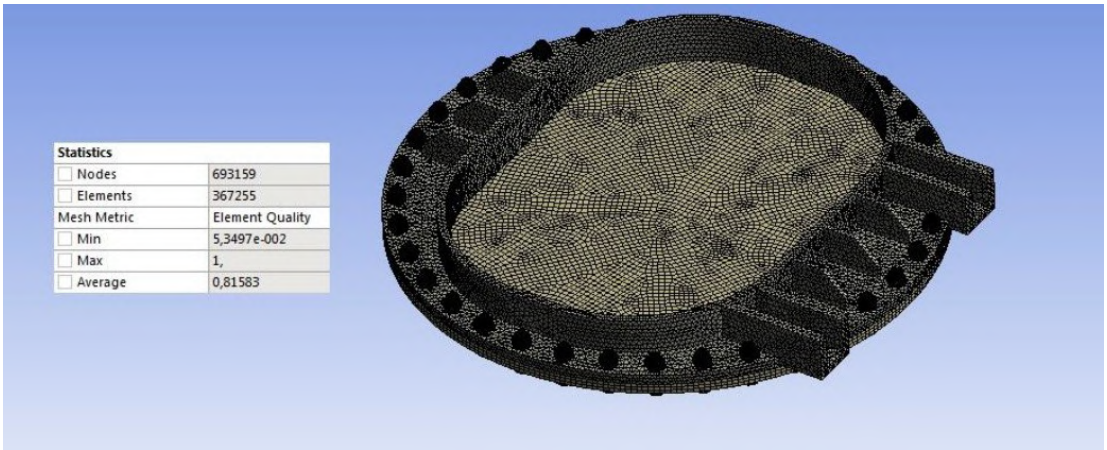

Fig. 2.86 Finite-element model of upper left flanged connection.

Calculation results of stress-strain state are presented in Fig. 2.87-2.91.

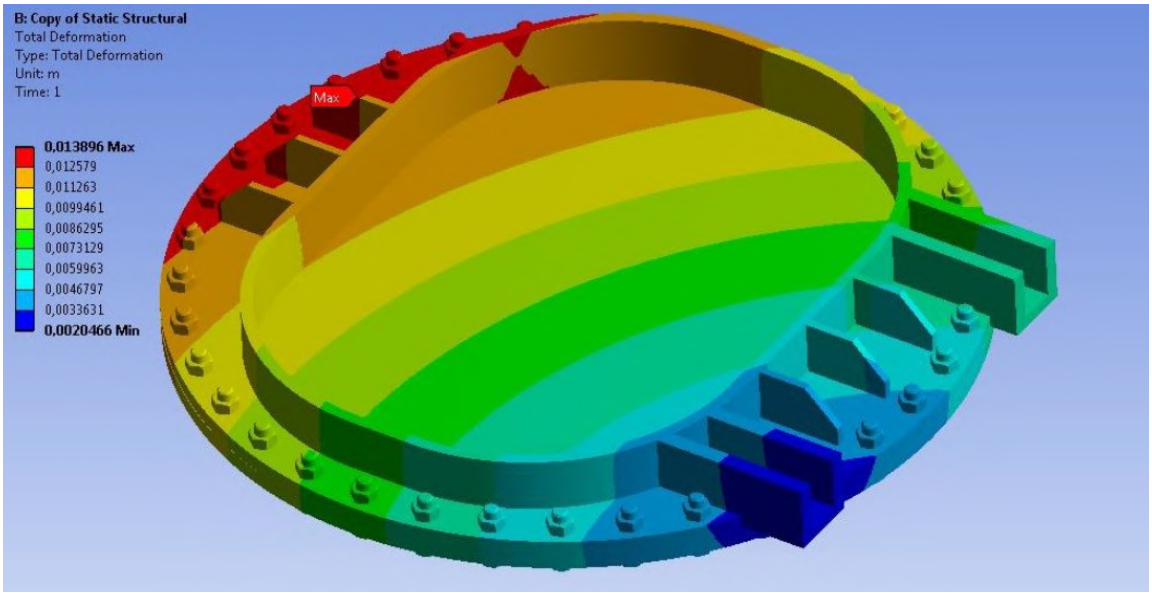

Fig. 2.87 Distribution of total strain arising in the structure.

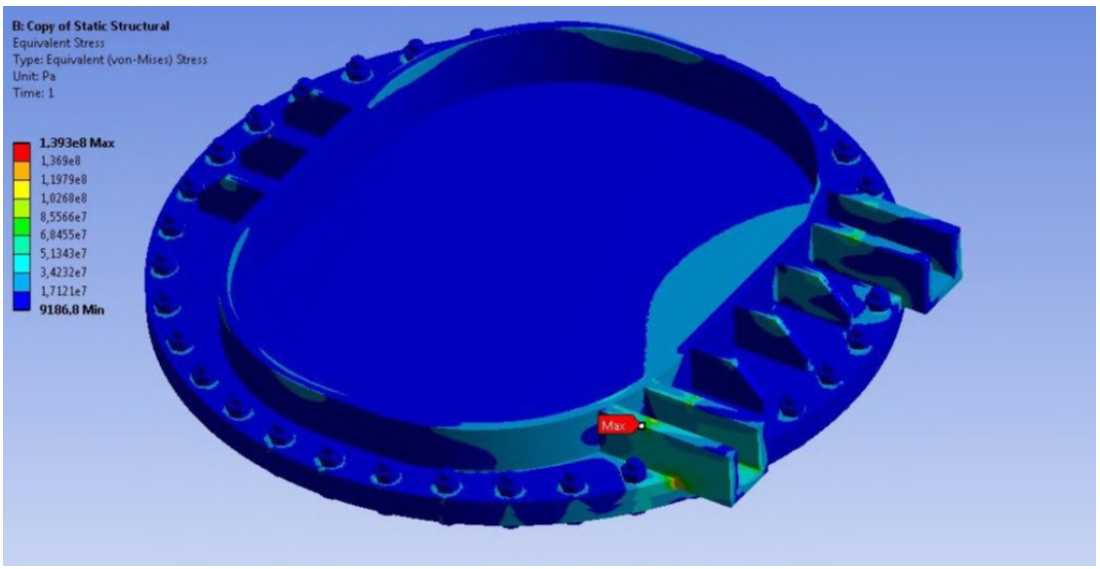

Fig. 2.88 Distribution of von Mises equivalent stresses in the left upper connection.

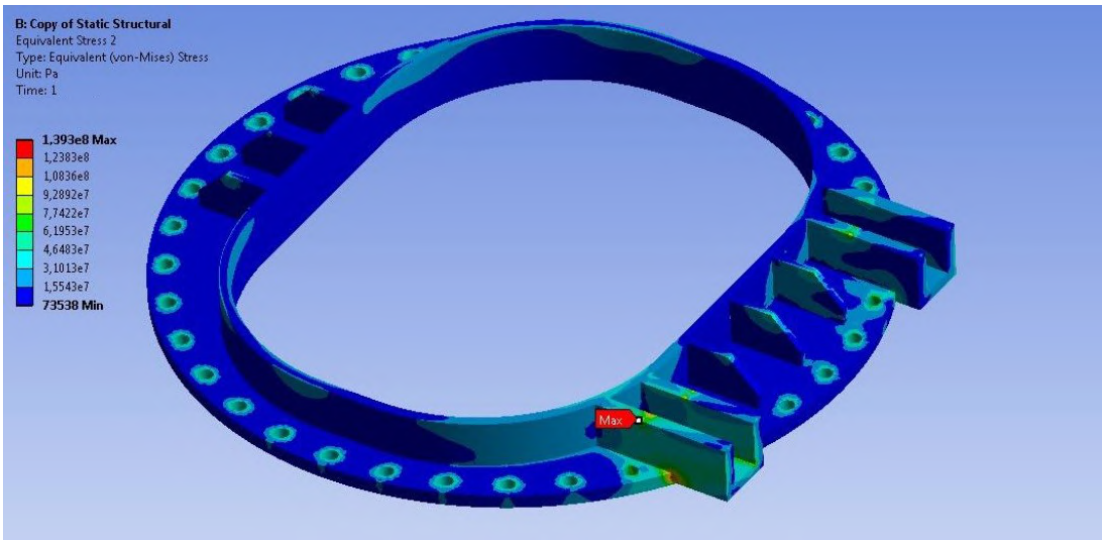

Fig. 2.89 Distribution of von Mises equivalent stresses in the flange.

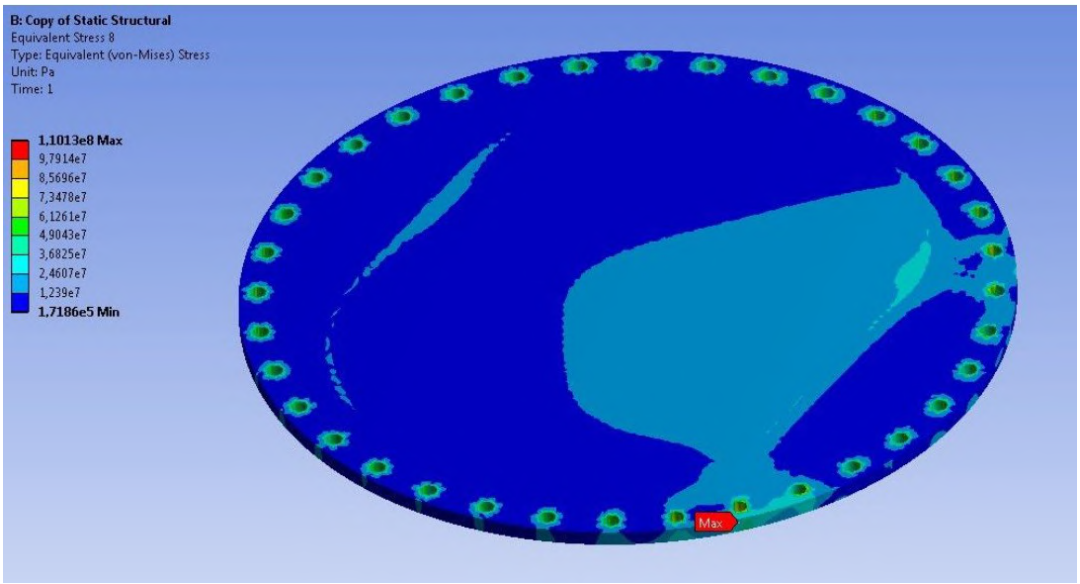

Fig. 2.90 Distribution of von Mises equivalent stresses in the lid.

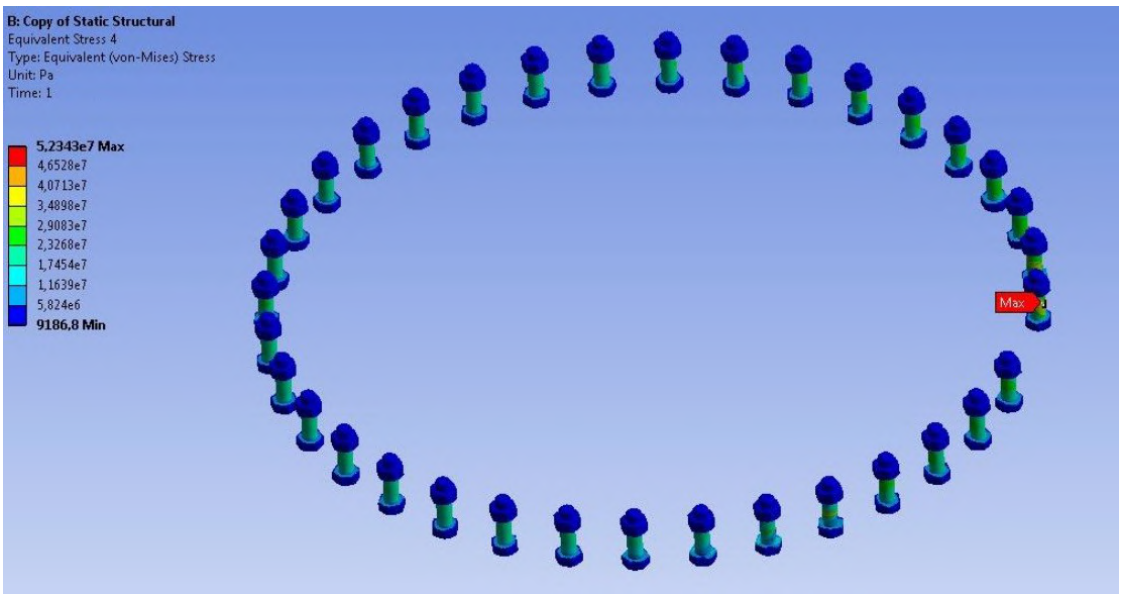

Fig. 2.91 Distribution of von Mises equivalent stresses in bolts.

2.3.5.2 Designing the lower flanged connection

The design pattern of lower flanged connection submodel is presented in Fig. 2.92.

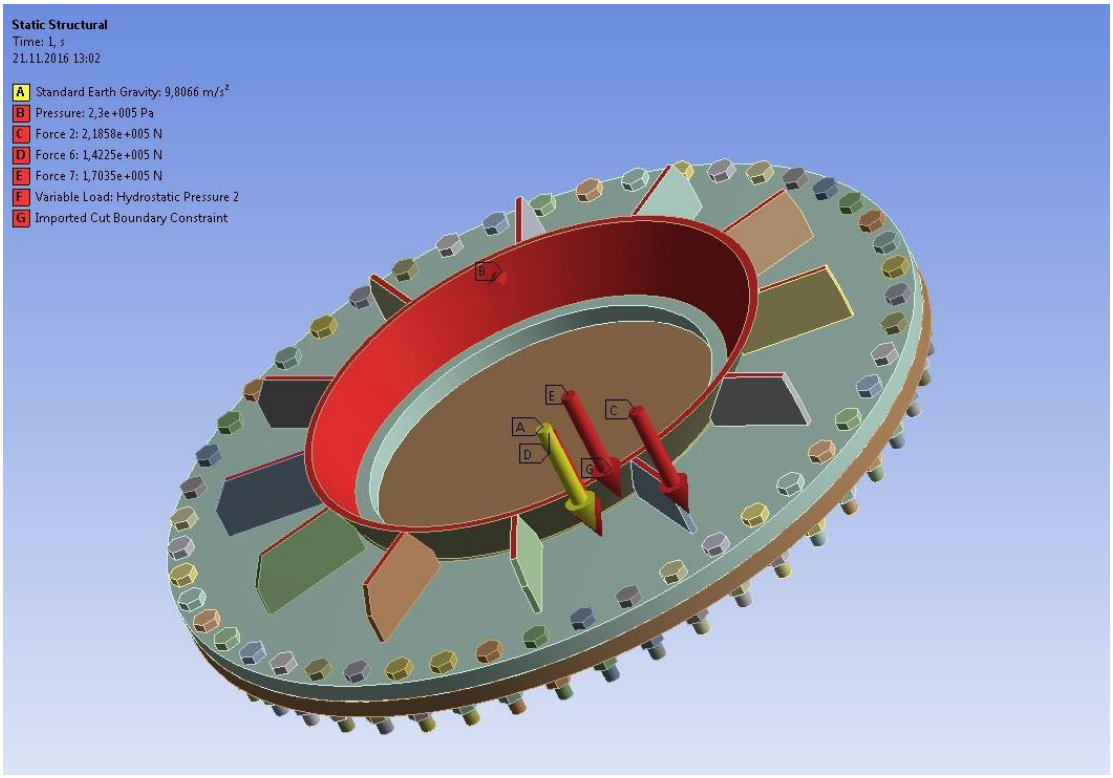

Fig. 2.92 Design case of lower flange loading.

Fig. 2.93 depicts imported strains from the general bin's model. The finite-element model is presented in Fig. 2.94. Calculation results of stress-strain state are presented in Fig. 2.95-2.99.

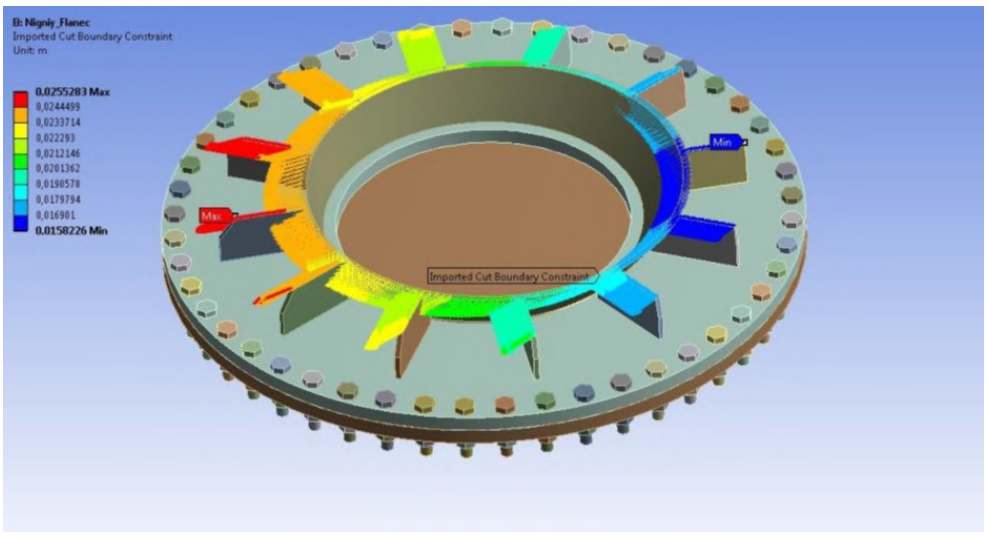

Fig. 2.93 Distribution of imported strain patterns in the lower flanged connection.

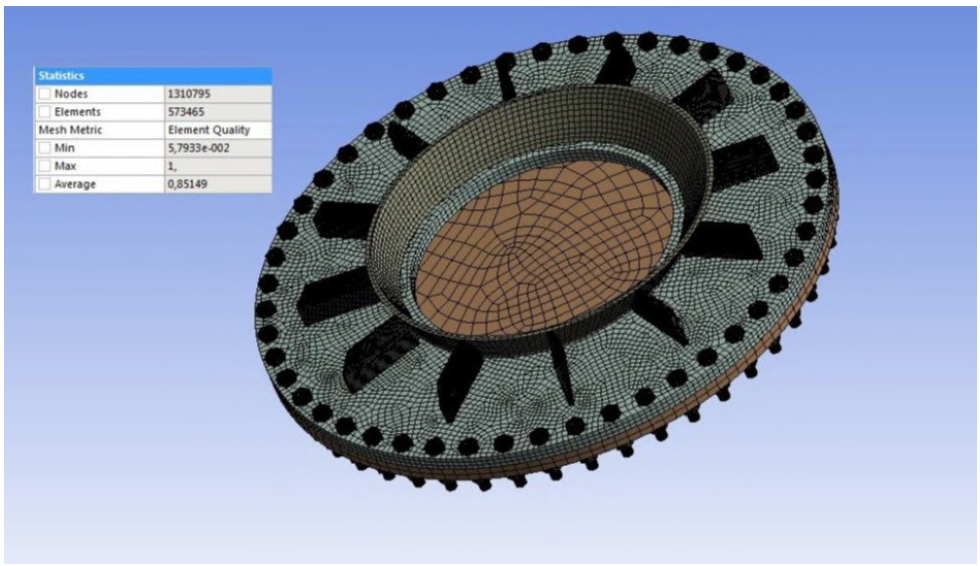

Fig. 2.94 Finite-element model of lower flanged connection.

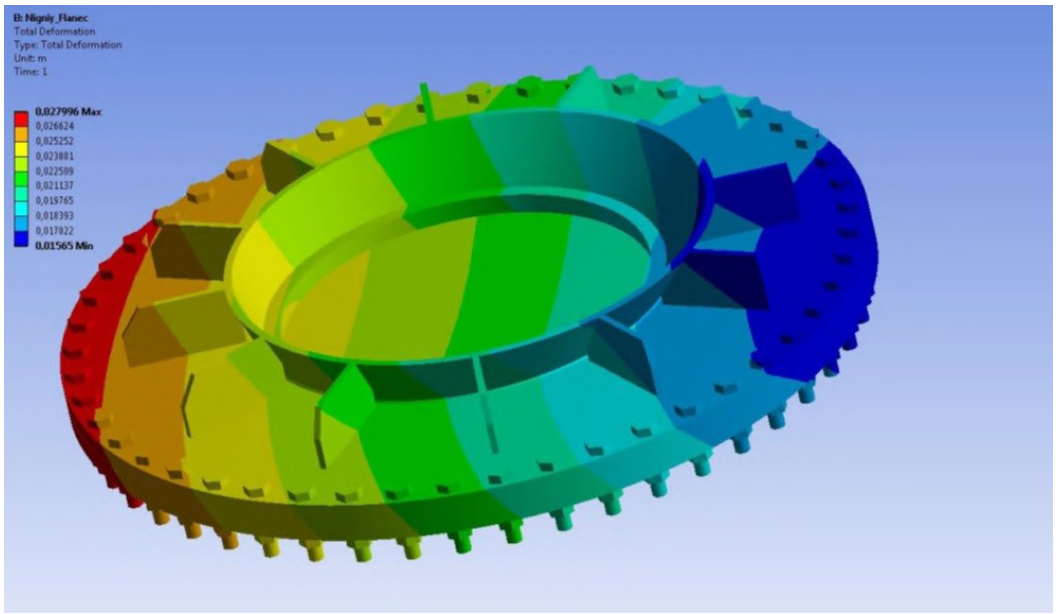

Fig. 2.95 Distribution of total strain arising in the structure.

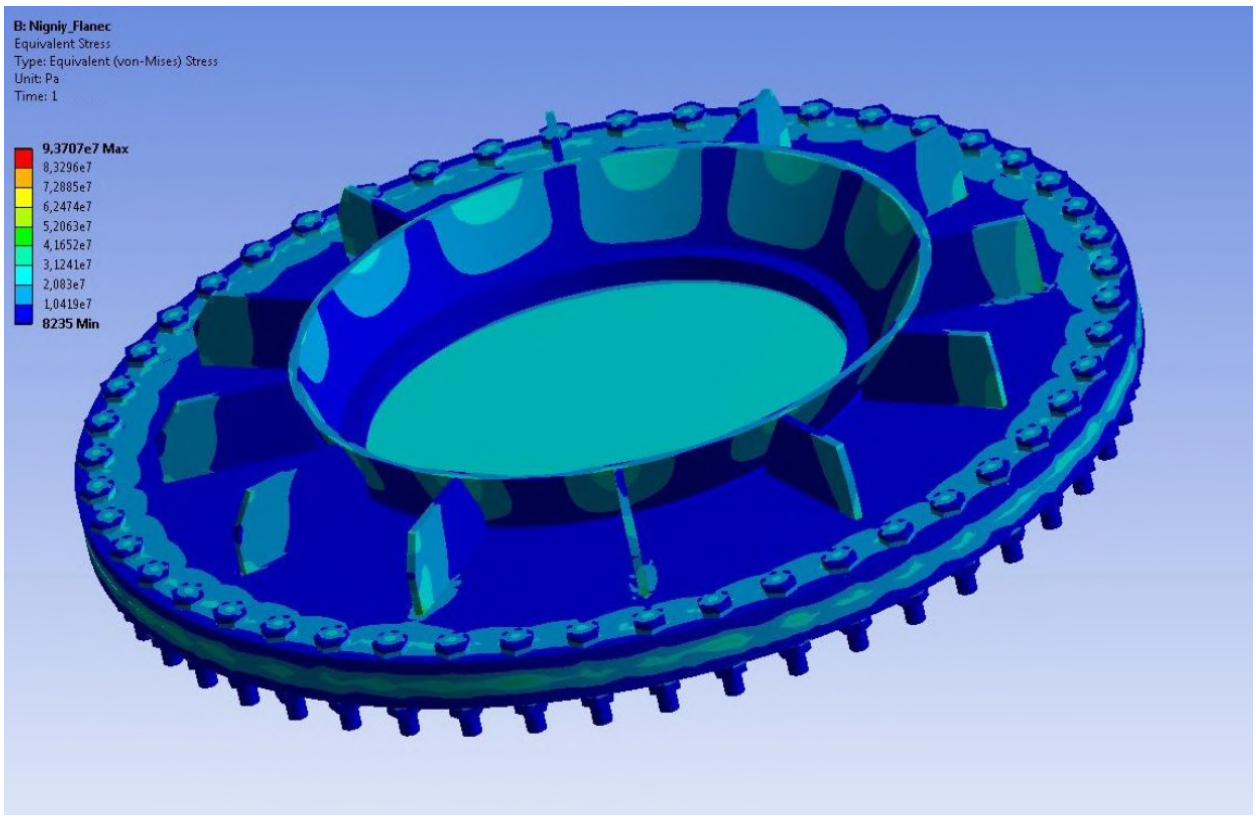

Fig. 2.96 Distribution of von Mises equivalent stresses.

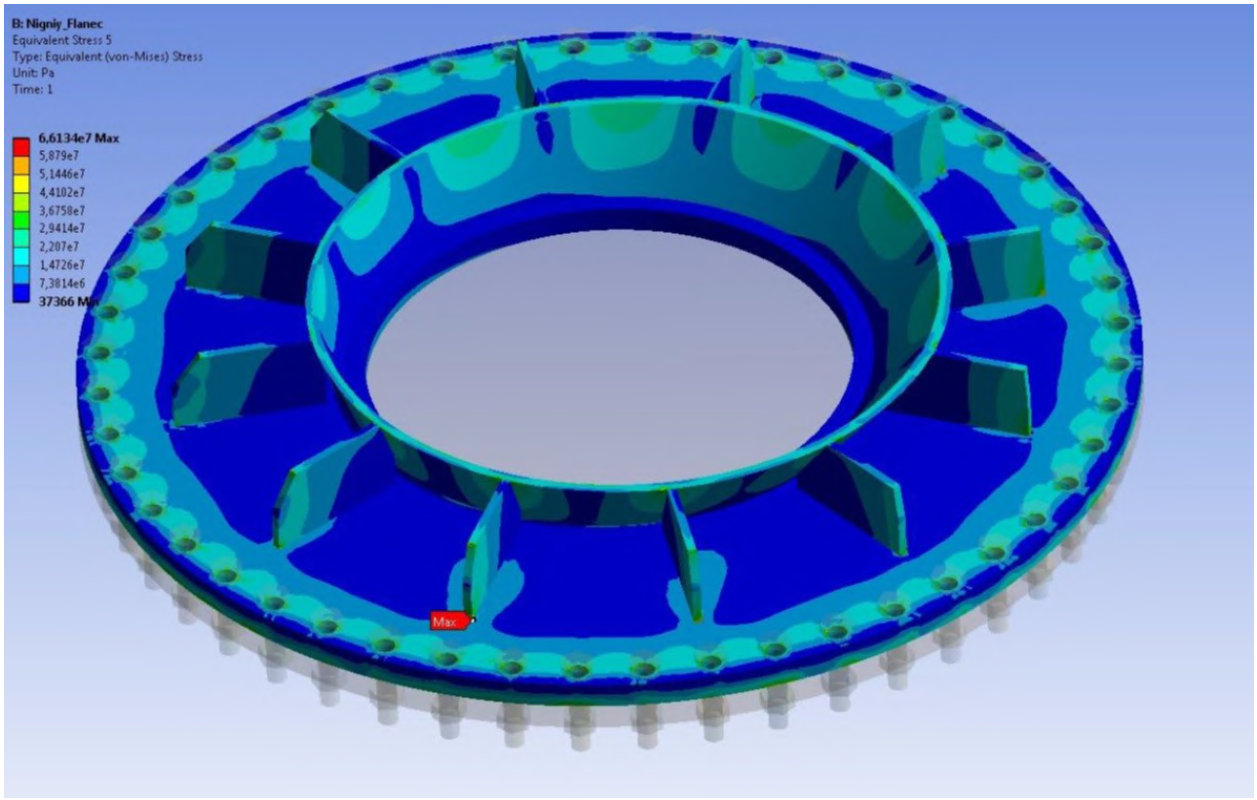

Fig. 2.97 Distribution of von Mises equivalent stresses in the flange.

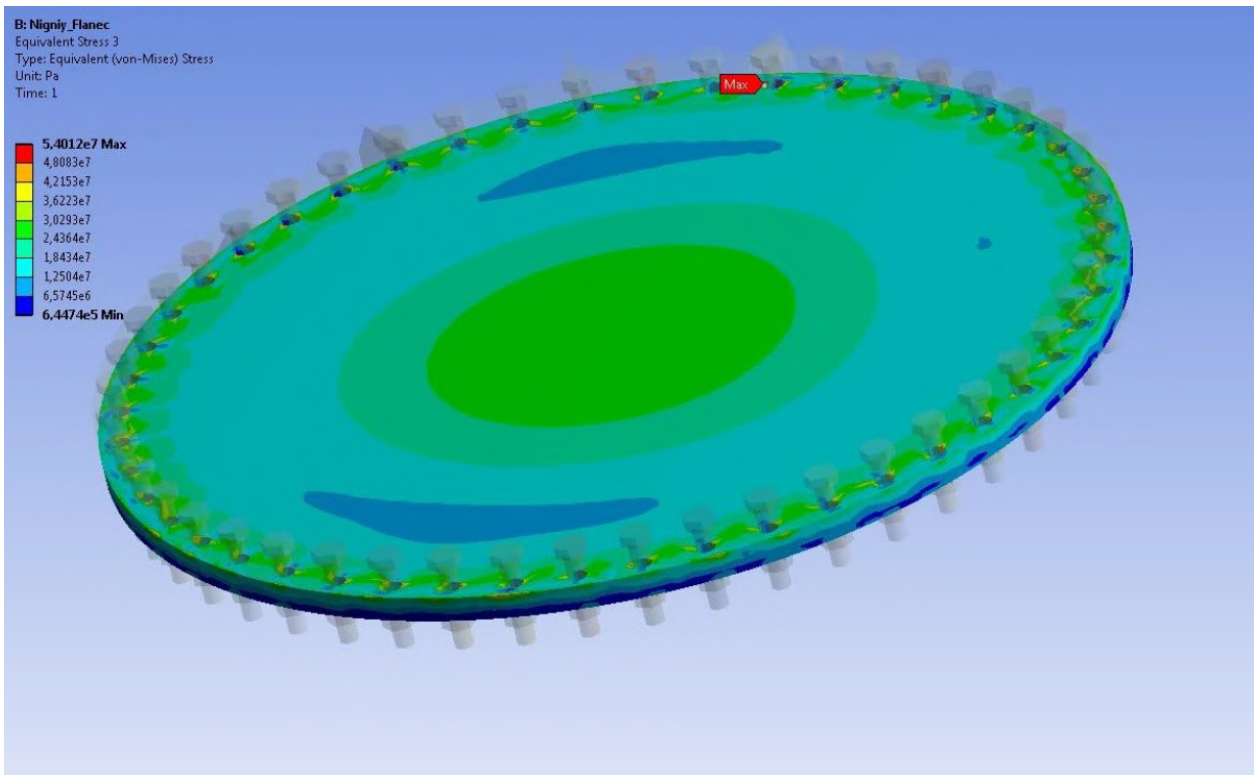

Fig. 2.98 Distribution of von Mises equivalent stresses in the lid.

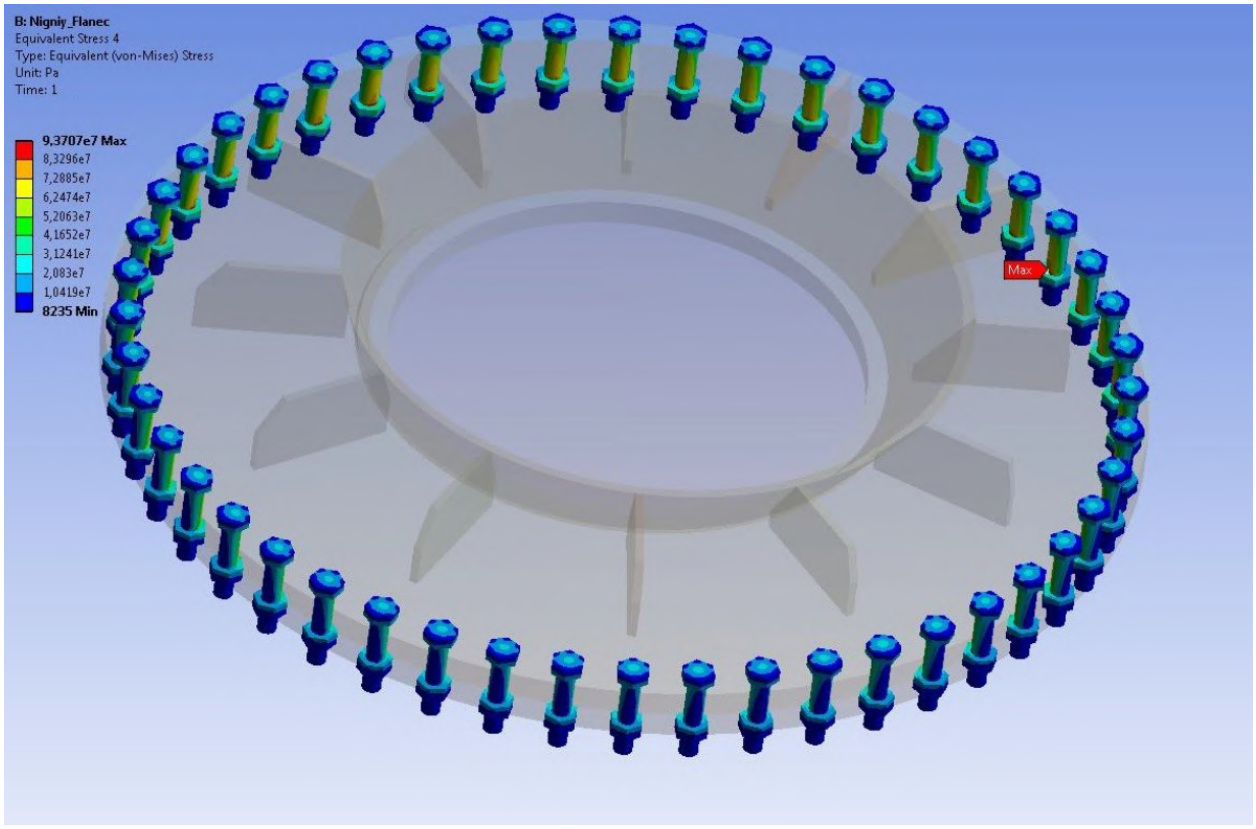

Fig. 2.99 Distribution of von Mises equivalent stresses in bolts.

2.3.5.3 Designing the lateral flanged connection

The submodeling pattern and design pattern of lower flanged connection sub-model is presented in Fig. 2.100-2.101.

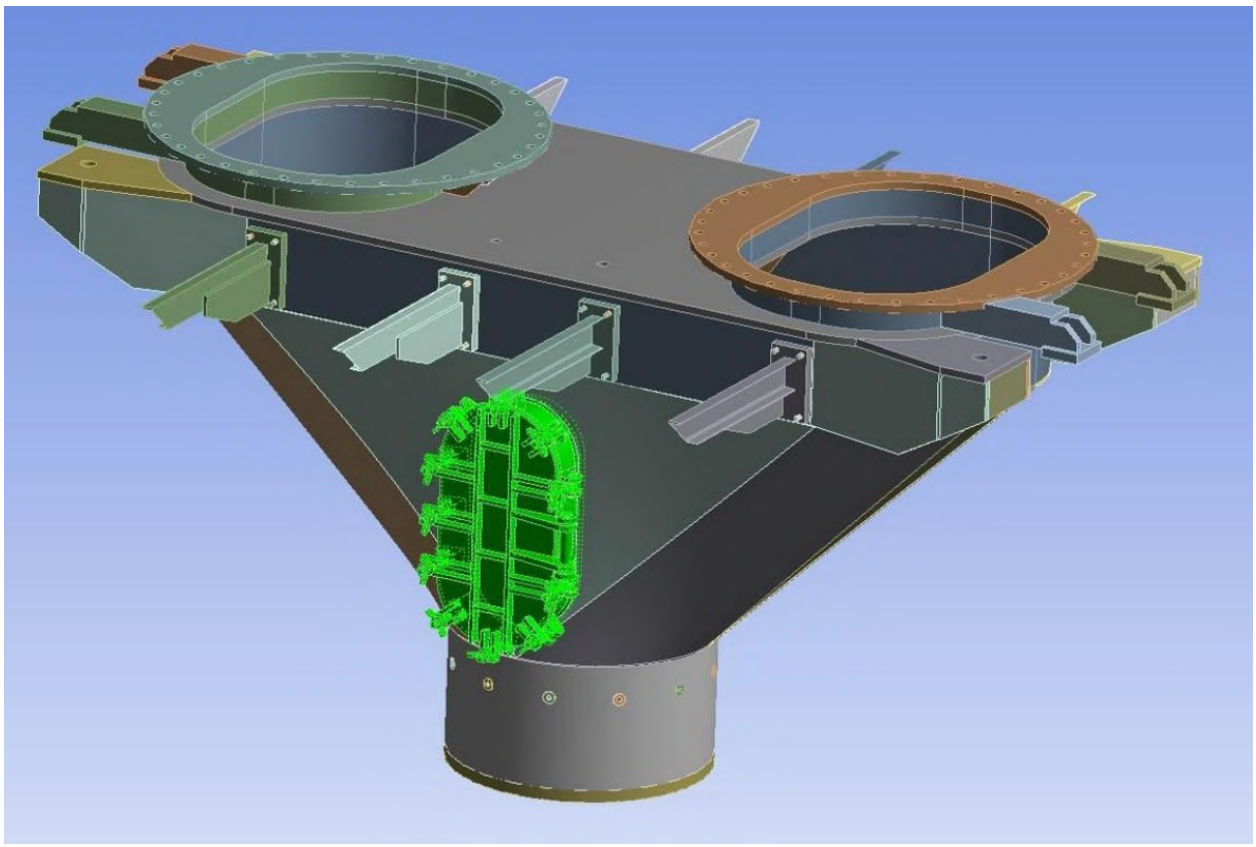

Fig. 2.100 Submodeling pattern of lateral flange.

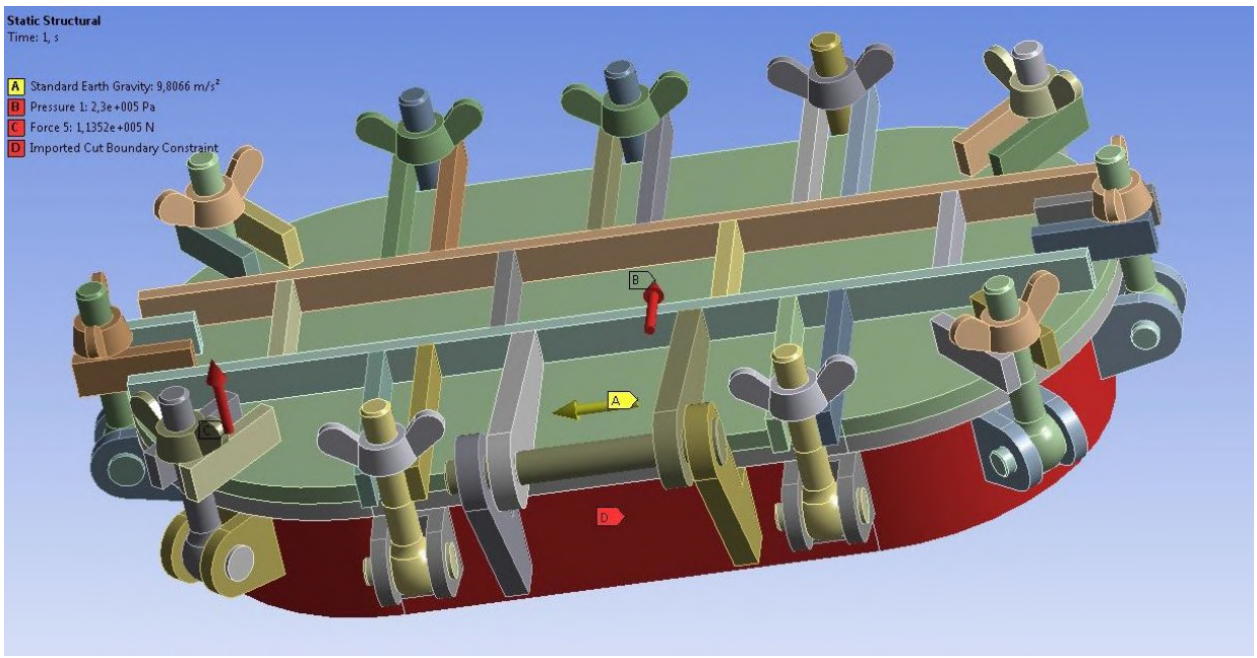

Fig. 2.101 Design case of lateral flange loading.

Fig. 2.102 depicts imported strains from the general bin's model. The finite-element model is presented in Fig. 2.103. Calculation results of stress-strain state are presented in Fig. 2.104-2.109.

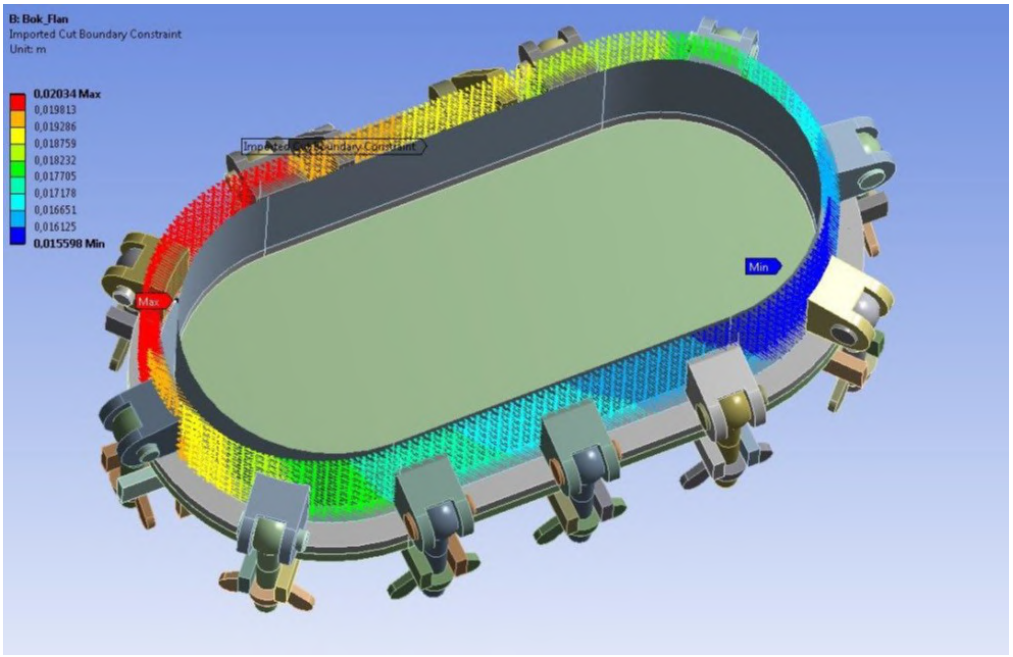

Fig. 2.102 Distribution of imported strain patterns in the lateral flanged connection.

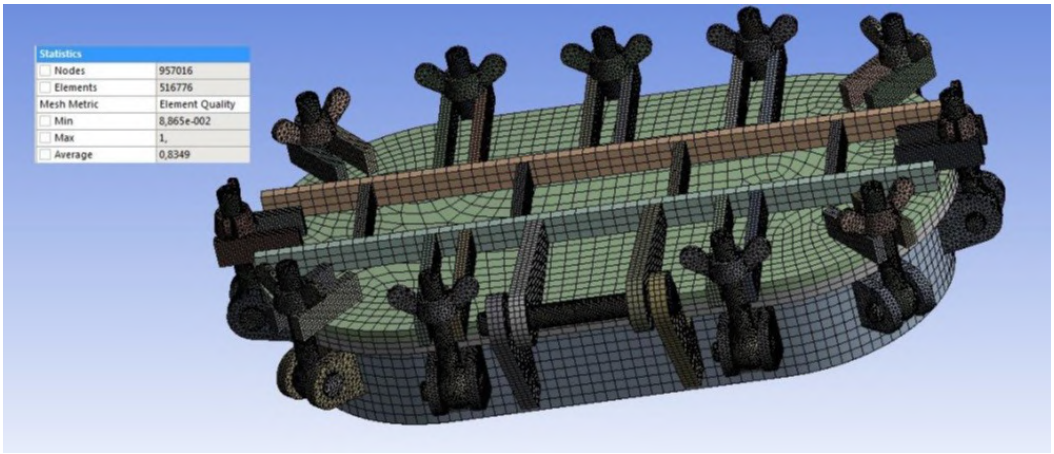

Fig. 2.103 Finite-element model of lower flanged connection.

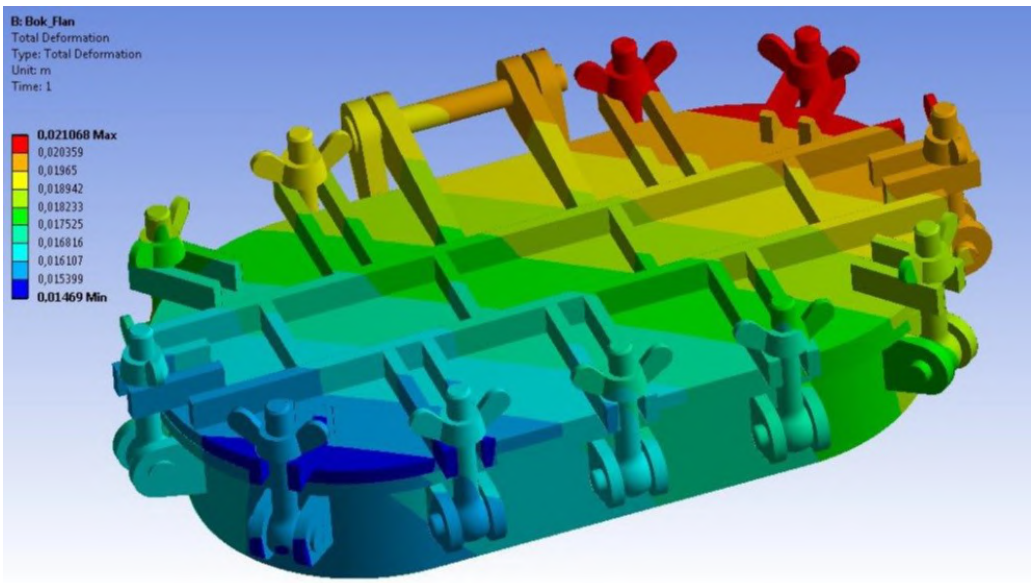

Fig. 2.104 Distribution of total strain arising in the structure.

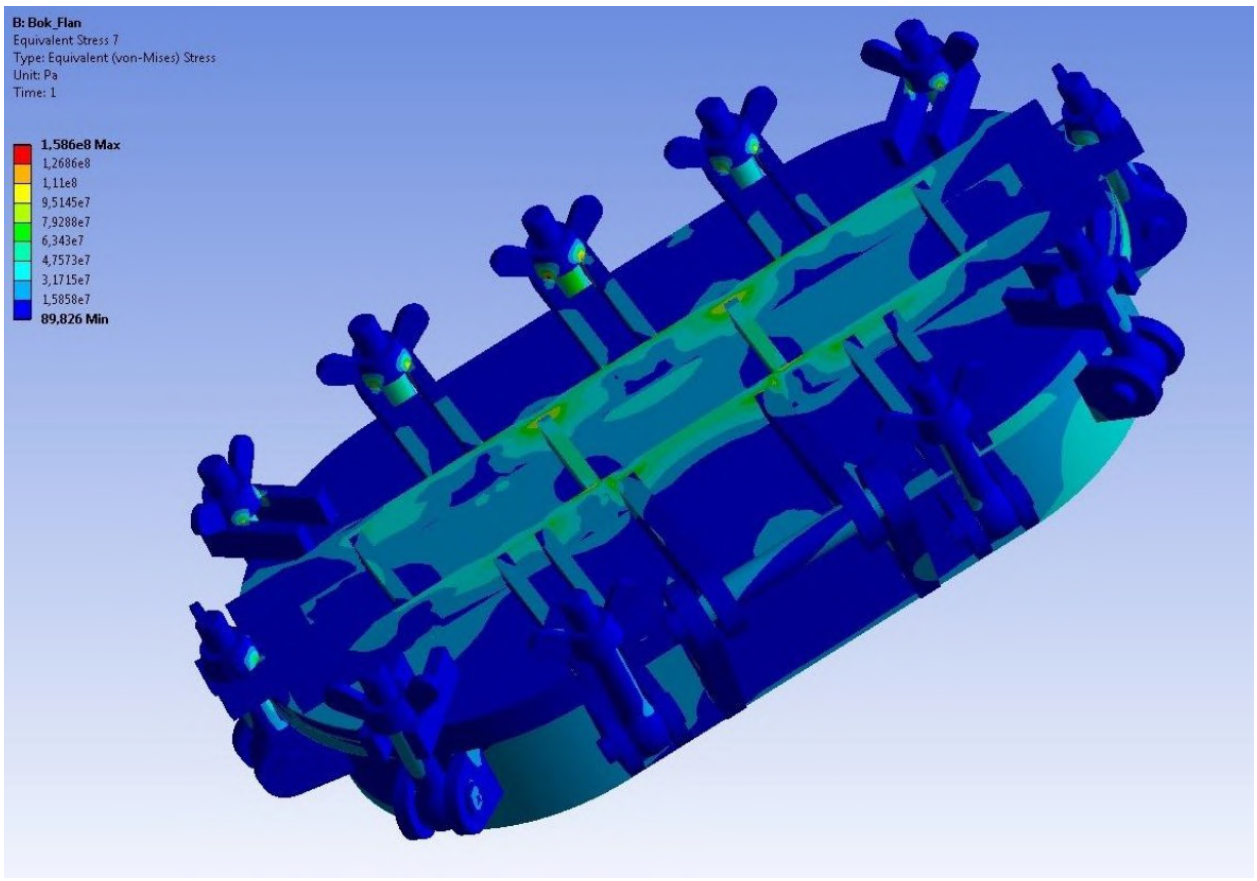

Fig. 2.105 Distribution of von Mises equivalent stresses.

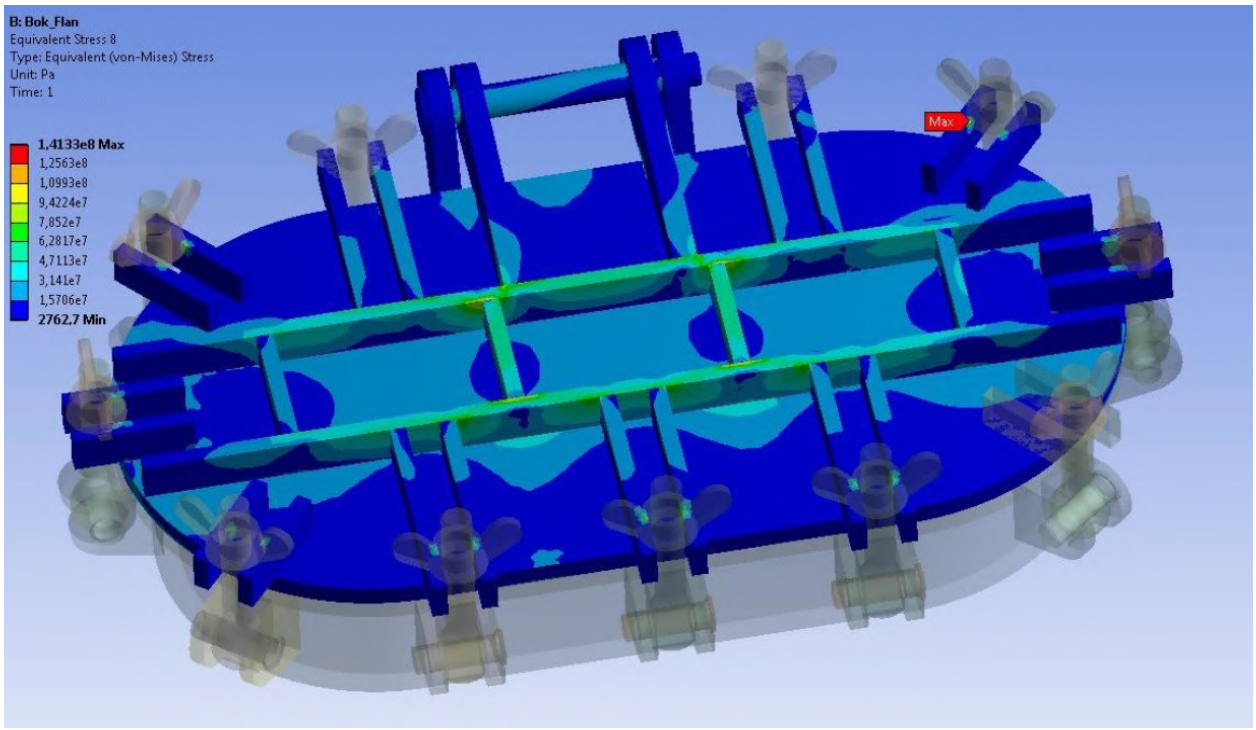

Fig. 2.106 Distribution of von Mises equivalent stresses in the lid.

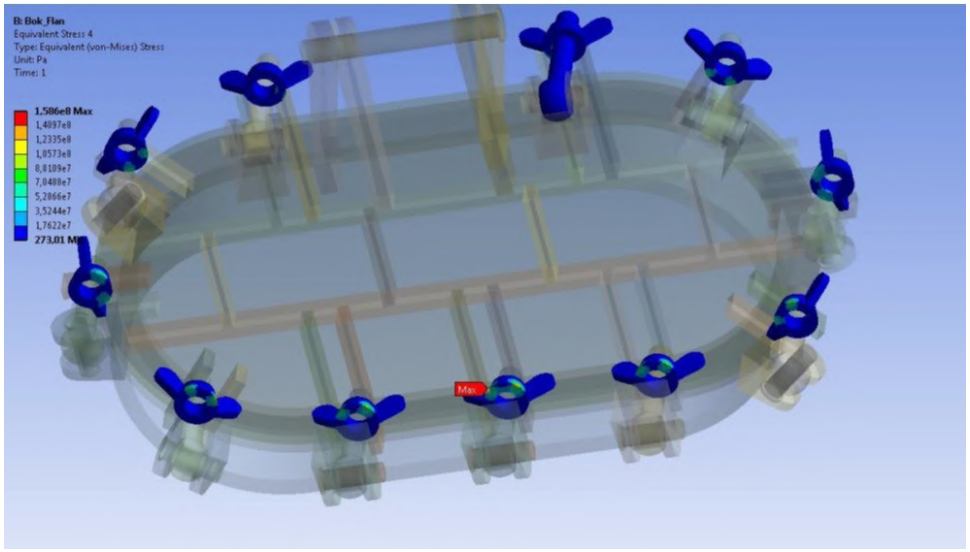

Fig. 2.107 Distribution of von Mises equivalent stresses in flange's nuts.

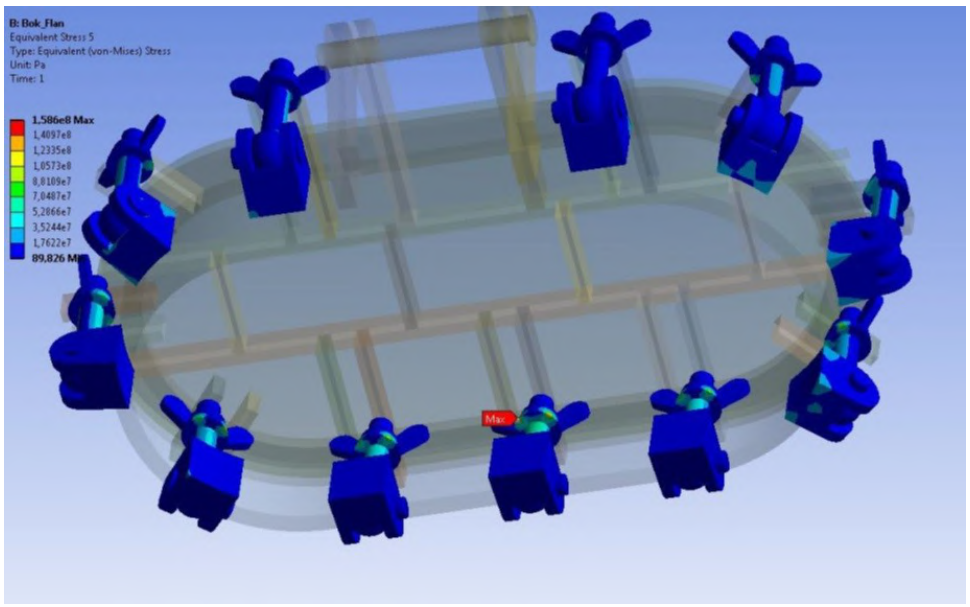

Fig. 2.108 Distribution of von Mises equivalent stresses in the ear lug.

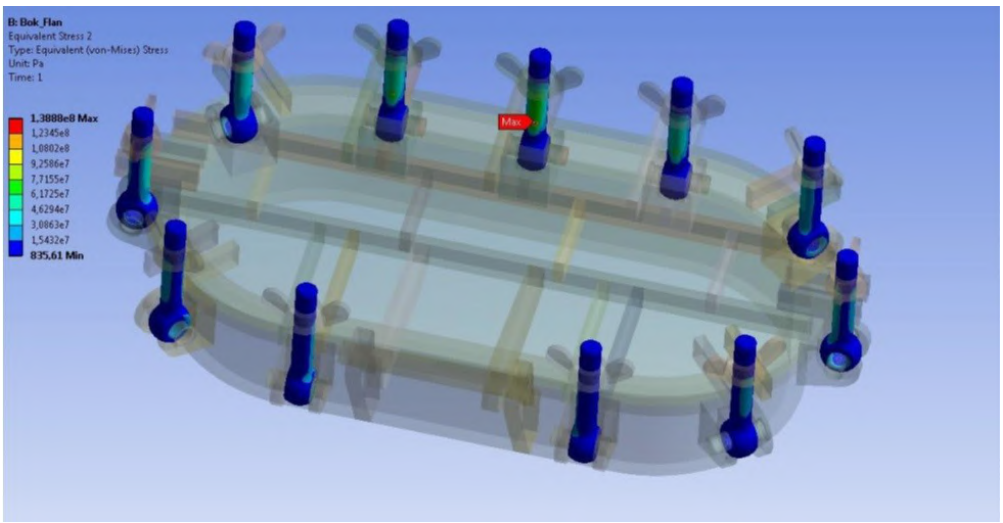

Fig. 2.109 Distribution of von Mises equivalent stresses in bolts.

2.3.6 Strength calculation of centering unit lugs for erection works

To assess the strength of centering unit's lugs when performing erection and transportation operations the case of structure's crane lift in vertical position has been considered. Fig. 2.1 presented the case of bin slinging. In the course of crane-lifting in vertical position the centering unit is fastened by ear lugs. The design model sets border shift conditions in all four lugs in form of shift limitation. The design load case for vertical lift of the bin is presented in Fig. 2.110. All design cases take into consideration the additional load equal to bin's weight and the weight of the upper sealing valve.

Calculation results of stress-strain state for bin's vertical lift in horizontal position are presented in Fig. 2.111-2.116.

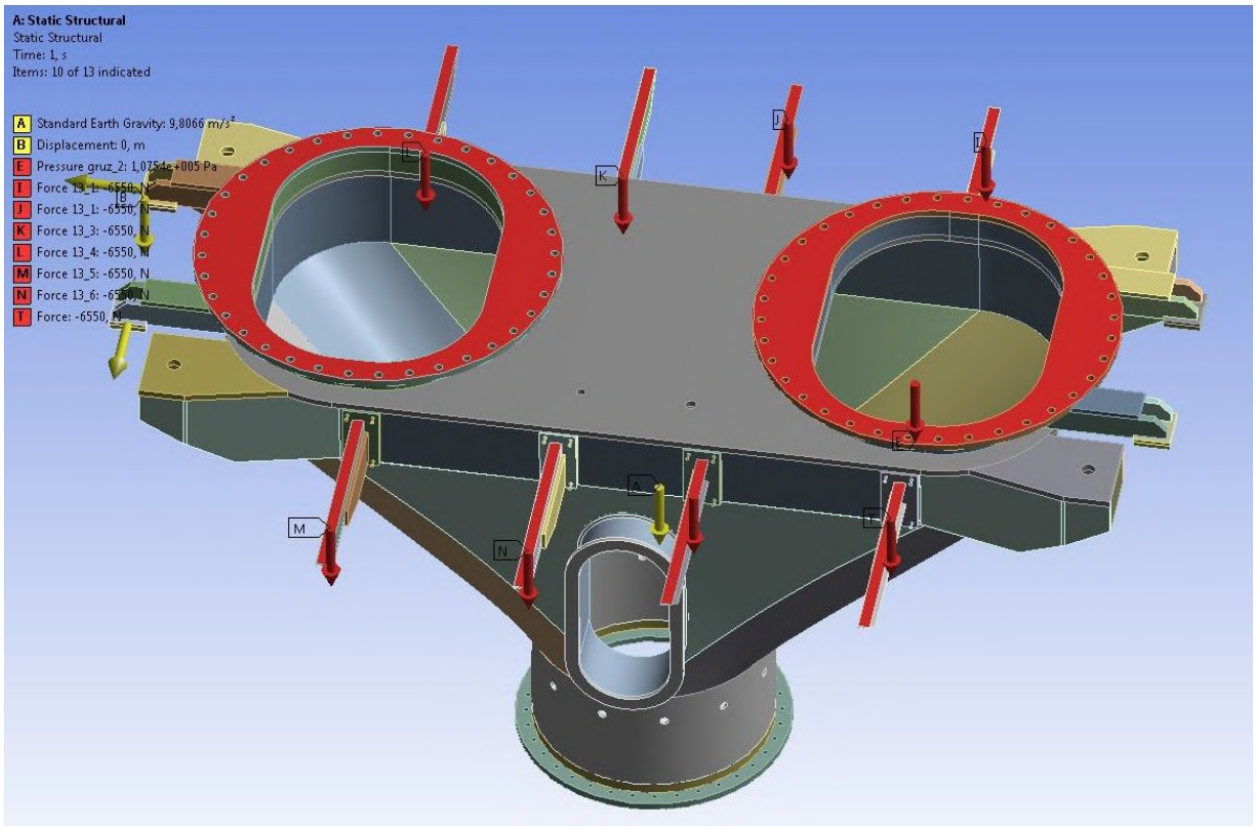

Fig. 2.110 Design case of centering unit's loading for calculation of support's lugs.

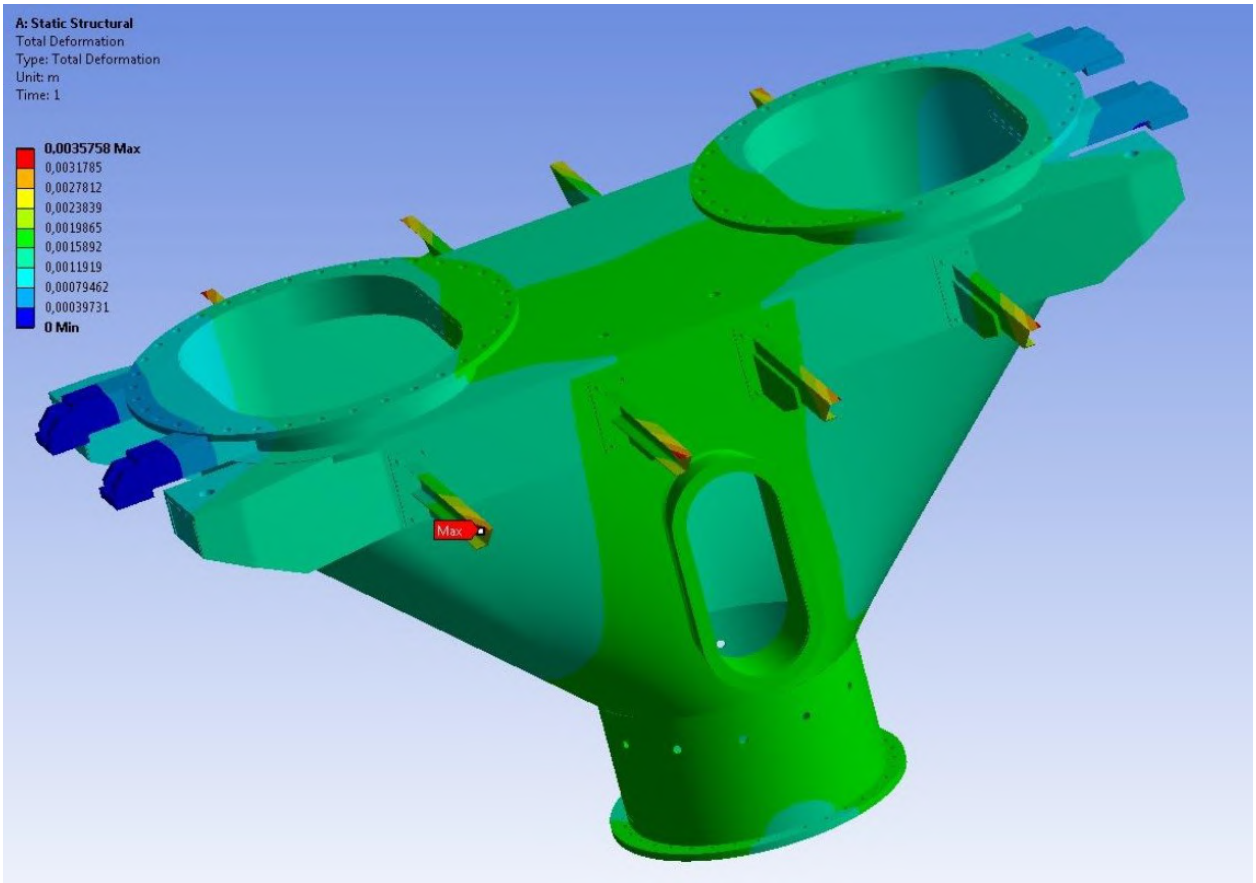

Fig. 2.111 Distribution of total strain arising in the centering unit.

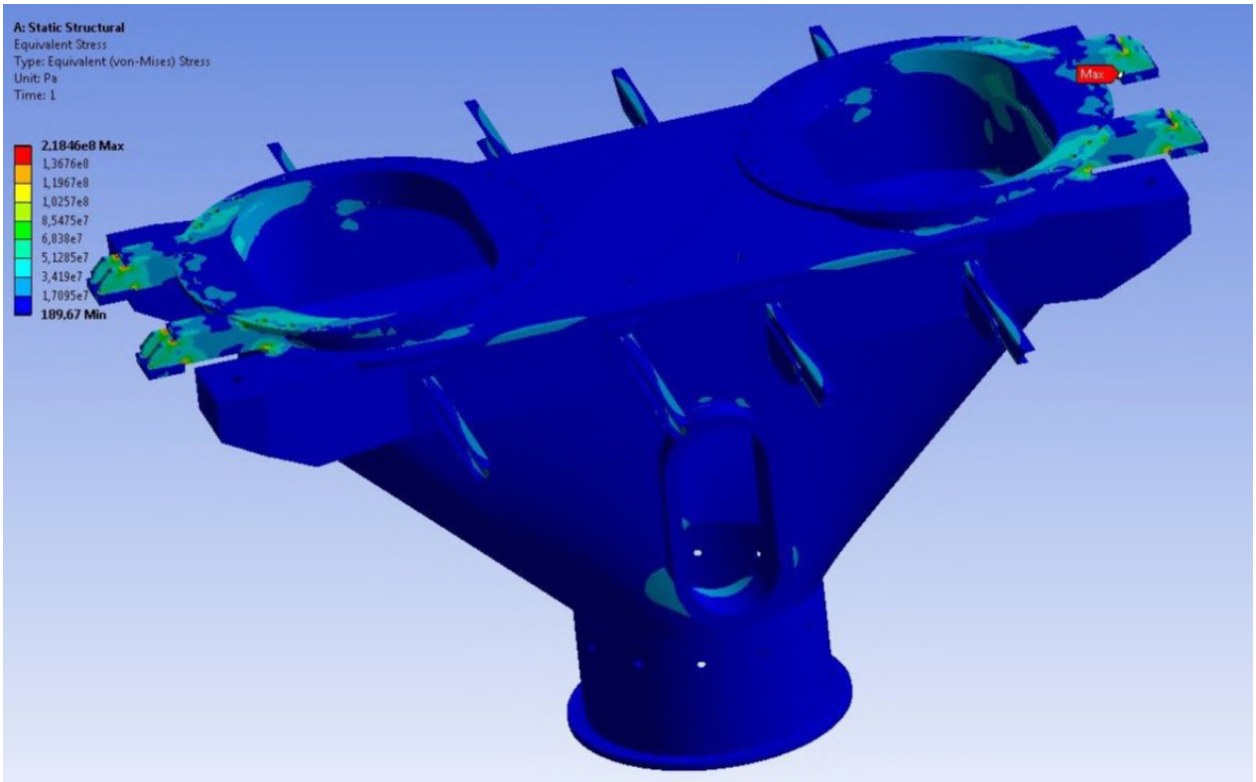

Fig. 2.112 Distribution of von Mises equivalent stresses when lifting in vertical position.

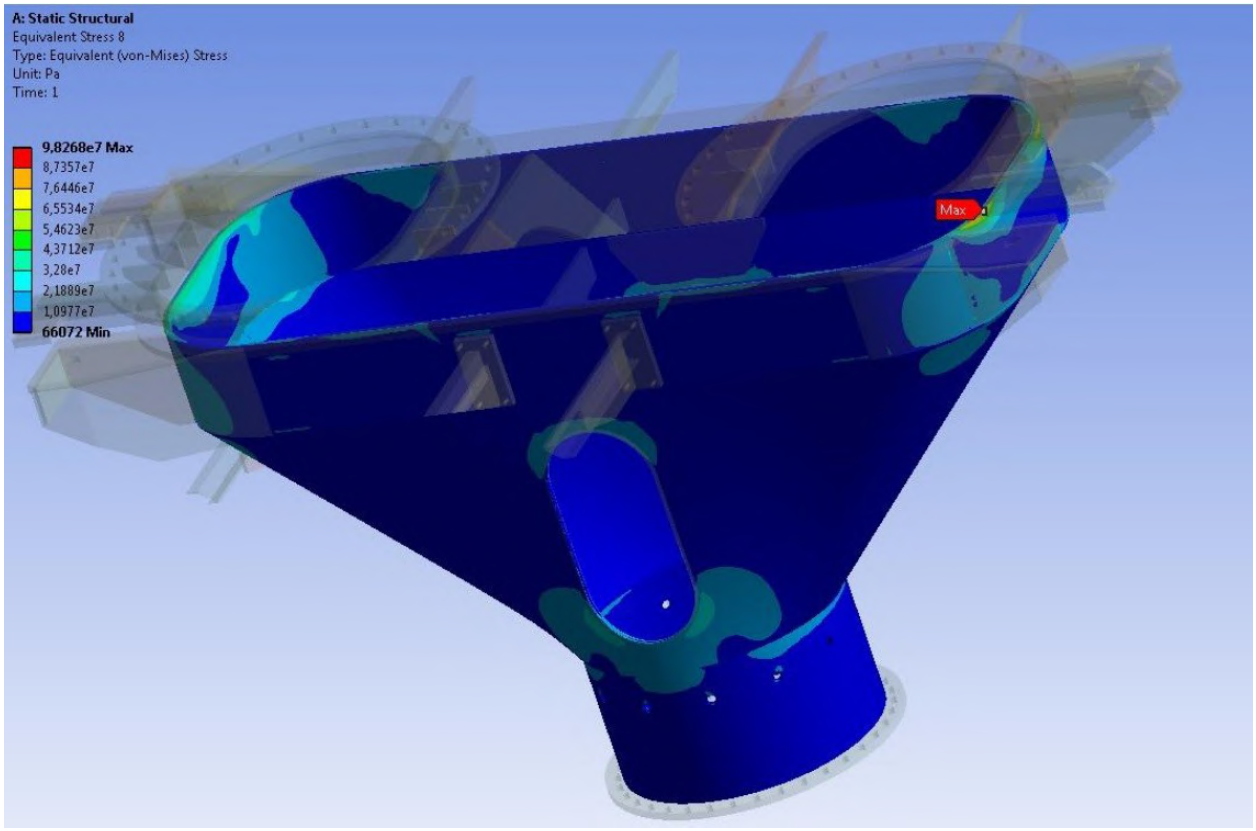

Fig. 2.113 Distribution of von Mises equivalent stresses in the cover when lifting in vertical position.

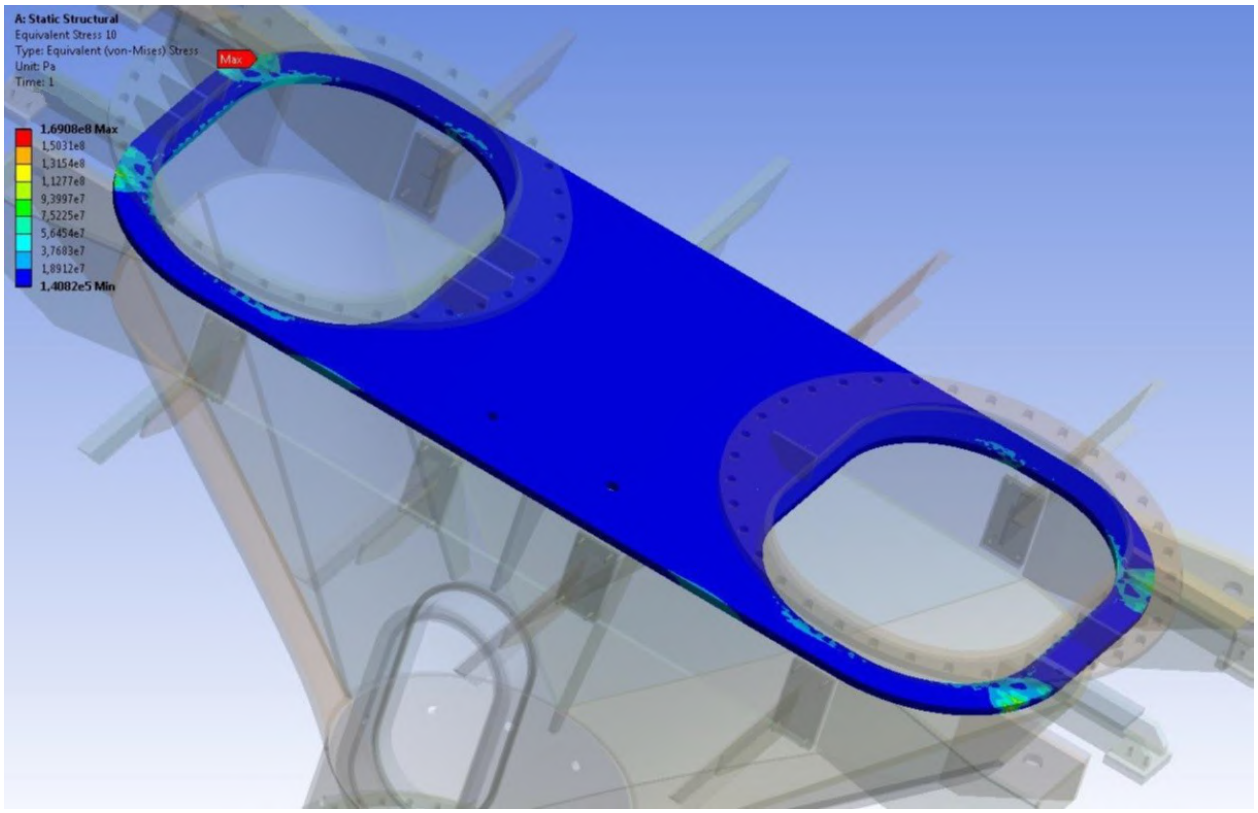

Fig. 2.114 Distribution of von Mises equivalent stresses in upper plate.

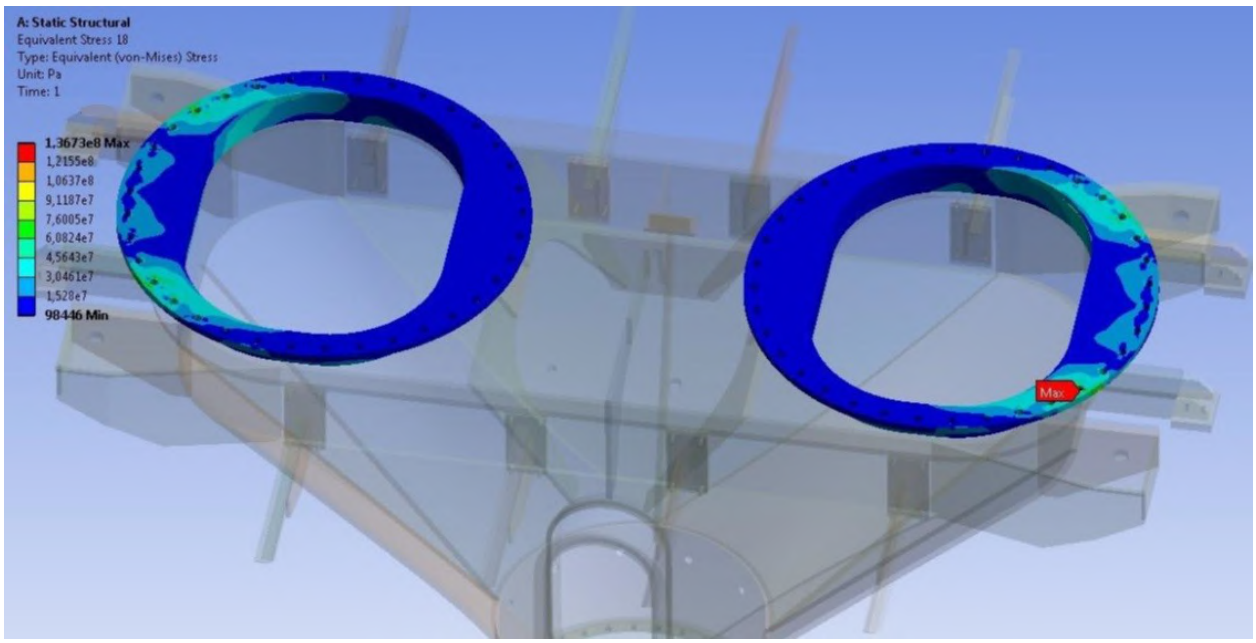

Fig. 2.115 Distribution of von Mises equivalent stresses in flanges.

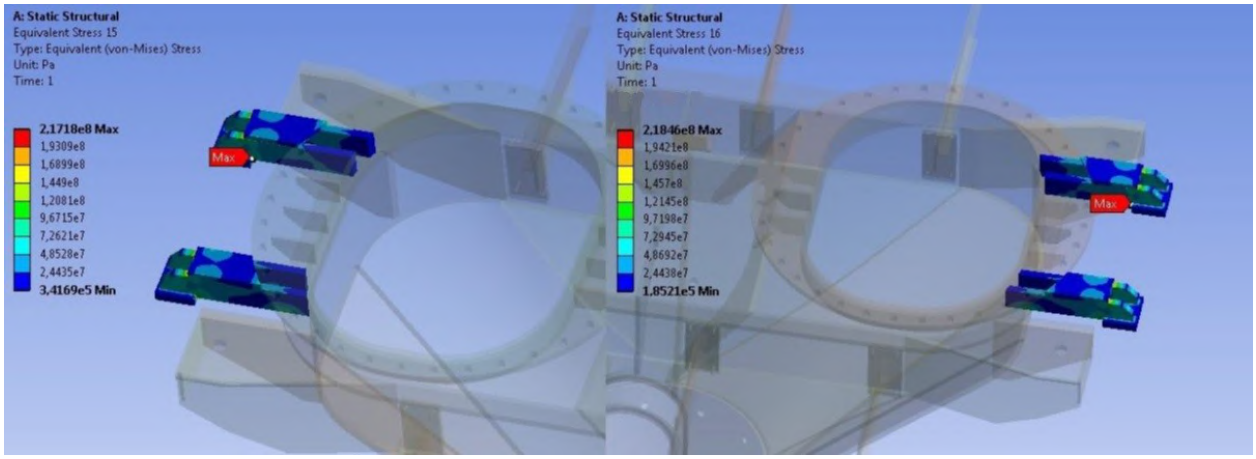

Fig. 2.116 Distribution of von Mises equivalent stresses in supports.

The centering unit meets strength and stiffness requirements when performing erection and transportation operations with the structure.

2.3.7 Design collective results

Calculation results obtained are presented as the summary Table 2.8. The table uses the following designations:

σ_{max}, the maximal stresses arising in structural member of material bin;

$[\sigma]$, permissible stresses in structural member of the bin;

n, safety factor of a structural member of material bin;

N, operational lifespan or number of cycles before appearance of fatigue cracks in bin's structure members. Time-related operational lifespan is calculated on the condition of making 57000 load cycles annually.

Table 2.8

Structural members of material bin	σ_{max} ***(MPa)***	***[σ] (MPa)***	***n***	***N***
Cylindrical wall	**90.8**	**136.9**	**1.5**	**$1x10^7$**
Curved wall	**117.4**	**191.6**	**1.63**	**$2.471x10^6$**
Top flange/ flange's cover	**109.1/49.6**	**188.8/191.6**	**1.73/3.86**	**$1x10^7$**
Bottom flange / flange's cover	**52.1/75.8**	**188.8/203.4**	**3.62/2.68**	**$1x10^7$**
Lateral flange / flange's cover	**86.7/57.7**	**184.4/191.6**	**2.12/3.32**	**$1x10^7$**
Top plate of the body frame	**144.3**	**188.8**	**1.3**	**$1.532x10^6$**
Support's lug	**149.6/152.7**	**188.8**	**1.26/1.23**	**$1.282x10^6$**
Bottom flange's bolts	**93.7**	**166.7**	**1.77**	**$1x10^7$**
Bolts of top right/left flanges	**51.2/52.3**	**166.7**	**3.25/3.18**	**$1x10^7$**
Bolts of lateral manhole	**138.0**	**166.7**	**1.2**	**$1.716x10^6$**

The presented results of designing show that charging bin's structure meets strength and stiffness requirements for all design loading cases. Structure's operation-al lifespan meets requirements of structure's period of operation. Since the charging bin operates under conditions of alternating load with symmetry factor equal to zero the structure's lifespan assessment has been carried out. Initiation of fatigue cracking is designed using SN-approach to description of Wehler curve. It should be noted that the biggest stresses in the structure arise in bin's support lug parts under conditions of joint loading due to maximal design earthquake of 6 points and normal service conditions. Operational lifespan of this part is lower as compared to operational lifespan of hopper body's load-bearing cover, but meets the requirements of service lifespan. Verification of selected Wehler SN curve is made on correspondence of the type of experimental dependence employed for lifespan assessment, and the type of stress state arising in the structure under study. These dependencies are presented for each design case in figures 2.19, 2.34, 2.60 and 2.76. Data presented in these figures show that for entire structure practically, and a danger zone in particular, stress state corresponds to tension state. This result means that employment of selected fatigue curve data obtained for the case of cyclic bending

was correct. Besides of that, the structure operates under conditions of tension for all design cases, thus allowing not performing structure buckling analysis.

The definitive design load case of the structure is impact of maximal design earthquake under normal service conditions, wherein maximal stresses arise in the centering unit's load-bearing cover.

2.4 CHAPTER CONCLUSIONS

Results of numerical calculation of the centering unit are as follows:

– the structure of the centering unit meets requirements to strength and stiffness;

– the most undesired design case of structure service is seismic impact under normal service conditions;

– the biggest stresses in centering unit's load-bearing cover arise at the joining of lateral flange and curved conical part of the structure;

– the structure's service lifespan till initiation of first fatigue cracking in the support's lug is 22.5years, thus meeting the service lifespan requirement.

CHAPTER III

3.1 INTRODUCTION

The purpose of this chapter is to calculate the strength of receiving hoppers with top-charging unit lining designed on the original prototype drawings "Ural metallurgical plant". These hoppers are the component part of the blast furnace top-charging unit.

The reference of hoppers to other parts of the entire charging unit is presented in introduction part monograph figure 0.3. The designs considered consist of upper hopper and lower hopper. The design features of the upper and lower receiving hoppers and operational service thereof as well, are determined by the following factors:

–overall weight of the entire structure as charged equals to 66000 kg;

–bottom elevation of the structure is at the level of 53898 mm, and the top elevation is at the level of 58848 mm. The top elevation is the place for charge loading, and the bottom level is the place for the upper sealing valve weighing 12,500 kg and flexible protection fitted to the silo's flange. The structure of the upper hopper is fitted with 4 external supports holding both the hopper itself and equipment fitted thereto. The structure of the lower hopper is fitted by the upper flange with the dosing unit, and by the lower flange is fitted with a sealing valve and flexible seal with total weight of 13,500 kg;

–receiving hoppers operate under conditions of steady-state thermal loading with the temperature of 450°C;

–the functional purpose of the discharging unit is batch mixture intake and charging thereof into the blast furnace. The calculations use the batch mixture (pellets) with maximum density of 2100 kg/m^3 as an example of a material to be charged;

–structures operate under conditions of static loading. The operational lifetime is 20 years;

–the blast furnace top-charging unit is located in Zaporozhye, Ukraine. The altitude of the land is 140 m, seismic zone corresponds to MSK-64.

3.2 INITIAL DATA, DESIGN CASES AND DESIGN ARRANGEMENTS OF RECEIVING HOPPERS

3.2.1 Characteristics of receiving hopper design

The geometrical dimensions of the upper receiving hopper metal structure and lower receiving hopper metal structure are specified according to the prototype drawing, presented in Fig. 3.1- 3.2.

The material of walls, bearing flanges, supporting brackets, upper weld-on linings and transportation lugs: plate steel 09G2S as per GOST19281-89.

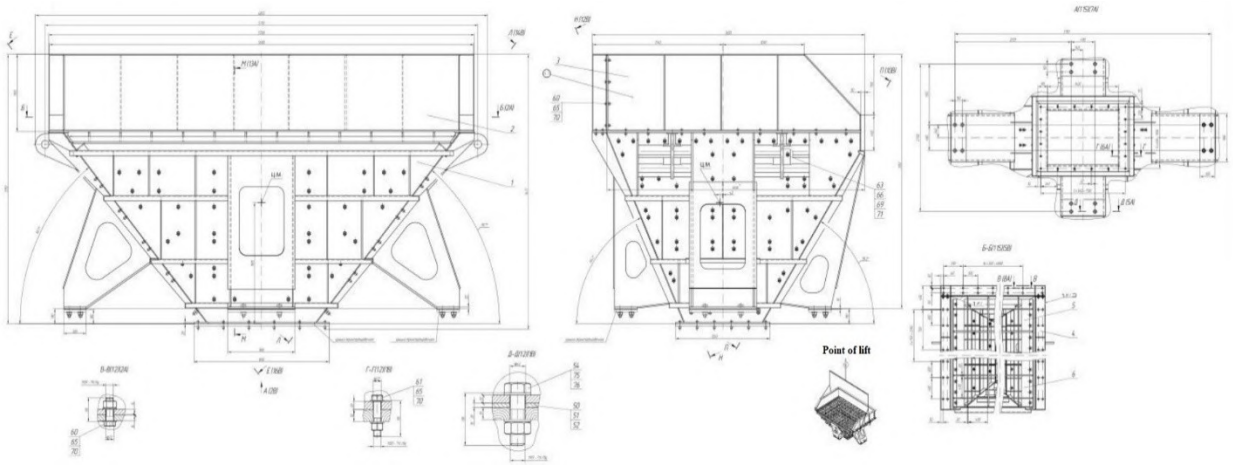

Fig.3.1 Geometrical parameters of the upper hopper

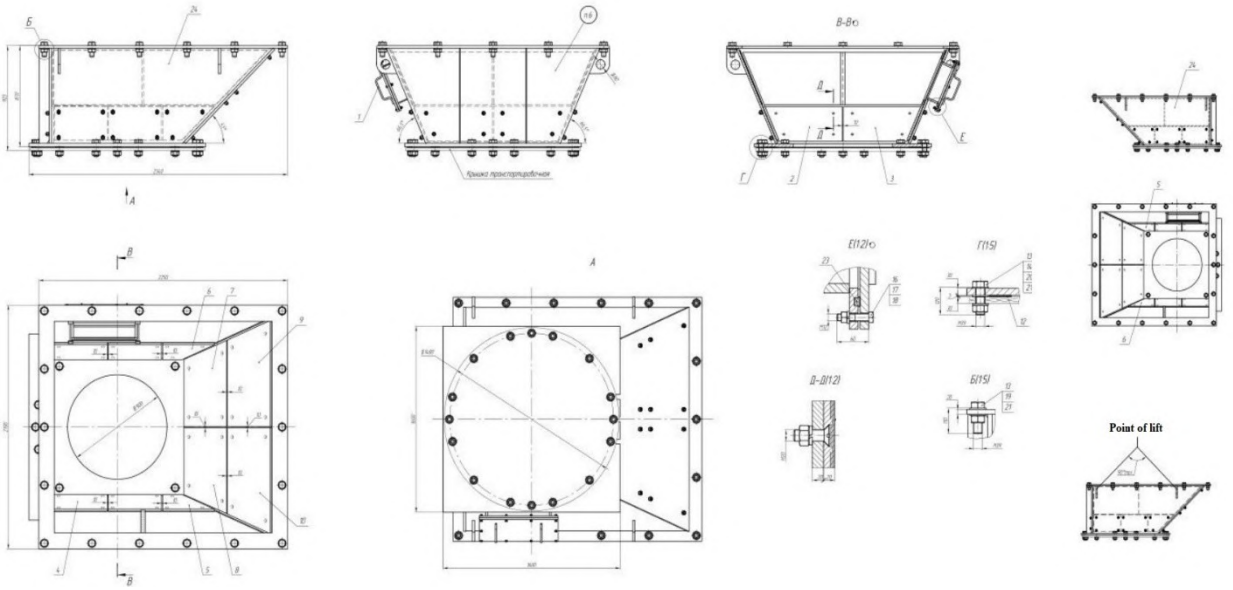

Fig. 3.2 Geometrical parameters of the lower hopper

3.2.2 The material properties and loading cases of receiving hoppers design

The operating conditions of the structure considered are determined by thermal steady-state field at the temperature of 450°C. The mechanical features of steel 09G2S based on GOST 1050-88 at 450°C are outlined in paragraph 1.2.2 of this work.

The normative documents mentioned in paragraph 1.2.3 of this work are used to determine loads, recommended design cases for centering top-charging unit and strength standards.

Besides thermal effect, the structure is further affected by the following loadings:

– weight of metal structure and batch mixture. Total weight of the entire structure shall not exceed 66000 kg;

– loose material loads acting on hopper's walls;

– wind effect;

– seismic impact.

3.2.2.1 Loose material loads on hopper's walls

The calculation of bulk material loads acting on hopper's walls is performed as per SNiP 2.09.03-85. Load safety indices $\mathbf{g_f}$ for structure dead weight, service loads on flooring, snow load and wind effect are taken as per SNiP 2.01.07-85 and are equal to:

– for horizontal and vertical pressures of bulk materials $\mathbf{g_f = 1.3}$;

– for specified angle of bulk material internal friction $\mathbf{g_f = 1.1}$.

The design bulk material vertical pressure at any point of the hopper for the case of loading up to the top elevation with loose material level surface shall be determined by the equation $\boldsymbol{p = n\gamma h}$, where $\boldsymbol{n}$ is the dynamic response factor, $\boldsymbol{\gamma}$ is material specific weight, $\boldsymbol{h}$ is material layer elevation above the given point.

The design horizontal (lateral) pressure onto vertical hopper's walls is specified by the equation $\boldsymbol{p_h = n*\lambda*\gamma*h}$, where $\boldsymbol{\lambda}$ is the lateral pressure factor that is taken as equal to $\boldsymbol{\lambda = p_h / p_\alpha = tg^2(45^0 - \phi/(2\, g_f))}$. Here $\boldsymbol{\phi}$ is material internal friction.

For the types of loose materials used the rated value of ϕ angle equals to 35°. The design value of the rated internal pressure angle is determined as the rated internal pressure angle deleted by the load safety factor $g_f = 1.1$. The value is $\lambda = 0.309564$.

Since the pressure from the loose material is determined by the maximum possible hopper filling degree, i.e. when material is over the hopper's top elevation at the natural degree of repose, the hopper is under the effect of the following loads:

– loose material pressure onto the receiving hopper's vertical wall. The rated lateral pressure for the case maximum possible loose material filling degree is determined by the equation $p_h = n \times \gamma \times z \times cos2\psi$, where n is the dynamic response factor (Table 1, Guidelines on calculation and designing of reinforced concrete, steel and combined bunkers, Moscow, Stroyizdat, 1983, 200 ps.). For the structures considered the values $n=1.2$, $\gamma=2100$, $\psi=35°$ (loose material repose angle), $cos2\psi=0.671$ are to be adopted;

– loose material pressure onto sloping wall in hopper's conical part. The angle of wall slope is adopted as constant and equal to α. The rated normal pressure on-to the sloping wall for the case of maximum possible loose material filling degree is determined as follows $p_h = n \times \gamma \times (z+h_0) \times cos^2\alpha + n \times \gamma \times z \times cos^2\psi \times sin^2\alpha$; where h_0 is the loose material height above hopper's top elevation level, and z is the coordinate of layer elevation from hopper's top edge;

– bin hopper pressure at lower flange aperture area shall be determined by the equation $p_\alpha = p_h / \lambda$.The pressures $p_h = n \times \gamma \times z \times cos^2\psi$, shall be determined by the value of bin hopper coordinate of the loose material top elevation in the hopper.

The calculations use the material with maximum specific weight of $2100\ kG/m^3$ as the batch mixture (pellets).

The values of operating pressures shall be determined for each receiving hopper in design cases for normal operating conditions.

3.2.2.2 Wind effect

The wind effect is an alternate load, for which two design values are set:

– limit design value;

– operating design value.

With respect to the norm the wind effect on the structure is set out as normal pressure preconditioned by general resistance of construction facility along *x* and *z* axes, and is conditionally applied to structure's projection on a plane square with appropriate axis. The limit design value of wind effect has been considered.

The limit design value of wind effect is determined by the formula:

$$W_m=\zeta_{FM}\times W_0\times C,$$

where, ζ_{FM} is the safety factor for the limit value of wind effect, determined by the time of equipment operation. The value of this factor is determined from the Table 9.1 of DBNV. 1.2-2:2006 and is adopted equal to $\zeta_{FM}= 0.90$.

W_0 is characteristic value of wind effect, and is defined by the wind region map 3 (Fig.1, annex E to design rules). For the city of Zaporozhye the wind effect characteristic value equals to 460Pa.

Coefficient C is calculated by the equation:

$$C = C_{aer}\times C_h\times C_{alt}\times C_{rel}\times C_{dir}\times C_d,$$

where C_{aer} is the aerodynamic factor of general air drag adopted as per DBNV.1.2-2:2006, and equals to 1.4;

C_h is the coefficient of construction facility height, determined by the annex 1 of the normative document and equals to $C_h=2.215$ for the upper receiving hopper and $Ch=2.175$ for the lower hopper**;**

C_{alt} is the coefficient of geographic height, equal to 1.0, since the geographic height of the construction facility is H = 150 m above sea level and under [H] = 500 m;

C_{rel} is the terrain relief factor, equal to 1.0**;**

C_{dir} is the coefficient of direction, equal 1.0;

C_d is the dynamic response factor, determined by Fig.9.6 of design rules and equals to 1.075. The value C is determined as follows:

$$C=1.4\times 2.175\times 1.0\times 1.0\times 1.0\times 1.075= 3.2734$$

$$C=1.4\times 2.2125\times 1.0\times 1.0\times 1.0\times 1.075= 3.3298$$

Accordingly, the limit design value of wind effect for hoppers equals to:

$$W_m = 0.9 \times 460 \times 3.198 = 1355.2 Pa;$$

$$W_m = 0.9 \times 460 \times 3.3298 = 1378.5 Pa.$$

Consideration of wind effect is performed for two load cases, namely: for wind effect lateral to the structure and for frontal wind pressure.

For the upper receiving hopper, the wind effect acts onto side shields. The area of side shields for side elevation equals to ***2.8719 m²***, and for back elevation the area is ***2.71 m²***. The wind effect, acting on the shield structure is replaced with an effect of a remote force. The remote force equals to the product of shield area and wind effect design value. These forces are applied to areas of hopper's top chord. Under conditions of frontal loading the remote force equals to ***3585 N*** and is applied with the following shield gravity center: ***x = –1.557 m, y=2.85 m, z = –1.4185m.*** Under conditions of lateral loading the remote force equals to ***3825 N*** and is applied with the following shield gravity center: ***x= 0.00634 m, y= 2.8289 m, z = –2.6557m.*** The coordinates of shield gravity centers were set out with reference to the global coordinate system.

3.2.2.3 Seismic impact, permissible stresses and design loading cases

The initial data for calculation of seismic strength of equipment designed are the seismic risk zoning of Ukraine (OSR-2004-A-B-C) developed by the Institute of Geophysics of the National Academy of Sciences of Ukraine. On the basis of construction norms "DBNV1.1-12:2006 Construction in seismic regions of Ukraine" the calculations are carried out for special load combination with consideration of seismic impact, i.e. design-basis earthquake (DE) and maximum design earthquakes (MDE).

The acceleration values for the given level of equipment mounting are determined by the method of linear interpolation in terms of vertical and horizontal oscillations with damping factor ***K= 0.02*** and site seismic intensity of 9 points (Fig. P9.1, Fig. P9.2 PNAE G-7-002-86). For seismic intensity of 6 points these parameters are multiplied by conversion factor equal to ***0.12*** (table P9.1). The initial parameters of accelerations for calculation on MDE are presented in tables 3.1, 3.2

and 3.3. The marks ***53.898 m*** and ***57.648 m*** correspond to lower and upper receiving hoppers of top-charging unit.

Table 3.1

Frequency, ***f, Hz***	**0**	**3**	**4**	**6**	**10**	**12**	**15**	**24**	**30**
Mark ***53.898 m***	**1.1**	**1.8**	**10.8**	**10.8**	**3.9**	**3.2**	**2.9**	**2.1**	**1.8**
Mark ***57.648 m***	**1.1**	**1.8**	**10.8**	**10.8**	**3.9**	**3.2**	**2.9**	**2.1**	**1.8**

Table 3.1 shows the generalized spectrum of horizontal oscillation response with damping factor 0.02 for the marks of equipment designed.

Table 3.2

Frequency, ***f, Hz***	**0**	**2**	**3**	**4**	**6**	**7**	**8**	**9**	**10**
Mark ***53.898 m***	**0.492**	**0.9**	**2.7**	**4.4**	**4.4**	**4.4**	**2.912**	**2.805**	**2.75**
Mark ***57.648 m***	**0.492**	**0.9**	**2.7**	**4.4**	**4.4**	**4.4**	**2.912**	**2.805**	**2.75**

Table 3.3

Frequency, ***f, Hz***	**10**	**12**	**13**	**15**	**17**	**19.5**	**24**	**30**
Mark ***53.898 m***	**2.75**	**2.595**	**2.54**	**2.43**	**2.328**	**2.169**	**1.906**	**1.59**
Mark ***57.648 m***	**2.75**	**2.595**	**2.54**	**2.43**	**2.328**	**2.169**	**1.906**	**1.59**

The tables 3.2 and 3.3 show the generalized spectrum of vertical vacillation response B with damping factor equal to 0.02 for the marks of the equipment designed.

The nominal permissible stress for receiving hoppers of the big charging unit of the blast furnace is adopted as per SNiP 2.04.12-86 equal to material yield strength at the temperature of 20°C reduced by the material and temperature adjustment safety factor. Material safety factor is adopted equal to $\gamma_м$***= 1.025***. Temperature adjustment factor is taken from the table 3 and equals to γ_m***= 2.2*** for the temperature of 450°C. Yield strength for 09G2S12 sheet steel 14mm thick at the temperature of 20°C is taken from the quality certificate No.21191dd. Oct.15, 2016 of Mariupol Ilyich Iron and Steel Works and equals to σ_{02}***= 465 MPa.*** The permissible stress is determined equal to: $[\sigma]_m = \sigma_{02}/(\gamma_м\gamma_m)$ ***= 206 МПа.*** Consideration of structure corrosion is made through reduction of permissible stress by the value proportional to sheet thickness variation. Corrosion wear is adopted equal to 3mm. The

permissible stress reduction factor due to corrosion is Δ= ***1,273***. Nominal permissible stress for receiving hoppers is adopted as equal to ***[σ] = [σ]$_m$/*** Δ = ***161МПа***.

Calculation of equipment static strength and structure performance capacity assessment under normal service conditions are performed as per IV theory of strength. Nominal permissible stress is used for assessment of structure performance capacity, both for calculation of seismic strength for the loading type "normal service conditions plus maximum design earthquakes" (NSC + MDE) and when taking into account the wind effect under loading type "normal service conditions + wind effect limit design " (NSC + LWE).

The required assessments of structure performance capacity define the following design cases and design loading patterns:

– structural design under conditions of NSC;

– structural design under conditions of NSC + LWE;

– structural design under conditions of seismic impact NSC + MDE;

– structural design under conditions of engineering assembly top-charging unit.

3.2.2.4 Design case for normal service conditions of the upper receiving hopper

The structure of the upper receiving hopper has one symmetry plane; therefore, the hopper design model represents one half of a structure with limiting symmetry conditions at symmetry plane. The hopper's structure has a protection grid weighing **2050kg** and lateral shields weighing **2058kg**. The protection grid rests on the structure's lateral board, and lateral shields are fixed to hopper's top chord. The design model does not take the protection grid and lateral shields into consideration, and the effect thereof is replaced with loads. The lateral board is under effect of the force equal to half of shield's weight, and at the top chord act the force equal to half of shield's weight. The design case for normal service conditions (NSC) is defined with the following loads acting on hopper's structure:

– grid weight force acting on hopper's lateral collar and equal to

$$G_{kl} = 1025kG = 10055N;$$

– shield's weight force acting the hopper's top collar and equal to ***1029 kG;***

– structure's bulk weight force equal to $G_к = 5915kG;$

– thermal stress upon application of steady-state heat up to 450°C;

– loose material pressure onto sloping lateral wall (angle of slope $\alpha=50.7°$) in hopper's conical part:

$$p_h = n \times \gamma \times (z+h_0) \times \cos^2\alpha + n \times \gamma \times z \times \cos^2\psi \times \sin^2\alpha;$$

Where, $h_0 = 0.96\ m,\ n = 1.4,\ \gamma = 2100\ kg/m^3,\ \psi=35°,\ \alpha=50.7°$, **z** is measured off from hopper's top elevation. Hopper's volume equals to $20\ m^3$, p_h is determined as follows:

$$p_h = 1132.26 + 2360.788 \times z;$$

– loose material pressure onto sloping back wall (angle of slope $\alpha=66.2°$) in hopper's conical part

$$p_h = n \times \gamma \times (z+h_0) \times \cos^2\alpha + n \times \gamma \times z \times \cos^2\psi \times \sin^2\alpha;$$

Where $h_0 = 0.96\ m,\ n = 1.4,\ \gamma = 2100\ kg/m^3,\ \psi=35°,\ \alpha=66.2°$,**z** is measured off from hopper's top elevation, and p_h is determined as follows:

$$p_h = 459.625 + 2130.281 \times z;$$

– loose material pressure onto sloping front wall (angle of slope $\alpha=66.2°$) in hopper's conical part:

$$p_h = n \times \gamma \times (z+h_0) \times \cos^2\alpha + n \times \gamma \times z \times \cos^2\psi \times \sin^2\alpha;$$

Where, $h_0 = 0.96\ m,\ n = 1.4,\ \gamma = 2100\ kg/m^3,\ \psi=35°,\ \alpha=66.2°$, **z** is measured off from hopper's top elevation, and p_h is determined as follows:

$$p_h = 783.731 + 2241.353 \times z.$$

Design model of the left hopper under normal service conditions is presented in Fig.1. The pattern of loose material pressure application onto hopper's conical sloping walls is presented in Fig. 3.3.

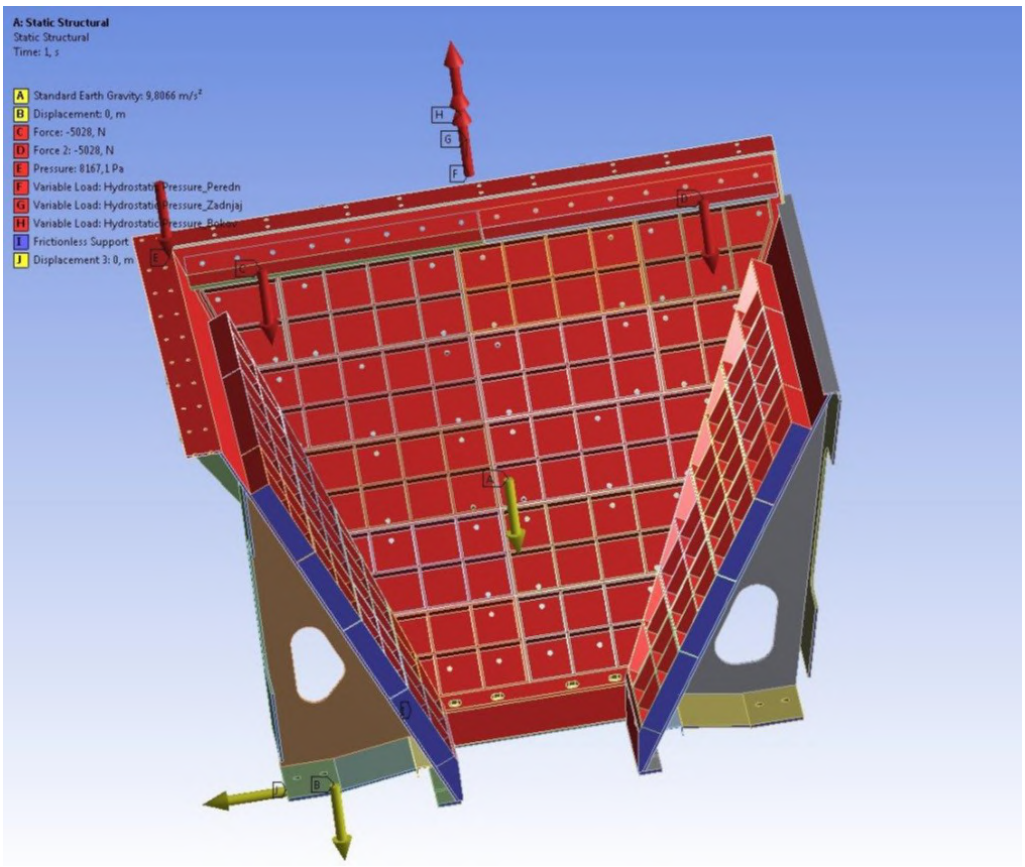

Fig.3.3. Design loading pattern of the upper hopper in NSC.

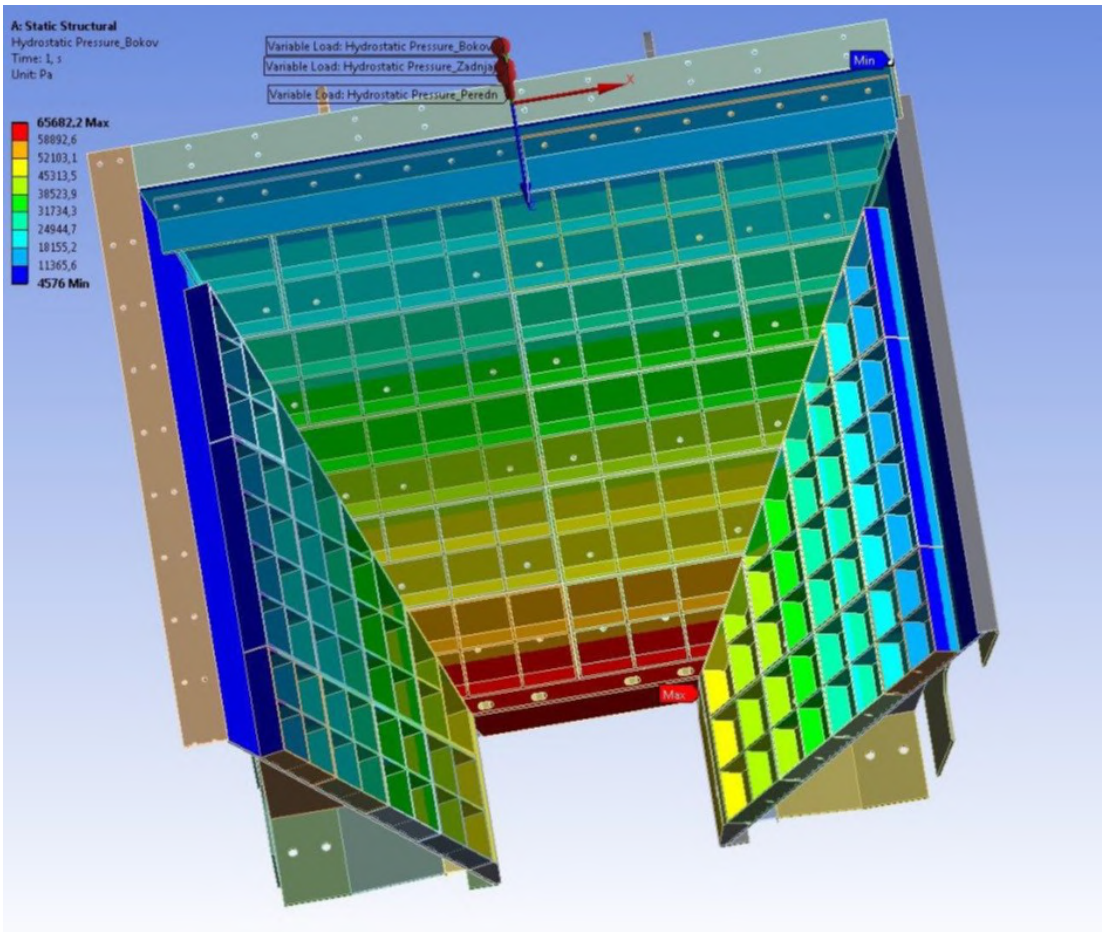

Fig.3.4. Loose material pressure distribution on hopper's walls.

3.2.2.5 Design case for normal service conditions of the lower receiving hopper

The structure of lower receiving hopper at the top reinforced collar is fixed with the top-charging unit, and at the bottom reinforced collar it is fixed with a flexible jumper connection and sealing valve. The design case for normal service conditions (NSC) is defined by the following loads acting on hopper's structure:

– structure's bulk weight force equal to $G_к$= ***2188 kG;***

– thermal stress upon application of steady-state heat up to 450°C;

– loose material pressure onto vertical hopper's wall: $p_h = n \times \lambda \times \gamma \times h$, where $\lambda = 0.309564$, n is the dynamic response factor,

for $n = 1.2$, $\gamma = 2\ 100\ kg/m^3$, p_h is determined as follows:

$$p_h = 780.1 \times z;$$

– design loose material pressure onto sloping wall in hopper's conical part is calculated as follows:

$p_\alpha = n \times m_o \times \gamma \times h$, where $m_o = \cos^2\alpha + \lambda \sin^2\alpha$; α is the angle of plane's slope relative to horizon.

For each segment's surface the design normal pressure is set out as follows:

Surface 1: $\alpha = 66.5^0$, $\lambda = 0.309564$, $m_o = 0{,}419344$,

$$p_h = 1215.1 \times z;$$

Surface 2: $\alpha = 45°$, $\lambda = 0.309564$, $m_o = 0.654782$,

$$p_h = 1650.1 \times z;$$

z is measured off from the hopper's top elevation.

Design model of the left hopper under normal service conditions is presented in figure 3.5. The pattern of loose material pressure application onto hopper's conical walls is presented in Fig. 3.6.

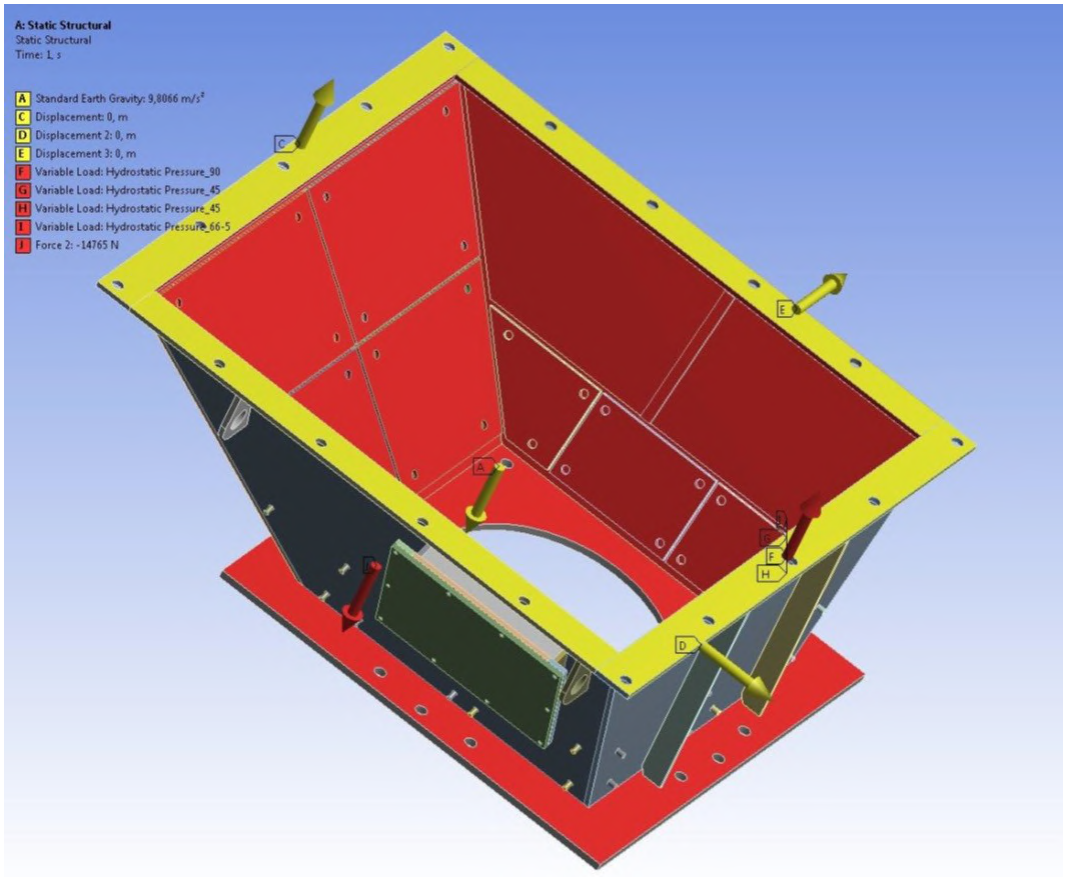

Fig.3.5 Design loading pattern of the lower hopper in NSC.

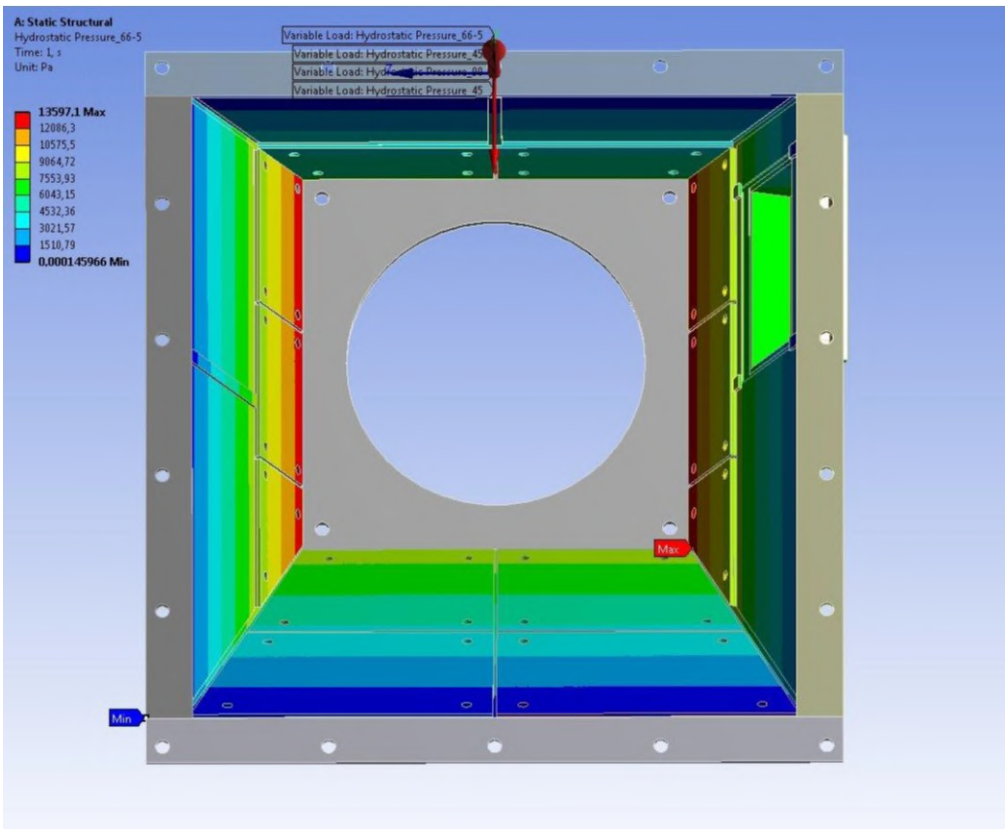

Fig.3.6 Loose material pressure distribution on hopper's walls.

3.2.3 Fundamental principles for performing calculations and analysis of calculation data.

Calculations of receiving hoppers are performed on a model with dimensions corresponding to design engineering product. The upper hopper design model takes the brickwork lining into consideration. The necessity to consider brickwork lining in a model is defined by conditions of hopper's loading. The brickwork lining is fixed at the pressure shell, and a contact may exist between sides of adjacent brickwork linings under the effect of external load. When performing calculations, the following features are to be taken into consideration:

– the geometrical model shall take into consideration all structure's stress risers caused by fillets and chamfers of component parts;

– structure's materials shall take into consideration, both linear-elastic isotropic materials with mechanical characteristics corresponding to operational temperature of 450°C. In case the yield strength stresses are exceeded, when solving inelastic problem, the bilinear deformation curve for the temperature of 450°C shall be used.

– an ideal contact interaction is adopted for all welded structure's surfaces. For bonded contact the metal-on-metal friction coefficient shall be adopted equal to 0.15;

– the IVth theory of strength shall be adopted as a criterion of strength. For all design cases the assessment of structure's performance capacity shall be performed by the permissible stress calculated as per item 2.3.4 and taken equal to ***[σ] = 161 MPa***.

– with regards for all erection and transportation operations with structures the design patterns shall adopt the value of overload factor as per GOST R 51282-99 (table 10) equal to **1.2.**

– when analyzing the calculation results the local extremums of equivalent stresses acting in areas within a finite element are not to be considered. This recommendation is related to numerical singularity of finite element method and can

be removed by means of submodelling of a structure the given area and corrective remeshing of the finite element model.

3.2.4 Description of hopper designing procedure.

Structure's geometric modeling has been performed using three-dimensional presentation of the hopper in SolidWorks software-package. Physical modeling has been carried out in ANSYS software-package. The calculation procedure of structure's stress-strain state is the finite-element method implemented by ANSYS WORKBENCH calculation package.

The upper hopper structure's finite-element model is presented in fig.3.7 and consists of 2534572 nodes united by 1008124 elements. The mesh quality is 0.7394. The lower hopper structure's finite-element model is presented in fig.3.8 and consists of 952749 nodes united by 307168 elements. The mesh quality is 0.815. Dimensions of a finite element for the presented models are within 151mm.

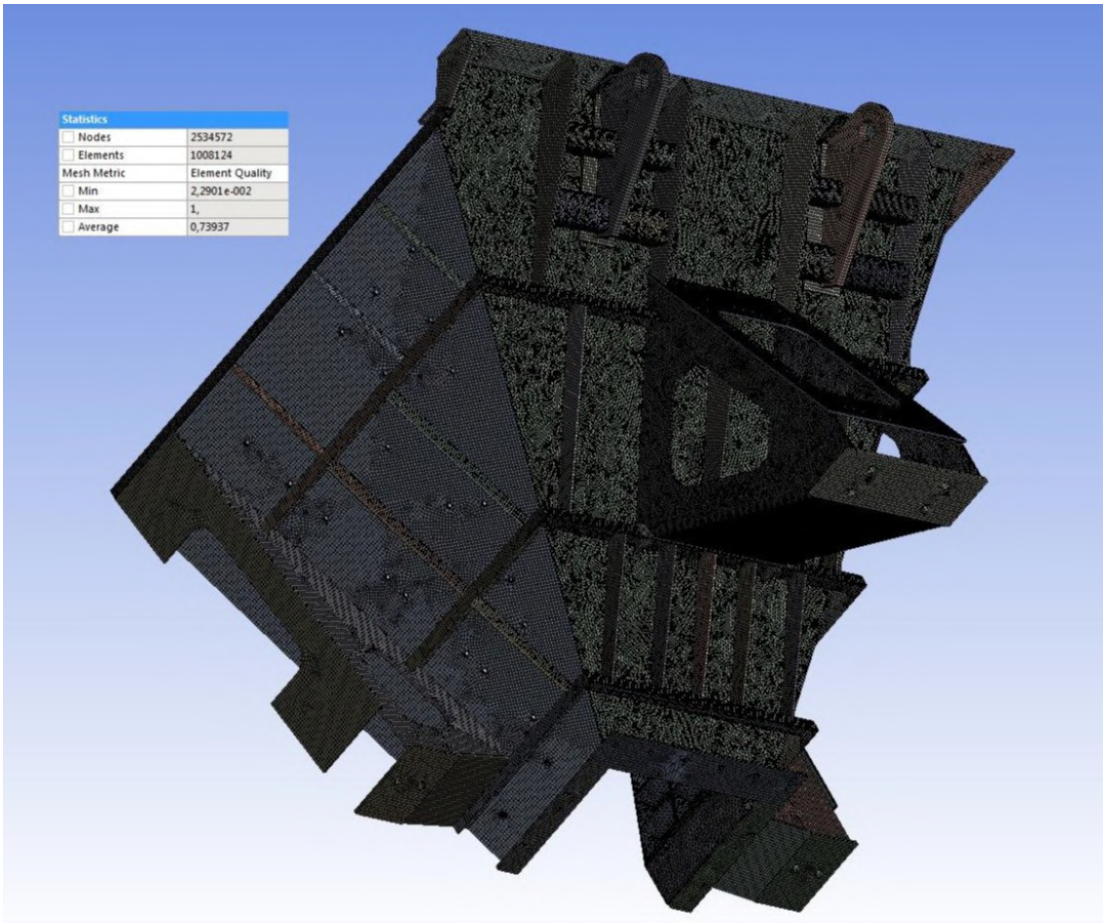

Fig. 3.7 Finite-element model for upper hopper designing.

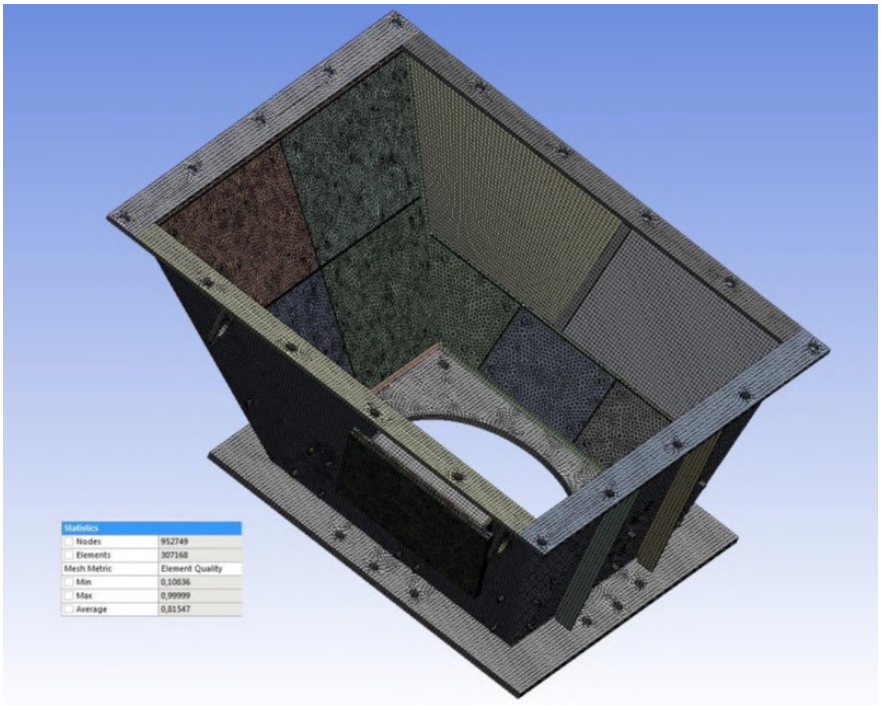

Fig. 3.8 Finite-element model for lower hopper designing

3.3 UPPER HOPPER DESIGN CALCULATION

3.3.1 Structural design for normal service conditions

Calculations results of the hopper under normal service conditions are presented in a form of stress and strain patterns in Fig. 3.9-3.17.

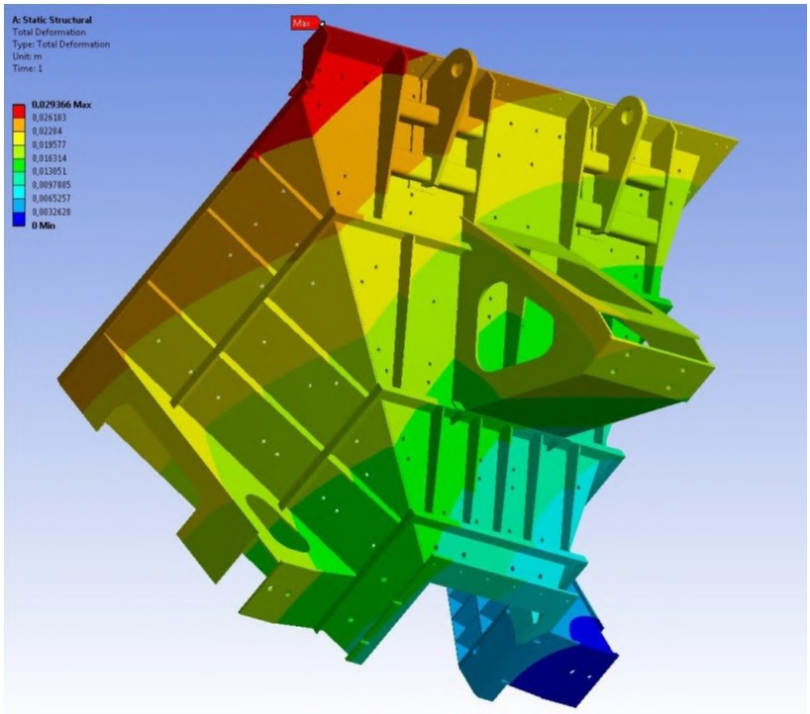

Fig. 3.9 Distribution of total strains arising in the structure

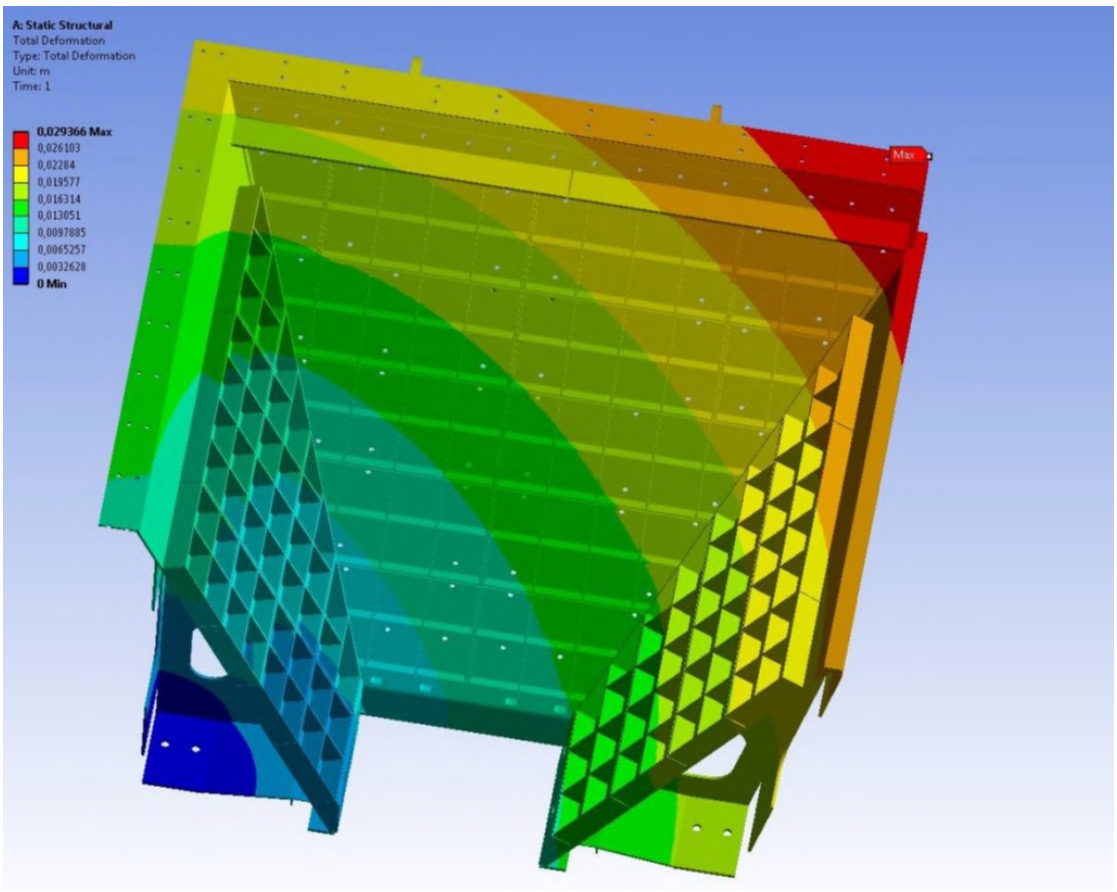

Fig. 3.10 Distribution of total strains arising in the structure.

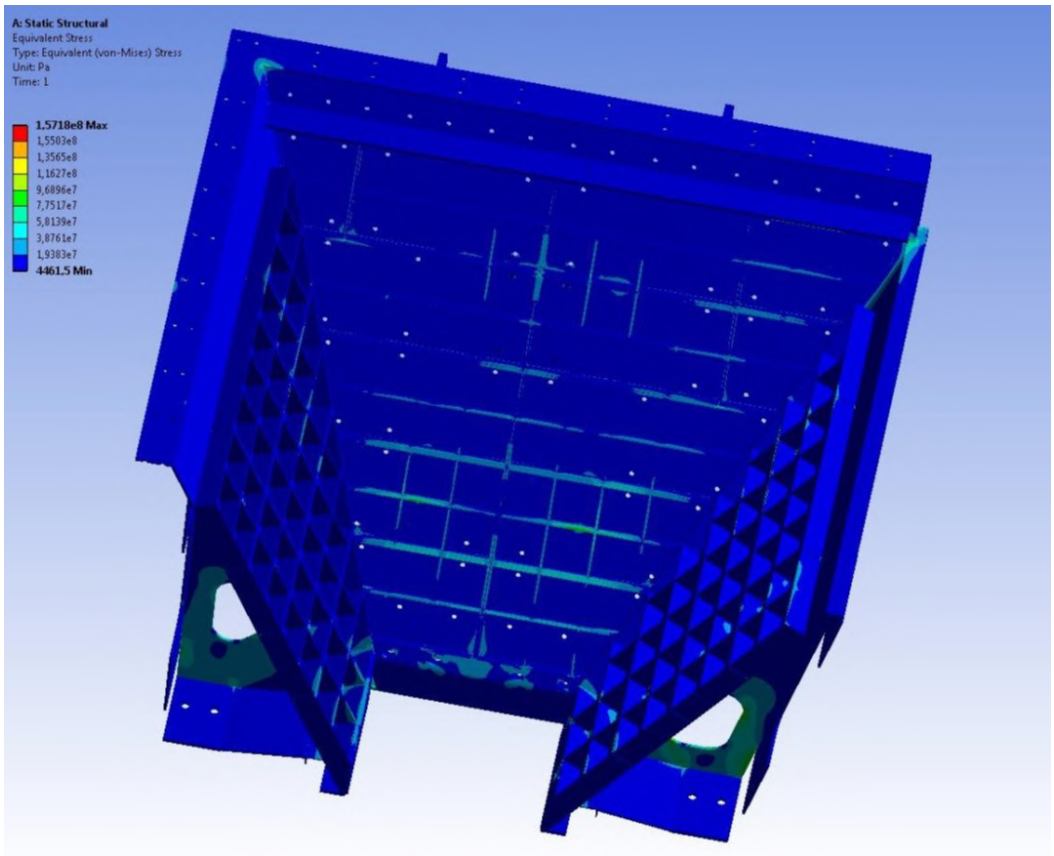

Fig. 3.11 Distribution of von Mises equivalent stresses in the hopper.

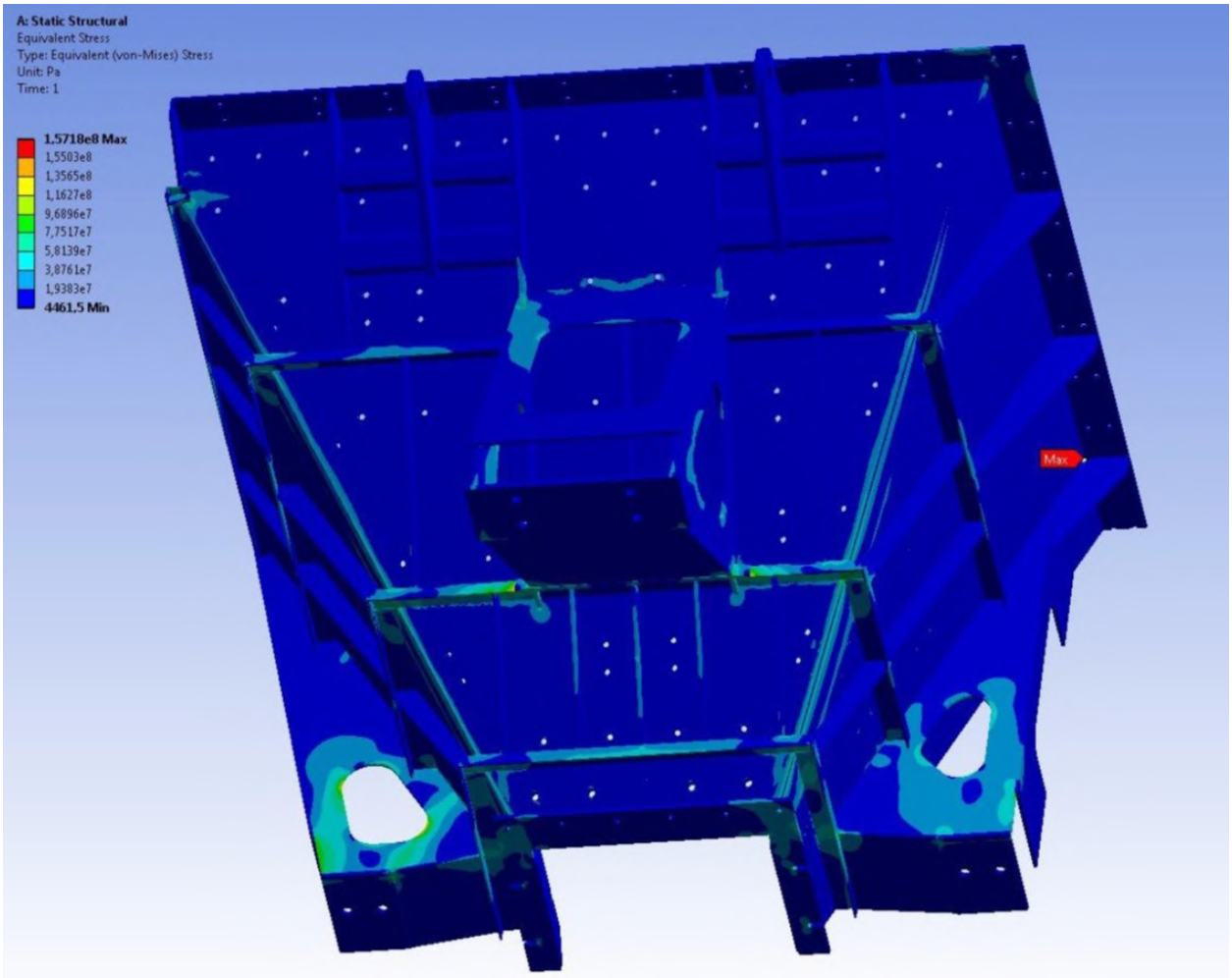

Fig. 3.12 Distribution of von Mises equivalent stresses in the hopper.

The biggest stresses of 157 MPa arise at the of rib's edge border. The value of this stress is local in nature and does not exceed the size of a finite element. The most loaded elements of the hopper are structure's supports and collars. The figures 3.13 - 3.17 present pictures of distribution of von Mises equivalent stresses in upper hopper elements in question. All load-bearing elements of the hopper show arising of stresses that do not exceed 146MPa, which is by 10.2% lower than material permissible stresses at hopper's operational temperature.

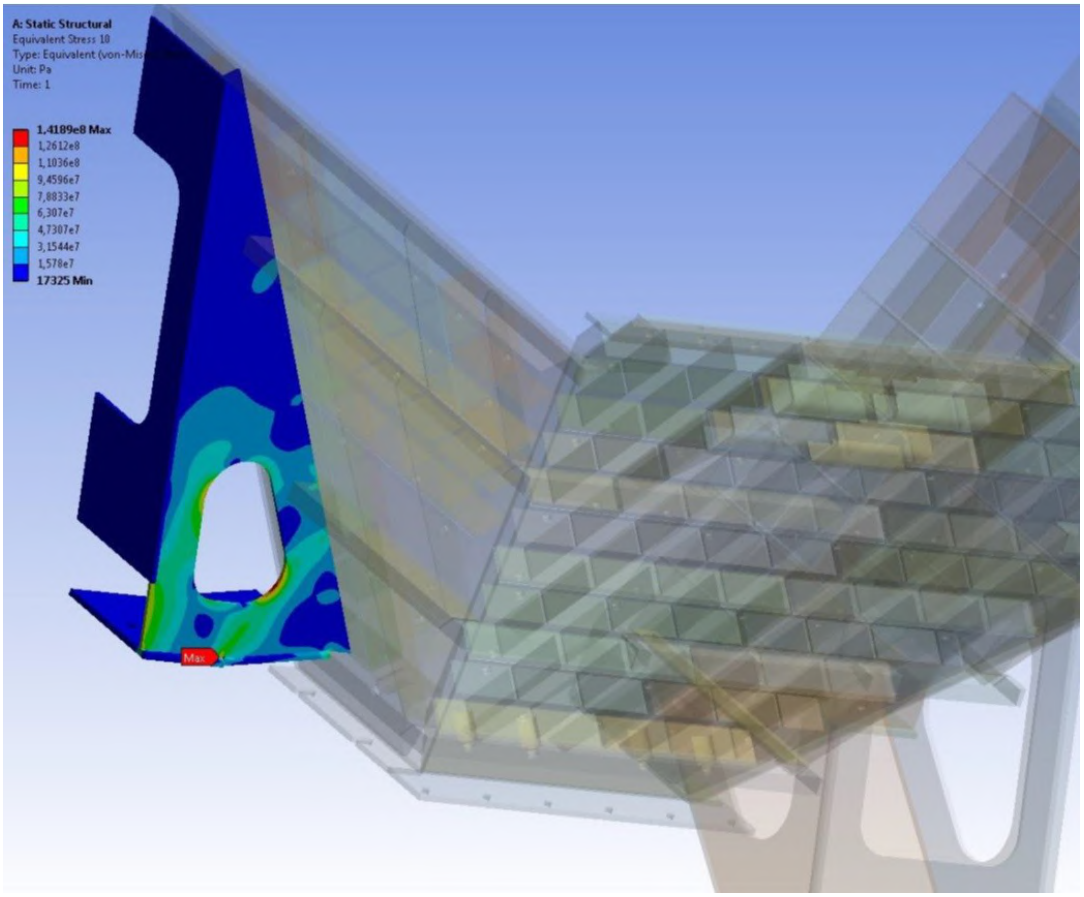

Fig. 3.13 Distribution of von Mises equivalent stresses in hopper's support.

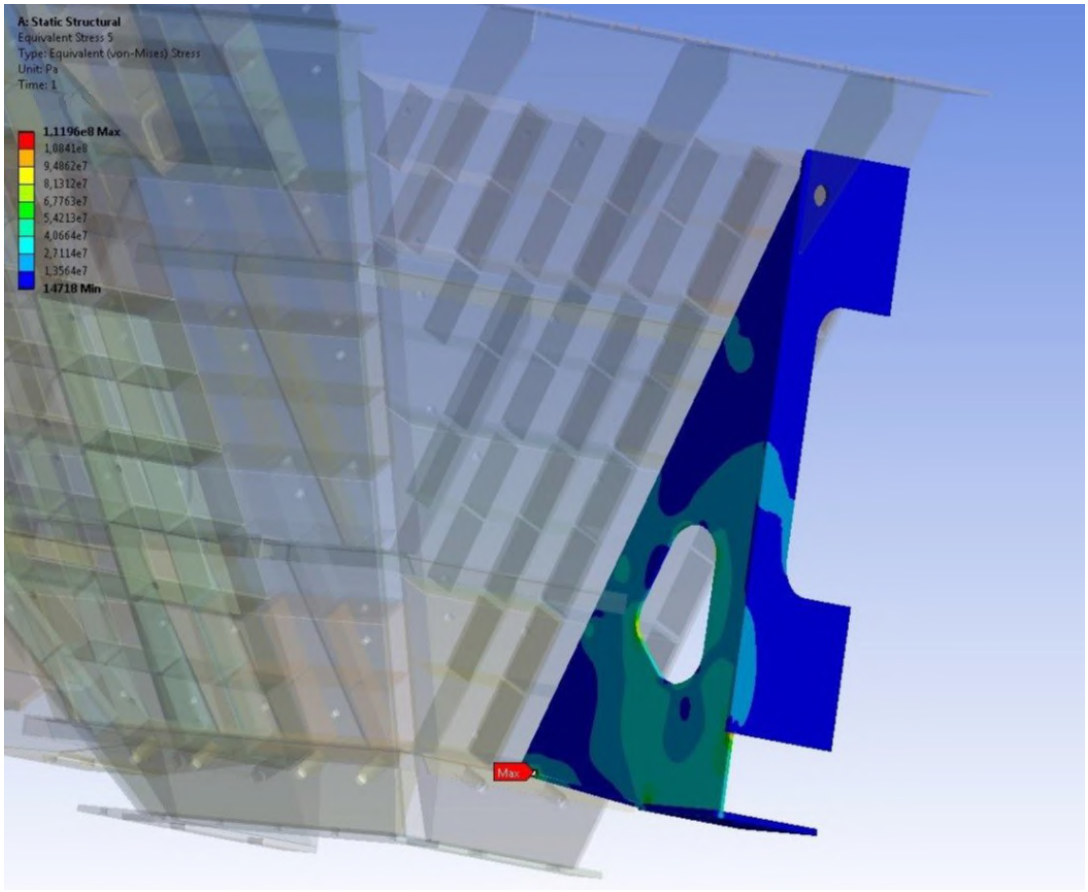

Fig. 3.14 Distribution of von Mises equivalent stresses in hopper's support.

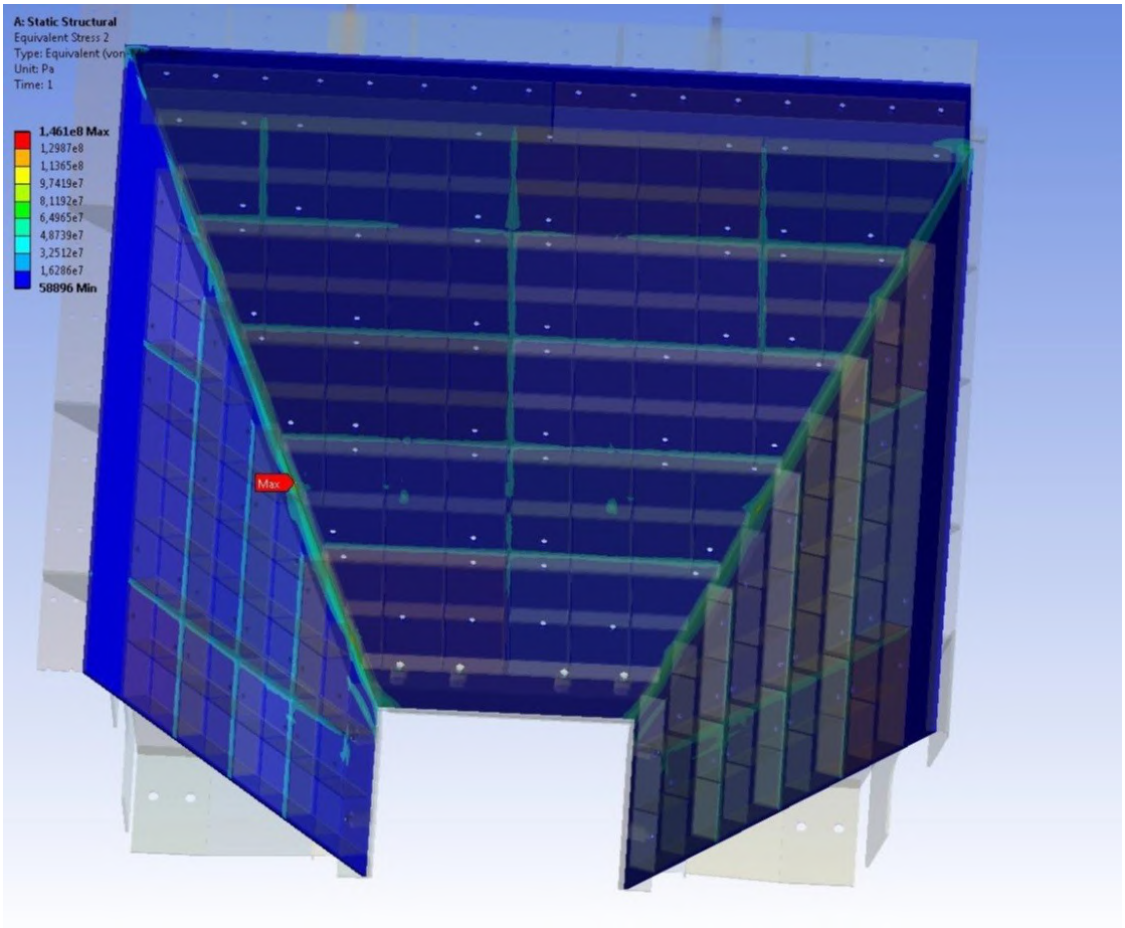

Fig. 3.15 Distribution of von Mises equivalent stresses in hopper's load-bearing cover.

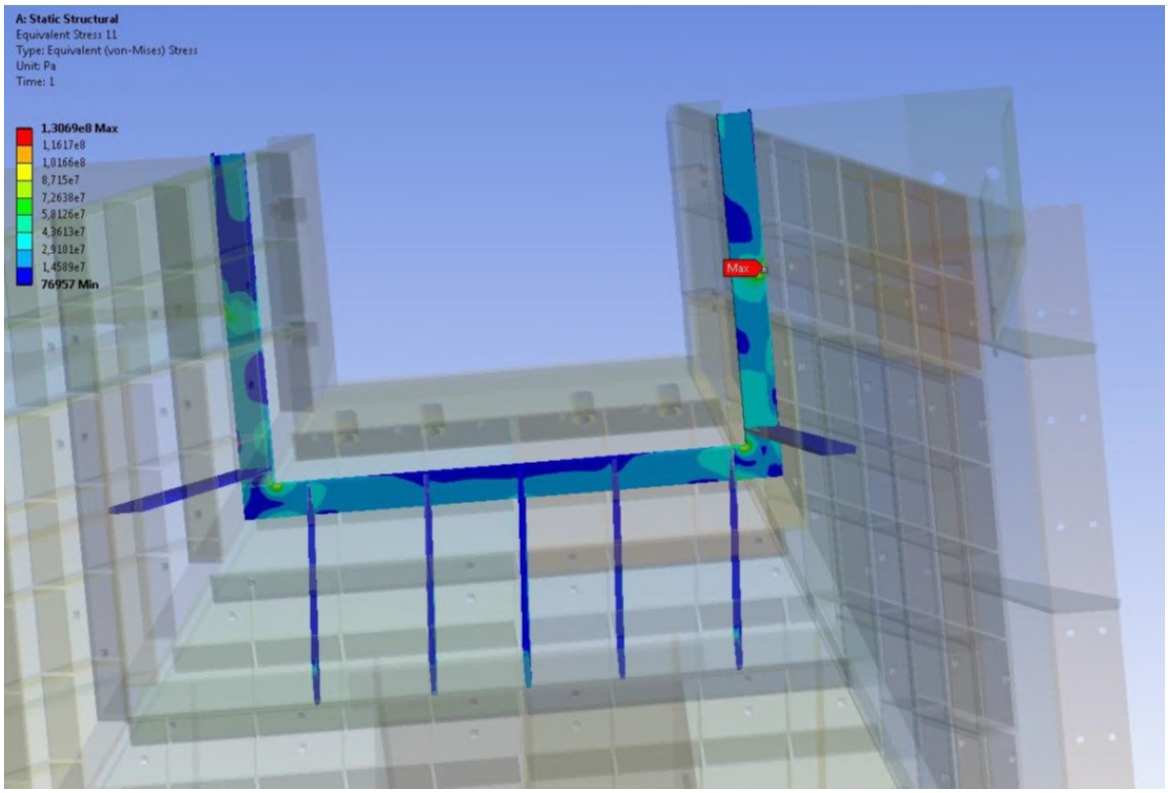

Fig. 3.16 Distribution of von Mises equivalent stresses in lower collar

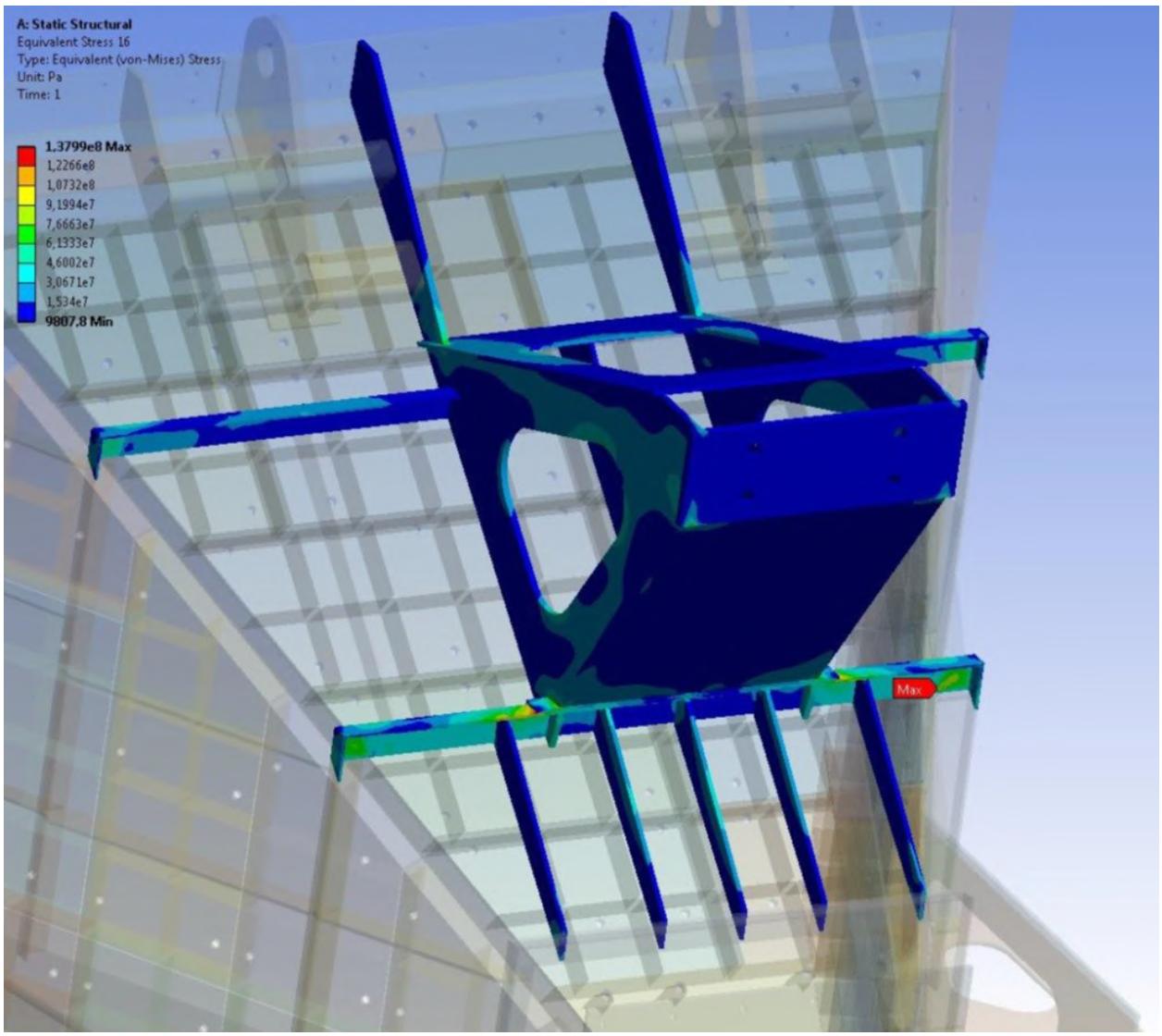

Fig.3.17. Distribution of von Mises equivalent stresses in lateral support, middle and top load-bearing collar of the hopper.

The presented results show that the structure meets strength and stiffness requirements for the load case in question.

3.3.2 Upper hopper structural design for wind effect conditions and normal service conditions

3.3.2.1 Upper hopper design under frontal wind effect

The design pattern of hopper's loading under normal service conditions and limit frontal wind effect is presented in Fig. 3.18.

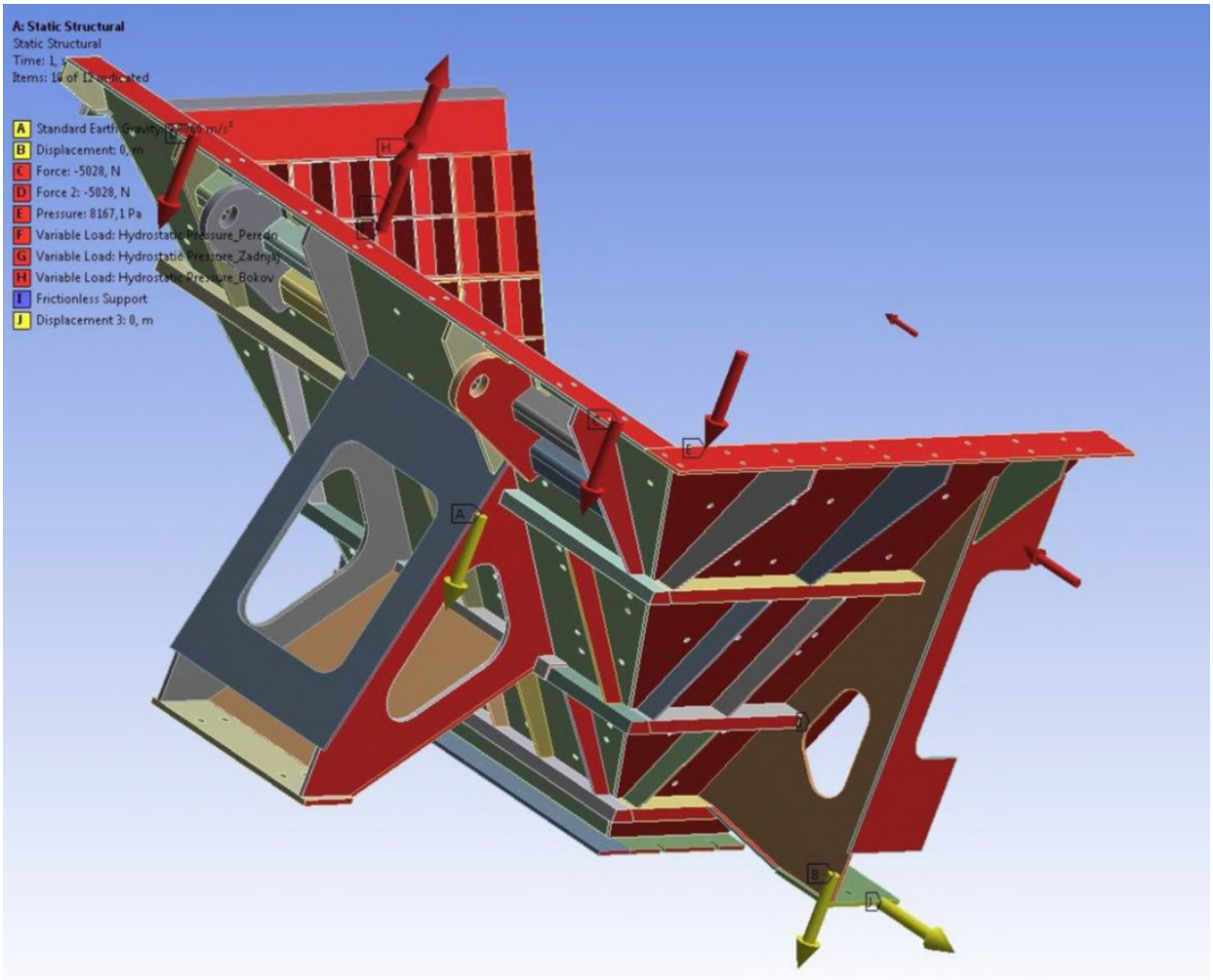

Fig. 3.18 Design pattern of hopper's loading under NSC+LWE

Results of hopper design are presented as stress and strain patterns in Fig.3.19-3.27. The most loaded elements of the hopper are load-bearing cover, structure's supports and collars. The figures 3.19-3.27 present pictures of distribution of von Mises equivalent stresses in upper hopper elements in question. All load-bearing elements of the hopper show the rise of stresses that do not exceed 155 MPa, which is by 3.8% lower than material permissible stresses at hopper's operational temperature.

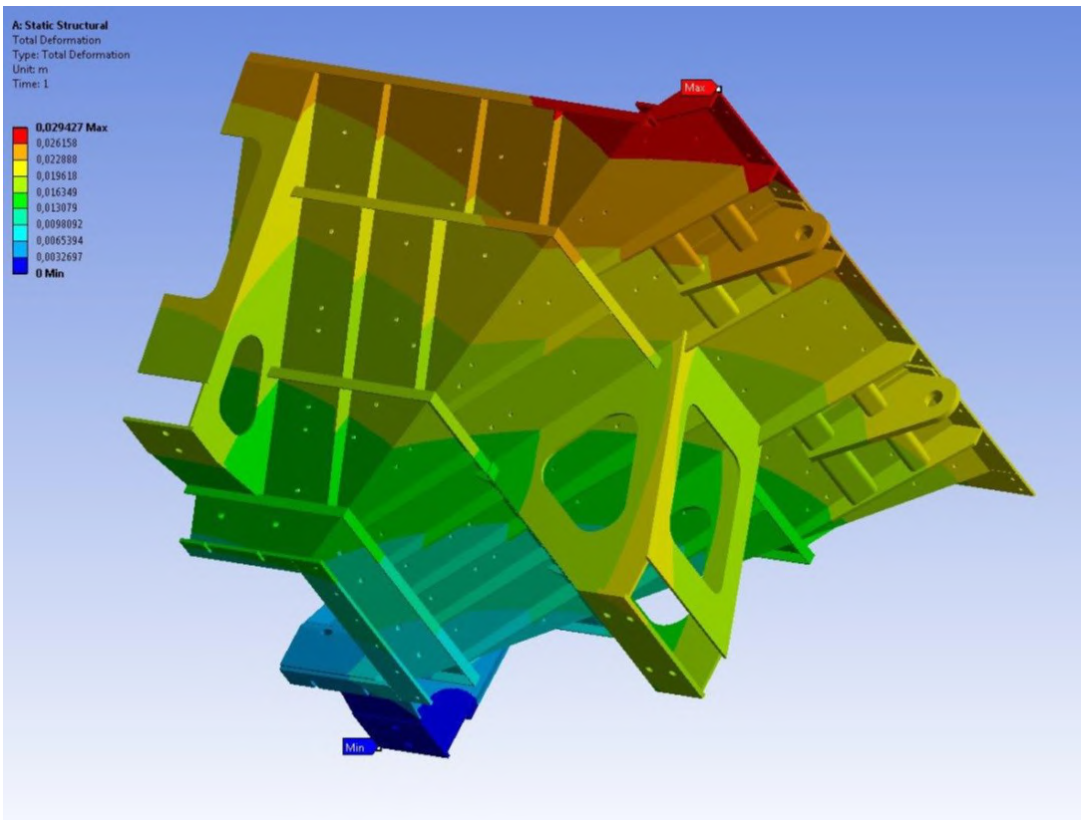

Fig. 3.19 Distribution of total strain arising in a structure

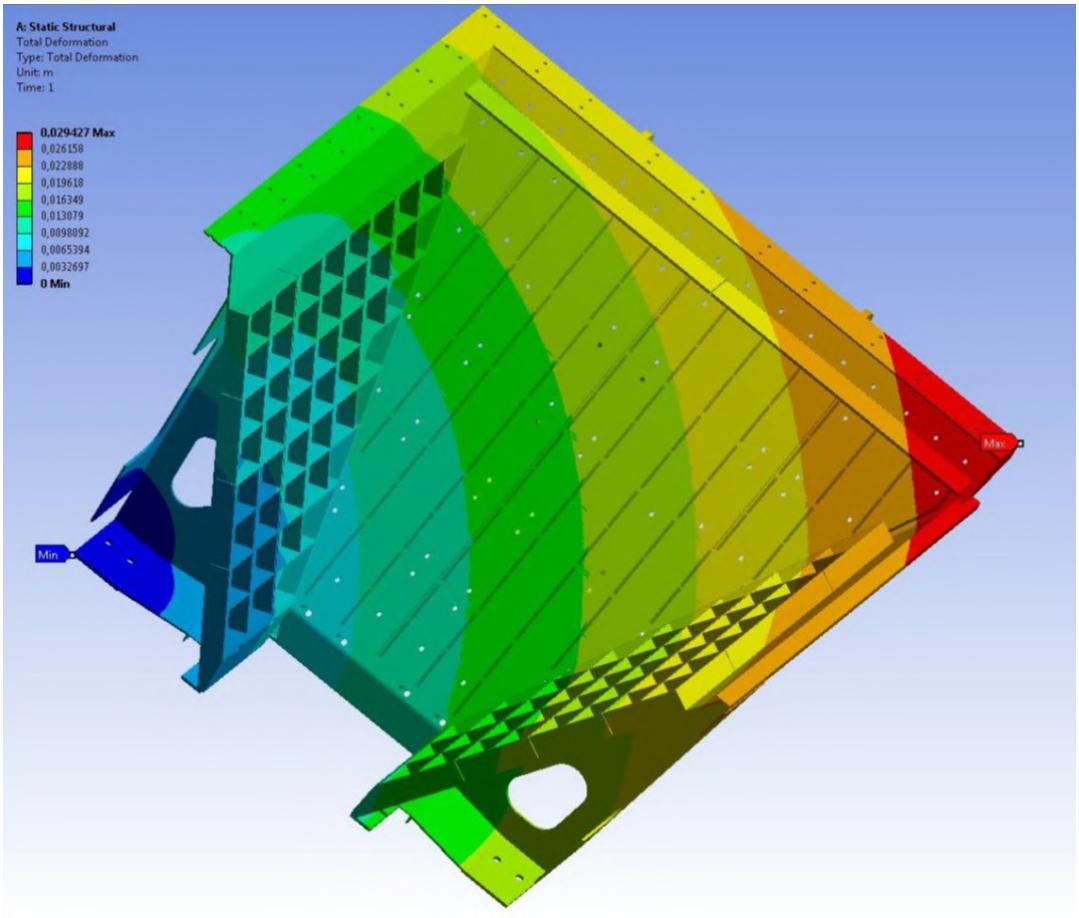

Fig. 3.20 Distribution of total strain arising in a structure

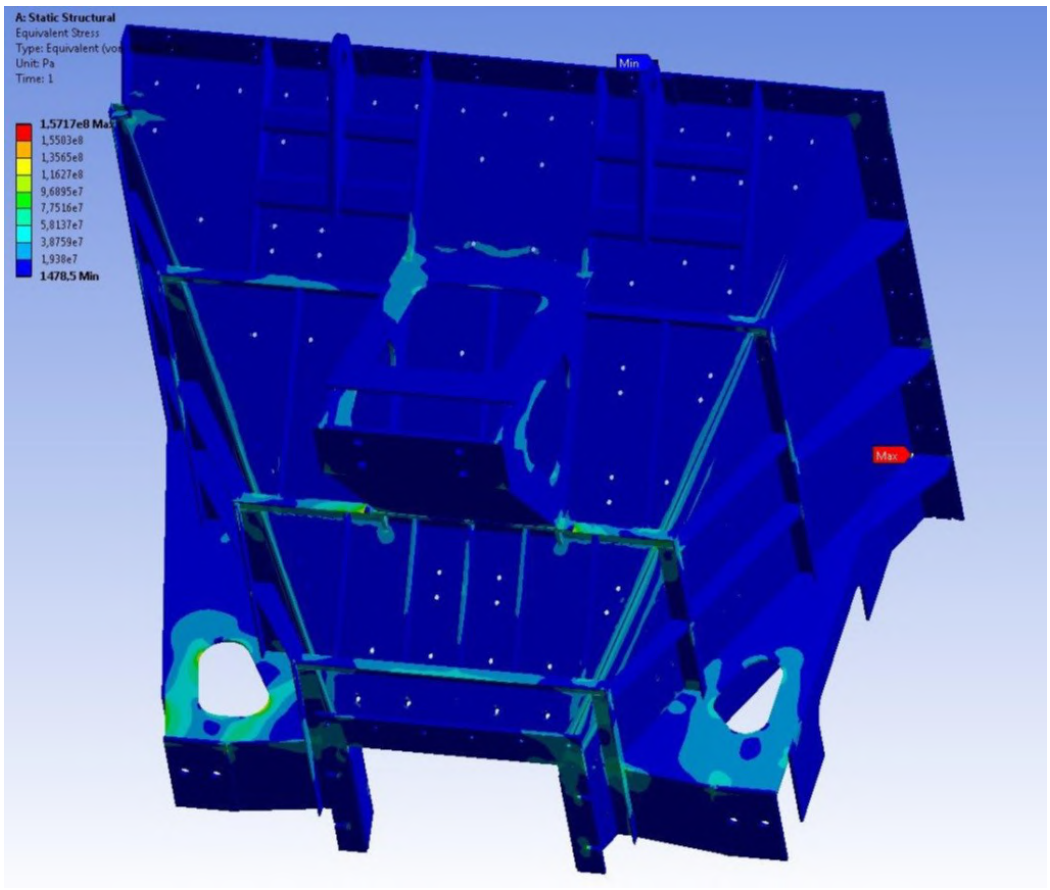

Fig. 3.21 Distribution of von Mises equivalent stresses in the hopper

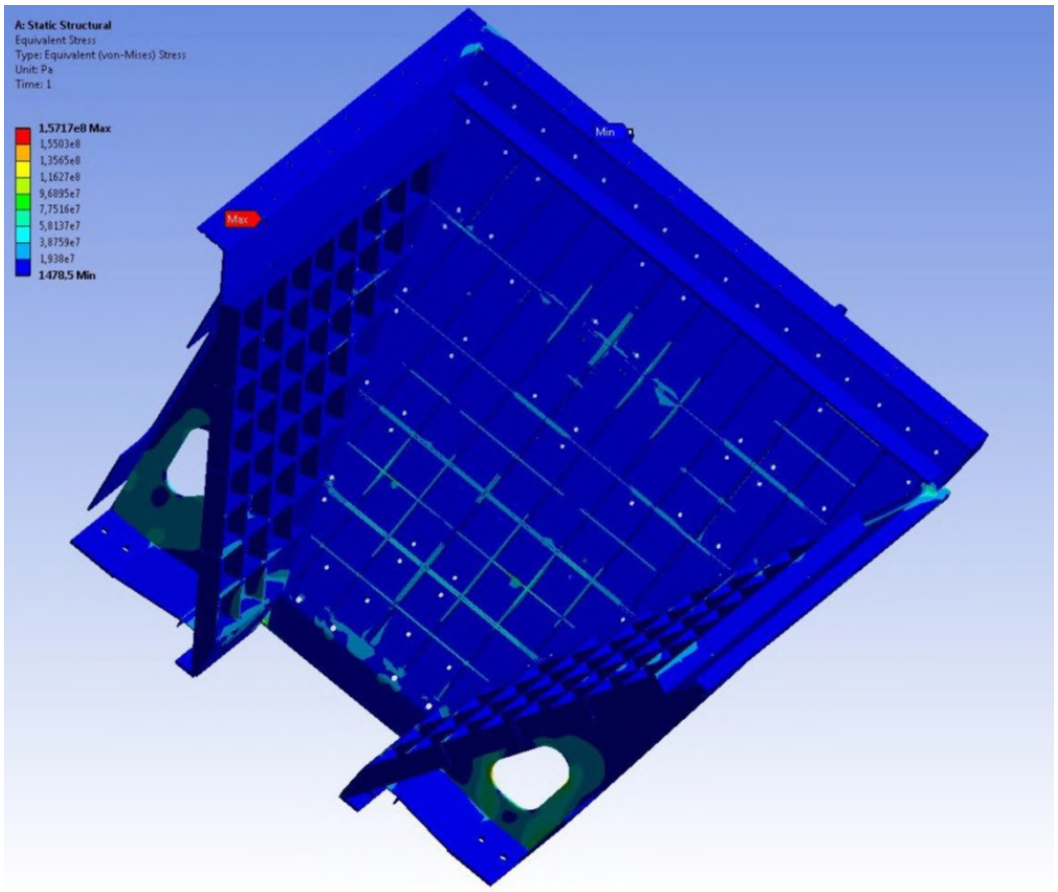

Fig. 3.22 Distribution of von Mises equivalent stresses in the hopper

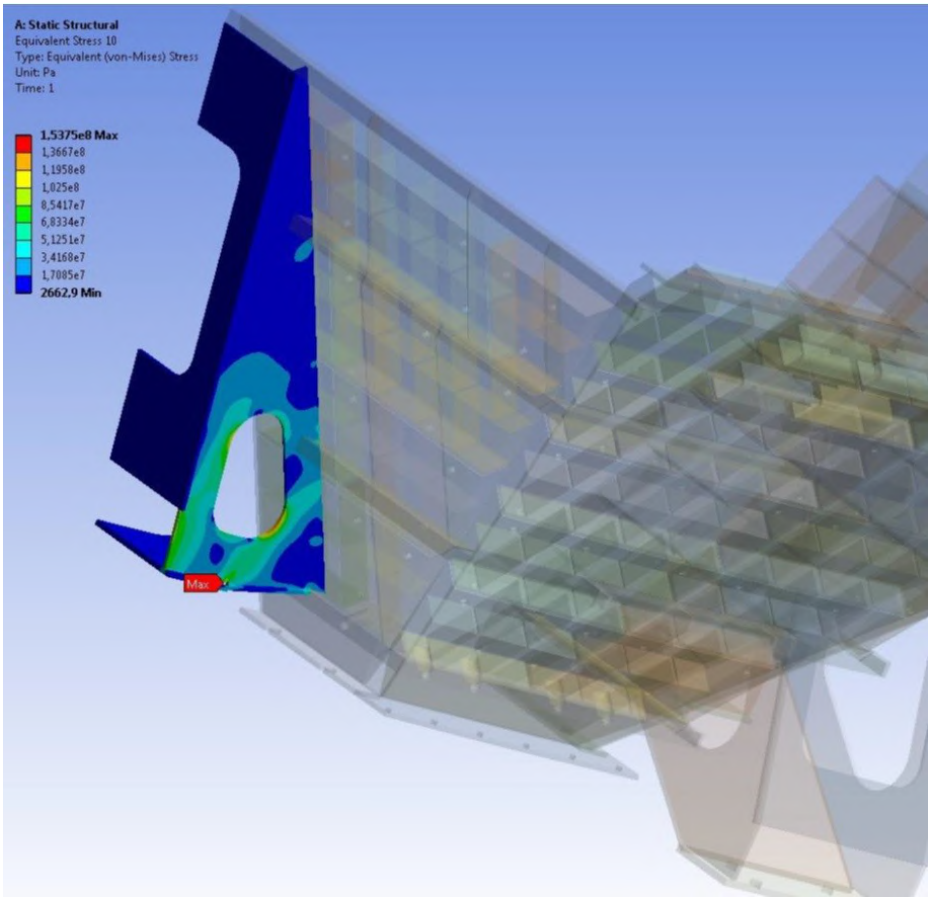

Fig. 3.23 Distribution of von Mises equivalent stresses in hopper's support

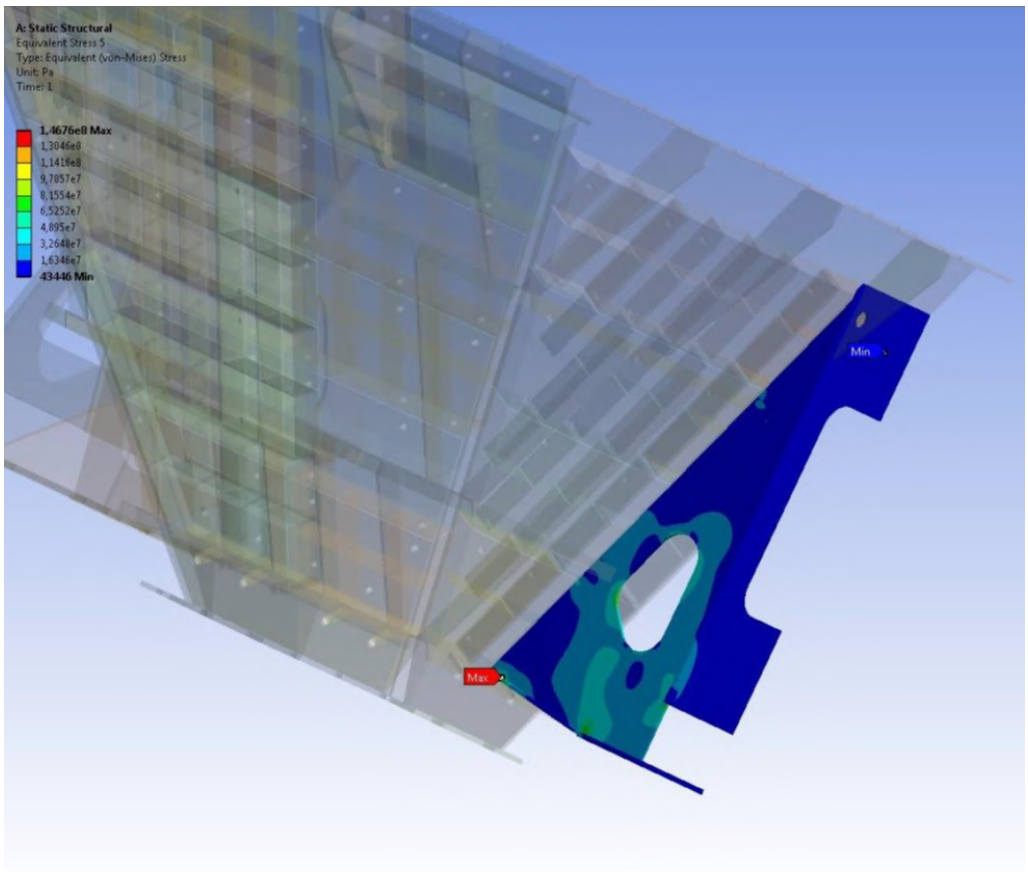

Fig. 3.24 Distribution of von Mises equivalent stresses in hopper's support

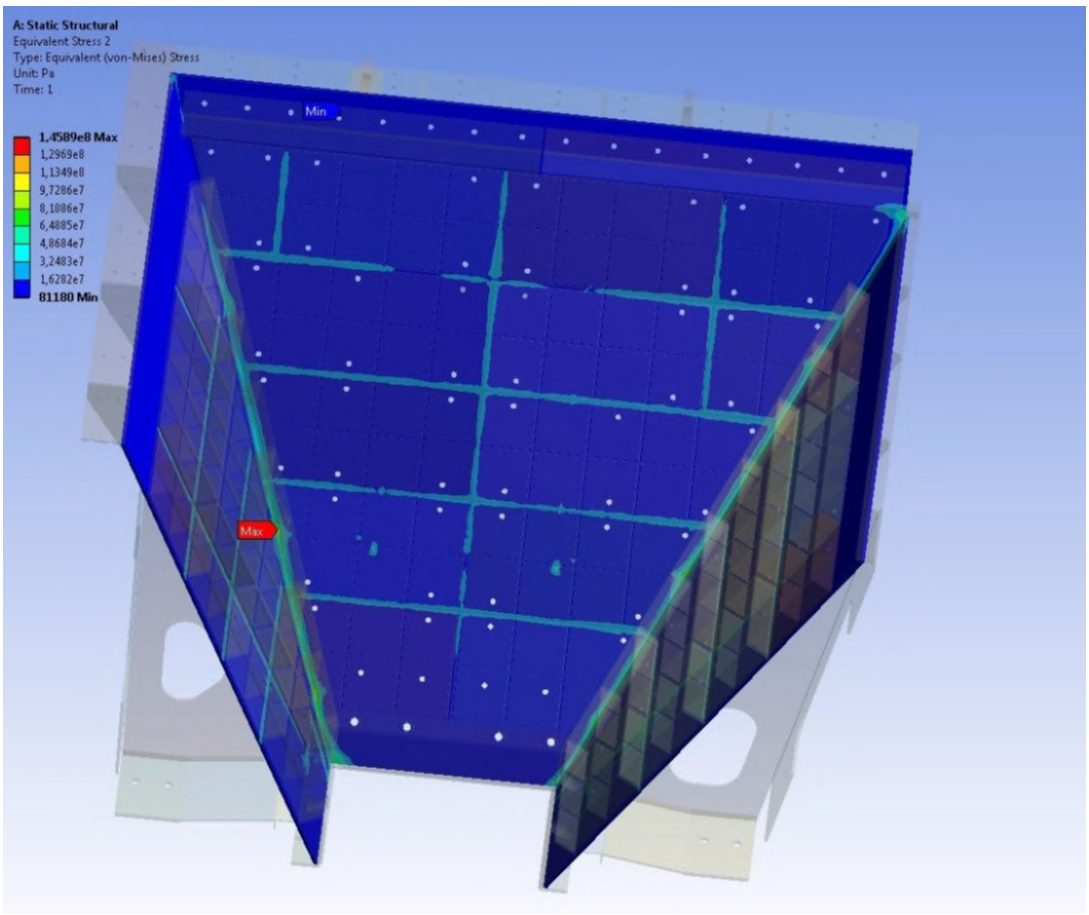

Fig. 3.25 Distribution of von Mises equivalent stresses in hopper's load-bearing cover.

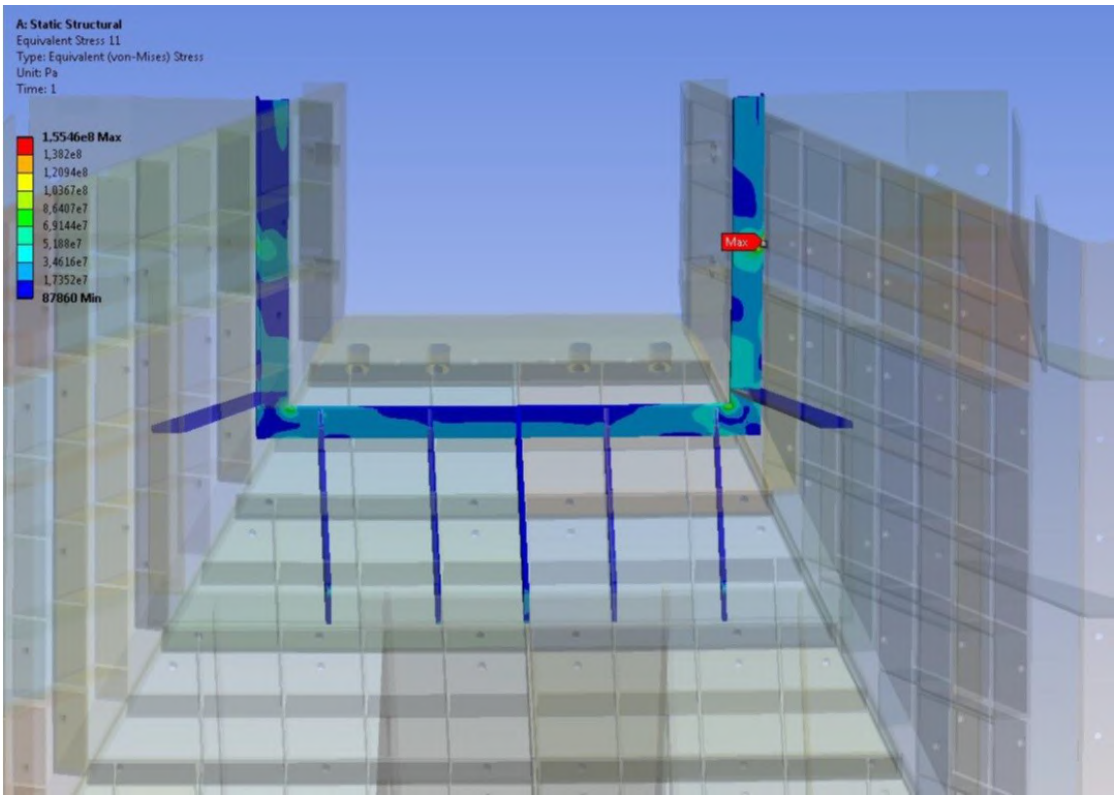

Fig. 3.26 Distribution of von Mises equivalent stresses in lower collar

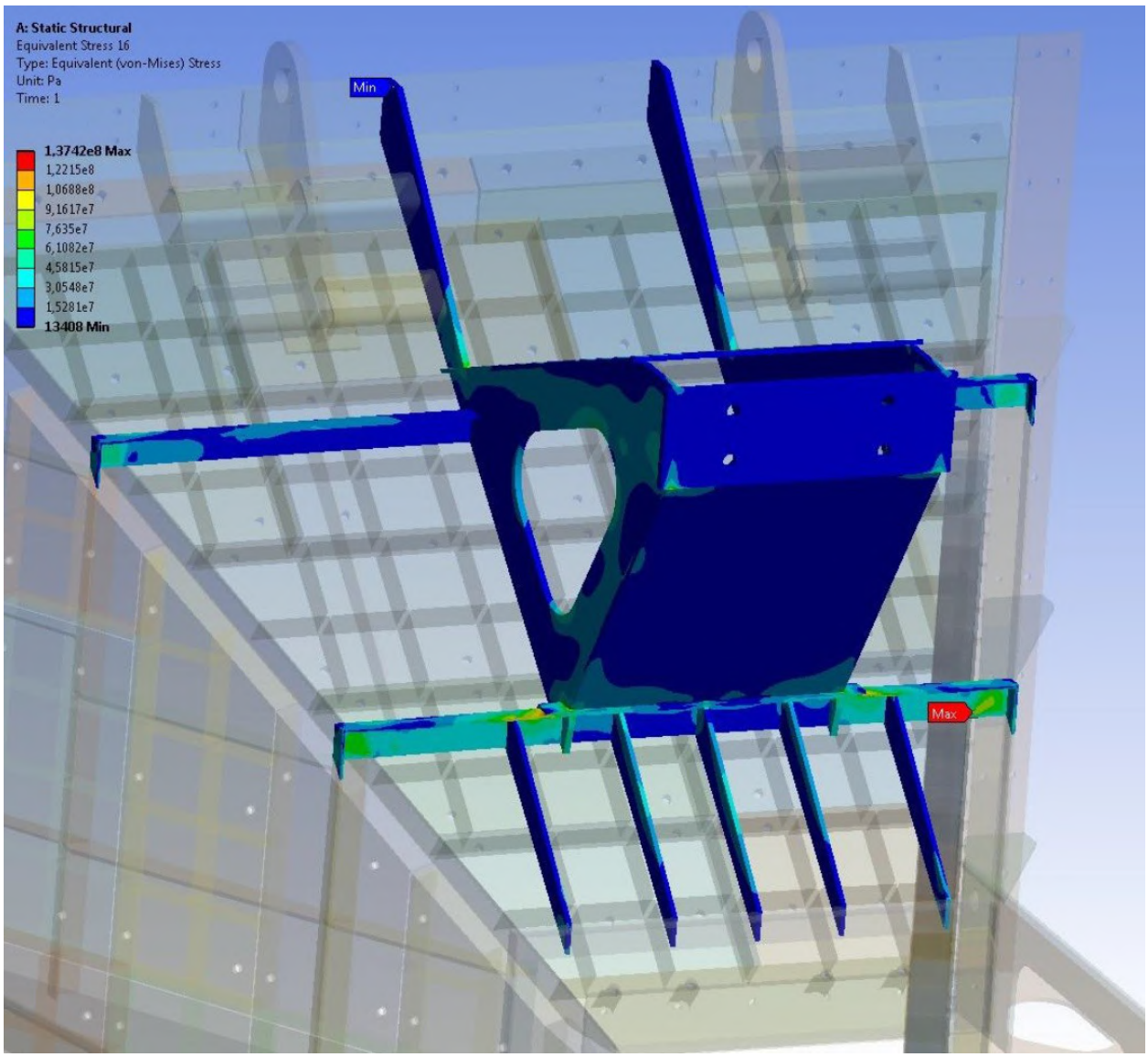

Fig. 3.27 Distribution of von Mises equivalent stresses in hopper's lateral support, middle and top load-bearing collar.

The biggest stresses of 157MPa arising at the of rib's edge border and acting locally within the limits of a finite element may be disregarded. The wind effect leads to arise in stresses in supports, load-bearing cover and load-bearing collars approximately by 2-10% as compared to normal service conditions. The biggest rise in stresses occurs at hopper's lower collar.

The results presented show that the structure meets requirements of strength and stiffness for the load case in question.

3.3.2.2 Upper hopper design under lateral wind effect

The design pattern of hopper's loading under normal service conditions and limit lateral wind effect is presented in Fig. 3.28.

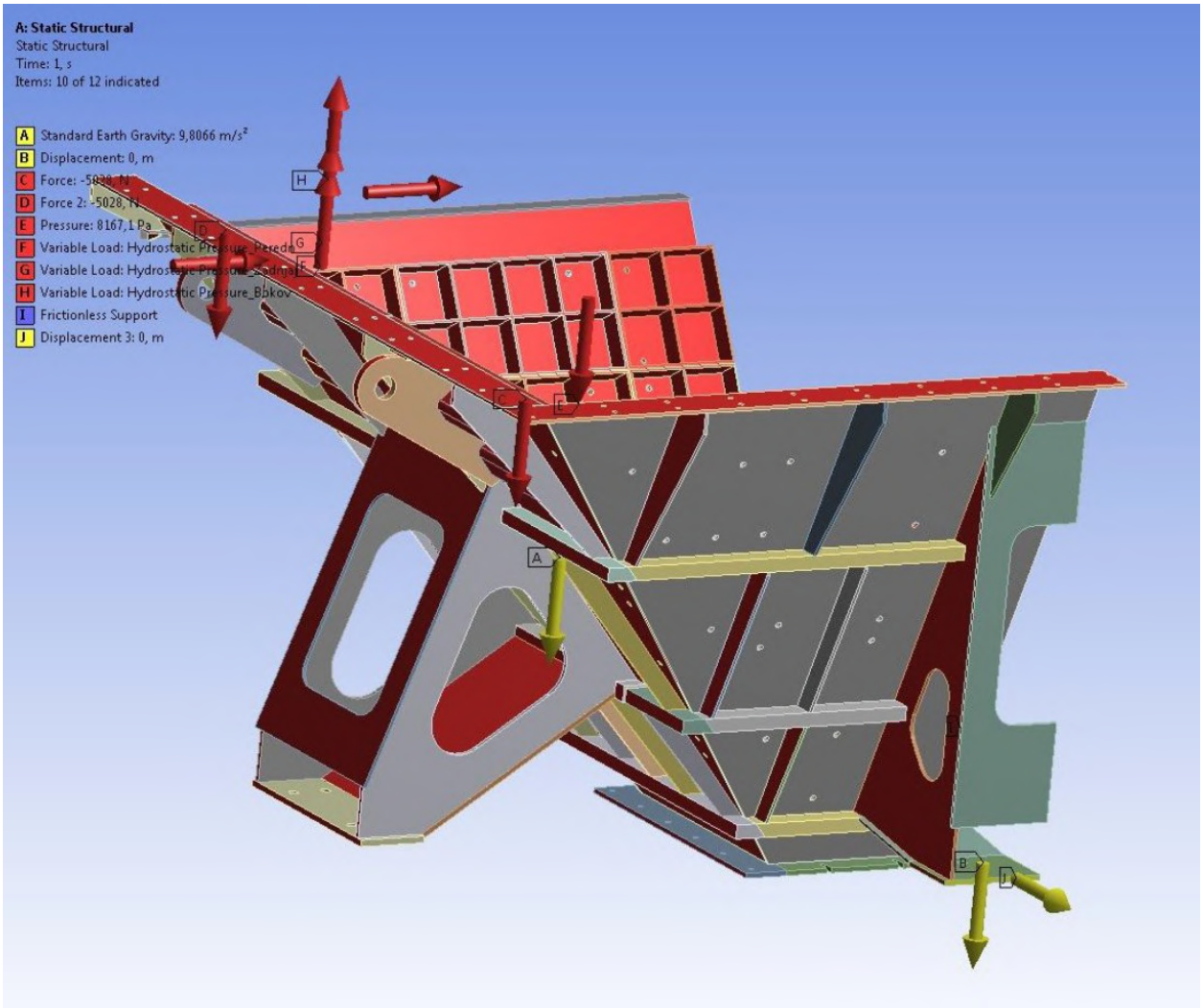

Fig. 3.28 Design pattern of hopper's loading under NSC+LWE

Results of hopper design for these conditions are presented as stress and strain patterns in Fig. 3.29-3.37. The most loaded elements of the hopper are structure's supports and collars. The figures 3.33-3.37 present pictures of distribution of von Mises equivalent stresses in upper hopper elements in question. All load-bearing elements of the hopper show the rise of stresses that do not exceed 149 MPa, which is by 8% lower than material permissible stresses at hopper's operational temperature.

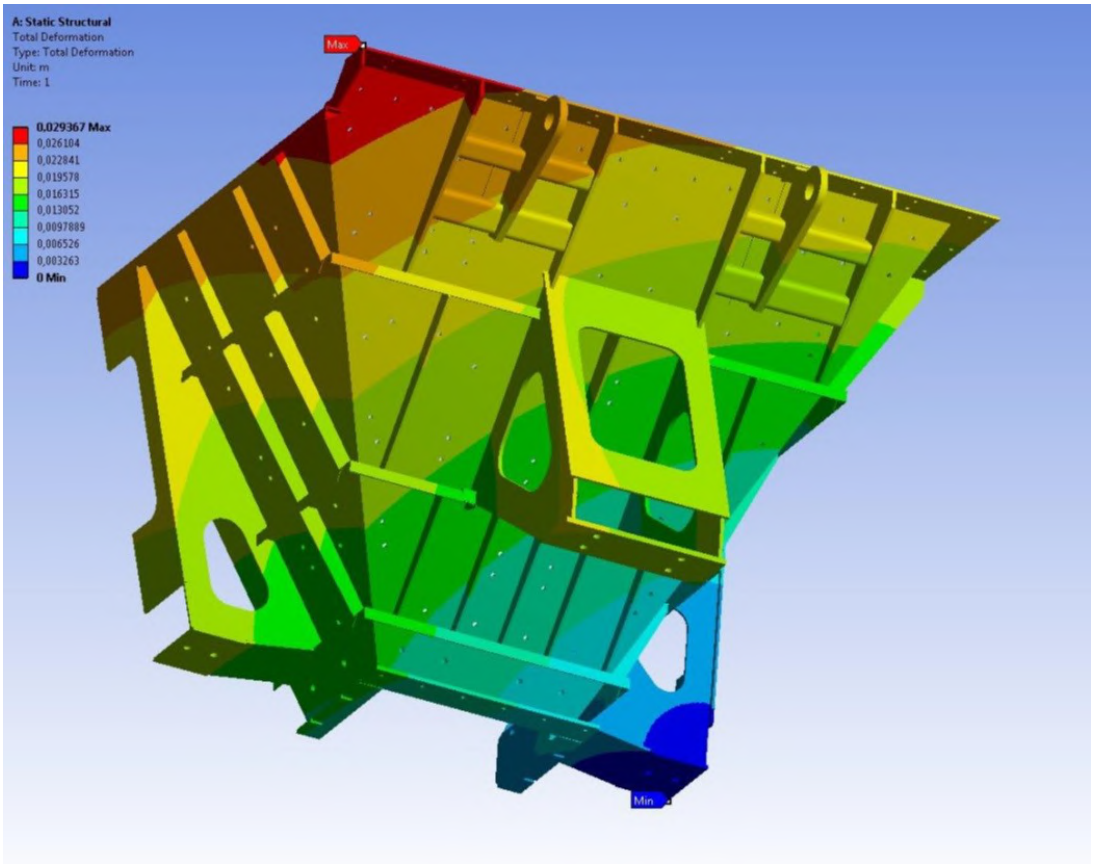

Fig. 3.29 Distribution of total strain arising in a structure

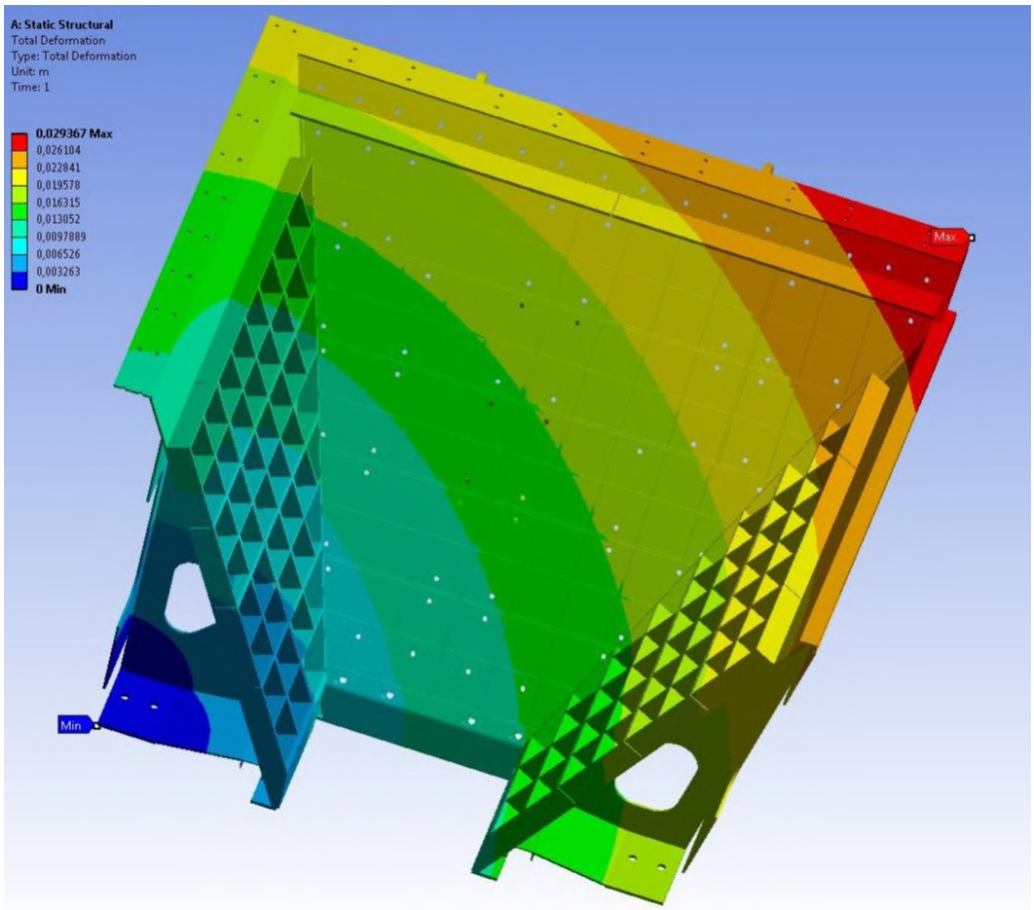

Рис. 3.30 Distribution of total strain arising in a structure

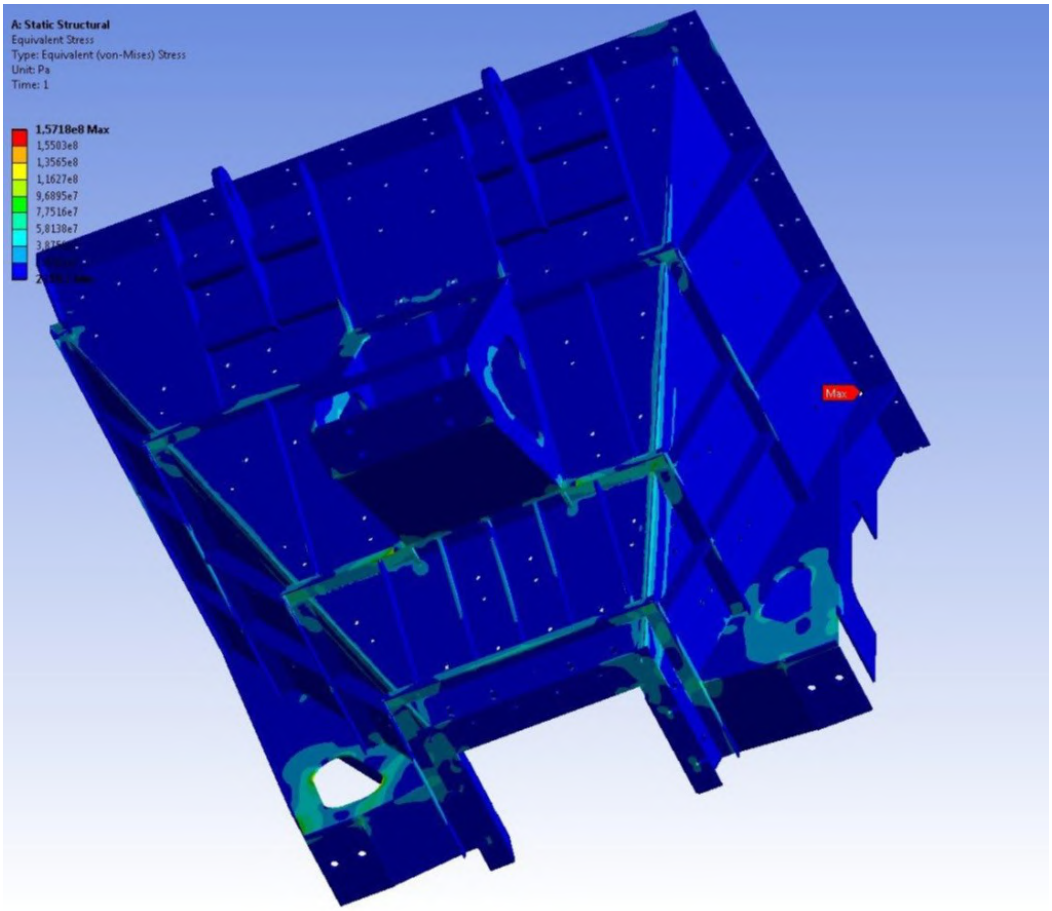

Fig. 3.31 Distribution of von Mises equivalent stresses in the hopper

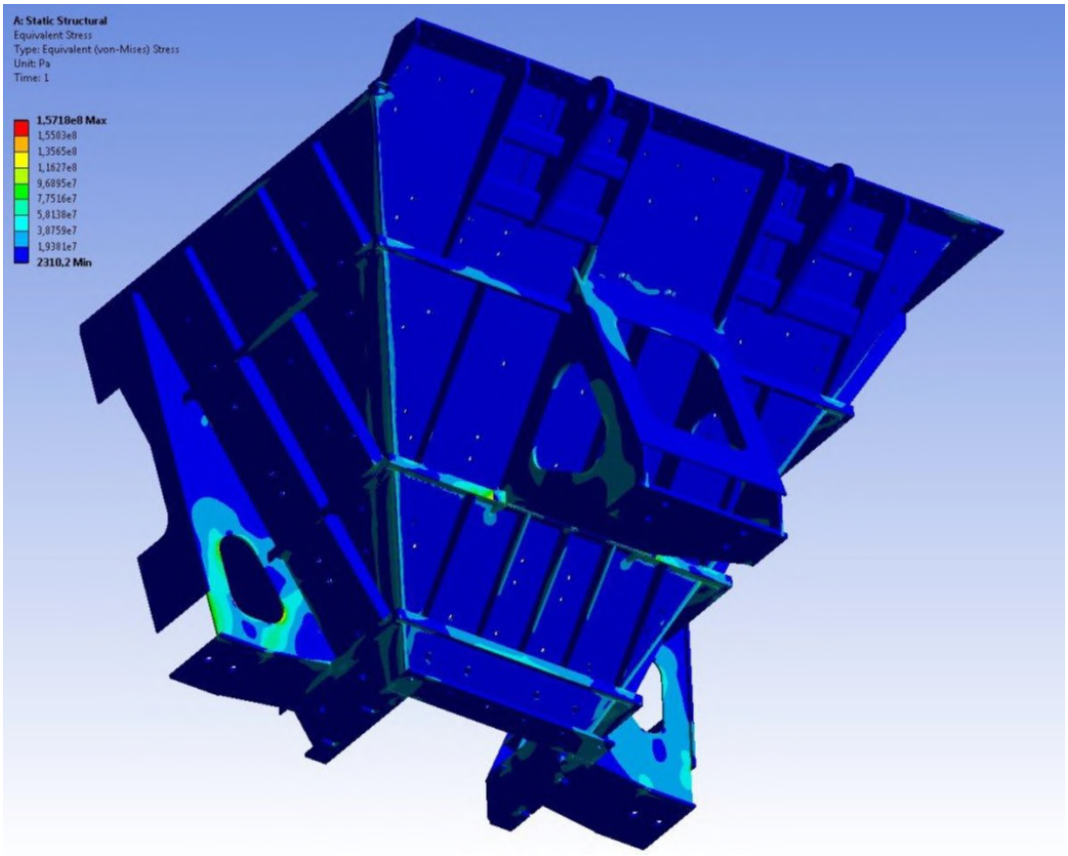

Fig. 3.32 Distribution of von Mises equivalent stresses in the hopper

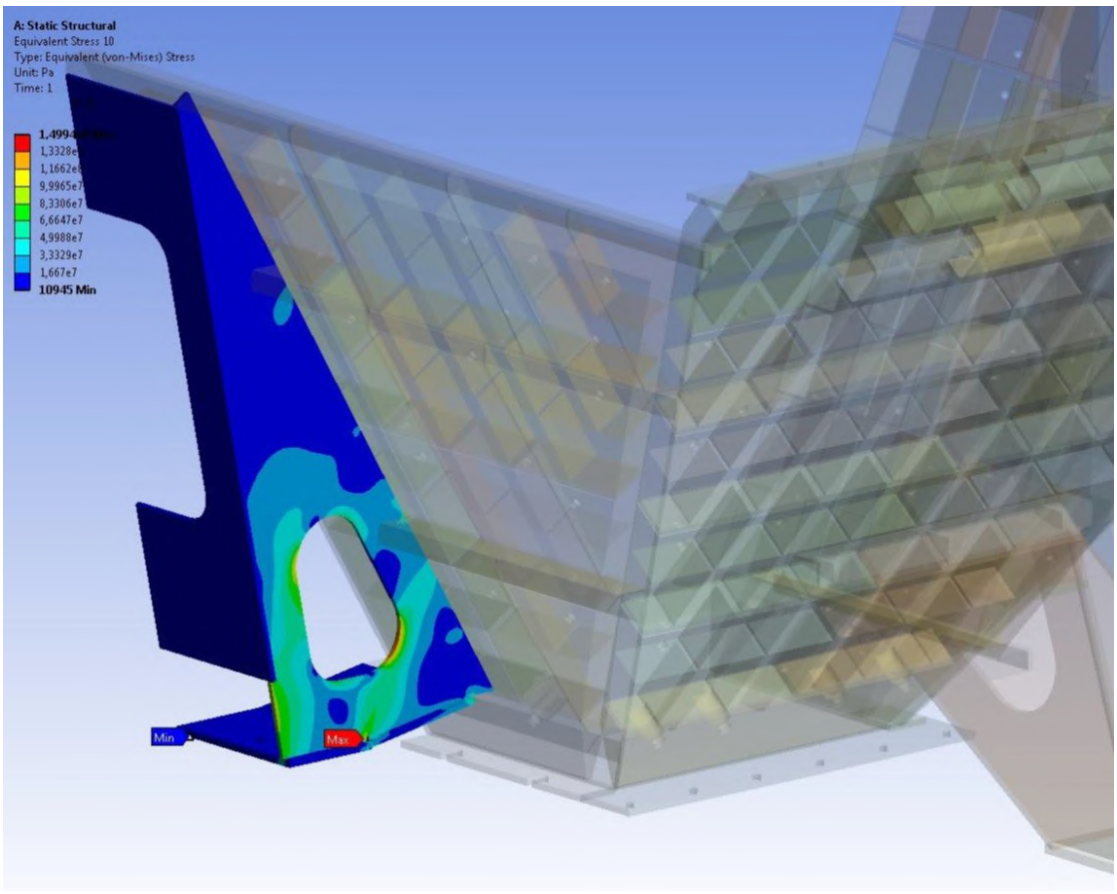

Fig. 3.33 Distribution of von Mises equivalent stresses in hopper's support

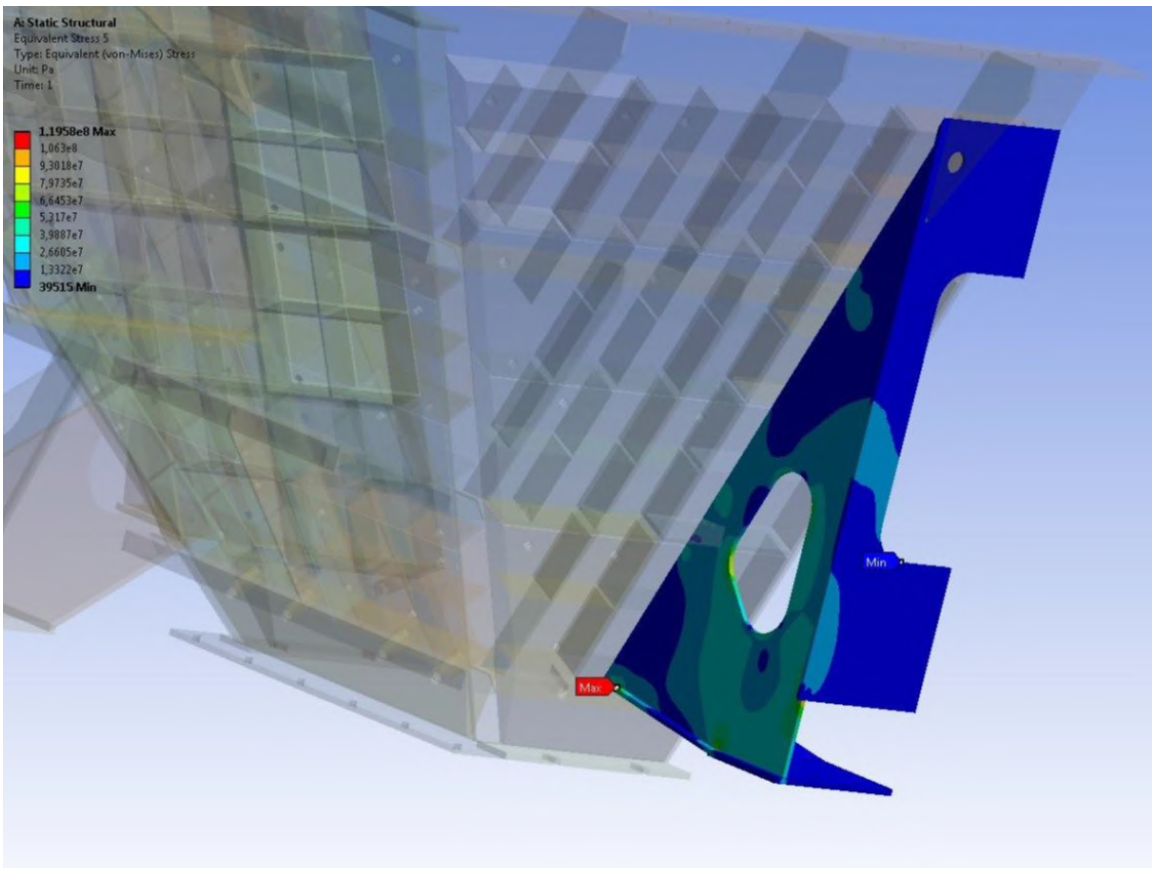

Fig. 3.34 Distribution of von Mises equivalent stresses in hopper's support

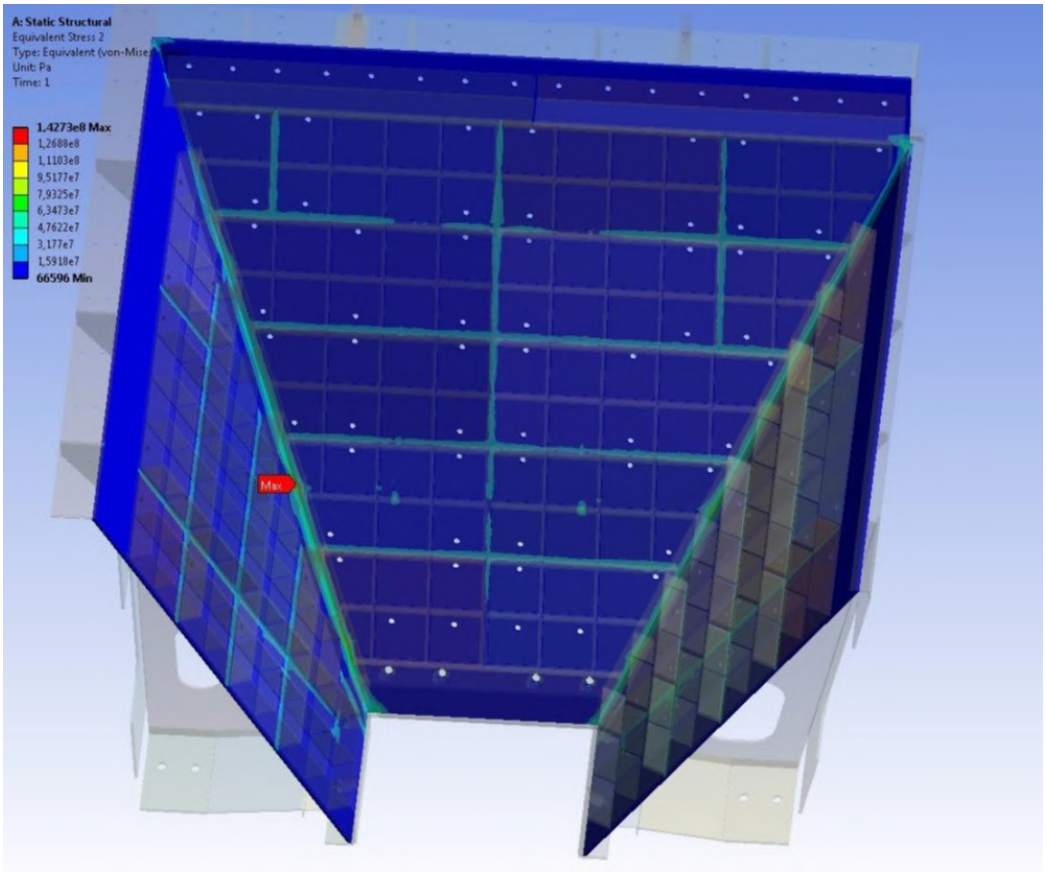

Fig. 3.35 Distribution of von Mises equivalent stresses in hopper's load-bearing cover.

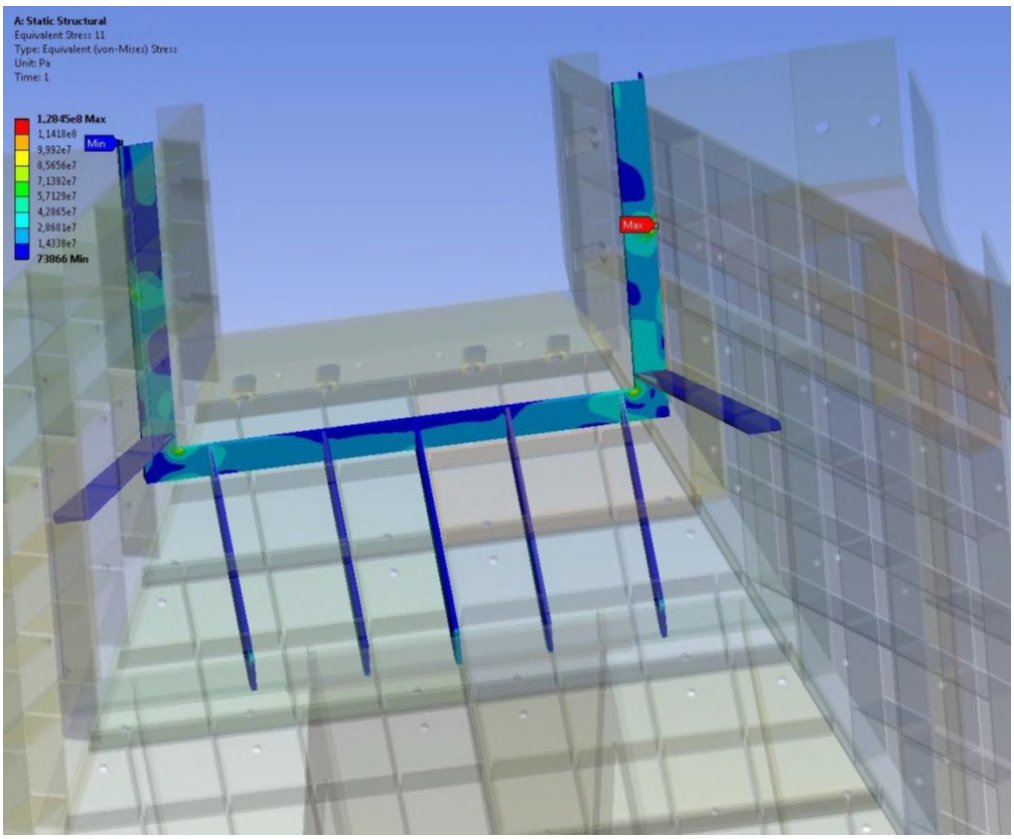

Fig. 3.36 Distribution of von Mises equivalent stresses in lower collar

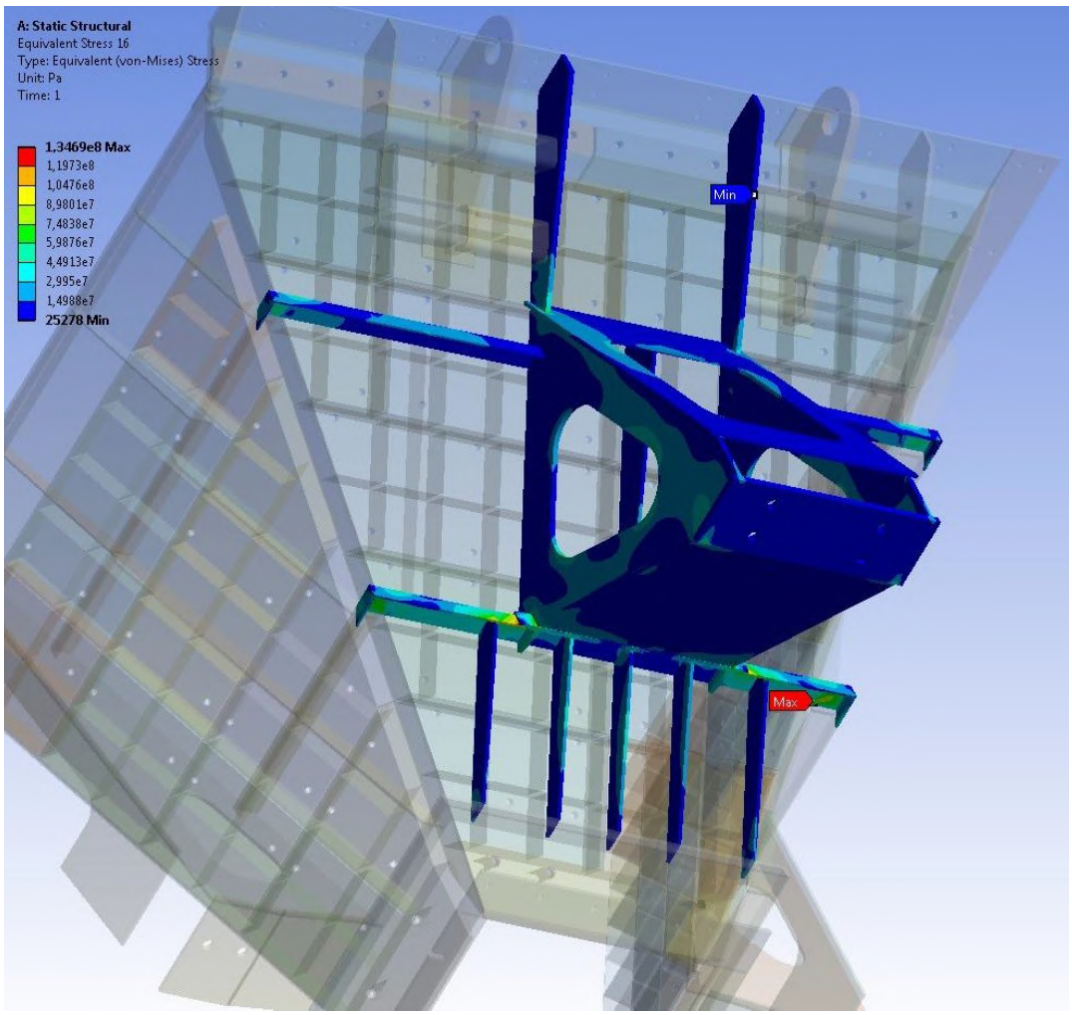

Fig. 3.37 Distribution of von Mises equivalent stresses in hopper's lateral support, middle and top load-bearing collar.

The biggest stresses of 157MPa arising at the of rib's edge border may be disregarded. The wind effect leads to arise in stresses in supports, load-bearing cover and load-bearing collars approximately by 2-5%. The biggest rise in stresses occurs at hopper's lateral support.

The results presented show that the structure meets requirements of strength and stiffness for the load case in question.

Out of two cases of wind direction considered the defining wind effect for the hopper is the frontal wind effect.

3.3.3 Structural design for seismic impact

Seismic impact calculation is performed using the response spectrum method. The initial data is the spectrum of structure's response to dynamic effect. The

response spectrum is taken to mean the absolute values of maximal response acceleration of linear-elastic system depending on impact frequency. The hopper response spectrum is specified with accelerograms and is presented in Tables 3.2-3.4 for the 57.648 m mark. To define this loading the structure's natural oscillation modes and quantity thereof shall be determined. The number of frequencies shall be determined out of the condition that the frequencies in question correspond to 90% of structure's reduced mass in accordance with the method of reduction. The values of natural oscillation frequency are determined out of structure's modal analysis.

3.3.3.1 Structure's modal analysis

Calculation results of modal analysis showed that it is sufficient to take into consideration the first 100 natural oscillation harmonics, and these are presented in Fig. 3.38.

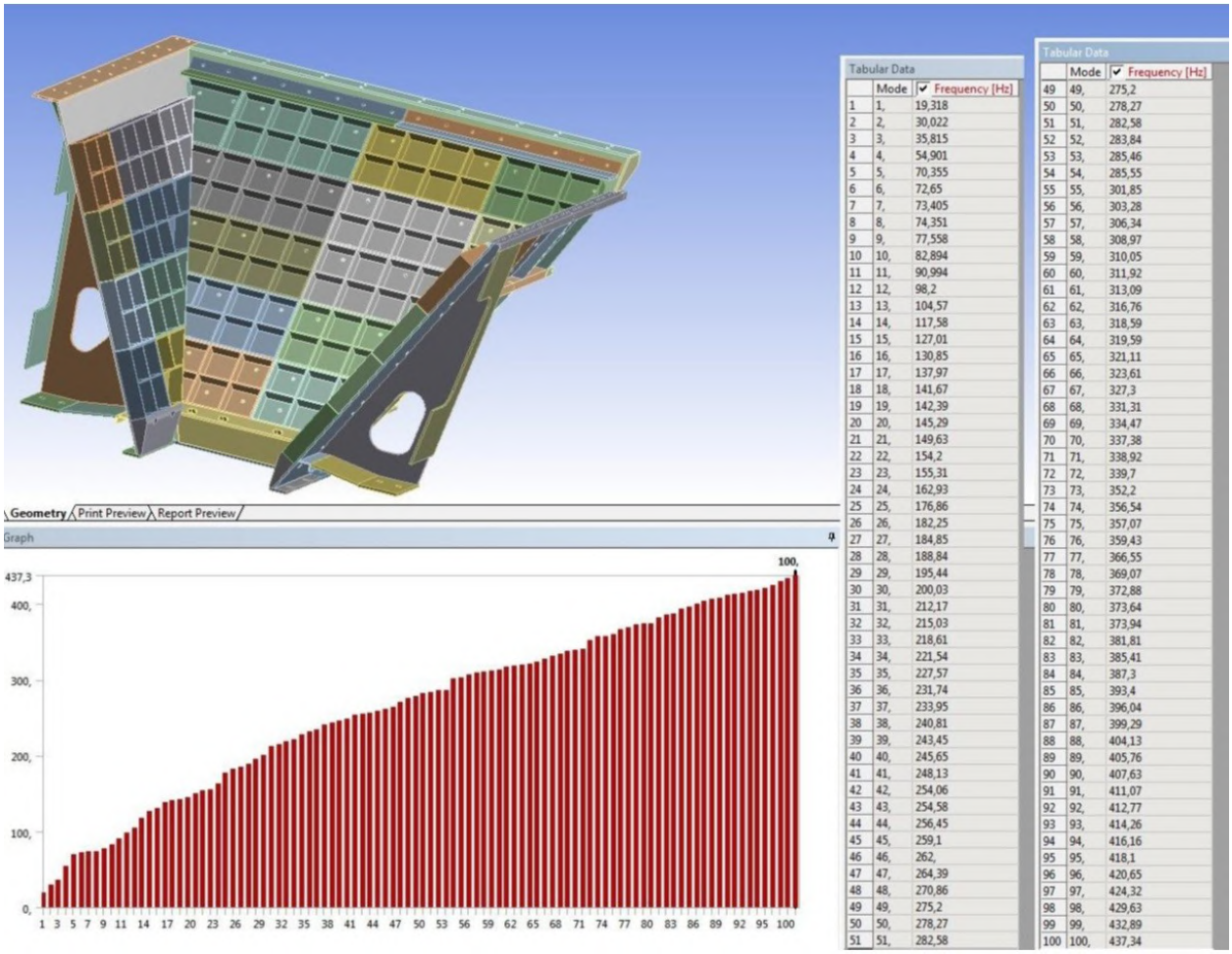

Fig. 3.38 Values of the first 100 natural oscillation frequencies.

Oscillation modes for certain natural frequencies are presented in Fig. 3.39.

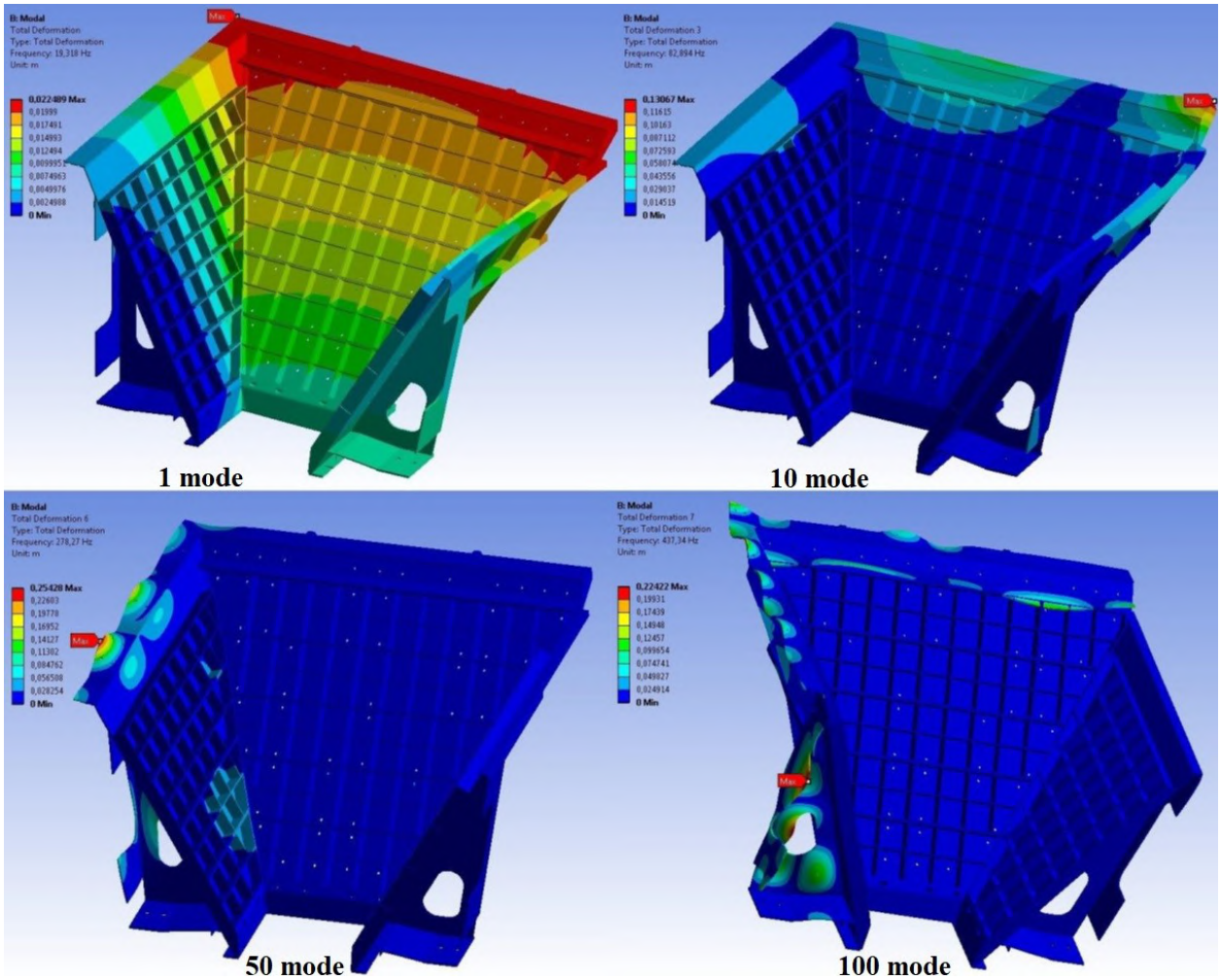

Fig. 3.39 Oscillation modes for 1, 10, 50 and 100 natural frequencies

When carrying out the linear-spectrum analysis the calculation results are obtained using the method of square-root out of sum of squares (SRSS). Field distribution of strains and von Mises equivalent stresses is presented in Fig. 3.40-3.41. The biggest stresses arise in the area of structure's securing, i.e. at structures lower collar.

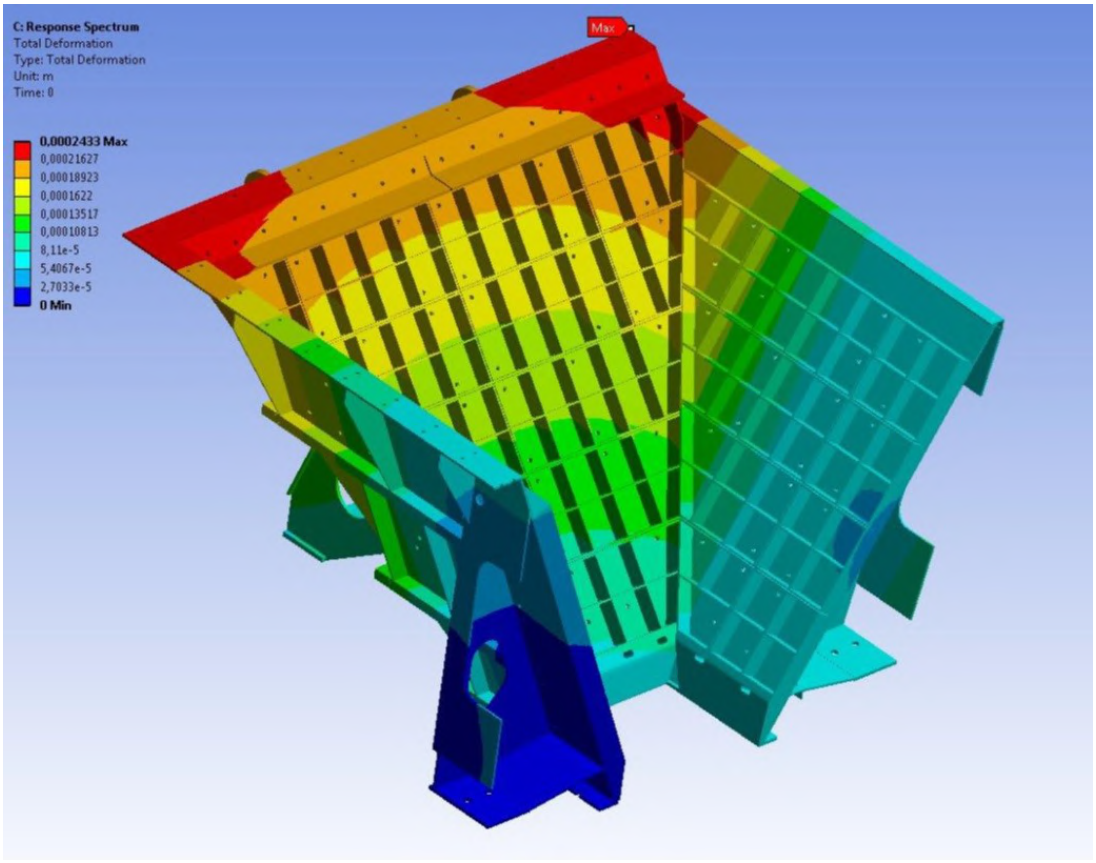

Fig. 3.40. Distribution of structure's total strain under seismic impact

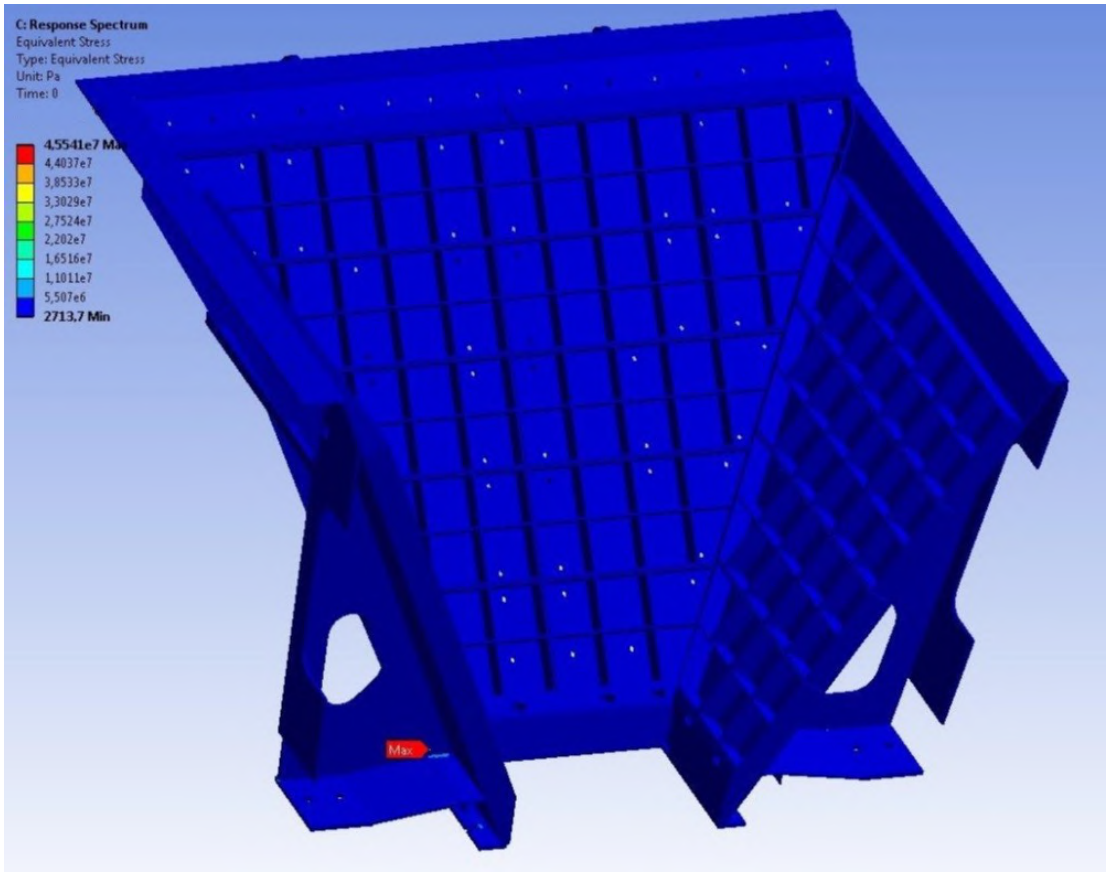

Fig. 3.41 Distribution of von Mises equivalent stresses in the hopper under seismic impact.

The Fig.3.42 shows distribution of von Mises equivalent stresses in hopper's structure lower collar.

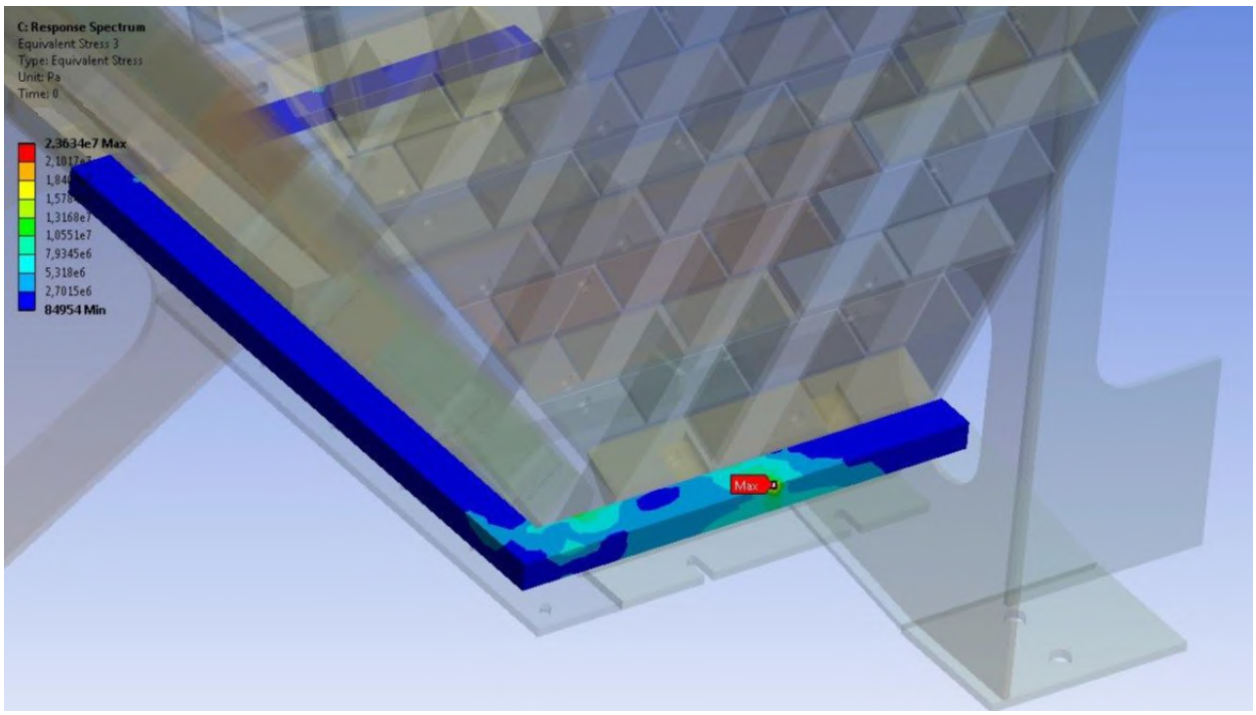

Fig. 3.42 Distribution of von Mises equivalent stresses in lower collar.

The maximal stresses in the area of joining the collar and support's rib. In the case under study the magnitude thereof does not exceed 17% of stresses for the case of normal service conditions. The resulting stresses have been summarized with stresses arising in normal service conditions. Total equivalent stresses in the lower collar do not exceed 154.5 MPa, and 156.4MPa in the support.

The results presented show that the structure meets requirements of strength and stiffness for the load case in question.

3.3.4 Strength calculation of upper hopper design lugs

To assess the strength of hopper's lugs the design case of crane lift of the fully loaded hopper holding the structure by lugs. On customer's demand the strength of shall withstand the additional load of 40000kg. The design model sets border shift conditions in all four lugs in form of cylindrical fixation and loading thereof with the total forces from fully loaded hopper and weight of additional load of 40000 kg. The design loading pattern is presented in Fig. 3.43.

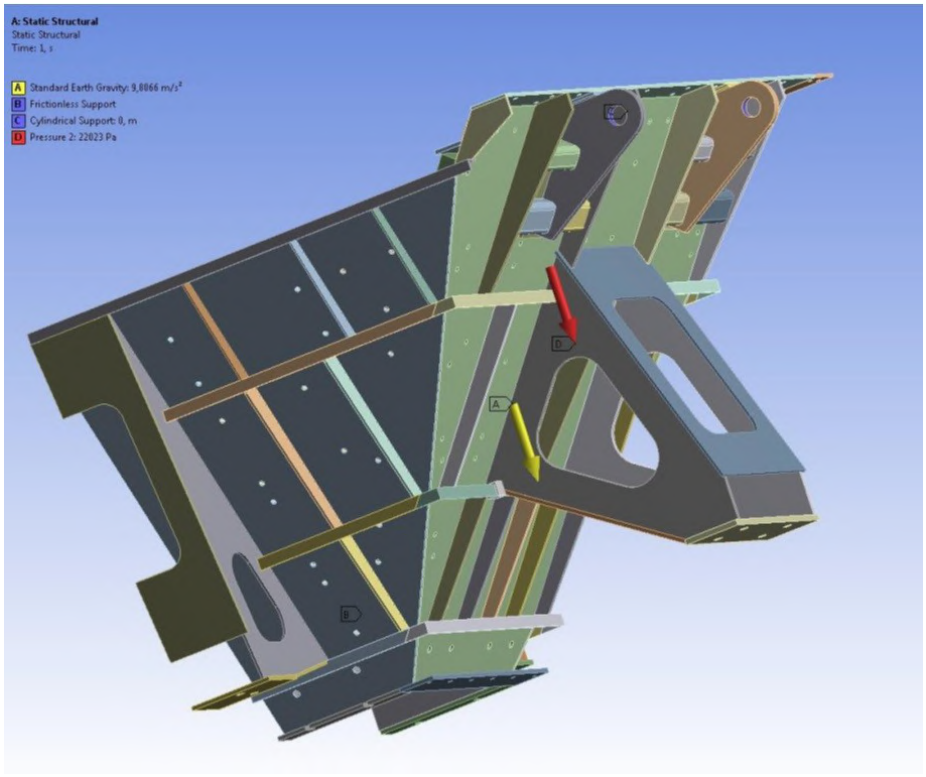

Fig. 3.43 Upper hopper design pattern for designing of lugs

Calculation results of stress-strain state are presented in Fig. 3.44-3.51.

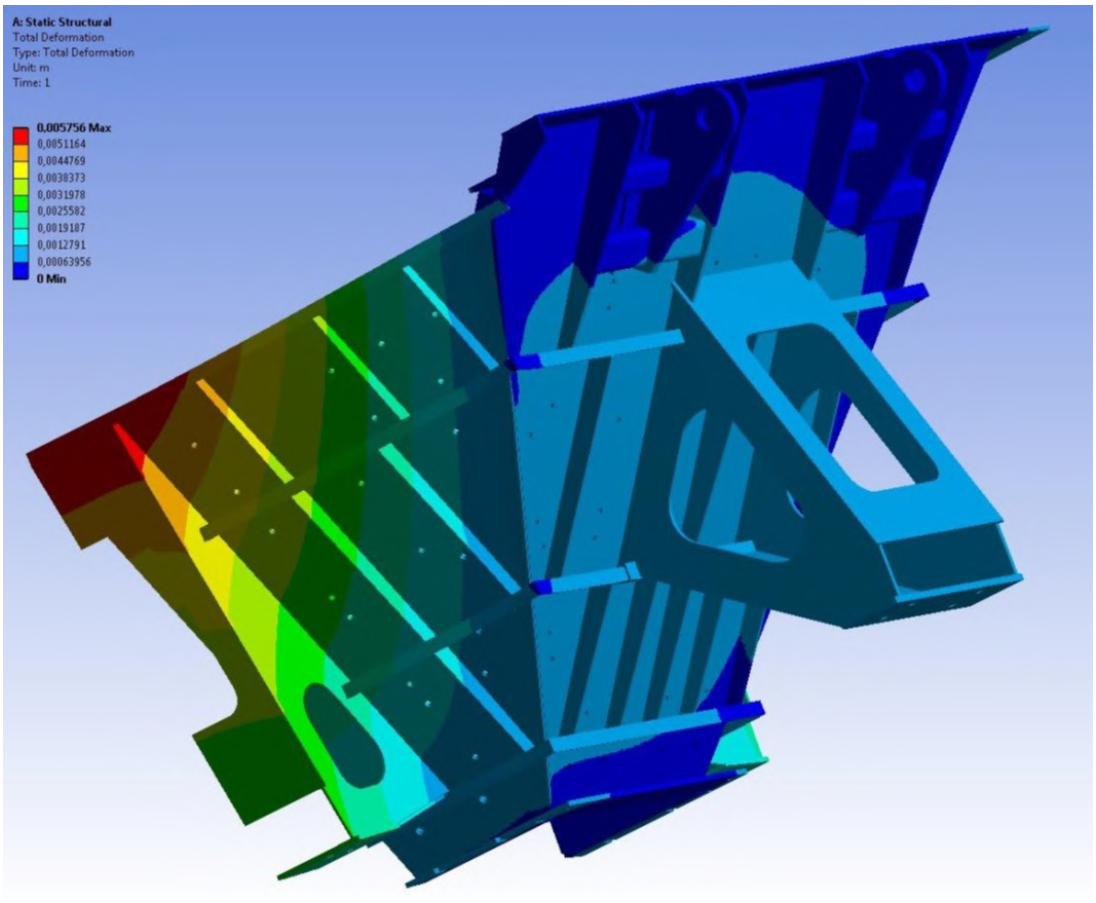

Fig. 3.44 Distribution of total strain arising in the structure

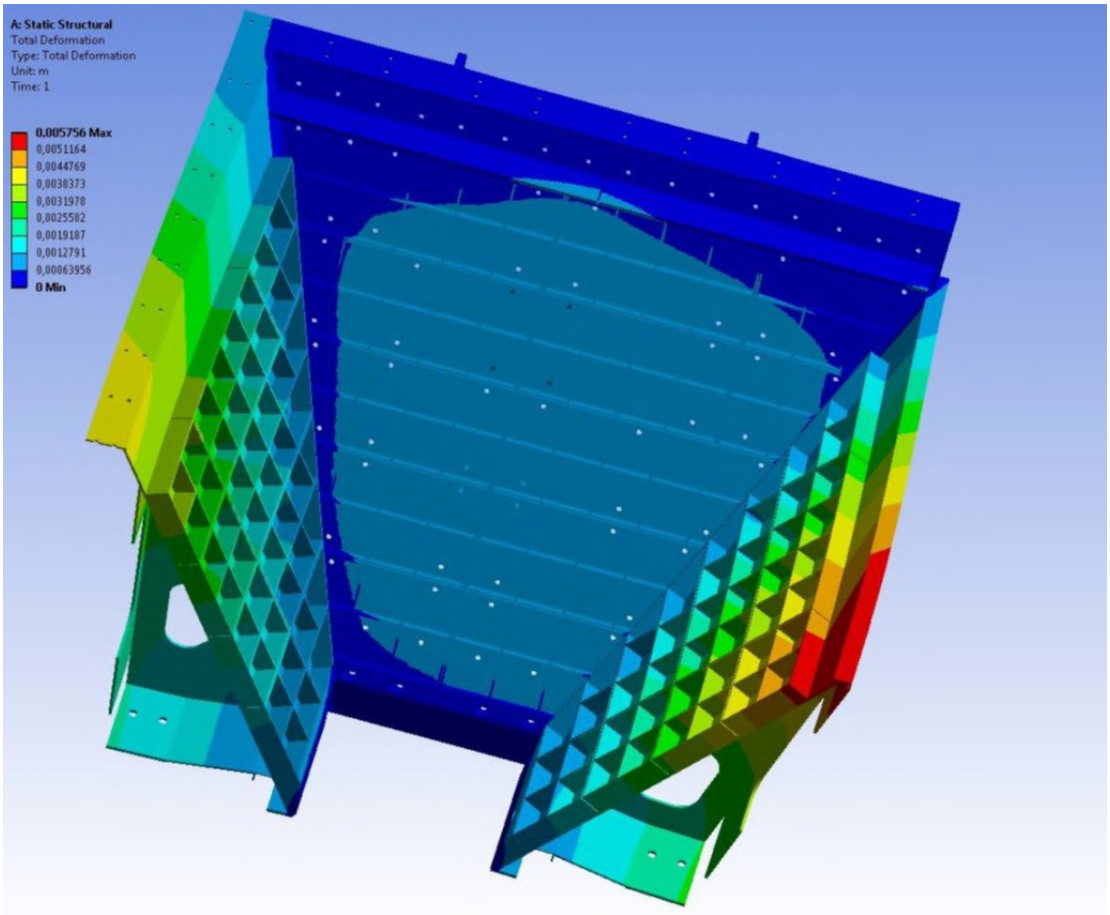

Fig. 3.45 Distribution of total strain arising in the structure

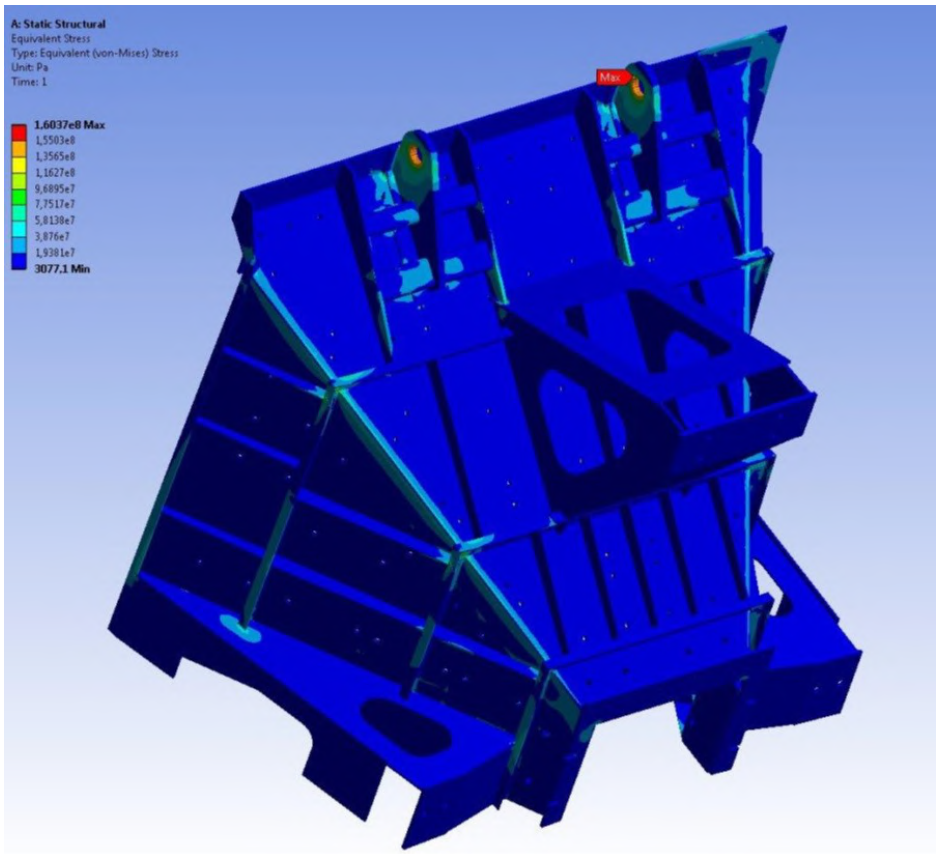

Fig. 3.46 Distribution of von Mises equivalent stresses.

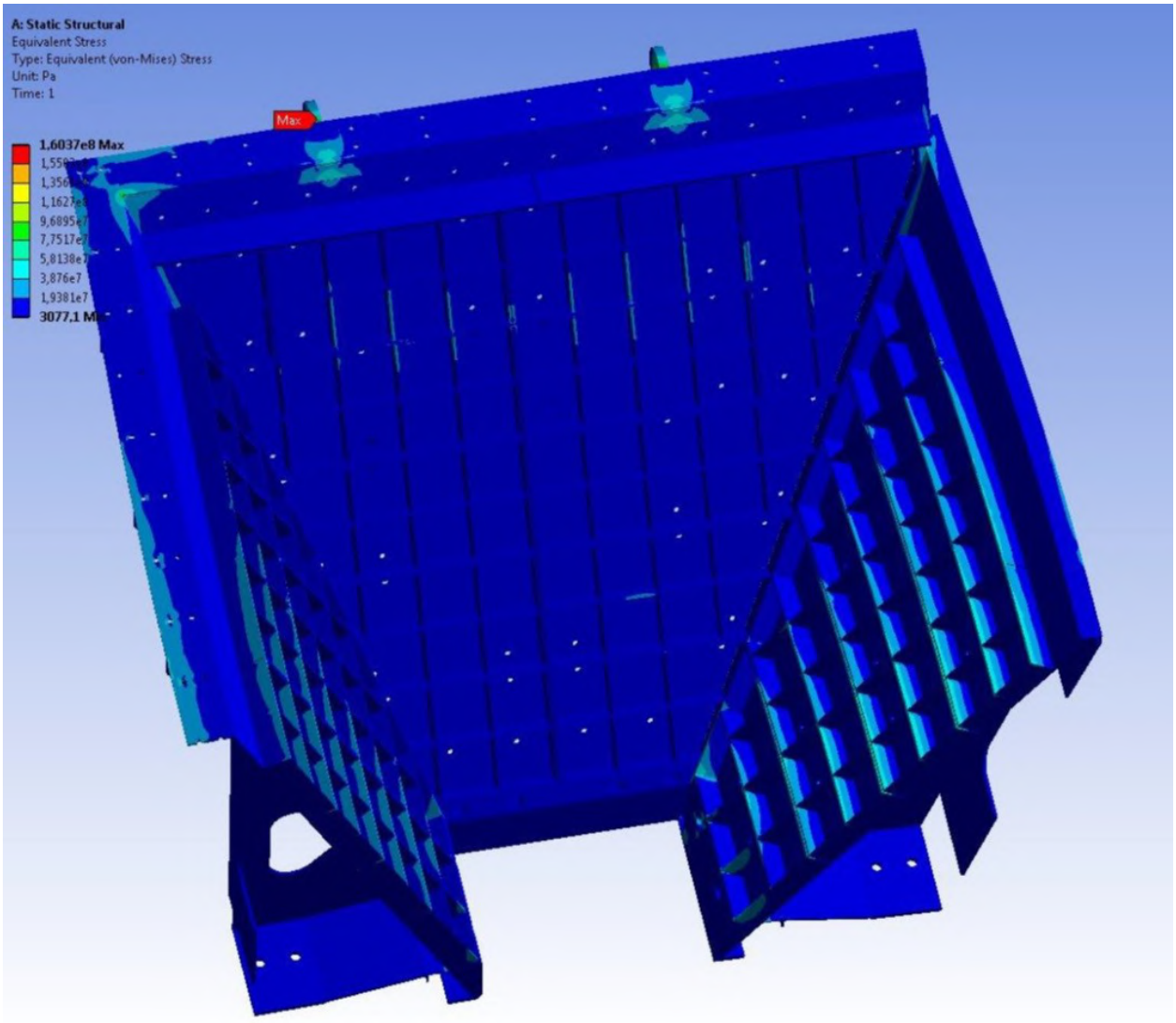

Fig. 3.47 Distribution of von Mises equivalent stresses.

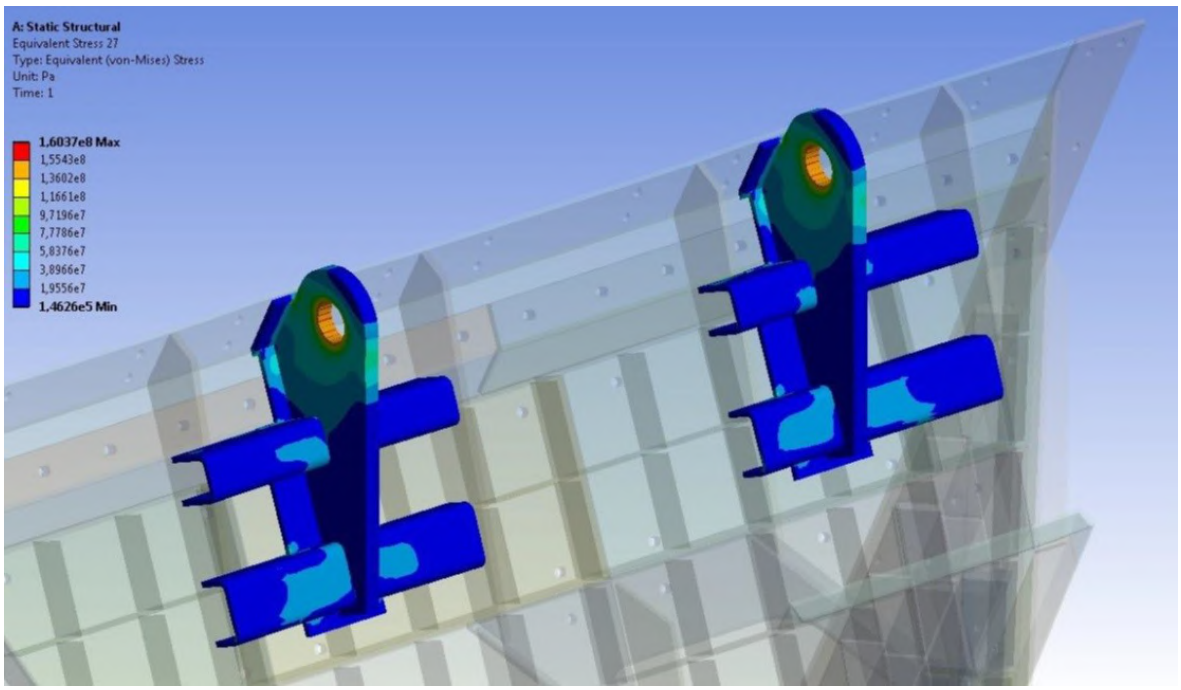

Fig. 3.48 Distribution of von Mises equivalent stresses in the lug

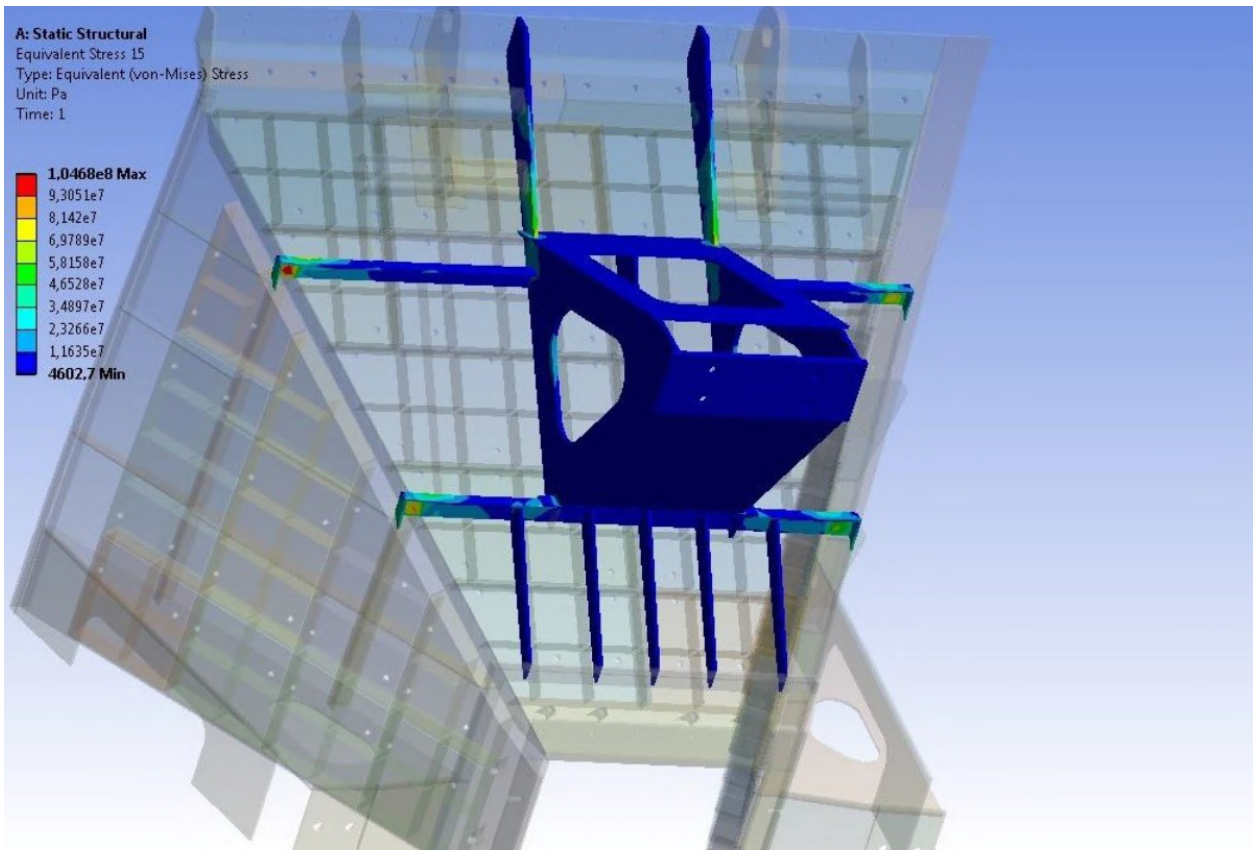

Fig. 3.49 Distribution of von Mises equivalent stresses in hopper's lateral support, middle and top load-bearing collar.

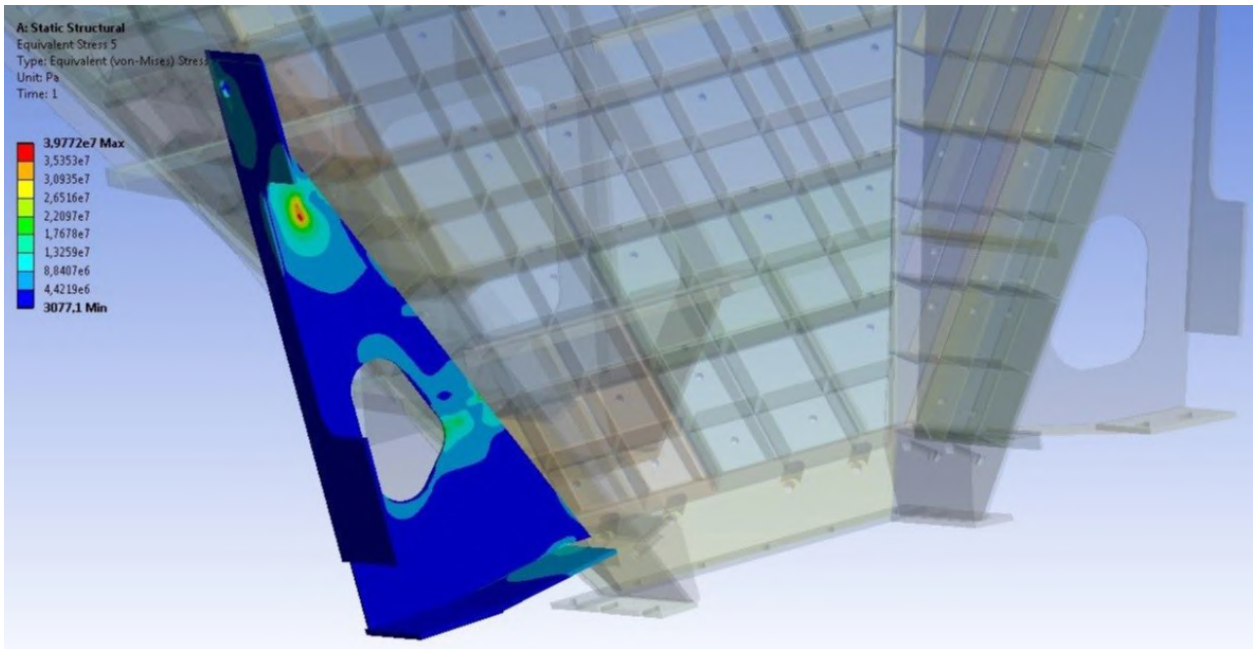

Fig. 3.50 Distribution of von Mises equivalent stresses in the support

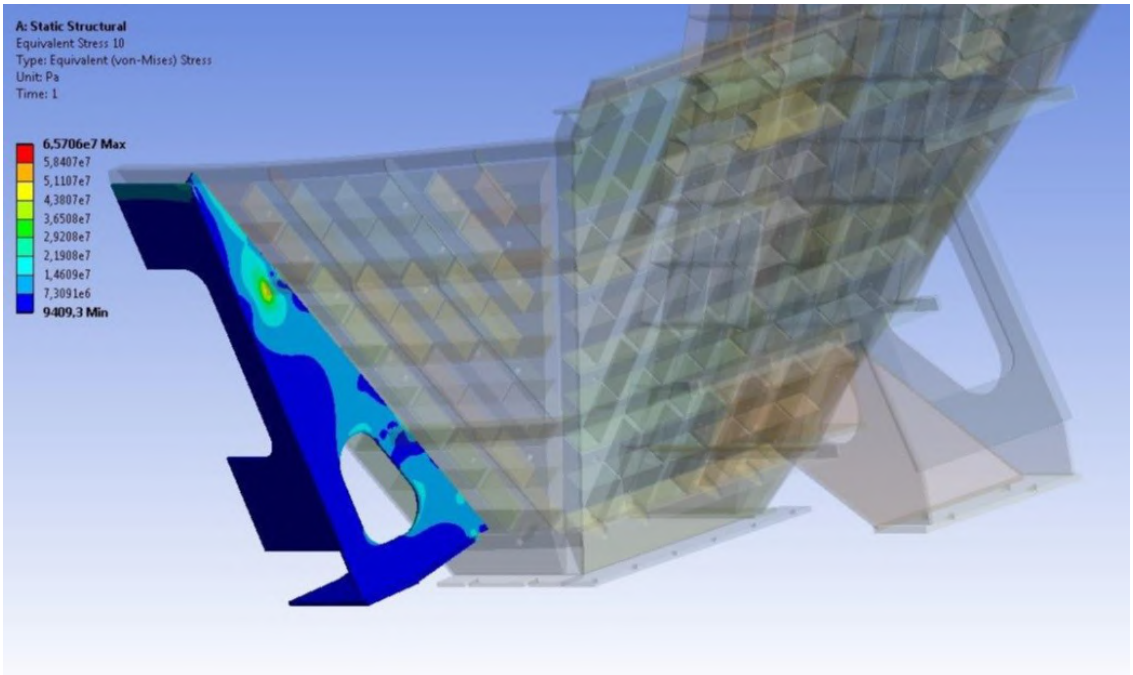

Fig. 3.51 Distribution of von Mises equivalent stresses in the support.

Maximum stresses in the structure do not exceed 160.5MPa. Whereas assembly and disassembly will be performed at normal temperature the structure meets strength and stiffness requirements.

3.3.5 Upper hopper design collective results

Calculation results obtained are presented as the summary Table 3.4 of design patterns and controlled variables.

Table 3.4

Design pattern	NSC	NSC+LWE frontal	NSC+LWE lateral	NSC+MDE
Maximum equivalent stresses in the hopper, MPa	**146.1**	**155.4**	**149.9**	**156.4**
Maximum equivalent stresses in the load-bearing cover, MPa	**146.1**	**145.9**	**142.7**	**146.6**
Maximum equivalent stresses in the hopper's back support, MPa	**111.9**	**146.7**	**119.5**	**156.4**
Maximum equivalent stresses in the hopper's front support, MPa	**141.9**	**153.7**	**149.9**	**144.8**
Maximum equivalent stresses in the lower load-bearing collar, MPa	**130.7**	**155.4**	**128.5**	**154.4**
Safety factor of the hopper	**1.102**	**1.036**	**1.074**	**1.029**
Safety factor of hopper's load-bearing cover	**1.102**	**1.103**	**1.128**	**1.098**
Safety factor of hopper's back support	**1.438**	**1.097**	**1.347**	**1.029**
Safety factor of hopper's frontal support	**1.134**	**1.047**	**1.074**	**1.111**
Safety factor of hopper's lower load-bearing collar	**1.231**	**1.036**	**1.252**	**1.036**

Calculation results show that the examined charging hopper's structure with consideration of potential corrosion meets strength and stiffness requirements for all design loading cases. The definitive design loading cases for the structure are normal service conditions plus design limit value of frontal wind effect and normal service conditions plus maximum design earthquake.

3.4 LOWER HOPPER DESIGN CALCULATIONS

3.4.1 Structural design for normal service conditions

Results of hopper design for normal service conditions are presented in Fig. 3.52-3.58 as von Moses equivalent stress and strain patterns.

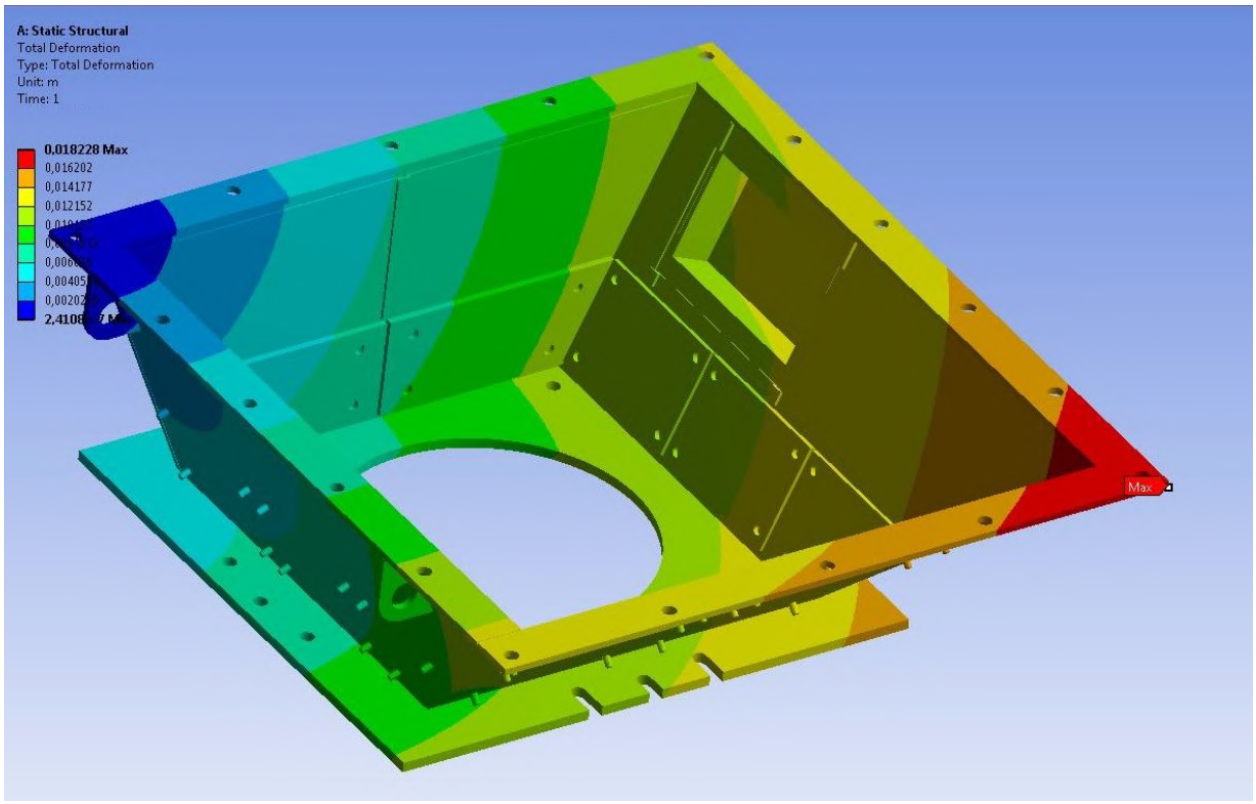

Fig. 3.52 Distribution of total strain arising in the structure

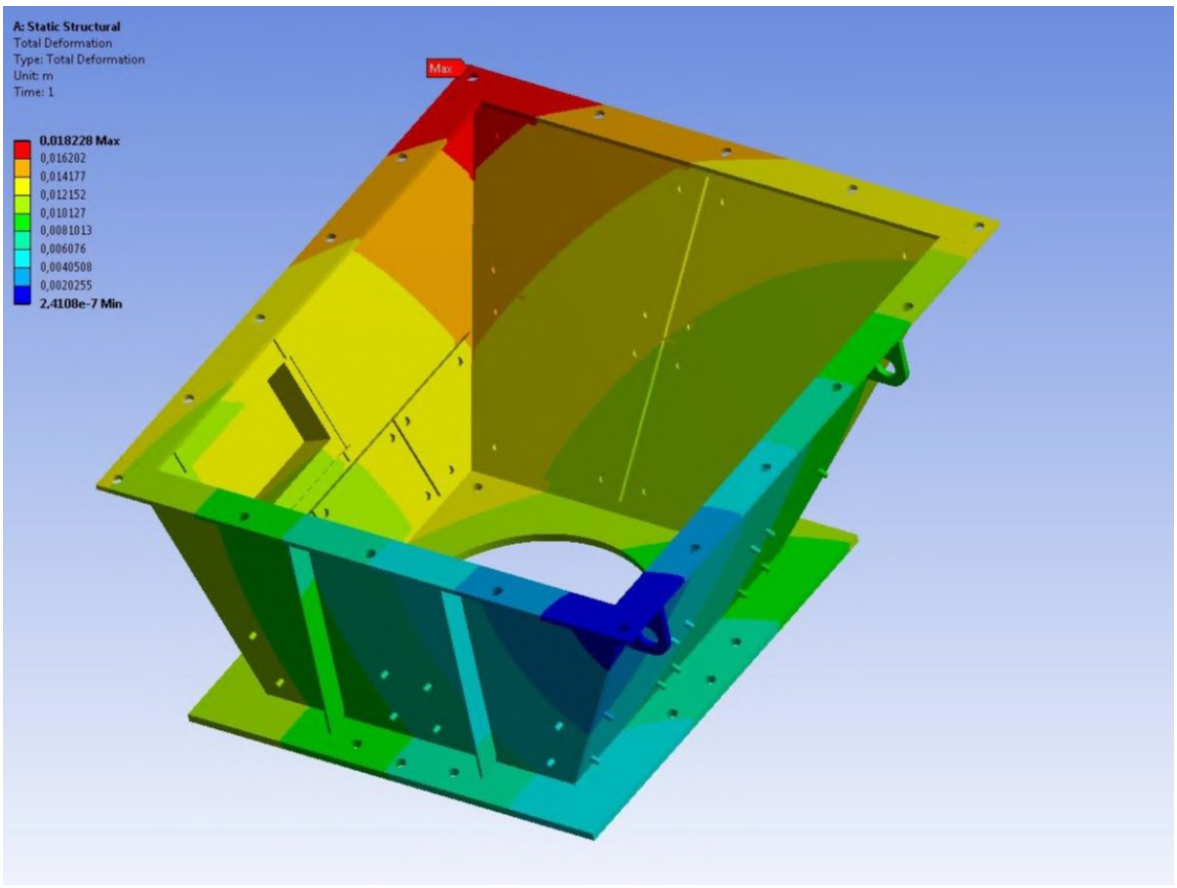

Fig. 3.53 Distribution of total strain arising in the structure

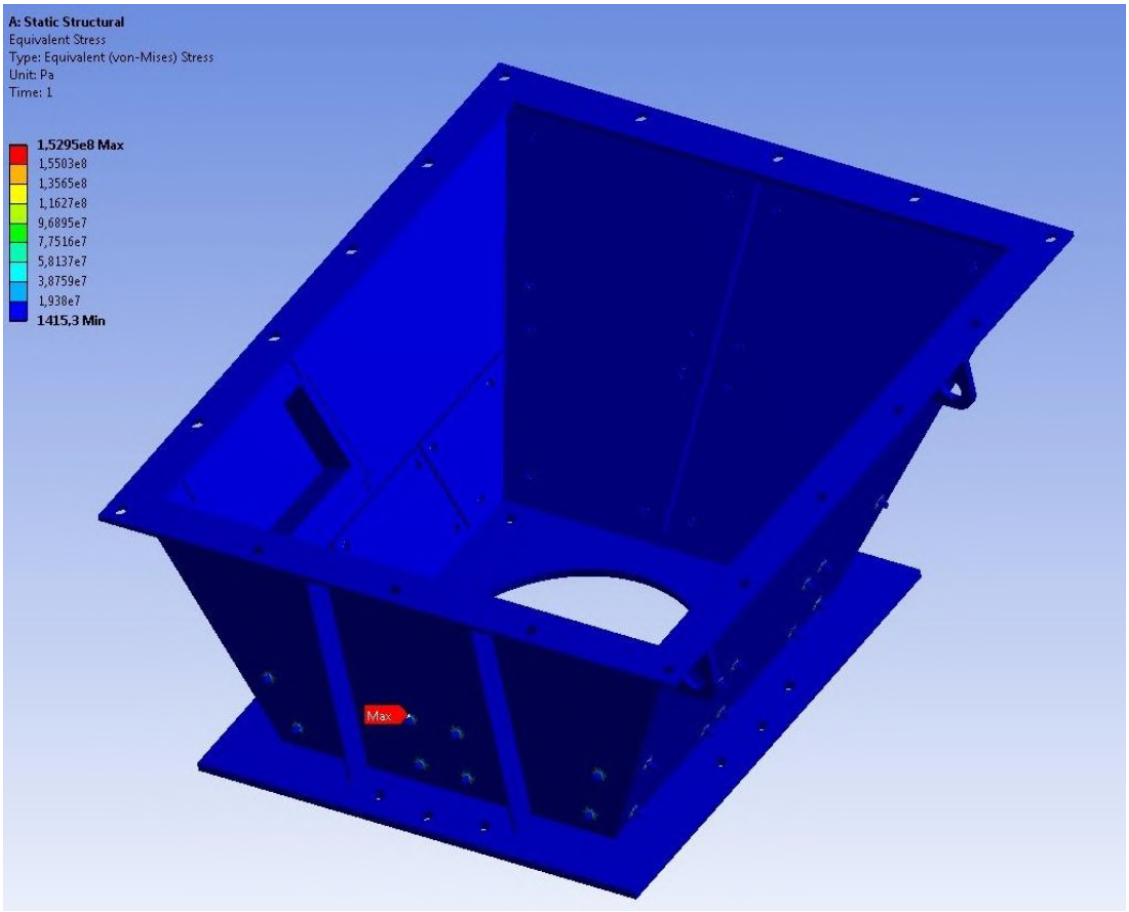

Fig. 3.54 Distribution of von Mises equivalent stresses in the hopper

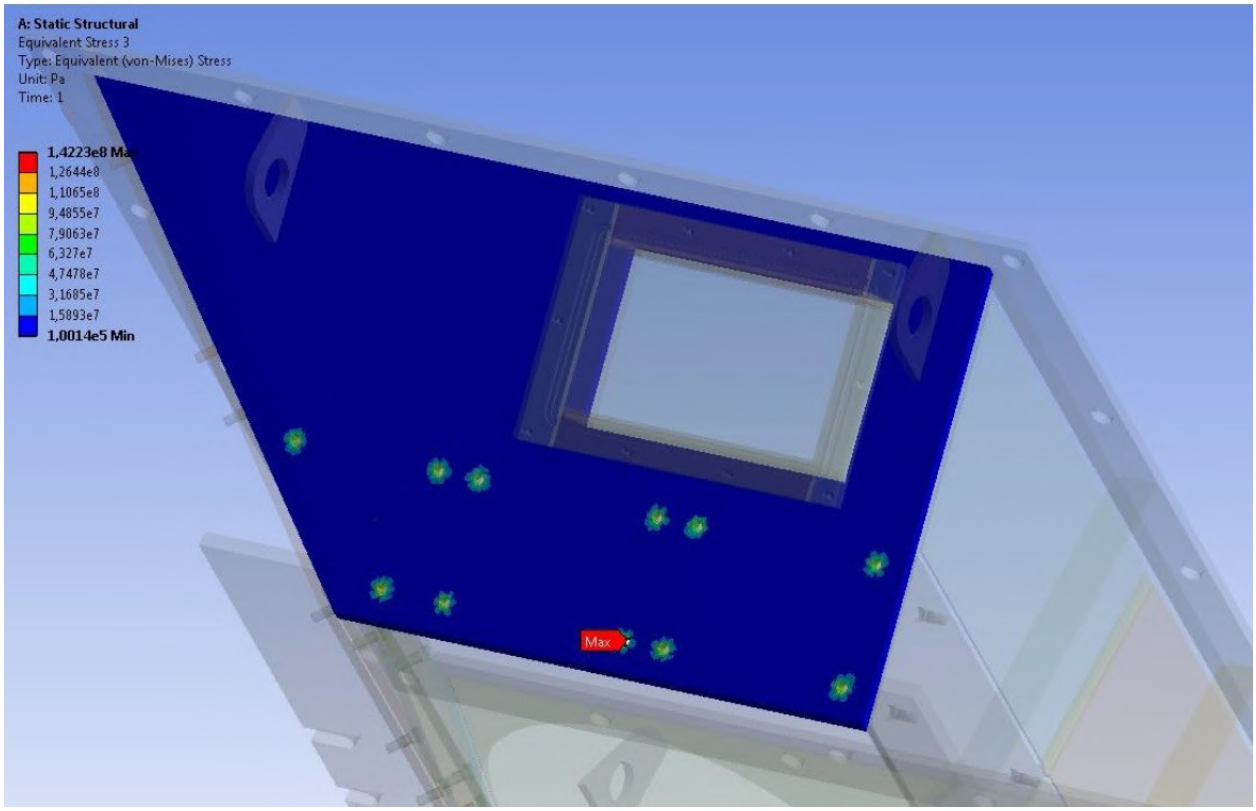

Fig. 3.55 Distribution of equivalent stresses in sheet 1 of the hopper

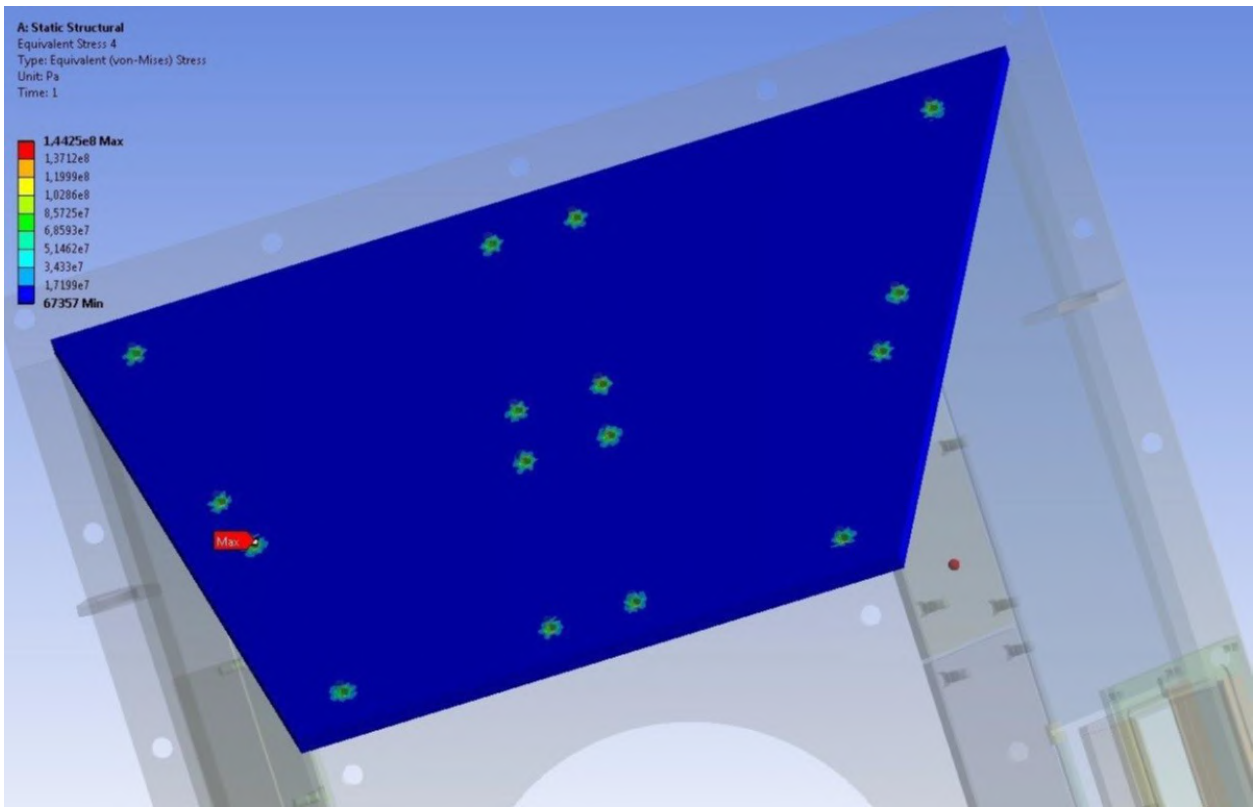

Fig. 3.56 Distribution of equivalent stresses in sheet 2 of the hopper

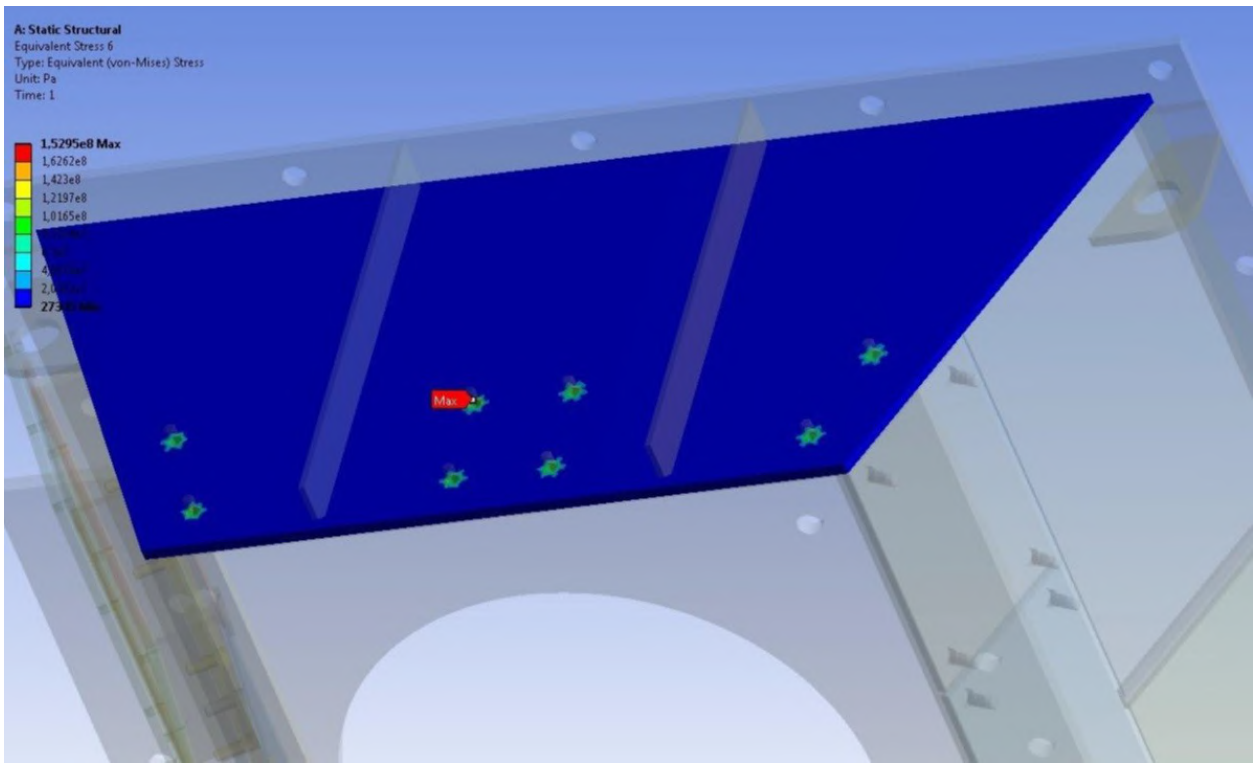

Fig. 3.57 Distribution of equivalent stresses in sheet 4 of the hopper

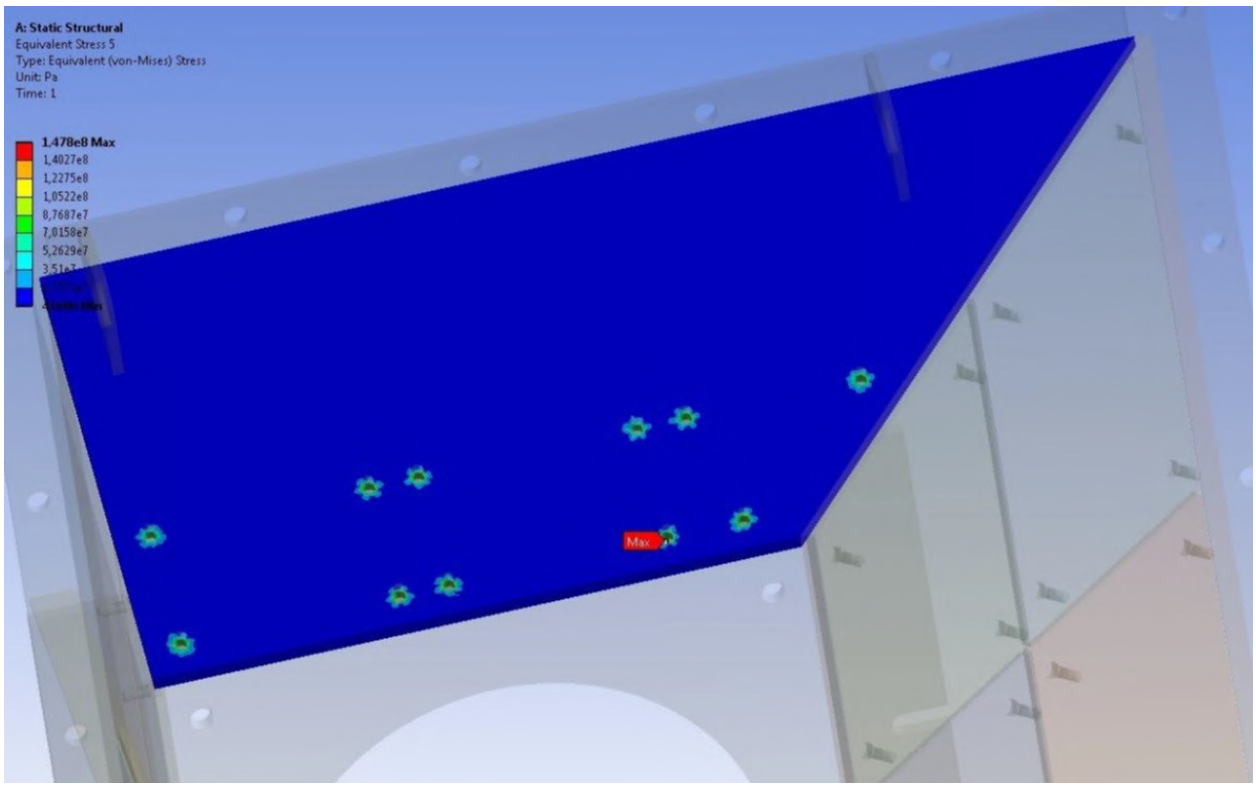

Fig. 3.58 Distribution of equivalent stresses in sheet 3 of the hopper.

The biggest stresses of 153MPa arising at the of aperture's edge border. The value of the biggest stresses distributed in the area is commensurate with sheet thickness and in certain cases does not exceed 92.3MPa.

The results presented show that the structure meets requirements of strength and stiffness for the load case in question.

3.4.2 Upper hopper structural design for wind effect conditions and normal service conditions

3.4.2.1 Lower hopper design under frontal wind effect

The design pattern of hopper loading under normal service conditions and limit frontal wind effect is presented in Fig.3.59.

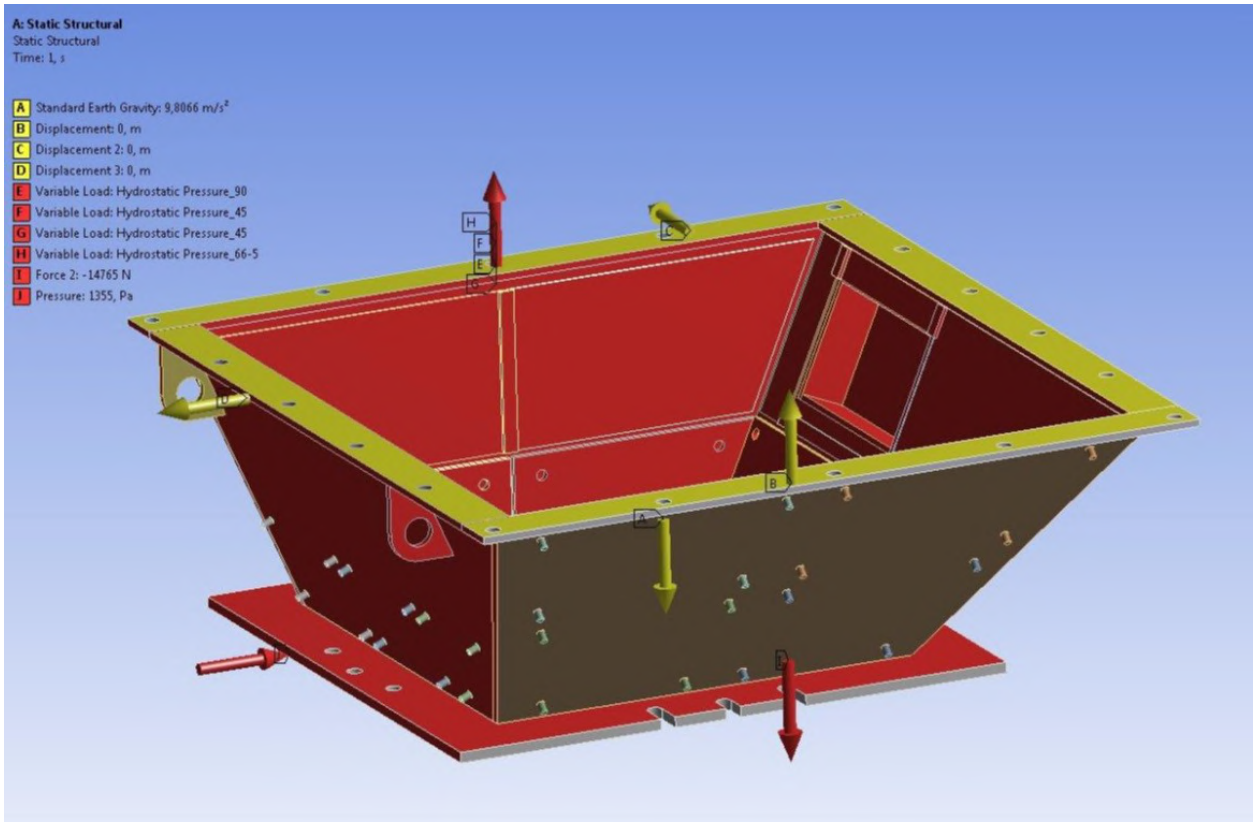

Fig. 3.59 Design pattern of hopper loading under NSC+LWE

Calculation results of the lower hopper for these service conditions are presented as stress-strain patterns in Fig.3.60-3.66. Fig. 3.63-3.66 represent distribution patterns of von Mises equivalent stresses in lower hopper lateral sheets.

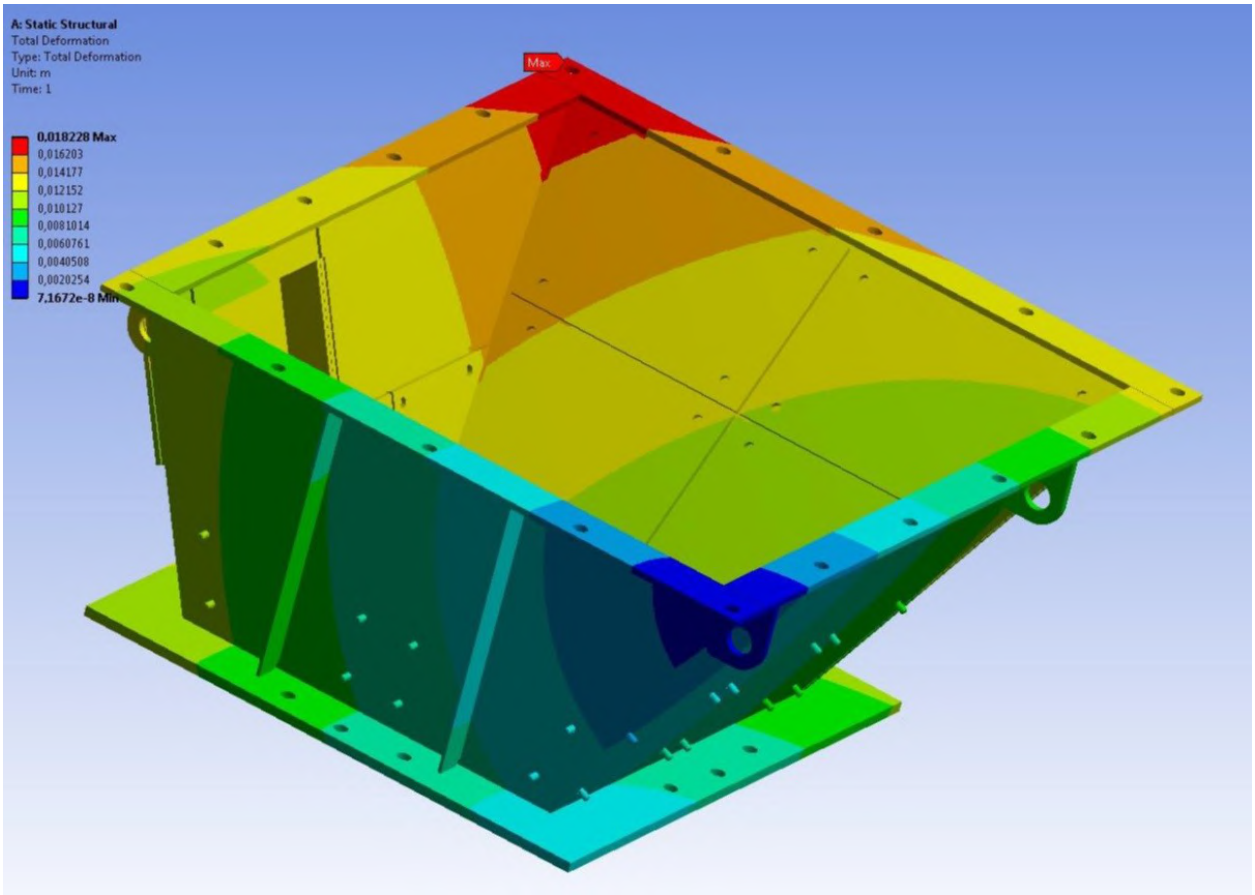

Fig. 3.60 Distribution of total strain arising in the structure

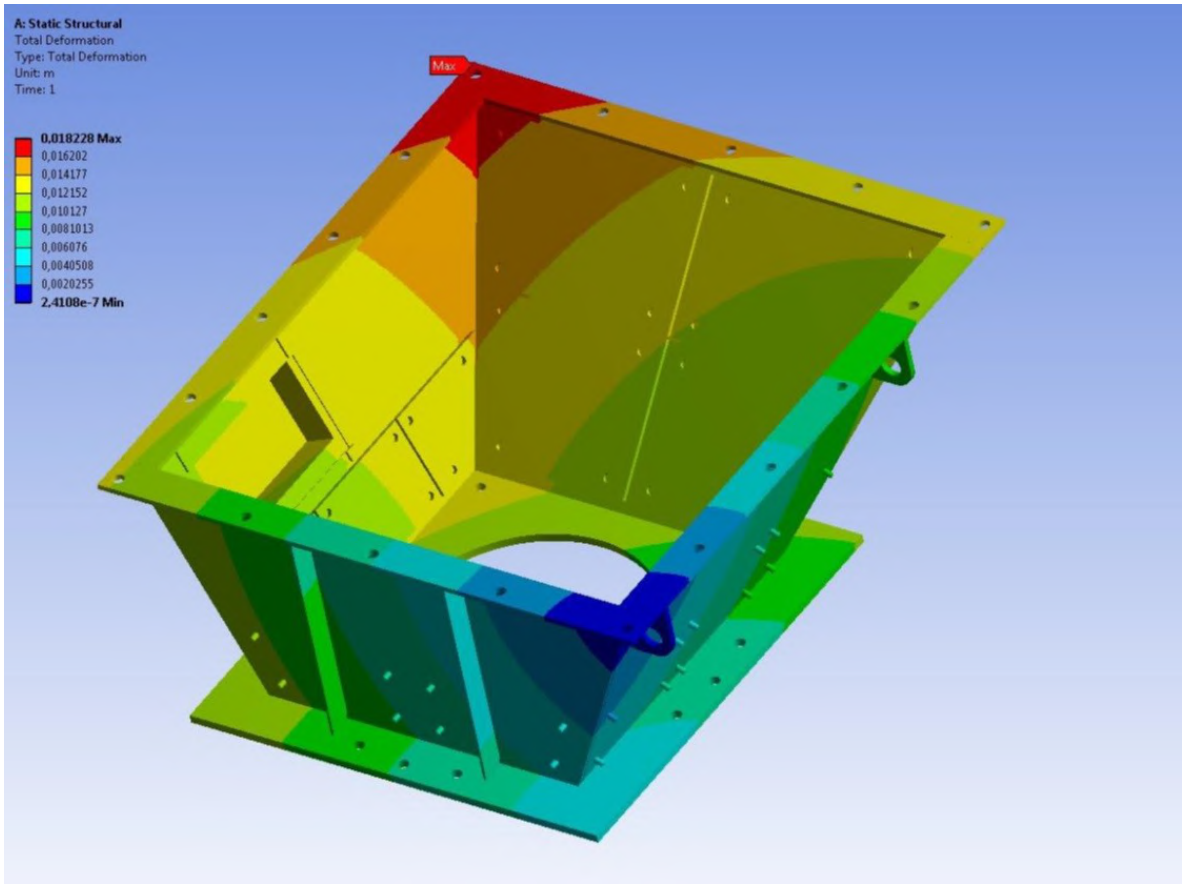

Fig. 3.61 Distribution of total strain arising in the structure

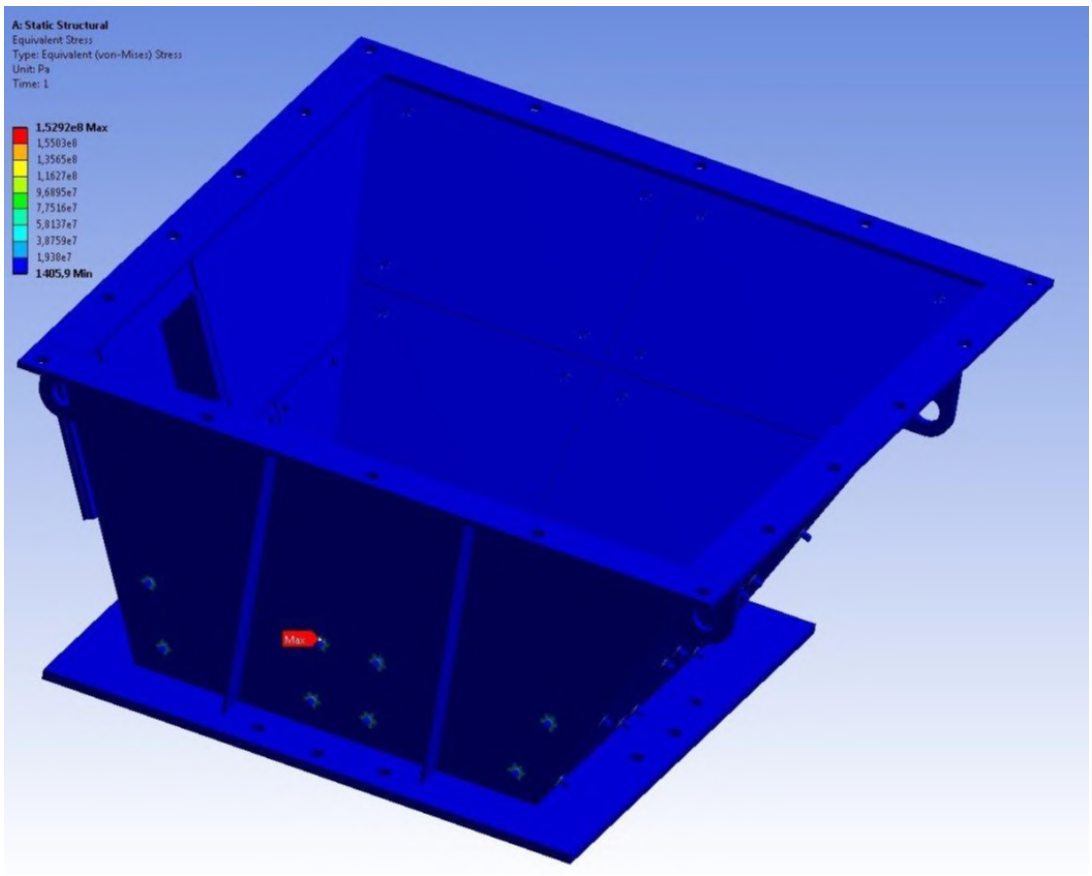

Fig. 3.62 Distribution of von Mises equivalent stresses in the structure

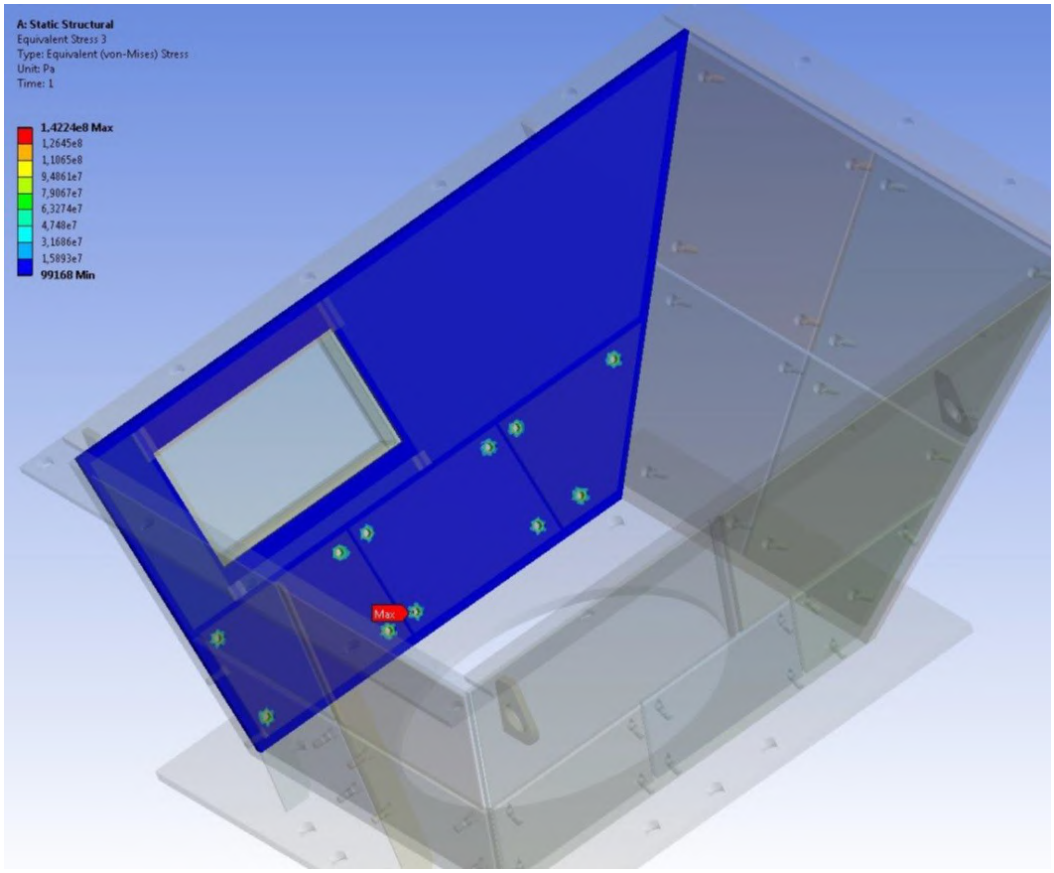

Fig. 3.63 Distribution of equivalent stresses in sheet 1 of the hopper

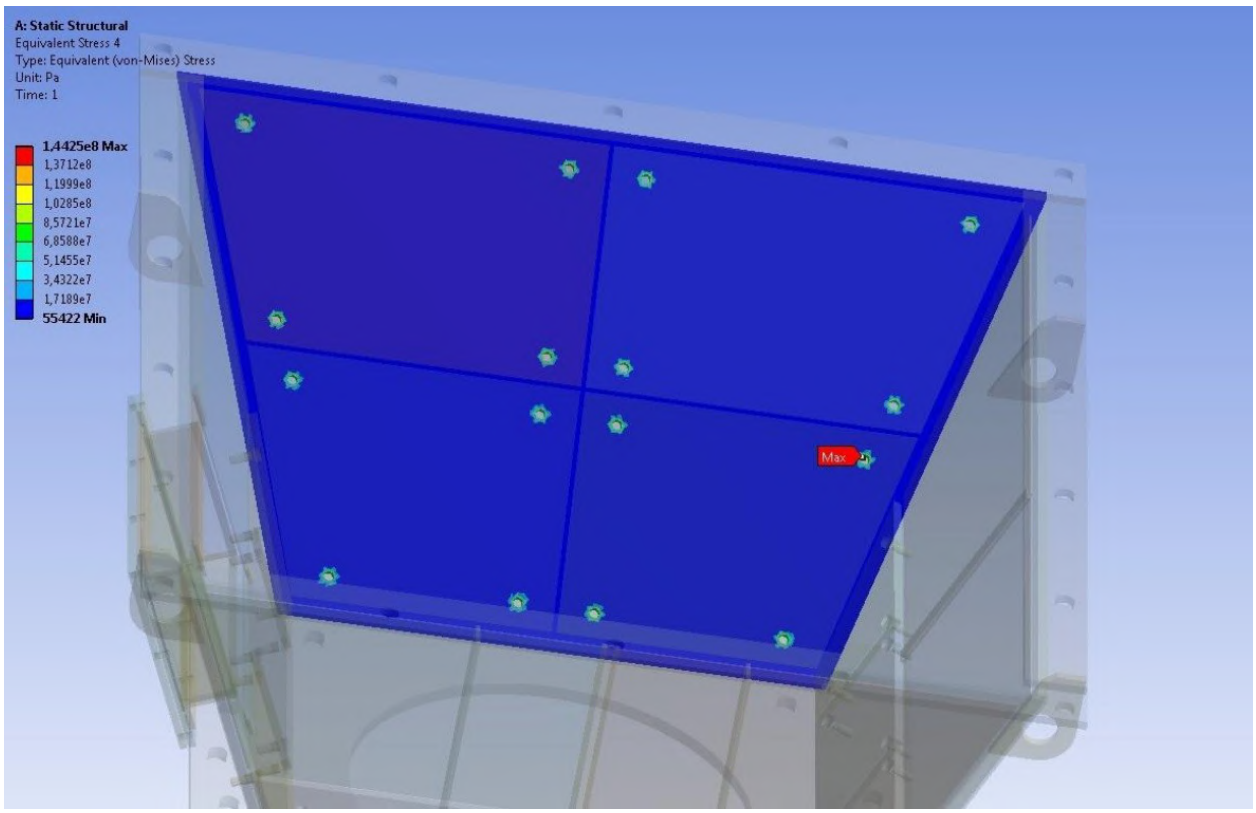

Fig. 3.64 Distribution of equivalent stresses in sheet 2 of the hopper

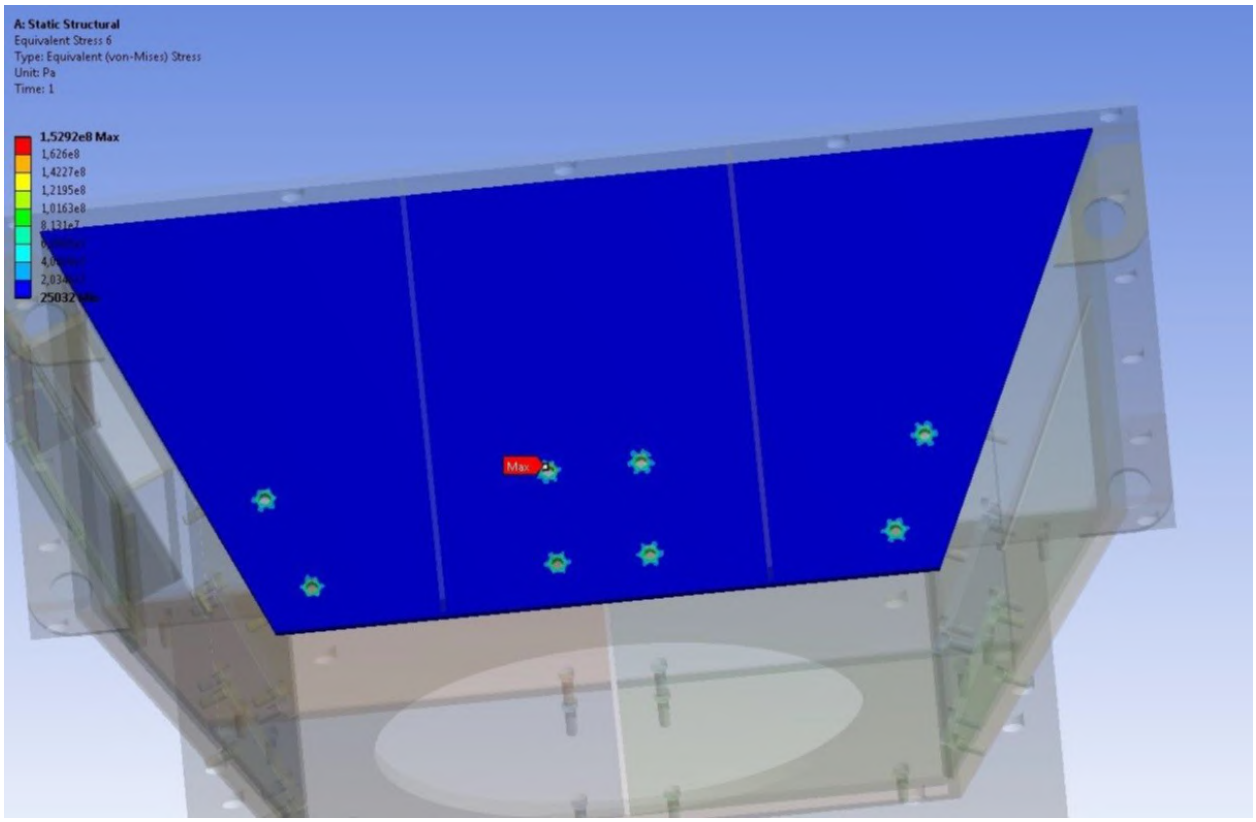

Fig. 3.65 Distribution of equivalent stresses in sheet 4 of the hopper

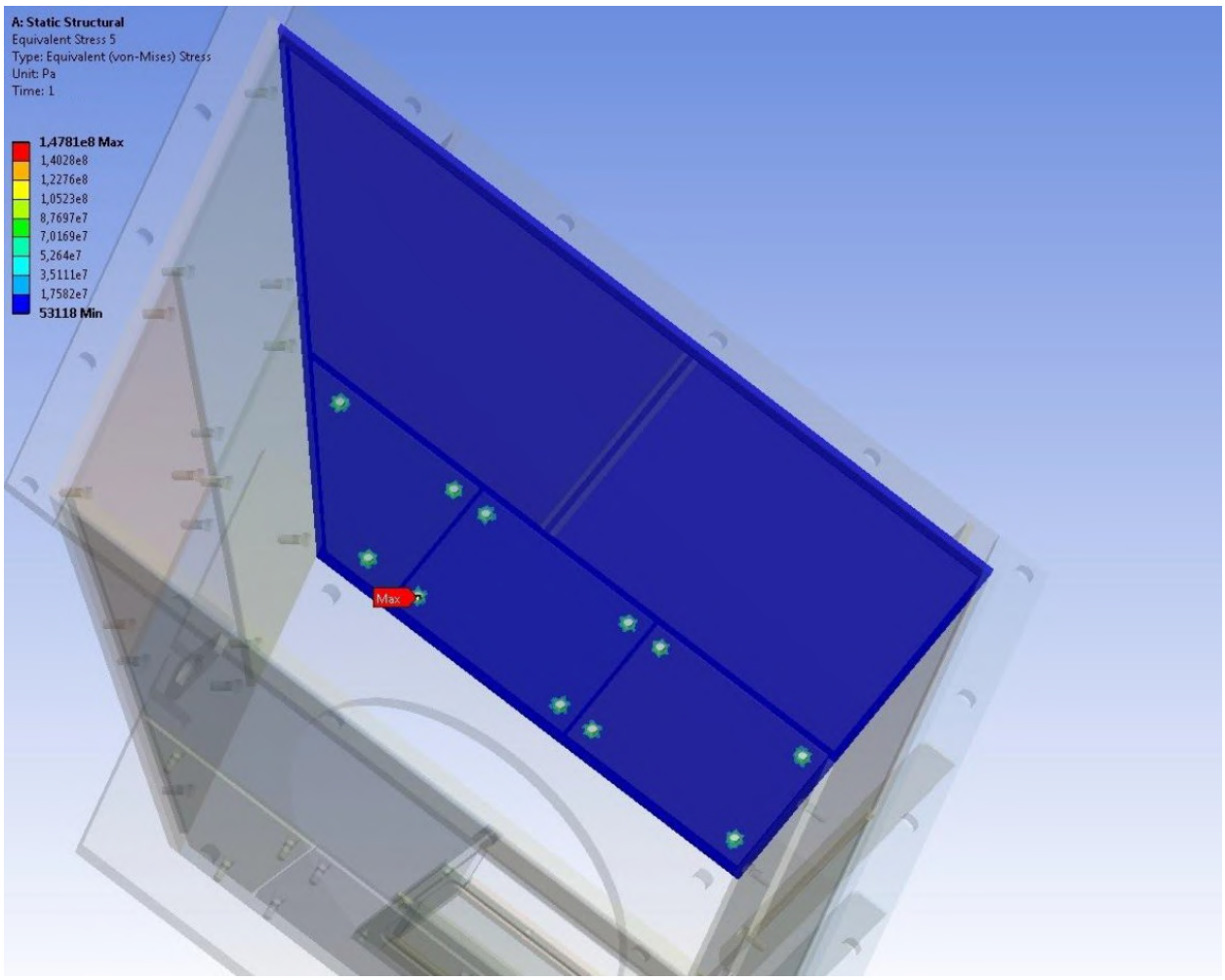

Fig. 3.66 Distribution of equivalent stresses in sheet 3 of the hopper

Analysis of results showed that wind effect insignificantly affects the stress-strain state of the lower receiving hopper, and arising stresses virtually concur with stresses for normal service conditions.

The results presented show that the structure meets requirements of strength and stiffness for the load case in question.

3.4.2.2 Lower hopper design under lateral wind effect

The design pattern of hopper loading under normal service conditions and limit frontal wind effect is presented in Fig.3.67.

Calculation results of the lower hopper for these service conditions are presented as stress-strain patterns in Fig.3.68-3.74. Fig. 3.71-3.74represent distribution patterns of von Mises equivalent stresses in lower hopper lateral sheets.

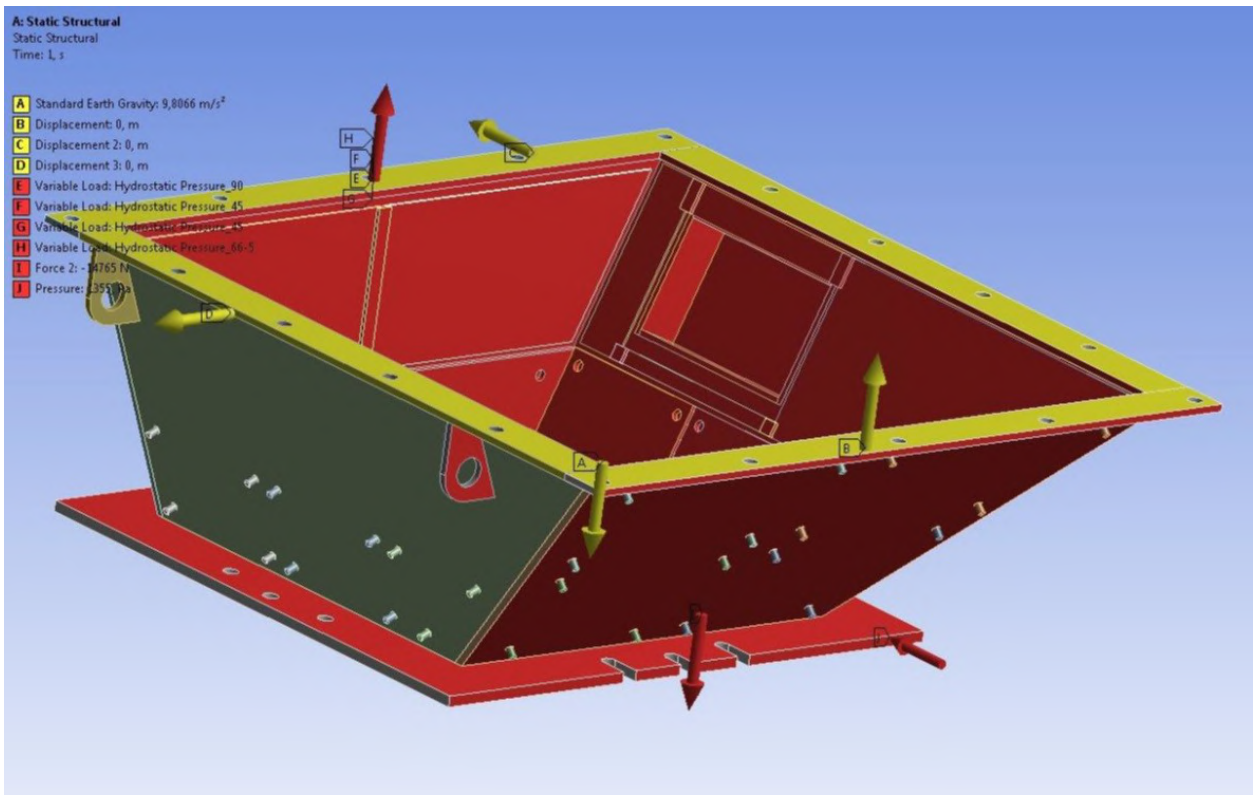

Fig. 3.67 Design pattern of hopper loading under NSC+LWE

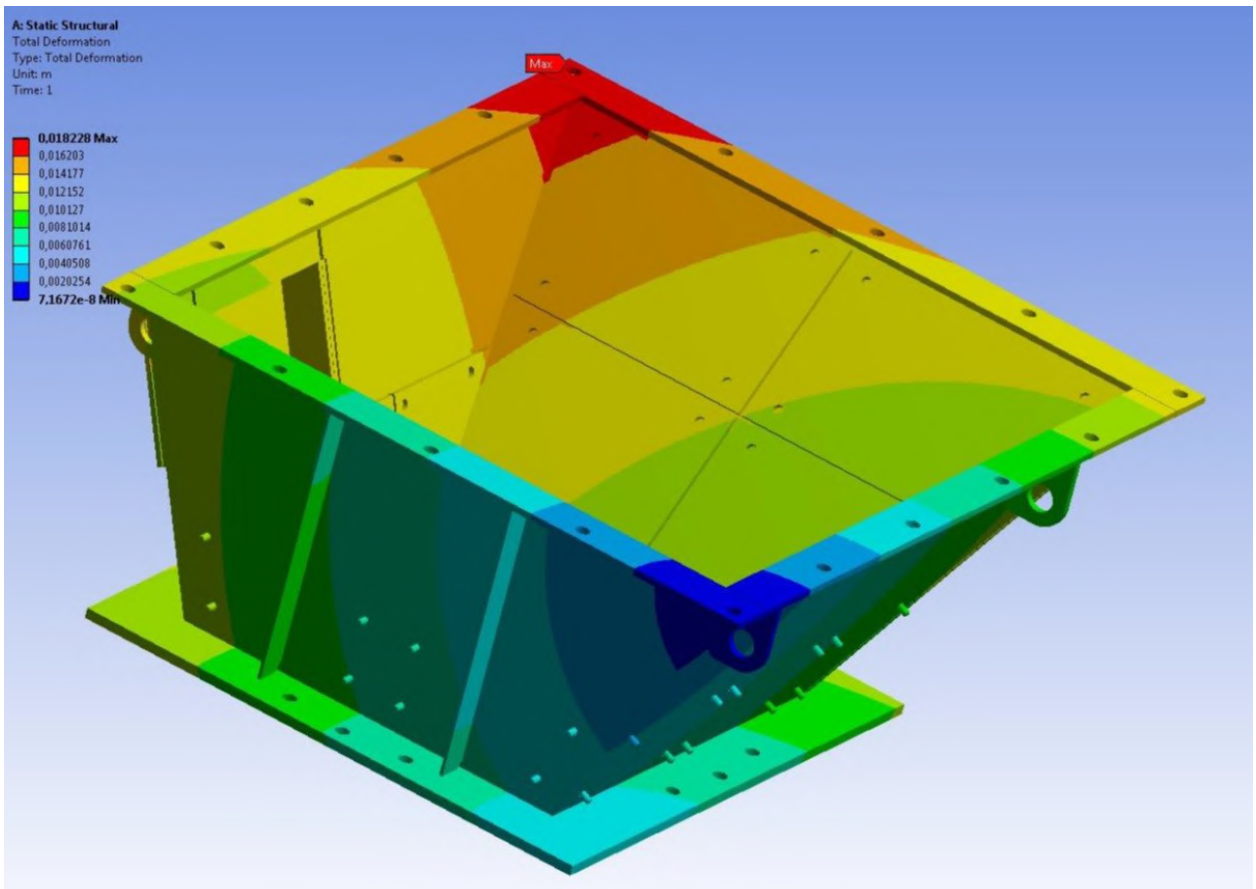

Fig. 3.68 Distribution of total strain arising in the structure

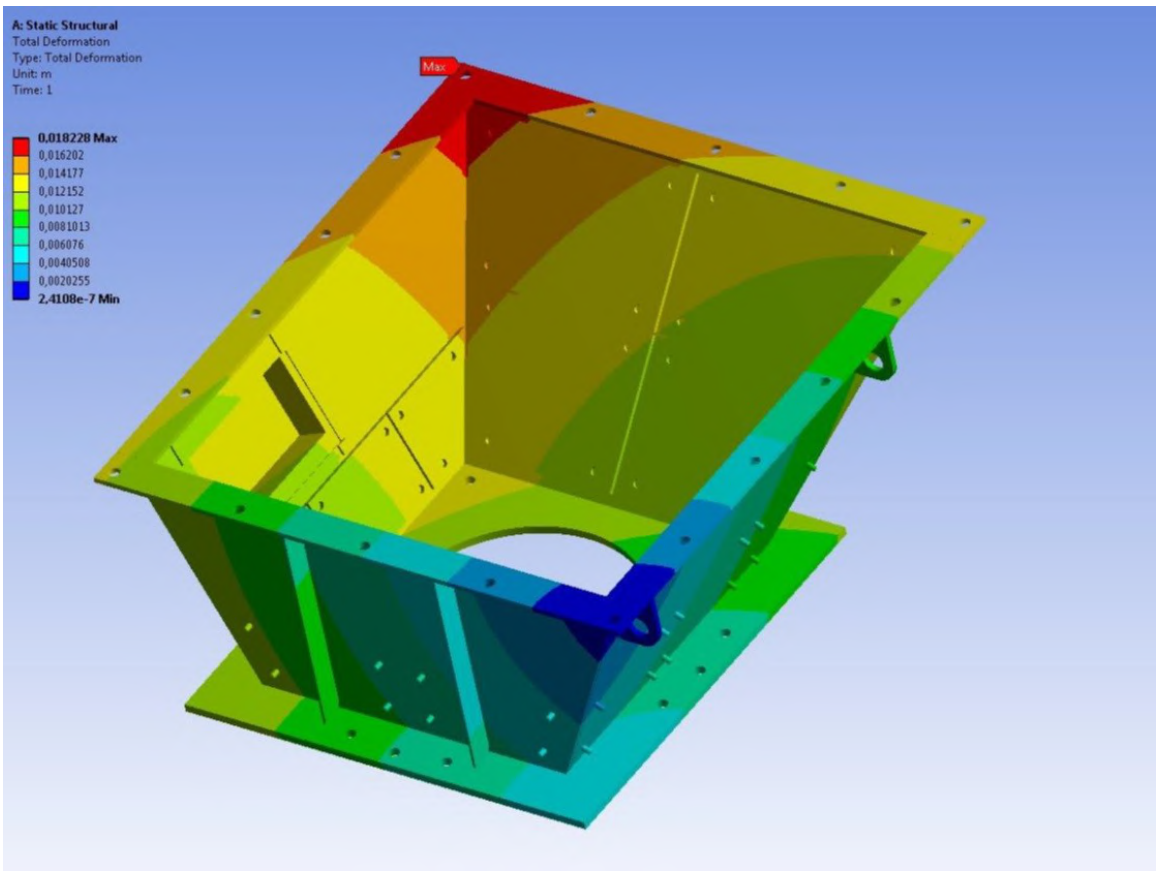

Fig. 3.69 Distribution of total strain arising in the structure

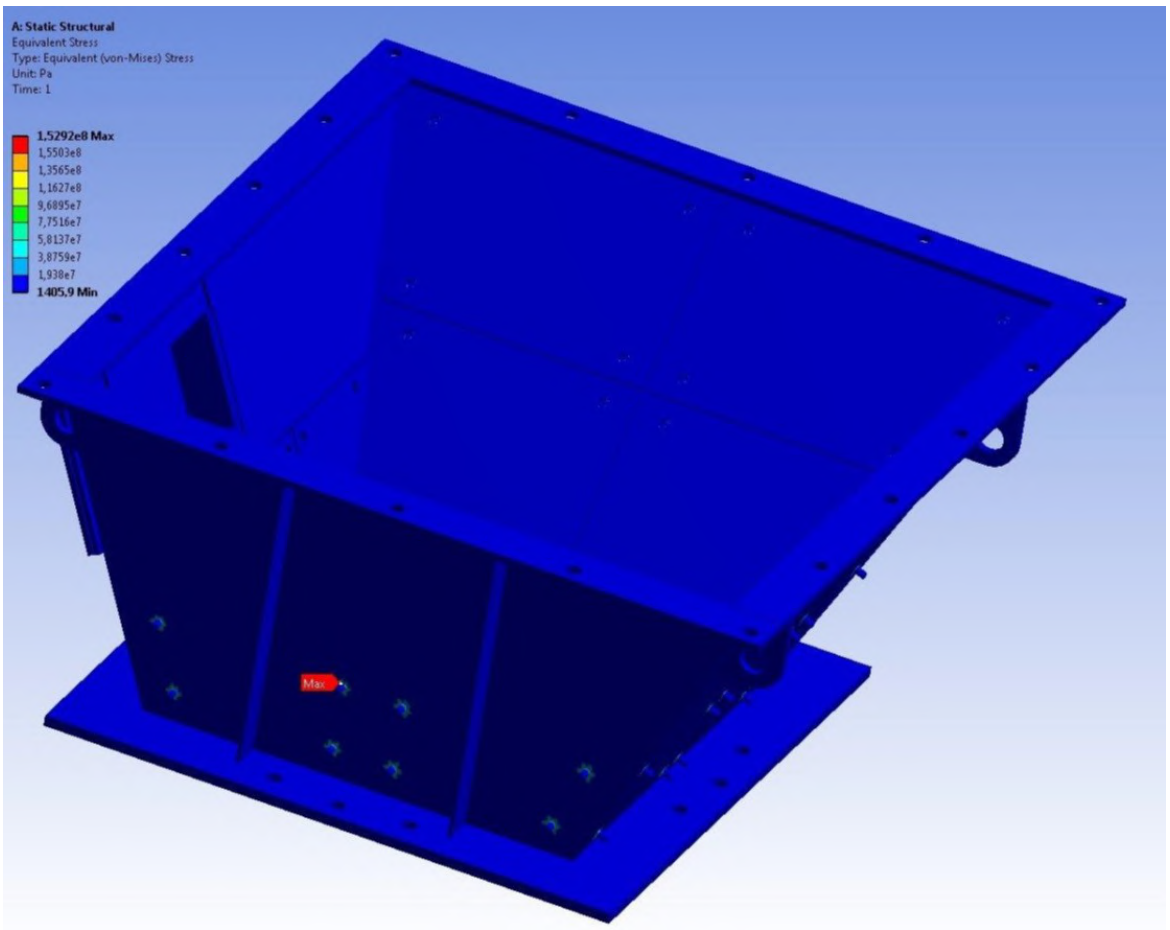

Fig. 3.70 Distribution of von Mises equivalent stresses in the hopper

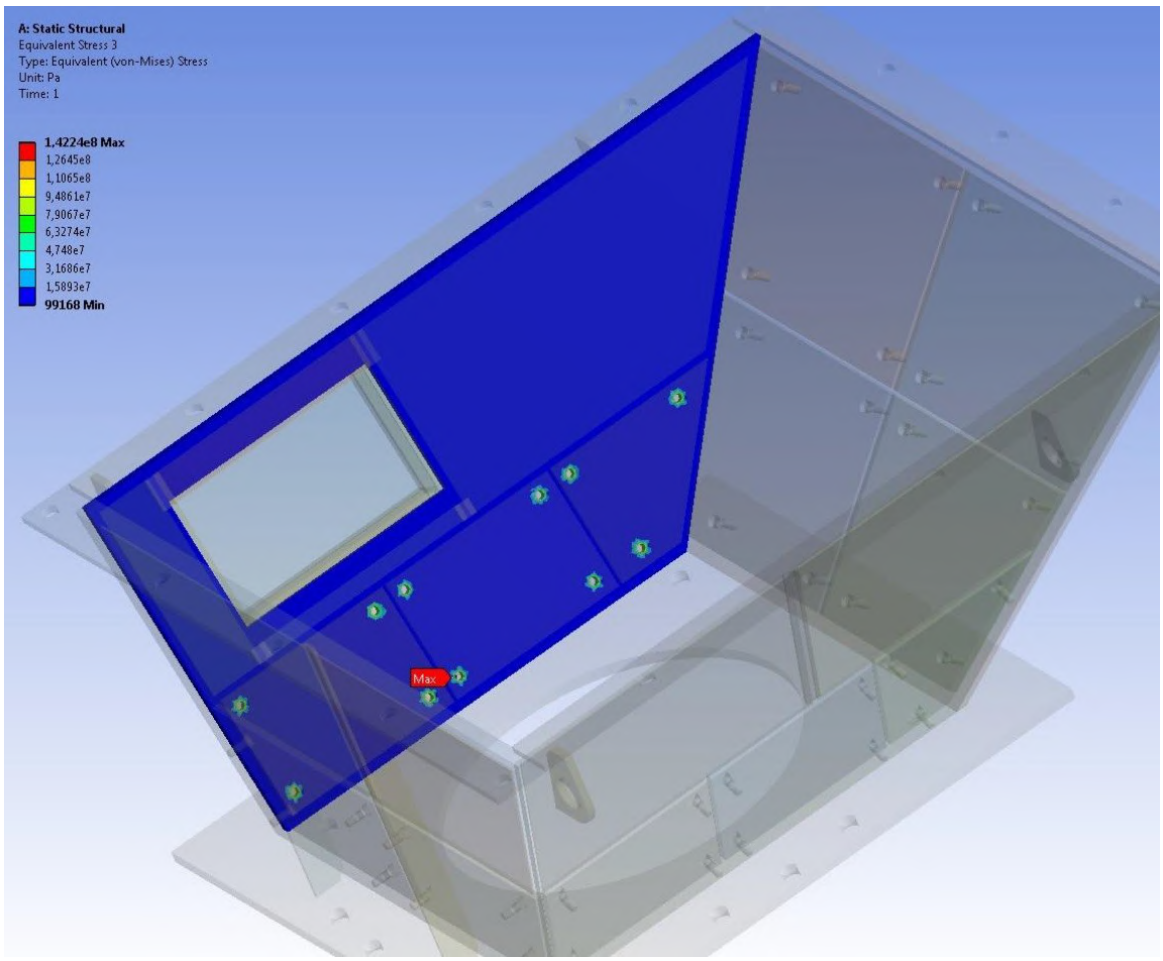

Fig. 3.71 Distribution of equivalent stresses in sheet 1 of the hopper

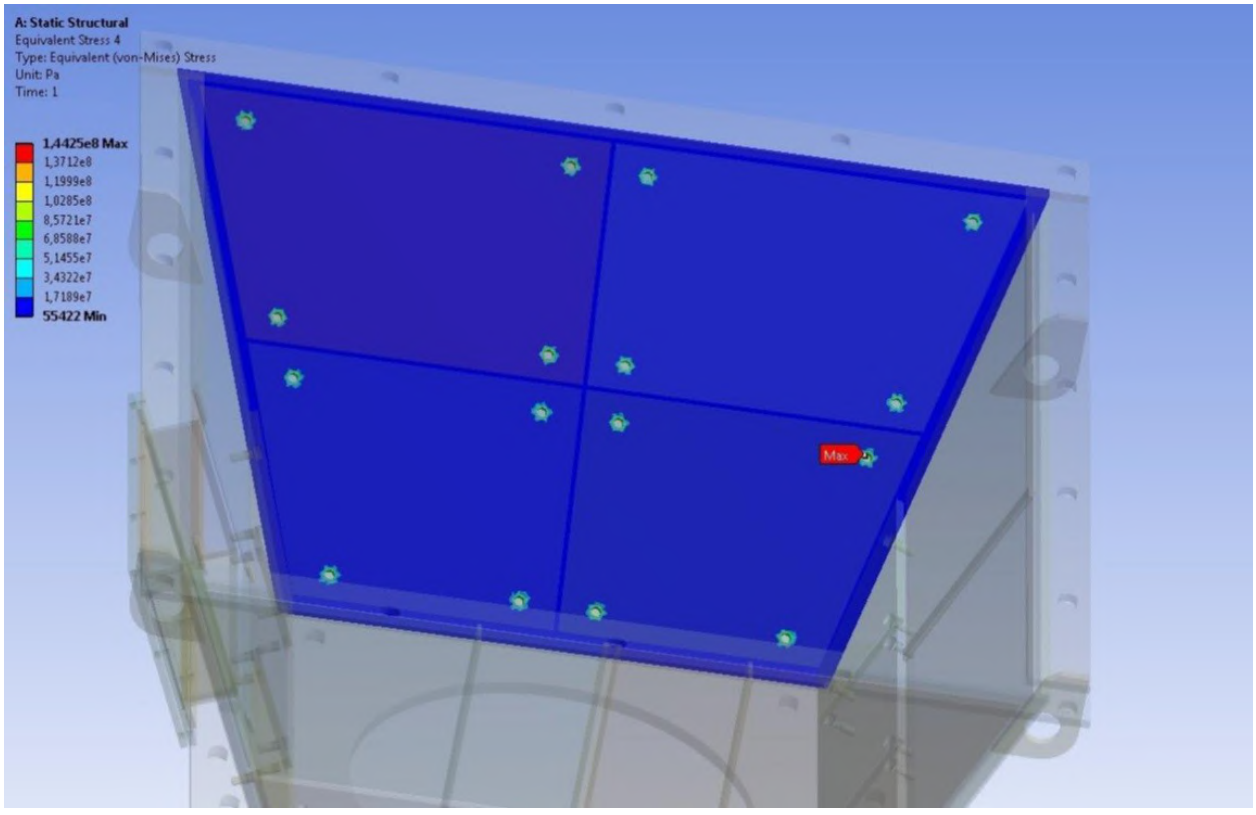

Fig. 3.72 Distribution of equivalent stresses in sheet 2 of the hopper

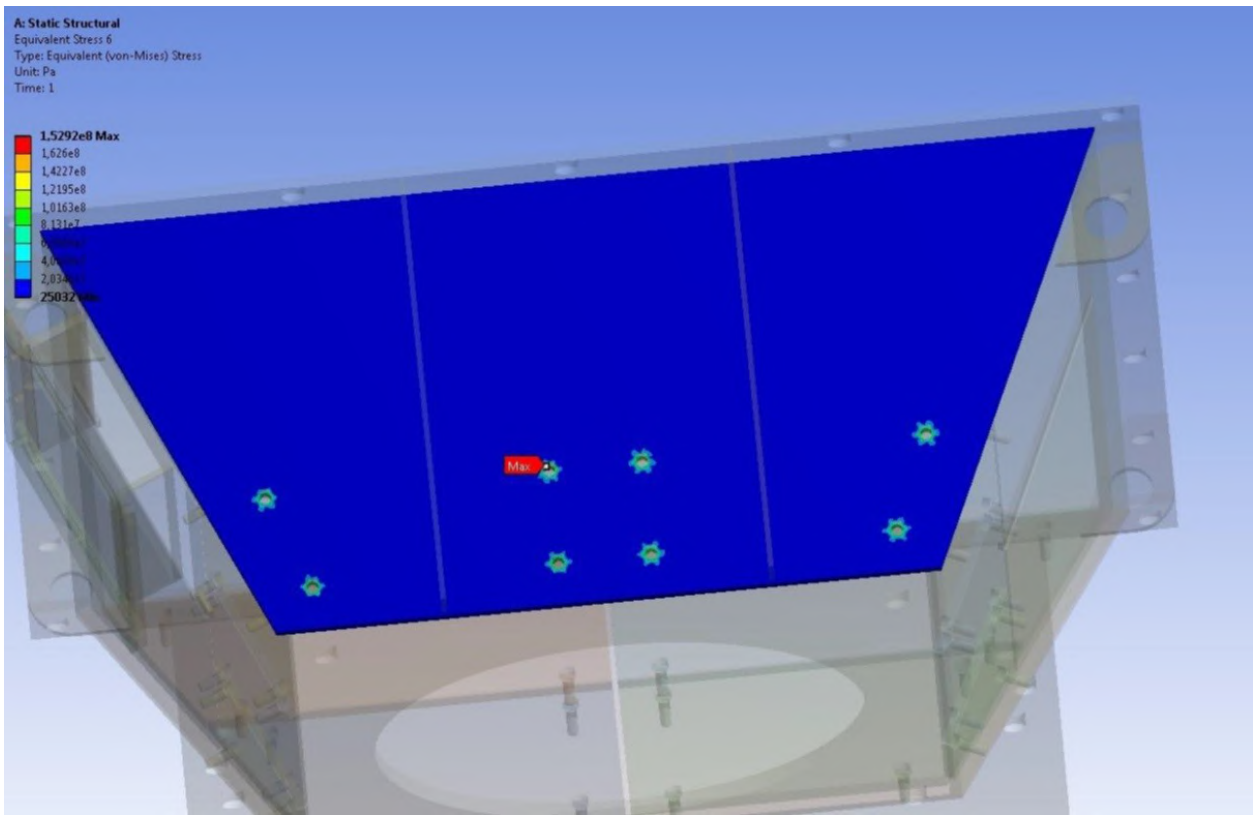

Fig. 3.73 Distribution of equivalent stresses in sheet 3 of the hopper

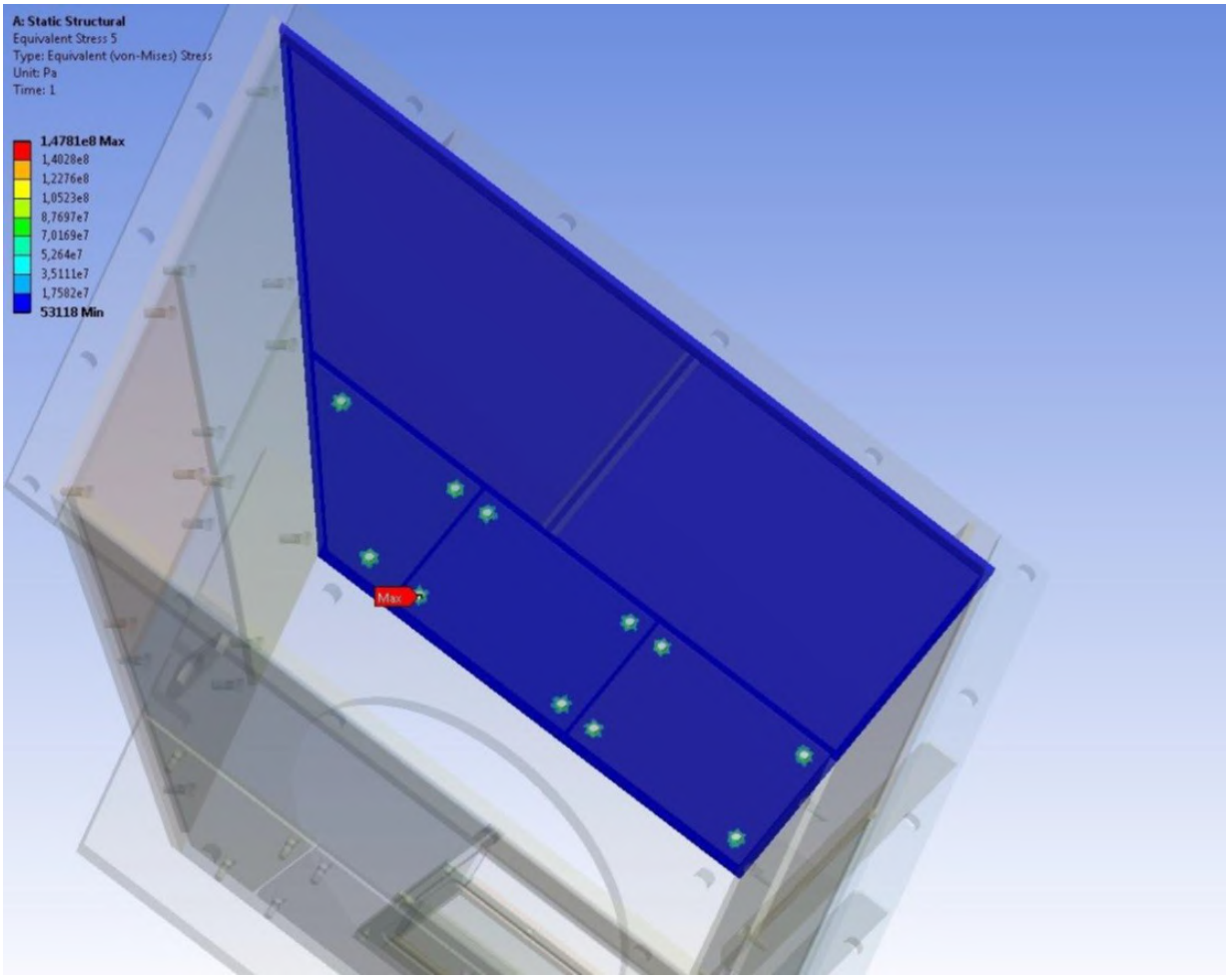

Fig. 3.74 Distribution of equivalent stresses in sheet 4 of the hopper

Assessment of the biggest stresses arising in the structure is performed for area1. Area 1 corresponds to a region commensurate with case thickness in vicinity maximal stresses and exceeds the boundaries of a finite element. According to results the wind effect insignificantly affects the stress-strain state of the lower receiving hopper.

The results presented show that the structure meets requirements of strength and stiffness for the load case in question.

3.4.3 Structural design for seismic impact

Calculation of seismic impact is performed using linear-spectrum method. The initial data is the spectrum of structure's response to dynamic effect. The spectrum is taken to mean a combination of absolute values of maximal response acceleration of linear-elastic system depending on impact frequency. The hopper response spectrum is specified with accelerograms and is presented in Tables 3.2-3.4 for the 53.898 m mark. To define this loading the structure's natural oscillation modes and quantity thereof shall be determined. The number of frequencies shall be determined out of the condition that the frequencies in question correspond to 90% of structure's reduced mass in accordance with the method of reduction. The values of natural oscillation frequency and modes are determined out of structure's modal analysis.

3.4.3.1 Structure's modal analysis

Calculation results of modal analysis showed that it is sufficient to take into consideration the first 100 natural oscillation harmonics, and these are presented in Fig. 3.75.

Oscillation modes for certain natural frequencies are presented in Fig. 3.76.

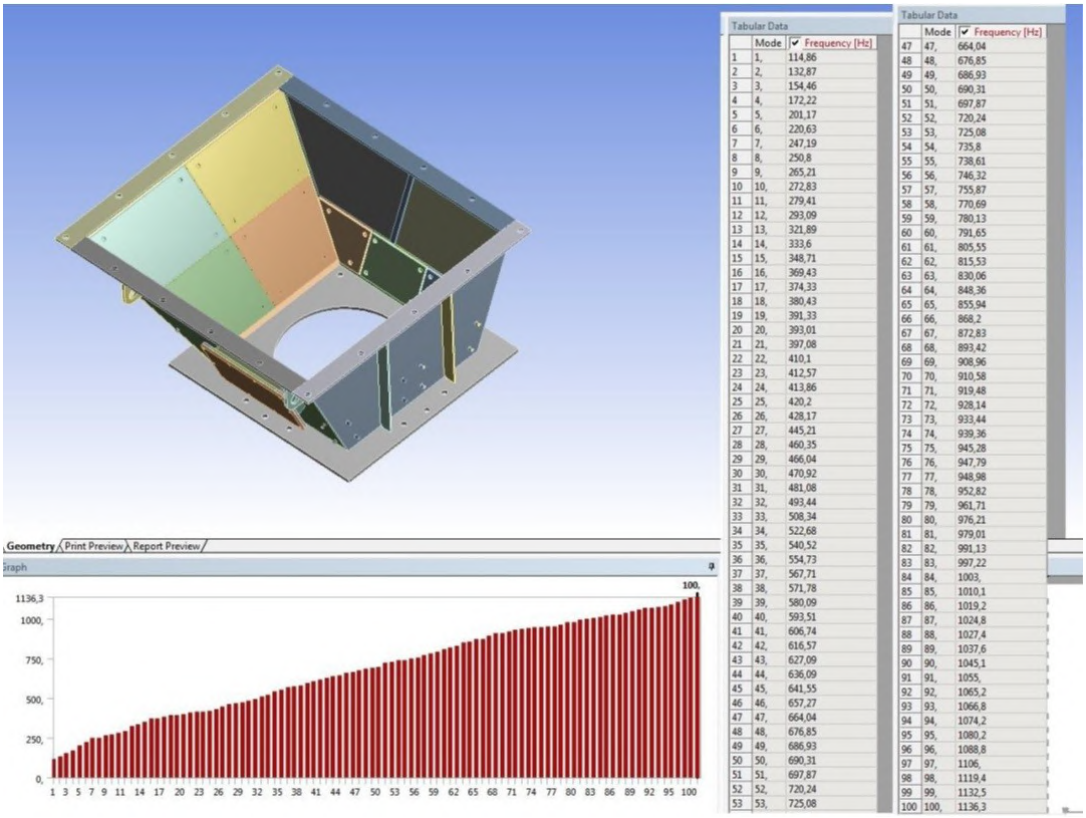

Fig. 3.75 Values of the first 100 natural structure's oscillation frequencies

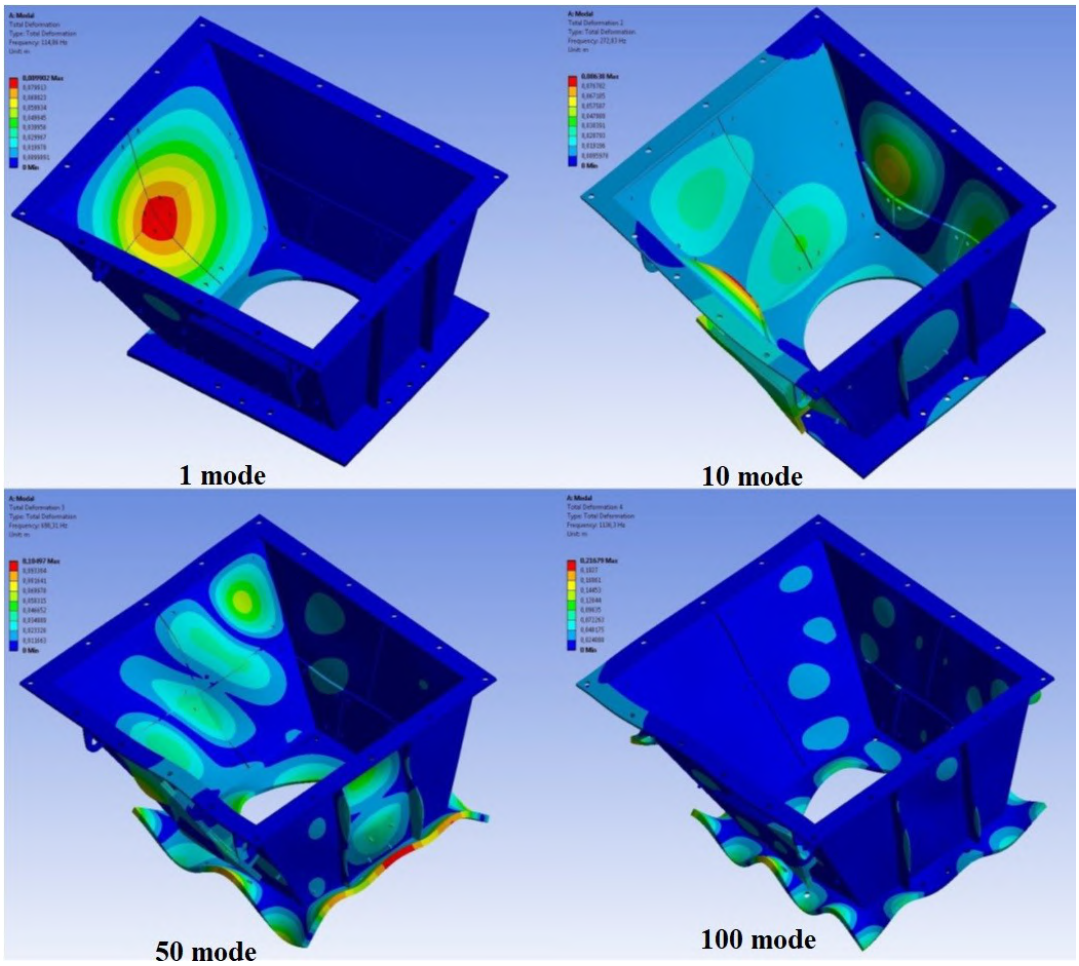

Fig. 3.76 Oscillation modes for 1, 10, 50 and 100 natural frequencies

When carrying out the linear-spectrum analysis the calculation results are obtained using the method of square-root out of sum of squares (SRSS). Field distribution of strains and von Mises equivalent stresses is presented in Fig. 3.77-3.78. The results presented show insignificant effect of seismic impact on stress-strain state of the structure.

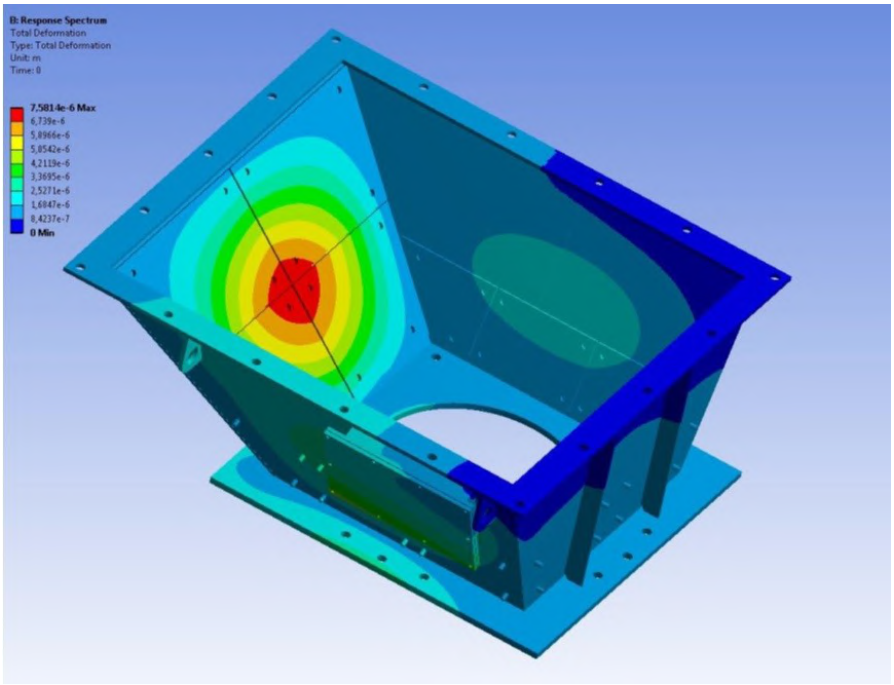

Fig. 3.77 Distribution of total strain in the structure under seismic impact

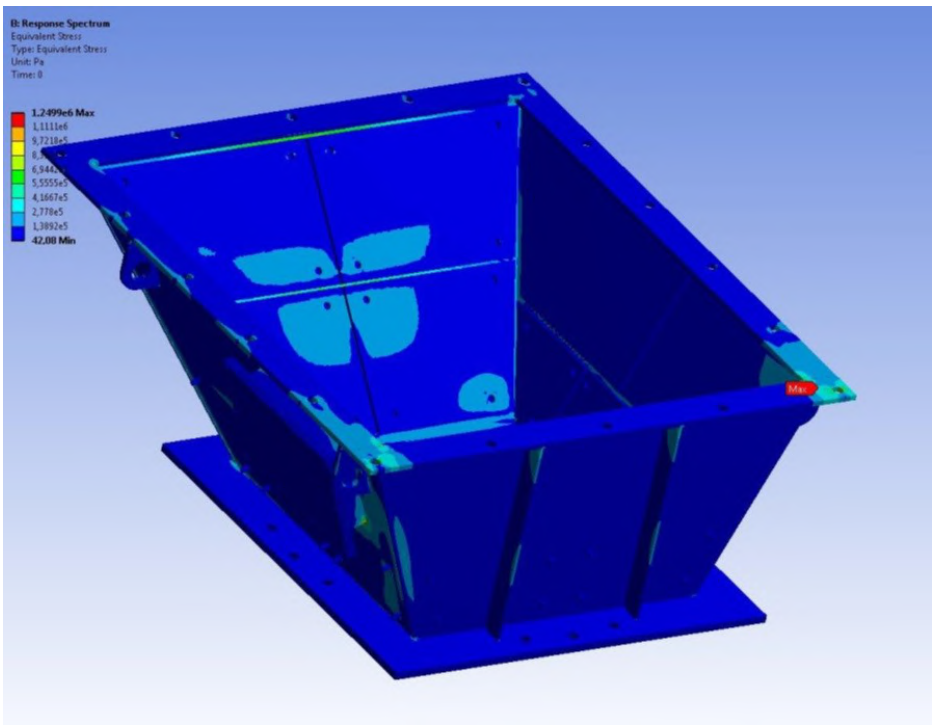

Fig. 3.78 Distribution of von Mises equivalent stresses in the hopper under seismic impact

3.4.4 Strength calculation of lower hopper design lugs

To assess the strength of lower hopper's lugs the design case of crane lift of the hopper holding the structure by lugs. The design model sets border shift conditions in all four lugs in form of cylindrical fixation. The structure has been additionally loaded and designed with consideration for conditions when in event of cable break the slinging by two lugs will ensure performance of erection works. The design loading pattern is presented in Fig.3.79. Calculation results of stress-strain state are presented in Fig. 3.80 -3.84.

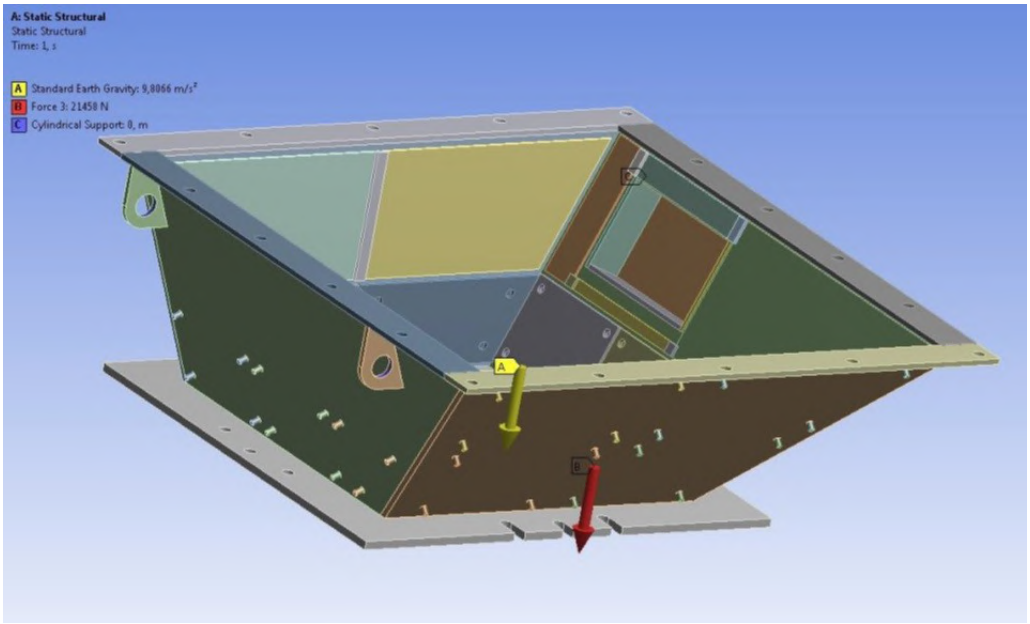

Fig. 3.79 Hopper design loading pattern for designing of lugs

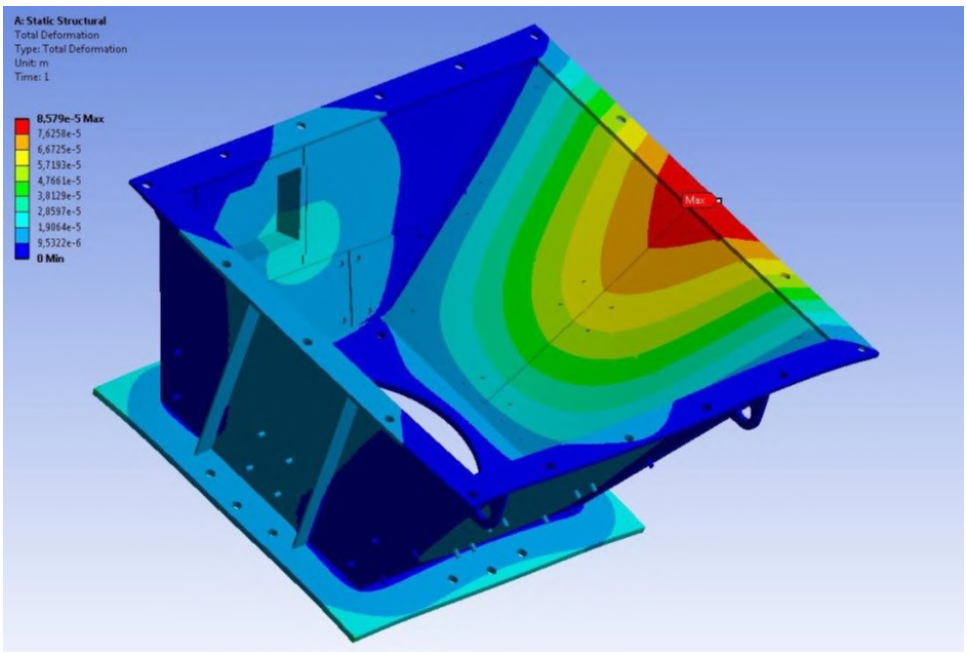

Fig. 3.80 Distribution of total strain arising in the structure

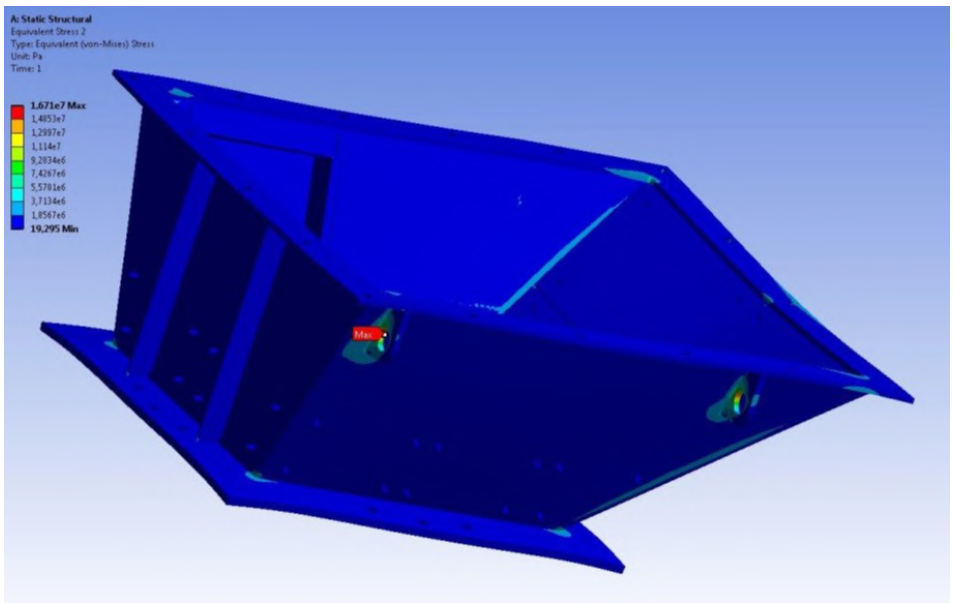

Fig. 3.81 Distribution of von Mises equivalent stresses

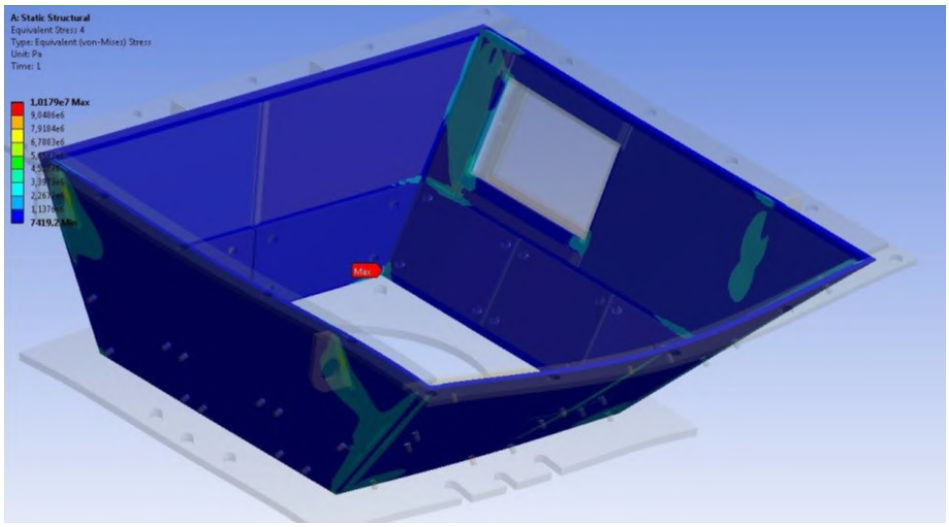

Fig. 3.82 Distribution of von Mises equivalent stresses in the lug

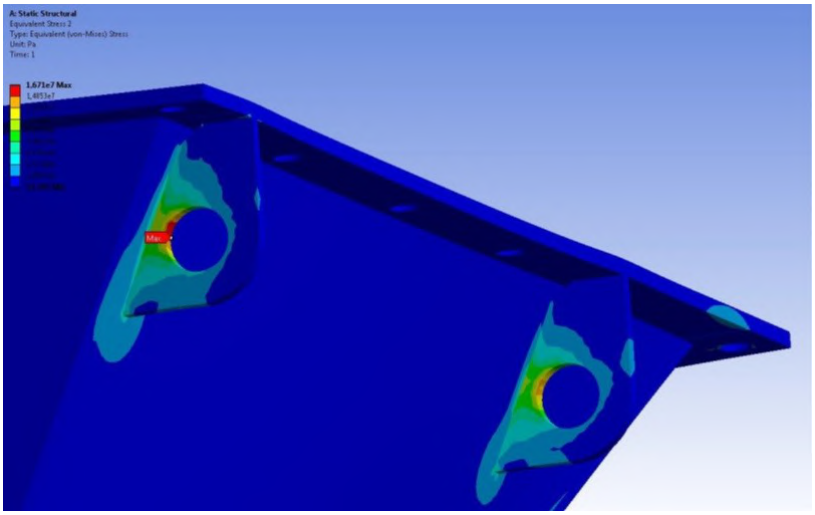

Fig. 3.83 Distribution of von Mises equivalent stresses in the right-hand pair of lugs

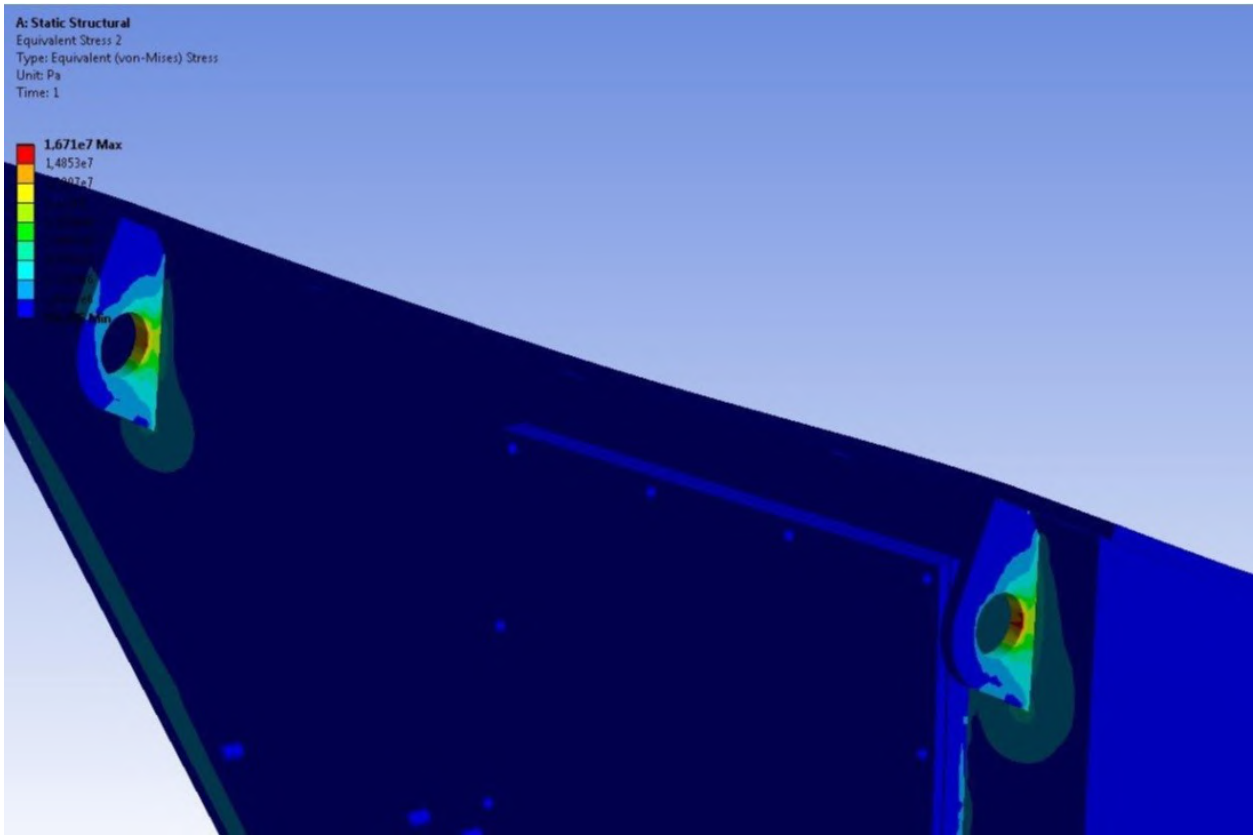

Fig. 3.84 Distribution of von Mises equivalent stresses in the left -hand pair of lugs

The results presented show that the structure meets requirements of strength and stiffness for the load case in question.

3.4.5 Lower hopper design collective results

Calculation results obtained are presented as the summary Table 3.5 of design patterns and controlled variables.

Table 3.5

Design pattern	NSC	NSC+ LWE frontal	NSC+ LWE lateral	NSC+ MDE
Maximum equivalent stresses in the hopper, MPa	**92.3**	**92.3**	**92.3**	**92.3**
Equivalent stresses in sheet 1 of the hopper, MPa, Area 1	**79.0**	**79.0**	**79.0**	**79.0**
Equivalent stresses in sheet 2 of the hopper, MPa, Area 1	**85.7**	**85.7**	**85.7**	**85.7**
Equivalent stresses in sheet 3 of the hopper, MPa, Area 1	**87.6**	**87.6**	**87.6**	**87.6**
Equivalent stresses in sheet 4 of the hopper, MPa, Area 1	**92.3**	**92.3**	**92.3**	**92.3**
Safety factor of the hopper	**1.744**	**1.744**	**1.744**	**1.744**
Safety factor in sheet 1 of the hopper (area 1)	**2.03**	**2.03**	**2.03**	**2.03**
Safety factor in sheet 2 of the hopper (area 1)	**1.878**	**1.878**	**1.878**	**1.878**
Safety factor in sheet 3 of the hopper (area 1)	**1.837**	**1.837**	**1.837**	**1.837**
Safety factor in sheet 4 of the hopper (area 1)	**1.744**	**1.744**	**1.744**	**1.744**

Calculation results presented show that the examined charging hopper's structure meets strength and stiffness requirements for all design loading cases. Wind effect and seismic impact insignificantly affect stress-strain state of the structure.

3.5 CHAPTER CONCLUSIONS

Results of numerical calculation of the hopper show are as follows:

- structures of upper and lower receiving hoppers meet strength and stiffness requirements;

- the definitive design cases of structure service are normal service conditions plus limit value of frontal wind effect and normal service conditions plus maximum design seismic loads;

- structure's elements, supports and lugs meet strength and stiffness requirements for erection and transportation operations with structures.

CONCLUSION

The advancement of technologies and numerical modeling methods is in continuous progress. Increasing computational capabilities and the implementation of artificial intelligence algorithms make it possible to create more complex models. These models allow for more accurate simulation and consideration of all possible external influences and technological changes. The software implementation of the finite element method within application software packages enables the calculation of the strength, stability, and durability of complex structures. Modern topology optimization methods, integrated into these packages, allow for the creation of more advanced designs. In turn, the improvement of metal smelting technologies necessitates changes in the requirements for existing structures. This dynamic of change has become a defining trend in the current development of emerging technologies.

The results presented in this monograph on the design of key elements of a bell-less charging device serve as an example of synthesizing modern numerical modeling tools with new technological developments. This work captures the current level of utilization of numerical modeling tools in the design of structures that implement innovative technologies. The designed structures have a projected service life cycle of 20 years. Each new blast furnace will incorporate emerging technologies and make use of improved structural solutions, developed using even more advanced tools. Life goes on.

The evolution of technology is motion without end.

"Per scientiam — ad progressum."

REFERENCE

1. Візінгер, Х. (n.d.). *Екологічна модернізація сталевої галузі України – довгий шлях*. GMK Center. Retrieved January 15, 2025, from https://gmk.center/ua/opinion/ekologichna-modernizaciya-stalevoi-galuzi-ukraini-dovgij-shlyah/
2. Іванова, К. (n.d.). *ЄБРР прокредитує «АрселорМіттал Кривий Ріг» на $100 млн*. The Page. Retrieved January 15, 2025, from https://thepage.ua/ua/news/yebrr-prokredituye-arselormittal-krivij-rig-na-dollar100-mln
3. Colibrium Additive. (n.d.). *A GE Aerospace company*. Retrieved January 15, 2025, from https://www.colibriumadditive.com/
4. HYBRIT. (n.d.). *Fossil-free steel – a joint opportunity*. Retrieved January 15, 2025, from https://www.hybritdevelopment.se/en/
5. ANSYS Inc. (2018). *Guide to ANSYS programmable features*. Canonsburg, PA.
6. Енциклопедичний словник з металургії. (n.d.). Retrieved January 15, 2025, from http://www.find-info.ru/doc/dictionary/metallurgy/index.htm
7. Paulus GMBH. (n.d.). *Garching, Germany*. Retrieved January 15, 2025, from https://www.northdata.com/Paulus%20GmbH,%20Garching/Amtsgericht%20M%C3%BCnchen%20HRB%2068331
8. Danieli Corus. (n.d.). *International presence*. Retrieved January 15, 2025, from https://www.danieli-corus.com
9. Primetals Technologies. (n.d.). *We pioneer the future of the metals industry*. Retrieved January 15, 2025, from https://www.primetals.com/about-us/who-we-are
10. ResearchGate. (n.d.). *Разработка мероприятий по продлению кампании доменных печей...* [Electronic resource]. Retrieved January 15, 2025, from https://www.researchgate.net/publication/336126543
11. ПАТ «Запорожсталь». (2016, July 4). *Выбросит на загрузочное устройство 165 млн грн*. Prompolit.info. Retrieved January 15, 2025, from https://prompolit.info/2016/07/04/pao-zaporozhstal-vybrosit-na-zagruzochnoe-ustrojstvo-165-mln-grn/
12. Ukrrudprom. (n.d.). *"ArcelorMittal Кривой Рог" посетили поставщики технологии и оборудования для реконструкции доменной печи № 9*. Retrieved January 15, 2025, from https://ukrrudprom.ua/news/ArcelorMittal_Krivoy_Rog_posetili_postavshchiki_tehnologii_i_obo.html
13. Danieli Corus. (n.d.). *Danieli Top Charging Unit with DANCU Distributor*. Retrieved January 15, 2025, from https://www.danieli-corus.com/ironmaking/top-charging-unit
14. Geerdes, M., et al. (2015). *Modern blast furnace ironmaking: An introduction* (3rd ed.). Amsterdam: IOS Press BV.

CONTENTS

INTRODUCTION 3

CHAPTER I

1.1 ASSESSMENT OF THE STRENGTH OF THE CHARGE BUNKER 12

1.1.1 Design features 12

1.2 INITIAL DATA, DEISGN CASES AND DESIGN ARRANGEMENT OF THE BIN 13

1.2.1 Characteristics of bin design 13

1.2.2 Physical and mechanical properties of materials 13

1.2.3 Loads and design loading cases 14

1.2.3.1 Loose material loads on bin's walls 15

1.2.3.2 Wind effect 17

1.2.3.3 Seismic impact 19

1.2.3.4 Permissible stresses and design loading cases 20

1.2.3.5 Design case for normal service conditions 23

1.2.4 Fundamental principles performing calculations and analyzing and calculation results 25

1.2.5 Description of bin designing procedure 27

1.3 BIN DESIGN CALCULATION 29

1.3.1 Structural design under estimated loading 29

1.3.2 Structural design for normal service conditions (NSC) 38

1.3.3 Structural design for seismic impact 47

1.3.3.1 Structure's modal analysis 48

1.3.4 Structural design for wind effect conditions and normal service conditions 52

1.3.5 Designing the bin structural members 68

1.3.5.1 Designing the upper flanged connection 68

1.3.5.2 Designing the lower flanged connection 72

1.3.5.3 Designing the lateral flanged connection 76

1.3.6 Strength calculation of bin design lugs 80
1.3.7 Design collective results 87
1.4 CHAPTER CONCLUSIONS 89

CHAPTER II

2.1 ASSESSMENT OF THE STRENGTH OF THE CENTERING TOP-CHARGING UNIT OF THE BLAST FURNACE 90
2.1.1 Design features 90
2.2 INITIAL DATA, DEISGN CASES AND DESIGN ARRANGEMENT OF THE BIN 91
2.2.2 The material properties and loading cases of the centering top-charging unit 91
2.2.2.1 Loose material loads on the centering top-charging unit walls 92
2.2.2.2 Wind effect 94
2.2.2.3 Seismic impact, permissible stresses and design loading cases 95
2.2.2.4 Design case for normal service conditions 96
2.2.3 Fundamental principles for carrying out calculations and analyzing and calculation results 98
2.2.4 Description of bin designing procedure 100
2.3 CENTERING UNIT DESIGN CALCULATION 100
2.3.1 Structural design under estimated loading 100
2.3.2 Structural design for normal service conditions (NSC) 110
2.3.3 Structural design for seismic impact 119
2.3.3.1 Structure's modal analysis 119
2.3.4 Structural design for wind effect conditions and normal service conditions 123
2.3.4.1 First case of frontal wind effect direction 123
2.3.4.2 Second case of lateral wind effect direction 133
2.3.5 Designing the bin structural members 144
2.3.5.1 Designing the upper flanged connection 144
2.3.5.2 Designing the lower flanged connection 150

2.3.5.3 Designing the lateral flanged connection 153
2.3.6 Strength calculation of centering unit lugs for erection works 158
2.3.7 Design collective results 161
2.4 CHAPTER CONCLUSIONS 163

CHAPTER III

3.1 INTRODUCTION 164
3.2 INITIAL DATA, DESIGN CASES AND DESIGN ARRANGEMENTS OF RECEIVING HOPPERS 165
3.2.1 Characteristics of receiving hopper design 165
3.2.2 The material properties and loading cases of receiving hoppers design 166
3.2.2.1 Loose material loads on hopper's walls 166
3.2.2.2 Wind effect 167
3.2.2.3 Seismic impact, permissible stresses and design loading cases 169
3.2.2.4 Design case for normal service conditions of the upper receiving hopper 171
3.2.2.5 Design case for normal service conditions of the lower receiving hopper 174
3.2.3 Fundamental principles for performing calculations and analysis of calculation data 176
3.2.4 Description of hopper designing procedure 177
3.3 UPPER HOPPER DESIGN CALCULATION 178
3.3.1 Structural design for normal service conditions 178
3.3.2 Upper hopper structural design for wind effect conditions and normal service conditions 183
3.3.2.1 Upper hopper design under frontal wind effect 183
3.3.2.2 Upper hopper design under lateral wind effect 190
3.3.3 Structural design for seismic impact 195
3.3.3.1 Structure's modal analysis 196
3.3.4 Strength calculation of upper hopper design lugs 199

3.3.5 Upper hopper design collective results 204
3.4 LOWER HOPPER DESIGN CALCULATIONS 205
3.4.1 Structural design for normal service conditions 205
3.4.2 Upper hopper structural design for wind effect conditions and normal service conditions 209
3.4.2.1 Lower hopper design under frontal wind effect 209
3.4.2.2 Lower hopper design under lateral wind effect 213
3.4.3 Structural design for seismic impact 218
3.4.3.1 Structure's modal analysis 218
3.4.4 Strength calculation of lower hopper design lugs 221
3.4.5 Lower hopper design collective results 223
3.5 CHAPTER CONCLUSIONS 224
CONCLUSION 225
REFERENCE 226
CONTENTS 227

Монографія містить результати рішень задач проектування конструкцій без конусного колошникового завантажувального пристрою доменної печі. Розглянуті всі розрахункові випадки навантажень конструкцій, а саме нормальних умов експлуатації, вітрового навантаження та сейсмічного впливу. Представлено результати розрахунку основних елементів завантажувального пристрою, а саме: бункерів шихти, центрувача, завантажувальних пристроїв. Результати отримані за допомогою моделювання методом скінченних елементів реалізованого в CAE системі ANSYS.

Для фахівців із механіки твердого деформованого тіла, механіки елементів конструкцій, механіки матеріалів, а також для викладачів, аспірантів і студентів відповідних спеціальностей.

ДНІПРОВСЬКИЙ НАЦІОНАЛЬНИЙ УНІВЕРСИТЕТ ІМЕНІ ОЛЕСЯ ГОНЧАРА

Ліповський Володимир Іванович

«ПРИКЛАДНІ ЗАДАЧІ ПРОЕКТУВАННЯ КОЛОШНИКОВОГО ЗАВАНТАЖУВАЛЬНОГО ПРИСТРОЮ ДОМЕННОЇ ПЕЧІ»

(англійською мовою)

Рецензенти:

Білодіденко Сергій Валентинович, доктор технічних наук, професор, завідувач. кафедри. Галузевого машинобудування Дніпровського металургійного інституту Українського державного університету науки і технологій.

Баюл Костянтин Васильович, доктор технічних наук, старший дослідник, старший науковий співробітник відділу технологічного обладнання систем управління Інституту чорної металургії імені З.І. Некрасова НАН України.

Авторське комп’ютерне оформлення

УДК 669.162.215.2:539.3]=111